



**School of Architecture, Planning and Landscape**

**The Effect of Asymmetrical Street Aspect Ratios on Urban Wind Flow  
and Pedestrian Thermal Comfort Conditions**

**Khalid Setaih**

**A Thesis**

**Submitted to the Graduate School of  
Architecture, Planning and Landscape**

**In Partial Fulfilment of the Requirements for the Degree of  
DOCTOR OF PHILOSOPHY**

**Newcastle University  
Newcastle Upon Tyne, UK**

**October, 2016**

## **Title Page**

**Thesis Title:** The Effect of Asymmetrical Street Aspect Ratios on Urban Wind Flow and Pedestrian Thermal Comfort Conditions

**Full name:** Khalid Mohammad Darweesh Setaih

**Qualification:** Doctor of Philosophy

**School:** School of Architecture, Planning and Landscape

**First supervisor:** Dr Neveen Hamza

**Second supervisor:** Professor Tim Townshend

**Submission Date:** October 2016

**Contact:** [setaih@hotmail.com](mailto:setaih@hotmail.com) ; +966 56 266 7733 (Saudi Arabia);  
[www.setaih.com](http://www.setaih.com) ; [www.diamond-umbrella.com](http://www.diamond-umbrella.com)



## Abstract

Over the last six decades, due to the discovery of oil and improvement in economic conditions in Saudi Arabia, the design of urban traditional neighbourhoods has changed from organic and pedestrian-oriented to geometric and vehicle-oriented, which has greatly influenced the pedestrian use of outdoor spaces. Combined with the high ambient air temperatures, these current trends affect wind flow patterns and pedestrian thermal comfort conditions in the hot arid region of Madinah in Saudi Arabia. Numerous studies were conducted correlating the configuration of urban street geometries (presented by height to width  $H/W$  aspect ratios) with thermal comfort, but mostly conducted in relation to exposure to solar radiation. Most of the previous studies have focused on symmetrical aspect ratios rather than asymmetrical ones, thus limit the available knowledge on asymmetrical canyon studies, which are more representative of actual urban areas. The study of multiple asymmetrical urban street aspect ratios (i.e. diverse buildings height to street width), based on optimising the buildings' height to influence wind flow rate, has not received much attention in the context of urban pedestrian thermal comfort, particularly in low wind speed environments within hot arid regions.

The present study aims to evaluate the effects of multi-asymmetrical street aspect ratios on urban pedestrian microclimate and outdoor thermal comfort conditions, through a case study of Quba Road, to find ways to enhance the thermal comfort level compared to the existing urban configuration. The road is a commercial/residential route linking two prominent religious sites in Madinah. Computational Fluid Dynamics (CFD) ANSYS Fluent 13.0 software is used as a numerical modelling tool to simulate the urban pedestrian microclimates for comparative studies, and results validated by field measurements. The CFD analysis is used for evaluating the air temperature and wind velocity measurements within the windward and leeward canyons of Quba Road. Thermal comfort is expressed by means of the physiologically equivalent temperature (PET) index using RayMan software, with a comfort range of  $21^{\circ}\text{C} - 31.3^{\circ}\text{C}$ .

The findings indicate that the strategy of leeward gradual increase in multiple asymmetrical aspect ratios, with  $H/W$  of 1 – 1.3 – 2.3 (building heights of 12m-15m-27m and streets width of 12m), improves wind velocity magnitudes at the pedestrian level by 169% (from 0.65m/s to 1.75m/s) and reduces ambient air temperatures by  $3.4^{\circ}\text{C}$ , which is recommended for enhancing urban pedestrian microclimates in low wind speed environments. The research predicts that possible changes to the configuration of the urban fabric can decrease urban heat stress for pedestrians by  $4.9^{\circ}\text{C}$  (PET).

**Keywords:** Multi-Asymmetrical street aspect ratio; CFD Numerical Modelling; Hot Arid; Pedestrian Microclimate; Thermal Comfort; Urban Canyon.

## **Related Academic Publications**

### **Conference Papers (published):**

- Setaih, K., Hamza, N. and Townshend, T. (2013a) 'Assessment of Outdoor Thermal Comfort in Urban Microclimate in Hot Arid Areas', *Proceedings of BS2013: 13th Conference of International Building Performance Simulation Association*. Chambéry, France, 26-28 of August. pp. 3153-3160.
- Setaih, K., Hamza, N. and Townshend, T. (2013b) 'Use of CFD Simulation in Urban Design for Outdoor Thermal Comfort in Hot and Dry Climates: A Review', *International PostGraduate Research Conference (IPGRC)*. April 2013. pp. 1069-1076.
- Setaih, K., Hamza, N. and Townshend, T. (2013c) 'Crafting and Assessing Urban Environments Using Computational Fluid Dynamics', *7<sup>th</sup> International Conference of the Arab Society for Computer Aided Architectural Design (Proceedings of ASCAAD)*. Saudi Arabia: Jeddah. ASCAAD, pp. 315-322.

### **Journal Papers (published):**

- Setaih, K., Hamza, N., Mohammed, M.A., Dudek, S. and Townshend, T. (2014) 'CFD Modeling as a Tool for Assessing Outdoor Thermal Comfort Conditions in Urban Settings in Hot Arid Climates', *Journal of Information Technology in Construction (ITcon)*, 19, pp. 248-269.

## Acknowledgements

First and foremost, I thank God, the Almighty, for His providence in my life throughout, especially during my PhD programme. This work could not have been done without the blessings of God.

As a Saudi Arabian citizen, the sponsorship from the government of the Kingdom of Saudi Arabia contributed to covering my living expenses in the UK which helped me in focusing more on my research. I would like to thank our Saudi government for the help and support.

Special thanks are due to both my supervisors, **Dr Neveen Hamza** and **Professor Tim Townshend**, for their academic input and support. Thanks to my friend, **Dr Mohammed Alhaji Mohammed**, for his detailed guidance and constructive comments.

I gratefully acknowledge the guidance of **Dr Mohammed Alhaji Mohammed**, **Dr John Kaiser Calautit**, **Mr. Giuseppe De Simone**, **Professor Bert Blocken**, **Mr. Guven Fidan**, **Dr Islam Abohella**, and **Dr Mohamed Mahgoub** during the setting of the computational part in this work. I emphasise my special thanks to my friends Dr Khalid Mandeli, Dr Mansour Helmi, Dr Mabrouk Alsheliby, Dr Yohannes Firzal, and Dr Chryssa Toufexi, Mr. Hamza Shararah, Mr. Wala Shaikh, Mr. Adil Hammas and Mr. Faisal Horaish, for their advice and instruction during my work.

I would like to express my sincere and deep appreciation and gratitude to my loving family. To my dad **Mohammad Setaih** and my mom **Jamila Bakhsh**, thank you for long years of prayers, caring and support, for always providing me with the needed support and encouragement. Words are inadequate to express my gratitude to my brothers and sisters, whose prayers and patience kept me going. Special thanks to my brother **Adil Setaih** for his patience and understanding in taking good care of my parents and our family while I am away doing my PhD. Very special thanks to my brother in law **Ali Abo Atteiah** for his effort and support during the field study. Thanks to Mrs. Dawn Johnson who accepted me as part of the family in the UK, with care and loving.

I would like to thank my wife **Ola Abo Atteiah** who has been a constant source of support, energy and motivation, experiencing all of the ups and downs of my research with patience, and helping me to be strong, positive and content.

And last but not least, thanks to a long list of friends who made the PhD journey an enjoyable and joyful experience, especially those who have engaged with me in countless thesis related conversations.

## Table of Contents

### **Chapter 1: Introduction**

Abstract.....	iii
Related Academic Publications .....	iv
Acknowledgements.....	v
Table of Contents.....	vi
List of Figures.....	xii
List of Tables .....	xxvii
List of Abbreviations and Nomenclature .....	xxviii
<b>CHAPTER 1: Introduction</b> .....	1
1.1. Introduction.....	2
1.2. Contribution to Knowledge.....	2
1.3. Outdoor Wind Flow and Pedestrian Thermal Comfort.....	6
1.4. The Research Aim and Objectives.....	7
1.5. Research Questions.....	8
1.5.1. Major Research Question.....	8
1.5.2. Minor Research Questions .....	8
1.6. Research Methodology .....	9
1.7. Research Limitation .....	12
1.8. The Organisation of the Thesis .....	14
<b>CHAPTER 2: Nature of the Case Study Area</b> .....	15
2.1. Introduction.....	16
2.2. The Context of Madinah .....	16
2.3. Official Plans for Extending the City Centre in Madinah.....	19
2.4. Local Planning and Regulations for Quba District .....	21
2.5. Initial Analysis of Quba Road.....	22
2.6. Selection of the Case Study Areas .....	27
2.7. Climate of Madinah .....	28
2.8. Summary .....	34
<b>CHAPTER 3: Literature Review on Outdoor Pedestrian Thermal Comfort</b> .....	35
3.1. Introduction.....	36
3.2. Background on Urban Thermal Discomfort .....	36
3.3. Thermal Comfort of Humans .....	38
3.4. Indoor and Outdoor Differences in Thermal Comfort Levels.....	38

3.5.	Outdoor Thermal Comfort Indices.....	41
3.6.	Thermal Comfort Interaction Factors .....	44
3.6.1.	Air Temperature.....	45
3.6.2.	Mean Radiant Temperature (MRT) .....	46
3.6.3.	Wind Speed.....	47
3.6.4.	Relative Humidity .....	47
3.6.5.	Clothing Insulation Ratio (Personal Factor) .....	49
3.6.6.	Activity Level (Metabolism Rate) .....	51
3.7.	Field Studies on Outdoor Thermal Comfort .....	53
3.8.	Assessment Approaches of Outdoor Pedestrian Thermal Comfort .....	62
3.9.	Summary .....	64
<b>CHAPTER 4: Literature Review on the Effects of Urban Street Canyon’s Configurations on Wind Flow .....</b>		<b>65</b>
4.1.	Introduction.....	66
4.2.	Importance of Urban Canyon Design with Microclimatic Awareness .....	66
4.3.	Effect of Urban Street Aspect Ratio on Pedestrian Wind Flow Rate.....	67
4.4.	Best Practice for Urban Heat Stress Mitigation Techniques in Urban Canyons.....	71
4.5.	Urban Roughness and Pedestrian Wind Flow Regime around Buildings.....	78
4.6.	Effect of Air Movement on Temperatures in Urban Contexts.....	82
4.7.	Assessment Approach of Urban Pedestrian Microclimates in a Street Canyon .....	89
4.8.	Previous Numerical Simulation Studies on Urban Microclimate and Thermal Comfort Using CFD Tool.....	92
4.9.	Summary .....	96
<b>CHAPTER 5: Research Methodology .....</b>		<b>97</b>
5.1.	Introduction.....	98
5.2.	Research Methodology Framework .....	98
5.3.	Desktop Survey: Preliminary Data Collection of the Case Study (Phase 1).....	100
5.4.	Field Measurement Procedures (Phase 2).....	101
5.4.1.	Time Selection of the Field Measurements.....	103
5.4.2.	Instruments for Field Measurements.....	105
5.5.	Technical Studies: Secondary Data Collection for Modelling Settings (Phase 3) .....	106
5.5.1.	Estimation of Metabolic Rate and Clothing Level.....	108
5.5.2.	CFD Guidelines on Setting the Simulation Model .....	108
5.5.2.1.	Boundary Conditions .....	111
5.5.2.2.	CFD Guidelines on Setting the Mathematical Models, Turbulent Scheme and Solver Method.....	113

5.5.2.3.	CFD Guidelines on Setting the S2S Radiation Model .....	113
5.5.2.4.	Grid Discretisation and Mesh Dependency Test.....	114
5.6.	CFD Numerical Simulation Procedures (Phase 4).....	117
5.6.1.	Validation of CFD ANSYS-Fluent 13.0 Model.....	118
5.6.2.	Simulation of the Base Model (Existing Conditions) .....	122
5.6.3.	Multi-Asymmetrical H/W Scenarios Based on Optimising the Base Case .....	126
5.6.4.	Scenarios Based on Optimising the Best Proposed Aspect Ratio Model .....	130
5.6.4.1.	Variations of Wind Flow at Night (S-17) and Noon (S-25) for the Best Proposed H/W Model 131	
5.6.4.2.	Increasing the Number of Building's Rows (S-18, S-19) .....	132
5.6.4.3.	Orientation of the Urban Canyon Geometry with Less Prevailing Wind Directions (S-20, S-21) 134	
5.6.4.4.	Configuration of New Streets Perpendicular to the Quba Canyons (S-22, S-23, S-24) 134	
5.6.4.5.	Removal of Buildings (S-26) Forming Open Spaces for a Local Hub .....	135
5.6.4.6.	Protruding Upper Floors for Shading (S-27 and S-28) .....	138
5.6.4.7.	Changes to Albedo Level for Surface Materials (S-29).....	140
5.6.4.8.	Changes to Block Patterns (S-30 and S-31).....	140
5.7.	Calculation of PET Index and MRT Temperatures (Phase 5) .....	141
5.8.	Summary .....	144
<b>CHAPTER 6: Field Measurements for the Assessment of Pedestrian Thermal Comfort ...</b>		<b>145</b>
6.1.	Introduction.....	146
6.2.	The High Urban Density Area (Case 1).....	147
6.2.1.	Pedestrians Number (Case 1).....	148
6.2.2.	Air Temperature.....	150
6.2.3.	Mean Radiant Temperature (Case 1) .....	151
6.2.4.	Wind Speed and Directions (Case 1) .....	155
6.2.5.	Relative Humidity (Case 1).....	160
6.2.6.	Pedestrian's Thermal Comfort Conditions (Case 1) .....	162
6.3.	The Intermediate Urban Density Area (Case 2).....	164
6.3.1.	Air Temperature and Relative Humidity (Case 2) .....	165
6.3.2.	Mean Radiant Temperature and Wind speed (Case 2).....	166
6.3.3.	Pedestrian's Thermal Comfort Conditions (Case 2) .....	169
6.4.	The Low Urban Density Area (Case 3).....	170
6.4.1.	Air Temperature and Wind Speed (Case 3) .....	171
6.4.2.	Mean Radiant Temperature and Relative Humidity (Case 3).....	174

6.4.3.	Pedestrian's Thermal Comfort Conditions (Case 3) .....	176
6.5.	Comparison between the Three Urban Density Levels (Case 1, 2, 3) .....	179
6.5.1.	Summer Results for the Three Urban Density Levels (Case 1, 2, 3) .....	180
6.5.1.1.	Air Temperature in Summer (in Case 1, 2, 3).....	180
6.5.1.2.	Wind Speed in Summer (in Case 1, 2, 3).....	181
6.5.1.3.	Relative Humidity in Summer (in Case 1, 2, 3).....	183
6.5.1.4.	Mean Radiant Temperature (MRT) in Summer (in Case 1, 2, 3) .....	184
6.5.1.5.	Pedestrian's Thermal Comfort Conditions in Summer (in Case 1, 2, 3).....	185
6.5.2.	Spring Results for the Three Density Areas (Case 1, 2, 3) .....	187
6.5.2.1.	Air Temperature during Spring (Case 1, 2, 3) .....	187
6.5.2.2.	Wind Speed during Spring (Case 1, 2, 3).....	189
6.5.2.3.	Relative Humidity during Spring (Case 1, 2, 3).....	190
6.5.2.4.	Mean Radiant Temperature (MRT) during Spring (Case 1, 2, 3) .....	191
6.5.2.5.	Pedestrian's Thermal Comfort Conditions during Spring (Case 1, 2, 3) .....	192
6.5.3.	Winter Results for the High and Low Urban Density Areas (Case 1 and 3) .....	194
6.5.3.1.	Air Temperature during Winter (Case 1 and 3) .....	194
6.5.3.2.	Wind Speed during Winter (Case 1 and 3) .....	195
6.5.3.3.	Relative Humidity during Winter (Case 1 and 3) .....	196
6.5.3.4.	Mean Radiant Temperature (MRT) during Winter (in Case 1 and 3).....	198
6.5.3.5.	Pedestrian's Thermal Comfort Conditions during Winter (Case 1 and 3).....	199
6.6.	Summary .....	200
<b>CHAPTER 7: The Effect of Asymmetrical Street Aspect Ratios on Urban Wind Flow and Pedestrian Thermal Comfort .....</b>		<b>205</b>
7.1.	Introduction.....	206
7.2.	Base Case Scenario (S-1).....	208
7.2.1.	Shading Level in Base Case (S-1).....	212
7.2.2.	Wind Velocity at the Pedestrian Level (S-1) .....	214
7.2.3.	Air Temperature at the Pedestrian Level (S-1) .....	220
7.3.	Symmetrical Aspect Ratios (S-2) Scenario.....	225
7.3.1.	Wind Velocity at the Pedestrian Level (S-2) .....	226
7.3.2.	Air Temperature at the Pedestrian Level (S-2) .....	231
7.4.	Multi-Asymmetrical Aspect Ratios Scenarios (S-3 to S-16) .....	236
7.4.1.	Lower Multi-Asymmetrical Aspect Ratios Scenarios (S-3 and S-4) .....	240
7.4.1.1.	Wind Velocity at the Pedestrian Level (S-3, S-4).....	241
7.4.1.2.	Air Temperature at the Pedestrian Level (S-3, S-4).....	243
7.4.2.	Medium Multi-Asymmetrical Aspect Ratios Scenarios (S-5, S-6, S-7) .....	245

7.4.2.1.	Wind Velocity at the Pedestrian Level (S-5, S-6, S-7) .....	247
7.4.2.2.	Air Temperature at the Pedestrian Level (S-5, S-6, S-7) .....	249
7.4.3.	Higher Multi-Asymmetrical Aspect Ratios Scenarios (S-8 through S-12).....	252
7.4.3.1.	Wind Velocity at the Pedestrian Level (S-8 through S-12) .....	253
7.4.3.2.	Air Temperature at the Pedestrian Level (S-8 through S-12) .....	258
7.4.4.	Leeward Gradual Increase in Asymmetrical Aspect Ratios (S-13 to S-16).....	261
7.4.4.1.	Wind Velocity at the Pedestrian Level (S-13, S-14, S-15, S-16).....	262
7.4.4.2.	Air Temperature at the Pedestrian Level (S-13, S-14, S-15, S-16).....	266
7.5.	Assessment of Pedestrian Thermal Comfort Conditions of the Best Aspect Ratios Model	269
7.5.1.	PET Temperature at the Pedestrian Level in the Base Case (S-1) .....	271
7.5.2.	PET Temperature at the Pedestrian Level in the Best Asymmetrical Aspect Ratio Model (S-11).....	272
7.6.	Summary .....	276
<b>CHAPTER 8: Further Analysis and Design Implications (based on the Best Proposed H/W Model)</b> .....		278
8.1.	Introduction.....	279
8.2.	Variation of Microclimate at Night (S-17) and at Noon (S-25) for the Best Proposed H/W Model .....	281
8.2.1.	Wind Velocity at the Pedestrian Level (S-17Night and S-25Noon) .....	282
8.2.2.	Air Temperature at the Pedestrian Level (S-17Night and S-25Noon) .....	286
8.3.	Increasing the Number of Buildings' Rows (S-18, S-19) .....	290
8.3.1.	Wind Velocity at the Pedestrian Level (S-18, S-19).....	291
8.3.2.	Air Temperature at the Pedestrian Level .....	295
8.4.	Orientation of the Urban Canyon Geometry (S-20, S-21) .....	298
8.4.1.	Wind Velocity at the Pedestrian Level (S-20, S-21).....	299
8.4.2.	Air Temperature at the Pedestrian Level (S-20, S-21).....	301
8.5.	Configuration of New Streets Perpendicular to the Quba Canyons (S-22, S-23, S-24)	303
8.5.1.	Wind Velocity at the Pedestrian Level (S-22, S-23, S-24) .....	304
8.5.2.	Air Temperature at the Pedestrian Level (S-22, S-23, S-24) .....	306
8.6.	Removal of Buildings (S-26) Forming Open Spaces for a Local Hub .....	308
8.6.1.	Wind Velocity at the Pedestrian Level (S-26: Removal of Buildings) .....	311
8.6.2.	Air Temperature at the Pedestrian Level (S-26: Removal of Buildings).....	313
8.7.	Protruding Upper Floors for Shading (S-27 and S-28) .....	315
8.7.1.	Shading Level (S-27 and S-28).....	316
8.7.2.	Wind Velocity at the Pedestrian Level (S-27 and S-28) .....	317
8.7.3.	Air Temperature at the Pedestrian Level (S-27 and S-28).....	320



8.8.	Changes to Albedo Level of Surface Materials (S-29) .....	323
8.8.1.	Wind Velocity at the Pedestrian Level (S-29) .....	324
8.8.2.	Air Temperature at the Pedestrian Level (S-29) .....	325
8.9.	Changes to Block Patterns (S-30 and S-31) .....	326
8.9.1.	Wind Velocity at the Pedestrian Level (S-30, S-31) .....	327
8.9.2.	Air Temperature at the Pedestrian Level (S-30, S-31) .....	329
8.10.	Implementation of the Research for Future Planning .....	332
8.10.1.	The Influence of Multi-Asymmetrical Aspect Ratios on Microclimate .....	332
8.10.2.	The Influence of Multi-Asymmetrical Aspect Ratios on Thermal Comfort .....	333
8.10.3.	The Influence of Increasing the Number of Buildings on Wind Flow in the Leeward Urban Areas .....	335
8.10.4.	The Replicability of the Proposed Asymmetrical Aspect Ratios .....	336
8.11.	Summary .....	337
<b>CHAPTER 9: Conclusions and Recommendations for Future Work</b> .....		339
9.1.	Introduction .....	340
9.2.	Main Conclusions .....	340
9.3.	Limitations of This Research and Implications for Future Research .....	348
9.4.	Recommendations .....	349
References .....		350
Appendices .....		371

## List of Figures

FIG. 1. 1: QUBA ROAD CANYONS, NORTH-SOUTH ORIENTATION, LINKING TWO MOST VISITED MOSQUES IN THE CITY. ....	5
FIG. 1. 2: METHODOLOGY AND OPERATIONAL FRAMEWORK OF THE CURRENT RESEARCH. ....	10
FIG. 2. 1: GEOGRAPHICAL SETTINGS OF MADINAH IN SAUDI ARABIA. SOURCE: MMM GROUP LIMITED ET AL. (2012D). ....	17
FIG. 2. 2: THE STRATEGIC MAP OF MADINAH CITY HIGHLIGHTING THE QUBA ROAD, THE SURROUNDING NATURAL FEATURES AND THE URBAN PATTERNS OF THE CITY. IT POINTS AT THE TWO MOST VISITED MOSQUES. ....	19
FIG. 2. 3: THE LOCATIONS OF THE EXISTING QUBA ROAD AND THE FUTURE NEW QUBA ROAD, AND THE FUTURE MAJOR PEDESTRIAN ROAD WITH NO CAR ACCESS. IT ALSO SHOWS THE EXTENDED BOUNDARY OF THE CITY CENTRE IN 30 YEARS. SOURCE: ADAPTED FROM MMM GROUP LIMITED ET AL. (2012D). ....	21
FIG. 2. 4: CROSS-SECTIONS OF THE QUBA ROAD. ....	23
FIG. 2. 5: ANALYSIS OF THE LAND USE, STRENGTHS AND WEAKNESSES OF QUBA ROAD, AND AREAS WITH URBAN DEVELOPMENT OPPORTUNITY. SOURCE: SETAIH (2010). ....	24
FIG. 2. 6: NUMBER OF PEDESTRIANS DURING THE 24 HOURS COMPARED WITH THE AIR & MEAN RADIANT TEMPERATURES. THE DATA OBTAINED IN THE HIGH URBAN DENSITY AREA (CASE 1) IN SPRING WERE, BASED ON AVERAGE HOURLY VALUES FOR THE MONITORING DURATION (1 <sup>ST</sup> TO THE 12 <sup>TH</sup> OF APRIL). SOURCE: SETAIH ET AL. (2013A). ....	26
FIG. 2. 7: THREE CASE STUDY AREAS SELECTED BASED ON DIFFERENT URBAN DENSITY LEVELS. THE CASE STUDY OF HIGH URBAN DENSITY AREA FALLS WITHIN THE FUTURE EXTENDED CITY CENTRE. ....	27
FIG. 2. 8: FIELD MEASUREMENTS (POINTS P1, P2, P3) LOCATIONS FOR THE CASE STUDY OF THE THREE URBAN DENSITIES, LOCATED AT A HEIGHT OF 2M ABOVE THE GROUND (I.E. PEDESTRIAN HEIGHT). ....	28
FIG. 2. 9: THE WEATHER READINGS IN MADINAH CITY OVER A 36-YEAR PERIOD FOR AVERAGE DAILY HIGH AND LOW RELATIVE HUMIDITY. SOURCE: WWW. WEATHERSPARK.COM (ACCESSED ON 10.09.2015). ....	29
FIG. 2. 10: CHANGES OF SEASONAL WIND DIRECTIONS REACHING THE ARABIAN PENINSULA, AND AVERAGE SEA LEVEL PRESSURE. SOURCE: VINCENT, 2008; CITED IN MMM GROUP LIMITED ET AL. (2012B). ....	29
FIG. 2. 11: THE FIGURE SHOWS THREE YEARLY PREVAILING WIND DIRECTIONS: SOUTH-WEST, WESTERLY, AND NORTH-WEST. YEARLY AVERAGE WIND SPEED IS AROUND 3.1M/S. SOURCE: IOWA (2015). ....	30
FIG. 2. 12: WIND ROSES SHOWING THE MONTHLY PREVAILING WIND SPEEDS AND DIRECTIONS. SOURCE: IOWA STATE UNIVERSITY OF SCIENCE AND TECHNOLOGY (ACCESSED ONLINE IN FEBRUARY, 2015). ....	31
FIG. 2. 13: AIR TEMPERATURE BASED ON MADINAH METEOROLOGICAL CENTRE (2012), SHOWING MONTHS OF APRIL AND OCTOBER WITH A TOLERABLE AIR TEMPERATURE SITUATED AT THE EDGES OF A CRITICAL HOT PERIOD, AND HIGHLIGHTING THE OUTDOOR THERMAL COMFORT ZONE IN HOT ARID CLIMATE (I.E. 21 <sup>0</sup> C TO 31.3 <sup>0</sup> C) BASED ON PHYSIOLOGICAL EQUIVALENT TEMPERATURE (PET) INDEX PROPOSED BY YAHIA AND JOHANSSON (2013A). ....	32
FIG. 2. 14: SUN POSITION IN MADINAH AT THE SIMULATION PERIOD (I.E. 1 <sup>ST</sup> OF APRIL 2013, REPRESENTING SPRING SEASON AT 15:00). PREVAILING WIND DIRECTION IS SOUTH WESTERLY. THE NAZIL AND TALI'E QUBA ROADS ARE ALSO HIGHLIGHTED.. SOURCE: CALCULATED USING THE FOLLOWING WEBSITE <a href="http://www.sunearthtools.com/">HTTP://WWW.SUNEARTHTOOLS.COM/</a> .....	33
FIG. 3. 1: THE COMPARISON BETWEEN AIR TEMPERATURES MEASURED IN AN URBAN CANYON, A SUBURBAN AREA, AND OPEN REFERENCE SITES. SOURCE: ERELL AND WILLIAMSON (2007:1249). ....	46
FIG. 3. 2: THE RELATIONSHIP BETWEEN THE AVERAGE RELATIVE HUMIDITY AND THE AIR TEMPERATURE LEVELS DURING THE YEAR (1961 TO 1990). SOURCE: YAHIA (2012). ....	49
FIG. 3. 3: SUMMER AND WINTER TRADITIONAL MALE CLOTHING AND THEIR CLO VALUE. NOTE THAT FEMALE CLOTHING INSULATION VALUES ARE MENTIONED WITHIN THE TEXT. SOURCE: AL-AJMIA ET AL. (2008). ..	51
FIG. 3. 4: RELATIONSHIP BETWEEN THE RADIATION INTENSITY RATE AND THE NUMBER OF PLACE USERS. THE PICTURE ON THE LEFT SHOWS LESS SOLAR INTENSITY THAN THE ONE ON THE RIGHT. SOURCE: ALJAWABRA AND NIKOLOPOULOU (2010). ....	55

FIG. 3. 5: COMFORT OUTDOOR TEMPERATURE CHART THAT SHOWS THE RECOMMENDED WIND SPEEDS FOR DIFFERENT SOLAR RADIATION LEVELS AS WELL AS FOR DIFFERENT AIR TEMPERATURES. SOURCE: CHENG AND NG (2006). .....	57
FIG. 3. 6: THE ESTIMATION THERMAL SENSATION AGAINST PET INDEX IN HOT ARID SUMMER OF RIYADH, SAUDI ARABIA. SOURCE: ABDEL-GHANY ET AL. (2013). .....	58
FIG. 3. 7: THE GRAPH SHOWS THE RANGES OF PET TEMPERATURE THAT IS APPLICABLE FOR HOT ARID CLIMATES. IT ALSO SHOWS PET FOR THE E–W-ORIENTED CANYON OF HEIGHT 5 AND WIDTH 10, FOR THE NO-GREEN AND WITH GREEN CASES, INSIDE THE CANYON AND ON THE ROOF, FOR RIYADH. SOURCE: ALEXANDRI AND JONES (2008). .....	59
FIG. 4. 1: INTERACTION BETWEEN URBAN MORPHOLOGY, MICROCLIMATE AND PEDESTRIAN'S THERMAL COMFORT. SOURCE: ADAPTED BY THE AUTHOR, SOURCE: AHMED-OUAMEUR AND POTVIN (2007). .....	67
FIG. 4. 2: THREE WIND FLOW REGIMES OVER ARRAYS OF BUILDINGS FOR DIFFERENT ASPECT RATIOS. SOURCE: OKE (1988). .....	69
FIG. 4. 3: STREAMLINES OF FLOW VORTICES WITHIN DIFFERENT ASPECT RATIOS OF; (A) 1.6, (B) 2.86 WITH TWO CIRCULATIONS (SOURCE: ADAPTED FROM JEONG AND ANDREWS, 2002), AND ASPECT RATIO OF 3.6 AND POTENTIAL TEMPERATURE DIFFERENCES OF (C) 0K, (D) 4K, WITH THREE-CIRCULATION REGIME (SOURCE: ADAPTED FROM KIM AND BAIK, 2001). .....	70
FIG. 4. 4: VELOCITY MAGNITUDE FOR ASWAN AND FARAFRA MODELS IN HOT ARID EGYPTIAN CLIMATE. DECREASING THE PASSAGE BETWEEN BUILDINGS WHILE USING WIDER STREET CANYONS. SOURCE: RIZK AND HENZE (2010). .....	73
FIG. 4. 5: SURFACE ALBEDO VALUES. SURFACES WITH WHITE PAINT USUALLY HAVE HIGHER ALBEDO THAN DARK MATERIALS, AND REFLECT MORE SOLAR RADIATION AND ARE GENERALLY COOLER. SOURCE: AKBARI ET AL. (1992). .....	74
FIG. 4. 6: REPRESENTATION OF WIND FLOW DIVERGENCE AROUND A RECTANGULAR BUILDING, WHICH IS CAUSED BY PRESSURE DIFFERENCE. SOURCE: RE-ILLUSTRATED FROM BLOCKEN AND CARMELIET (2004B). .....	79
FIG. 4. 7: WIND VELOCITY PROFILES REFLECTING DEFERENT TERRAINS ROUGHNESS AS WELL AS AERODYNAMIC ROUGHNESS ( $z_0$ ) REGARDING THE HEIGHT FROM THE GROUND AND THE USE OF A REQUIRED DISPLACEMENT LENGTH (D). SOURCE: STANKOVIC ET AL. (2009:78). .....	81
FIG. 4. 8: WIND SPEED CONTOURS EXTRACTED FROM CFD SIMULATION AT 3.5M ABOVE THE GROUND FOR URBAN STREETS ORIENTATIONS WITH THREE WIND FLOW DIRECTIONS (0o, 45o, AND 90o) IN HONG KONG. SOURCE: YUAN AND NG (2012). .....	84
FIG. 4. 9: OBLIQUE WIND DIRECTION AT 45°. SOURCE: LEE AND WONG (2014). .....	86
FIG. 4. 10: DIFFERENT STREET PATTERNS (E.G. A) GRID BLOCK POSITION STYLE, B) CHESS-BOARD STYLE) CAN AFFECT THE WIND VELOCITY AND BLOCKING RATIO OF DUSTY WINDS. SOURCE: GOLANY (1996). .....	87
FIG. 4. 11: ORIENTATION OF URBAN PATTERN DIAGONALLY TO EAST-WEST AXIS. A) IS A GRID PATTERN; B) NARROW ZIGZAGGING ALLEYS; AND C) BLOCKING STREETS OR PERPENDICULAR. SOURCE: GUT AND ACKERKNECHT (1993). .....	88
FIG. 4. 12: MOVEMENT OF MARKERS IN THE VENTILATION PATH: (A) BEFORE THE REARRANGEMENT; (B) AFTER THE REARRANGEMENT. SOURCE: OGURO ET AL. (2002); CITED IN MURAKAMI (2006). .....	89
FIG. 5. 1: METHODOLOGY AND OPERATIONAL FRAMEWORK OF THE CURRENT RESEARCH. ....	99
FIG. 5. 2: MEASUREMENTS SITES ALONG QUBA ROAD, IN THE SOUTHERN PART OF THE CITY, CHARACTERISED BY DIFFERENT URBAN DENSITY ZONES. ....	101
FIG. 5. 3: FIELD MEASUREMENTS POINTS (P1, P2, P3) LOCATIONS FOR THE CASE STUDY OF THE THREE URBAN DENSITIES, LOCATED AT A HEIGHT OF 2M ABOVE THE GROUND (I.E. PEDESTRIAN HEIGHT). .....	102
FIG. 5. 4: AIR TEMPERATURE BASED ON MADINAH METEOROLOGICAL CENTRE (2012), SHOWING MONTHS OF APRIL AND OCTOBER WITH A TOLERABLE AIR TEMPERATURE SITUATED AT THE EDGES OF A CRITICAL HOT PERIOD, AND HIGHLIGHTING THE OUTDOOR THERMAL COMFORT ZONE FOR HOT ARID CLIMATE (I.E. 21°C TO 31.3°C) BASED ON PHYSIOLOGICAL EQUIVALENT TEMPERATURE (PET) INDEX PROPOSED BY YAHIA AND JOHANSSON (2013A). .....	104

FIG. 5. 5: A PORTABLE INTEGRATED WEATHER STATION KESTREL 4400 HEAT STRESS TRACKER WAS LOCATED AT 2M OF HEIGHT. THE PICTURES WERE TAKEN AT THE INTERMEDIATE URBAN DENSITY AREA WITHIN NAZIL QUBA ROAD. ....	106
FIG. 5. 6: PEDESTRIANS IN QUBA ROAD ARE OBSERVED WEARING HEAVY CLOTHING LAYERS IN COLD WINTER AND LIGHTER IN HOT SEASONS. ....	108
FIG. 5. 7: COMPUTATIONAL DOMAIN DIMENSION AND THE BOUNDARY CONDITIONS IN THE CURRENT RESEARCH. H IS THE HEIGHT OF THE TALLEST BUILDING. ....	110
FIG. 5. 8: REFINED MESH WAS APPLIED AT THE AREA OF INTEREST AND THE SURROUND BUILDINGS. THE CELLS SIZE IS 0.2M X 0.4 M AND THE STRETCHING RATIO ON THE MESH RESOLUTION IS 1.2. THE TOTAL NUMBER OF CELLS IN THE COMPUTATIONAL DOMAIN IS 3,385,643 CELLS. 10 LAYERS WITH 0.2M OF CELLS WERE APPLIED NEAR WALL SURFACES. ....	116
FIG. 5. 9: THE CURRENT RESEARCH DEPENDENCY TEST OF THE COARSE CELLS, FINE CELLS AND FINER CELLS. ....	117
FIG. 5. 10: A TYPICAL EXAMPLE FOR CONVERGENCE THAT WAS OBTAINED WITHIN THE CURRENT STUDY. ....	121
FIG. 5. 11: HIGH URBAN DENSITY CASE (BASE MODEL). INTEREST AREA OF THE STUDY IS 120 X 90M AND THE WIDTH OF THE TALİ'E AND NAZIL QUBA ROADS IS 12M. ....	122
FIG. 5. 12: ASYMMETRIC ASPECT RATIOS OF THE EXISTING (E) CASE IN THE INTEREST AREA, PARTICULARLY ALONG THE FIVE CROSS-SECTIONS OF MEASUREMENTS POINTS. NOTE THAT MOST OF THE NUMBERS IN H/W ARE ROUNDED UP. ....	124
FIG. 5. 13: THE FIGURE SHOWS 15 MEASUREMENTS POINTS EXTRACTED FOR EACH OF THE TWO QUBA CANYONS. EACH CANYON CONTAINS OF THREE ROWS OF MEASUREMENTS POINTS, I.E. ALONG THE MIDDLE OF THE ROAD, NEAR LEEWARD ELEVATIONS (LEFT) AND NEAR WINDWARD ELEVATIONS (RIGHT). ....	125
FIG. 5. 14: A SIMPLIFIED CONCEPT SHOWING THE LOCATIONS OF THREE ROWS OF MEASUREMENT POINTS (LEFT, MIDDLE AND RIGHT; WITH 15 POINTS IN EACH CANYON) BETWEEN THE THREE ROWS OF BUILDINGS IN THE INTEREST AREA. ....	125
FIG. 5. 15: SYMMETRICAL ASPECT RATIO (S-2) SCENARIO WITH FIVE SIMULATED LOCATIONS OF MEASUREMENT POINTS, SHOWING UNIFIED BUILDINGS HEIGHT OF 12M FOR THE THREE ROWS OF BUILDINGS. ....	126
FIG. 5. 16: THE BEST PROPOSED MULTI-ASYMMETRICAL ASPECT RATIOS SCENARIO (S-11) WITH FIVE SET OF MEASUREMENT LOCATIONS FOR EACH OF THE TWO MAIN CANYONS AT THE PEDESTRIAN LEVEL. ....	132
FIG. 5. 17: INCREASING THE NUMBER OF ROWS OF BUILDINGS ON THE BEST ASPECT RATIO SCENARIO FROM 3 ROWS TO 6 ROWS. THE LAST THREE ROWS ARE POSITIONED AS GRID STYLE IN S-18, WHILE AS CHESS-BOARD IN S-19. ....	133
FIG. 5. 18: ORIENTATION OF URBAN CANYON GEOMETRY WITH THE WESTERLY SECOND PREVAILING WIND DIRECTION (S-20 SCENARIO) AND NORTH-WESTERLY THIRD PREVAILING WIND DIRECTION (S-21 SCENARIO). ....	134
FIG. 5. 19: THREE SCENARIOS ON THE CONFIGURATION OF NEW STREETS THAT ARE PARALLEL WITH THE MAIN PREVAILING WIND DIRECTION, WHILE IT IS APPROXIMATELY PERPENDICULAR TO THE NORTH-SOUTH AXIS OF QUBA CANYONS. ....	135
FIG. 5. 20: SCENARIO S-26 BASED ON REMOVING BUILDINGS AND OR CREATING OPEN SPACES AND PASSAGES, PARTICULARLY AT SIMULATION LOCATION NUMBER 4 IN THE LEEWARD CANYON (I.E. NAZIL QUBA ROAD). ....	136
FIG. 5. 21: CONCEPTUAL DIAGRAM FOR PROPOSED COMMUNAL NODES AND LOCAL HUBS IN QUBA ROAD BASED ON ACCEPTABLE MAXIMUM WALKING TIME (IN MINUTES) AND DISTANCE (IN METRES). ADAPTED FROM SETAIH (2010). ....	137
FIG. 5. 22: PROTRUDING UPPER FLOORS SCENARIO IN S-27 AND S-28 SCENARIOS, WITH 9M STREET OPENESS TO THE SKY. ....	138
FIG. 5. 23: CHANGES TO BLOCK PATTERNS IN S-30 WITH GRID BUILDING POSITION AND S-31 WITH CHESS BOARD BUILDING POSITION, AND INCREASING THE NUMBER OF ROWS TO BE TOTAL OF 6 ROWS. ....	141
FIG. 5. 24: INTERFACE OF RAYMAN SOFTWARE V. 1.3. TO OBTAIN PET THERMAL COMFORT VALUES. THE REQUIRED SIX MAIN INPUTS ARE NUMBERED IN THIS IMAGE FROM 1 TO 6. ....	142
FIG. 6. 1: MEASUREMENTS SITES ALONG QUBA ROAD, CHARACTERISED BY DIFFERENT URBAN DENSITY ZONES. ....	147

FIG. 6. 2: IN-SITU MEASUREMENTS POINT LOCATION IN A HIGH URBAN DENSITY AREA (CASE1) IN THE NAZIL QUBA ROAD (I.E. LEEWARD CANYON). .....	148
FIG. 6. 3: NUMBER OF PEDESTRIANS IN HIGH URBAN DENSITY AREA, DURING SPRING, AUTUMN, AND WINTER. HIGHLIGHTED THE 5 PRAYER TIMES. ....	149
FIG. 6. 4: AIR TEMPERATURE PATTERN AT A HEIGHT OF 2M ABOVE THE GROUND FOR THE FOUR CLIMATIC SEASONS IN THE HIGH URBAN DENSITY AREA (CASE 1), BASED ON AVERAGE HOURLY VALUES DURING THE WHOLE MONITORING DURATION. ....	150
FIG. 6. 5: SOME OF THE HOURLY AIR TEMPERATURES VALUES (I.E.4 TO 7 DAYS ) REPRESENTING THE TEMPERATURE PATTERN FOR THE FOUR CLIMATIC SEASONS IN THE HIGH URBAN DENSITY AREA (CASE 1) AT 2M HEIGHT ABOVE THE GROUND. ....	151
FIG. 6. 6: MRT PATTERN AT A HEIGHT OF 2M ABOVE THE GROUND FOR THE FOUR CLIMATIC SEASONS IN THE HIGH URBAN DENSITY AREA (CASE 1), BASED ON AVERAGE HOURLY VALUES DURING THE WHOLE MONITORING DURATION. ....	152
FIG. 6. 7: SOME OF THE HOURLY MRT VALUES (I.E.4 TO 7 DAYS ) REPRESENTING THE MRT PATTERN FOR THE FOUR CLIMATIC SEASONS IN THE HIGH URBAN DENSITY AREA (CASE 1) AT 2M HEIGHT ABOVE THE GROUND. ....	152
FIG. 6. 8: DIFFERENCE IN VALUES BETWEEN MEAN RADIANT TEMPERATURE (MRT) AND AIR TEMPERATURE IN THE HIGH URBAN DENSITY AREA (CASE 1). ....	153
FIG. 6. 9: AMOUNT OF SHADING IN THE QUBA ROAD CANYONS OVER A YEAR AT 09:00, 12:00 AND 15:00 HOURS .....	154
FIG. 6. 10: WIND SPEED VALUES FOR THE FOUR CLIMATIC SEASONS IN THE HIGH URBAN DENSITY AREA (CASE 1). THE FIGURE HIGHLIGHTS THE RECOMMENDED WIND SPEED ZONE FOR PEDESTRIANS. ....	155
FIG. 6. 11: SOME OF THE HOURLY WIND SPEED VALUES (I.E.4 TO 7 DAYS ) REPRESENTING THE SPEED PATTERN FOR THE FOUR CLIMATIC SEASONS IN THE HIGH URBAN DENSITY AREA (CASE 1) AT 2M HEIGHT ABOVE THE GROUND. ....	156
FIG. 6. 12: WIND ROSE FOR AUTUMN SEASON (OCTOBER, 2012) IN THE HIGH URBAN DENSITY AREA (CASE 1). ....	158
FIG. 6. 13: WIND ROSE FOR WINTER SEASON (JANUARY, 2013) IN THE HIGH URBAN DENSITY (CASE 1). ....	158
FIG. 6. 14: WIND ROSE FOR SPRING SEASON (APRIL, 2013) IN THE HIGH URBAN DENSITY (CASE 1). ....	159
FIG. 6. 15: WIND ROSE FOR SUMMER SEASON (JUNE, 2013) IN THE HIGH URBAN DENSITY AREA (CASE 1). ....	159
FIG. 6. 16: COMPARISON BETWEEN THE RELATIVE HUMIDITY VALUES OF THE FOUR CLIMATIC SEASONS IN THE HIGH URBAN DENSITY AREA (CASE 1). ....	160
FIG. 6. 17: SOME OF THE HOURLY RELATIVE HUMIDITY VALUES (I.E.4 TO 7 DAYS ) REPRESENTING THE HUMIDITY PATTERN FOR THE FOUR CLIMATIC SEASONS IN THE HIGH URBAN DENSITY AREA (CASE 1) AT 2M HEIGHT ABOVE THE GROUND. ....	161
FIG. 6. 18: COMPARISON BETWEEN THE PHYSIOLOGICALLY EQUIVALENT TEMPERATURE (PET) INDEX VALUES OF THE FOUR CLIMATIC SEASONS IN THE HIGH URBAN DENSITY AREA (CASE 1). THE UPPER LIMIT IN SUMMER AND LOWER LIMIT IN WINTER COMFORT ZONE IN HOT ARID AREAS ARE 31.3°C AND 21°C, RESPECTIVELY. ....	162
FIG. 6. 19: MEASUREMENT LOCATION FOR THE INTERMEDIATE URBAN DENSITY AREA (CASE 2), BETWEEN TWO SYMMETRICAL BUILDINGS (21M HEIGHT), AND DISTANCED 2.5M FROM THE WINDWARD ELEVATION. ....	165
FIG. 6. 20: COMPARISON BETWEEN THE AIR TEMPERATURE AND RELATIVE HUMIDITY VALUES FOR THE SPRING AND SUMMER SEASONS IN THE INTERMEDIATE URBAN DENSITY AREA (CASE 2). ....	166
FIG. 6. 21: THE MRT VALUES IN THE SPRING AND SUMMER SEASONS IN THE INTERMEDIATE URBAN DENSITY AREA (CASE 2). ....	167
FIG. 6. 22: THE DIFFERENCE IN VALUES BETWEEN THE MRT AND AIR TEMPERATURE IN THE INTERMEDIATE URBAN DENSITY AREA (CASE 2). ....	167
FIG. 6. 23: COMPARISON BETWEEN THE WIND SPEED VALUES OF THE SPRING AND SUMMER SEASONS IN THE INTERMEDIATE URBAN DENSITY AREA (CASE 2). ....	168
FIG. 6. 24: COMPARISON BETWEEN THE PHYSIOLOGICALLY EQUIVALENT TEMPERATURE (PET) INDEX VALUES OF THE SPRING AND SUMMER SEASONS IN THE INTERMEDIATE URBAN DENSITY AREA (CASE 2). THE UPPER LIMIT IN SUMMER AND LOWER LIMIT IN WINTER COMFORT ZONE IN HOT ARID AREAS ARE 31.3°C AND 21°C, RESPECTIVELY. ....	169

FIG. 6. 25: FIELD MEASUREMENT LOCATION AT THE LOW URBAN DENSITY AREA (CASE 3) ALONG QUBA ROAD.	170
FIG. 6. 26: COMPARISON BETWEEN THE AIR TEMPERATURE VALUES OF THE SPRING, SUMMER, AND WINTER SEASONS IN THE LOW URBAN DENSITY AREA (CASE 3), BASED ON AVERAGE HOURLY DATA.	171
FIG. 6. 27: COMPARISON BETWEEN THE WIND SPEED VALUES OF THE SPRING, SUMMER, AND WINTER SEASONS IN THE LOW URBAN DENSITY AREA (CASE 3), BASED ON AVERAGE HOURLY DATA.	172
FIG. 6. 28: THE MRT VALUES OF THE SPRING, SUMMER, AND WINTER SEASONS IN THE LOW URBAN DENSITY AREA (CASE 3).	174
FIG. 6. 29: THE RELATIVE HUMIDITY VALUES OF THE SPRING, SUMMER, AND WINTER SEASONS IN THE LOW URBAN DENSITY AREA (CASE 3).	175
FIG. 6. 30: DIFFERENCE BETWEEN MEAN RADIANT TEMPERATURE (MRT) AND AIR TEMPERATURE IN THE LOW URBAN DENSITY AREA (CASE 3).	176
FIG. 6. 31: THE PET INDEX VALUES IN THE LOW URBAN DENSITY AREA (CASE 3).	177
FIG. 6. 32: FIELD MEASUREMENTS LOCATIONS FOR THE THREE URBAN DENSITY CASES, LOCATED AT A HEIGHT OF 2M	179
FIG. 6. 33: COMPARISON BETWEEN THE AIR TEMPERATURE VALUES OF THE HIGH URBAN DENSITY (CASE 1), INTERMEDIATE DENSITY (CASE 2) AND LOW DENSITY (CASE 3), MEASURED SIMULTANEOUSLY DURING THE SUMMER SEASON.	181
FIG. 6. 34: COMPARISON BETWEEN THE WIND SPEED VALUES OF THE HIGH URBAN DENSITY (CASE 1), INTERMEDIATE DENSITY (CASE 2) AND LOW DENSITY (CASE 3), MEASURED SIMULTANEOUSLY DURING THE SUMMER SEASON.	182
FIG. 6. 35: COMPARISON BETWEEN THE RELATIVE HUMIDITY VALUES OF THE HIGH URBAN DENSITY AREA, INTERMEDIATE DENSITY AREA AND LOW DENSITY AREA, MEASURED SIMULTANEOUSLY DURING THE SUMMER SEASON.	183
FIG. 6. 36: : COMPARISON BETWEEN THE MRT VALUES OF THE HIGH URBAN DENSITY (CASE 1), INTERMEDIATE DENSITY (CASE 2) AND LOW DENSITY (CASE 3), MEASURED SIMULTANEOUSLY DURING THE SUMMER SEASON.	184
FIG. 6. 37: COMPARISON BETWEEN THE PHYSIOLOGICALLY EQUIVALENT TEMPERATURE (PET) INDEX VALUES OF THE HIGH URBAN DENSITY (CASE 1), INTERMEDIATE DENSITY (CASE 2) AND LOW DENSITY (CASE 3) DURING THE SUMMER SEASON.	185
FIG. 6. 38: COMPARISON BETWEEN THE AIR TEMPERATURE VALUES OF THE HIGH URBAN DENSITY (CASE 1), INTERMEDIATE DENSITY (CASE 2) AND LOW DENSITY (CASE 3), MEASURED SIMULTANEOUSLY DURING THE SPRING SEASON.	188
FIG. 6. 39: COMPARISON BETWEEN THE WIND SPEED AVERAGE HOURLY VALUES OF THE HIGH URBAN DENSITY (CASE 1), INTERMEDIATE DENSITY (CASE 2) AND LOW DENSITY (CASE 3), MEASURED SIMULTANEOUSLY DURING THE SPRING SEASON.	190
FIG. 6. 40: COMPARISON BETWEEN THE RELATIVE HUMIDITY AVERAGE HOURLY VALUES OF THE HIGH URBAN DENSITY AREA, INTERMEDIATE URBAN DENSITY AND LOW URBAN DENSITY AREA, MEASURED SIMULTANEOUSLY DURING THE SPRING SEASON.	191
FIG. 6. 41: COMPARISON BETWEEN THE MRT AVERAGE HOURLY VALUES OF THE HIGH URBAN DENSITY (CASE 1), INTERMEDIATE DENSITY (CASE 2) AND LOW DENSITY (CASE 3) DURING THE SPRING SEASON.	192
FIG. 6. 42: COMPARISON BETWEEN THE PHYSIOLOGICALLY EQUIVALENT TEMPERATURE (PET) INDEX VALUES OF THE HIGH URBAN DENSITY (CASE 1), INTERMEDIATE DENSITY (CASE 2) AND LOW DENSITY (CASE 3) DURING SPRING.	193
FIG. 6. 43: AIR TEMPERATURE VALUES IN AREAS OF HIGH URBAN DENSITY (CASE 1) AND LOW URBAN DENSITY (CASE 3) DURING THE WINTER SEASON.	195
FIG. 6. 44: WIND SPEED VALUES AND WIND DIRECTIONS IN AREAS OF HIGH URBAN DENSITY (CASE 1) AND LOW URBAN DENSITY (CASE 3) DURING THE WINTER SEASON.	196
FIG. 6. 45: RELATIVE HUMIDITY VALUES IN AREAS OF HIGH URBAN DENSITY (CASE 1) AND LOW URBAN DENSITY (CASE 3) DURING THE WINTER SEASON.	197
FIG. 6. 46: MRT VALUES IN AREAS OF HIGH URBAN DENSITY (CASE 1) AND LOW URBAN DENSITY (CASE 3) DURING THE WINTER SEASON.	198

FIG. 6. 47: COMPARISON BETWEEN THE PHYSIOLOGICALLY EQUIVALENT TEMPERATURE (PET) INDEX VALUES OF THE HIGH URBAN DENSITY (CASE 1) AND LOW URBAN DENSITY (CASE 3) DURING THE WINTER SEASON. THE UPPER LIMIT IN SUMMER AND LOWER LIMIT IN WINTER COMFORT ZONE IN HOT ARID AREAS ARE 31.3°C AND 21°C, RESPECTIVELY. ....	199
FIG. 7. 1: HIGH URBAN DENSITY CASE (BASE MODEL). INTEREST AREA OF THE STUDY IS 120 X 90M AND THE WIDTH OF THE TALİ'E AND NAZIL QUBA ROADS IS 12M. ....	209
FIG. 7. 2: ASYMMETRIC ASPECT RATIOS OF THE EXISTING (E) CASE IN THE INTEREST AREA, PARTICULARLY ALONG THE FIVE CROSS-SECTIONS OF MEASUREMENTS POINTS. ....	210
FIG. 7. 3: THE FIGURE SHOWS 15 MEASUREMENTS POINTS EXTRACTED FOR EACH OF THE TWO QUBA CANYONS. EACH CANYON CONTAINS OF THREE ROWS OF MEASUREMENTS POINTS, I.E. ALONG THE MIDDLE OF THE ROAD, NEAR LEEWARD ELEVATIONS (LEFT) AND NEAR WINDWARD ELEVATIONS (RIGHT). ....	211
FIG. 7. 4: THE LEVEL OF SHADING IN THE BASE CASE (S-1) SCENARIO BASED ON YEARLY SUN PATH AT 15:00 HOURS. IN APRIL, THE WINDWARD CANYON (TALİ'E Q. RD.) HAS LESS SHADING THAN THE LEEWARD CANYON (NAZIL Q. RD.). ....	213
FIG. 7. 5: CONTOURS OF VELOCITY MAGNITUDE (M/S) AT PEDESTRIAN HEIGHT FOR THE BASE CASE (S-1) OF THE HIGH URBAN DENSITY AREA. HIGHLIGHTING THE 30 SIMULATION POINTS AT THE LEFT, MIDDLE AND RIGHT (L,M,R) LOCATIONS OF THE CANYONS. VERTICAL WIND VELOCITY WITHIN THE CANYON IS PRESENTED FOR THE E-3 CROSS-SECTION LOCATION. ....	215
FIG. 7. 6: WIND SPEED FOR THE BASE CASE (S-1) IN THE TALİ'E QUBA ROAD ALONG FIVE CROSS-SECTIONS. ....	217
FIG. 7. 7: WIND SPEED FOR THE BASE CASE (S-1) IN THE NAZIL QUBA ROAD ALONG FIVE CROSS-SECTIONS... ..	218
FIG. 7. 8: CONTOURS OF AIR TEMPERATURE IN DEGREE (°C) AT PEDESTRIAN HEIGHT FOR THE BASE CASE (S-1 SCENARIO). ....	221
FIG. 7. 9: AIR TEMPERATURE FOR THE BASE CASE (S-1) IN THE TALİ'E QUBA ROAD ALONG FIVE CROSS-SECTIONS. ....	222
FIG. 7. 10: AIR TEMPERATURE FOR THE BASE CASE (S-1) IN THE NAZIL QUBA ROAD ALONG FIVE CROSS-SECTIONS. ....	223
FIG. 7. 11: SYMMETRICAL ASPECT RATIO (S-2) MODEL WITH UNIFIED BUILDINGS HEIGHT OF 12M (H/W OF 1). THE FIGURE SHOWS A CROSS-SECTION THAT REPRESENTS THE FIVE LOCATIONS OF THE SIMULATION MEASUREMENTS. ....	225
FIG. 7. 12: CONTOURS OF VELOCITY MAGNITUDE (M/S) AT PEDESTRIAN HEIGHT FOR THE SYMMETRICAL ASPECT RATIO (S-2) OF $H_1/W - H_2/W - H_3/W = 1$ , SHOWING MEASUREMENT POINTS LOCATIONS. ....	227
FIG. 7. 13: WIND SPEED IN THE TALİ'E QUBA ROAD FOR THE MULTI-SYMMETRICAL ASPECT RATIOS (S-2) SCENARIO AT MEASUREMENTS LOCATIONS, AND COMPARED WITH THE BASE CASE S-1 SCENARIO AT THE PEDESTRIAN LEVEL. ....	228
FIG. 7. 14: WIND SPEED IN THE NAZIL QUBA ROAD FOR THE MULTI-SYMMETRICAL ASPECT RATIOS (S-2) SCENARIO AT MEASUREMENTS LOCATIONS, AND COMPARED WITH THE BASE CASE S-1 SCENARIO AT THE PEDESTRIAN LEVEL. ....	229
FIG. 7. 15: CONTOURS OF AIR TEMPERATURE DEGREE (°C) AT PEDESTRIAN HEIGHT FOR THE SYMMETRICAL ASPECT RATIO (S-2) OF $H_1/W - H_2/W - H_3/W = 1$ . ....	231
FIG. 7. 16: SHADING LEVEL IN THE S-2 (SYMMETRICAL BUILDING HEIGHT OF 12M), IN THE MORNING, NOON AND AFTERNOON PERIODS IN APRIL. AT THE SIMULATION TIME (15:00 HOURS) THE CANYONS ARE IN SHADE AT THE MEASUREMENT LOCATIONS. ....	232
FIG. 7. 17: AIR TEMPERATURE IN THE TALİ'E QUBA ROAD FOR THE MULTI-SYMMETRICAL ASPECT RATIOS SCENARIO (S-2) AT MEASUREMENTS LOCATIONS, AND COMPARED WITH THE BASE CASE S-1 SCENARIO AT THE PEDESTRIAN LEVEL. ....	233
FIG. 7. 18: AIR TEMPERATURE IN THE NAZIL QUBA ROAD FOR THE MULTI-SYMMETRICAL ASPECT RATIOS SCENARIO (S-2) AT MEASUREMENTS LOCATIONS, AND COMPARED WITH THE BASE CASE S-1 SCENARIO AT THE PEDESTRIAN LEVEL. ....	234
FIG. 7. 19: LOW MULTI-ASYMMETRICAL ASPECT RATIOS (S-3 AND S-4) SCENARIOS SHOWING A UNIFIED ASPECT RATIO $H_1/W$ OF 1 ON THE FIRST ROW OF BUILDINGS, AND UNIFIED INTERCHANGEABLE ASPECT RATIOS $H_2/W$ AND/OR $H_3/W$ OF 0.8 AND 1.3 FOR THE SECOND AND THIRD ROWS OF BUILDINGS. ....	240

FIG. 7. 20: CONTOURS OF VELOCITY MAGNITUDE (M/S) AT PEDESTRIAN HEIGHT (2M) FOR THE LOW CASE ASPECT RATIO SCENARIOS OF S-3 AND S-4 AND COMPARED WITH THE BASE CASE (S-1). .....	242
FIG. 7. 21: OVERALL WIND VELOCITY FOR THE BASE CASE AND THE LOWER MULTI-ASYMMETRICAL H/W SCENARIOS (S-3, S-4) IN THE NAZIL AND TALİ'E QUBA ROADS (I.E. LEEWARD AND WINDWARD CANYONS, RESPECTIVELY). .....	243
FIG. 7. 22: CONTOURS OF AIR TEMPERATURE DEGREES ( $^{\circ}$ C) AT PEDESTRIAN HEIGHT (2M) FOR THE LOW CASE ASPECT RATIO SCENARIOS OF S-3 AND S-4 AND COMPARED WITH THE BASE CASE (S-1) SCENARIO. ....	244
FIG. 7. 23: : OVERALL AIR TEMPERATURE IN THE NAZIL AND TALİ'E QUBA ROADS FOR THE LOW H/W MULTI-ASYMMETRICAL ASPECT RATIOS CASES AT FIVE MEASUREMENT LOCATIONS, & COMPARED WITH THE BASE CASE (S-1). ....	245
FIG. 7. 24: MEDIUM MULTI-ASYMMETRICAL ASPECT RATIOS (S-5, S-6 AND S-7) SCENARIOS SHOWING A UNIFIED ASPECT RATIO $H_1/W$ OF 1 ON THE FIRST ROW OF BUILDINGS, AND UNIFIED INTERCHANGEABLE ASPECT RATIOS $H_2/W$ AND/OR $H_3/W$ OF 1.3, 1.5 AND 1.8 FOR THE SECOND AND THIRD ROWS OF BUILDINGS. ....	246
FIG. 7. 25: CONTOURS OF VELOCITY MAGNITUDE (M/S) AT PEDESTRIAN HEIGHT (2M) FOR THE MEDIUM CASE ASPECT RATIO SCENARIOS OF S-5, S-6 AND S-7 AND COMPARED WITH THE BASE CASE (S-1) SCENARIO. ....	247
FIG. 7. 26: OVERALL WIND SPEED IN THE NAZIL AND TALİ'E QUBA ROADS FOR THE MEDIUM TYPE OF H/W MULTI-ASYMMETRICAL ASPECT RATIOS CASES AT FIVE MEASUREMENT LOCATIONS, & COMPARED WITH THE BASE CASE (S-1). .....	248
FIG. 7. 27: CONTOURS OF AIR TEMPERATURE DEGREES ( $^{\circ}$ C) AT PEDESTRIAN HEIGHT (2M) FOR THE MEDIUM CASE ASPECT RATIO SCENARIOS OF S-5, S-6 AND S-7 AND COMPARED WITH THE BASE CASE (S-1) SCENARIO. ....	250
FIG. 7. 28: OVERALL AIR TEMPERATURE IN THE NAZIL AND TALİ'E QUBA ROAD FOR THE MEDIUM H/W MULTI-ASYMMETRICAL ASPECT RATIOS CASES AT FIVE MEASUREMENT LOCATIONS, & COMPARED WITH THE BASE CASE (S-1). ....	251
FIG. 7. 29: FIVE SCENARIOS OF HIGHER MULTI-ASYMMETRICAL ASPECT RATIOS (S-8 TO S-12), SHOWING A UNIFIED ASPECT RATIO $H_1/W$ OF 1 ON THE FIRST ROW OF BUILDINGS, AND UNIFIED INTERCHANGEABLE ASPECT RATIOS $H_2/W$ AND/OR $H_3/W$ OF 1.3, 1.5, 1.8, 2 AND 2.3 FOR THE SECOND AND THIRD ROWS OF BUILDINGS. ....	252
FIG. 7. 30: CONTOURS OF VELOCITY MAGNITUDE (M/S) AT PEDESTRIAN HEIGHT (2M) FOR THE HIGH CASE ASPECT RATIO SCENARIOS OF S-8, S-9, S-10, S-11 AND S-12 AND COMPARED WITH THE BASE CASE (S-1) SCENARIO. ....	255
FIG. 7. 31: OVERALL WIND SPEED WITHIN THE TALİ'E QUBA ROAD FOR THE HIGH TYPE OF MULTI-ASYMMETRICAL ASPECT RATIOS CASES AT FIVE AVERAGE MEASUREMENT LOCATIONS, AND COMPARED WITH THE BASE CASE (S-1). ....	256
FIG. 7. 32: OVERALL WIND SPEED WITHIN THE NAZIL QUBA ROAD FOR THE HIGH TYPE OF MULTI-ASYMMETRICAL ASPECT RATIOS CASES AT FIVE AVERAGE MEASUREMENT LOCATIONS, AND COMPARED WITH THE BASE CASE (S-1). ....	257
FIG. 7. 33: CONTOURS OF AIR TEMPERATURE DEGREES ( $^{\circ}$ C) MAGNITUDE AT PEDESTRIAN HEIGHT IN FIVE DIFFERENT HIGH ASYMMETRICAL SCENARIOS ACROSS FIVE SECTIONS AND EXTRACTED 30 POINTS. ....	258
FIG. 7. 34: AIR TEMPERATURE IN THE TALİ'E QUBA ROAD FOR THE HIGHER TYPE OF H/W MULTI-ASYMMETRICAL ASPECT RATIO CASES AT FIVE AVERAGE MEASUREMENT LOCATIONS, AND COMPARED WITH THE BASE CASE (S-1). ....	259
FIG. 7. 35: AIR TEMPERATURE IN THE NAZIL QUBA ROAD FOR THE HIGHER TYPE OF H/W MULTI-ASYMMETRICAL ASPECT RATIO CASES AT FIVE AVERAGE MEASUREMENT LOCATIONS, AND COMPARED WITH THE BASE CASE (S-1). ....	260
FIG. 7. 36: LEEWARD GRADUALLY INCREASED MULTI-ASYMMETRICAL ASPECT RATIOS (S-13 TO S-16). THE BUILDING HEIGHTS STARTS FROM 12M IN S-13, S-14 AND S-15, WHILE IT STARTS FROM 15M IN S-16. ....	262
FIG. 7. 37: CONTOURS OF VELOCITY MAGNITUDE AT THE PEDESTRIAN LEVEL FOR THE CASES OF LEEWARD GRADUAL INCREASE IN ASPECT RATIOS ON THE THREE ROWS OF BUILDINGS, & COMPARED WITH THE BASE CASE (S-1). ....	263
FIG. 7. 38: OVERALL WIND SPEED WITHIN THE TALİ'E QUBA ROAD FOR THE LEEWARD GRADUAL INCREASE IN MULTI-ASYMMETRICAL ASPECT RATIOS CASES AT FIVE MEASUREMENT LOCATIONS, & COMPARED WITH THE BASE CASE (S-1). .....	264



FIG. 7. 39: OVERALL WIND SPEED WITHIN THE NAZIL QUBA ROAD FOR THE LEEWARD GRADUAL INCREASE IN MULTI-ASYMMETRICAL ASPECT RATIOS CASES AT FIVE MEASUREMENT LOCATIONS, & COMPARED WITH THE BASE CASE (S-1).	265
FIG. 7. 40: CONTOURS OF AIR TEMPERATURE IN DEGREES ( $^{\circ}$ C) AT THE PEDESTRIAN LEVEL FOR THE CASES OF LEEWARD GRADUAL INCREASE IN ASPECT RATIOS ON THE THREE ROWS OF BUILDINGS, & COMPARED WITH THE BASE CASE (S-1).	266
FIG. 7. 41: OVERALL AIR TEMPERATURE WITHIN THE TALİ'E QUBA ROAD FOR THE LEEWARD GRADUAL INCREASE IN MULTI-ASYMMETRICAL ASPECT RATIOS CASES AT FIVE MEASUREMENT LOCATIONS, & COMPARED WITH THE BASE CASE.	267
FIG. 7. 42: OVERALL AIR TEMPERATURE WITHIN THE NAZIL QUBA ROAD FOR THE LEEWARD GRADUAL INCREASE IN MULTI-ASYMMETRICAL ASPECT RATIOS CASES AT FIVE MEASUREMENT LOCATIONS, & COMPARED WITH THE BASE CASE.	268
FIG. 7. 43: PET PATTERN FOR THE WINDWARD CANYON IN THE BASE CASE (S-1) SCENARIO.	271
FIG. 7. 44: PET PATTERN FOR THE LEEWARD CANYON IN THE BASE CASE (S-1) SCENARIO.	272
FIG. 7. 45: PET INDEX TEMPERATURE WITHIN THE NAZIL QUBA ROAD FOR THE BEST MULTI-ASYMMETRICAL ASPECT RATIO SCENARIO (S-11), AT THREE SIDES OF THE CANYON ALONG FIVE MEASUREMENT LOCATIONS, & COMPARED WITH THE BASE CASE.	275
FIG. 8. 1: THE BEST MULTI-ASYMMETRICAL ASPECT RATIOS SCENARIO (S-11).	279
FIG. 8. 2: THE NUMBER OF PEDESTRIANS IN A HIGH URBAN DENSITY AREA IN QUBA ROAD, DURING SPRING, AUTUMN, AND WINTER SEASONS PER 24 YOURS (EXCEPT IN AUTUMN, BETWEEN 06:00 TO 17:00 HOURS). IT SHOWS INCREASE OF QUBA ROAD USERS WITHIN THE FIVE PRAYERS TIME AS WELL AS DURING EVENING TILL 23:00 HOURS AT NIGHT.	281
FIG. 8. 3: CONTOURS OF VELOCITY MAGNITUDE (M/S) AT PEDESTRIAN HEIGHT (2M) FOR S-17 THAT REPRESENTS THE NIGHT TIME (21:00PM) CASE BASED ON THE BEST H/W OF (1-1.3-2.3), & COMPARED WITH THE NIGHT BASE CASE.	282
FIG. 8. 4: CONTOURS OF VELOCITY MAGNITUDE (M/S) AT PEDESTRIAN HEIGHT (2M) FOR S-25NOON THAT REPRESENTS THE H/W OF 1 – 1.3 – 2.3 AT 12:00PM, & COMPARED WITH THE BASE CASE OF THE EXISTING SITUATION AT NOON.	283
FIG. 8. 5: WIND VELOCITY PATTERN AT PEDESTRIAN HEIGHT (2M) FOR S-17 THAT REPRESENTS THE NIGHT TIME (21:00PM) CASE WITH THE BEST H/W OF (1 – 1.3 – 2.3), AND COMPARED WITH THE EXISTING CONDITIONS DURING THE NIGHT (S-1 NIGHT), PARTICULARLY FOR THE NAZIL QUBA ROAD (LEEWARD CANYON) ALONG FIVE MEASUREMENT LOCATIONS.	284
FIG. 8. 6: WIND VELOCITY PATTERN AT PEDESTRIAN HEIGHT (2M) FOR S-25NOON THAT REPRESENTS THE RESULTS AT NOON (12:00PM) CASE WITH THE OPTIMUM H/W OF (1 – 1.3 – 2.3), AND COMPARED WITH THE EXISTING CONDITIONS DURING THE MID-DAY (S-1 NOON), PARTICULARLY FOR THE NAZIL QUBA ROAD (LEEWARD CANYON).	285
FIG. 8. 7: CONTOURS OF AIR TEMPERATURE ( $^{\circ}$ C) AT PEDESTRIAN HEIGHT (2M) FOR S-17 THAT REPRESENTS THE NIGHT TIME CASE (21:00PM) BASED ON THE OPTIMUM H/W OF 1-1.3-2.3, & COMPARED WITH THE EXISTING CASE AT NIGHT.	286
FIG. 8. 8: AIR TEMPERATURE AT PEDESTRIAN HEIGHT (2M) FOR S-17 THAT REPRESENTS THE NIGHT TIME CASE (21:00PM) BASED ON THE OPTIMUM H/W OF 1-1.3-2.3, AND COMPARED WITH THE S-1 NIGHT (THE EXISTING CASE AT NIGHT) IN THE LEEWARD CANYON.	286
FIG. 8. 9: CONTOURS OF AIR TEMPERATURE ( $^{\circ}$ C) AT PEDESTRIAN HEIGHT (2M) FOR S-25NOON THAT REPRESENTS THE NOON TIME CASE (12:00PM) BASED ON THE OPTIMUM H/W OF 1-1.3-2.3, & COMPARED WITH THE EXISTING CASE AT NOON.	287
FIG. 8. 10: AIR TEMPERATURE IN THE LEEWARD CANYON FOR S-25NOON THAT REPRESENTS THE NOON TIME CASE (12:00PM) BASED ON THE OPTIMUM H/W OF 1-1.3-2.3, AND COMPARED WITH THE S-1 NOON (EXISTING CASE AT NOON).	287
FIG. 8. 11: AIR TEMPERATURE IN THE WINDWARD CANYON FOR S-25NOON THAT REPRESENTS THE NOON TIME CASE (12:00PM) BASED ON THE OPTIMUM H/W OF 1-1.3-2.3, AND COMPARED WITH THE S-1 NOON (EXISTING CASE AT NOON).	288

FIG. 8. 12: INCREASING THE NUMBER OF ROWS OF BUILDINGS TO THE LEEWARD AREA IN THE BEST PROPOSED ASPECT RATIO SCENARIO IN THIS STUDY. IN S-18 SCENARIO, THE BUILDINGS IN THE NEW ROWS ARE POSITIONED AS GRID STYLE, WHILE IN S-19 SCENARIO HAVING A CHESS-BOARD BUILDING POSITION. ....	290
FIG. 8. 13: CONTOURS OF VELOCITY MAGNITUDE (M/S) AT PEDESTRIAN HEIGHT FOR INCREASE ROWS OF BUILDINGS MODELS IN THE S-18 SCENARIO (GRID STYLE) AND S-19 SCENARIO (CHESS-BOARD STYLE)..	292
FIG. 8. 14: WIND VELOCITY (M/S) PATTERN IN FIVE CANYONS FOR INCREASED NUMBER OF ROWS OF BUILDINGS IN S-18 (GRID STYLE) AND S-19 (CHESS-BOARD STYLE) SCENARIOS. ....	293
FIG. 8. 15: WIND FLOW STREAMLINE AND PRESSURE AT WALL SURFACES FOR URBAN CANYONS WITH VARIATION OF BUILDING HEIGHT. SOURCE: HANG ET AL. (2015). ....	294
FIG. 8. 16: CONTOURS OF AIR TEMPERATURE AT PEDESTRIAN HEIGHT FOR INCREASE ROWS OF BUILDINGS MODELS IN THE S-18 SCENARIO (GRID STYLE) AND S-19 SCENARIO (CHESS-BOARD STYLE). ....	295
FIG. 8. 17: AIR TEMPERATURE PATTERN IN FIVE CANYONS FOR INCREASED NUMBER OF ROWS OF BUILDINGS IN S-18 (GRID STYLE) AND S-19 (CHESS-BOARD STYLE). ....	296
FIG. 8. 18: ORIENTATION OF URBAN CANYON GEOMETRY WITH THE WESTERLY SECOND PREVAILING WIND DIRECTION (S-20 SCENARIO) AND NORTH-WESTERLY THIRD PREVAILING WIND DIRECTION (S-21 SCENARIO), AND COMPARED TO THE SOUTH-WESTERLY MAIN PREVAILING WIND DIRECTION WITH THE BEST ASPECT RATIO SCENARIO (S-11). ....	298
FIG. 8. 19: CONTOURS OF VELOCITY MAGNITUDE (M/S) AT PEDESTRIAN HEIGHT (2M) IN S-20 (W DIRECTION) AND S-21 (NW DIRECTION), AND COMPARED WITH THE BEST ASPECT RATIO S-11 SCENARIO (SW DIRECTION). ....	299
FIG. 8. 20: WIND SPEED AT THE PEDESTRIAN HEIGHT (2M) IN S-20 (W DIRECTION) AND S-21 (NW DIRECTION), AND COMPARED WITH THE BEST ASPECT RATIO S-11 SCENARIO (SW DIRECTION), WITH H/W OF 1 – 1.3 – 2.3. ....	300
FIG. 8. 21: CONTOURS OF AIR TEMPERATURE ( $^{\circ}$ C) AT THE PEDESTRIAN LEVEL FOR THE BEST ASPECT RATIO WITH SCENARIOS OF WESTERLY PREVAILING WIND DIRECTION (S-20) AND NORTH-WESTERLY PREVAILING WIND (S-21), AND COMPARED WITH THE BEST ASPECT RATIO (S-11) SCENARIO WITH SOUTH-WESTERLY WIND DIRECTION. ....	301
FIG. 8. 22: AIR TEMPERATURE IN THE NAZIL QUBA ROAD FOR THE BEST ASPECT RATIO WITH STRATEGY (H/W OF 1-1.3-2.3) IN S-20 SCENARIO WITH WESTERLY PREVAILING WIND DIRECTION, AND IN S-21 SCENARIO WITH NORTH-WESTERLY PREVAILING WIND, AND COMPARED TO S-11 WITH SOUTH-WESTERLY WIND DIRECTION. ....	302
FIG. 8. 23: THREE SCENARIOS ON THE CONFIGURATION OF NEW STREETS THAT ARE PARALLEL WITH THE MAIN PREVAILING WIND DIRECTION, WHILE IT IS APPROXIMATELY PERPENDICULAR TO THE NORTH-SOUTH AXIS OF QUBA CANYONS. ....	303
FIG. 8. 24: CONTOURS OF WIND VELOCITY (M/S) AT THE PEDESTRIAN LEVEL FOR THE CONFIGURATION OF NEW STREETS PERPENDICULAR TO QUBA CANYONS STRATEGY (S-22: LOWER STREET, S-23: UPPER STREET, S-24: UPPER & LOWER STREET CONFIGURATIONS), AND COMPARED WITH THE BASE MODEL OF BEST H/W SCENARIO (S-11). ....	304
FIG. 8. 25: WIND SPEED PATTERN AT THE PEDESTRIAN LEVEL FOR THE CONFIGURATION OF NEW STREETS PERPENDICULAR TO QUBA CANYONS STRATEGY (S-22: LOWER STREET, S-23: UPPER STREET, S-24: UPPER & LOWER STREET CONFIGURATIONS), AND COMPARED WITH THE BASE MODEL OF BEST H/W SCENARIO (S-11). ....	305
FIG. 8. 26: CONTOURS OF AIR TEMPERATURE AT THE PEDESTRIAN LEVEL FOR THE CONFIGURATION OF NEW STREETS PERPENDICULAR TO QUBA CANYONS STRATEGY (S-22: LOWER STREET, S-23: UPPER STREET, S-24: UPPER & LOWER STREET CONFIGURATIONS), AND COMPARED WITH THE BASE MODEL OF BEST H/W SCENARIO (S-11). ....	306
FIG. 8. 27: AIR TEMPERATURE PATTERN AT THE PEDESTRIAN LEVEL FOR THE CONFIGURATION OF NEW STREETS PERPENDICULAR TO QUBA CANYONS STRATEGY (S-22: LOWER STREET, S-23: UPPER STREET, S-24: UPPER & LOWER STREET CONFIGURATIONS), AND COMPARED WITH THE BASE MODEL OF BEST H/W SCENARIO (S-11). ....	307
FIG. 8. 28: SCENARIO S-26 BASED ON REMOVING BUILDINGS AND OR CREATING OPEN SPACES AND PASSAGES, PARTICULARLY AT SIMULATION LOCATION NUMBER 4 IN THE LEEWARD CANYON (I.E. NAZIL QUBA ROAD). ....	308

FIG. 8. 29: CONCEPTUAL DIAGRAM FOR PROPOSED COMMUNAL NODES AND LOCAL HUBS IN QUBA ROAD BASED ON ACCEPTABLE MAXIMUM WALKING TIME (IN MINUTES) AND DISTANCE (IN METRES). ADAPTED FROM SETAIH (2010). .....	310
FIG. 8. 30: CONTOURS OF WIND VELOCITY (M/S) AT THE PEDESTRIAN LEVEL FOR THE STRATEGY OF REMOVAL OF BUILDINGS IN S-26 SCENARIO, AND COMPARED WITH THE BASE MODEL OF THE OPTIMUM H/W IN S-11.	311
FIG. 8. 31: THE WIND VELOCITY PATTERNS AT THE PEDESTRIAN LEVEL FOR THE STRATEGY OF REMOVAL OF BUILDINGS IN S-26 SCENARIO, AND COMPARED WITH THE BASE MODEL OF THE OPTIMUM H/W IN S-11 AT FIVE AVERAGED SIMULATED LOCATIONS. ....	312
FIG. 8. 32: CONTOURS OF AIR TEMPERATURE AT THE PEDESTRIAN LEVEL FOR THE STRATEGY OF REMOVAL OF BUILDINGS IN S-26 SCENARIO, AND COMPARED WITH THE PROPOSED MODEL OF THE OPTIMUM H/W IN S-11. ....	313
FIG. 8. 33: AIR TEMPERATURE PATTERN AT THE PEDESTRIAN LEVEL FOR THE STRATEGY OF REMOVAL OF BUILDINGS IN S-26 SCENARIO, AND COMPARED WITH THE PROPOSED MODEL OF THE OPTIMUM H/W IN S-11. ....	313
FIG. 8. 34: PROTRUDING UPPER FLOORS SCENARIO IN S-27 AND S-28 SCENARIOS, WITH 9M STREET OPENESS TO THE SKY. ....	315
FIG. 8. 35: THE LEVEL OF SHADING DURING THE DAY IN APRIL (SIMULATION TIME IN SPRING SEASON) FOR THE CONFIGURATION OF THE PROTRUDING UPPER FLOORS MODELS, WITH BUILDING HEIGHTS OF 12M (FIRST ROW), 15M (SECOND ROW) AND 27M (THIRD ROW). ....	317
FIG. 8. 36: VELOCITY CONTOURS AT THE PEDESTRIAN LEVEL IN THE S-27 SCENARIO (I.E. PROTRUDING FLOORS) AT 15:00 HOURS, AND COMPARED WITH THE OPTIMUM ASPECT RATIO SCENARIO S-11 AT 15:00 HOURS. ....	318
FIG. 8. 37: VELOCITY CONTOURS AT THE PEDESTRIAN LEVEL IN THE S-28 SCENARIO (I.E. PROTRUDING FLOORS, H/W OF 1.3 – 1.7 – 3) AT 12:00 HOURS, AND COMPARED WITH S-25 SCENARIO (H/W OF 1 – 1.3 – 2.3) AT 12:00 HOURS. ....	318
FIG. 8. 38: WIND VELOCITY PATTERN AT THE PEDESTRIAN LEVEL IN THE LEEWARD CANYON FOR THE S-27 SCENARIO (I.E. PROTRUDING FLOORS AT 15:00 HOURS) AND S-28 SCENARIO (I.E. PROTRUDING FLOORS AT 12:00 HOURS), AND COMPARED WITH THE S-11 AND S-25 SCENARIOS (I.E. H/W OF 1 – 1.3 – 2.3 AT 15:00HOURS AND 12:00 HOURS, RESPECTIVELY). ....	319
FIG. 8. 39: AIR TEMPERATURE CONTOURS AT THE PEDESTRIAN LEVEL IN THE S-27 SCENARIO (I.E. PROTRUDING FLOORS) AT 15:00 HOURS, AND COMPARED WITH THE OPTIMUM ASPECT RATIO SCENARIO S-11 AT 15:00 HOURS. ....	320
FIG. 8. 40: AIR TEMPERATURE CONTOURS AT THE PEDESTRIAN LEVEL IN THE S-28 SCENARIO (I.E. PROTRUDING FLOORS, H/W OF 1.3 – 1.7 – 3) AT 12:00 HOURS, AND COMPARED WITH S-25 SCENARIO (H/W OF 1 – 1.3 – 2.3) AT 12:00 HOURS. ....	320
FIG. 8. 41: AIR TEMPERATURE PATTERN AT THE PEDESTRIAN LEVEL IN THE LEEWARD CANYON FOR THE S-27 SCENARIO (I.E. PROTRUDING FLOORS AT 15:00 HOURS) AND S-28 SCENARIO (I.E. PROTRUDING FLOORS AT 12:00 HOURS), AND COMPARED WITH THE S-11 AND S-25 SCENARIOS (I.E. H/W OF 1 – 1.3 – 2.3 AT 15:00HOURS AND 12:00 HOURS, RESPECTIVELY). ....	322
FIG. 8. 42: VELOCITY CONTOURS AT THE PEDESTRIAN LEVEL IN THE S-29 SCENARIO (I.E. CHANGING TO A HIGHER ALBEDO LEVEL), AND COMPARED WITH THE OPTIMUM ASPECT RATIO SCENARIO S-11 (LOWER ALBEDO LEVEL) AT 15:00 HOURS. ....	324
FIG. 8. 43: WIND VELOCITY PATTERN AT THE PEDESTRIAN LEVEL IN THE LEEWARD CANYON FOR THE S-29 SCENARIO (I.E. CHANGING TO HIGHER ALBEDO LEVEL), COMPARED TO THE S-11 (I.E. LOWER ALBEDO) AT 15:00 HOURS. ....	324
FIG. 8. 44: AIR TEMPERATURE CONTOURS AT THE PEDESTRIAN LEVEL IN THE S-29 SCENARIO (I.E. HIGHER ALBEDO LEVEL), AND COMPARED WITH THE OPTIMUM ASPECT RATIO SCENARIO S-11 (LOWER ALBEDO LEVEL) AT 15:00 HOURS. ....	325
FIG. 8. 45: AIR TEMPERATURE PATTERN AT THE PEDESTRIAN LEVEL IN THE LEEWARD CANYON FOR THE S-29 SCENARIO (I.E. CHANGING TO HIGHER ALBEDO LEVEL), COMPARED TO THE S-11 (I.E. LOWER ALBEDO) AT 15:00 HOURS. ....	325
FIG. 8. 46: CHANGES TO BLOCK PATTERNS IN S-30 WITH GRID BUILDING POSITION AND S-31 WITH CHESS BOARD BUILDING POSITION, AND INCREASING THE NUMBER OF ROWS TO BE TOTAL OF 6 ROWS. ....	326

FIG. 8. 47: WIND VELOCITY CONTOUR AT THE PEDESTRIAN LEVEL FOR THE CHANGING BLOCK PATTERNS IN S-30 AND S-31 SCENARIOS, COMPARED WITH S-18 AND S-19 THAT SHARE THE SAME ASPECT RATIO CONFIGURATIONS. ....	327
FIG. 8. 48: WIND VELOCITY PATTERN AT THE PEDESTRIAN LEVEL FOR THE CHANGING BLOCK PATTERNS IN S-30 WITH GRID STYLE POSITION OF BUILDINGS. ....	328
FIG. 8. 49: WIND VELOCITY PATTERN AT THE PEDESTRIAN LEVEL FOR THE CHANGING BLOCK PATTERNS IN S-31 WITH CHESS-BOARD STYLE POSITION OF BUILDINGS. ....	328
FIG. 8. 50: AIR TEMPERATURE CONTOURS AT THE PEDESTRIAN LEVEL FOR THE CHANGING BLOCK PATTERNS IN S-30 AND S-31 SCENARIOS, COMPARED WITH S-18 AND S-19 THAT SHARE THE SAME ASPECT RATIO CONFIGURATIONS. ....	329
FIG. 8. 51: AIR TEMPERATURE PATTERN AT THE PEDESTRIAN LEVEL FOR THE CHANGING BLOCK PATTERNS IN S-30 WITH GRID STYLE POSITION OF BUILDINGS. ....	330
FIG. 8. 52: AIR TEMPERATURE PATTERN AT THE PEDESTRIAN LEVEL FOR THE CHANGING BLOCK PATTERNS IN S-31 WITH CHESS-BOARD STYLE POSITION OF BUILDINGS. ....	331
FIG. 8. 53: THE BEST MULTI-ASYMMETRICAL ASPECT RATIOS SCENARIO (S-11). ....	332
FIG. 8. 54: PROPOSED IMPLEMENTATION ASPECT RATIOS FOR THREE TO SIX ROWS OF BUILDINGS. ....	335
A5. 1: CONVERGENCE OBTAINED FOR S-1 MODEL (BASE CASE). ....	372
A5. 2: CONVERGENCE OBTAINED FOR S-5 MODEL (H/W OF 1 - 1 - 1). ....	372
A5. 3: CONVERGENCE OBTAINED FOR S-3 MODEL (H/W=1-0.8-1.3). ....	372
A5. 4: CONVERGENCE OBTAINED FOR S-4 MODEL (H/W=1-1.3-0.8). ....	372
A5. 5: CONVERGENCE OBTAINED FOR S-5 MODEL (H/W=1-1.5-1.5). ....	372
A5. 6: CONVERGENCE OBTAINED FOR S-6 MODEL (H/W=1-1.3-1.8). ....	372
A5. 7: CONVERGENCE OBTAINED FOR S-7 MODEL (H/W=1-1.8-1.3). ....	372
A5. 8: CONVERGENCE OBTAINED FOR S-8 MODEL (H/W=1-2-2). ....	372
A5. 9: CONVERGENCE OBTAINED FOR S-9 MODEL (H/W=1-1.8-2.3). ....	373
A5. 10: CONVERGENCE OBTAINED FOR S-10 MODEL (H/W=1-2.3-1.8). ....	373
A5. 11: CONVERGENCE OBTAINED FOR S-11 MODEL (H/W=1-1.3-2.3). ....	373
A5. 12: CONVERGENCE OBTAINED FOR S-12 MODEL (H/W=1-2.3-1.3). ....	373
A5. 13: CONVERGENCE OBTAINED FOR S-13 MODEL (H/W=1-1.3-1.5). ....	373
A5. 14: CONVERGENCE OBTAINED FOR S-14 MODEL (H/W=1-1.3-2). ....	373
A5. 15: CONVERGENCE OBTAINED FOR S-15 MODEL (H/W=1-1.5-2.3). ....	373
A5. 16: CONVERGENCE OBTAINED FOR S-16 MODEL (H/W=1.3-1.5-2.3). ....	373
A5. 17: CONVERGENCE OBTAINED FOR S-17 MODEL (MICROCLIMATE AT NIGHT FOR H/W=1.3-1.5-2.3). ....	374
A5. 18: CONVERGENCE OBTAINED FOR S-18 MODEL (LEEWARD INCREASE IN BUILDING' ROWS WITH GRID POSITION). ....	374
A5. 19: CONVERGENCE OBTAINED FOR S-19 MODEL (LEEWARD INCREASE IN BUILDING'S ROWS WITH CHESS-BOARD POSITION). ....	374
A5. 20: CONVERGENCE OBTAINED FOR S-20 MODEL (WESTERLY WIND DIRECTION). ....	374
A5. 21: CONVERGENCE OBTAINED FOR S-21 MODEL (NORTH-WESTERLY WIND DIRECTION). ....	374
A5. 22: CONVERGENCE OBTAINED FOR S-22 MODEL (LOWER STREET). ....	374
A5. 23: CONVERGENCE OBTAINED FOR S-23 MODEL (UPPER STREET). ....	374
A5. 24: CONVERGENCE OBTAINED FOR S-24 MODEL (UPPER AND LOWER STREETS). ....	374
A5. 25: CONVERGENCE OBTAINED FOR S-25 MODEL (OPTIMUM H/W AT NOON). ....	375
A5. 26: CONVERGENCE OBTAINED FOR S-26 MODEL (REMOVAL OF BUILDINGS). ....	375
A5. 27: CONVERGENCE OBTAINED FOR S-27 MODEL (PROTRUDING FLOORS AT 15:00 HOURS). ....	375
A5. 28: CONVERGENCE OBTAINED FOR S-28 MODEL (PROTRUDING FLOORS AT NOON). ....	375
A5. 29: CONVERGENCE OBTAINED FOR S-29 MODEL (CHANGES TO ALBEDO AT 15:00 HOURS). ....	375
A5. 30: CONVERGENCE OBTAINED FOR S-30 MODEL (CHANGES TO BLOCK PATTERNS, GRID STYLE). ....	375
A5. 31: CONVERGENCE OBTAINED FOR S-31 MODEL (CHANGES TO BLOCK PATTERNS, CHESS-BOARD STYLE). ....	375

A6. 1: AVERAGE HOURLY MICROCLIMATIC DATA MONITORED IN THE HIGH URBAN DENSITY AREA (CASE 1).	376
A6. 2: DETAILED HOURLY MICROCLIMATIC DATA IN THE HIGH URBAN DENSITY AREA (OCTOBER)	377
A6. 3: DETAILED HOURLY MICROCLIMATIC DATA IN THE HIGH URBAN DENSITY AREA (WINTER)	383
A6. 4: DETAILED HOURLY MICROCLIMATIC DATA IN THE HIGH URBAN DENSITY AREA (SPRING)	387
A6. 5: DETAILED HOURLY MICROCLIMATIC DATA IN THE HIGH URBAN DENSITY AREA (SUMMER)	393
A6. 6: AVERAGE HOURLY MICROCLIMATIC DATA MONITORED IN THE INTERMEDIATE URBAN DENSITY AREA (CASE2)	397
A6. 7: DETAILED HOURLY MICROCLIMATIC DATA IN THE INTERMEDIATE URBAN DENSITY AREA (SPRING).	398
A6. 8: DETAILED HOURLY MICROCLIMATIC DATA IN THE INTERMEDIATE URBAN DENSITY AREA (SUMMER).	401
A6. 9: AVERAGE MICROCLIMATIC DATA MONITORED IN THE LOW URBAN DENSITY AREA (CASE3).	404
A6. 10: DETAILED HOURLY MICROCLIMATIC DATA IN THE LOW URBAN DENSITY AREA (WINTER).	405
A6. 11: DETAILED HOURLY MICROCLIMATIC DATA IN THE LOW URBAN DENSITY AREA (SPRING).	409
A6. 12: DETAILED HOURLY MICROCLIMATIC DATA IN THE LOW URBAN DENSITY AREA (SUMMER).	415
A7. 1: CONTOURS OF VELOCITY MAGNITUDE FOR SYMMETRICAL URBAN CANYONS WITH $H/W$ OF 1, WIND DIRECTION OF -105 FROM NORTH. THE GRAPH SHOWS LOWER WIND VELOCITIES IN LEEWARD CANYONS COMPARED TO WINDWARD CANYON. SOURCE: ADAPTED FROM HANG ET AL. (2015).	418
A7. 2: WIND VELOCITY AT THE LEFT (LEEWARD) SIMULATION POINTS IN THE LOW ASYMMETRICAL ASPECT RATIO SCENARIOS, PARTICULARLY IN THE TALÍ'E QUBA ROAD, AND COMPARED WITH THE BASE CASE S-1 SCENARIO.	419
A7. 3: WIND VELOCITY AT THE LEFT (LEEWARD) SIMULATION POINTS IN THE LOW ASYMMETRICAL ASPECT RATIO SCENARIOS, PARTICULARLY IN THE NAZIL QUBA ROAD, AND COMPARED WITH THE BASE CASE S-1 SCENARIO.	419
A7. 4: WIND VELOCITY AT THE MIDDLE SIMULATION POINTS IN THE LOW ASYMMETRICAL ASPECT RATIO SCENARIOS, PARTICULARLY IN THE TALÍ'E QUBA ROAD, AND COMPARED WITH THE BASE CASE S-1 SCENARIO.	420
A7. 5: WIND VELOCITY AT THE MIDDLE SIMULATION POINTS IN THE LOW ASYMMETRICAL ASPECT RATIO SCENARIOS, PARTICULARLY IN THE NAZIL QUBA ROAD, AND COMPARED WITH THE BASE CASE S-1 SCENARIO.	420
A7. 6: WIND VELOCITY AT THE RIGHT (WINDWARD) SIMULATION POINTS IN THE LOW ASYMMETRICAL ASPECT RATIO SCENARIOS, PARTICULARLY IN THE TALÍ'E QUBA ROAD, AND COMPARED WITH THE BASE CASE S-1 SCENARIO.	420
A7. 7: WIND VELOCITY AT THE RIGHT (WINDWARD) SIMULATION POINTS IN THE LOW ASYMMETRICAL ASPECT RATIO SCENARIOS, PARTICULARLY IN THE NAZIL QUBA ROAD, AND COMPARED WITH THE BASE CASE S-1 SCENARIO.	421
A7. 8: AIR TEMPERATURE AT THE LEFT (LEEWARD) SIMULATION POINTS IN THE LOW ASYMMETRICAL ASPECT RATIO SCENARIOS, PARTICULARLY IN THE TALÍ'E QUBA ROAD, AND COMPARED WITH THE BASE CASE S-1 SCENARIO.	422
A7. 9: AIR TEMPERATURE AT THE LEFT (LEEWARD) SIMULATION POINTS IN THE LOW ASYMMETRICAL ASPECT RATIO SCENARIOS, PARTICULARLY IN THE NAZIL QUBA ROAD, AND COMPARED WITH THE BASE CASE S-1 SCENARIO.	422
A7. 10: AIR TEMPERATURE AT THE MIDDLE SIMULATION POINTS IN THE LOW ASYMMETRICAL ASPECT RATIO SCENARIOS, PARTICULARLY IN THE TALÍ'E QUBA ROAD, AND COMPARED WITH THE BASE CASE S-1 SCENARIO.	423
A7. 11: AIR TEMPERATURE AT THE MIDDLE SIMULATION POINTS IN THE LOW ASYMMETRICAL ASPECT RATIO SCENARIOS, PARTICULARLY IN THE NAZIL QUBA ROAD, AND COMPARED WITH THE BASE CASE S-1 SCENARIO.	423
A7. 12: AIR TEMPERATURE AT THE RIGHT (WINDWARD) SIMULATION POINTS IN THE LOW ASYMMETRICAL ASPECT RATIO SCENARIOS, PARTICULARLY IN THE TALÍ'E QUBA ROAD, AND COMPARED WITH THE BASE CASE S-1	423
A7. 13: AIR TEMPERATURE AT THE RIGHT (WINDWARD) SIMULATION POINTS IN THE LOW ASYMMETRICAL ASPECT RATIO SCENARIOS, PARTICULARLY IN THE NAZIL QUBA ROAD, AND COMPARED WITH THE BASE CASE S-1	424
A7. 14: WIND VELOCITY AT THE LEFT (LEEWARD) SIMULATION POINTS IN THE MEDIUM ASYMMETRICAL ASPECT RATIO SCENARIOS IN THE TALÍ'E QUBA ROAD, AND COMPARED WITH THE BASE CASE S-1 SCENARIO.	425
A7. 15: WIND VELOCITY AT THE LEFT (LEEWARD) SIMULATION POINTS IN THE MEDIUM ASYMMETRICAL ASPECT RATIO SCENARIOS IN THE NAZIL QUBA ROAD, AND COMPARED WITH THE BASE CASE S-1 SCENARIO.	425
A7. 16: WIND VELOCITY AT THE MIDDLE SIMULATION POINTS IN THE MEDIUM ASYMMETRICAL ASPECT RATIO SCENARIOS IN THE TALÍ'E QUBA ROAD, AND COMPARED WITH THE BASE CASE S-1 SCENARIO.	426
A7. 17: WIND VELOCITY AT THE MIDDLE SIMULATION POINTS IN THE MEDIUM ASYMMETRICAL ASPECT RATIO SCENARIOS IN THE NAZIL QUBA ROAD, AND COMPARED WITH THE BASE CASE S-1 SCENARIO.	426
A7. 18: WIND VELOCITY AT THE RIGHT (WINDWARD) SIMULATION POINTS IN THE MEDIUM ASYMMETRICAL ASPECT RATIO SCENARIOS IN THE TALÍ'E QUBA ROAD, AND COMPARED WITH THE BASE CASE S-1 SCENARIO.	426

A7. 19: WIND VELOCITY AT THE RIGHT (WINDWARD) SIMULATION POINTS IN THE MEDIUM ASYMMETRICAL ASPECT RATIO SCENARIOS IN THE NAZIL QUBA ROAD, AND COMPARED WITH THE BASE CASE S-1 SCENARIO. ....	427
A7. 20: AIR TEMPERATURE AT THE LEFT (LEEWARD) SIMULATION POINTS IN THE MEDIUM ASYMMETRICAL ASPECT RATIO SCENARIOS IN THE TALÍ'E QUBA ROAD, AND COMPARED WITH THE BASE CASE S-1 SCENARIO. ....	428
A7. 21: AIR TEMPERATURE AT THE LEFT (LEEWARD) SIMULATION POINTS IN THE MEDIUM ASYMMETRICAL ASPECT RATIO SCENARIOS IN THE NAZIL QUBA ROAD, AND COMPARED WITH THE BASE CASE S-1 SCENARIO. ....	428
A7. 22: AIR TEMPERATURE AT THE MIDDLE SIMULATION POINTS IN THE MEDIUM ASYMMETRICAL ASPECT RATIO SCENARIOS IN THE TALÍ'E QUBA ROAD, AND COMPARED WITH THE BASE CASE S-1 SCENARIO. ....	429
A7. 23: AIR TEMPERATURE AT THE MIDDLE SIMULATION POINTS IN THE MEDIUM ASYMMETRICAL ASPECT RATIO SCENARIOS IN THE NAZIL QUBA ROAD, AND COMPARED WITH THE BASE CASE S-1 SCENARIO. ....	429
A7. 24: AIR TEMPERATURE AT THE RIGHT (WINDWARD) SIMULATION POINTS IN THE MEDIUM ASYMMETRICAL ASPECT RATIO SCENARIOS IN THE TALÍ'E QUBA ROAD, AND COMPARED WITH THE BASE CASE S-1 SCENARIO. ....	429
A7. 25: AIR TEMPERATURE AT THE RIGHT (WINDWARD) SIMULATION POINTS IN THE MEDIUM ASYMMETRICAL ASPECT RATIO SCENARIOS IN THE NAZIL QUBA ROAD, AND COMPARED WITH THE BASE CASE S-1 .....	430
A7. 26: WIND VELOCITY AT THE LEFT SIMULATION POINTS (LEEWARD) IN THE HIGH ASYMMETRICAL ASPECT RATIO SCENARIOS, PARTICULARLY IN THE TALÍ'E QUBA ROAD (BETWEEN THE FIRST AND THE SECOND ROWS OF BUILDINGS). ....	432
A7. 27: WIND VELOCITY AT THE LEFT SIMULATION POINTS (LEEWARD) IN THE HIGH ASYMMETRICAL ASPECT RATIO SCENARIOS, PARTICULARLY IN THE NAZIL QUBA ROAD (BETWEEN THE SECOND AND THE THIRD ROWS OF BUILDINGS). ....	432
A7. 28: WIND VELOCITY AT THE MIDDLE SIMULATION POINTS IN THE HIGH ASYMMETRICAL ASPECT RATIO SCENARIOS, PARTICULARLY IN THE TALÍ'E QUBA ROAD (BETWEEN THE FIRST AND THE SECOND ROWS OF BUILDINGS). ....	433
A7. 29: WIND VELOCITY AT THE MIDDLE SIMULATION POINTS IN THE HIGH ASYMMETRICAL ASPECT RATIO SCENARIOS, PARTICULARLY IN THE NAZIL QUBA ROAD (BETWEEN THE SECOND AND THE THIRD ROWS OF BUILDINGS). ....	434
A7. 30: WIND VELOCITY NEAR THE WINDWARD WALLS (RIGHT POINTS) IN THE HIGH ASYMMETRICAL ASPECT RATIO SCENARIOS, PARTICULARLY IN THE TALÍ'E QUBA ROAD (BETWEEN THE FIRST AND THE SECOND ROWS OF BUILDINGS). ....	434
A7. 31: WIND VELOCITY NEAR THE WINDWARD WALLS (RIGHT POINTS) IN THE HIGH ASYMMETRICAL ASPECT RATIO SCENARIOS, PARTICULARLY IN THE NAZIL QUBA ROAD (BETWEEN THE SECOND AND THE THIRD ROWS OF BUILDINGS). ....	435
A7. 32: AIR TEMPERATURE AT THE LEFT SIMULATION POINTS (LEEWARD) IN THE HIGH ASYMMETRICAL ASPECT RATIO SCENARIOS, PARTICULARLY IN THE TALÍ'E QUBA ROAD (BETWEEN THE FIRST AND THE SECOND ROWS OF BUILDINGS). ....	436
A7. 33: AIR TEMPERATURE AT THE LEFT SIMULATION POINTS (LEEWARD) IN THE HIGH ASYMMETRICAL ASPECT RATIO SCENARIOS, PARTICULARLY IN THE NAZIL QUBA ROAD (BETWEEN THE SECOND AND THE THIRD ROWS OF BUILDINGS). ....	437
A7. 34: AIR TEMPERATURE AT THE MIDDLE SIMULATION POINTS IN THE HIGH ASYMMETRICAL ASPECT RATIO SCENARIOS, PARTICULARLY IN THE TALÍ'E QUBA ROAD (BETWEEN THE FIRST AND THE SECOND ROWS OF BUILDINGS). ....	438
A7. 35: AIR TEMPERATURE AT THE MIDDLE SIMULATION POINTS IN THE HIGH ASYMMETRICAL ASPECT RATIO SCENARIOS, PARTICULARLY IN THE NAZIL QUBA ROAD (BETWEEN THE SECOND AND THE THIRD ROWS OF BUILDINGS). ....	438
A7. 36: AIR TEMPERATURE NEAR THE WINDWARD WALLS (RIGHT POINTS) IN THE HIGH ASYMMETRICAL ASPECT RATIO SCENARIOS, PARTICULARLY IN THE TALÍ'E QUBA ROAD (BETWEEN THE FIRST AND THE SECOND ROWS OF BUILDINGS). ....	439
A7. 37: AIR TEMPERATURE NEAR THE WINDWARD WALLS (RIGHT POINTS) IN THE HIGH ASYMMETRICAL ASPECT RATIO SCENARIOS, PARTICULARLY IN THE NAZIL QUBA ROAD (BETWEEN THE SECOND AND THE THIRD ROWS OF BUILDINGS). ....	439
A7. 38: WIND VELOCITY AT THE LEFT SIDE (NEAR LEEWARD ELEVATIONS) OF TALÍ'E QUBA ROAD (WINDWARD CANYON) IN THE THE GRADUAL INCREASE IN ASPECT RATIOS MODELS (S-13 TO S-16) AND COMPARED WITH THE BASE CASE S-1 SCENARIO. ....	440
A7. 39: WIND VELOCITY IN THE MIDDLE OF TALÍ'E QUBA ROAD (WINDWARD CANYON) IN THE THE GRADUAL INCREASE IN ASPECT RATIOS MODELS (S-13 TO S-16) AND COMPARED WITH THE BASE CASE S-1 SCENARIO. ....	440
A7. 40: WIND VELOCITY AT THE RIGHT SIDE (NEAR WINDWARD ELEVATIONS) OF TALÍ'E QUBA ROAD (WINDWARD CANYON) IN THE THE GRADUAL INCREASE IN ASPECT RATIOS MODELS (S-13 TO S-16) AND COMPARED WITH THE BASE CASE S-1 SCENARIO. ....	440
A7. 41: WIND VELOCITY AT THE LEFT SIDE (NEAR LEEWARD ELEVATIONS) OF NAZIL QUBA ROAD (LEEWARD CANYON) IN THE THE GRADUAL INCREASE IN ASPECT RATIOS MODELS (S-13 TO S-16) AND COMPARED WITH THE BASE CASE S-1 SCENARIO. ....	441

A7. 42: WIND VELOCITY IN THE MIDDLE OF NAZIL QUBA ROAD (LEEWARD CANYON) IN THE THE GRADUAL INCREASE IN ASPECT RATIOS MODELS (S-13 TO S-16) AND COMPARED WITH THE BASE CASE S-1 SCENARIO. ....	441
A7. 43: WIND VELOCITY AT THE RIGHT SIDE (NEAR WINDWARD ELEVATIONS) OF NAZIL QUBA ROAD (LEEWARD CANYON) IN THE THE GRADUAL INCREASE IN ASPECT RATIOS MODELS (S-13 TO S-16) AND COMPARED WITH THE BASE CASE S-1 SCENARIO. ....	441
A7. 44: AIR TEMPERATURE AT THE LEFT SIDE (NEAR LEEWARD ELEVATIONS) OF TALİ'E QUBA ROAD (WINDWARD CANYON) IN THE THE GRADUAL INCREASE IN ASPECT RATIOS MODELS (S-13 TO S-16) AND COMPARED WITH THE BASE CASE S-1 SCENARIO. ....	442
A7. 45: AIR TEMPERATURE IN THE MIDDLE OF TALİ'E QUBA ROAD (WINDWARD CANYON) IN THE THE GRADUAL INCREASE IN ASPECT RATIOS MODELS (S-13 TO S-16) AND COMPARED WITH THE BASE CASE S-1 SCENARIO. ....	442
A7. 46: AIR TEMPERATURE AT THE RIGHT SIDE (NEAR WINDWARD ELEVATIONS) OF TALİ'E QUBA ROAD (WINDWARD CANYON) IN THE THE GRADUAL INCREASE IN ASPECT RATIOS MODELS (S-13 TO S-16) AND COMPARED WITH THE BASE CASE S-1 SCENARIO. ....	442
A7. 47: AIR TEMPERATURE AT THE LEFT SIDE (NEAR LEEWARD ELEVATIONS) OF NAZIL QUBA ROAD (LEEWARD CANYON) IN THE THE GRADUAL INCREASE IN ASPECT RATIOS MODELS (S-13 TO S-16) AND COMPARED WITH THE BASE CASE S-1 SCENARIO. ....	443
A7. 48: AIR TEMPERATURE IN THE MIDDLE OF NAZIL QUBA ROAD (LEEWARD CANYON) IN THE THE GRADUAL INCREASE IN ASPECT RATIOS MODELS (S-13 TO S-16) AND COMPARED WITH THE BASE CASE S-1 SCENARIO. ....	443
A7. 49: AIR TEMPERATURE AT THE RIGHT SIDE (NEAR WINDWARD ELEVATIONS) OF NAZIL QUBA ROAD (LEEWARD CANYON) IN THE THE GRADUAL INCREASE IN ASPECT RATIOS MODELS (S-13 TO S-16) AND COMPARED WITH THE BASE CASE S-1 SCENARIO. ....	443
A7. 50: PET TEMPERATURE IN THE WINDWARD CANYON (I.E. TALİ'E QUBA ROAD) NEAR THE WINDWARD WALLS (RIGHT POINTS), LEEWARD WALLS (LEFT POINTS) AND MIDDLE OF THE CANYON IN THE HIGH ASYMMETRICAL ASPECT RATIO SCENARIO OF S-11. ....	444
A8. 1: WIND VELOCITY AT PEDESTRIAN HEIGHT (2M) FOR S-13 THAT REPRESENTS THE NIGHT TIME (21:00PM) CASE BASED ON THE BEST H/W OF (S-11), AND COMPARED WITH THE BASE CASE (S-1) AT NIGHT IN THE TALİ'E QUBA ROAD ALONG FIVE CROSS-SECTIONS AT THE LEFT (LEEWARD), MIDDLE AND RIGHT (WINDWARD) ROWS OF POINTS .....	445
A8. 2: AIR TEMPERATURE AT PEDESTRIAN HEIGHT (2M) FOR S-13 THAT REPRESENTS THE NIGHT TIME (21:00PM) CASE BASED ON THE BEST H/W OF (S-11), AND COMPARED WITH THE BASE CASE (S-1) AT NIGHT IN THE TALİ'E QUBA ROAD ALONG FIVE CROSS-SECTIONS AT THE LEFT (LEEWARD), MIDDLE AND RIGHT (WINDWARD) ROWS OF POINTS. ....	445
A8. 3: CONTOURS OF VELOCITY MAGNITUDE (M/S) AT PEDESTRIAN HEIGHT (2M) FOR THE BASE CASE WITH SOUTH-WESTERLY WIND DIRECTION (S-1 SOUTH-WEST) AND WESTERLY WIND DIRECTION (S-1 WEST) SCENARIOS. ....	446
A8. 4: WIND VELOCITY IN THE TALİ'E Q. RD. AT PEDESTRIAN HEIGHT (2M) FOR THE BASE CASE WITH SOUTH-WESTERLY WIND DIRECTION (S-1 SOUTH-WEST) AND WESTERLY WIND DIRECTION (S-1 WEST) SCENARIOS. ....	446
A8. 5: WIND VELOCITY IN THE NAZIL Q. RD. AT PEDESTRIAN HEIGHT (2M) FOR THE BASE CASE WITH SOUTH-WESTERLY WIND DIRECTION (S-1 SOUTH-WEST) AND WESTERLY WIND DIRECTION (S-1 WEST) SCENARIOS. ....	447
A8. 6: CONTOURS OF AIR TEMPERATURE DEGREES (OC) AT PEDESTRIAN HEIGHT (2M) FOR THE BASE CASE WITH SOUTH-WESTERLY WIND DIRECTION (S-1 SOUTH-WEST) AND WESTERLY WIND DIRECTION (S-1 WEST) SCENARIOS. ....	447
A8. 7: AIR TEMPERATURE IN THE TALİ'E Q. RD. AT PEDESTRIAN HEIGHT (2M) FOR THE BASE CASE WITH SOUTH-WESTERLY WIND DIRECTION (S-1 SOUTH-WEST) AND WESTERLY WIND DIRECTION (S-1 WEST) SCENARIOS. ....	447
A8. 8: AIR TEMPERATURE IN THE NAZIL Q. RD. AT PEDESTRIAN HEIGHT (2M) FOR THE BASE CASE WITH SOUTH-WESTERLY WIND DIRECTION (S-1 SOUTH-WEST) AND WESTERLY WIND DIRECTION (S-1 WEST) SCENARIOS. ....	448
A8. 9: CONTOURS OF VELOCITY MAGNITUDE (M/S) AT PEDESTRIAN HEIGHT (2M) FOR THE BASE CASE WITH A HYPOTHESISED SOUTH WIND DIRECTION (S-1 SOUTH) PARALLEL WITH THE URBAN CANYONS, AND COMPARED WITH SOUTH-WESTERLY WIND DIRECTION. ....	449
A8. 10: WIND VELOCITY IN THE TALİ'E Q. RD. AT PEDESTRIAN HEIGHT (2M) FOR THE BASE CASE WITH HYPOTHESISED SOUTH WIND DIRECTION (S-1 SOUTH) I.E. PARALLEL WITH THE URBAN CANYONS, AND COMPARED WITH THE PREVAILING SOUTH-WESTERLY DIRECTION. ....	449

A8. 11: WIND VELOCITY IN THE NAZIL Q.RD. AT PEDESTRIAN HEIGHT (2M) FOR THE BASE CASE WITH HYPOTHESISED SOUTH WIND DIRECTION (S-1 SOUTH) PARALLEL WITH THE URBAN CANYONS, AND COMPARED WITH THE PREVAILING SOUTH-WESTERLY DIRECTION. ....	449
A8. 12: CONTOURS OF AIR TEMPERATURE DEGREES (OC) AT PEDESTRIAN HEIGHT (2M) FOR THE BASE CASE WITH A HYPOTHESISED SOUTH WIND DIRECTION (S-1 SOUTH) PARALLEL WITH THE URBAN CANYONS, AND COMPARED WITH SOUTH-WESTERLY WIND DIRECTION. ....	450
A8. 13: AIR TEMPERATURE IN THE TALÍ'E Q.RD. AT PEDESTRIAN HEIGHT (2M) FOR THE BASE CASE WITH HYPOTHESISED SOUTH WIND DIRECTION (S-1 SOUTH) PARALLEL WITH THE URBAN CANYONS, AND COMPARED WITH THE PREVAILING SOUTH-WESTERLY WIND DIRECTION. ....	450
A8. 14: AIR TEMPERATURE IN THE NAZIL Q.RD. AT PEDESTRIAN HEIGHT (2M) FOR THE BASE CASE WITH HYPOTHESISED SOUTH WIND DIRECTION (S-1 SOUTH) PARALLEL WITH THE URBAN CANYONS, AND COMPARED WITH THE PREVAILING SOUTH-WESTERLY WIND DIRECTION. ....	450
A8. 15: WIND SPEED AT PEDESTRIAN HEIGHT (2M) IN THE TALÍ'E QUBA ROAD FOR THE BEST ASPECT RATIO WITH SCENARIOS OF WESTERLY PREVAILING WIND DIRECTION (S-16) AND NORTH-WESTERLY PREVAILING WIND (S-17), AND COMPARED WITH THE BEST ASPECT RATIO (S-11) SCENARIO WITH SOUTH-WESTERLY PREVAILING WIND. ....	451
A8. 16: AIR TEMPERATURE AT PEDESTRIAN HEIGHT (2M) IN THE TALÍ'E QUBA ROAD FOR THE BEST ASPECT RATIO WITH SCENARIOS OF WESTERLY PREVAILING WIND DIRECTION (S-16) AND NORTH-WESTERLY PREVAILING WIND (S-17), AND COMPARED WITH THE BEST ASPECT RATIO (S-11) SCENARIO WITH SOUTH-WESTERLY PREVAILING WIND. ....	451
A8. 17: WIND VELOCITY FOR THE STREETS CONFIGURATION WITH DIFFERENT PREVAILING WIND DIRECTIONS.....	452
A8. 18: AIR TEMPERATURES FOR THE STREETS CONFIGURATION WITH DIFFERENT PREVAILING WIND DIRECTIONS .....	452



## List of Tables

TABLE 2. 1: THE WEATHER READINGS IN MADINAH CITY IN 2010, ADAPTED FROM WWW.TUTTIEMPO.NET .....	32
TABLE 3. 1: PREVIOUS STUDIES ON OUTDOOR THERMAL COMFORT. ....	60
TABLE 4. 1: PREVIOUS STUDIES ON URBAN STREET GEOMETRY (I.E. ASPECT RATIO AND ORIENTATION OF AN URBAN STREET CANYON). ....	75
TABLE 4. 2: EXTENDED LAND BEAUFORT SCALE SHOWING WIND EFFECTS ON PEOPLE. SOURCE: LAWSON AND PENWARDEN (1975). ....	82
TABLE 4. 3: PREVIOUS NUMERICAL STUDIES ON URBAN MICROCLIMATE USING CFD SIMULATION. ....	95
TABLE 5. 1: GEOMETRICAL PROPERTIES AT THE THREE MEASUREMENT POINTS' URBAN ZONES ALONG THE NAZIL QUBA ROAD IN THE CITY OF MADINAH (39.7°N, 24.55°E). ....	102
TABLE 5. 2: PERFORMANCE OF KESTREL DATA LOGGER. DIFFERENCE IN ERROR BASED ON PENTZ AND SHOTT (1988). ....	106
TABLE 5. 3: BOUNDARY CONDITIONS AND INITIAL SETTING OF ANSYS-FLUENT 13.0 MODELLING. ....	119
TABLE 5. 4: DATA INPUTS AND THE SIMULATED AND MEASURED AIR TEMPERATURE (°C) AND WIND SPEED (M/S) DIFFERENCES AT THE NAZIL QUBA STREET (LEEWARD CANYON). THE RESULTS OF WIND VELOCITY ARE WITHIN THE ACCEPTABLE ERROR MARGIN OF 20% RECOMMENDED BY WILLEMSSEN AND WISSE (2002). ....	120
TABLE 5. 5: INTERCHANGEABLE MULTI-ASYMMETRICAL ASPECT RATIOS SCENARIOS SPECIFICATIONS FOR THE SECOND AND THIRD ROWS OF BUILDINGS FOR S-3 THROUGH S-12, WITH THE FIRST ROW ARE CONSTANT AS IN S-2 SCENARIO. NOTE THAT THE NUMBERS UNDERLINED IN H/W ARE ROUNDED UP.....	128
TABLE 5. 6: MATERIAL SPECIFICATIONS BASED ON ASHRAE (2009) AND QU (2011). ....	140
TABLE 6. 1: AVERAGE VALUES OF URBAN MICROCLIMATE AND PET THERMAL COMFORT CONDITIONS OBTAINED AT PEDESTRIAN HEIGHT IN DIFFERENT URBAN DENSITY AND CLIMATIC SEASONS IN THE NAZIL QUBA ROAD, IN MADINAH. ....	203
TABLE 7. 1: BOUNDARY CONDITIONS AND INITIAL SETTING OF ANSYS-FLUENT 13.0 MODELLING. ....	207
TABLE 7. 2: INTERCHANGEABLE MULTI-ASYMMETRICAL ASPECT RATIOS SCENARIOS SPECIFICATIONS FOR THE SECOND AND THIRD ROWS OF BUILDINGS FOR S-3 THROUGH S-12, WITH THE FIRST ROW ARE CONSTANT AS IN S-2 SCENARIO. NOTE THAT THE NUMBERS UNDERLINED IN H/W ARE ROUNDED UP.....	238
TABLE 7. 3: LEVEL OF IMPROVEMENT IN THERMAL COMFORT PET TEMPERATURE IN THE WINDWARD AND LEEWARD CANYONS FOR THE PROPOSED ASPECT RATIO SCENARIOS COMPARED TO THE BASE CASE. ....	273
TABLE 8. 1: PROPOSED LEVEL OF THERMAL COMFORT PERFORMANCE IN THE CURRENT RESEARCH BASED ON THE URBAN STREET CANYON H/W SIMULATION ANALYSIS COMPARED TO THE BASE CASE. ....	334

## List of Abbreviations and Nomenclature

ABL Atmospheric Boundary Layer

CFD Computational Fluid Dynamics.

This is “*a branch of fluid mechanics that uses numerical methods and algorithms to solve and analyse problems that involve fluid flows*” (Masnavi et al., 2012:117).

Compact Urban Form

This is “*a city that is concentrated and firmly unified with a consolidation of land uses in a close and tight physical relationship with each other and the structures within themselves*” (Golany, 1995:155).

H/W Buildings’ Height to Street Width aspect ratio

MRT Mean Radiant Temperature

This is a rationally derived environmental index defined as the uniform black-body temperature that would result in the same radiant energy exchange as in the actual environment.

PET Physiological Equivalent Temperature

It is defined as the Physiological Equivalent Temperature at any given place (outdoors or indoors) and is equivalent to the air temperature at which, in a typical indoor situation (with no wind and solar radiation), the heat balance of the human body is maintained with core and skin temperatures equal to those under the complex outdoor conditions to be assessed (Höppe, 1999).

RANS Reynolds Averaged Navier-Stokes

RH Relative Humidity

S2S Surface-to-Surface (radiation model in Ansys CFD FLUENT)

S-1 Scenario 1

UHI Urban Heat Island

UDF User Defined Function

Cs Roughness Constant

$\varepsilon$  Turbulence dissipation rate

k Kinetic energy

$K$	von Karman constant ( $K=0.42$ )
$k_s$	Sand-grain roughness height
$U, V$	Wind velocity
$U^*$	Friction velocity
$Z_0$	Urban Roughness Length

# CHAPTER 1: Introduction

## **Chapter Structure**

- 1.1. Introduction
- 1.2. Contribution to Knowledge
- 1.3. Outdoor Wind Flow and Pedestrian Thermal Comfort
- 1.4. The Research Aim and Objectives
- 1.5. Research Questions
- 1.6. Research Methodology
- 1.7. Research Limitation
- 1.8. The Organisation of the Thesis

# Chapter 1: Introduction

---

## 1.1. Introduction

Due to the discovery of oil and improvement in economic conditions in Saudi Arabia, the design of urban traditional neighbourhoods has changed over the last six decades from organic and pedestrian-oriented to geometric and vehicle-oriented, which has greatly influenced the pedestrian use of outdoor spaces (Eben Saleh, 1997). One of the major issues facing many outdoor pedestrian spaces in hot arid regions of Saudi Arabia, including Madinah city, is the high ambient temperatures combined with current trends in urbanisation which affect pedestrian thermal comfort (Eben Saleh, 1997; Abdel-Ghany et al., 2013).

The thesis aims to investigate the effects of multi-asymmetrical street aspect ratios (i.e. diverse building heights to street width  $H_1/W - H_2/W - H_3/W$ ) on urban pedestrian microclimate and outdoor thermal comfort conditions of a residential and commercial urban canyon (i.e. Quba Road) in the low wind speed environment and hot arid region of Madinah in Saudi Arabia. This is to find ways to enhance the thermal comfort level in the existing urban configuration of Quba Road canyons (i.e. Tali'e Quba canyon and Nazil Quba canyon) in Madinah. The focus is particularly during mid-seasons (spring and autumn), as they are positioned at the edge of the extremely hot summer season, with an average daily air temperature range of 32.6 °C – 45.8 °C in August (summer), 22.4 °C – 36.1 °C in April (spring), and 23.6 °C – 38.7 °C in October (autumn). Thus, to extend the use of outdoor spaces by shifting the thermal conditions from a range of thermal discomfort into a range of critical thermal comfort as much as possible, passively without the introduction of any mechanical system for cooling (e.g. Erell et al., 2011; Oke, 1988; Pearlmutter et al., 2007).

## 1.2. Contribution to Knowledge

The relative impact of city planning and structural height can positively or negatively affect the street level microclimates, and as a result influences the thermal sensation of humans (Oke, 1988). Thus, there is an interrelationship between urban street canyon design, microclimatic parameters, and human thermal comfort (Ahmed-Ouameur and Potvin, 2007; Krüger, et al., 2011; Nikolopoulou et al., 2004; Shishegar, 2013; Martins et al., 2012; Yahia, 2012). The urban street canyon design can include

altering the canyon's H/W aspect ratios (building's height to street's width ratio), orientation with prevailing wind directions and exposure to solar radiation.

Numerous studies were conducted in relation to the configuration of urban geometries presented by H/W aspect ratio with microclimate, but mostly conducted in relation to exposure to solar radiation (Xi et al., 2012; Johansson, 2006; Ali-Toudert and Mayer, 2006). The majority of previous studies on thermal comfort have focused on symmetrical aspect ratios rather than asymmetrical ones, thus limit the available knowledge on asymmetrical canyon studies, which are more representative of actual urban areas. The study of multiple asymmetrical urban street aspect ratios (i.e. diverse buildings height to street width;  $H_1/W - H_2/W - H_3/W$ ), based on optimising the buildings' height to influence wind flow rate, has not received much attention in the context of urban pedestrian thermal comfort, particularly in low wind speed environments and in hot arid regions.

This study deviated from previous research and studies of Ali-Toudert and Mayer (2007) and Qaid and Ossen (2014). For example, Ali-Toudert and Mayer (2007) investigated the effects of asymmetrical urban canyons on thermal comfort, by manipulating an asymmetrical urban canyon with a wide opening to the sky and compared an asymmetrical urban canyon with smaller opening to the sky (i.e. overhanging facades or balconies). The simulation outcomes revealed that the larger the openness of the canyon to the sky, the greater the heat stress. This study was conducted under hot arid climatic condition of Ghardaia in the Algerian Sahara, using Envi-met model and PET index for the simulation and calculation of thermal comfort, respectively. However, the study did not consider testing different aspect ratios ( $H/W$ ) of the asymmetrical canyon in terms of altering buildings height. Instead, they have considered the openness to the sky, which seriously lacks in information on the effect of different asymmetrical aspect ratios on pedestrian wind environment, thus on pedestrian thermal comfort.

On the other hand, Qaid and Ossen (2014) studied the effects of asymmetrical street aspect ratios for two rows of buildings on outdoor microclimates. The study was conducted in hot humid region of Malaysia with northeast to southwest street axis orientation instead of hot arid climate with north-south street orientation like the current research case study. The researchers investigated three interchangeable asymmetrical aspect ratios ( $H_1/W - H_2/W$  of 0.8 – 1; 0.8 – 1.5; and 0.8 – 2) for both sides of the street (i.e. six scenarios). It was found that aspect ratios of 0.8-2 can reduce the morning

microclimate and night heat stress level, yet the negative impacts during the day are greater than the positive impacts in the night. On the other hand, it was found that by interchanging the aspect ratios to 2 – 0.8 it can reduce the air temperature by 4.7°C and surfaces temperature by 10 to 14°C. This research neither considered north-south canyon orientation, nor the effects of multi asymmetrical aspect ratios ( $H_1/W$ - $H_2/W$ - $H_3/W$ ). In addition, it was not conducted under hot arid conditions and did not calculate the pedestrian thermal comfort conditions, which the current research attempts to cover.

Since the study aims to predict the effects of configuring different street aspect ratios on pedestrian level urban wind velocity, a numerical simulation is an appropriate method and CFD ANSYS-Fluent is suited for this task (e.g. Bottillo et al., 2014; De Lieto Vollaro et al., 2014; Ahranjani, 2010; Ali-Toudert and Johansson, 2006; Qaid and Ossen, 2014). The software is capable of predicting air temperature, wind velocity, relative humidity, and solar radiation. Solar radiation contributes considerably to diurnal heat stress in clear sky conditions, as partly of solar radiation is absorbed and partly reflected by urban surfaces. However, limited urban wind simulation studies were conducted using radiation models coupled with CFD, due to lack of information on the scattering medium of different materials for the radiative transfer equation, while this equation is CPU-intensive. This current research aims to use S2S (surface-to-surface) radiation model, which was recently validated by Bottillo et al. (2014); De Lieto Vollaro et al. (2014) and Ahranjani (2010). S2S radiation scheme is available in CFD ANSYS-Fluent, and it models the enclosure radiative transfer without participating scattering medium, as it simplifies the net radiation budget to surfaces within a street canyon based on sky view factor.

The present study aims to evaluate the effects of multi-asymmetrical street aspect ratios on urban pedestrian microclimate and outdoor thermal comfort conditions, through a case study of Quba Road. The thesis also explores the urban pedestrian microclimate and outdoor thermal comfort conditions of the three urban density types (high, intermediate and low urban densities) along Quba Road, during the four climatic seasons. This is to understand the relationships between the microclimatic variables, and thermal comfort conditions during the day and at night periods, and between the three urban densities and the four climatic seasons.

Quba Road (north-south axis) is a commercial/residential route linking between two prominent religious sites in Madinah, Saudi Arabia. It contains three different urban density types, which are a high urban density area (Case 1), intermediate urban density

area (Case 2) and low urban density area (Case 3). Quba Road suffers from low wind flow rate and high air temperature during the day, which could be due to the approximately perpendicular prevailing wind direction (from south-westerly direction) to the urban canyon with  $-112.5^\circ$  angle of attack, and exposure to extreme solar radiation that increases air temperature at ground level.

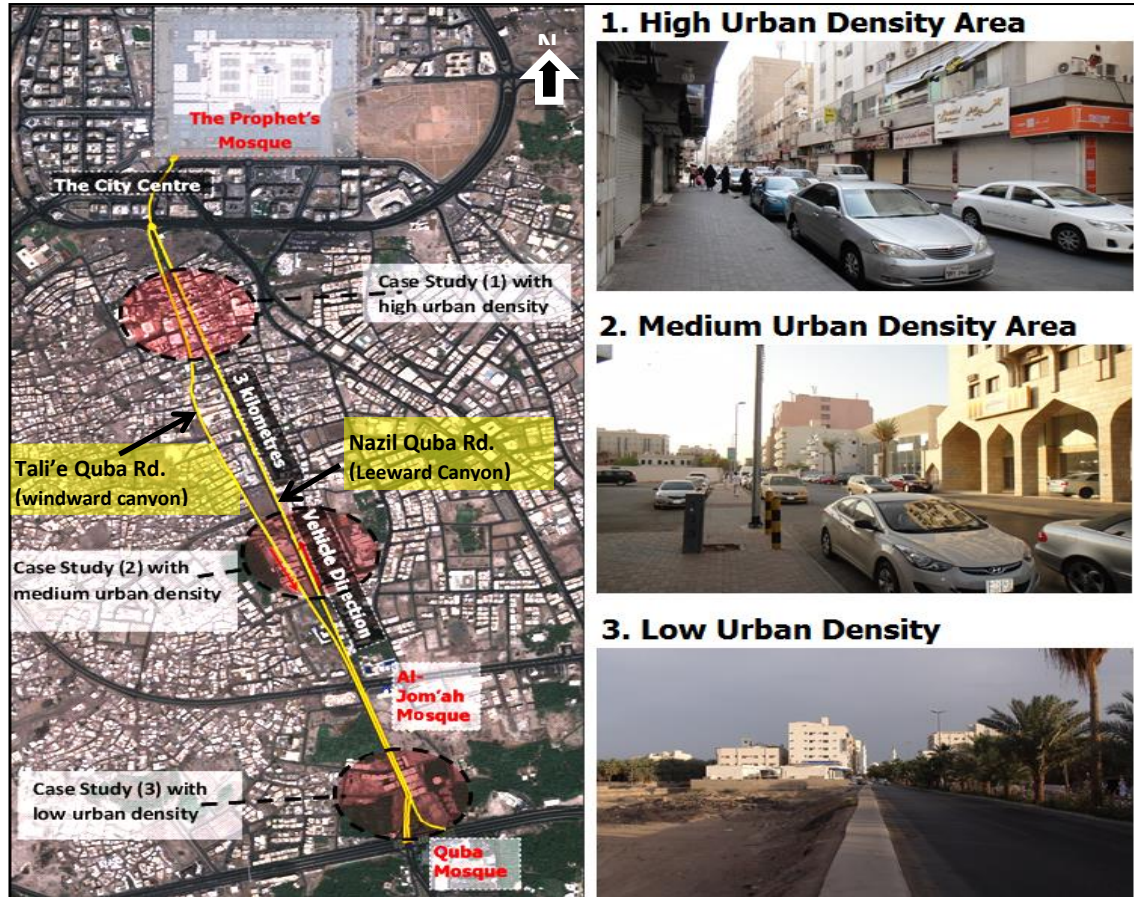


Fig. 1. 1: Quba Road canyons, North-South orientation, linking two most visited mosques in the city.

Quba Road divides the urban area into three rows of buildings, with two urban canyons, namely Tali'e Quba Road (i.e. windward canyon) and Nazil Quba Road (i.e. leeward canyon). Although the Tali'e Quba Road (i.e. windward canyon) experiences less thermal stress than the leeward canyon (refer to simulation results in Chapter 7), the number of shops in the Nazil Quba Road (leeward canyon) is higher than the Tali'e Quba Road (windward canyon) with increased number of pedestrian. This could be because of the Nazil Quba road being the direct urban physical linkage between the two most visited sites in Madinah, namely the Prophet Mosque in the city centre and the Quba Mosque in the South (3km in between). Many small mosques are situated every 200m along the windward elevation side of the Nazil Quba Road, which attract pedestrian during praytime, while the Tali'e Quba Road lacks these religious venues.



### 1.3. Outdoor Wind Flow and Pedestrian Thermal Comfort

According to Stavrakakis et al. (2012), the improvement of wind movement can enhance the effects of thermal environments at pedestrian level. With respect to the urban microclimate modelling, Errell et al. (2011) indicated that the integration of computational fluid dynamics (CFD) with urban design can enable the simulation and prediction of fluid fluxes (e.g. heat and wind) and the effects of urban geometry on thermal environments. Ali-Toudert and Mayer (2006) have simulated the effects of urban street aspect ratio and orientation of urban street on pedestrian thermal comfort, under hot arid conditions, using a computer simulation method (e.g. CFD). However, their study was based on the degree of exposure to solar radiation, but not on the wind flow rate and prevailing wind directions. Golany (1996) suggests that higher buildings results in higher wind speeds at pedestrian levels due to high wind catchment objects, and vice versa. Qaid and Ossen (2014) suggest that, although in cold climates the high rise buildings are not recommended, however, in hot climates these are preferable due to their potential for increasing convective heat transfer, thus enhancing thermal comfort. In addition, orientation of an urban street in relation to wind flow direction leads to different effects on the wind flow rate (Golany, 1996; Ali-Toudert and Mayer, 2006).

In order to evaluate the effects of urban street aspect ratio on pedestrian thermal comfort in a certain location of a city, the definition of appropriate indices based on human thermal comfort criteria is necessary. Despite the widespread research conducted to define indoor comfort indices, limited studies have been carried out on defining outdoor thermal comfort indices, particularly under hot arid conditions. Air temperature, mean radiant temperature, relative humidity and wind speed are microclimatic parameters that have been mostly addressed with regard to pedestrian thermal comfort in outdoor environment. The relationship between pedestrian thermal comfort and characteristics of urban street canyons is widely studied in literature; however, most of these studies were based on exposure degree of street surfaces to solar radiation. Therefore, pedestrian thermal comfort can be investigated based on the effects of altering urban street canyon designs on airflow regime. These designs include aspect ratio ( $H/W$ ) and orientation of urban street canyons with prevailing wind directions.

Although few studies on outdoor thermal comfort were conducted in hot arid climate, relatively limited research has been conducted in Saudi Arabia (e.g. Abdel-Ghany et al., 2013), while no research on thermal comfort has been conducted in the context of Madinah. Thus, the field study approach combined with urban simulations

has been employed to assess the outdoor human thermal comfort perceptions and identify the urban microclimate conditions during the mid-seasons in Madinah. However, modelling of pedestrian thermal comfort within multiple street canyons of a large urban environment still has limitations due to the computational time and cost.

#### **1.4. The Research Aim and Objectives**

This study aims to evaluate the effects of multi-asymmetrical street aspect ratios on urban pedestrian microclimate and outdoor thermal comfort, particularly in a low wind speed environment, through a case study of Quba Road, in order to find ways to improve the urban wind flow and pedestrian thermal comfort conditions in the hot arid climate of Madinah.

To achieve this aim, the following objectives were derived:

1. Understanding the context of the case study area and the climatic characteristics (Chapter 2).
2. To understand the outdoor thermal comfort interaction factors and the pedestrian thermal comfort criteria for hot arid regions (Chapter 3).
3. To understand the effect of urban configurations on pedestrian level wind flow in urban street canyons (Chapter 4).
4. To explore the urban pedestrian microclimate and thermal comfort conditions of a residential and commercial urban canyon (i.e. Quba Road) in Madinah, through field measurements during the four climatic seasons (discussed in Chapter 6).
5. To examine the effects of the optimisation of the urban H/W aspect ratios to the existing urban configurations on the urban wind flow rate during the day, and to evaluate the pedestrian thermal comfort conditions for the proposed best H/W scenario (discussed in Chapter 7).
6. To study the variation of wind flow for the optimum proposed H/W model, considering scenarios on time variations, different orientations of urban canyons with wind directions, increasing the number of buildings' rows, configuring new streets perpendicular to the existing canyons, removal of buildings, providing cantilevers, and changing material colours and changing the block patterns (discussed in Chapter 8).
7. To propose guidelines for improving the wind flow and outdoor thermal comfort based on a case study of Quba Road in Madinah (Chapter 8).

## **1.5. Research Questions**

### **1.5.1. Major Research Question**

What is the influence of the multi-asymmetrical street aspect ratios on urban pedestrian microclimate and outdoor thermal comfort conditions, in a low wind speed environment of Madinah?

### **1.5.2. Minor Research Questions**

To answer the above major research question, the following minor research questions were addressed.

1. What is the existing urban and climatic characteristics of the study area in Madinah?
2. What are the outdoor pedestrian thermal comfort interaction factors and the comfort criteria for the hot arid climates?
3. How do different urban configurations affect the variations of wind flow in urban street canyons at the pedestrian level?
4. What are the characteristics of the existing urban pedestrian microclimate and thermal comfort conditions in Madinah?
5. What are the effects of different street aspect ratios in relation to the existing conditions on wind flow and pedestrian thermal comfort?
6. What are the effects of different urban configurations in relation to the proposed optimum street aspect ratios model on wind flow and pedestrian thermal comfort, considering scenarios on: time variation, different orientations, increasing the number of rows of buildings, configuration of new perpendicular streets, removal of buildings, providing cantilevers, and changing material colours and changing the block patterns?
7. How will the research be implemented for future planning?

## 1.6. Research Methodology

This research methodology employed a systematic procedure to gather field and numerical simulation data to assess outdoor pedestrian thermal comfort, and to quantitatively compare and evaluate the effects of various asymmetrical street aspect ratios strategies on urban wind flow (Figure 1.2). The methodology was developed from previous relevant researches of Chen and Ng (2012) and Wei (2014), which is quantitative in character and summarises the overall processes and procedures employed in order to achieve the current research aim and objectives, including the following five phases:

- Desktop Survey: preliminary data collection of the case study area (Phase 1).
- Field Measurement Procedures (Phase 2).
- Technical Studies: secondary data collection of PET and CFD (Phase 3).
- CFD Numerical Simulation Procedures (Phase 4).
- Calculation of PET Index and MRT Temperatures (Phase 5).

In Phase 1, the desktop survey (preliminary data collection) was conducted concerned with gathering information about the case study area, through mapping and reviewing local planning regulations documents (discussed in Chapter 2), and reviewing the relevant literature to understand the thermal comfort indices (discussed in Chapter 3) and the effect of wind flow in urban areas (discussed in Chapter 4). Based on this information, a general concept of the case study was developed and the categorisation of Quba Road into three major zoning areas, which are based on built up density, named as: high urban density area (Case 1), intermediate urban density area (Case 2) and low urban density area (Case 3). All the gathered information was used later in preparing for the subsequent phases (Phase 2 through Phase 5).

In Phase 2, weather data were obtained from World Meteorological Organisation using Meteonorm software, including data for solar radiation, air temperature, wind speed, prevailing wind directions, location coordinate (discussed in Chapter 5). The gathered information was used later in preparing for the subsequent phases (Phase 3 through Phase 5). In this phase, four field measurement campaigns were carried out in order to record the variations in the microclimate and the outdoor thermal comfort for the four climatic seasons within the Quba Road (discussed in Chapter 5 and 6). This contains measurements of microclimatic parameters: air temperature, globe temperature (to calculate the mean radiant temperature, MRT), relative humidity, and wind speed.

Field measurement method is a validated method for the assessment of urban microclimate and pedestrian thermal comfort in outdoor spaces (Yahia and Johansson, 2013a; Aljawabra and Nikolopoulou, 2010; Lenzholzer and Koh, 2010).

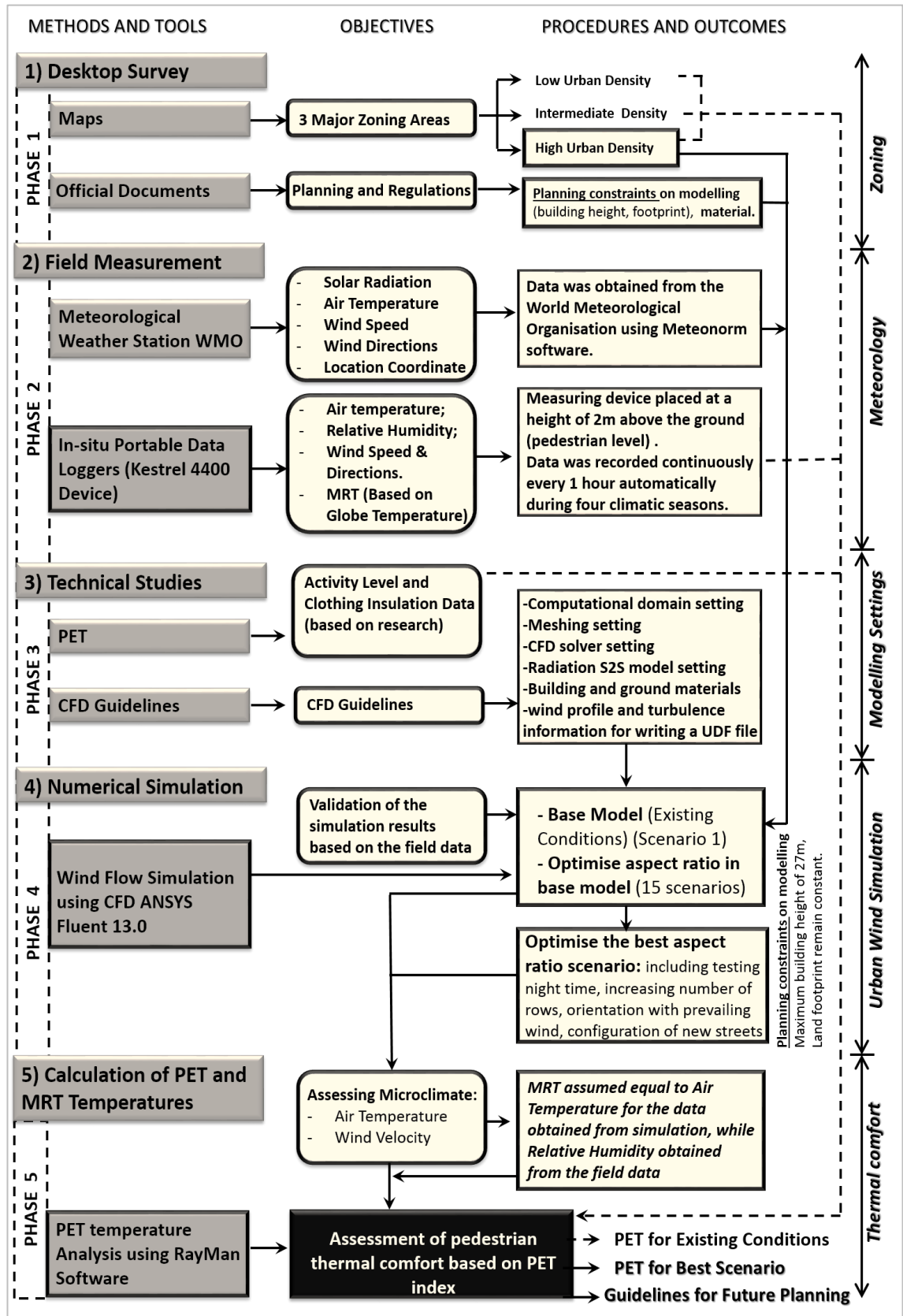


Fig. 1. 2: Methodology and operational framework of the current research.

The four campaigns were handled in the three different locations of the road, including the high urban density area, the intermediate urban density area and the low urban density area during the same time period. The field measurements were taken during autumn (the 14<sup>th</sup> to 25<sup>th</sup> of October 2012), winter (the 1<sup>st</sup> to 7<sup>th</sup> of January 2013), spring (the 1<sup>st</sup> to 12<sup>th</sup> of April 2013), and summer (the 17<sup>th</sup> to 29<sup>th</sup> of June 2013). The duration of measurements for each day was 24 hours. However, some microclimatic data for the intermediate urban density and low urban density areas were lost during the research, due to damage and theft of two measuring devices, in particular during the autumn and winter in Case 2, and autumn in Case 3. Thus, only the high urban density area (Case 1) has complete data for the four climatic seasons.

In Phase 3, technical studies (secondary data collection) were conducted on setting the RayMan software and CFD ANSYS Fluent 13.0 simulation software, through reviewing the literature on pedestrian activity level data, summer and winter clothing insulation data and CFD basic guidelines (discussed in Chapter 5). The gathered information was used later in preparing for the subsequent phases (Phase 4 and Phase 5). The CFD basic guidelines were obtained to set up the numerical simulation software (Phase 4), including information of computational domain setting, meshing setting, CFD solver setting, Radiation S2S (surface to surface) model setting, building and ground materials' properties, and wind profile and turbulence information for the writing a UDF file that can be read by ANSYS Fluent 13.0 program. The activity level and clothing insulation data were required in the calculation of PET thermal comfort index (Phase 5).

In Phase 4, numerical simulation was conducted using urban geometry information of the case study, data obtained from the meteorological station and CFD setting guideline provided in Phase 1, Phase 2 and Phase 3, respectively (discussed in Chapter 7 and 8). The meteorological data were applied as input data to simulate the different urban design scenarios for the high urban density area in this research (Case 1). The simulations have been performed with the academic CFD code ANSYS-Fluent 13.0, 3D double precision, pressure based version and the steady RANS equations have been solved in combination with the realisable  $k-\varepsilon$  model base on the best CFD practice guidelines. Weather information from the meteorological station was required to statistically provide boundary conditions for the numerical model. This process was required to enable the validation of the numerical model by comparing the extracted results from the simulation model with the results obtained from field measurements of

the existing situation. After the validation procedure, testing different modifications in the urban street canyon model (proposed scenarios) were applied, to find ways to mitigate the negative effects of urban microclimates and to enhance the outdoor pedestrian thermal comfort levels.

In Phase 5, evaluating the existing outdoor pedestrian thermal comfort conditions in the four climatic seasons of Madinah, and evaluating the outdoor pedestrian thermal comfort conditions in the proposed urban street aspect ratios model were conducted (discussed in Chapter 7 and 8). The pedestrian thermal comfort was expressed by means of the physiologically equivalent temperature (PET) index. PET was calculated using the RayMan model (Matzarakis et al., 2007). PET index has been calibrated for a hot arid climate in built up areas by Yahia and Johansson (2013a), with an upper limit of 31.3°C and lower limit of 21°C. The factors that were necessary for calculating the PET index was obtained in Phase 2 and 3 and 4, which were: air temperature, mean radiant temperature, relative humidity, wind speed, pedestrian metabolic rate (i.e. activity level; 192.5 W for walking) and clothing insulation level (e.g. 0.59clo for summer clothing and 1.3clo for winter clothing). In this phase, the data for MRT in the existing situation were calculated based on the globe temperature obtained in Phase 2 (i.e. field study).

### **1.7. Research Limitation**

The simulation and field studies are conducted within the urban canopy layer at urban microclimatic scale, and the results are limited to the pedestrian level (i.e. 2m above the ground). This allows for better understanding of pedestrian microclimate and thermal comfort conditions. Therefore, the investigations incorporated the influence of multi-asymmetrical street aspect ratios design on urban wind flow and pedestrian thermal comfort conditions.

The study is limited to the hot arid climate of Madinah. Although some of the findings may be generalised, the conclusions of the study are not necessarily valid throughout the hot arid regions, since there are microclimatic variations between different zones within a city or different cities in terms of urban street orientation, local planning regulations, topography, and proximity to the sea, etc.

The field study was carried out during the four climatic seasons, including Autumn (between the 14<sup>th</sup> to 25<sup>th</sup> of October 2012), Winter (between the 1<sup>st</sup> to 7<sup>th</sup> of January 2013), Spring (between the 1<sup>st</sup> to 12<sup>th</sup> of April 2013), and Summer (between the 17<sup>th</sup> to 29<sup>th</sup> of June 2013). The microclimatic data were measured for 24 hours continuously during the monitoring period. However, some microclimatic data were lost during the research, due to damage and theft of two measuring devices, particularly during the autumn and winter seasons in Case 2 (i.e. the intermediate urban density area), and autumn in Case 3 (i.e. the low urban density area). Thus, only the high urban density area (Case 1) has obtained complete data for the four climatic seasons.

The simulation investigations of the proposed multi-asymmetrical aspect ratios are limited to the hot mid-season of spring rather than in the summer peak period. This is to extend the use of outdoor space by shifting the thermal conditions from a range of thermal discomfort into a range of critical thermal comfort as much as possible passively without the introduction of any mechanical system for cooling. The peak times in hot countries are thermally stressful, thus it is difficult to implement the investigated urban interventions on their own and subsequently alter the conditions passively from discomfort to comfort.

Due to limitations in computing time and resource, the steady state CFD RANS numerical simulation was applied instead of the unsteady method. Thus, the simulation time was at 15:00 hours on the 1<sup>st</sup> of April (i.e. average reading of the first 12 days of April, taken from the City's weather file) was analysed to represent mid seasons, but this may not represent the whole spring season months. The simulation model is limited to an urban area with no source of water or vegetation, thus relative humidity is excluded from the simulation due to computational time constraints.

The research is limited to the local planning and regulation constraints for the maximum buildings height (27m) and the existing footprints for buildings. This research is limited to north-south axis orientation of the investigated urban street canyon, while approximately perpendicular to the prevailing wind directions.



## **1.8. The Organisation of the Thesis**

This thesis is divided into nine chapters. The first chapter establishes the introduction to the main concept of the study. The second chapter initially analyses and explains the research case study areas in Quba Road in Madinah and the local planning and regulations. The third chapter reviews the relevant literature concerning the interaction factors of pedestrian thermal comfort, indoor and outdoor differences in thermal comfort, and pre-established criteria for outdoor thermal comfort that can be applied to the hot dry microclimates. The fourth chapter is about reviewing the effects of urban street aspect ratios and orientations with prevailing winds on pedestrian microclimates, and best practice for urban heat stress mitigation strategies in outdoor urban canyons. The fifth chapter outlines the research methodology for the assessment of outdoor pedestrian thermal comfort, introduces the use of an empirical study as the research validation mechanism and validates the CFD simulation tool used in the research. Chapter six analyses and discusses the microclimatic data collected in the field study and calculates the existing pedestrian thermal comfort conditions in the selected outdoor spaces within the Quba Road. Chapters seven and eight analyse the microclimatic data extracted from the CFD model and discuss the findings of testing different proposed modifications in the urban street canyon model (i.e. optimising the urban configurations of the high urban density area along Quba Road). The final chapter is the conclusion which provides an overview of the study, highlights the questions posed, summarises the methods used for the assessment of outdoor pedestrian thermal comfort, the important findings of the research, and the conclusions reached as well as recommendations for future research.

## **CHAPTER 2: Nature of the Case Study Area**

### **Chapter Structure**

2.1. Introduction

2.2. The Context of Madinah

2.3. Official Plans for Extending the City Centre in  
Madinah

2.4. Local Planning and Regulations for Quba District

2.5. Initial Analysis of Quba Road

2.6. Selection of the Case Study Areas

2.7. Climate of Madinah

2.8. Summary

# Chapter 2:

## Nature of the Case Study Area

---

### 2.1. Introduction

This chapter focuses on understanding urban patterns in Madinah, the local planning and regulations, selection of the case study zones based on their urban density levels and meteorological data of the city.

### 2.2. The Context of Madinah

Madinah, also called Medina or officially called Al-Madinah Al-Monawarah, is the capital city of Al-Madinah Province, with a population size of about 1.3 million in 2013 projected to increase to 2.5 million in 2038 (MMM Group Limited et al., 2012f). Madinah is the fourth largest city in Saudi Arabia after the capital city of Riyadh, the commercial capital and main port of Saudi Arabia, i.e. Jeddah, and after the holiest city of pilgrimage among the Islamic world, i.e. Makkah (Mecca). Madinah is the second most visited city in Saudi Arabia, embracing the history of the prophet Mohammad and his companions since 622 AD; however, to visit Madinah is not a pilgrimage rite, but the unique merits of the Prophet Mohammad's city, his Mosque, his tomb and the city's religious history attract Muslim pilgrims to visit it (Iqbal, 2013). The Prophet Mosque and Quba Mosque are the first two most visited sites in Madinah, and are linked directly by Quba Road (the case study route in this research).

Madinah is characterised by a hot arid climate, and is located in the western region of Saudi Arabia (longitude of 39.7°N and latitude of 24.55°E), with altitude of 597-639 metres above the sea level, and lies approximately 160 kilometres inland from the eastern side of the Red Sea coast and 350 kilometres north of Makkah (Figure 2.1). There are many large green areas within Madinah, as a result of the junction of three valleys – Al-Aql, Al-Aqiq, and Al-Himdh (MMM Group Limited et al., 2012b). The terrain of Madinah city is fertile with the presence of a volcanic hill that rises in the direction of the north; its environment is characterised by basalt and andesite rocks, metamorphosed schist and granite rocks; and natural conditions have donated Madinah's several features that made the city more important; water supplies in Madinah are abundant, its land is fertile with high and abundant productivity (Hanqie Production, 2010).



Fig. 2. 1: Geographical settings of Madinah in Saudi Arabia. Source: MMM Group Limited et al. (2012d).

The prevailing urban configurations in Madinah is a compact form with flat buildings' roofs. Golany (1996) found that the preferred urban form in hot dry regions as in most Middle Eastern cities, with respect to thermal performance, is the compact morphology with flat roofs. Flat roofs and low density open squares are the most comfortable spaces at summer nights, as a result of released heat in a form of radiation from the flat surfaces and the formation of cool air on the surfaces that are exposed to the clear sky (de Schiller and Evans, 2000).

Madinah consists of farm lands that cut through the Northern part of the city, with pockets of green land in the centre and large green spaces to the South, wadis in and around the city, and mountains, as shown in Figure 2.2. The mountains are located in the western (W), north-western (NW) and south-western (SW) areas of the city, which form a large natural barrier that filters the effects of sands, which is not a usual case in Madinah compared to desert cities (e.g. Riyadh). However, this barrier may slow down the prevailing wind speeds (NW, W and SW directions) that are blown from the Red Sea direction (i.e. 160km west of Madinah).

In addition, much of the land within Madinah is fertile as a result of surrounding volcanic ash and wadis which irrigate key locations. Date farms are one of the major industries within Madinah and offer relief from a densely built city. Recently, the Madinah municipality has restricted the lands with soil that are suitable for agriculture from being used for urban development, which is due to the conversions of such lands in the past and resulting in the reduction of farm numbers in the city (MMM Group Limited et al., 2012d). Many studies that focused on the importance of vegetation in an urban environment, found that an appropriate vegetation design strategy can control the effects of wind flow (Shahidan and Jones, 2008; Robinette, 1972), radiation and shading (Fahmy et al., 2010; Mochida and Lun, 2006; Murakami, 2006; Brown and Gillespie, 1995; Shahidan et al., 2007), pollution concentration level (Litschke and Kuttler, 2008; Fujii et al., 2005), and moisture in the surrounding air (Shahidan and Jones, 2008; Robinson, 2004; Kotzen, 2003). Nevertheless, increasing the amount of vegetation in hot arid regions is clearly resource intensive. Therefore, it is impractical to be considered in the present study.



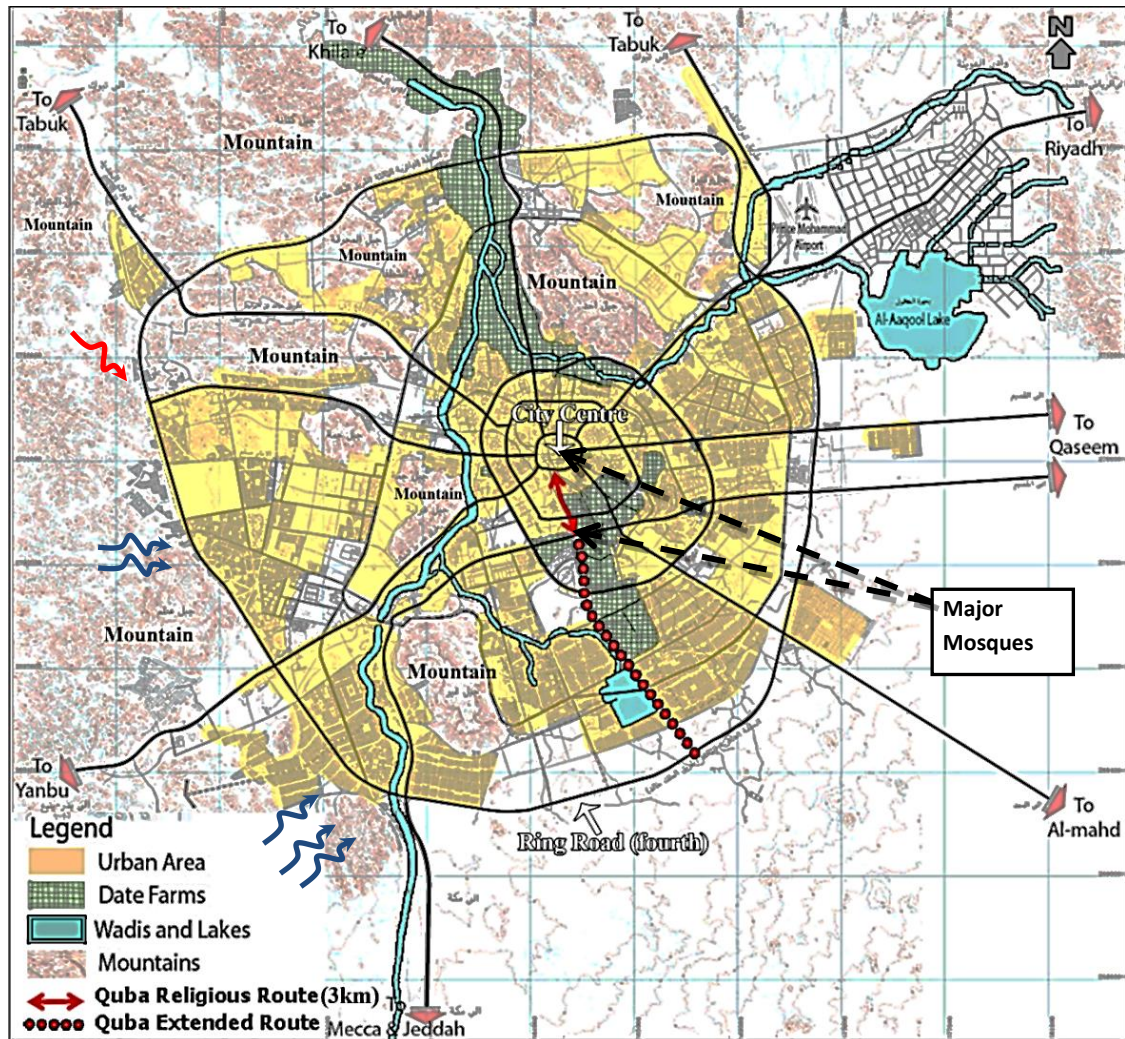


Fig. 2. 2: The Strategic Map of Madinah city highlighting the Quba Road, the surrounding natural features and the urban patterns of the city. It points at the two most visited mosques.

Many of the street patterns within Madinah are irregular at the neighbourhood level and differ greatly throughout the city. Madinah is served through four well-established major ring roads allowing accessibility to the city centre. There are also radial roads in and out of the city, but these are less well established and navigation can be problematic. All roads in the city are intended for vehicular traffic, so any pedestrianisation would be completely new to Madinah. This research studies one of the key radial routes (i.e. Quba road) from the southern barrier of the city centre into the South of Madinah (less than 3km) which is highlighted in Figure 2.2.

### 2.3. Official Plans for Extending the City Centre in Madinah

*“The city of Madinah has a clear hierarchy of streets with multiple well-defined connections to the Prophet’s Mosque and its Plaza. A series of past plans have effectively shaped the City’s built form and public realm. The future growth of the Prophet’s Mosque will necessitate change to the built form and the public realm, as the*

*growth will place new demands on building forms and their surrounding public spaces”* (MMM Group Limited et al., 2012d: 17).

Madinah municipality proposed new planning strategies for redevelopment of many areas in Madinah, including a multimodal network made up of metro lines, pedestrian walkways, and roads, such as Sunnah Path (i.e. used to be the Prophet’s walkway that links between his mosque and the Quba Mosque), serving as the primary pedestrian boulevard in the south (MMM Group Limited et al., 2012e). This network is parallel to the Quba Road, i.e. the current research case study area, with less than 200 metres of distance apart. The Madinah Municipality has proposed a new concept for pedestrianising several streets of Quba district (this includes Sunnah Path and Quba Road) (Figure 2.3). The Municipality has also proposed a new major route called the New Quba Road (located about 600m parallel with the western side of the existing Quba Road), with the aim to strengthen the link between the city centre and the southern edge of the city, which will also reduce the traffic on the existing Quba Road and encourage more pedestrians flow (MMM Group Limited et al., 2012c).

A ‘U’ shape road has also been proposed in the governmental plans, which forms a ring road linked with the western part of the second existing ring road, which will form the new boundary of the enlarged city centre within 30 years (MMM Group Limited et al., 2012c), as illustrated in Figures 2.3.



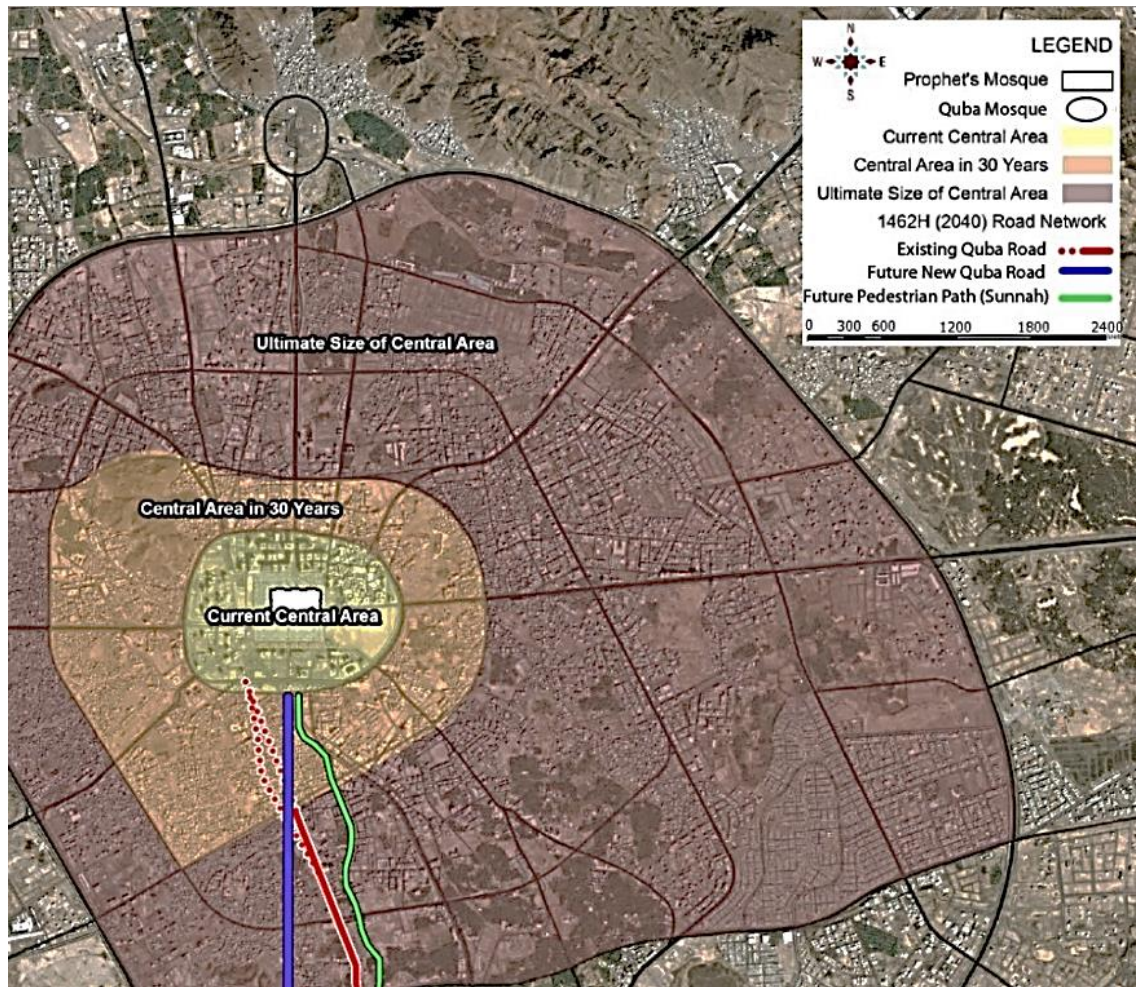


Fig. 2. 3: The locations of the existing Quba Road and the future New Quba Road, and the future major pedestrian road with no car access. It also shows the extended boundary of the city centre in 30 years. Source: adapted from MMM Group Limited et al. (2012d).

In addition, major investment projects are planned to take place in the extended area of the city centre, particularly targeting private sector investments, including the half length of Quba Road that falls within the enlargement barrier of the central area (MMM Group Limited et al., 2012g). According to the local planning and regulation documents, most of the investment locations in Madinah are well planned but there is a need to strengthen the economic investments within the new central area (MMM Group Limited et al., 2012e).

#### 2.4. Local Planning and Regulations for Quba District

The development concept mentioned in the above section, strengthens the purpose for conducting the current research, as it suggests a major redevelopment plan of Quba Road and the surrounding neighbourhoods, and the need for planned pedestrian spaces and networks; but so far there are no studies that have been presented on pedestrian thermal comfort enhancement methods in Madinah.



There are no series of policies from national planning through regional that can control the local planning and regulations, but rather planners are guided by masterplans. The recent plan for urban development of Madinah is a valuable opportunity for this study on the assessment of pedestrians thermal comfort conditions, and thus the aim to find out ways to mitigate the urban heat stress in outdoor urban canyons (streets).

The local planning and regulations limit the maximum building height to 27m, while the urban footprints will be leased to private investors to strengthen the economic benefit in the city (MMM Group Limited et al., 2012g). Thus, the current research will consider these constraints of the existing planned area (i.e. buildings and street footprints and maximum buildings height), as the construction permission in Madinah is usually approved based on the local planning and regulations that is drawn up by most updated masterplan.

## **2.5. Initial Analysis of Quba Road**

Quba Road is the targeted axis in the case study of the current research with the neighbourhood grid rotated approximately  $22.5^\circ$  counter-clockwise from the cardinal directions. The orientation of the Quba Road is one of the best in terms of how the road direction intersects with the sun path. For example, a numerical study was conducted in a hot and dry climate of Algeria on evaluating the effects of an urban street height-to-width ratio ( $H/W = 0.5, 1, 2, \text{ and } 4$ ; with a constant street width of 8m and symmetrical buildings heights) and orientations with solar radiation (E-W, N-S, NE-SW and NW-SE) on outdoor thermal comfort (Ali-Toudert and Mayer, 2006). It was found that thermal sensation at street level depends strongly on urban street orientation, building heights and street width. N-S streets showed a trend to be slightly cooler than E-W streets, particularly as the aspect ratio increases (i.e. by shading effect).

Quba Road is a significant and active link between the southern side of the first ring road (which embeds the prophet's mosque and the city centre), and the Quba mosque with the length of 2400 m from the southern part of the first ring road. In addition to these two most visited historic mosques in Madinah, another important historical religious site called Al-Jom'ah mosque is located in between with a distance of 720 metres away from Quba Mosque (Fig. 2.4). The area along the length between al-Jom'ah and Quba mosques is a low built-up area, with many vacant plots and palm tree farms in the surroundings. The part of this Road closer to the city centre has a

higher urban density, while the medium urban density area is located in the middle length of the road, as shown on the aerial map below.

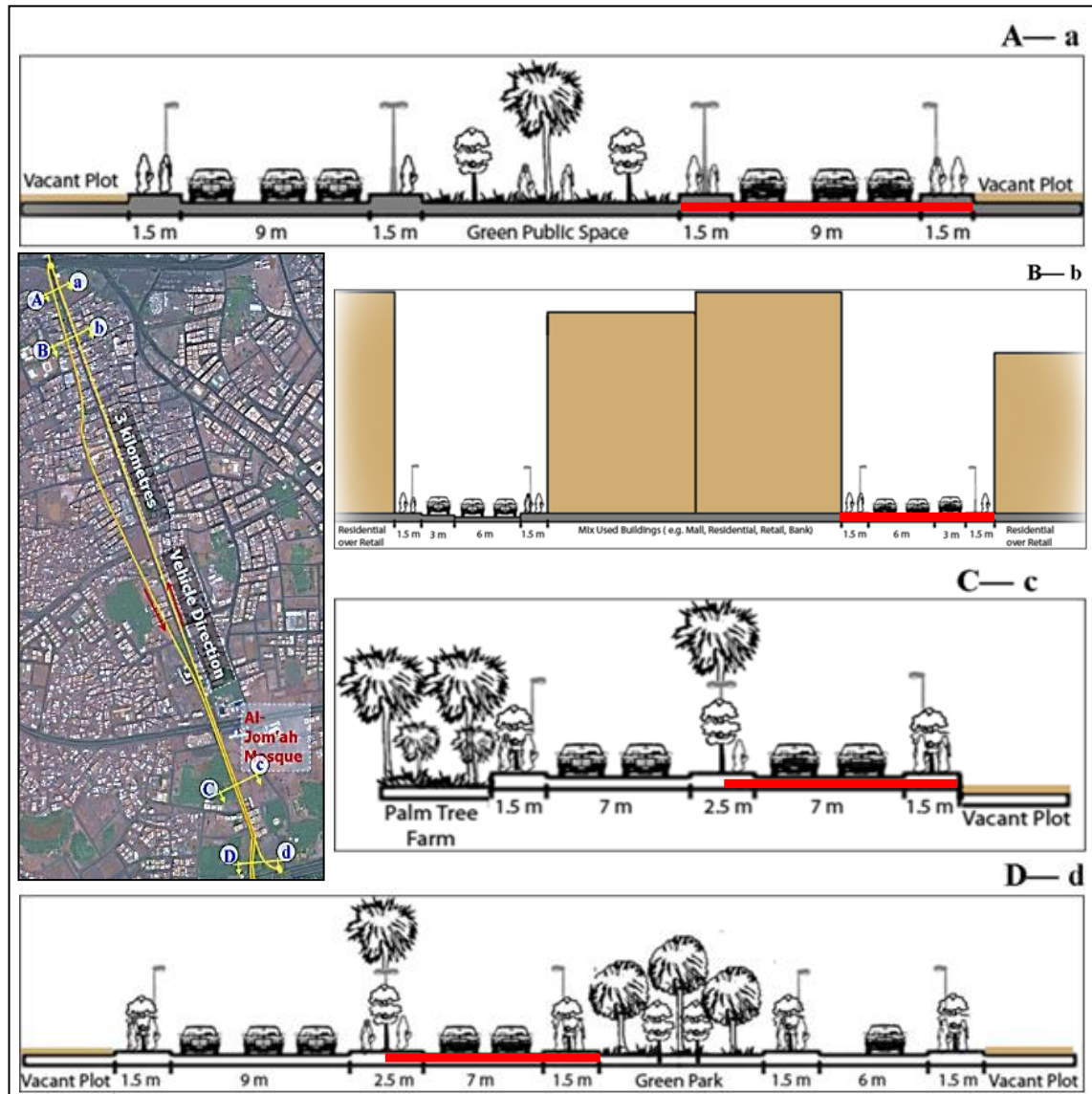


Fig. 2. 4: Cross-Sections of the Quba Road.

The Quba road is divided into two canyons (windward canyon, i.e. Tali'e Quba Road and leeward canyon, i.e. Nazil Quba Road) with buildings blocks in between, particularly the northern half of the road, while they join in the southern half with small green spaces in between, as illustrated in the cross-sections in Figure 2.4. The case study measurements were conducted in the leeward canyon, i.e. Nazil Quba Road (discussed in section 2.6). The canyon's width is 12m, with pedestrian paths on both sides of the canyon, but does not account for pedestrian comfort or safety, as some parts of these pavements are 0.5 metres high from the ground and some areas are not paved, while this canyon lacks trees and vegetation, which are important elements for shading and evaporative cooling.



Figure 2.5 demonstrates the conceptual diagram of the existing urban fabric in relation to land uses along Quba Road, their strengths and weaknesses, and their opportunities for redevelopment. The conceptual diagram shows that there are high percentages of undeveloped areas (low density) located around the southern part of the road, then the middle length of the road is characterised with medium density (Setaih, 2010). This includes vacant plots and farm lands. Most residential buildings and residential over retails are located in highly dense areas near the city centre.

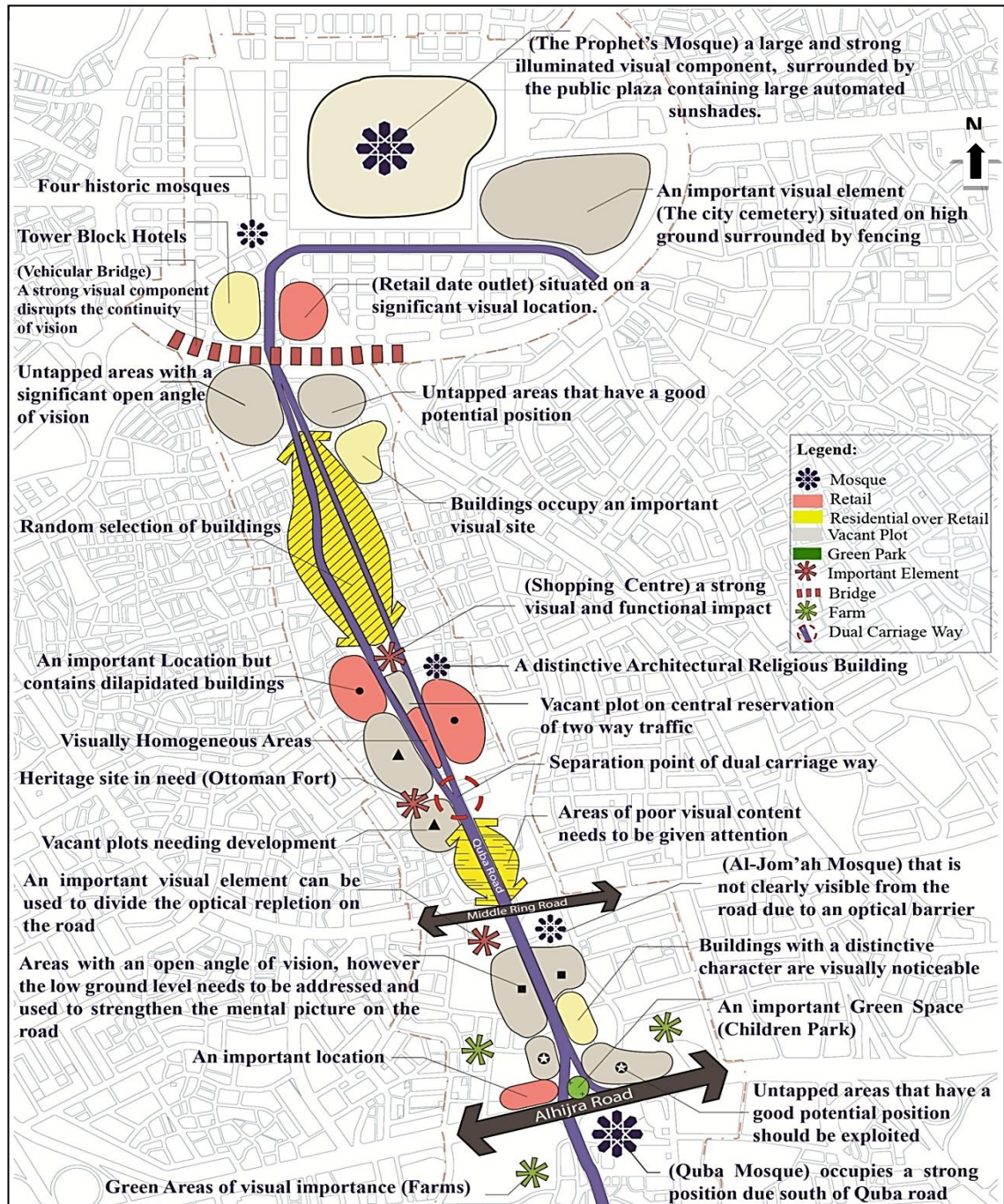


Fig. 2. 5: Analysis of the land use, strengths and weaknesses of Quba Road, and areas with urban development opportunity. Source: Setaih (2010).

The absence of vegetation along the Quba Road remains an issue for pedestrians comfort, as vegetation can protect people from hot sun radiation by providing shades and evaporative coolness. However, this research will focus only on optimising urban geometry, excluding the study of vegetation due to the time constraint. The northern part of the Quba Road accommodates a strong commercial catchment area that can encourage visitors to use pedestrian spaces, particularly along the Nazil Quba Road (i.e. the leeward canyon). This area has a strong advantage in attracting even more visitors due to its location close to the city centre, and its position as a desirable link between the Prophet's Mosque (in the city centre) and Quba Mosque (in the south).

The height of buildings along this Road varies from 1 storey to 9 storeys, with an average of 7 storeys. The level of maintenance of buildings along Quba Road is mostly medium condition, with some places of poor and others of very good level of maintenance. The materials used in the area are concrete for buildings and pavements, and asphalt on the road. The traditional wooden windows called 'Roshan' are rarely found in the area, especially since the last 10 years, which used to be utilised for aesthetics and privacy purpose, as well as for protection from solar radiation while allowing proper ventilation in the building. However, Quba road will experience a redevelopment strategy due to the poor urban fabric of irregular building blocks (MMM Group Limited et al., 2012d).

Although pedestrians in the existing Quba Road are not given sufficient space and priority (e.g. some areas are not paved, no seating furniture, lack of trees, etc.), many pedestrians and vehicles travel through this street to and from the Haram (Prophet's Mosque). Most of them occupy the street after the five prayer times for a very short period at the daytime and longer periods at nights and evenings when the sun cools down. The number of existing pedestrians that cross the 1<sup>st</sup> Ring Road (i.e. the boundary of the city centre) during the peak hour has reached 15000 people immediately following the weekly Friday Noon Prayer on the 30<sup>th</sup> of October 2009, i.e. corresponding to early weeks of the Hajj pilgrimage season MMM Group Limited et al., 2012c). The Quba Road is surrounded by many vacant plots, which has a great opportunity for the (re)development. The lack of community nodes and insufficient spaces for pedestrian along Quba Road, and poor condition of the informal buildings in the district have led the Madinah Municipality to suggest redevelopment strategy of this route and the surrounding neighbourhoods (MMM Group Limited et al., 2012a).

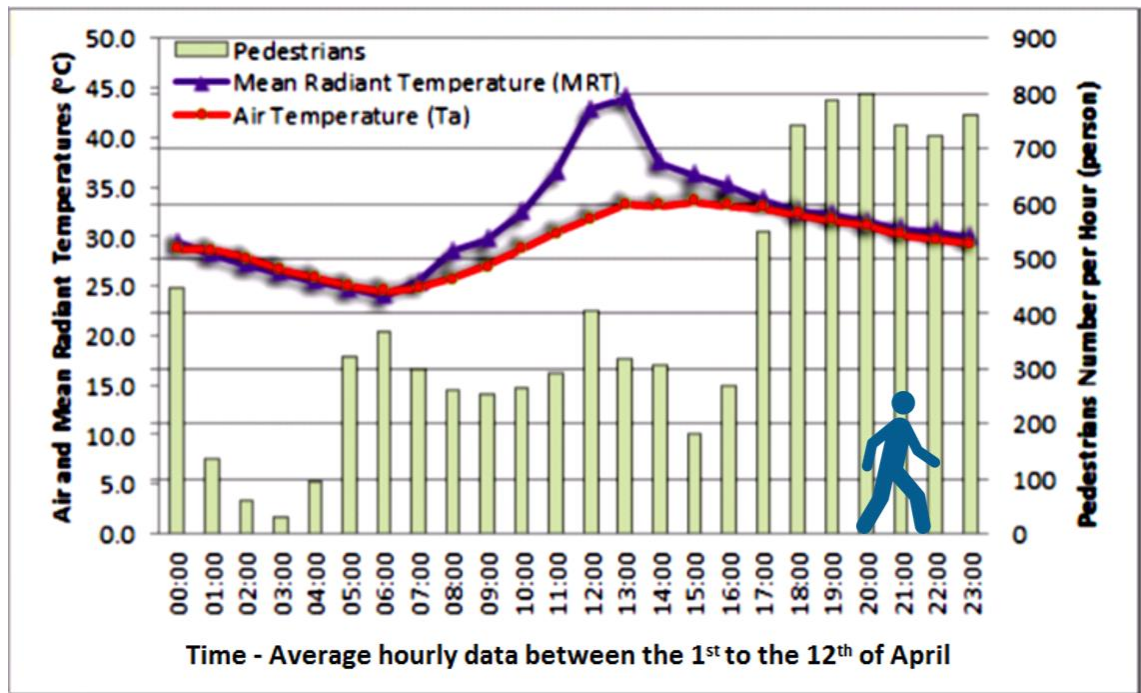


Fig. 2. 6: Number of pedestrians during the 24 hours compared with the air & mean radiant temperatures. The data obtained in the high urban density area (Case 1) in spring were, based on average hourly values for the monitoring duration (1<sup>st</sup> to the 12<sup>th</sup> of April). Source: Setaih et al. (2013a).

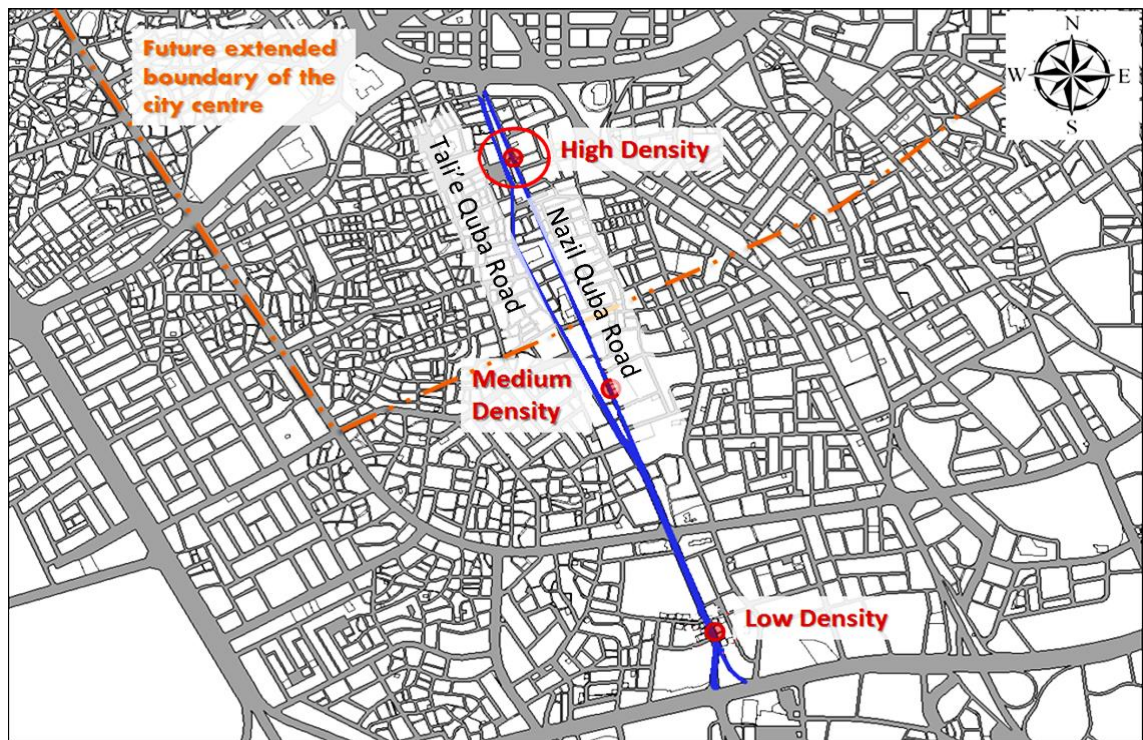
Figure 2.6 shows an initial field study of the pedestrian numbers and microclimatic parameters in the high urban density area of the Quba Road, near the city centre (Setaih et al., 2013a). The data for the microclimate and pedestrian numbers were obtained between the 1<sup>st</sup> to the 12<sup>th</sup> of April 2013, using a Kestrel 4400 Heat Stress Tracker (i.e. data logger) and an observational method, respectively. The study demonstrates a significant increase of pedestrians at 5:00-5:30 a.m. before the sun rises, at 12:00pm during the hot peak period, and after 17:00 hours just before the sun sets, which is as a result of walking to and from the nearby mosques to perform Dawn Prayer and Noon Prayer, as well as to spend more time outdoors during the absence of the sun.

However, a gradual decline in the number of the pedestrians in Quba Road during most of the daytimes is due to the increase in the heat stress levels outdoors. Consequently, the increase in the air temperature that reaches its maximum of 34°C in the midday with higher mean radiant temperature (MRT) value of 44°C, leads to more pedestrian and shoppers to prefer walking outdoors during the evening and night times rather than during hot sunny days. This is similar to a study by Abdel-Ghany et al. (2013), but for the summer period of Riyadh city, where extreme heat stress is experienced with 10°C higher in summer during the peak hours than in spring.



## 2.6. Selection of the Case Study Areas

This study was conducted in Quba Road under the four climatic seasons in Madinah. The length of the Road is 2.4km, which links Quba Mosque at the southern end and the city centre at the northern end. Municipality plans show interest for implementing major roads that are mainly for pedestrians, linking the city centre with southern areas (MMM Group Limited et al., 2012d). The plans also indicate the need for enlargement of the city centre barrier which will extend until about half the length of the Quba Road, including the high urban density area (Case 1), as illustrated in Figure 2.7.



*Fig. 2. 7: Three case study areas selected based on different urban density levels. The case study of high urban density area falls within the future extended city centre.*

Figure 2.8 shows the three case study zones, selected based on different urban densities, including high urban density (Case 1), intermediate urban density (Case 2) and low urban density (Case 3) (also see section 5.4). These three major zoning areas were selected with the aim of exploring the existing urban pedestrian microclimate and thermal comfort conditions in Quba Road, through conducting field measurements (refer to the results in Chapter 6). The figure also demonstrates the selected locations of the field measurement points, representing open spaces between buildings.

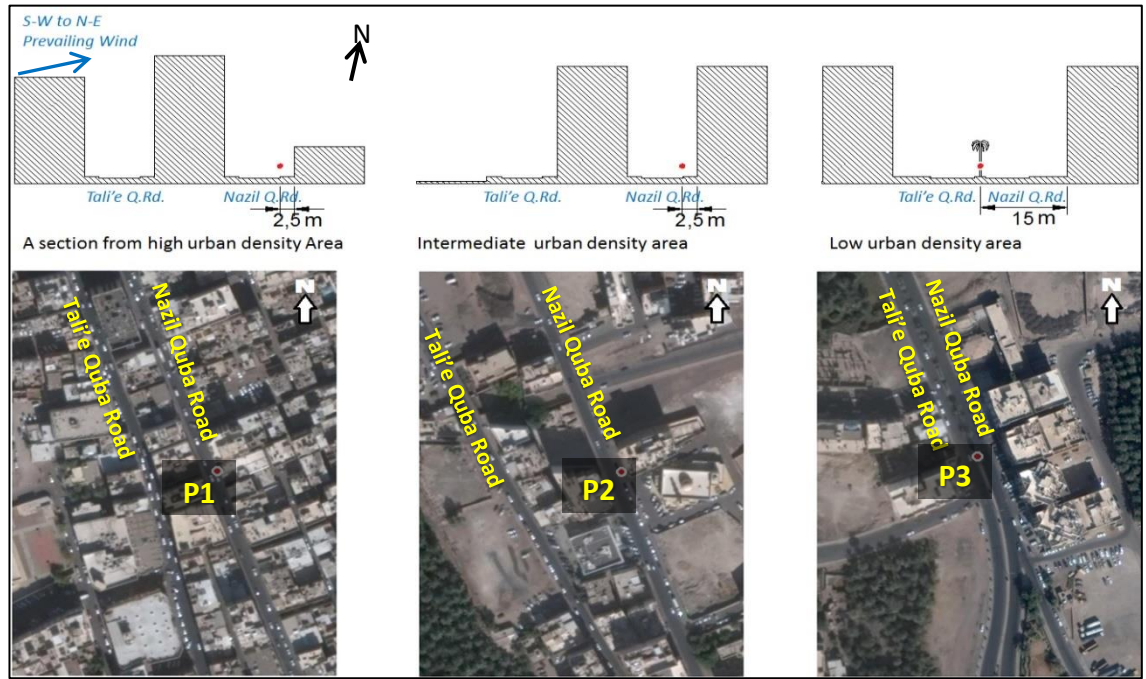


Fig. 2. 8: Field measurements (Points P1, P2, P3) locations for the case study of the three urban densities, located at a height of 2m above the ground (i.e. pedestrian height).

## 2.7. Climate of Madinah

The climate of Madinah is hot and arid, characterised by intense solar irradiance and extreme air temperatures during most of the year, with an average maximum yearly temperature of 36.9°C, and minimum of 22.7°C. The city experiences an average yearly relative humidity of 17.5%, as illustrated in Figure 2.9. The annual rainfall on average is scarce as Madinah is a subtropical desert city influenced by the Tropic of Cancer and has no major periods of humidity, due to the decline of air pressure in winters and the monsoon during summers (Al-Madinah Regional Municipality, 2011).

The wind speeds in Madinah are very low and calm with a yearly average value of 3.1m/s, an average lowest air speed of 2.5m/s recorded in winters and average maximum of 3.5m/s recorded in summer at the city's airport (Iowa State University of Science and Technology, 2015). Wind speed in Madinah is very low due to the small variation in wind pressure throughout the year (MMM Group Limited et al., 2012d). Figure 2.10 demonstrates change of wind directions that shifts from season to season, particularly from January to July, and average sea level pressure (Source Vincent, 2008, cited in MMM Group Limited et al., 2012b).

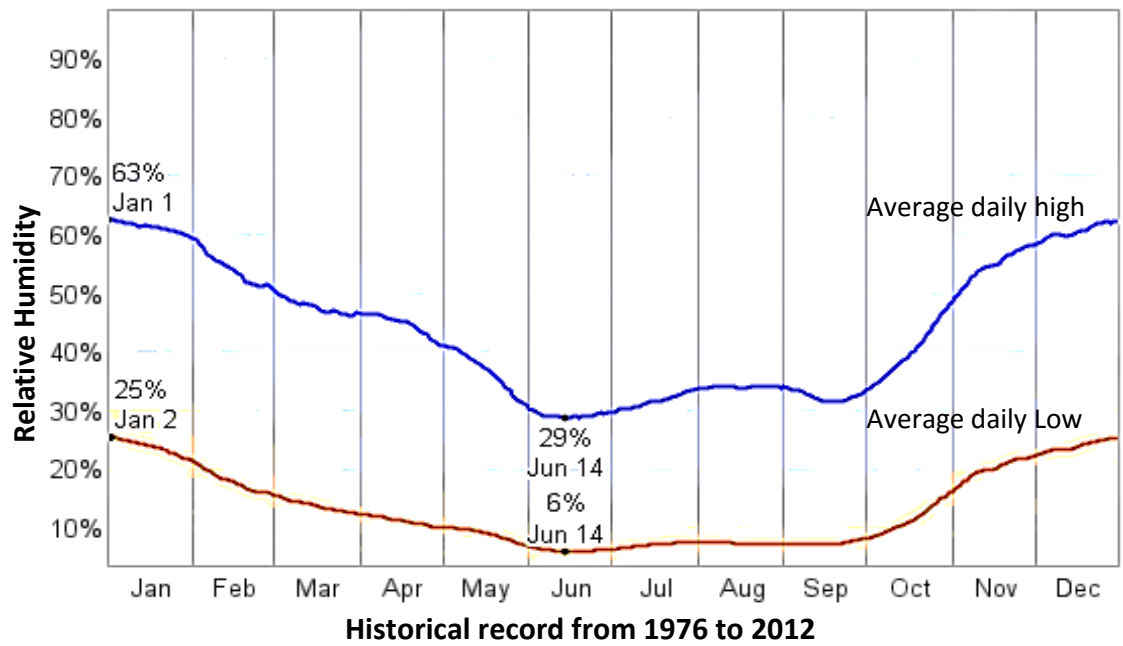


Fig. 2. 9: The weather readings in Madinah city over a 36-year period for average daily high and low relative humidity. Source: [www. weatherspark.com](http://www.weatherspark.com) (accessed on 10.09.2015).

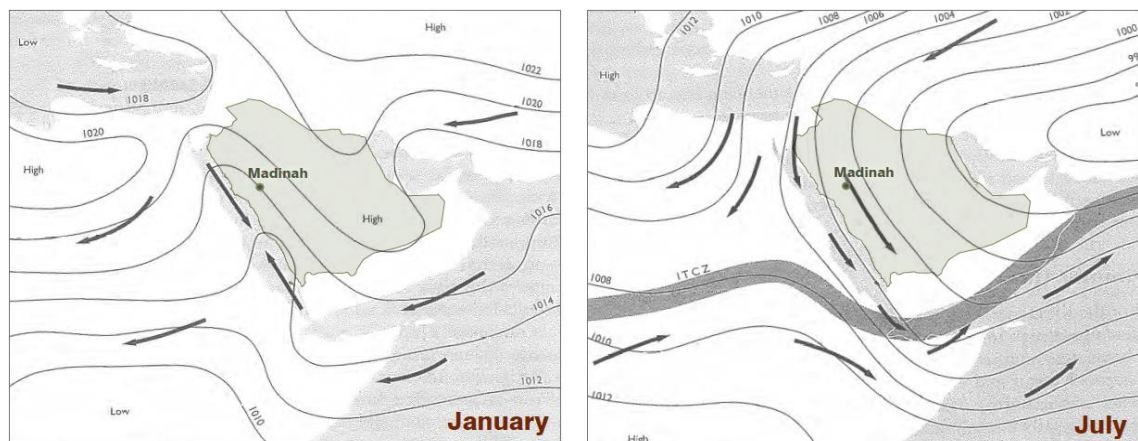


Fig. 2. 10: Changes of seasonal wind directions reaching the Arabian Peninsula, and average sea level pressure. Source: Vincent, 2008; cited in MMM Group Limited et al. (2012b).



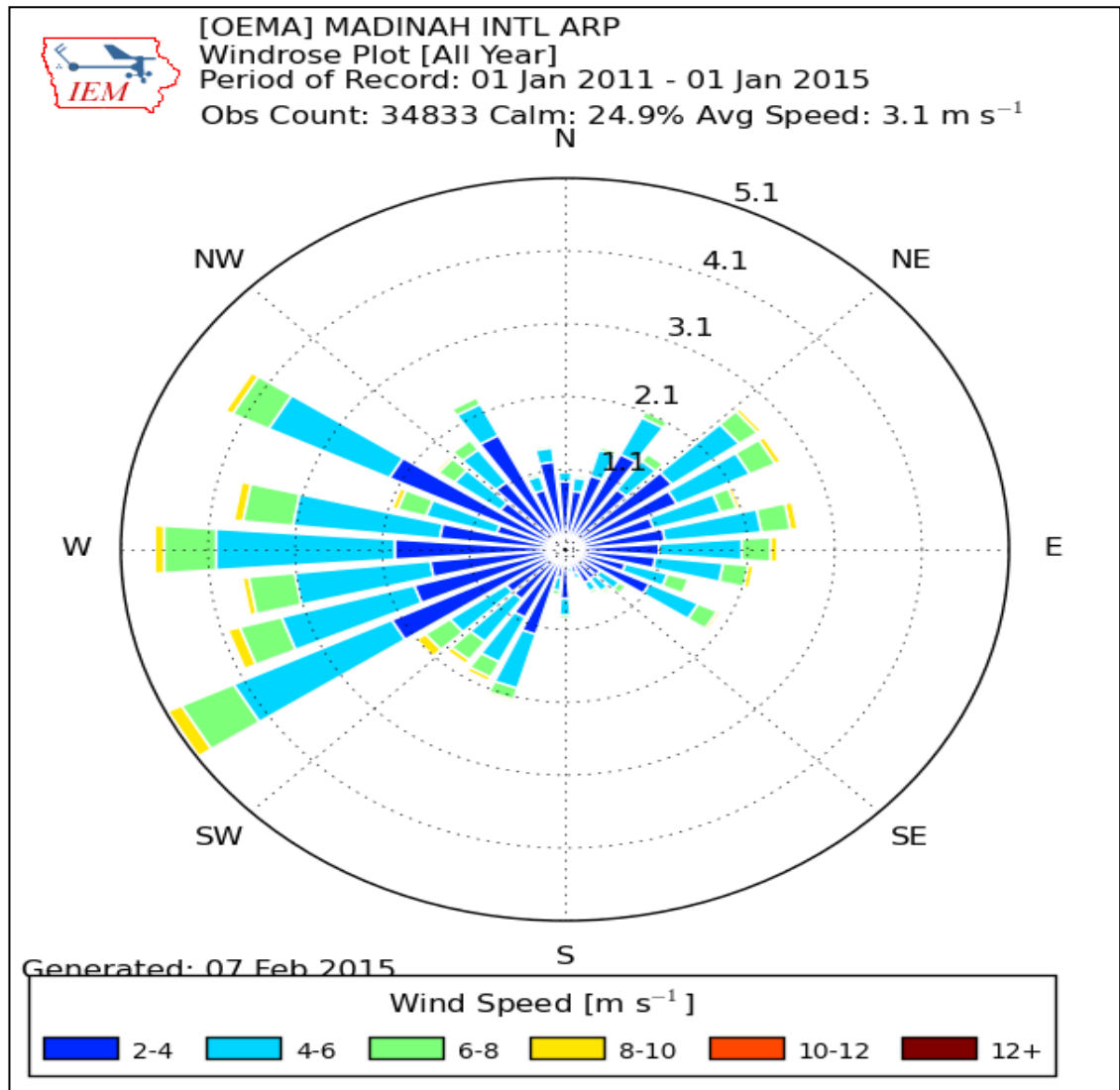


Fig. 2. 11: The figure shows three yearly prevailing wind directions: south-west, westerly, and north-west. Yearly average wind speed is around 3.1m/s. Source: Iowa (2015).

Figure 2.11 shows that there are three yearly prevailing wind directions in Madinah. The main prevailing wind is from the South-West direction, followed by less prevailing wind from the West direction, then the North-West direction, for roughly 6 to 10 months each year, starting from February (Weather Underground, 2010).

Figure 2.12 shows the monthly wind roses for Madinah. The month of April was chosen for the numerical investigation in the current research. The wind rose for April indicates that the undisturbed average daily wind speed in Madinah is about 3.2m/s from south westerly direction, with higher afternoon speed value of 4.7m/s (i.e. at 15:00 hours). The latter value will be considered in this study for the CFD simulation purpose (discussed in Chapter 7).

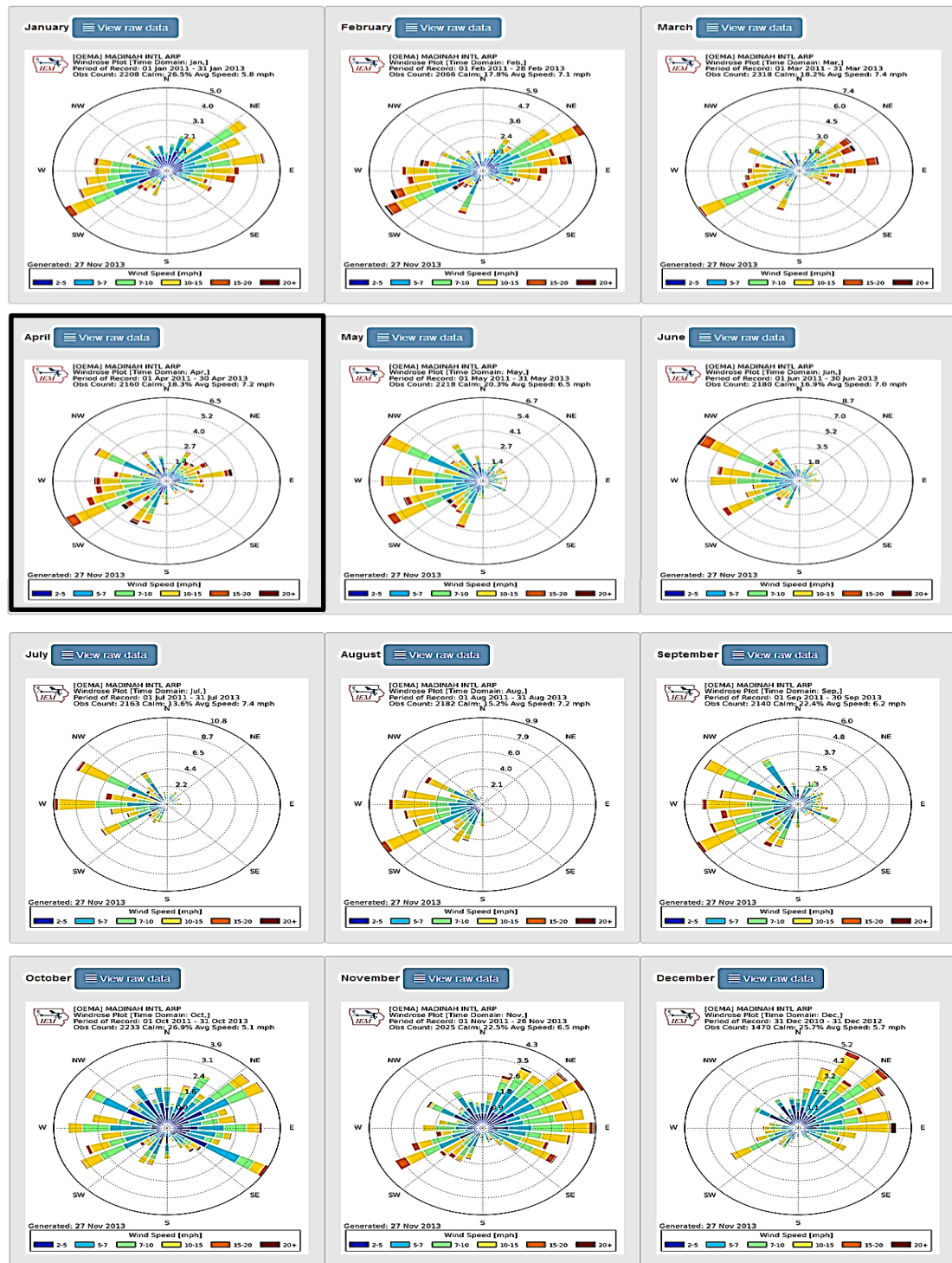


Fig. 2. 12: Wind roses showing the monthly prevailing wind speeds and directions. Source: Iowa State University of Science and Technology (accessed online in February, 2015).

As is typical for many arid zones, the climate of Madinah region is characterised by wide diurnal and seasonal thermal fluctuations, accompanied by very low daytime relative humidity and intense solar radiation. The average daily air temperature in Madinah varies with a range of 32.6°C – 45.8°C in August (summer), 22.4°C – 36.1°C in April (spring), and 23.6°C – 38.7°C in October (autumn), as shown in Figure 2.13

and Table 2.1. This research aims to find ways to enhance the thermal comfort level in Quba Road, during mid-seasons (spring and autumn), as they are positioned at the edge of the extremely hot summer season. Thus, it aims to extend the use of outdoor space by shifting the thermal conditions from a range of thermal discomfort into a range of critical thermal comfort as much as possible, passively without the introduction of any mechanical system for cooling (e.g. Erell et al., 2011; Oke, 1988; Pearlmutter et al., 2007). In winter, while minimum daily temperatures occasionally reach freezing and winds are strong, clear skies and abundant solar radiation prevail in the daytime.

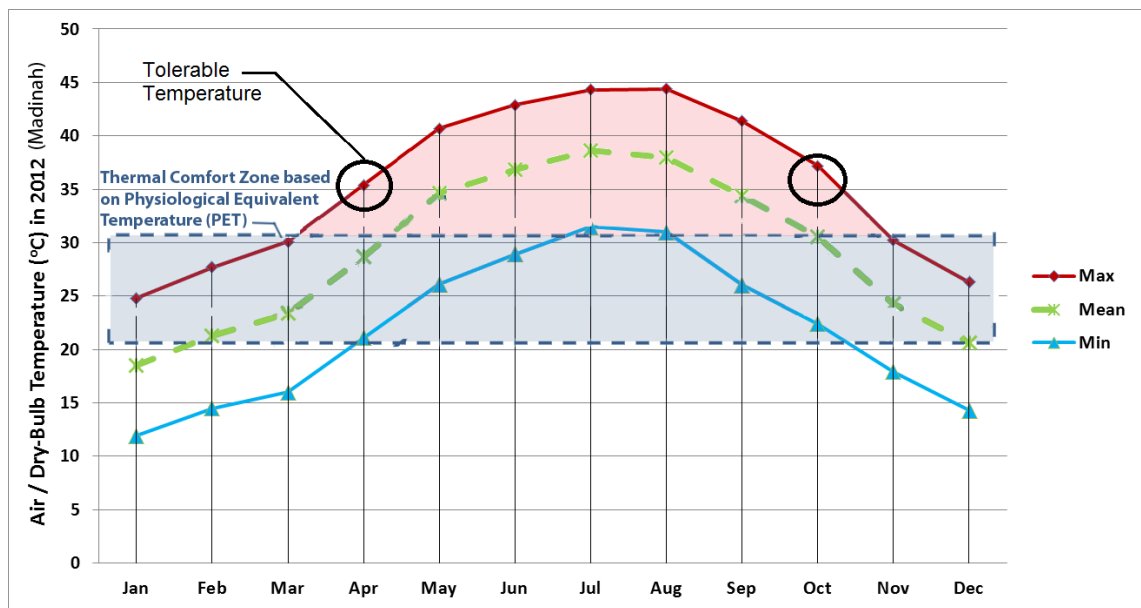


Fig. 2. 13: Air temperature based on Madinah Meteorological Centre (2012), showing months of April and October with a tolerable air temperature situated at the edges of a critical hot period, and highlighting the outdoor thermal comfort zone in hot arid climate (i.e. 21°C to 31.3°C) based on physiological equivalent temperature (PET) index proposed by Yahia and Johansson (2013a).

Table 2. 1: The weather readings in Madinah city in 2010, adapted from [www.tutiempo.net](http://www.tutiempo.net)

		Mean Temp (°C)	Max Temp (°C)	Minimum Temp (°C)	Mean Humidity (%)	Precipitation amount (mm)	Mean Visibility (km)	Mean Wind Speed (km/h)	Maximum Sustained wind speed (km/h)	Indicator for occurrence of Rain or Drizzle
Winter	Jan	20.6	28	13	27.7	1.02	9.7	7.9	20.1	1
	Feb	23.2	29.9	15.7	23.4	0	9.1	10.2	24.1	0
	Mar	25.9	33.1	17.7	19.2	20.83	8.8	10.8	24.3	2
Spring	Apr	29.5	36.1	22.4	22.6	58.67	9.4	12.2	25.8	3
	May	34.7	41.1	26.9	12.6	0	9	11	23.5	0
	Jun	37.8	44.1	30	8.9	0	9.6	9.9	23.3	0
Summer	Jul	38.1	44.4	30.9	15	20.32	9.2	11.8	26.8	1
	Aug	39.5	45.8	32.6	12.1	0	9.7	9.8	24.3	1
	Sep	36.4	43.3	28.5	11.4	0	10	8.3	21.8	0
Autumn	Oct	31.5	38.7	23.6	13.8	0	10.1	6.7	18.5	0
	Nov	25.1	31.9	17.8	17.5	0	10.1	9.9	21	0
	Dec	20.1	26.8	13	25.8	13.97	8.7	8.1	19.1	1
Average (year 2010)		30.2	36.9	22.68	17.5	9.57	9.45	9.71	22.71	0.75

Due to the City's location (at 39° 36' 6" N and 24° 28' 6" E) which lies in the Northern and Eastern hemisphere and the lacking of cloud cover, considerable solar radiation affects ground level conditions (Construction Group, 1972). The sun elevation ranges from a low angle of 42° at noon on December 21<sup>st</sup> (i.e. in winter) to a high angle of 84° at noon on June 21<sup>st</sup> (Sun Design, Undated). High temperatures have resulted in the widespread use of air conditioning, thus increased energy consumption and heat released to the city (MMM Group Limited et al. (2012d). The sunrise in Madinah occurs at about 6:30 a.m. and sunset is at about 6:30 p.m. Due to clear sky conditions, the city receives about 12 hours sunshine over most of the year. In the spring season, the peak air temperature reaches 33°C at the airport. Figure 2.14 illustrates the sun position in Madinah, highlighting its position at 15:00 hours in April 2013, representing the spring season, and showing the prevailing wind direction of South Westerly (i.e. the information used in this research for numerical modelling).

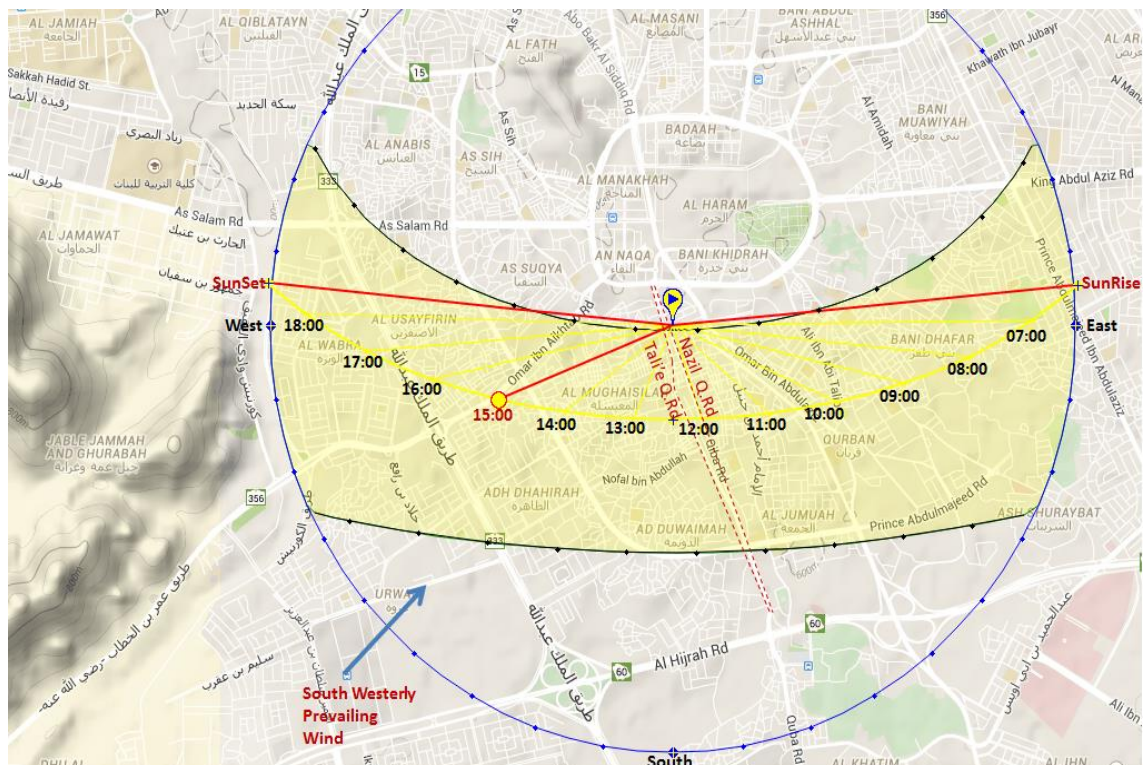


Fig. 2. 14: Sun position in Madinah at the simulation period (i.e. 1<sup>st</sup> of April 2013, representing spring season at 15:00). Prevailing wind direction is South Westerly. The Nazil and Tali'e Quba Roads are also highlighted.. Source: calculated using the following website <http://www.sunearthtools.com/>

## 2.8. Summary

This chapter discussed the characteristics of Madinah, including its geographical, economic and religious importance. The climate in Madinah indicated that the major issue of the city is the low wind speed and extreme hot dry climate. The new redevelopment plans of Madinah have been discussed, highlighting the potential for conducting this research on Quba Road. The local planning and regulations limit the maximum building heights to 27m, while the urban footprints will be remained and leased to private investors to strengthen the economic benefit in the city. The Quba Road has been highlighted as one of the areas falls within the redevelopment plan and future major investment projects.. Three locations were selected for the investigations based on their urban density, which are: the high urban density area (Case 1), intermediate urban density area (Case 2) and low urban density area (Case 3). More information about these locations will be found in the Methodology in Chapter 5 and the Field Results in Chapter 6. The initial study of Quba Road has reflected the opportunity of conducting the current study due to availability of many vacant plots, while the area that has higher urban density level falls within the official redevelopment plans.



# CHAPTER 3: Literature Review on Outdoor Pedestrian Thermal Comfort

## **Chapter Structure**

- 3.1. Introduction
- 3.2. Background on Urban Thermal Discomfort
- 3.3. Thermal Comfort of Humans
- 3.4. Indoor and Outdoor Differences in Thermal Comfort Levels
- 3.5. Outdoor Thermal Comfort Indices
- 3.6. Thermal Comfort Interaction Factors
- 3.7. Field Studies on Outdoor Thermal Comfort
- 3.8. Assessment Approaches of Outdoor Pedestrian Thermal Comfort
- 3.9. Summary

# Chapter 3:

## Literature Review on Outdoor Pedestrian Thermal Comfort

---

### 3.1. Introduction

This chapter presents a literature review pertinent to studies on outdoor urban pedestrian microclimate and thermal comfort. It focuses on the importance of designing urban pedestrian microclimates with thermal comfort enhancement approach. It discusses previous field studies on outdoor thermal comfort and the relevant thermal comfort criteria that are applicable for hot arid climates. The knowledge gaps based on the literature review are also identified and summarised at the end of this chapter.

### 3.2. Background on Urban Thermal Discomfort

One of the major issues facing many outdoor pedestrian spaces in hot arid regions of Saudi Arabia, including Madinah city, is the absence of thermal comfort (Eben Saleh, 1997). Madinah is located in a transitional zone where monsoon and Mediterranean climatic types are experienced; thus it is extremely hot and arid during summer (temperature ranges between 36-45°C), and it experiences low temperatures with very slight rainfall throughout winter (temperature ranges between 15-20°C) (MMM Group Limited et al., 2012d). This issue of thermal discomfort is further aggravated by the urbanisation process, which involves a decline in vegetation in the urban areas, absorption of solar energy gained by paved concrete and asphalt surfaces, use of dark materials with low reflectivity or albedo level, anthropogenic heat release from man-made constructions and air-conditioners (Mochida and Lun, 2006; Chalfoun, 2001).

Moreover, due to the modernisation of the Saudi community over the last six decades, with the discovery of oil and improvement in economic conditions, the design of traditional urban neighbourhoods has changed from organic and pedestrian-oriented to geometric and vehicle-oriented, which has greatly influenced the use of outdoor spaces (Eben Saleh, 1997). This issue, for example, has led people to spend less time in outdoor spaces during day-time, and therefore spend most of their time in air conditioned buildings and vehicles (Eben Saleh, 1997). Thus, with the increase in population the amount of urban energy consumption for indoors is vast and becoming

burdensome, accompanying with the consequence of urban thermal environment being getting worse (Zhang et al., 2009). In addition, *“due to the improper and unreasonable planning of city structure, materials used in the city construction and building settlements and arrangements, thermal environment of cities has been getting worse, e.g. air pollution and heat island of cities has been significantly existed”* (Zhang et al., 2009:36). This urban heat accumulation would aggravate the UHI (Urban Heat Island) effects that can lead to increased usage of air conditioning for internal spaces, and indirectly results in people preferring to stay in comfortable indoor environments and leaving outdoor spaces under-utilised, especially in hot arid areas (Givoni, 1998; Chung and Choo, 2011).

Increasing the albedo level (i.e. reflectivity property) of materials, planting trees, vegetation, reducing released anthropogenic heat, and designing efficient urban street canyons to facilitate air movement are common techniques to mitigate the heat stress and enhance outdoor thermal comfort. However, the implementation of these techniques in urban design with thermal comfort is not always practical or economical. Furthermore, the consequences of these strategies greatly differ according to characteristics and climate of the city. In best practise for planning an urban route with microclimate awareness, planners and urban designers should refer to these mitigation strategies as passive technologies due to the fact that further control of them is either difficult after their implementation or very expensive (Ahranjani, 2010). For example, urban street orientation with prevailing wind direction is an effective strategy against the urban heat stress, but it could inversely elevate the sand storm level in some places. In contrast, the orientation of urban streets perpendicular to wind direction can significantly reduce airflow rate and consequently the levels of pedestrian comfort. Another effective strategy against urban heat stress is designing a street aspect ratio ( $H/W$ , ratio of average building heights to a street width) with high rise buildings (Priyadarsini et al., 2008). This can increase the air ventilation and reduce air temperature, but it could inversely cause wind discomfort or danger in certain locations. However, in low wind speed environments, high rise buildings can be preferable to enhance wind velocity magnitudes in urban areas.

Vanos et al. (2010) indicated that outdoor thermal comfort (or discomfort) in urban open spaces is a complex matter and has become an increasingly debated topic. However, empirical data from in-situ measurements on urban microclimate and the subjective human perception level in the outdoor context are still needed, as this would



provide a broader thermal comfort perspective in urban spaces (Nikolopoulou and Lykoudis, 2006). However, there is very little on-site research that has been conducted during all the four main climatic seasons in hot arid areas in the context of thermal comfort.

### **3.3. Thermal Comfort of Humans**

Human thermal comfort is a subjective state of mind from the psychological perspective that expresses satisfaction with the surrounding thermal microclimates (ASHRAE, 2009; 1985). Thermal comfort depends mainly on the heat exchange between the human body and the surrounding thermal environments by convection, conduction, radiation and evaporation. According to Bouyer et al. (2007) and Szokolay (2008), convective mode of heat transfer and the exchange of dry and humid air can be influenced by air temperature ( $^{\circ}\text{C}$ ). The radiation mode of heat exchange can be influenced by mean radiant temperature (MRT) ( $^{\circ}\text{C}$ ). The heat convection and latent exchange can be influenced by air velocity (m/s). The evaporative mode of heat exchange can be influenced by relative humidity (%).

However, it is not only these microclimatic parameters that can influence heat exchange but also personal behavioural factors, including clothing insulation ratio (clo) and metabolic heat (met) generated from the body activity level (Pickup and de Dear, 1999; Bouyer et al., 2007; Auliciems and Szokolay, 2007). These microclimatic and personal factors (also discussed in section 3.6) are convincing measurable relationships between thermal comfort conditions and the surrounding urban microclimates that must be addressed when calculating conditions for the evaluation of thermal comfort (Givoni, 2010; Ali-Toudert and Mayer, 2006; Nicol et al., 2012; Gaitani et al., 2007; Nikolopoulou and Lykoudis, 2007; CIBSE, 2006a; HSE, 2012; Aihua et al., 2011; Prek, 2006; Leduc et al., 2006; etc.).

### **3.4. Indoor and Outdoor Differences in Thermal Comfort Levels**

According to Murakami (2006), calculating the value of a human thermal comfort index is a key process not only for evaluating human comfort conditions but also for designing urban pedestrian streets. Most of the human thermal comfort indices require inputs of air temperature, mean radiant temperature (MRT), relative humidity, wind speed, human activity level and clothing insulation ratio levels, in urban open

spaces (Nicol et al., 2012). However, the indices for calculating the thermal comfort conditions can differ for the indoor and outdoor environments.

Indoor condition is often defined as “*the collective whole of all the physical properties in a room which influence a person via his heat loss and respiration*” (Fanger, 1970:13). Most of the recent indices for predicting thermal comfort are based on redevelopment of the PMV (Predictive Mean Vote) equation, which was proposed by Fanger (1970). The PMV index is based on human heat balance, and includes all the six key variables influencing thermal comfort conditions (mentioned above). The PMV index predicts the mean response of a large group of people on the ASHRAE 7-point thermal sensation scale. Although PMV index has become the most commonly used comfort index in the field of human thermal comfort, it is prescribed for indoor air conditioned circumstances. Potter and de Dear (2000) have investigated several outdoor scenarios experimentally using the indoor PMV (Predicted Mean Vote) model. However, they found that a PMV value of 27°C was observed in outdoor spaces, while it should have had a predicted thermal neutrality value at 24.1°C. Thus, PMV is not suitable for the prediction of outdoor thermal comfort conditions, due to the variable thermal environment under outdoor complex conditions (Zhang et al., 2007; Humphreys et al., 2007; Wong and Khoo, 2003).

Similar results were found from extensive structural interviews and field measurements of five public places in central Taiwan (with 8077 sets of data), which were conducted from the cold humid winter of 2004 through the hot humid summer of 2005. It was found that occupants of outdoor and semi-outdoor environments were more tolerant regarding thermal comfort than occupants of naturally ventilated indoor environments (Hwang and Lin, 2007). The thermal sensation conditions were obtained by SET\* (standard effective temperature) index based on the thermal sensation vote and thermal preference vote of the occupants. However, this research was considered in humid areas and not under hot arid climatic regions.

Moreover, findings of a study on different aspects of assessing indoor and outdoor thermal comfort asserted that different approaches are necessary for evaluating thermal comfort of outdoors than the commonly used indoor thresholds (Höppe, 2002). Furthermore, in an assessment of the bioclimatic comfort in an outdoor public space under a warm dry region, the results of a PET comfort index (i.e. physiologically equivalent temperature index) showed that thermal comfort under outdoor conditions can be maintained with temperatures well above the standard values defined for indoor

conditions (Oliveira and Andrade, 2007). Thus, it can be concluded that indoor thermal comfort indices are not applicable to the outdoor situations (Potter and de Dear, 2000). However, application of an outdoor thermal comfort index may differ from one climate to another climatic condition. Thus, careful selection of an appropriate thermal comfort index should be considered, particularly for hot arid regions to achieve the current research initial objective (i.e. assessing thermal comfort conditions in Madinah).

Höppe (2002) defined three approaches for the differences between outdoor and indoor thermal comfort, which are: a psychological approach, a thermos-physiological approach, and an approach that is based on the heat balance of the human body. Psychologically, the difference between indoor and outdoor thermal comfort is related to the subject's expectation. In outdoor environmental conditions, people can tolerate a larger variation than the indoor spaces, which is as a result of possibilities for adaptive behaviour in outdoors (Emmanuel, 2005). Potter and de Dear (2000) and Spagnolo and de Dear (2003a) indicate that due to different expectation of climatic conditions between indoors and outdoors, the acceptable outdoor temperature range should be wider than the indoor context. Therefore, Nikolopoulou et al. (2001) found in their study on understanding the human parameter that people (397 people out of 767 interviewed) did not mind warmer than usual conditions in outdoor urban spaces. However, their research was conducted in a cold region, during hot summer as well as mild spring and cold winter, and the time of exposure to the specific environmental conditions was short, since the study concerned with people choosing to sit in resting places. It could therefore be speculated that in warmer regions, the situation would be reversed and fewer people would be found outdoors when temperatures would be higher than average (Nikolopoulou et al., 2001).

Secondly, the thermo-physiological differences that diverge between outdoor and indoor thermal exposure are clothing insulation ratio, human activity levels, the exposure time ranges (Höppe, 2002). During warm conditions, people tend to wear lighter clothing and do light activities, while in cold conditions they tend to wear winter clothing and do activities that increase metabolic heat production in their body (Nicol et al., 2012). According to Emmanuel (2005) usually exposure to indoor environments can last hours, while outdoor exposure times are in the ranges of minutes. It has been suggested that the period for the maximum acceptable walking distance of 1600m under the shade in a hot arid region is 20 minutes (Setaih, 2010).

The third aspect is the heat balance differences between outdoor and indoor thermal comfort. Indoor comfort indices such as PMV are based on assumptions of thermal steady-state between subject and thermal environment. Thus, Höppe (2002) and Emmanuel (2005), argue that in actual conditions, steady comfort model cannot provide realistic predictions under outdoor conditions, thus thermal steady state is never reached even when people spend some hours outdoors. Thus, these three aspects of thermal comfort conclude that outdoor thermal comfort is distinguished from the indoor thermal exposure. Therefore, the thermal comfort indices that are purely based on heat balance would not be suitable to predict outdoor thermal comfort conditions in this current study.

Alternatively, depending on the six key factors in thermal comfort (mentioned earlier), several researchers have modified the energy balance based models for indoors with the attempt to develop useful models that can estimate human thermal comfort conditions for outdoor environments as discussed in the following section.

### **3.5. Outdoor Thermal Comfort Indices**

This section discusses the outdoor thermal indices that have been used in hot climate studies. Several integrative thermal indices derived from the human energy balance, e.g., PET (physiologically equivalent temperature) index was developed by Höppe (1999 and 2002); OUT\_SET\* (outdoor standard effective temperature) index was proposed by Pickup and de Dear (1999); and UTCI (Universal Thermal Climate Index) developed by the COST Action 730 (2009). According to Wei (2014), the obvious need for a thermal comfort model suitable for outdoor applications has prompted the International Society of Biometeorology (ISB) and the World Meteorological Organization (WMO) to form a specialist Working Commission to develop a Universal Thermal Climatic Index (UTCI). The UTCI index is a thermal perception scale developed to predict thermal comfort conditions under different climates. UTCI is based on an equivalent temperature for a given combination of air temperature, radiation, relative humidity and wind speed (McGregor, 2012). Błażejczyk et al. (2010) reported that the associated evaluation scale for the UTCI was based on simulated physiological responses and includes 10 categories that range from: extreme heat stress, very strong heat stress, strong heat stress, moderate heat stress, no thermal stress, slight cold stress, moderate cold stress, strong cold stress, very strong cold stress, and extreme cold stress. However, since the UTCI is newly developed, relatively few corrections have been conducted (e.g. Bröde et al., 2012). Thus, larger samples may be

required in order to calibrate the UTCI in the future. Moreover, calculating the UTCI can be time consuming as it requires expert knowledge to operate with the complex simulation software (WEI, 2014). Besides, the predictive ability of UTCI is also needed to be calibrated in hot arid climates.

Pickup and de Dear (1999) proposed Outdoor Standard Effective Temperature index (OUT\_SET\*), which is adapted from new Standard Effective Temperature (SET\*) that was proposed by Gagge et al. (1986). In 1967, Gagge presented Standard Effective Temperature (SET\*) which is defined as “*the temperature of an imaginary enclosure at 50% RH [relative humidity] in which a sedentary human occupant, dressed in standard clothing [0.09m<sup>2</sup>K/W or 0.6clo] in still air, would lose the same total heat by sensible and insensible heat transfer as he would in the actual environment*” (Gagge, 1981:87). In the outdoor version (OUT\_SET\*), the actual mean radiant temperature is calculated using a human thermoregulatory model (e.g. Spagnolo and de Dear, 2003a&b; Emmanuel, 2005). Spagnolo and de Dear (2003a) found that the thermal neutrality in terms of the thermal comfort index OUT\_SET\* of 26.2°C was significantly higher than the indoor SET\* counterpart of 24.0°C. Nevertheless, according to Johansson et al. (2014) OUT\_SET\* index is less widely used in comparison with PET index.

PET (Physiological Equivalent Temperature) index, which is an up-to-date thermal index, has been widely used for outdoor case studies of thermal comfort (e.g. Mayer and Höppe, 1987; Bouyer et al., 2007; Thorsson et al., 2007; Alexandri and Jones, 2008; Setaih et al., 2013a; Abdel-Ghany et al., 2013). PET index is based on the Munich Energy-balance Model for Individual (MEMI), which was developed and defined by Höppe (1999) to compare the actual outdoor conditions with the indoor environmental conditions in order to assess the outdoor thermal comfort in terms of indoor standards. PET index (expressed in °C) is defined as the Physiological Equivalent Temperature at any given place (outdoors or indoors) and is equivalent to the air temperature at which, in a typical indoor situation (with no wind and solar radiation), the heat balance of the human body is maintained with core and skin temperatures equal to those under the complex outdoor conditions to be assessed (Höppe, 1999). In other words, PET was designed in a physiologically relevant way to model the thermal conditions of the human body in any given environment. For example, PET value may be more than 20 K higher than air temperature on hot summer days with direct solar irradiation, while it can be up to 15 K lower on a windy day in winter. Thus, it takes into the account of wind and solar radiation values which are the

two most important thermal comfort interaction factors. Thus, this may suggest that PET index can be a useful tool for the current case study of outdoor thermal comfort.

The PET index has been utilised in hot arid climate studies (e.g. Yahia and Johansson, 2013a&b; Ali-Toudert et al., 2005; Ali-Toudert and Mayer, 2006; Mahmoud, 2011; Abdel-Ghany, 2013). According to Matzarakis and Mayer (1996), the PET index comprises of 9 bands, including very hot (extreme heat stress); hot (strong heat stress); warm (moderate heat stress); slightly warm (slight heat stress); neutral or thermally comfortable (no heat stress); slightly cool (slight cool stress); cool (moderate cool stress); cold (strong cold stress) and very cold (extreme cold stress). A PET value range of 18°C to 23°C is characterised as thermally comfortable outdoor environmental conditions. In general, higher values indicate increasing probability of heat stress, and lower values indicate the increasing probability of cold stress (Matzarakis and Mayer, 1996). However, a question may arise as to whether this comfort range has been calibrated in hot arid climates. For instance, in the Mediterranean climate of Heraklion, the threshold criteria that have been chosen are the thermal acceptance of physiological equivalent temperature (PET) index between 18°C to 29°C; the degree above 35°C in PET will make a person to feel uncomfortably hot with heat stress; and if PET goes lower than 8°C will result in cold stress state (Matzarakis, 2007).

In contrast, an analysis of human thermal comfort conditions in an urban landscape zone in Cairo (Egypt) found that, in hot dry climate, the comfort sensation levels has extended to between the range of 22-30°C for PET temperature, while in cold season of winter thermal comfort found within a range of 21-29°C PET (Mahmoud, 2011). Although this range was validated by this researcher for hot arid regions, the main concern is that the study in Cairo was conducted only in a park, which maybe not valid for different urban environment that lacks vegetation.

On the other hand, Yahia and Johansson (2013a) conducted a study in the hot dry city of Damascus in Syria, to evaluate the behaviour of different thermal indices by investigating various outdoor urban environments. In their study, the subjects (920 people in both summer and winter) were asked to report their sensation based on a 9-point scale, which are: very hot (+4), hot (+3), warm (+2), slightly warm (+1), comfortable (0), slightly cool (-1), cool (-2), cold (-3) and very cold (-4). The researchers found that at 80% acceptability for PET comfort range during summer defined to upper limit of 31.3°C, and the lower comfort limit in winter defined to 21°C. In light of this study, the urban configurations investigated are typical example to the

urban fabric in the current research case study areas, particularly within the high and intermediate urban density areas (see Chapter 2). However, these estimated PET values for hot arid urban areas are proposed for Damascus, which is not necessarily transferable to Madinah. Nevertheless, the estimated upper PET thermal comfort limit of 31.3°C and lower limit of 21°C have been used as a reference in this study since no other reference values calibrated for Madinah.

Thus, the assessment of thermal comfort in this current study is expressed by means of the physiologically equivalent temperature (PET). However, it should not be confused between the PET sensation temperature and air temperature degrees, although both of them are expressed in °C, as PET is a calculation of several microclimatic variables including air temperature. PET can be calculated easily by using the RayMan model (Available online), which was developed by Matzarakis et al. (2007), and it is recommended by German VDI-guidelines (Thom, 1998) for urban and regional planning. RayMan software takes inputs of the six thermal comfort key factors (i.e. air temperature, MRT, wind speed, etc.), and it is valid for hot and sunny climate in which values of MRT exceed 60°C at around noon (Abdel-Ghany et al., 2013; Matzarakis et al., 2007).

### **3.6. Thermal Comfort Interaction Factors**

This section discusses the thermal comfort interaction factors, including the microclimatic factors such as: air temperature, mean radiant temperature, relative humidity and air velocity; and personal factors including: clothing insulation ratio and metabolic rate (activity level).

According to Nikolopoulou and Lykoudis (2006), in an analysis of thermal comfort in outdoor urban spaces across different European countries, their findings confirm a strong relationship between microclimatic and comfort conditions. Air temperature and solar radiation were found the most determinants of thermal comfort, while the convective cooling of the winds is desired at high air temperatures. The latter statement may suggest the importance of designing urban streets with wind movement in hot arid climatic regions. Ali-Toudert et al. (2005) demonstrated that in hot arid regions cooling effects through increased wind speed as well as evaporation (i.e. increasing relative humidity ratio) are recommended to enhance the heat stress levels. Thus, this should be investigated in the case study area (i.e. Madinah) of the current

research where wind flow rate is critically low, by testing different urban street design scenarios with prevailing wind speed directions.

In a study by Ali-Toudert et al. (2005) on outdoor thermal comfort in a hot dry region of Beni-Isguen, Algeria, it was found that heat stress in hot arid regions is very high in wide open spaces (i.e. unobstructed sites) in contrast to sheltered urban locations. This is because the level of exposure to solar radiation is larger in unobstructed locations. These factors are the main consideration in calculating the PET value, as they affect the heat balance of the human body. Nevertheless, in the current research the main focus is to enhance thermal comfort level through improving wind flow pattern. Johansson (2006) studied the influence of urban geometry on outdoor thermal comfort in a hot dry climate of Fez, Morocco. The researcher used PET index based on field measurements, but the PET values were obtained based on steady state condition and did not take into the account walking condition. In addition, the study did not consider the clothing and activity levels, which can affect the accuracy of the PET results.

When analysing the microclimate of urban spaces, the primary objective for researchers is to determine quality of life in daily occupation or operation of these areas. Observations of the use of outdoor spaces revealed that the reduction in users' presence appears as a result of thermal discomfort, when air temperature increases significantly (Nikolopoulou and Lykoudis, 2007; Bruse, 2009). However, air temperature is not the only microclimatic parameter that influences human thermal perceptions but also the MRT, wind speed and relative humidity.

### **3.6.1. Air Temperature**

Air temperature is a central microclimatic factor that affects the evaporative and convective mode of heat exchange to and from the body, and thus influencing thermal comfort (Gaitani et al., 2007; CIBSE, 2006a). Air temperature is usually different from rural areas compared to urban areas. For example, Djenane et al. (2008) have found that air temperature measured empirically in an urban area was 3.5°C higher than the meteorological station readings at the nearest airport (i.e. usually located in suburban areas). The reason for such higher temperatures in a city (i.e. urban heat island, UHI) is because of the progressive modification of surface covers, with dense concentrations of low albedo materials like asphalt, and structures which absorb more heat than natural ground covers, as well as anthropogenic heat release causing UHI (Hu and Brunzell, 2015; Radhi et al., 2013 and 2015).



For example, researchers such as Erell and Williamson (2007) conducted a micro-climatic study for a number of locations in the city of Adelaide, Australia, and compared the air temperatures at an urban street canyon, a suburban site (about 1.7 km away from the urban canyon), and an open reference site (in the green belt of parklands and 100 m distanced from a river) on a typical clear day in May 2000. It was found that the maximum temperature differences were recorded just before the sunrise time; where a difference of 5.1°C monitored between the urban canyon and the suburban site, and 6.7°C found between the urban canyon and the open reference site (Fig. 3.1). This difference in the temperature may affect the calculation of realistic human thermal comfort conditions in an outdoor urban microclimate, therefore in the current study the in-situ measurement was considered for actual urban microclimate studies in Madinah.

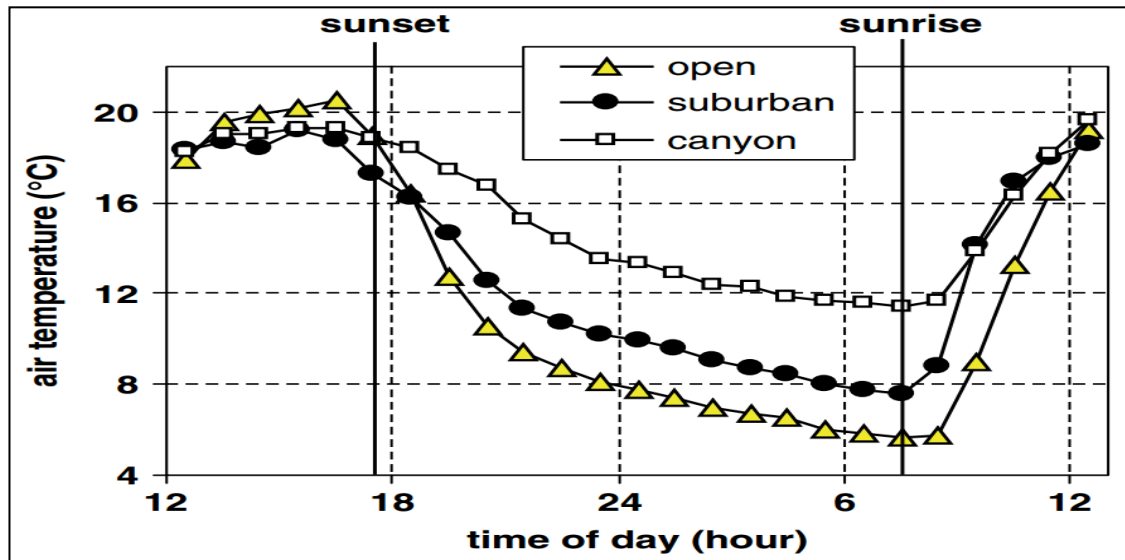


Fig. 3. 1: The comparison between air temperatures measured in an urban canyon, a suburban area, and open reference sites. Source: Erell and Williamson (2007:1249).

### 3.6.2. Mean Radiant Temperature (MRT)

Mean Radiant Temperature (MRT) is defined as the uniform surface temperature of black enclosure with which an individual exchanges the same heat by radiation as the actual non-uniform environment (Gaitani et al., 2007; CIBSI, 2006b). MRT is a key factor in pedestrian thermal comfort, but is more complex than the air temperature as it affects the radiation mode of heat transfer, and thus it is a measure of radiation exchange of “the average temperature of the surrounding surface elements” (Szokolay, 2008:18; CIBSE, 2006a:8). Moreover, the difference between air temperature and MRT is that the latter has a greater influence on the body heat gain or loss to the environment, as our skin absorbs as much radiant energy as a matt black body, even though this can be decreased by reflective clothing (Streinu-Cercel et al., 2007).

### 3.6.3. Wind Speed

Wind environment is one of the most considerable factors in urban microclimate study as it has a direct influence on conveying heat from the thermal urban environment as well as from our body (Mochida & Lun, 2006). Naturally, air flow is caused by pressure difference, as it flows from a higher pressure zone towards a lower pressure one (Szokolay, 2008). For example, *“on the windward side of a building a positive pressure field will develop, where the pressure is proportional to the square of the velocity. At the same time a negative (reduced) pressure field may develop on the leeward side and the difference between the two pressures can generate quite a strong cross-ventilation”* (Szokolay, 2008: 16).

Moving air can result in a favourable cooling effect in hot season when the heat is removed from the body by convection and evaporation, however completely still (i.e. less than 0.1m/s) or too fast (i.e. greater than 6 m/s) air movement may cause discomfort (Gaitani et al., 2007; and CIBSE, 2006a; Streinu-Cercel et al., 2007) or even wind danger (Blocken and Carmeliet, 2004a). Cheng and Ng (2006) recommended that for a person under shade, with solar radiation intensity of around 100 W/m<sup>2</sup>, and air temperature range of 27-34°C, one needs around 0.1-2.5m/s for sitting activity to remain in comfort; 2.5-4m/s for standing activity; and 4-5m/s for walking activity. However, this recommendation was based on conditions under the hot humid climate of Hong Kong and not hot arid. Rizk and Henze (2010) suggest the acceptable wind velocity range in hot arid climates to achieve thermal comfort for air temperatures that exceed 32°C in shade, with a lower limit threshold of 1.6m/s (based on ASHREA Standard 55, 2004), and upper limit of 3.8m/s (based on Beaufort Scale).

### 3.6.4. Relative Humidity

According to CIBSE (2006a:10), the amount of moisture in the air depends mainly on the air temperature and pressure, i.e. air holds more water vapour when the pressure and temperature increase, and vice versa. Thus, *“it is widely accepted that higher humidity and air temperature intensifies thermal sensation and reduces perspiration and evaporation of the body’s capacity, consequently the body cannot be cooled by evaporation”* (Djamila et al., 2014; Holm and Engelbrecht, 2005). Since the efficiency of evaporation is decreased as the relative humidity increases, in hot conditions the relative humidity becomes a much more essential factor (Stathopoulos, 2006). However, in winter seasons or cold conditions, humidity has little direct effect

on thermal comfort. According to Gaitani et al. (2007), relative humidity (RH) is an indirect influence exacerbated by the latent respiratory exchange and the insensible skin perspiration, as it affects sweat evaporation and incidental skin wetness. It affects evaporation mode of heat transfer as it depends on the amount of moisture in the air, so if the air holds too much moisture (the maximum moisture content that air could support is said to be saturated) or too little (dry air) may cause discomfort to the human body (CIBSE, 2006a).

Humidity in rural and suburban areas is usually higher than the urban areas, which is as a result of the evaporation caused by surface temperatures of dense urban environments (Yahia, 2012). Relative humidity is usually found maximum in the morning, due to low air temperature, and minimum during the afternoon as a result of high temperature. Thus, watering plants is more effective when relative humidity is high, that is because of less evaporation process from the ground occurs during morning and evening hours. In addition, an assessment of the influence of air temperature on relative humidity in the hot dry climate of Damascus across the whole year (1961 to 1990) is represented in Figure 3.2. Summer temperatures can reach 35°C during a hot sunny day, while cold winter temperature reaches as low as 2°C at night. Spring and autumn seasons are the most comfortable periods as the temperature reaches 22°C during the day. However, the inverse relationship between the temperature and relative humidity demonstrates that relative humidity increases when there is a decline in air temperature, and it significantly drops where there is a significant rise in temperature. In addition, rain can enhance the level of relative humidity as it increase the amount of water surfaces and thus the humidity rate (Yahia, 2012).

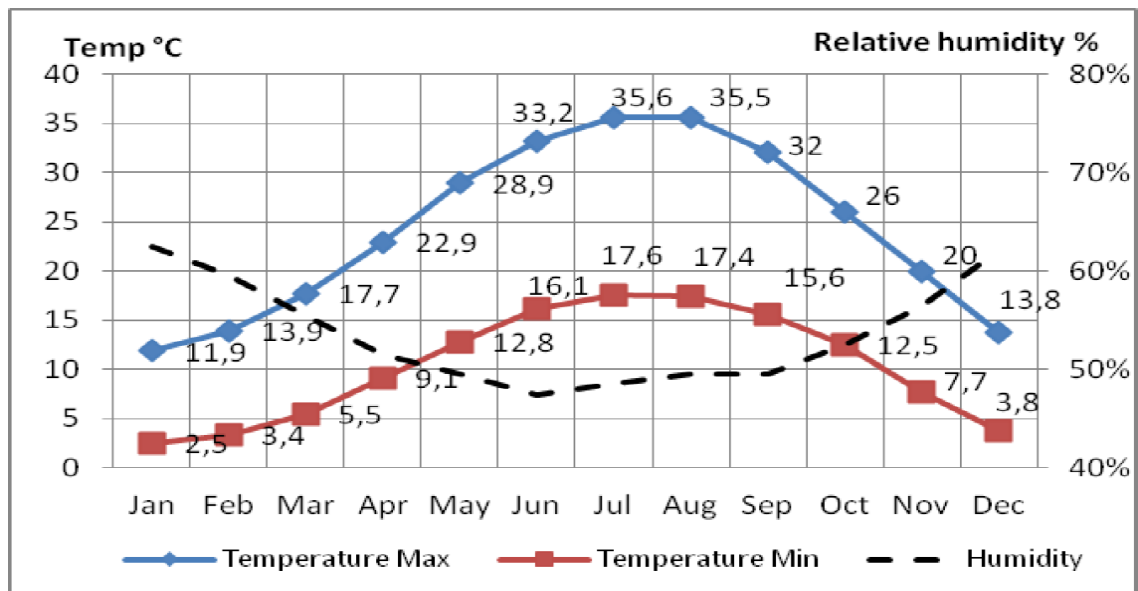


Fig. 3. 2: The relationship between the average relative humidity and the air temperature levels during the year (1961 to 1990). Source: Yahia (2012).

Szokolay (2008) recommends the range of between 30-70% as suggested air humidity for natural ventilated areas. Streinu-Cercel et al. (2007:127) and CIBSE (2006b:1-4) recommend that the acceptable relative humidity is in the range between 40 - 70% as it has a minor impact on thermal comfort “with the optimum being around 65% RH at comfort temperature.” Ahmed (2003) found that thermal comfort can be obtained under still air in a shaded area when the air temperature is at maximum of 32.5°C with the relative humidity range of between 50-75%, and at minimum of 27.5°C with 50-85% of relative humidity.

### 3.6.5. Clothing Insulation Ratio (Personal Factor)

The adaptive principle of thermal comfort in Nicol et al. (2012:8) states a fact that “if a change occurs such as to produce discomfort, people react in ways which tend to restore their comfort.” Thorsson et al. (2004) studied the thermal bioclimatic conditions and patterns of behaviour in an urban park in Göteborg, Sweden. The main focus of their research was on personal adaptation under cold humid conditions. It was found that people enhance their thermal comfort status by changing their normal clothing to thermal clothes. However, this study was not conducted under hot arid conditions. The function of clothing is to insulate or keep the high environmental temperatures and solar radiation (in hot climates) away from the skin, whilst still allowing heat loss by evaporation as air is pumped over the body surface and through

the clothing when the person moves (Berger, 1988). Nicol et al. (2012: 6) stated that *“we expect different thermal experiences in summer and winter, and we modify our behaviour accordingly”*; however, *“temperatures that are ‘right’ in summer when wearing a T-shirt and shorts could be oppressively hot in winter clothing.”* Thus, clothing value (i.e. expressed in term of Clo) is an important behavioural adjustment that a person might consciously or unconsciously make to modify heat and mass fluxes governing the thermal balance of the body (Wohlwill, 1975).

A study by Yahia (2012) has found that in hot dry summer of Damascus city the insulation value of people’s clothing tend to decrease with increasing air temperatures (clothing values varied between 0.4 to 0.8 clo), whereas in winter is the opposite (ranged between 0.5 to 2.5 clo). Similarly, Oliveira and Andrade (2007) found that with increase in the PET thermal sensation value the predominant type of clothing changes and Clo values are reduced. However, the level of clothing insulation can vary according to culture (e.g. Thowb in the Middle East, or suit in Europe) as well as to climate (hot, cold, etc.). Yahia (2012) have found that some people adjust their clothing according to the weather, while others use heavy clothing in fairly warm condition, as the latter choice is to some extent found linked to cultural aspects. Therefore, its function is not purely thermal but also cultural.

The figure below (Fig. 3.3) shows the local/cultural type of clothing insulation for Gulf region. In Saudi Arabia, male summer clothing usually consists of white cotton fabric of T-shirt with 1/3 sleeves, short serwal (underwear), long serwal, thawb (light long loosely fitting gown), kuffiya (hat), white ghutra or red shemagh worn on the head with equal (i.e. black head ring), and sandals. The clo value for this is between 0.69-0.79, whereas in winter the value reaches 0.84-1.29 clo (Al-Ajmia et al., 2008; Nicol et al., 2012). In addition, gulf female summer clothing usually consists of abaya (long black dress), hijab, bra, pants, and sandals (with clo value of 0.80); whereas winter clothing (with clo value of 1.17-1.34) consists of abaya, long trouser, bra, pants, socks, and shoes (Al-Ajmia et al., 2008). These values that were measured in laboratories (with error of around 20%) can be used as assumption in the thermal comfort studies (Nicol et al., 2012). Thus, in the current research, these values will be considered for the calculation of human thermal comfort conditions.

Ensemble type	Ensemble description	$f_{cl}$	clo	$f_a$ $m^2.K.W^{-1}$	clo	$f_{cl}$ $m^2.K.W^{-1}$	clo	$f_T$ $m^2.K.W^{-1}$
Male summer clothing	T-shirt with 1/3 sleeves, short serwal, thawb and sandals	1,30	0,594	0,092	0,59	0,092	1,05	0,163
	T-shirt with 1/3 sleeves, short serwal, thawb, kuffiya, white ghutra, equal, sandals	1,35	0,594	0,092	0,69	0,107	1,13	0,175
	T-shirt with 1/3 sleeves, short serwal, long serwal, thawb, kuffiya, white ghutra, equal, sandals	1,36	0,594	0,092	0,79	0,123	1,23	0,191
Male winter clothing	T-shirt with 1/3 sleeves, short serwal, long cotton serwal, thawb, kuffiya, ghutra shemagh, equal, shoes	1,46	0,594	0,092	0,84	0,131	1,25	0,194
	T-shirt with 1/3 sleeves, short serwal, long cotton serwal, thawb, ghutra shemagh, equal, jacket, shoes	1,45	0,594	0,092	1,29	0,200	1,70	0,264

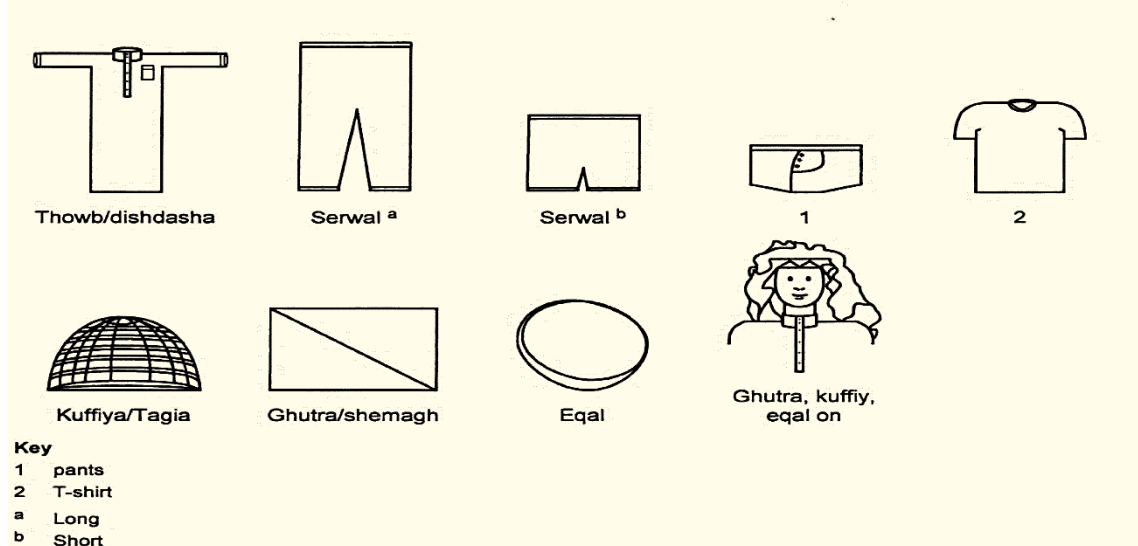


Fig. 3. 3: Summer and winter traditional male clothing and their clo value. Note that female clothing insulation values are mentioned within the text. Source: Al-Ajmia et al. (2008).

### 3.6.6. Activity Level (Metabolism Rate)

Human body generates heat by its metabolic system; and a various amount of metabolic heat can be lost from the person's body depending on the levels of activity and the characteristics of a body (Erell et al., 2011). To normally maintain the thermal balance of the body, the produced metabolic heat must be dissipated to the environment, otherwise the body will be thermally unbalanced with an increased temperature, and thus the person would feel thermal discomfort (Nicol et al., 2012; Szokolay, 2008). Erell et al. (2011) reported that our body attempts to maintain thermal equilibrium under hot or warm conditions through several mechanisms of evaporative cooling, in particular through the production and secretion of sweat.

To achieve the body's thermal balance and thus thermal comfort condition, the stored heat in the body (i.e. 37°C) must equal the sum of the following heat based factors: metabolic heat production, net radiation exchange, convection, conduction, and evaporation (including sweat and respiration) (Szokolay, 2008). It is acknowledged that human normal inner-body temperature is always 37°C, whereas the skin can vary

between the temperatures of 31 to 34°C (Szokolay, 2008). According to Givoni (2010), cooling of the skin by sweat evaporation is dependent on the ambient air temperature, while the sweat evaporation rate from the skin can be affected by the air speed around the human body. In addition, higher humidity can intensify thermal sensation and reduce perspiration and evaporation of the body's capacity, which can cause thermal discomfort (Djamila et al., 2014; Holm and Engelbrecht, 2005). Convection is defined as *“the process of heat exchange between the skin and the surrounding air”*, which can be either by heat gain from the air to the body's skin or heat loss from the skin (Givoni, 2010:87). It is not only the activity levels that can produce heat through our body, but also the food we eat will convert into energy (heat) (Nicol et al., 2012).

The heat production of an average body (with mean surface area of approximately 1.8m<sup>2</sup>) of a seated person is often taken as 100 W (i.e. 1 met or 58.2 W/m<sup>2</sup>), but it can vary from about 70 W (in sleep) to over 700 W in vigorous activity or heavy work (Szokolay, 2008). The more active we are, the more heat we produce; thus, *“a complication that may arise is that people can vary their activity from time to time, and a particular activity can affect the thermal sensation for some time afterwards”* (Nicol et al., 2012: 100). The metabolic value for a person walking on the level of 2km/h is 198 W (i.e. 1.9 Met or 110 W/m<sup>2</sup>), which was adopted in this current study due to the nature of the research that is based on assessment of outdoor pedestrian thermal comfort. However, according to Nicol et al (2006) and Humphreys (1979), although activity level and clothing choice will provide an adaptive opportunity for comfort, complete adaptation to the extreme thermal microclimates is not generally achieved by its own in outdoors without the support of urban design with microclimate (discussed in Chapter 4).



### 3.7. Field Studies on Outdoor Thermal Comfort

Over the years, many studies on urban microclimate and thermal comfort have become a specific interest to many researchers in the fields of architectural design, urban planning and urban street design, focussing on different outdoor thermal environments, pedestrian comfort and various climatic types (Honjo, 2009). Previous studies provided valuable information on understanding the impacts of outdoor microclimatic parameters on pedestrian thermal comfort and the use of outdoor spaces. A summary of the findings from previous outdoor thermal comfort field studies is listed in Table 3.1.

Some studies on outdoor thermal comfort focused on tropical hot humid climates (e.g. Lin, 2009; Ahmed, 2003; Emmanuel et al., 2007; Krüger et al., 2011; Chen and Ng, 2012), cold climate (e.g. Mayer and Höppe, 1987; Thorsson et al., 2004; Nikolopoulou et al., 2001; Nikolopoulou and Lykoudis, 2006), and temperate climate (Spagnolo and de Dear, 2003a). Many researches have been conducted on hot arid climates (e.g. Yahia and Johansson, 2013a&b; Givoni et al., 2003; Ali-Toudert and Mayer, 2006; Djenane et al., 2008; Bourbia and Awbi, 2004a&b; Aljawabra and Nikolopolou, 2010; Pearlmutter et al., 2007; Abdel-Ghany et al., 2013; Shashua-Bar et al., 2009; Mahmoud, 2011). However, there is very limited research on outdoor thermal comfort under hot arid conditions especially in Saudi Arabia (Abdel-Ghany et al., 2013), whereas no relevant research has been done in the city of Madinah.

In hot arid areas, the major climatic issues are the extreme dryness with high day temperatures and dusty storms. However, unlike many cities in Saudi Araba, Madinah is protected from dusty storms by its nature of being surrounded by mountains, particularly in the south, west and north areas of the city, while the prevailing winds are mainly from the south-westerly direction, followed by the less prevailing wind from the westerly direction, then the north-westerly direction. Thus, these mountains have reduced the effect of dusty storms on urban areas but have raised an issue of low wind speed environment. According to de Schiller and Evans (2000), hot arid climate is characterised by intense solar radiation, large temperature amplitude between day and night, dusty storm, torrential rain, low cloudy days, intense dehydration, high salinization, and evaporation exceeding precipitation. These basic profiles reflect the climate of the Middle East as well as North Africa, most part of Australia and South-Western United States. However, regarding the introduction of modern urban settlements, Al-Ibrahim (1990: 65) has critically argued that “*the environmental*

*performance of modern architecture is inferior to that of traditional architecture, and that modern building materials are not well suited to the hot arid environment of Saudi Arabia. A frequently cited example is that of concrete blocks, that material out of which most walls are presently made and which is much more heat conductive than the traditional mud walls”.*

In the hot dry city of Damascus, Yahia and Johansson (2013a) have conducted in-situ microclimate measurements and structured interviews (i.e. questionnaire survey) in summer and winter. The microclimatic measurements were taken to compare between the actual thermal sensation and the calculated human thermal comfort indices (e.g. PET index and OUT\_SET\* index, see Section 3.5). This was performed to evaluate the interviewees’ thermal sensation and other parameters such as age and gender, clothing insulation value, reason for being in the place, duration of time spent in outdoor spaces, emotional state of the place, their thermal preference, assessment of the microclimate indicators, aesthetic qualities of the place, and assessing the attitude to urban outdoor exposure (Yahia and Johansson, 2013a). However, their study’s objective was to calibrate the thermal comfort indices under hot dry conditions for Damascus, which is time consuming as it requires structural interviews (mentioned above).

Aljawabra and Nikolopoulou (2010) studied the influence of hot arid climate on the use of outdoor urban spaces and thermal comfort in Phoenix and in Marrakech, illustrated in Figure 3.4. They conducted field surveys including structured interviews (total of 429 interviews from both cities in summer and winter) interview with a standard questionnaire and observations of people and their activities on site, while monitoring microclimatic data during the summer and winter seasons. One of the main advantages of this method in outdoor pedestrian thermal comfort studies is that it can involve direct observation of social behaviour, and thus this may promote the understanding of social actual behaviour in relation to the other interaction factors of pedestrian thermal comfort (i.e. environmental factor; activity level; period of space usage; and clothing insulation). However, their research focussed on work towards understanding the relationship between place microclimate and human behaviour, but did not consider finding ways to mitigate urban heat stress. Further, they used the combination of structural interviews and in-situ measurements which is time consuming. Nevertheless, the findings revealed that *“improvement of microclimatic conditions in urban spaces can enable people to spend more time outdoors”* (Aljawabra and Nikolopoulou, 2010:198).

Furthermore, the analysis of the data collected by observation and questionnaire survey concluded that:

- High mean air temperature during hot arid summers between 35°C (e.g. in Marrakech in North Africa) to 39°C (e.g. in Phoenix, Arizona in the USA) can clearly reduce the duration of use of public spaces, thus economic activities.
- The mean air temperature around 20 or 22°C in low-humid winter is voted as a more comfortable condition in the study of Phoenix and Marrakech.
- The intensity of solar radiation has a strong negative impact on the number of people using the space (as shown in Figure 3.4) and the number of activities (e.g. chatting, reading, eating, walking, etc.), as higher the intensity the more number of users decreases in hot arid summers (refer to Chapter 4).
- However, in shaded parks and urban plazas, negative but medium correlations were found between the users' number in such hot dry climate and the solar radiation (Aljawabra and Nikolopoulou 2010).



*Fig. 3. 4: Relationship between the radiation intensity rate and the number of place users. The picture on the left shows less solar intensity than the one on the right. Source: Aljawabra and Nikolopoulou (2010).*

It is evident, given the data collected by these researchers, that there are temporal, spatial, and climatic variables which all must be considered when designing open spaces. In fact, this particular investigation provided evidence of a general standard of microclimate analysis, echoed by such researchers as Gaitani et al. (2007) and Lenzholszer and Koh (2010), and others. The dominant research method used across varying spaces involves case study analysis that consists of environmental readings and social feedback. On the basis of this widespread standardisation of method

and increasingly consistent results retrieved from such data collection techniques, it is proposed that the methodological foundation for this research be slightly differentiated in order to contribute analysis and discussion that expands theory within this industry, not simply mimicking it. Thus, this current research proposed to conduct a numerical simulation study together with the field measurement methods, with the aim to investigate the effects of multi-asymmetrical aspect ratios on urban pedestrian microclimate and thermal comfort conditions, as discussed in the second part of the literature in Chapter 4.

Extrapolating the principles underlying the case study research methodology, Mirzaei and Haghighat (2010) clarified that there are validated approaches that are used to enable the assessment of outdoor pedestrian thermal comfort conditions, such as in-situ microclimate measurements method, and the numerical simulation approach (using wind tunnel, or computational fluid dynamics). According to Erell et al. (2011), these two methods are the most common research tools used to assess the wind comfort and thermal comfort within the built environments. In addition, both methods may require the distribution of the human thermal comfort indices (e.g. PET or Physiological Equivalent Temperature, etc.) for the assessment and prediction of human thermal comfort conditions (Erell, 2005). Such indices can be alternative to structural interviews, thus reducing efforts and time consumption. Although most evaluation tools have advantages and disadvantages, the three above mentioned methods (comfort indices, CFD numerical simulation and in-situ measurements) can give promising results once used properly, leading to a good urban space design decision making, thus finding ways for the enhancement of urban microclimates and thermal comfort of outdoor pedestrian environments (Campos-Arriaga, 2009; Erell, 2005) (refer to section 3.8, and Chapters 4 and 5 for details on these methods). However, people's satisfaction levels vary to a great extent, which can make it difficult to determine their thermal comfort levels (Jacobs, 1993; Worpole and Knox, 2007; and Watson and Studdert, 2006).

Cheng and Ng (2006) constructed the Hong Kong outdoor air temperature comfort chart, which was based on collated data of previous researchers conducting work elsewhere that are similar to Hong Kong climatic conditions. The chart demonstrates that for a person under shade, with solar radiation intensity of around 100 W/m<sup>2</sup>, and air temperature range of 27-34°C, one needs around 0.1-2.5m/s for sitting activity to remain in comfort; 2.5-4m/s for standing activity; and 4-5m/s for walking activity, as illustrated in Figure 3.5. It is deduced from meteorological studies that the

maximum air temperature in Madinah for April (in spring) is 35°C, which is situated outside the comfort outdoor temperature zone. However, this outdoor comfort temperature zone chart was developed under hot and humid conditions, which might not be applicable for hot arid conditions of Madinah. Rizk and Henze (2010) suggest the acceptable wind velocity range in hot arid climates to achieve thermal comfort for air temperatures that exceed 32°C in shade, with a lower limit threshold of 1.6m/s (based on ASHREA Standard 55, 2004), and upper limit of 3.8m/s (based on Beaufort Scale).

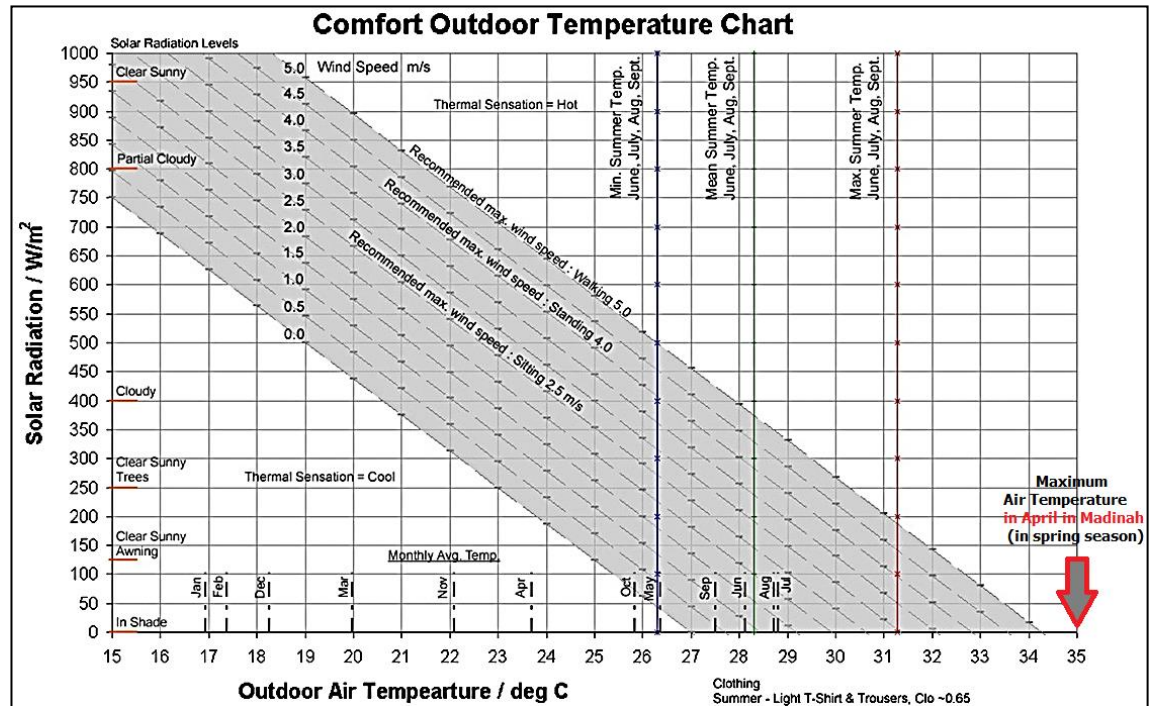


Fig. 3. 5: Comfort outdoor temperature chart that shows the recommended wind speeds for different solar radiation levels as well as for different air temperatures. Source: Cheng and Ng (2006).

Alternatively, Abdel-Ghany et al. (2013) have performed PET (physiologically equivalent temperature) index on outdoor spaces to study the human thermal comfort conditions and heat stress levels during the hot arid summer in Riyadh, Saudi Arabia. The findings revealed that a person would feel thermally uncomfortable, or very hot with extreme heat stress, during most of the day hours (9:30 - 17:00), and the person's thermal sensation drops to the range between hot to slightly warm during the early morning and at night periods (see Figure 3.6). The researchers have compared the PET results with the universal thermal climatic index (UTCI), and found almost similar results of corresponding heat stress and thermal sensation, which might indicate that PET is suitable index for predicting thermal comfort in Saudi Arabia, particularly for hot arid regions. In a different climatic region, the PET comfort sensation index has

shown a good agreement with the perception of interviewees in a study conducted in the hot humid region of Japan on the relation between the thermal comfort conditions and outdoor activity levels (Thorsson et al., 2007). However, these two studies of hot arid and hot humid have applied a uniform PET comfort band range of 18-23°C, which was proposed in a study by Matzarakis and Mayer (1996) under hot humid conditions of Athens, in Greece. Thus, this PET comfort range was not calibrated for hot arid conditions. For the assessment of thermal comfort in Madinah, the PET index is more relevant; as it has been calibrated for hot arid regions with a comfort threshold range of 21°C to 31.3°C proposed by Yahia and Johansson (2013a) (refer to section 3.5 for more detail).

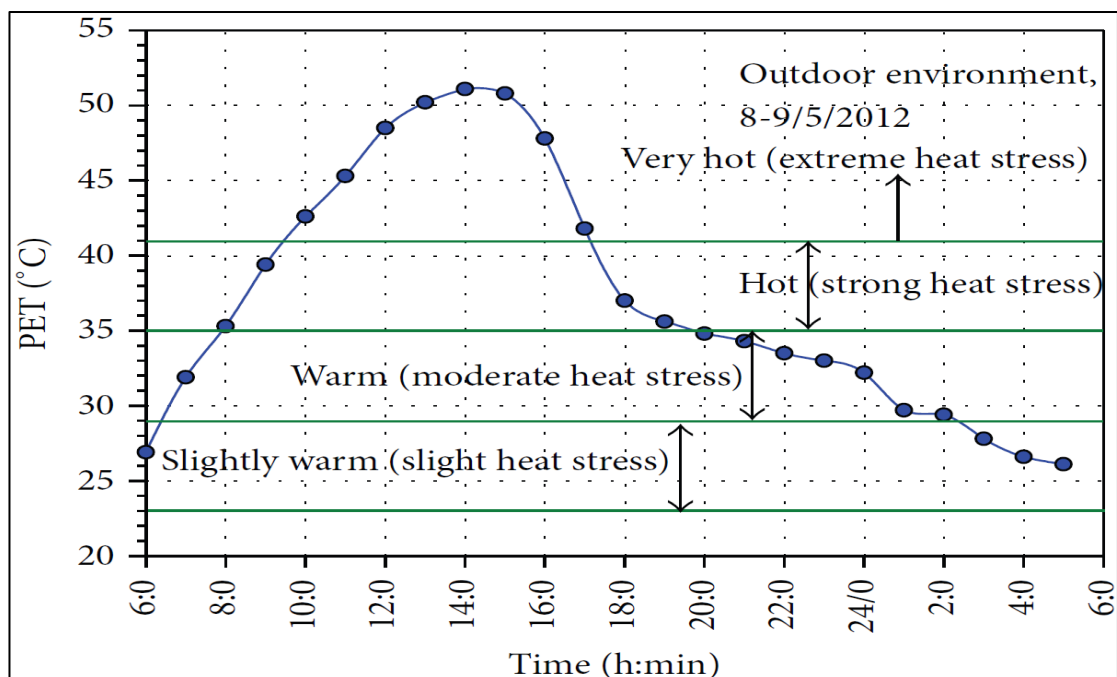


Fig. 3. 6: The estimation thermal sensation against PET index in hot arid summer of Riyadh, Saudi Arabia. Source: Abdel-Ghany et al. (2013).

Another study was conducted on several climatic regions, including the hot arid climate of Riyadh in Saudi Arabia by Alexandri and Jones (2008), using meteorological data to calculate the thermal comfort conditions by PET index. The researchers have also obtained the PET values in diverse climatic regions, including Riyadh, Montrea, Brasilia, Mumbai, London, Beijing, Moscow, Hong Kong and Athens. However, they have used the PET comfort band range of 18-23°C under diverse climates. The main issue in this study is that the comfort range has not been calibrated under hot arid



conditions, which may result in less accurate results. Nevertheless, the study focussed on evaluating the effects of vegetated and non-vegetated building roofs and elevations on street and roof levels microclimates, with an East-West (E-W) oriented urban street and aspect ratio of 0.5 (i.e.  $H/W = 5m/10m$ ). It was found that in Riyadh, a person standing above the bare concrete roof can feel the thermal perception of “very hot” in the afternoon, but when covered with vegetation, the sensation level of “warm” is obtained in the duration of 5 hours (Fig. 3.7). In most of the daytime under a hot arid climate, the green roof reaches the “slightly warm” condition and “comfortable” zone. While for the thermal sensation inside the urban canyon, it improves from “hot” to “slightly warm” and “comfortable” conditions in the early morning and late evening hours.

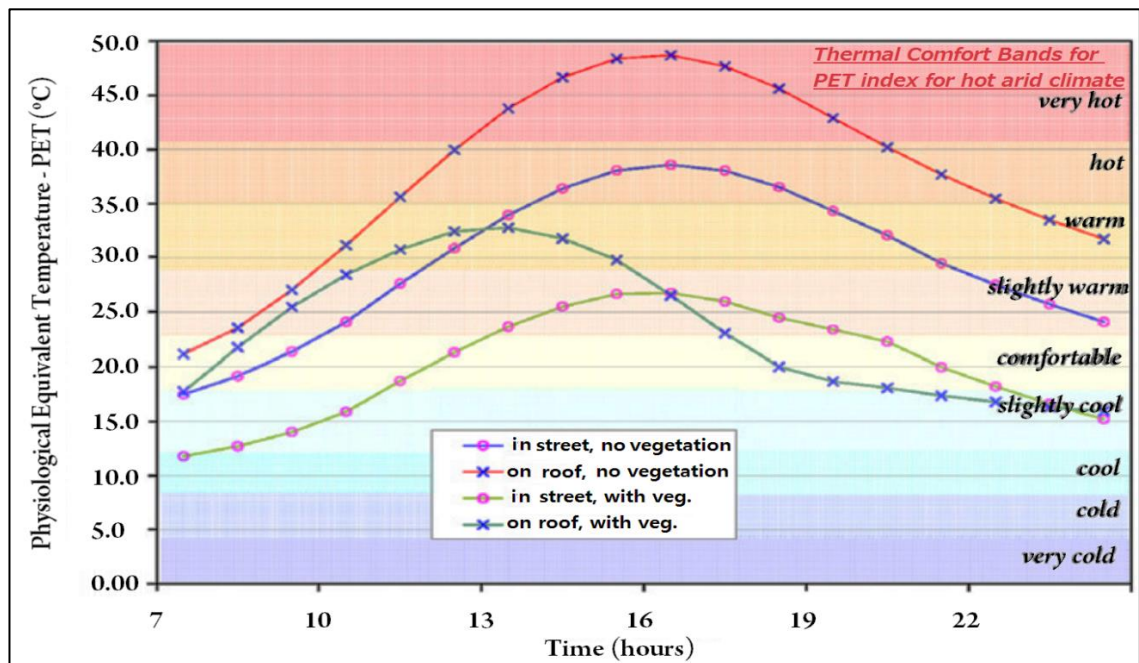


Fig. 3. 7: The graph shows the ranges of PET temperature that is applicable for hot arid climates. It also shows PET for the E–W-oriented canyon of Height 5 and Width 10, for the no-green and with green cases, inside the canyon and on the roof, for Riyadh. Source: Alexandri and Jones (2008).



Table 3. 1: Previous studies on outdoor thermal comfort.

Researcher	Climate Region	Research Title	Comments
Thorsson et al. (2004)	Goteborg, Sweden (Cold Humid)	Thermal bioclimatic conditions and patterns of behaviour in an urban park in Göteborg, Sweden.	People enhance their thermal comfort status by changing their normal clothing to thermal clothes and by choosing the most supportive thermal opportunities available within the place. Psychological aspects may influence the subjective assessment. The main focus of this research was on personal adaptation in cold humid region, but not under hot arid conditions.
Ali-Toudert et al. (2005)	Beni-Isguen, Algeria (Hot Dry)	Outdoor thermal comfort in the Old Desert City of Beni-Isguen, Algeria.	The thermal comfort was expressed by means of the physiologically equivalent temperature (PET) index. Heat stress in a hot arid region is very high in wide open spaces (i.e. unobstructed sites) in contradiction of sheltered urban locations, which is due to the level of exposure to solar radiation is larger in unobstructed locations.
Johansson (2006)	Fez, Morocco (Hot Dry)	Influence of urban geometry on outdoor thermal comfort in a hot dry climate: A study in Fez, Morocco.	PET index was used in this study based on field measurements, but the PET values were obtained based on steady state condition and did not take into the account for walking condition. The study also did not consider the clothing and activity levels, which have effects on the accuracy of calculation of thermal comfort conditions.
Nikolopoulou & Lykoudis (2006)	Europe	Thermal comfort in outdoor urban spaces: analysis across different European countries.	The findings confirm a strong relationship between microclimatic and comfort conditions, with Air temperature and solar radiation were found the most determinants of comfort, while the convective cooling of the winds is desired at high air temperatures. Thus, this should be investigated in the current research case study area (i.e. Madinah) where wind flow rate is critically low, by testing different urban street design scenarios with prevailing wind speed directions.
Cheng & Ng (2006)	Hong Kong, China	Thermal comfort in urban open spaces for Hong Kong.	The researchers has constructed the Hong Kong outdoor comfort chart under shade, which was based on collated data of previous researchers conducting work elsewhere that are similar to Honk Kong climatic conditions. However, this comfort zone was developed under hot and humid conditions, which may not be applicable for hot arid climates.
Hwang & Lin (2007)	Taiwan (Hot Humid)	Thermal comfort requirements of occupants of semi-outdoor and outdoor environments in hot humid regions.	The results show that occupants of semi-outdoor and outdoor environments are more tolerant regarding thermal comfort than are occupants of naturally ventilated indoor environments.
Thorsson et al. (2007)	Tokyo, Japan (Hot Humid)	Thermal comfort and outdoor activity in Japanese urban public places.	PET index has shown a good agreement with the perception of interviewees in outdoor public places. But the study was conducted under hot humid conditions and not under hot arid environment.

Pearlmutter et al. (2007)	Negev Highlands, Israel (Hot arid)	Integrated modeling of pedestrian energy exchange and thermal comfort in urban street canyons	In hot arid region, compact urban street canyons (H/W in the range of 1.0 - 2.0) can substantially reduce overall thermal discomfort at pedestrian levels if their axis orientation is approximately north-south (or is not rotated by more than 45° from N-S).
Oliveira & Andrade (2007)	Lisbon, Portugal (during warm dry days)	An initial assessment of the bioclimatic comfort in an outdoor public space in Lisbon	The results of PET index showed that thermal comfort under outdoor conditions can be maintained with temperatures well above the standard values defined for indoor conditions. Women showed a stronger negative reaction to high wind speed than men. In addition, with increase in PET value, the predominant type of clothing changes and Clo values are reduced.
Alexandri and Jones (2008)	Riyadh, Saudi Arabia (Hot Arid)	Temperature decreases in an urban canyon due to green walls and green roofs in diverse climates.	PET index was performed for an urban street. The results indicated that, by introducing vegetation on building facades as well as on roof tops, the thermal sensation within the urban canyon improved from hot to slightly warm as well as comfortable conditions in the early morning and late evening.
Abdel-Ghany et al. (2013)	Riyadh, Saudi Arabia (Hot Arid)	Human thermal comfort and heat stress in an outdoor urban arid environment: A case study.	The findings showed that a person would feel thermally uncomfortable during most of the day hours in summer. PET index was validated for hot arid regions by comparing its values with UTCI index. However, the comfort band of 18°C-23°C was based on hot humid studies and not for hot arid conditions, thus this may affect the accuracy of their results.
Yahia & Johansson (2013a)	Damascus, Syria (Hot dry)	Evaluating the Behaviour of Different Thermal Indices by Investigating Various Outdoor Urban Environments in the Hot Dry City of Damascus, Syria	The study defined upper limit in hot dry summer to 31.3°C for PET index, and the lower comfort limit in winter to 21°C.
Ndetto and Matzarakis (2014)	Dar es Salaam, Tanzania	Urban atmospheric environment and human biometeorological studies in Dar es Salaam, Tanzania	The afternoon period from December to February is relatively the most thermal stressful period to pedestrians where PET values of above 35°C were found.

### 3.8. Assessment Approaches of Outdoor Pedestrian Thermal Comfort

There are a number of ways in which the thermal comfort of outdoor spaces can be assessed in order to facilitate the design of suitable mitigation measures, including full scale field measurements and numerical simulations. Even though in-situ measurement (i.e. field study) approach is the most reliable technique, a continuous and urban-scale implementation of them is not practical or economical. Alternatively, the computer simulation method has been extensively used due to the recent advancement in the computer technology. However, modelling of pedestrian thermal comfort within multiple street canyons of a large urban environment is still limited due to the computational time and cost (discussed in Chapter 4).

Observational method includes field measurements, thermal remote sensing, and small-scale modelling. Thermal remote sensing involves the remote observation of UHI (Urban Heat Island) using satellites and aircraft. However, this technique can only provide data on surface temperature, the effects of surface radiation, and thermodynamic properties, but it is not possible to observe the wind speeds and relative humidity. In addition, the disadvantages of this technique are that it is very expensive and because of atmospheric interactions, it is not always possible to obtain steady images of the urban surface (Mirzaei and Haghighat, 2010). Another technique is to use small scale modelling in which a prototype of the urban area is constructed, and tested using a wind tunnel. It is acknowledged that this technique can be useful in studying some impacts of the urban street canyon on its environment, such as visual impact or pollution dispersion (Poreh, 1996). However, the difficulty in this technique is creating an accurate model and the process can be expensive.

An alternative approach is conducting empirical studies or in-situ measurements technique. In the “*field measurement approach, the near surface temperature pattern in urban area is generally compared with rural area*” (Mirzaei and Haghighat 2010, p.2191). There are a variety of empirical studies that have explored the implications of thermal comfort in outdoor spaces, emphasising the fundamental influence on microclimate perception and visit frequency. Lenzhölzer and Koh (2010), for example, conducted recent experiments in Holland to investigate whether or not particular spatial configurations generate unique microclimates experiences for visitors. Interviews with individuals occupying the square, at various times of day, yielded results that argue definitively for the occurrence of microclimate conditions in various places throughout the test site, as the context of the spatial orientation of structures immediately

surrounding open spaces, building alignment, spacing, and architecture had a direct and measurable impact on the microclimate of that particular area. Comparative analysis of other spaces was able to prove the distinctive nature of these findings.

The field measurement technique involves an analysis of urban microclimatic parameters, thermal variations, air velocity, and turbulence, relative humidity, and pollution concentrations, based on data collected by mobile stations (Gaitani et al., 2007; Lenzholzer and Koh, 2010). This technique is a simple and easy method to monitor urban microclimate situations in a city (Nikolopoulou and Lykoudis, 2006 & 2007). Moreover, Mochida et al. (2006b) have argued that for specifying the boundary conditions of numerical modelling domain, the use of meteorological data is important; however its data are inadequate when simulating the urban spatial distributions of microclimate for accurately evaluating the thermal comfort and wind effects, which thus the integration of in-situ measurements in the urban environment is strongly recommended. This method is more precise for the analysis of existing urban microclimates and calculation of outdoor pedestrian thermal comfort conditions. Therefore, some field measurements were conducted for the validation of results obtained from numerical simulations (e.g. Tominaga et al., 2008; Blocken et al., 2007).

Researchers such as Yahia (2012) and Lenzhölzer (2010) asserted that conducting in-situ measurements by using appropriate weather stations is of importance in thermal comfort studies to gain awareness of accurate characteristics of urban microclimates. However, some of the issues of the in-situ measurement can be that it is time consuming, uses expensive instruments, and involves man-power (e.g. Shashua-Bar et al., 2009; Ahmed-Ouameur and Potvin, 2007). Moreover, only a limited number of parameters can be measured simultaneously, and it is not always possible to produce all three-dimensional spatial distribution of the relevant factors in an urban environment. In addition, it is necessary to conduct the measurements for a long period of time, as this would allow filtering the effect of unpredictable errors. Therefore, the process can also be time consuming and costly (Mirzaei and Haghighat, 2010). Furthermore, it is embedded with errors, especially for wind speed measurement at pedestrian level in the built environment, which may reach the acceptable maximum error of 20% (Willemssen and Wisse, 2002). However, measurements are only valid at the point of measurement, which may be because of variation of wind value from one point to another adjacent point that are affected by urban roughness, pressure between shaded areas and sunny areas, etc. Moreover, due to insufficient equipment, cost constraints and time limitation,

the measurements in the current research were conducted only in a single point for each of the three case studies based on different urban densities along Quba Road.

### 3.9. Summary

This chapter has discussed the outdoor pedestrian microclimate and thermal comfort. It has highlighted some of the main factors causing urban thermal discomfort. It has reviewed the previous field studies on outdoor thermal comfort and relevant thermal comfort criteria. To obtain the microclimatic data, field measurements are conducted as a potential for obtaining more reliable reading for urban microscale studies. For the assessment of thermal comfort in Madinah, the PET (Physiological Equivalent Temperature) index is more relevant; as it has been calibrated for hot arid regions with a comfort threshold range of 21°C to 31.3°C proposed by Yahia and Johansson (2013a). The factors that are necessary for calculating the PET index has been discussed, which are: air temperature, mean radiant temperature, relative humidity, wind speed, pedestrian metabolic rate and clothing insulation level. The values for the latter two have also been identified which will be used as assumption in the current research. RayMan software has been identified in this chapter for calculation of PET temperature.

In addition, the knowledge gap based on the literature review has been identified. There is a lack of field studies on urban microclimate and assessment of outdoor thermal comfort in Saudi Arabia, while no such research has been conducted in Madinah. Few studies have focused on the assessment of urban microclimate and outdoor pedestrian thermal comfort during the four climatic seasons, based on different urban density levels, particularly under hot arid conditions and low wind speed environments, continuously for periods of 24 hours. Thus, the current research focusses on exploring the urban pedestrian microclimate and thermal comfort in Madinah during the four microclimatic seasons for continuous periods of 24 hours in each season based on field measurement method (refer to Chapter 6).

It is acknowledged here that temperatures in peak summer season fall out of tolerable and critical thermal comfort ranges. Therefore, applying any possible urban mitigation measures would rationally aim at improving thermal conditions in intermediate seasons (spring, autumn), where there is a possibility to find passive means to reduce sensations of near critical thermal comfort conditions (refer to Chapter 7 and 8).

# **CHAPTER 4: Literature Review on the Effects of Urban Street Canyon's Configurations on Wind Flow**

## **Chapter Structure**

- 4.1. Introduction
- 4.2. Importance of Urban Canyon Design with Microclimatic Awareness
- 4.3. Effect of Urban Street Aspect Ratio on Pedestrian Wind Flow Rate
- 4.4. Best Practice for Urban Heat Stress Mitigation Techniques in Urban Canyons
- 4.5. Urban Roughness and Pedestrian Wind Flow Regime around Buildings
- 4.6. Effect of Air Movement on Temperatures in Urban Context
- 4.7. Assessment Approach of Outdoor Pedestrian Microclimates in a Street Canyon
- 4.8. Previous Numerical Simulation Studies on Urban Microclimate and Thermal Comfort Using CFD Tool
- 4.9. Summary

# CHAPTER 4:

## Literature Review on the Effects of Urban Street Canyon's Configurations on Wind Flow

---

### 4.1. Introduction

This chapter presents a literature review pertinent to studies on effects of urban street canyon's configuration on urban pedestrian microclimate and thermal comfort. It focuses on best practice for planning urban route configuration, limited to the following two aspects: the effect of urban street canyon's aspect ratio on microclimatic conditions at the pedestrian level and the effects of orientation of urban canyons on pedestrian thermal comfort level. It also discusses the previous CFD numerical simulation studies on urban microclimate and thermal comfort. The knowledge gaps based on the literature review are also identified and summarised at the end of this chapter.

### 4.2. Importance of Urban Canyon Design with Microclimatic Awareness

The first part of the literature review (Chapter 3) highlighted that thermal comfort is an important factor that needs to be considered when designing outdoor urban pedestrian spaces in either hot or cold microclimates, as it forms an important factor for the usability and attractiveness of public places (e.g. Lenzhölzer and Koh, 2010). Thermal comfort in outdoor pedestrian microclimates is a factor that encourages people to visit these places and/or to prolong their usage of the space, which in turn provides increased opportunities for sociability and economic activity as well as other benefits (Eben Saleh, 1997; Aljawabra and Nikolopoulou, 2010; Nasir et al., 2012). Givoni et al. (2003:77) pointed that *“thermal comfort of persons staying outdoors is one of the factors influencing outdoor activities in streets, plazas, playgrounds, urban parks, etc.”* Therefore, Carmona et al. (2003:185) have argued that *“if spaces are not comfortable, they are unlikely to be used.”* However, despite the fact that urban designers must create comfortable urban spaces for the users, there is a lack of understanding of the appropriate design process for the enhancement of outdoor thermal comfort.

In an urban canyon's design, the relative impact of city planning and structural height can positively or negatively affect the ground level microclimate (Oke, 1988).



There is an interrelationship between urban street canyon design (e.g. urban aspect ratios and street orientations), microclimatic parameters (e.g. air temperature, solar radiation, air speed and humidity), and adaptive personal factors (e.g. activity level and clothing insulation level). This is shown to have direct impact on pedestrians' thermal comfort conditions in outdoor urban spaces (Ahmed-Ouameur and Potvin, 2007; Krüger, et al., 2011; Nikolopoulou et al., 2004; Shishegar, 2013; Martins et al., 2012; Yahia, 2012).

Therefore, Ahmed-Ouameur and Potvin (2007) stated that urban configuration is an independent variable of urban microclimate and human's thermal comfort factors (Figure 4.1); while microclimate can be influenced by urban morphology and climatology. On the other hand, human's thermal comfort factors depend on both attributes of the urban morphology and urban microclimate, as well as on the adaptive behaviour opportunity for enhancing thermal comfort levels (Givoni, 2010; Emmanuel and Johansson, 2006; Vasilikou and Nikolopoulou, 2014; Yahia, 2012; Thani et al., 2013).

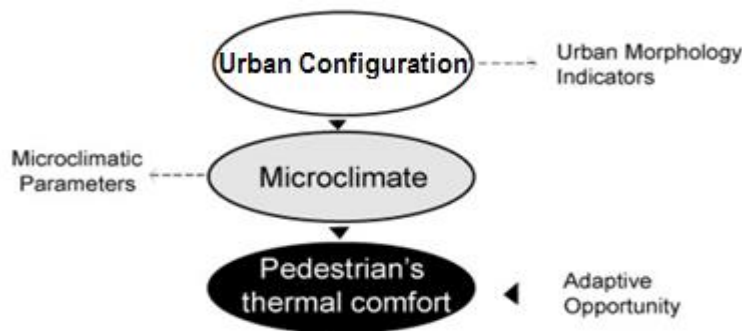


Fig. 4. 1: Interaction between urban morphology, microclimate and pedestrian's thermal comfort. Source: adapted by the author, source: Ahmed-Ouameur and Potvin (2007).

#### 4.3. Effect of Urban Street Aspect Ratio on Pedestrian Wind Flow Rate

The wind flow within an urban street is strongly affected by the urban street canyon geometry (H: height, L: length, W: width) and the street orientation (Ali-Toudert, 2005; Ahranjani, 2010; Oke, 1988). Therefore, one can develop the relationship between the street canyon parameters and the airflow pattern. The street canyon can be called deep, regular or avenue canyons when the aspect ratio (H/W) is greater than two, one, or half, respectively (Ahranjani, 2010). An urban canyon is called symmetric when the height of buildings at the sides of a street is equal in a cross-section, and an asymmetric canyon is called when one building height at one side of the street width is taller than the opposite building on the other side of the street (Ahranjani,

2010). However, in urban numerical studies simplification of urban aspect ratio is often recommended, due to the limitation of computational power and turbulence issues. Therefore, Nakamura and Oke (1988) recommend assumption of averaging buildings heights and performing roughly symmetrical types of urban canyons. However, many studies have conducted symmetrical aspect ratio (e.g. Ali-Toudert and Mayer, 2006; Georgakis and Santamouris, 2006), while limited number of studies have performed on asymmetrical aspect ratio, particularly for pedestrian wind field studies.

Many researchers studied the effects of street aspect ratio ( $H/W$ ) with the degree of exposure to solar radiation to control the amount of radiation from reaching the ground and different solar orientations in relation to street level radiant temperatures, particularly during extreme hot conditions. However, most of these studies have focused on symmetrical building heights to width ratios, but did not consider the effect of multi-asymmetrical street aspect ratios on pedestrian thermal comfort. Ali-Toudert and Mayer (2006) conducted a numerical study in a hot and dry climate of Algeria on the effects of a symmetrical urban street height-to-width ratio ( $H/W = 0.5, 1, 2, \text{ and } 4$ ; with a constant street width of 8m) and orientations with solar radiation (E-W, N-S, NE-SW and NW-SE) on outdoor thermal comfort. It was found that thermal sensation at street level depends strongly on street orientation and building heights and street width. N-S streets showed a trend to be slightly cooler than E-W streets, particularly as the aspect ratio increases.

However, the simulated wind speed in their study was perpendicular incidence on the street axis, which led to a skimming flow regime and found to be strongly reduced at pedestrian level. Nevertheless, their study mainly focused on the orientation in relation to solar radiation rather than with prevailing wind directions, as well as the aspect ratio was symmetrical and focused on exposure to solar angle instead of wind flow rate. Considering wind flow perpendicular to different urban street aspect ratios, for example, three regimes of wind flow over buildings arrays can occur based on the aspect ratios ( $H/W$ ). These are isolated roughness flow ( $H/W < 0.3$ ), wake interference flow ( $0.3 < H/W < 0.7$ ) and skimming flow ( $H/W > 0.7$ ) (Oke, 1988), as illustrated in Figure 4.2.

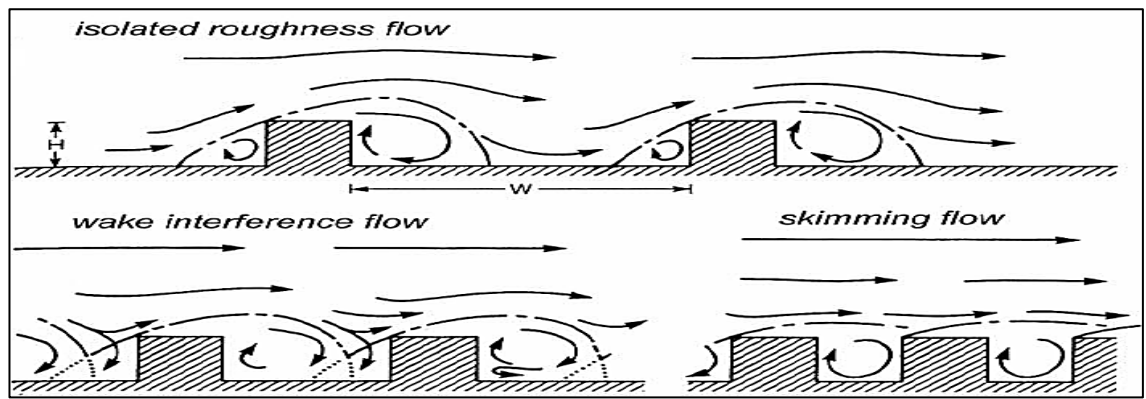


Fig. 4. 2: Three wind flow regimes over arrays of buildings for different aspect ratios. Source: Oke (1988).

Hussain and Lee (1980) have also found similar results but in the gap between two buildings that are arranged along the prevailing wind direction. According to Ali-Toudert (2005) and Oke (1988), the isolated roughness flow regime occurs between well-spaced buildings when there is no interaction at the windward and leeward flows. The wake interference flow occurs when  $H/W$  increases, as a result of disturbed wakes. The skimming flow regime occurs with further increase in  $H/W$ , which is the case in many dense urban contexts, as the urban deep street becomes isolated from the above circulating air and a stable circulatory vortex is established in-canyon, thus influencing the microclimate conditions at street and pedestrian levels (Oke, 1988).

Moreover, Jeong and Andrews (2002) suggested that for increasing from a one-circulation regime to a two counter-rotating circulation, a threshold aspect ratio of  $1.60 < H/W < 2.86$  is observed. This would generally move the main circulation to the upper part of the urban street, while a secondary weak circulation can generate in the bottom part (Fig. 4.3a and 4.3b respectively). For the evolution of the airflow to a three-circulation regime in the canyon, Kim and Baik (2001) reported the threshold aspect ratio of 3.40-3.60 (see Fig. 4.3c). In addition, the researchers found that by heating street-bottom (e.g. temperature difference of 4K), the characteristic of the latter mentioned flow regime changes to two counter-rotating vortices in the lower layer and a mechanically induced upper vortex (Fig. 4.3d).

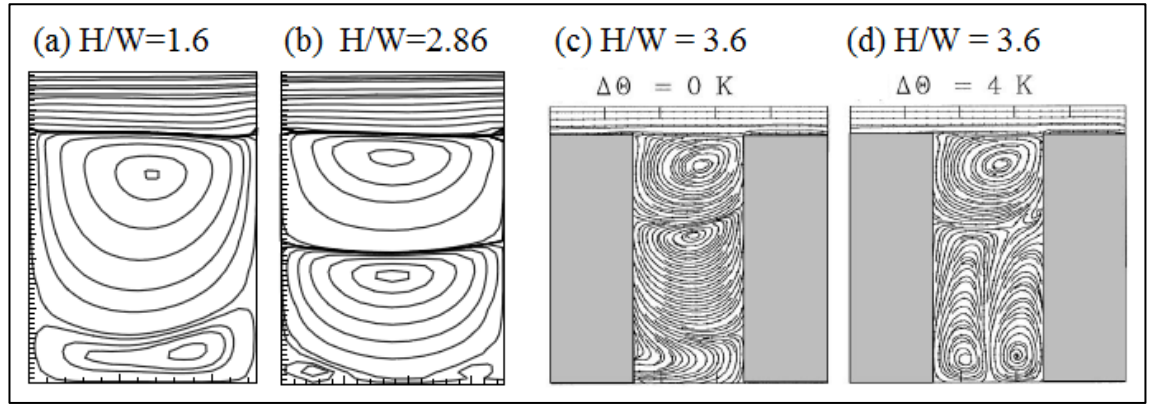


Fig. 4. 3: Streamlines of flow vortices within different aspect ratios of; (a) 1.6, (b) 2.86 with two circulations (source: adapted from Jeong and Andrews, 2002), and aspect ratio of 3.6 and potential temperature differences of (c) 0K, (d) 4K, with three-circulation regime (source: adapted from Kim and Baik, 2001).

However, in the current research, only flow speed of vortices at pedestrian level will be analysed, due to the nature of the investigation seeking for enhancing pedestrian level wind comfort, thus improving the outdoor pedestrian thermal comfort conditions. Nevertheless, increasing circulation regime within the urban street canyon may lead to pedestrian wind discomfort, as a result of increased wind speed. For example, Al-Sallal and Al-Rais (2011) found that when wind speed is higher than 5m/s wind can reach deeper inside the narrow streets. Although this case improved the circulation of wind flow in some places maximising thermal comfort, while creating vortices at the building corners causing wind discomfort to some extent at pedestrian level. However, in the current research the yearly average maximum wind speed in Madinah city was found to be 3.5m/s at the airport (Iowa State University of Science and Technology, 2015), while urban areas suffer from very low wind speed. Therefore, methods for increasing wind speeds should be investigated for such regions.

Jeong and Andrews (2002:1137) stated that “*compared with the better ventilation characteristics associated with better parallel flow, cross-flow produces partial isocirculation formed by a cascade of vortices that descends from the rooftop to the street*”. However, DePaul and Sheih (1986) argue that these type of vortices can limit air flow movement to funnel within the urban canyon to the crossing free stream, leading to trapped pollutants concentration. Nevertheless, this limitation may occur when parallel wind speed with street canyon is lower than perpendicular wind flow (e.g. Al-Sallal and Al-Rais, 2012).

#### 4.4. Best Practice for Urban Heat Stress Mitigation Techniques in Urban Canyons

The living conditions of people are very difficult in hot arid climates (Ali-Toudert et al., 2005), because of the extreme climatic conditions. However, the microclimate of an urban street in hot arid regions can be enhanced by using appropriate urban configuration strategies (e.g. urban ventilation, shading, urban materials alteration, anthropogenic heat release reduction, etc.), which can be regulated by adjusting urban design and planning policies (Ahranjani, 2010). However, the main limitation of these mitigation strategies is that their implementation is not always economically practical in the existing unplanned urban areas. Moreover, even after adapting proper mitigation strategies for different locations, the outcome could vary from one part of a city to another, which makes the mitigation strategies ineffective.

Many studies on different urban design strategies have been performed for outdoor thermal environments, which provide understanding of their effects on the thermal sensation of a person at street and pedestrian levels (as discussed in Chapter 3, also see Table 4.1). However, only a few have studied the effect of asymmetrical urban street canyon's aspect ratios (different heights to width ratio,  $H/W$ ) in relation to prevailing wind flow directions under different climatic conditions (e.g. Qaid and Ossen, 2014), while very little research on asymmetrical urban canyons' aspect ratio has been conducted in hot arid regions. Appropriate urban street geometry design can have a positive effect on airflow regime in hot climates, thus increased wind speed can reduce the urban heat stress and enhance pedestrian thermal comfort levels (Qaid and Ossen, 2014).

Various studies were conducted on the configuration of urban geometries (e.g.  $H/W$  height to width aspect ratios and street orientations) with urban microclimates but in relation to exposure to solar radiation (Xi et al., 2012; Johansson, 2006; Santamouris et al., 1999; Ali-Toudert et al., 2005; Ali-Toudert and Mayer, 2006; Coronel and Álvarez, 2001; Swaid et al., 1993). However, most of the previous studies have focused on symmetrical aspect ratios rather than asymmetrical ones, which limit the available knowledge on asymmetrical canyon studies. Very limited research has been conducted in hot arid climates on asymmetry urban street, particularly in a form of two building blocks (Ali-Toudert and Mayer, 2007; Todhunter, 1990) rather than rows of multiple buildings. However, the study of multi asymmetrical urban streets aspect ratios, i.e. diverse height-to-width ( $H_1/W - H_2/W - H_3/W$ ) ratios for at least three rows of multiple

buildings was not discussed in the context of urban and pedestrian microclimates in hot arid regions.

This represents a fundamental difference between the aim of the present research and the previous studies of Ali-Toudert and Mayer (2007) and Qaid and Ossen (2014). Further, Ali-Toudert and Mayer's study (2007) followed a different method of investigating the effects of asymmetrical urban canyons on thermal comfort, which is by manipulating an asymmetrical urban canyon with a wide opening to the sky and comparing an asymmetrical urban canyon with overhanging facades (i.e. smaller opening to the sky). The simulation outcomes revealed that the larger the openness of the canyon to the sky, the greater the heat stress. This study was conducted under hot arid climatic conditions of Ghardaia in the Algerian Sahara, using Env-met model and PET index for the simulation and calculation of thermal comfort, respectively. However, the study did not consider testing different aspect ratios (H/W) of the asymmetrical canyon in terms of altering buildings height. Instead, they have considered the openness to the sky, which seriously lacks in information on the effect of different asymmetrical aspect ratios on pedestrian wind environment, thus on pedestrian thermal comfort.

Other researchers studied the effects of both building shapes and arrangement of buildings in a chess-board design on airflow around multiple rows of buildings (particularly, three rows) in hot arid climates of Aswan and Farafra in Egypt (Figure 4.4), using CFD numerical simulation method (Rizk and Henze, 2010). They focused on the effect of narrow passages between buildings, canyons between rows of buildings and shapes of windward elevations on wind speed ratio. It was found that by creating a narrow passages of 6m between buildings at the same row and wider canyon (10m) between the buildings rows, the Aswan model, which uses rectangular shapes that have slope exterior wall in two directions at the windward elevations and wide distances between passages of buildings at the same row, can achieve 60-80% of wind velocity at the windward side of buildings at the second and third rows.

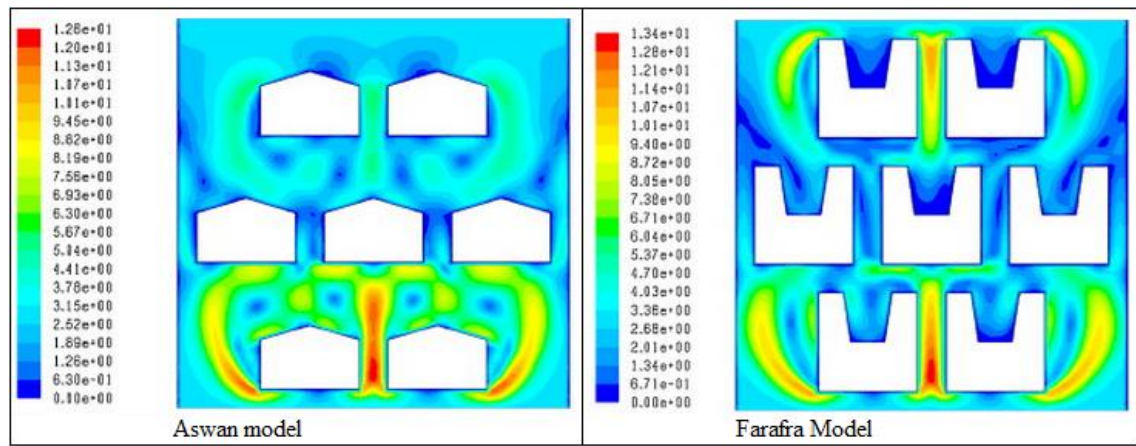


Fig. 4. 4: Velocity magnitude for Aswan and Farafra Models in hot arid Egyptian climate. Decreasing the passage between buildings while using wider street canyons. Source: Rizk and Henze (2010).

However, the model's results were based on high wind velocity input values of between about 12 to 13m/s, which may not be applicable for the current research of Madinah where the yearly average maximum wind speed was found to be 3.5m/s (refer to Chapter 2 for more detail). Nevertheless, the researchers found that a chess-board design arrangement for buildings rows can also increase wind velocity at both windward surfaces and narrow passages of the next row by increasing street canyon width to as much as 20m (Rizk and Henze, 2010). Similarly, it was found that in the Farafra model, which uses narrow distances between passages of buildings (i.e. 6m) at the same row and rectangular shapes that have trapezoid courtyards that face the wind, it is possible to achieve 33-41% of wind velocity at the windward surfaces and 38-70% at the second and third row, by using the chess-board design arrangement and increasing the canyons width. This evidence emphasises the importance of narrow passages which can increase wind velocity by venturi effect (channel effect, i.e. the effect where wind speed increases as it passes through a smaller openings) (e.g. Blocken and Carmeliet, 2004b), as increasing wind speeds is demanding in areas that suffer from very low wind to achieve thermal comfort (Qaid and Ossen, 2014). However, these case studies of Egypt of multiple rows of buildings did not consider the effect of increasing the urban street H/W aspect ratios (particularly increasing the height of buildings) on urban pedestrian microclimate or pedestrian thermal comfort conditions.

Other researchers studied the effects of building materials on outdoor urban thermal microclimates to control the reflectivity and absorption levels of solar radiation (e.g. Oke, 1982; Oke et al., 1991; Tan and Fwa, 1992; Ramadhan and Al-Abdul Wahhab, 1997; Priyadarsini et al., 2008; Taha, 1997; Akbari et al., 2009). For instance, Priyadarsini et al. (2008) have studied the effects of urban surface materials on air

temperature within an urban street canyon in a hot humid region of Singapore. It was found that air temperature in the canyon was significantly different when using high reflectance and low reflectance building surface materials. The results revealed that the high reflectance values will reduce the air temperature within the canyons. Hence, they have concluded that the type of surface materials and their colour are among the most important factors that can control the thermal microclimatic conditions. Surfaces of concrete, asphalt, bricks and other dark urban structures absorb more heat than lighter colour materials during the daytime, increase more heat in the air by convection, and re-radiate the absorbed heat back into the urban environment during the night (Oke, 1982; Oke et al., 1991). Therefore, in the current study, the effect of changing materials on urban microclimate will be considered, to improve the thermal comfort conditions in Madinah.

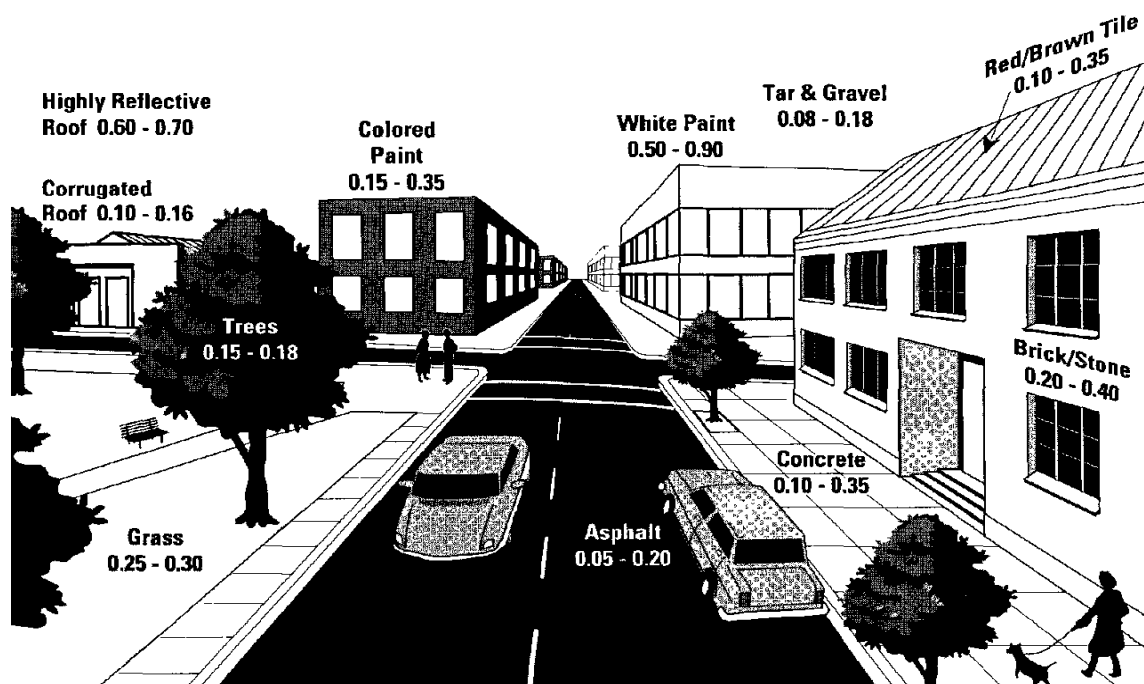


Fig. 4. 5: Surface albedo values. Surfaces with white paint usually have higher albedo than dark materials, and reflect more solar radiation and are generally cooler. Source: Akbari et al. (1992).

According to Ahranjani (2010), urban heat stress mitigation strategy of urban materials alteration may include using green elements, greening exterior walls and rooftops of buildings, reducing the asphalt-paved area, and using higher solar reflectance (albedo) materials on buildings. The latter two will be considered in the present study. However, increasing the number of vegetation in hot and arid regions is clearly resource intensive, as high evaporation rates may occur, and it requires water and maintenance. Akbari et al. (1992) have studies the albedo range in urban areas, as



highlighted in Figure 4.5, with higher albedo level is found in white paint with value range of 0.5 to 0.9.

Summaries of the findings from previous studies on urban microclimate design strategies and assessment of thermal comfort are listed in Table 4.1, and discussed in this chapter.

*Table 4. 1: Previous Studies on Urban Street Geometry (i.e. aspect ratio and orientation of an urban street canyon).*

<b>Researcher</b>	<b>Climate Region</b>	<b>Main Research Findings</b>	<b>Comments</b>
Mayer & Höppe (1987)	Munich, Germany (Hot Summer season).	Significant heat stress was found in the urban street canyon that is exposed to south. In contrast, highest amount of shading were found in the "trunk space of the tall spruce forest" exposed to north.	The research did not consider the effect of street orientation and aspect ratio.
Nakamura & Oke (1988)	Japan (Hot Humid)	This paper demonstrated that a number of useful relationships exist between the urban geometry and the urban microclimate of street canyons. In terms of H/W: a lower limit of about 0.4 is set by the need to provide some degree of shelter and to retain a reasonable proportion of the heat island warmth. An upper limit of 0.60-0.65 ensures that both atmospheric dispersion and solar access is maintained within the street canyons.	Hypothetical average of building heights can be based on this paper, which suggests for simplification of urban geometry.
Gut & Ackerknecht (1993)	Hot Arid	The straight streets with parallel buildings can maximise solar radiation, but by orienting the urban pattern diagonally to the east-west axis can provide both potential shade on the street and support the dynamic movement of air.	This study did not consider the effects urban street orientations with prevailing wind direction. It also did not consider the effect of aspect ratio.
Golany (1996)	Hot Dry	Straight and parallel urban streets with prevailing wind direction is better than perpendicular urban pattern to reduce the urban roughness, thus to support wind movement within the urban areas. However, the city boundary receives hot and dusty wind during the day and colder wind towards the latter part of the night. Perpendicular urban street to wind direction reduces the wind speeds and dust.	This study gives generic guidelines for urban designers. It focused on urban street orientation parallel with prevailing wind direction and perpendicular to wind. However, it neither took into the account for the effects of orientation of street on pedestrian wind flow rate, nor it considered the aspect ratio.
Pearlmutter (1998)	Negev in Israel (Hot Arid)	North-south axis orientated urban streets get cool air from the shaded north-northwest wind. Highest air temperatures observed in the E-W street.	This research focused on perpendicular and parallel street canyons that were symmetrical with a H/W ratio close to unity (single-storey row houses with a 3m width of narrow pedestrian rows). It did not consider the effect of different aspect ratios on air flow ratio.

Nishimura et al. (1998)	Japan (Hot Humid)	The effectiveness of water features in reducing the urban heat stress. Introducing artificial waterfall and spray fountain and urban canal facility in hot and humid urban spaces in Japan has reduced 11°C of surrounding air temperature.	This study did not consider the effects of building heights and urban street orientations on urban microclimate.
Santamouris et al. (1999)	Hot Summer of Athen	During the night period, the distribution of the street temperature across the canyon shows clearly that surface temperatures are higher in the middle of the canyon than in the area close to the building walls. The study of the air flow characteristics points out that for wind speed perpendicular to the canyon axis, the air flow inside the canyon is mainly characterized by either a circulatory vortex or a double vortex. Moreover, a strong relation between the velocity inside the canyon with the velocity above the buildings when wind flows parallel to the axis of the canyon, was found.	However, the buildings heights were symmetrical in the simulation. Only one aspect ratio H/W of 2.4 was studied base on field measurement, and no numerical study was conducted on various aspect ratios and orientation of streets.
Givoni et al. (2003)	Negev and Tel Aviv, Israel (Hot Arid)	The paper discusses methodological issues and carrying out problems in outdoor comfort research. The paper also summarises several studies going on presently in Israel and presents some of the actual experimental results from these studies.	This study did not consider methodological issues relating to urban street orientation and aspect ratio and their effects on outdoor pedestrian microclimate.
Ahmed (2003)	Dhaka, Bangladesh (Hot Humid)	Factors affecting thermal comfort in outdoor spaces and a comfort zone based on environmental parameters for outdoor urban spaces are presented.	This study was conducted in hot humid and not in hot arid region. It also did not consider the effect of urban street aspect ratio and orientation with prevailing wind speed.
Ali-Toudert & Mayer (2006)	Ghardaia, Algeria (Hot Dry)	The results show contrasting patterns of thermal comfort between shallow and deep urban streets, and between the various orientations studied. The comparison of all case studies reveals that the time and period of day during which extreme heat stress occurs, as well as the spatial distribution of PET index at street level; depend strongly on aspect ratio and street orientation.	In this study the wind direction was perpendicular to street axis. The results of the street orientation was based on different solar orientations (i.e. E-W, N-S, NE-SW and NW-SE) rather than orientation with prevailing wind directions. The aspect ratios H/W of 0.5, 1, 2, and 4 were simulated, but it was simplified to symmetrical urban street rather than variation of heights around the street.
Johansson & Emmanuel (2006)	Colombo, Sri Lanka (Hot Humid)	The study proposed several strategies to improve outdoor thermal comfort in the city of Colombo. To encourage airflow within an urban street, the research suggested using irregular positioning of buildings and creating variations in building height.	The research used PET index with maximum comfort band of 33°C. However, this study was conducted under hot humid conditions, and such comfort band may not apply to hot arid zones. This study has neither considered the effects of orientation of urban street with wind movements, nor did perform numerical simulation on the effects of aspect ratios on pedestrian wind flow patterns.

Johansson (2006)	Fez, Morocco (Hot Dry)	The comfort PET index indicated that deeper the street canyon (i.e. highly shaded street), which means higher aspect ratio (H/W) of urban streets, the lower the air temperature and fairly comfortable thermal conditions in summer. However, if there is a cold season as in Fez, the urban design should include some wider streets or open spaces or both to provide solar access.	However, this study was restricted to one type of urban design (i.e. aspect ratios), but has not considered orientation of urban streets with prevailing winds, which might contribute to enhance air movement pattern as well as thermal comfort levels, and no numerical simulation was conducted.
Shahidan & Jones (2008)	Proposed Concept (Hot Dry)	Three layers of plant cover will create a high quality shaded area, promote high humidity level, provide an optimum evaporative and convective comfort cooling and reduce the overall surrounding air temperature in urban area. The creation of landform will generate high wind speed that blow away warm dry air at the upper part of the canopy and provide a cooler moistened air underneath the canopy.	This theoretical based landscape design, which may need further investigation, has neither considered urban aspect ratio nor urban street orientations with prevailing winds.
Priyadarsini et al. (2008)	Singapore (Hot Humid)	It was found that the effect of facade materials and their colours was very significant and the temperature at the middle of a narrow canyon increased up to 2.5°C with the facade material having lower albedo. It was also found that strategically placing a few high-rise towers will enhance the air flow inside the canyon thereby reducing the air temperature.	This study considered both urban street orientation with prevailing wind speed and the aspect ratio. However, the study was conducted in a hot humid climate and did not focus on hot arid climate.
Al-Sallal & Al-Rais (2011)	Dubai, UAE (Hot Humid)	Traditional urban context resists funnelling of airflow inside the streets at pedestrian level when the prevailing wind is as lower than 3m/s, however, when wind speed is higher than 5m/s wind can reach deeper inside the traditional narrow streets. The latter case improved the circulation of wind flow in some places maximising thermal comfort, while creating vortices at the building corners causing wind discomfort to some extent at pedestrian level.	This numerical study (based on CFD analysis) did not consider the effects of different aspect ratios and orientation with wind directions.
Al-Sallal & Al-Rais (2012)		In modern urban context, airflow funnelled more rigorously between the urban blocks and dispersed randomly in the street canyons, improving the circulation of wind flow to some extent, while creating vortices. However, wind flow decreased when faced the buildings, funnelled by the wider street canyons, then increased once again when reached the free stream area. The wind velocities were more comfortable in wider street canyons with aspect ratio H/W of 1.75.	However, this study was based on CFD simulation analysis of existing situation, while did not consider testing the effects of altering urban geometry (i.e. various aspect ratios and orientation with prevailing wind directions).

Zhang et al. (2011)	Hong Kong, China (Hot Humid)	This study investigated the ventilation and thermal comfort of the environment surrounding a new university building under construction. The results indicated that wind availability was determined by effective building shape, building locations and wind direction.	However, the focus of the study was on the effect of annual average wind speed in eight prevailing wind direction around one building, but it did not analyse the effect of orientation of an urban street.
Yuan & Ng (2012)	Hong Kong, China (Hot Humid)	Wind speed is significantly decelerated, especially in deep street canyons across the wind direction of 90°. When the input wind direction is changed from 90° to 45° air flow can enter into the streets from both directions. Therefore, areas with stagnant air are decreased. In the input wind direction of 0°, air flow can penetrate more deeply into the streets than those in the prevailing wind direction (90°).	However, this study was based on testing different wind speed value with three wind direction for two parallel cubic buildings, but it did not consider the effects of these values with different urban aspect ratios.

#### 4.5. Urban Roughness and Pedestrian Wind Flow Regime around Buildings

Airflow regime can directly influence pedestrian's thermal sensation levels. For example, Priyadarsini et al. (2008) have studied the effects of high rise buildings on wind environment. They found that strategically placing a few high-rise towers will enhance the air flow inside the canyon thereby reducing the air temperature. However, their study on the effects of different aspect ratios focused only on two building blocks, but did not consider the effects of multiple blocks in each row of buildings along the street canyon. According to Santamouris et al. (1999), in a deep urban street, wind flow at street level is influenced by the prevailing wind speed above the building roof, the vertical stratification of air inside the canyon and the advection mechanism from the buildings corners.

According to Oke (1988), there are three main zones of flow disturbance in an envelope surrounding an isolated building, including: 1) a bolster eddy vortex caused by flow down a windward building façade; 2) a lee eddy drawn into the cavity of low pressure behind the building caused by flow separation from the building corners and its top roof (i.e. sharp edges); and 3) further downstream is the building wake that have higher turbulence by lower horizontal speeds than the undisturbed wind flow. The vertical air stratification inside the canyon and vortices types have further illustrated by Blocken and Carmeliet (2004b) and explained in the following context, which are important for the study of pedestrian wind environments, particularly for the current

case study of Madinah where wind speed in compact urban areas is very low (i.e. lower than 1m/s).

According to Blocken and Carmeliet (2004b), knowledge of urban aerodynamics has explained that as the wind approaches a wide high-rise rectangular building block it gradually diverges, due to the high pressure differences around the building. Figure 4.6 shows that the wind in the upstream separates as it approaches the building into parts, where some flows deviate over and around the block. Other parts of the approaching wind deviate from the maximum pressure at the stagnation point of the windward façade (situated at 70% of the building) to the lower pressure areas situated in the followings: the upward (i.e. top of the building), downward (at the ground level) and sideward of the building façade. Blocken and Carmeliet (2004b) have also explained that the downward flow feeds vortices near the ground (i.e. standing vortex, base vortex or horseshoe vortex), which also separates from the stagnation point at the ground level and flows to the lower pressure at the sideways, forming corner streams (i.e. vortex wrapping around corners) with high speed values. Flow direction near ground or pedestrian levels is opposite to the approach flow direction. Thus, these vortices are important to be considered in the analysis of pedestrian level microclimate.

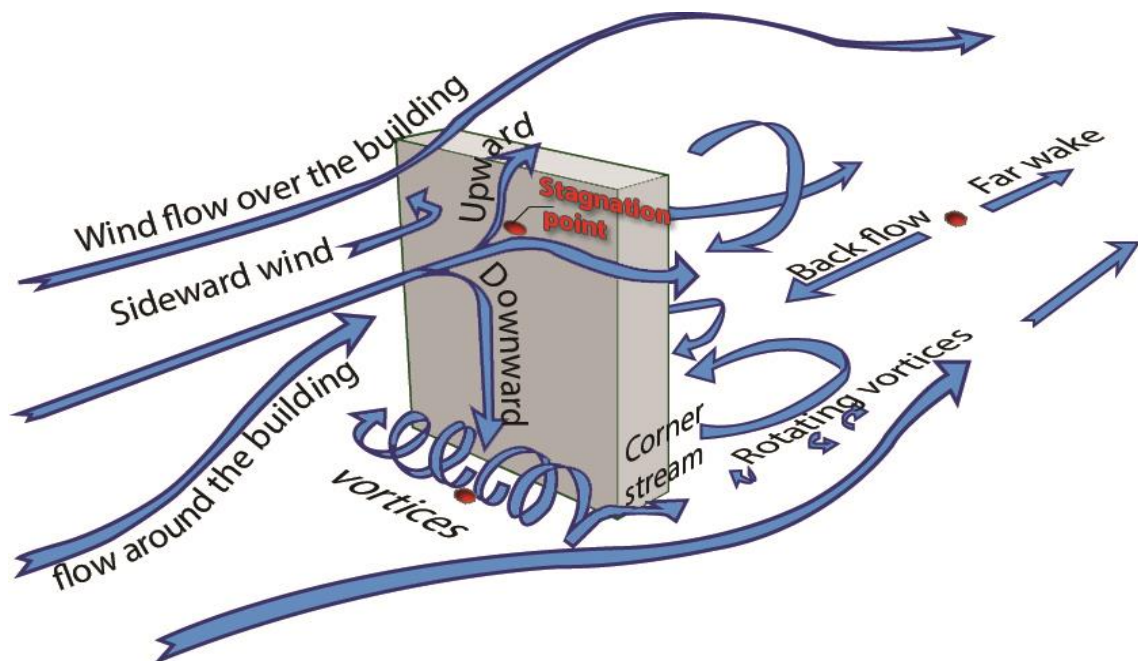


Fig. 4. 6: Representation of wind flow divergence around a rectangular building, which is caused by pressure difference. Source: re-illustrated from Blocken and Carmeliet (2004b).

At the leeward side of the building, a separation bubble occurs due to its under-pressure zone. Thus, this would influence the wind flow in the downstream at a stagnation zone at ground level by creating back flow recirculation, thus large rotating

vortices are created behind the building. For oblique wind at  $45^\circ$ , corners streams are more severe, while a jet with increased wind speeds can be found at a passage between buildings and behind the buildings, while the bar effect is observed behind the building when the wind direction is about  $45^\circ$  (Blocken and Carmeliet, 2004b). In contrast, a tall building with narrow windward façade can deflect the flow side-ways. Thus, the standing vortex very rarely occurs and the normal direction of the flow would resume rapidly. The current research should validate its simulation results based on the above mentioned description of previous researchers on pedestrian wind environment. However, it should be acknowledged that the study by Blocken and Carmeliet (2004b) is for flow around an isolated building and more complex when many are considered as in the current research.

The total array of roughness elements (e.g. buildings, trees, etc.) influences the production of mechanical turbulence and the form of the vertical wind profile (Oke, 1988). According to Lam (2010:57), the growing number of buildings as the urbanisation process “*increases the roughness of the surface underlying the atmosphere and exerts a drag on the low-level winds*”, which can decrease the wind speed near the ground in the long run. Thus, according to Clarke et al. (1982), the aerodynamic roughness length ( $z_0$ ) is the critical surface parameter governing the production of turbulence in the urban boundary layer. According to Blocken et al. (2007), this is an important parameter when evaluating wind environments at pedestrian as well as urban levels using numerical models.

The terrain roughness of urban constructions, geographic and natural features has great transforming effects on the aerodynamics of the wind, including effects on air velocity, air direction and turbulence intensity (ASCE, 1996; Mochida & Lun, 2006). Stankovic et al. (2009) have specified three deferent types of aerodynamic roughness length ( $z_0$ ), which are: (1) city centre terrain, ( $z_0 > 0.7$ ); (2) suburban terrain, ( $z_0 = 0.25 - 0.3$ ); (3) an open field terrain, ( $z_0 = 0.01 - 0.03$ ). These are reflected in following graph (Fig. 4.7), with the use of a required displacement length ( $d$ ) by each profile, and reflecting the way the profile is displaced relating to the height and density of the obstacles. Thus, in the current research the roughness length of between 0.25 and 1.0m will be considered in the simulation modelling (e.g. Blocken and Carmeliet, 2004b; Oke, 1988).

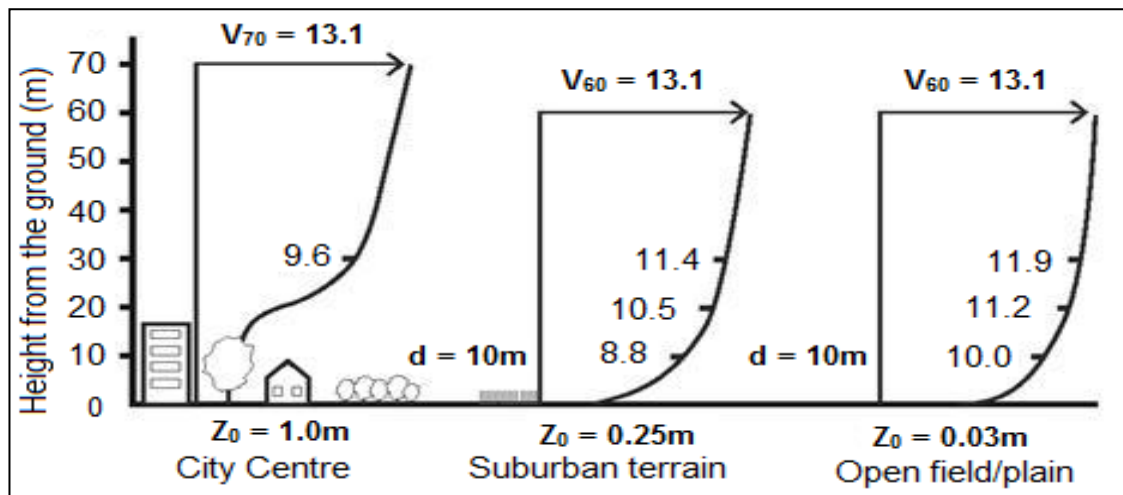


Fig. 4. 7: Wind velocity profiles reflecting deferent terrains roughness as well as aerodynamic roughness ( $z_0$ ) regarding the height from the ground and the use of a required displacement length ( $d$ ). Source: Stankovic et al. (2009:78).

According to Klemm (2007), the common problems of airflow in urban areas on microclimatic scale are the excessive air flow in buildings vicinity, the formation of strong turbulences in certain areas, and sometimes lack of ventilation in areas concentrated with high-rise buildings, which may result in concentration of pollutants and trapped heat, and can lead to pedestrian wind and thermal discomfort. Blocken et al. (2009b) indicated that uncomfortable high wind speed and wind danger can be introduced at pedestrian level by improper planning of high-rise buildings. This phenomenon was reported by Wise (1970) leading to shops being untenanted due to the windy environment that discouraged people from shopping.

Table 4.2 lists the Extended Land Beaufort Scale for wind effects on people. In this table, Lawson and Penwarden (1975) described wind speed at 1m/s or less as light air to calm air with no noticeable wind effect. This level of speed is common in urban pedestrian microclimates in Madinah (Setaih et al., 2013a). However, Rizk and Henze (2010) suggest the acceptable wind velocity range in hot arid climates to achieve thermal comfort for air temperatures that exceed 32°C in shade, with a lower limit threshold of 1.6m/s (based on ASHREA Standard 55, 2004), and upper limit of 3.8m/s (based on Beaufort Scale). The suggested upper and lower wind velocity limits have been used as reference in the current research. However, it is acknowledged that it may not be possible for wind velocity alone to achieve thermal comfort, as there are other microclimatic factors (e.g. mean radiant temperature, relative humidity, etc.) that can have effects on pedestrian thermal comfort conditions. Nevertheless, the estimated upper PET thermal comfort limit of 31.3°C and lower limit of 21°C have been used as a reference in this study since no other reference values calibrated for Madinah.



Moreover, moving air can result in a favourable cooling effect in the hot season when the heat is removed from the body by convection and evaporation, however completely still (i.e. less than 0.1m/s) or too fast (i.e. greater than 6 m/s), air movement may cause discomfort (Gaitani et al., 2007; and CIBSE, 2006a; Streinu-Cercel et al., 2007) or even wind danger (Blocken and Carmeliet, 2004b).

Table 4. 2: Extended Land Beaufort Scale showing wind effects on people. Source: Lawson and Penwarden (1975).

Beaufort Number	Description	Wind Speed at 1.75 m height (m/s)	Effect
0	Calm	0.0–0.1	
1	Light air	0.2–1.0	No noticeable wind
2	Light breeze	1.1–2.3	Wind felt on face
3	Gentle breeze	2.4–3.8	Hair disturbed, clothing flaps, newspaper difficult to read
4	Moderate breeze	3.9–5.5	Raises dust and loose paper, hair disarranged
5	Fresh breeze	5.6–7.5	Force of wind felt on body, danger of stumbling when entering a windy zone
6	Strong breeze	7.6–9.7	Umbrellas used with difficulty, hair blown straight, difficult to walk steadily, sideways wind force about equal to forwards walking force, wind noise on ears unpleasant
7	Near gale	9.8–12.0	Inconvenience felt when walking
8	Gale	12.1–14.5	Generally impedes progress, great difficulty with balance in gusts
9	Strong gale	14.6–17.1	People blown over

However, according to Bottema (2000: 2&3) “*pedestrian discomfort occurs when wind effects become so strong and occur so frequently (say on time scales up to 1h), that people experiencing those wind effects will start to feel annoyed, and eventually will act in order to avoid these effects.*” However, this definition suggests that wind effects do not necessarily indicate wind discomfort (Blocken and Carmeliet, 2004b). Thus, Bottema (2000) proposed wind discomfort criterion (Wind Discomfort = mean wind speed + turbulence intensity > 6m/s) which agrees with previous researchers that the discomfort threshold value at pedestrian height is greater than 6m/s. However, this threshold is more suitable for walking, while different threshold may apply for other human activities.

#### 4.6. Effect of Air Movement on Temperatures in Urban Contexts

Wind speed and direction plays a large role in mitigating the heat stress in the urban thermal environment (Blocken and Persoon, 2009). For example, Cheng et al. (2007) studied the effects of wind on human thermal comfort for the people of Hong Kong during the summer. Their results of the experimental study have shown that by

increasing the wind speed from 0.3 m/s to 1 m/s a 2°C of air temperature was dropped at 1.75m height (i.e. presuming the pedestrian level). This demonstrates the strong relationship between air speed and air temperature in urban microclimate. Variation of buildings' height and orientation of urban street with wind direction can control the speed of air movement. Givoni (1998) emphasised that the wind conditions can be controlled by the density of the urban area, appropriate size and height of single buildings, proper implementation of high-rise buildings and the orientation and width of the urban canyons.

Zhang et al. (2011) have conducted a numerical study (using CFD Fluent code) to study the ventilation and thermal comfort of the environment surrounding a new university building under construction. The results indicated that wind availability was determined by effective building shape, locations and wind direction. However, the focus of the study was on the effect of annual average wind speed in eight prevailing wind directions around one building in an urban area on the surrounding pedestrian microclimate, but it did not consider the analysis of an urban street.

Al-Sallal and Al-Rais (2011 & 2012) studied outdoor airflow analysis and potential for passive cooling in the traditional urban context and modern urban context of Dubai. The findings revealed that the traditional urban context resists funnelling of airflow inside the streets at pedestrian level when the prevailing wind is lower than 3m/s, however, when wind speed is higher than 5m/s, wind can reach deeper inside the traditional narrow streets. The latter case improved the circulation of wind flow in some places maximising thermal comfort, while creating vortices at the building corners causing wind discomfort to some extent at pedestrian level. In the modern urban pattern, airflow funnelled more rigorously between the urban blocks and dispersed randomly in the street canyons, improving the circulation of wind flow to some extent, while creating vortices. However, wind flow decreased when faced the buildings, funnelled by the wider street canyons, then increased once again when reached the free stream area. The wind velocities were more comfortable in wider street canyons with aspect ratio  $H/W$  of 1.75. Moreover, the wind velocity remains stable in the longer urban street canyons at low values of 0.5m/s and 1.5m/s in the winter and the summer, respectively. However, these studies were based on CFD simulation analysis of existing situation, while did not consider testing the effects of altering urban geometry (i.e. various aspect ratios and orientation with prevailing wind directions).

According to Santamouris (2001) and the findings revealed by Priyadarsini et al. (2008), it was concluded that the temperature in the urban canyon is strongly influenced by the surface temperature of the canyon, and it is mainly controlled by the process of air movement through convection. The researchers also pointed out that the orientation of urban street has a minor effect on the air temperature in the middle of urban canyons. However, the appropriate orientation of urban street might promote driving the wind into the thermal space, which may lead to the reduction in the temperature of the urban surfaces.

For example, Yuan and Ng (2012) studied the effects of different urban morphologies on the pedestrian-level natural ventilation in high-density areas in a hot humid region of Hong Kong, using a computational fluid dynamics (CFD) simulation method. They conducted many testing scenarios for regular urban streets surrounded by random cubic buildings in three wind directions ( $0^\circ$ ,  $45^\circ$ , and  $90^\circ$ ). The  $90^\circ$  is the prevailing wind direction (i.e. along small buildings wall arrays), while  $0^\circ$  (i.e. wind direction along longer buildings wall arrays) and  $45^\circ$  (wind direction along both buildings walls) were simulated to describe comprehensively the natural ventilation performance in different wind directions.

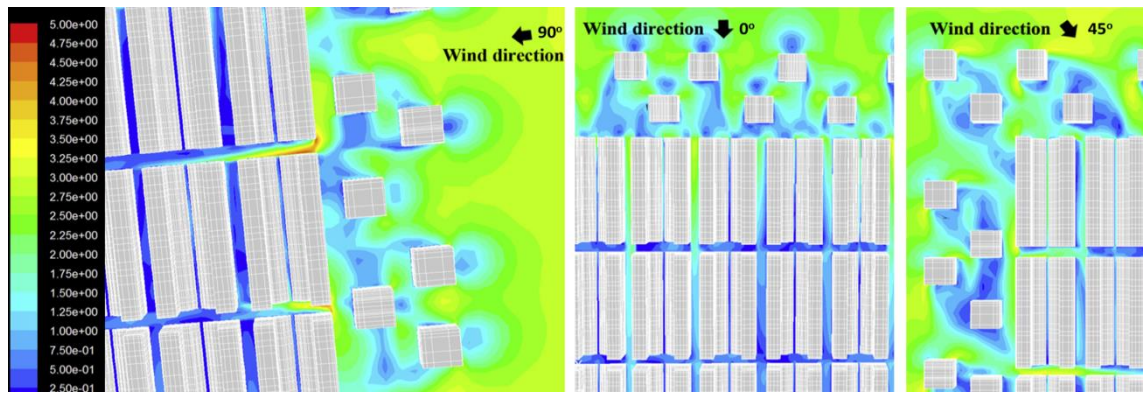


Fig. 4. 8: Wind speed contours extracted from CFD simulation at 3.5m above the ground for urban streets orientations with three wind flow directions ( $0^\circ$ ,  $45^\circ$ , and  $90^\circ$ ) in Hong Kong. Source: Yuan and Ng (2012).

Their findings revealed that wind speed for the  $90^\circ$  orientation in the urban area was accelerated at some street canyons along with the prevailing wind direction, while at further street canyons wind speed was significantly decelerated. However, when the orientation of urban street with wind direction was changed from  $90^\circ$  to  $0^\circ$ , air flow penetrated more deeply into the urban streets than those in the prevailing wind direction of  $90^\circ$ . This could be because of the length of buildings wall is larger in case of  $0^\circ$  than the smaller walls in case of  $90^\circ$  that are parallel with wind direction, as illustrated in

Figure 4.8. Whereas with the orientation of  $45^\circ$ , air flow was entered into the streets from both directions and has improved the air speed in comparison to the other two simulated scenarios. However, these data were obtained for high rise buildings, but at 3.5m above the ground and not at normal pedestrian's height (i.e. between 1.5 to 2m). The study also did not consider the effects of different aspect ratios on wind environment, and it was limited to the urban wind environment in a regular street grid.

According to Pearlmutter et al. (2007:2408), findings of a semi-empirical study have indicated that *“in a hot-arid environment, the thermal comfort of pedestrians may be modified dramatically by street geometry alone. Such modification, however, are contingent on both the aspect ratio and the directional orientation of the street. While daytime comfort may be drastically improved by compact sectional proportions ( $H/W$  in the range of 1.0-2.0) when the street is oriented north-south or close to it, corresponding modifications in east-west streets are not evident”*. In a hot arid Algerian case study, it appears that the air temperature is more sensitive to the aspect ratio than the orientation, which is due to the shading effect from adjacent buildings (Ali-Toudert and Mayer, 2006). As it was observed that the differences in air temperature between the same aspect ratio of both the orientations (E-W and N-S) are small. However, this case study was conducted with wind direction that was perpendicular to both street axes, and has not taken into account the effects of parallel wind direction on the air temperature of these orientations and aspect ratios. Therefore, the perpendicular incidence on street axis has led to a skimming flow regime and a strongly reduced wind speed in all streets at pedestrian level (i.e. from 5m/s to 0.3m/s) (Ali-Toudert and Mayer, 2006).

On the other hand, Pearlmutter (1998) asserted that a parallel urban canyon with prevailing wind direction has higher wind flow rate than the perpendicular canyon to prevailing wind direction. Lee and Wong (2014) observed that for oblique wind at  $22.5^\circ$ ,  $45^\circ$ , and  $67^\circ$  from north have slightly higher speeds in the canyons than at  $0^\circ$  and  $90^\circ$  (from north), at pedestrian level. However, this was due to absence of clear straight canyons in their simulated study, as illustrated in Figure 4.9, which has reduced wind speed magnitudes in  $0^\circ$  and  $90^\circ$  wind directions cases.

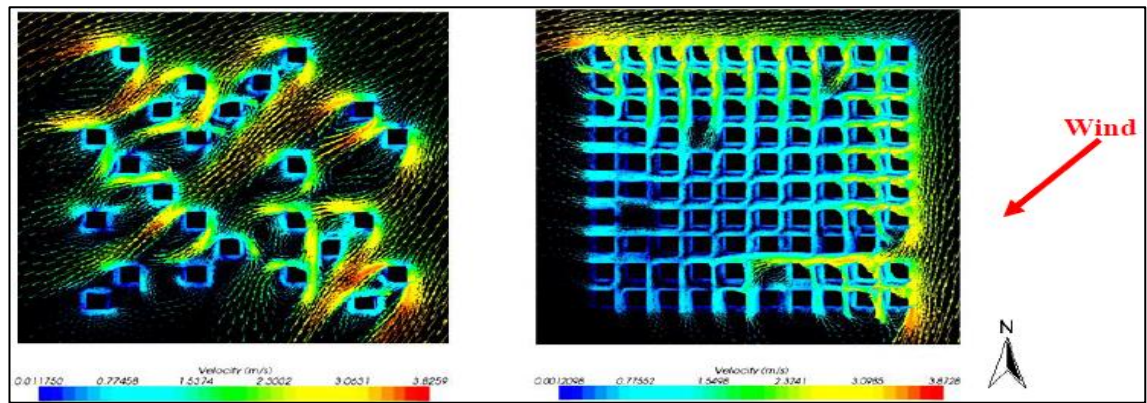
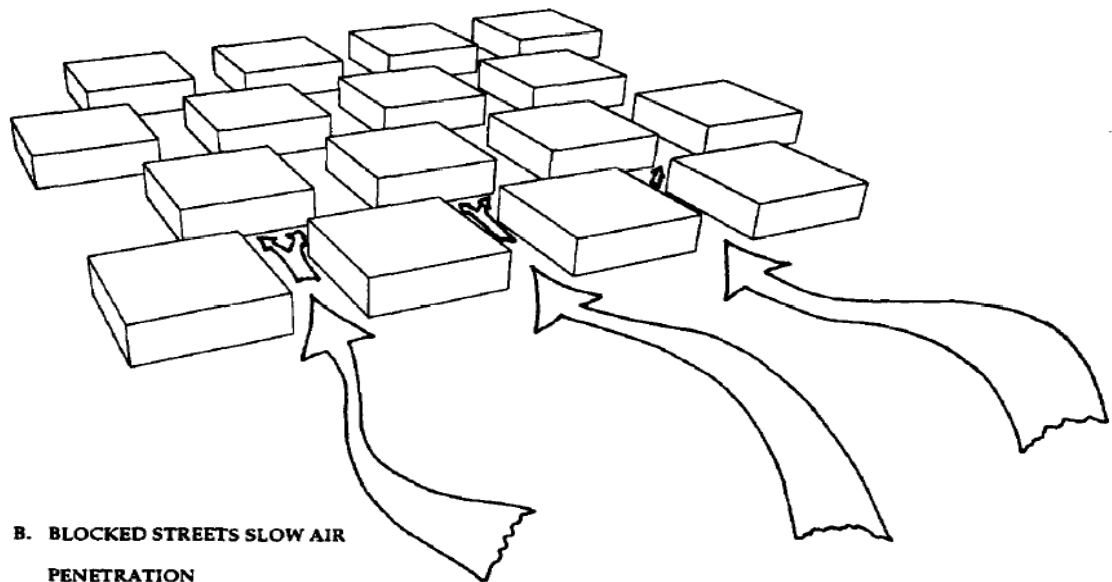
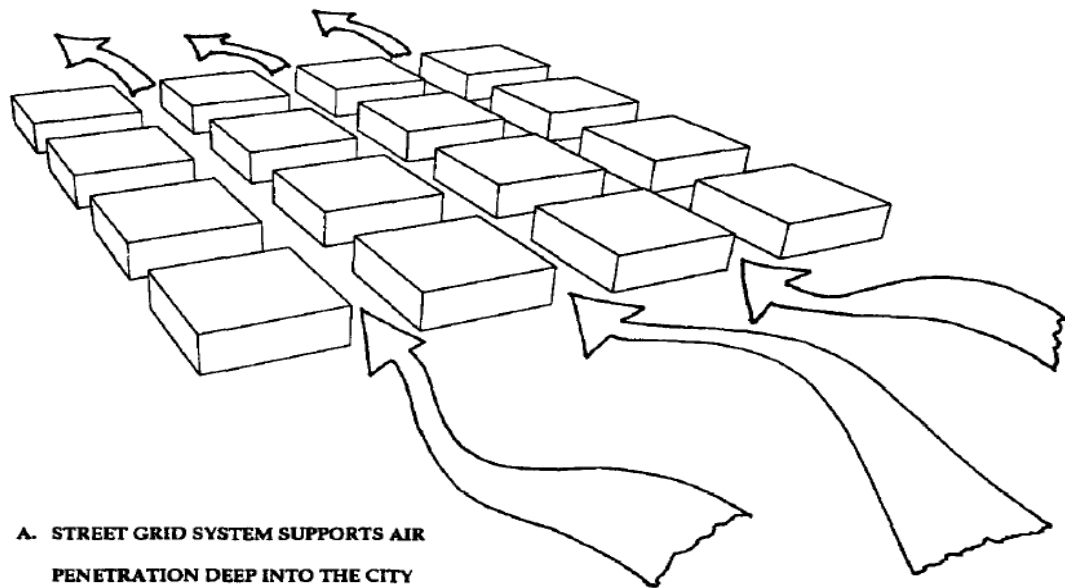


Fig. 4. 9: Oblique wind direction at  $45^\circ$ . Source: Lee and Wong (2014).

The guidelines assumed by Golany (1996) for the design of urban residential streets suggest that: to support air movement into and within the urban areas, urban streets should be designed straight and parallel to each other (figure 4.10a); however, the city boundary receives hot and dusty wind during the day and colder wind towards the latter part of the night. On the other hand, the wind blowing through the sandy streets or vacant plots (i.e. unpaved sections of the city) with no vegetation covers may cause dust turbulence and bring intense heat. Whereas, perpendicular urban streets to each other (Figure 4.10b) can reduce dusty winds, but still bring warmer winds during the daytime and cooler at night at decreased wind velocity (Golany, 1996).



*Fig. 4. 10: Different street patterns (e.g. A) grid block position style, B) chess-board style) can affect the wind velocity and blocking ratio of dusty winds. Source: Golany (1996).*

Other researchers (i.e. Gut and Ackerknecht, 1993) also agree with Golany's suggestions, however, they argue that the straight streets with parallel buildings can maximise solar radiation, but by orienting the urban pattern diagonally to the east-west axis can provide both potential shade on the street and support the dynamic movement of air (Fig. 4.11a). However, most importantly is the form of alleys and buildings such as narrow zigzagging alleys and alleys with blocked streets. For example, zigzagging narrow alleys receive minimum radiation within the above mentioned diagonal urban grid, as it can also reduce the effect of stormy winds, and provide shaded spaces throughout the day, thus the provision of a cool and enhanced microclimate in summer,

while relatively warm during cold nights and in winter (Fig. 4.11b) (Gut and Ackerknecht, 1993). Similarly, blocking streets or perpendicular streets to each other with the concept of diagonal urban pattern to east-west axis can retain ventilation in closed patios open to the sky, reduce the effects of sandy storms, and minimise radiation or maximise shade (Fig. 4.11c).

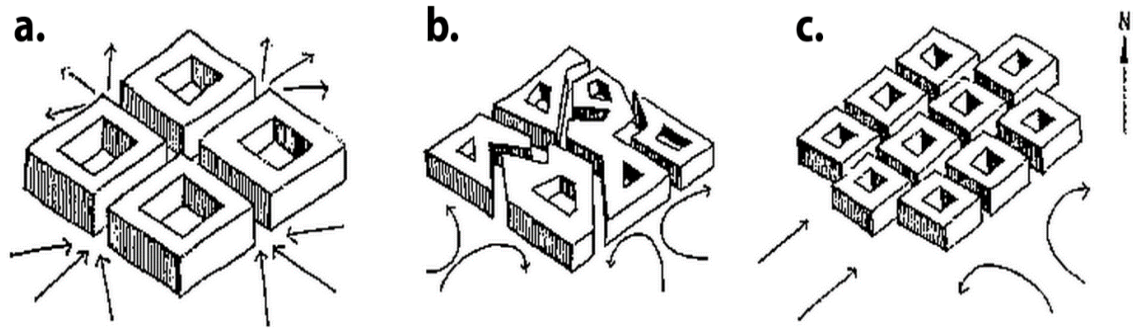


Fig. 4. 11: Orientation of Urban pattern diagonally to east-west axis. a) Is a grid pattern; b) Narrow zigzagging alleys; and c) Blocking streets or perpendicular. Source: Gut and Ackerknecht (1993).

According to Erell et al. (2011), the average wind flow over ground level is usually in a horizontal direction especially in flat and smooth areas; however, in urban areas, where physical obstacles usually occur, the wind gets obstructed causing the modification of the flow pattern (this proportion of obstructed air is known as the boundary-layer). According to Blocken and Carmeliet (2004b) the construction of buildings and other obstacles such as trees etc. can change the wind speed and wind direction, as well as air pollution, driving rain, radiation and daylight; and they are mainly dependant on physical aspects including the shape, size, and orientation of the structure.

Oguro et al. (2002 in Japanese, cited in Murakami (2006)) simulated the effect of orientation of buildings with prevailing wind directions. The results indicated that after the rearrangement of several buildings with wind direction (from Fig. 4.12a to 4.12b), the movement of markers in the ventilation path through the urban complex (adjacent to a river during summer) has become efficiently active, with increased air speed. Moreover, findings of numerical simulation studies have shown that the appropriate urban arrangement with wind can favourably cause wind speed acceleration near buildings corners, which can improve the process of ventilation (Klemm, 2007). Priyadarsini et al. (2008) have analysed that 90% of air velocities of three points along a length of 250m of urban canyon, in Singapore, were increased by structuring high-rise buildings at the entrance of the street, which have enhanced the air temperature by reducing 1°C. This is another example that shows the strong relationship between air



speed and air temperature. However, inappropriate location of high-rise towers may lead to increase in the temperature as well as the wind discomfort between the buildings, which can be as a result of the heat dissipation from the condensing air conditioners that generate thermal buoyancy effect, which causes an internal hot air flow (Priyadarsini et al., 2008).

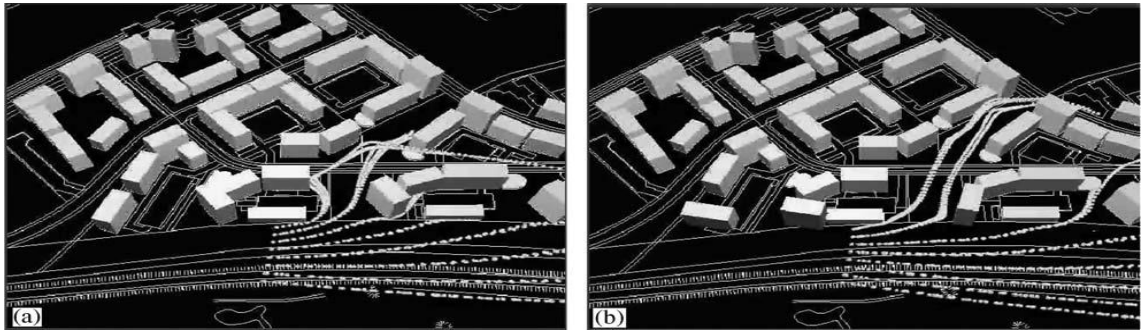


Fig. 4. 12: Movement of Markers in the ventilation path: (a) before the rearrangement; (b) after the rearrangement. Source: Oguro et al. (2002); cited in Murakami (2006).

The assessment method detected from the previous researches have used CFD numerical simulations, thus the following section evaluates this method.

#### 4.7. Assessment Approach of Urban Pedestrian Microclimates in a Street Canyon

There are different methods used to analyse urban heat stress and to enable the design of adaptive thermal comfort, including observational approaches (discussed in the previous chapter 3 in section 3.8) and simulation methods (Mirzaei and Haghighat 2010). Recent technologies have introduced new opportunities to integrate computational fluid dynamics (CFD) simulation system in urban design studies (e.g. Ansys Fluent and CFX, ENVI-met, etc.) to understand the patterns of wind flow through the built environment and its effects on human thermal comfort conditions (Chung & Choo, 2011; Tominaga et al., 2008). According to Arnfield (2003), numerical modelling has the apparent benefits over comprehensive field measurement on justification of their controllability and frugality of time and resource. The research also stated that numerical simulation is a perfectly suited methodology to dealing with the difficulties of urban complex environment system. Energy balance models and computational fluid dynamics (CFD) are among these models, which showed the most reliable and satisfactory outcomes.

Energy balance models take account of the energy exchanges with surfaces and ambient air in the urban canopy. These models can be used to predict the ambient temperature and surfaces temperatures of buildings, pavements, and streets. These types



of models are quick to run and can provide accurate results. However according to Mirzaei and Haghighat (2010), a major drawback is that the technique does not include air velocity, and separates temperature and velocity fields, such that the assumptions used do not always accurately represent the interaction of velocity and temperature in reality. Moreover, the geometry and buildings complexity are approximated in this model with limited grids on the wall surfaces. Thus, this makes the spatial resolution of the energy conservation method very weak, particularly when it is required to investigate the thermal comfort at pedestrian level.

Alternatively, computational fluid dynamics (CFD) can solve simultaneously all the governing equations of fluid flux inside the urban street canyons, including velocity, temperature, etc. Researchers have asserted that CFD is a validated method and its outcomes are quite reliable when compared with in-situ measurements and wind tunnel results (Chung et al., 2011:39; Tominaga et al., 2008:1759; Yoshie et al., 2007:1572). However, existing knowledge has not yet defined how such systems should be operated to enhance the thermal comfort level for outdoor pedestrian spaces. Such a definition may require inputs of environmental parameters, urban interventions and behaviour of space users.

Thus, CFD is capable of predicting more accurate environmental information required for the prediction of thermal comfort and solving wind issues in urban canyons. Lists of advantages and disadvantages of CFD are explored in Setaih et al. (2013a;b;c & 2014). However, in order to obtain accurate results, each boundary layer must be modelled in detail, which requires complex high-resolution grids and makes the process complicated and difficult (Blocken et al., 2009a). Erell et al. (2011) also corroborated the difficulty of modelling the boundary conditions in an urban area with a high degree of accuracy in order to obtain useful results from CFD. According to Mirzaei and Haghighat (2010), the main problem with CFD is that the atmospheric interactions of a city are complicated and their analysis requires a vast number of nodes to simulate a city. Another problem is that it is difficult to match the temporal and spatial resolution of the interactions within a city. For example, the different scales of atmospheric turbulence and canopy-scale turbulence. These factors must be simplified and modelled separately in the CFD process, which affects the accuracy of the results. Erell et al., (2011) add that the calculations obtained from CFD are limited to short periods of time and the methodology cannot be applied to problems requiring time scales longer than a few days.

According to Erel et al. (2011), the CFD technique has been used for analysing the air movement around buildings (e.g. Gousseau et al., 2013), wind comfort conditions at pedestrian level (e.g. Stathopoulos, 2006), to study the effects of wind driven rain (e.g. Blocken and Carmeliet, 2004a), and many other urban applications including the impact of vegetation, water ponds and surface materials on urban thermal environment (e.g. Robitu et al., 2006). Many researchers have validated the use of CFD, as it was found that the microclimatic results obtained from CFD are very reliable when compared with the results of field measurements and wind tunnel (Tominaga et al., 2008; Yoshie et al., 2007).

However, Mirzaei and Haghighat (2010) imply that one of the difficulties in analysing a specific urban micro-climate, within an urban street canyon, and designing suitable mitigation measures, is that this micro-climate is being the result of a multitude of micro-scale processes such as human metabolism, and middle-scale interactions including wind, temperature, humidity and other atmospheric forces. Thus, in analysing this type of climate, it is not always possible to integrate all the contributing factors accurately and therefore a designer must make certain assumptions and simplifications in the analysis process. Therefore, many studies simplified their simulation model to non-homogeneous buildings shape and material, ignoring small details of stationary and mobile objects within the street canyon, and discrepancy in providing boundary conditions (Mirzaei and Haghighat, 2010). However, these simplifications can make the results less effective.

#### **4.8. Previous Numerical Simulation Studies on Urban Microclimate and Thermal Comfort Using CFD Tool**

There are very limited on-site and numerical integrated studies for the assessment of outdoor urban thermal behaviour in general (e.g. Gómez et al., 2012; Hataya et al., 2006; Priyadarsini et al., 2008; Fintikakis et al., 2011; Shahidan et al., 2012), whereas the majority of the integrated studies were performed for the validation purpose in wind comfort studies at pedestrian level (e.g. Blocken et al., 2012; Mochida et al., 2006b; etc.), and wind studies at building level (e.g. van Hooff and Blocken, 2010; etc.). This gap in the literature is even wider when considering pedestrian thermal comfort in particular (e.g. Stavrakakis et al., 2012). CFD simulation tool is a very powerful tool for modelling complex fluid flows in urban areas and around buildings, with no limitation on the number of measurement point locations in the model comparing with the wind tunnel tests (other tools are compared and explored in Setaih et al., 2014 & 2013c). Summaries of the findings from previous numerical studies on urban microclimate using CFD technique are listed in Table 4.3, and discussed in the following paragraphs.

Researchers such as Stavrakakis et al. (2012) have investigated in detail the prediction of outdoor thermal comfort. They have created a new methodology for effective bioclimatic-design applications in the urban environment through implementing a human thermal comfort index into a computational fluid dynamics (CFD) code. However, the data used in their study was based on the meteorological station (located on the roof of a city-hall building), and not directly from urban street or pedestrian levels of the case study, which can lead to less accurate results than the actual in-situ measurements method. The most current research on outdoor thermal comfort has used both approaches of field study and CFD simulation (e.g. Zoras et al., 2014). This research has validated CFD with in-situ measurements in the field of heat mitigating strategy and enhancement of thermal comfort in urban open spaces, which was conducted in the Greek city centre of Florina. However, the main focus of their research was only on the effect of surface materials on the urban microclimate, and does not include the assessment of thermal or cooling effect of other urban interventions on the environment (e.g. buildings arrangement with the cooling effects of wind movement and direction; as well as shading effects of urban H/W ratios). Furthermore, the study lacks the use of a human thermal comfort index that is necessary for the prediction of pedestrian thermal comfort conditions. Thus, the current research seeks to cover these gaps in the research. Nevertheless, the methodology for conducting CFD simulation to

obtain microclimatic data of the existing situation as well as the data for modified urban microclimate design is fundamental, which is explored further as methodology guidelines in Chapter 5.

Bottillo et al. (2014) conducted microclimatic analysis in a typical urban configuration, using a CFD (Ansys-Fluent code) method for a N-S oriented urban street canyon with a given H/W aspect ratio. Their study used the standard  $k-\varepsilon$  model to simulate a three-dimensional flow field with the aim to investigate the effect of solar radiation on the flow field within the canyon. However, their focus was to compare between transient and stationary simulations to evaluate the importance of considering the thermal inertia effects in an urban street canyon study. In addition, the orientation of urban street canyon and the fixed aspect ratio were based on exposure to solar radiation rather than with prevailing wind directions. The street canyon in the study was chosen to be isolated from the urban environment. Despite these differences from the current research, the setting of the computational boundary conditions can be similar to the current research investigation, due to the focus of the research on H/W and orientation of street (but with wind direction), setting of the incoming solar radiation, and wind profile settings.

Blocken et al. (2012) have performed CFD simulation for pedestrian wind comfort and wind safety in irregular urban streets, for the North-South oriented Eindhoven University Campus, in the Netherlands. They have used CFD Fluent Code and RANS equation with the realisable  $k-\varepsilon$  turbulence model. The findings of the simulation were compared with the field measurements results of the wind speed at pedestrian level (i.e. 1.75m).

In CFD modelling approach, there are four main solvers for turbulence models, which namely are Reynolds-Averaged Navier-Stokes, Large Eddy Simulation, Direct Numerical Simulation (DNS) and Detached Eddy Simulation (DES). The DES solver is a combination of RANS and LES, which was driven by the quest to address the challenge of high-Reynolds number, for massively separated flows that RANS and LES are powerless to solve the simulation problem on their own (Spalart, 2009). The DNS model is the most accurate solver of fluid turbulence, as it solves the Navier-Stokes equations without any approximation of the turbulence except numerical discretization (Furbo et al., 2009) using a fine mesh when the whole flow scales (temporal and spatial) are resolved (Sengupta et al., 2008).

According to Blocken et al. (2009b), RANS solves only the mean flow, while it models all the scales of turbulence, whereas the LES (e.g. He and Song, 1999) solves the large and most important turbulent eddies, while it models only the small eddies. Nielsen et al. (2007) have stated that, in the RANS model, this approach divides temperature and velocity and other major variables into time-averaged and turbulent fluctuation. This model is commonly used in research on urban complex environments. For example, Blocken and Persoon (2009) have used RANS to assess wind comfort conditions around a football stadium on pedestrian and building levels. However, it is not as accurate as Large Eddy Simulation (LES) model. Despite of this the advantages of RANS are its availability in all CFD codes, inexpensive and widely validated.

According to Yoshie et al. (2007), the LES model is difficult to implement in urban environment for wind studies at pedestrian-level. This is because the grids in LES are more refined than RANS and requires larger computational power for simulation (Franke et al., 2007). In addition, Santiago et al. (2010) have used both LES and RANS to study the effect of incident wind direction on the dispersion of flow plume, and have found that LES is about two orders of magnitude is greater than RANS in terms of computational cost. Therefore, the use of RANS with  $k-\varepsilon$  (turbulent kinetic energy) model is quite suitable for modelling wind flow around buildings, and has become popular for wind studies at pedestrian level (e.g. Blocken et al., 2004; Blocken and Carmeliet, 2008; Blocken and Persoon, 2009; Yoshie et al., 2007; Takakura et al., 1993; Stathopoulos and Baskaran, 1996; Richards et al., 2002). However, the main deficiency of modelling by using steady RANS is its incompetence to inherently transient calculations of the flow-field features, including “*separation and recirculation downstream of windward edges and vortex shedding in the wake*” (Blocken et al., 2009b:490).

In general, Catalano and Amato (2003) have stated that “*the responsibility of a turbulence model in CFD simulation is to close the RANS equations by computing the components of the Reynolds stress tensor*” (cited in Setaih et al., 2014). Examples of such turbulence models include the Renormalization Group (RNG) kinetic energy,  $k-\varepsilon$  realisable model,  $k-\omega$  model, Shear Stress Transport (SST) model, etc., which the selection of these models are based on the context of the flow problem. (More information and an example of using RANS with different model has been published in Setaih et al., 2014).

Table 4. 3: Previous numerical studies on urban microclimate using CFD simulation.

Researcher	Research Title	Comments
Bottillo et al. (2014)	Fluid dynamic and heat transfer parameters in an urban canyon.	RANS equations have been solved with the standard k-e model. Computational domain was based on guidelines by Franke et al. (2007) and Tominaga et al. (2008). Solar load module was activated to obtain the surfaces temperature. The study has presented environmental parameters settings. The researchers used surface to surface (S2S) radiation model provided in CFD Fluent to account for the solar energy exchange parameters.
De Lieto Vollaro et al. (2014)	Numerical study of urban canyon microclimate related to geometrical parameters.	CFD Fluent code was used to study the microclimate of a street canyon in an urban environment, taking into account three different aspect ratios (H/W). The CFD settings for Solar Radiation and environmental parameters were based from Bottillo et al. (2014). Other computational settings were based on CFD guidelines by Franke et al. (2007) and Tominaga et al. (2008).
Ramponi & Blocken (2012)	CFD simulation of cross-ventilation for a generic isolated building: Impact of computational parameters.	The aerodynamic roughness ( $z_0$ ) value in relation to the roughness parameters in the found surface boundary conditions has be presented in an equation that take into account for the sand-grain roughness height (Ks) and the roughness constant (Cs). The researcher recommended changing the constant roughness in CFD Fluent to 0.5 using UDF format. These recommendations have been validated in urban microclimate studies by other researchers (e.g. Bottillo et al., 2014; and De Lieto Vollaro et al., 2014).
Saneinejad et al. (2012)	Coupled CFD, radiation and porous media transport model for evaluating evaporation cooling in an urban environment	MRT (mean radiant temperature) was calculated based on Fanger (1970) equation, which takes into account for combined effect of the long-wave radiation and the short-wave radiation received by a person. However, this study used a coupled model that consists of three sub-models: a CFD model; BE-HAM; and RAD. In addition, coupled method of the three software can be time consuming, thus alternative method to obtain the solar parameters is provided in Bottillo et al. De Lieto Vollaro et al. (2014).
Zhang et al. (2011)	A study of the ventilation and thermal comfort of the environment surrounding a new university building under construction	CFD Fluent code was used in this study with steady RANS equations and Standard k-e model. The results were obtained when the scaled residuals dropped below $10^{-4}$ , as the study was performed by using the standard k-epsilon turbulent model and second-order upwind scheme.

Ahranjani (2010)	Systematic simulation method to quantify and control pedestrian comfort and exposure during urban heat island	It was proven that aspect ratio is the most important and effective parameter on the ventilation efficiency. One of the aspects of this research was to study the influence of radiation fluxes on street canyon at pedestrian level. The researcher demonstrated that using a surface-to-surface (S2S) radiation model is an appropriate technique for modelling the enclosure radiative transfer. Residuals of $10^{-4}$ were applied as convergence criteria. A SIMPLE algorithm was also performed as a numerical procedure to solve the NS equation.
------------------	---	---

#### 4.9. Summary

This chapter discussed the importance of enhancing outdoor pedestrian microclimate and thermal comfort for the usability and attractiveness of public places. It discussed strategies for urban heat mitigation in an urban canyon, with the main focus on street aspect ratios and orientation of urban streets with prevailing wind directions. It has reviewed the previous numerical simulation studies on urban pedestrian microclimates and outdoor thermal comfort. To achieve the research aim of finding ways to mitigate heat stress through urban geometry design, it was found that CFD numerical simulation is appropriate for this task.

In addition, the knowledge gap based on the literature review has been identified. Numerous studies were conducted in relation to the configuration of urban street aspect ratios with thermal comfort, but mostly conducted in relation to exposure to solar radiation. However, most previous studies focused on symmetrical aspect ratios rather than asymmetrical ones, which limit the available knowledge on asymmetrical canyon studies. The study of multiple asymmetrical urban street aspect ratios (i.e. diverse buildings heights to street width  $H_1/W - H_2/W - H_3/W$ ) for at least three rows of buildings, based on optimising the building heights to adapt wind flow rate numerically, has not received much attention in the context of urban pedestrian thermal comfort, particularly in low wind speed environments within hot arid regions.

## **CHAPTER 5: Research Methodology**

### **Chapter Structure**

- 5.1. Introduction
- 5.2. Research Methodology Framework
- 5.3. Desktop Survey: Preliminary Data Collection of the Case Study (Phase 1)
- 5.4. Field Measurements Procedures (Phase 2)
- 5.5. Technical Studies: Secondary Data Collection for Modelling Settings (Phase 3)
- 5.6. CFD Numerical Simulation Procedures (Phase 4)
- 5.7. Calculation of PET Index and MRT Temperatures (Phase 5)
- 5.8. Summary



# Chapter 5:

## Research Methodology

---

### 5.1. Introduction

In order to improve the urban wind flow and pedestrian thermal comfort conditions in the hot arid climate of Madinah, this thesis aims to evaluate different multi-asymmetrical street aspect ratios strategies in a low wind speed environment. Based on the following research methodology framework, data obtained from meteorological reports, field measurements and through numerical simulation model were used to address the study's objectives.

### 5.2. Research Methodology Framework

This research methodology employed a systematic procedure to gather field and numerical simulation data to assess outdoor pedestrian thermal comfort, and to quantitatively compare and evaluate the effects of various asymmetrical street aspect ratios strategies on urban wind flow (Figure 5.1). The methodology was developed from previous relevant researches of Chen and Ng (2012) and Wei (2014), which is quantitative in character and summarises the overall processes and procedures employed in order to achieve the current research aim and objectives, including the following five phases:

- Desktop Survey: preliminary data collection of the case study area (Phase 1)
- Field Measurement Procedures (Phase 2)
- Technical Studies: secondary data collection for Modelling Settings (Phase 3)
- CFD Numerical Simulation Procedures (Phase 4)
- Calculation of PET Index and MRT Temperatures (Phase 5)

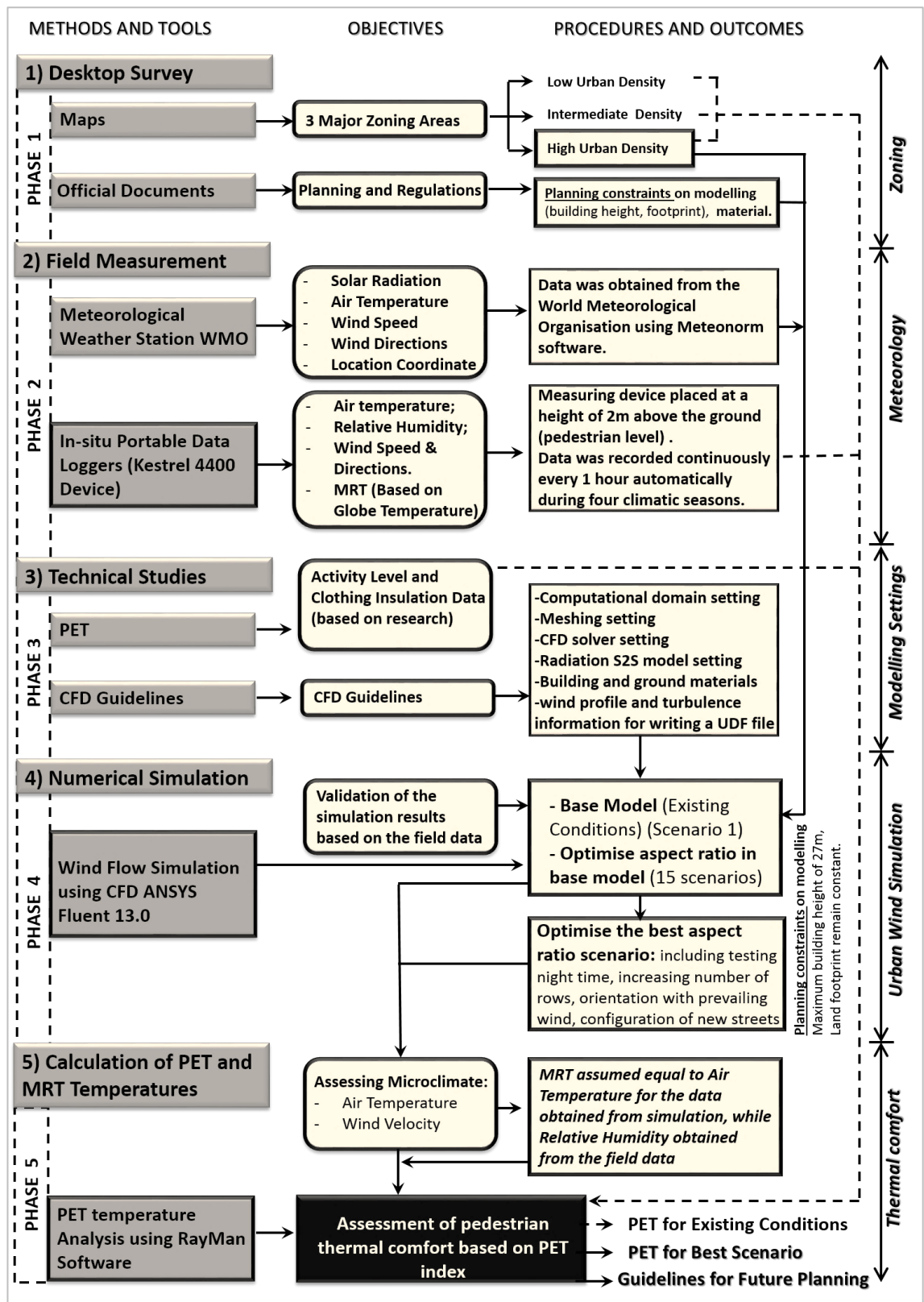


Fig. 5. 1: Methodology and operational framework of the current research.

### 5.3. Desktop Survey: Preliminary Data Collection of the Case Study (Phase 1)

In Phase 1, the objective number 1 (stated in section 1.4) was addressed, which was about understanding the context of the case study area and the climatic characteristics (Chapter 2).

The desktop survey (preliminary data collection) was conducted concerned with gathering information on the case study area, through mapping using the satellite images and observations, reviewing local planning regulations documents (discussed in Chapter 2), reviewing the relevant literature to understand the thermal comfort indices (discussed in Chapter 3) and understanding the effect of wind flow in urban areas on urban pedestrian microclimate (discussed in Chapter 4). The aim was to map the variation of Quba Road's characteristics, including, land cover, building heights, urban densities, development opportunities and the limitation of the redevelopment of the street. Thus, an overall concept of the locations and timing of the field measurements and numerical simulations were generated; and the planning constraints on modelling were reported in this phase. All the gathered information were used later in preparing for the subsequent phases.

Based on Phase 1, the case study was categorised into three major zones of varying urban densities along Quba Road (North-South axis with  $-22.5^{\circ}$  orientation from North). These were a high urban density area (Case 1), intermediate urban density area (Case 2), and low urban density area (Case 3), as illustrated in Figure 5.2. There is no series of policies from national planning through regional that can control the local planning and regulations, but rather planners are guided by masterplans. The recent plan for urban development of Madinah is a valuable opportunity for this study on the assessment of pedestrians thermal comfort conditions and thus the aim to find out ways to mitigate the urban heat stress in outdoor urban canyons (refer to section 2.3). The local planning and regulations limit the maximum building height to 27m, while the urban footprints will be leased to private investors to strengthen the economic benefit in the city. Thus, the current research considered these constraints of a previously planned area (i.e. buildings and street footprints and maximum buildings height) (e.g. Islam, 2011), as in Madinah the buildings permission is usually approved based on the local planning and regulations that are drawn up by most updated masterplan.

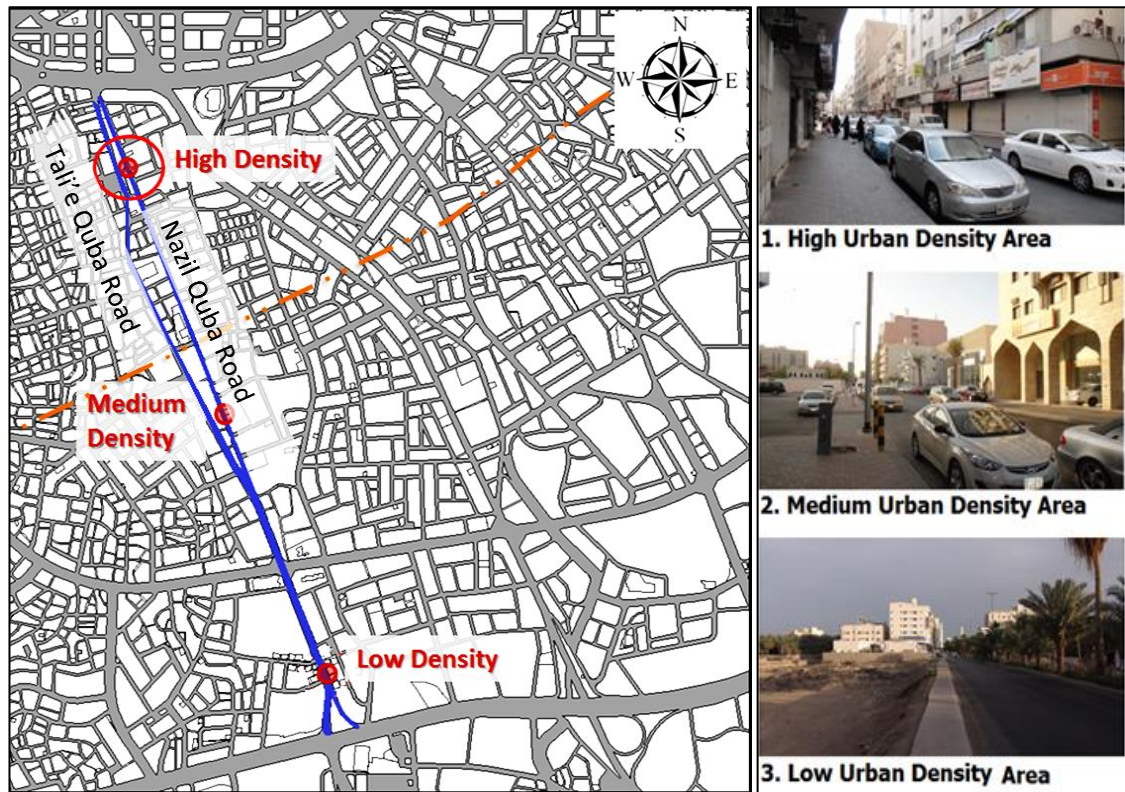


Fig. 5. 2: Measurements sites along Quba Road, in the southern part of the city, characterised by different urban density zones.

#### 5.4. Field Measurement Procedures (Phase 2)

In Phase 2, the objectives number 2 and 4 in this research were addressed (refer to section 1.4), which were: to understand the outdoor thermal comfort interaction factors and the pedestrian thermal comfort criteria for hot arid regions (Chapter 3); and to assess the urban pedestrian microclimate and thermal comfort conditions of a residential and commercial urban canyon (i.e. Quba Road) in Madinah, through field measurements during the four climatic seasons (Chapter 6). Thus, four field measurement campaigns were carried out in order to explore the variation in the microclimate and the outdoor thermal comfort in the urban canyon. The four field measurement campaigns were undertaken in three different locations of the street base on their built up density, including high urban density area (Case 1), intermediate urban density area (Case 2) and low urban density area (Case 3) (reference to their geometrical properties in Table 5.1, and Chapter 2).

The field measurements were selected in the Nazil Quba Road (i.e. the leeward canyon), due to the position of the canyon as a main commercial route in the Quba district, and as a straight urban physical linkage between the two most visited mosques in Madinah. The field measurement locations were selected to represent the urban open



spaces within the Road, based on different levels of urban density, including: the high urban density area (Case 1), intermediate urban density area (Case 2) and low urban density area (Case 3), as illustrated in Figure 5.3.

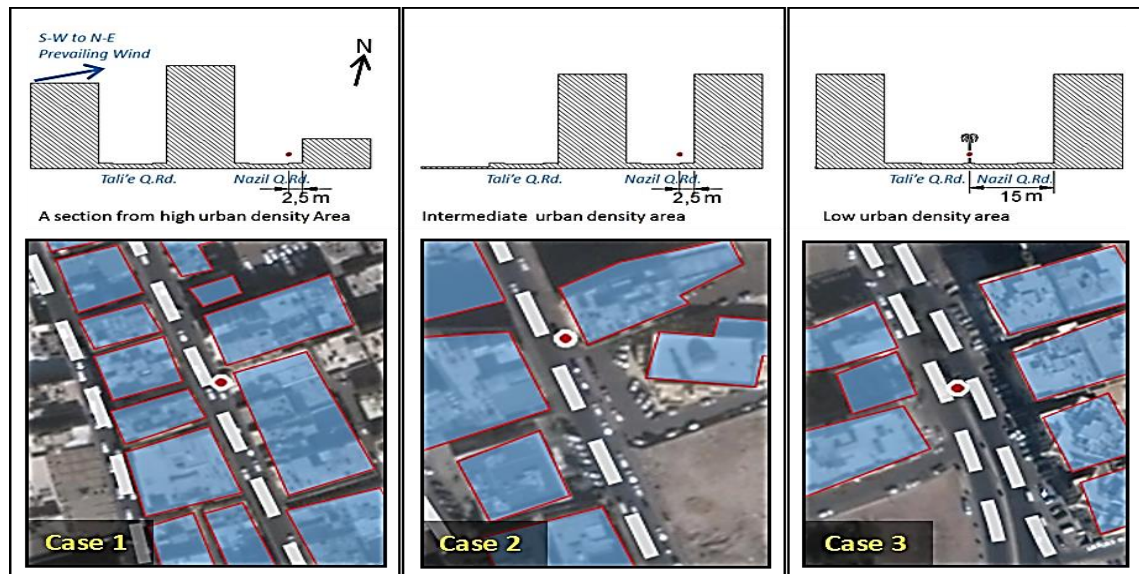


Fig. 5. 3: Field measurements Points (P1, P2, P3) locations for the case study of the three urban densities, located at a height of 2m above the ground (i.e. pedestrian height).

Table 5.1 summarises the geometrical characteristics of the three field measurement cases, and their locations between two buildings along Quba Road, at the pedestrian level (2m).

Table 5. 1: Geometrical properties at the three measurement points' urban zones along the Nazil Quba Road in the city of Madinah (39.7°N, 24.55°E).

Cases	Urban Density Type	Street Width	Location of Measurements Points between Two Street Aspect Ratios (H/W)	Route Axis Orientation (angle from N)
Case 1	High (with no vegetation and vacant plots)	12 m	$H_1/W = 1.9$ ; $H_2/W=0.5$ Located 2m above the ground, near windward elevation	22.5° anticlockwise North-South Urban Canyon
Case 2	Intermediate (with vacant plots)	12m	$H_1/W = 1.8$ ; $H_2/W=1.8$ Located 2m above the ground, near windward elevation	22.5° anticlockwise North-South Urban Canyon
Case 3	Low (with vacant plots and farms)	30m	$H_1/W = 0.7$ ; $H_2/W=0.7$ Located 2m above the ground, in the middle of two canyons	22.5° anticlockwise

#### 5.4.1. Time Selection of the Field Measurements

The field measurements were taken for 12 days in autumn (between the 14<sup>th</sup> to 25<sup>th</sup> of October 2012), 7 days in winter (between the 1<sup>st</sup> to 7<sup>th</sup> of January 2013), 12 days in spring (between the 1<sup>st</sup> to 12<sup>th</sup> of April 2013), and up to 13 days in summer (between the 17<sup>th</sup> to 29<sup>th</sup> of June 2013). The field measurements were conducted for 24 hours continuously over the monitoring period. Field measurement method is a validated method for the assessment of urban microclimate and pedestrian thermal comfort in outdoor spaces (Yahia and Johansson, 2013a; Aljawabra and Nikolopoulou, 2010; Lenzholzer and Koh, 2010) (refer to Chapter 3, section 3.7). The instrument used in this study for the field measurements process has been discussed below in section 5.4.1.

However, some microclimatic data for the intermediate urban density and low urban density areas were lost during the research, due to damage and theft of two measuring devices, in particular during the autumn and winter in Case 2, and autumn in Case 3. Thus, only the high urban density area (Case 1) has obtained complete data of the four climatic seasons. The main microclimatic data gathered were air temperature, relative humidity, wind speed and direction and globe temperature. The globe temperatures were obtained to calculate the MRT based on the literature (e.g. Thorsson et al., 2007; Johansson et al., 2014; Yahia and Johansson, 2013a; refer to section 5.7). The measurement data were also used to calculate the pedestrian thermal comfort conditions in the targeted road and to validate the results of the numerical simulation, as discussed in section.

Weather data were obtained from the World Meteorological Organisation (WMO) using Meteonorm software, to collect the data inputs for the CFD numerical simulation including data for solar radiation, air temperature, wind speed, prevailing wind directions, location coordinate. The gathered information were used later in preparing for the subsequent phases.

This research aims to find ways to enhance the thermal comfort level in Quba Road, during mid-seasons (spring and autumn), as they are positioned at the edge of the extremely hot summer season, with an average daily air temperature range of 32.6 °C – 45.8 °C in August (summer), 22.4 °C – 36.1 °C in April (spring), and 23.6 °C – 38.7 °C in October (autumn), as shown in Figure 2.13 and Table 2.1.

According to Ahmed (2003) and Ng and Cheng (2012), pedestrians in hot humid climates can tolerate air temperatures of up to 34°C in shaded outdoor spaces when airflow within a canyon is 4-5m/s. However, this proposed upper limit is not necessarily transferable to the hot arid climate of Madinah. In addition, wind velocities in Madinah's urban areas are predominantly 0.1-2m/s (Setaih et al., 2013a). Based on these temperatures, the current research attempted to focus on the peak temperature of around 34°C as the upper limit of tolerance. In Madinah, air temperature during April (spring) peaks slightly above the limit of tolerance with difference value of 2°C, and higher in October (autumn) with difference value of 5°C (Figure 5.4).

Thus, the month of April (mid-season), having a lower average daily air temperature than October, was chosen as a primary period for performing the numerical simulation studies, to extend the use of outdoor space by shifting the thermal conditions from a range of thermal discomfort into a range of critical thermal comfort as much as possible, passively without the introduction of any mechanical system for cooling (e.g. Erell et al., 2011; Oke, 1988; Pearlmutter et al., 2007).

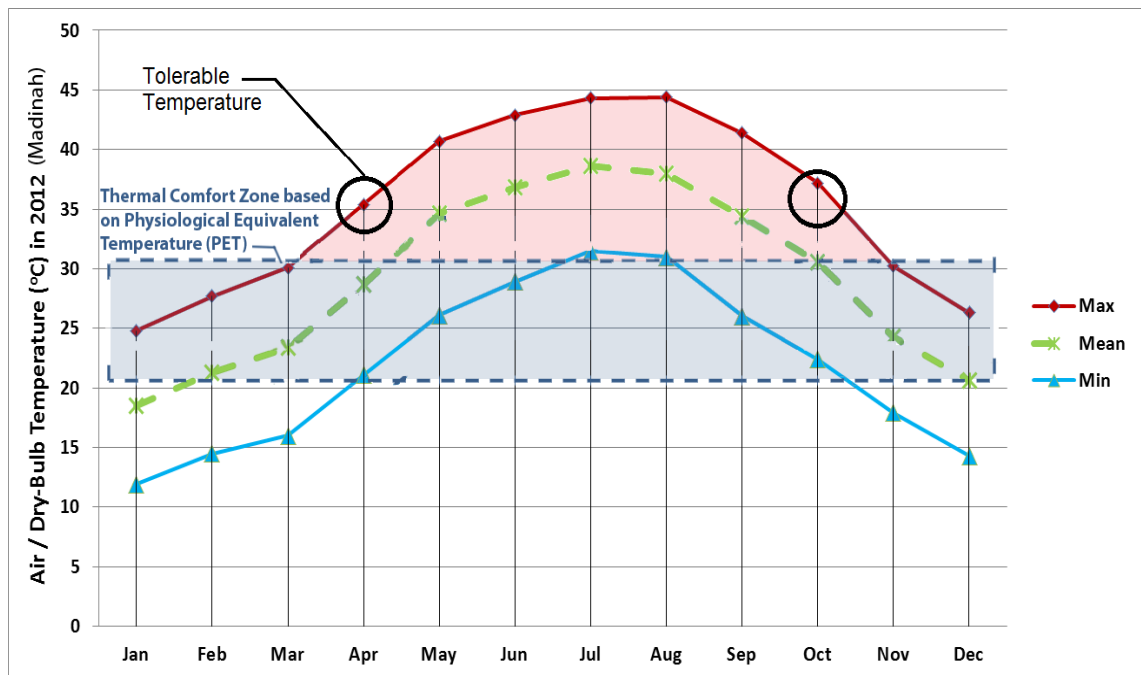


Fig. 5. 4: Air temperature based on Madinah Meteorological Centre (2012), showing months of April and October with a tolerable air temperature situated at the edges of a critical hot period, and highlighting the outdoor thermal comfort zone for hot arid climate (i.e. 21°C to 31.3°C) based on physiological equivalent temperature (PET) index proposed by Yahia and Johansson (2013a).

#### 5.4.2. Instruments for Field Measurements

For the assessment of outdoor pedestrian thermal comfort within a specific urban environment, the required data are related to the following four main variables: ambient air temperature, mean radiant temperature (MRT), relative humidity and wind velocity. The instruments used to collect these data respectively are: thermometer, black globe thermometer, hygrometer, and anemometer (Auliciems and Szokolay, 2007; Ali-Toudert et al., 2005; Yahia and Johansson, 2013a). Researchers in the field of urban microclimate have used variant series of a portable Kestrel data-logging weather station (e.g. Kestrel 4400 heat stress tracker by Nielsen Kellerman Corporation) (e.g. Yang et al., 2010; Traum et al., 2008; Giridharan et al., 2007). The Kestrel 4400 Heat Stress Tracker device integrates the required sensors for the assessment of thermal environment, and its sensors performance and reading accuracy are presented in Table 5.2.

In order to assess the main microclimatic parameters and thermal comfort conditions simultaneously along Quba Road, three Kestrel 4400 heat stress tracker devices were used and positioned within the three selected urban density areas, representing the open space. Each of the field measurement instruments (Kestrel 4400) was attached to an existing column (lighting column) found in the Nazil Quba Road, within the case study zones, with a distance of 1m from the column, 2m above the ground level and at least 2.5m from the nearest building wall, as illustrated in Figure 5.5. This corresponds to the suggested pedestrian height in urban studies (e.g. Blocken et al., 2009b), and acceptable distance from the wall surfaces, as the air temperature within urban streets has found to be insignificant compared to near urban surfaces (Ali-Toudert and Mayer, 2006). In addition, hanging the data loggers at the height of 2m was necessary for the pedestrian safety and convenience purpose.





Fig. 5. 5: A portable integrated weather station Kestrel 4400 Heat Stress Tracker was located at 2m of height. The pictures were taken at the intermediate urban density area within Nazil Quba Road.

Table 5. 2: Performance of Kestrel data logger. Difference in Error based on Pentz and Shott (1988).

	Accuracy	△ Error	Notes
Wind Speed	±0.1m/s	± 0.14m/s	25mm diameter Impeller with high precision axle and low-friction Zytel® bearings
Ambient Temperature	±0.5°C	± 0.7°C	Air, water or snow temperature. Hermetically-sealed, precision thermistor mounted externally and thermally isolated for rapid response. Airflow of 1 m/s or greater provides fastest response and reduction of insulation effect.
Relative Humidity	±3%	± 4%	Polymer capacitive sensor, mounted externally in thin-walled chamber
Globe Temperature	±1.4°C	± 2°C	25mm black globe thermometer, copper, externally mounted. Calibrated to achieve same measurements as standard 150mm globe

The device is based on the ISO 7243 standard for hot environments (e.g. Parsons, 2003 & 2006), and it contains a data logger to record the microclimatic variables simultaneously and stores them automatically.

In order to calibrate the equipment, the three Kestrel data loggers were tested prior to the field study, by comparing the air temperature results in a room, and the difference in values was negligible (i.e. 0.1°C). The acceptable difference in error for ambient temperature as a result of using these field equipment was found to be 0.7°C based on Pentz and Shott (1988:p25), as demonstrated in Table 5.2.

### 5.5. Technical Studies: Secondary Data Collection for Modelling Settings (Phase 3)

In Phase 3, technical studies (secondary data collection) were conducted to set the CFD ANSYS Fluent 13.0 model for urban wind simulation and to set the RayMan model for calculating PET index. This phase was conducted through reviewing the

literature on the CFD guidelines for modelling urban complex environments, and the required inputs for the calculation of human thermal comfort in outdoor spaces. The gathered information was used later in preparing for the subsequent phases (Phase 4 and Phase 5).

The CFD guidelines include information of computational domain setting, meshing setting, CFD solver settings, Radiation S2S model setting, building and ground materials' properties, and wind profile and turbulence information for the writing a UDF file that can be read by ANSYS Fluent 13.0 program. Pedestrian activity level and clothing insulation data were required in the calculation of PET thermal comfort index, which were obtained here from the literature on hot arid regions (e.g. Yahia and Johansson, 2013a).

### 5.5.1. Estimation of Metabolic Rate and Clothing Level

Activity level and clothing level values were required inputs in RayMan software for the calculation of the PET thermal comfort index. In a study conducted by Yahia and Johansson (2013a) on 920 people under hot arid summer and cold winter seasons, it is found that the value for the walking activity was 192.5 W (i.e. 1.9 met or  $106.94\text{W/m}^2$ ) and the clothing insulation ratio was 0.6 clo for summer clothing and 1.3 clo for winter clothing. These researchers used the clo and met values and calibrated for the calculating of thermal comfort and calibrated the comfort threshold for PET in hot arid climate of Damascus.

Therefore, in the current research, these values were used for the calculation of PET index based on an assumption that Madinah share somewhat similar pedestrian thermal behaviour, as during the field measurement it was observed that most people wear variety of light clothing during the hot seasons (i.e. 0.6clo) and heavier ones in cold winter (i.e. 1.3clo), as illustrated in Figure 5.6. The clo and met levels were verified in ANSI/ASHRAE Standard 55-2013 (ASHRAE, 2013) (refer to section 3.6.5 in Chapter 3).



*Fig. 5. 6: pedestrians in Quba Road are observed wearing heavy clothing layers in cold winter and lighter in hot seasons.*

### 5.5.2. CFD Guidelines on Setting the Simulation Model

Since the study aims to predict the effects of different street aspect ratios on pedestrian level urban wind velocity, a numerical simulation is an appropriate method and CFD ANSYS-Fluent is suited for this task (e.g. Bottillo et al., 2014; De Lieto Vollaro et al., 2014; Ahranjani, 2010; Ali-Toudert and Johansson, 2006; Qaid and Ossen, 2014). According to Arnfield (2003), numerical modelling has the apparent benefits over comprehensive field measurement on justification of their controllability

and frugality of time and resource. The research also stated that numerical simulation is a suited methodology to dealing with the difficulties of urban complex environment systems. ANSYS-Fluent code has been validated and used in many urban canyons and aspect ratios studies (Bottillo et al., 2014; De Lieto Vollaro et al., 2014; Ahranjani, 2010), as well as in thermal comfort (Stavarakakis et al., 2012 & 2010) and pedestrian wind environments studies (Ramponi and Blocken, 2012; etc.). This study uses version 13.0 of ANSYS-Fluent.

Settings of the boundary conditions were based on literature (e.g. Tominaga et al., 2008; Blocken et al., 2007; Ramponi and Blocken, 2012; Reiter, 2008; Franke, 2007; De Lieto Vollaro et al., 2014; Bottillo et al., 2014). The modelling settings were validated for the current research by comparing the wind velocity simulation results at different hours (e.g. 0.6m/s at 15:00 hours) with the field measurement data (e.g. 0.65m/s at 15:00 hours) (discussed in section 5.6.1). The outcome of the wind velocity, with error margin around 8%, confirmed the ability of the CFD simulation (Fluent 13.0) in accurately simulating and predicting wind flow behaviour in outdoor urban thermal environment.

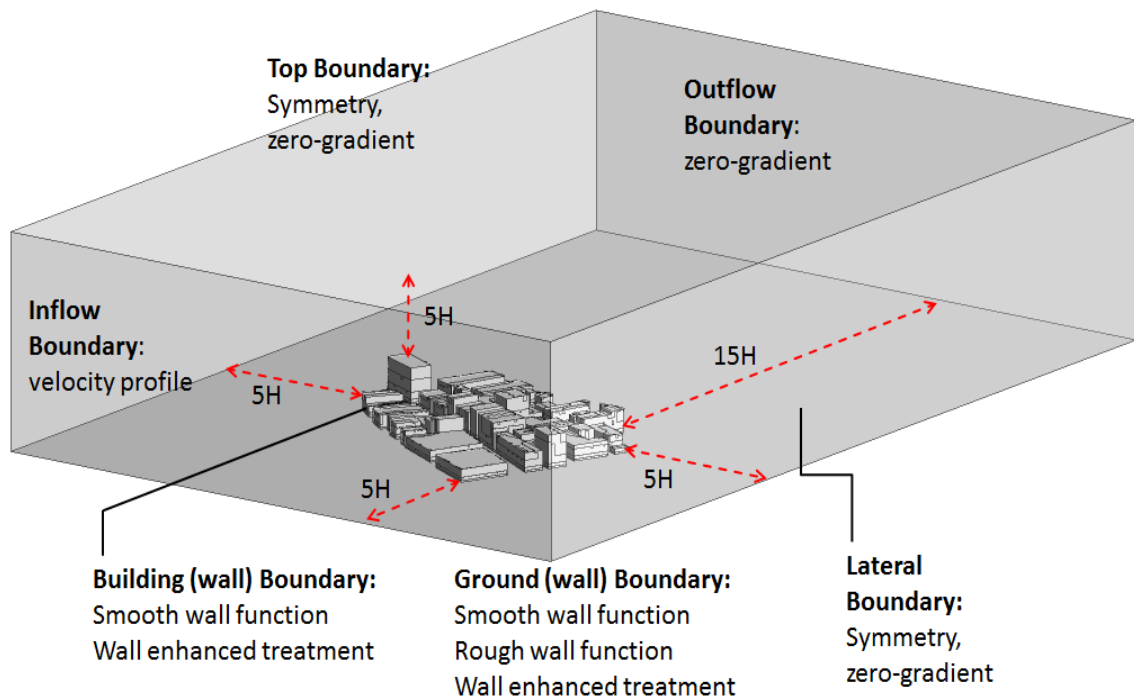
Blocken et al. (2012) have performed CFD simulation for pedestrian wind comfort and wind safety in urban streets, for the North-South oriented Eindhoven University Campus, in the Netherlands. They have used CFD Fluent Code and RANS equation with the realisable  $k-\varepsilon$  turbulence model. Their findings of the simulation were compared with the field measurements results of the wind speed at pedestrian level.

A cuboid computation domain was allocated around the studied buildings area to investigate the pedestrian thermal comfort (Figure 5.7). To set the appropriate dimensions of the cuboid as well as the mesh size, the meshing dependency test and the base model geometry test were applied, respectively. In the meshing dependency test, the mesh size of 0.2m x 0.4m (fine mesh) with about 3.4 million of cells, and the finer mesh size of 0.2m x 0.2m with about 9.1 million of cells achieved higher accuracy of wind velocity results than the coarser mesh (0.2m x 0.6m). The fine and finer cell sizes validated the use of the mesh for the simulation, thus the models were conducted based on the fine mesh size (i.e. 0.2m x 0.4m) (refer to section 5.5.5).

The cuboid computational domain dimension was based on recommendations by Franke et al. (2004), Blocken et al., (2007) and Tominaga et al., (2008). Thus, five times the height (5H) of the tallest building in the study area were applied for the height

of the domain from the tallest building and from the two sides of the urban area that forms the width of the computational domain, as illustrated in Figure 5.7. Blocken et al. (2007) and Tominaga et al. (2008) have also recommended  $5H$  for the upstream and  $15H$  for the downstream that forms the domain's length. These dimensions should reduce the errors of the wind profile from all the directions. Thus, these dimensions were verified and validated for the current research simulation, as illustrated in Figure 5.6. The height of tallest building ( $H$ ) was used as 28m, as it is located around the area of interest and included in the modelling.

A profile of wind speed varying with the height at the air entrance of the simulation field was developed from an empty computational domain and used for the simulation of the case study area. This process is recommended in the best practice guidelines for the homogeneity of the air flow at upstream and downstream of the domain (Franke et al., 2007). The following sub-section present the settings that were in this study for the boundary conditions of the cuboid computational domain.



*Fig. 5. 7: Computational domain dimension and the boundary conditions in the current research.  $H$  is the height of the tallest building.*

### 5.5.2.1. Boundary Conditions

Inlet flow condition is the appropriate function at inflow surface. Thus, this was considered with inputs of metrological data of air temperature and wind speed. For the wind velocity ( $U$ ), kinetic energy ( $k$ ) and turbulence dissipation rate ( $\varepsilon$ ), as well as urban roughness length ( $Z_0$ ) and friction velocity ( $U^*$ , which equals 0.5. in this study), the following equations were coded in user defined function (UDF) file:

$$U_{(z)} = \frac{U_{ABL}^*}{\kappa} \ln\left(\frac{z+Z_0}{Z_0}\right) \quad (1)$$

$$k_{(z)} = \frac{U_{ABL}^{*2}}{\sqrt{C_\mu}} \quad (2)$$

$$\varepsilon_{(z)} = \frac{U_{ABL}^{*3}}{\kappa(z+Z_0)} \quad (3)$$

$$U_{ABL}^* = \frac{\kappa U_z}{\ln\left(\frac{z+Z_0}{Z_0}\right)} \quad (4)$$

These profiles are often used as inlet profiles for CFD simulations when measured profiles of  $U$  and  $k$  are available (Blocken et al., 2007). The velocity profile  $U$  at specified heights  $z$ , and roughness length  $z_0$  has been validated in COST (Franke et al., 2004), WMO (Oke, 1999) and Blocken et al. (2012), which takes into account the von Karman constant ( $\kappa = 0.42$ ; constant shear stress with height), which is calculated within the low portion of the atmospheric boundary layer (ABL) with the friction velocity ( $U^*$ ).

Many researchers, including Janssen et al. (2013), have implemented this formula of wind profile in CFD for wind studies at pedestrian height, as well as turbulence kinetic energy and turbulence dissipation rate that are linked to the roughness length parameter. Numerous methods have been conducted as turbulence boundary condition. The turbulent kinetic energy  $k_{(z)}$  can be estimated using the ABL friction velocity  $U_{ABL}^*$  and a model empirical constant ( $C_\mu=0.09$ ) of the realisable  $k-\varepsilon$  model (Blocken et al. 2007; Ramponi and Blocken, 2012).

Outflow surface is a condition of zero pressure gradients, as it requires free pressure specification with zero static pressure (Tominaga et al., 2008). According to AIJ guidelines for practical applications of CFD to pedestrian wind environment, this could be a reasonable assumption if the outlet boundary is positioned far from the region where the impact of the target building is negligible (Tominaga et al., 2008). Therefore, the boundary condition in FLUENT for this surface was important to be specified as “outlet” condition, by which air leaves the computational domain.

According to Blocken et al. (2007), the roughness of the implicit terrain, in the upstream and downstream parts of the domain, is either expressed in  $z_0$  (i.e. the aerodynamic roughness length, in the range 0.03-2m), or in terms of the equivalent sand-grain roughness height for the atmospheric boundary layer ( $k_{S,ABL} \approx 30z_0$ , in the range of 0.9 to 60m). Blocken et al. (2007) stated that in the centre part of the computational domain, where it explicitly models the actual geometrical terrain, the roughness is most often expressed in terms of the equivalent sand-grain roughness height ( $k_S$ , in the range of 0-0.1m). The sand-grain roughness height ( $k_S$ ) was specified in the current research at the ground boundary condition based on aerodynamic roughness length ( $z_0$ ) and roughness constant ( $C_s=5$ , this was coded in the UDF due to the limitation of CFD Fluent software), using the following equation (Ramponi and Blocken, 2012):

$$k_{S,ABL} = \frac{9.793z_0}{C_s} \quad (5)$$

Blocken et al. (2007) argue that if sand-grain roughness height ( $k_S$ ) is used in the wall functions, then the following four requirements should be satisfied simultaneously:

- High mesh resolution should be used sufficiently in the vertical direction within one metre of the cell height in the bottom layer of the domain, or according to Franke et al. (2004) structuring 2 to 3 layers bellow pedestrian height (e.g. 2m);
- A horizontally homogeneous ABL flow is required in the upstream and downstream areas by using a wall function;
- Distance ( $z_P$ ) from the centre point ( $P$ ) of wall-adjacent cell to the bottom wall of the domain should be kept larger than the sand-grain roughness height ( $k_S$ ); and
- The relationship between the roughness of the sand-grain ( $k_S$ ) and the aerodynamic roughness length ( $z_0$ ) is important to be identified; concerning “*the relationship that results from matching the ABL mean velocity profile and the wall function in the CFD code*”.

These requirements were applied in the current research and the sand-grain value was calculated from equation 5 to the value 0.98, which was based on the roughness length ( $z_0$ ) value of 0.5m for urban areas based on Stankovic et al. (2009) and Wieringa (1992), as discussed in the literature review (Chapter 4).



Franke et al. (2007), Blocken et al. (2012) and Reiter (2008) have recommended using symmetry boundary conditions for the lateral and top computational domain surfaces. This would enforce a parallel flow by forcing the velocity component normal to the boundary. This is because the specification for the inlet flow boundary of the computational domain requires profile conditions of neutral vertical wind velocity profile  $U$  on flat terrain, vertical distribution of turbulent kinetic energy  $k$ , and turbulent dissipation rate  $\varepsilon$ ; whereas the outlet boundary requires free pressure specification with zero static pressure.

#### **5.5.2.2. CFD Guidelines on Setting the Mathematical Models, Turbulent Scheme and Solver Method**

Since fine resolution and contribution of wind velocity are necessary to study pedestrian thermal comfort within an urban street canyon, the Navier-Stokes (NS) equation is solved in CFD-Fluent 13.0 as the governing equation for this study. The RANS (i.e. Reynolds-averaged Navier-Stokes) model is also applied as the turbulence model to predict the effects of turbulence. To evaluate the impact of buoyancy effects, the boussinesq module has been used for air density.

The  $k-\varepsilon$  model, which includes two transport equations to resolve turbulent kinetic energy ( $k$ ) and its dissipation rate ( $\varepsilon$ ), is employed in this study. There are several reliable  $k-\varepsilon$  models for urban environmental studies, including standard, realisable and renormalization group theory (RNG) models. Standard  $k-\varepsilon$  model has been widely used in microclimatic scale studies. This is because of its low computational cost, robustness, and reasonable accuracy (De Lieto Vollaro et al., 2014; Bottillo et al., 2014). However, realisable  $k-\varepsilon$  model gives better convergence of the residuals than the simplified standard  $k-\varepsilon$  model. Therefore, in the current research the realisable  $k-\varepsilon$  model was used because its good performance has been validated for urban microclimate analysis (e.g. Blocken et al., 2012).

#### **5.5.2.3. CFD Guidelines on Setting the S2S Radiation Model**

The CFD ANSYS Fluent 13.0 software is capable of predicting air temperature, wind velocity, relative humidity, and solar radiation. Solar radiation contributes considerably to diurnal heat stress in clear sky conditions, as partly of solar radiation is absorbed and partly reflected by urban surfaces to the urban environment. However, the use of radiation models in studies within urban areas, limits the validity of results, due



to lack of information on the scattering medium of different materials for the radiative transfer equation, while this equation is CPU-intensive (Ahraanjani, 2010).

Ahraanjani (2010) studied the effect of the urban canyon aspect ratio on the ventilation efficiency using a surface-to-surface (S2S) radiation Model provided in ANSYS Fluent software. One of the aspects of Ahraanjani's research was to study the influence of radiation fluxes on street canyon at pedestrian level. S2S radiation scheme models the enclosure radiative transfer without participating scattering medium, as it simplifies the net radiation budget to surfaces within a street canyon based on sky view factor. The model simulates the sun's position for a given time and date, and geometry position. However, the main limitation of this model is that it assumes all surfaces are diffuse.

Bottillo et al. (2014) and De Lieto Vollaro et al. (2014) also used a S2S model with solar load module to account for the solar energy exchange parameters within urban canyon microclimate related to geometrical parameters (e.g. urban street aspect ratio). These researchers demonstrated that using a surface-to-surface (S2S) radiation model, is an appropriate technique for studying the influence of radiation fluxes on street canyon at pedestrian level. The S2S model is a simplified and a view-factor based model, which calculates solar radiation in the computational domain separately so it can be coupled with CFD simulation, and has been validated for urban canyon studies (e.g. Bottillo et al., 2014; De Lieto Vollaro et al., 2014; Ahraanjani, 2010).

Thus, in the current study, the S2S model is coupled with CFD simulation, which includes the solar ray tracing algorithm and simulates the sun's location in the sky for a given time and day of the measurements as well as the global position (e.g. latitude, longitude, and time zone), grid orientation, and sunshine factor. Residuals of  $10^{-4}$  were applied as convergence criteria (e.g. Bottillo et al., 2014; De Lieto Vollaro et al., 2014; Ahraanjani, 2010).

#### **5.5.2.4. Grid Discretisation and Mesh Dependency Test**

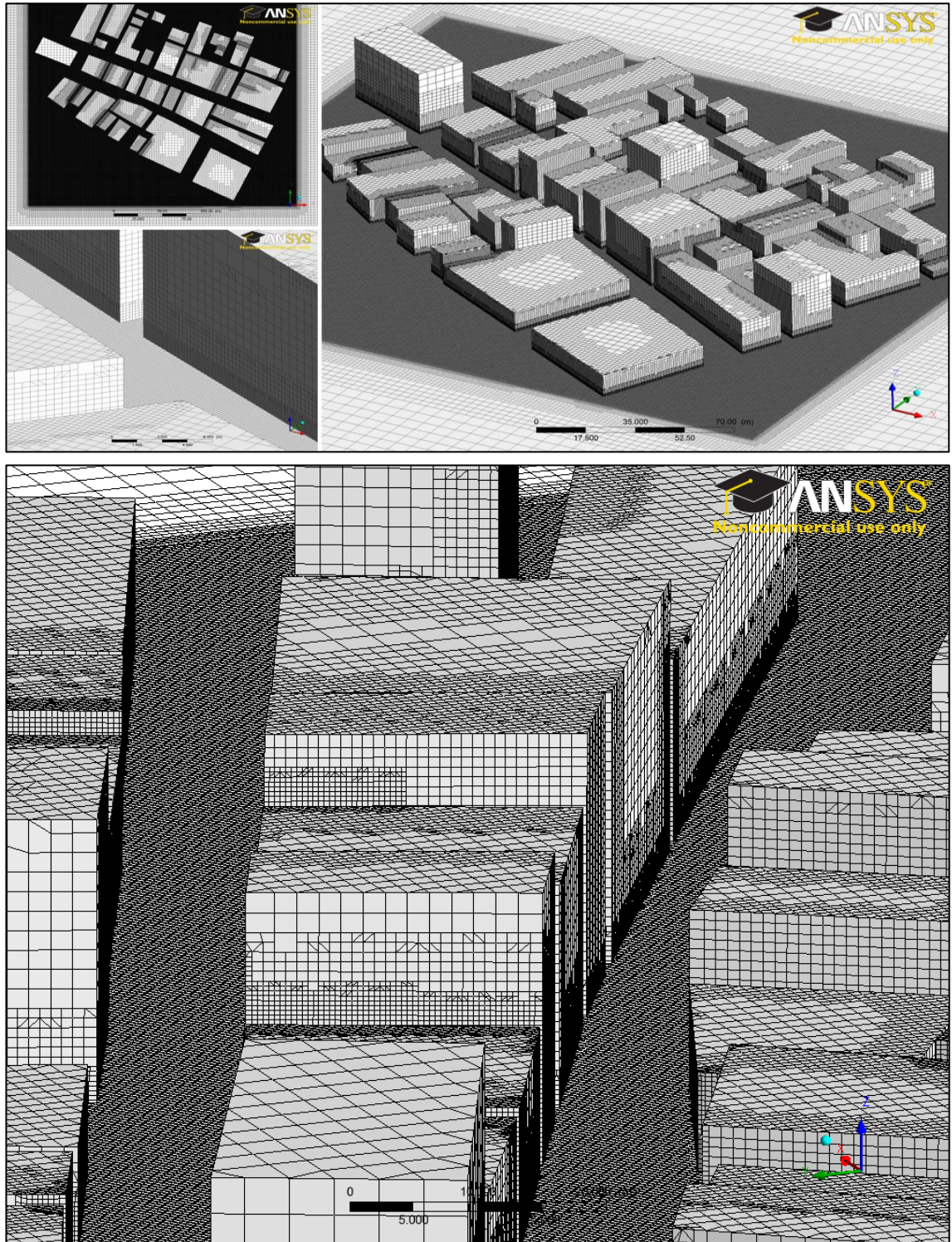
For the accurate prediction of the flow pattern within the urban geometry at pedestrian level as well as around buildings, it is important that the characteristic of separating flows near walls and the roof to be reproduced correctly. It is recommended that to reproduce this separation, the minimum of 10 fine grids to be applied at the interest area (Tominaga et al., 2008; Reiter, 2008). It is also recommend to apply

stretching ratios of maximum of 1.3 (Franke et al., 2007; Tominaga et al., 2008) or even less than 1.2 (Bartzis et al., 2004) of adjacent grids to set up grid shapes with similar widths, especially in areas with a steep velocity gradient. For the study of pedestrian microclimate in urban areas, it is advised to test the sensitive of the results of using this stretching ratio on mesh resolution, as it may change according to the building shape and the surroundings (Franke et al., 2007).

Moreover, Franke et al. (2004) assert that regarding the cell resolution for actual building, the calculation of wind speed at pedestrian height of 1.5 to 2 metres should be arranged at the 3<sup>rd</sup> or 4<sup>th</sup> grid higher from the ground surface, with 10 grid layers at least to be set to building side. This is comparable to the AIJ guidelines where it is stated that the cell location should be set to at least at the third or above from the height of the ground surface, with the minimum resolution grid of about 0.5 – 5 metres within the area of interest (i.e. one tenth of the building scale) (Tominaga et al., 2008).

In the current research, these recommendations were considered; and a highly refined mesh was applied in the interest urban area. ANSYS Meshing software was used in this research; applying minimum and maximum grid sizes of 0.20m x 0.40m in the interest area, respectively. The growth ratio of 1.2 and 10 layers near the ground surfaces were obtained in the current research based on the above mentioned recommendations, as illustrated in Figure 5.8.

Figure 5.9 shows the current research dependency test of three different cell sizes, including coarse, fine and finer grids. Hexahedral cell shape was chosen to ensure a high quality of the computational grid (e.g. Botillo et al., 2014; de Lieto Vollaro et al., 2014). The size of the course mesh was 0.2m x 0.6m of resolution with about 2.5 million of cells, the fine mesh was 0.2m x 0.4m with about 3.4 million of cells, and the finer mesh was 0.2m x 0.2m with about 9.1 million of cells. The test was performed on air velocity from the ground level to the pedestrian height of 2m. The test results were compared with the field measurement reading of the air velocity in spring at 15:00 hours, i.e. 0.6m/s. The results illustrated that the finer cells (0.2m x 0.2m) achieved the higher dependency level recording 0.59m/s at the pedestrian height, followed by the fine cells (0.2m x 0.4m) with 0.57m/s, while the coarser mesh (0.2m x 0.6m) having lowest level with a value of 0.54m/s. The fine and finer cell sizes validated the use of the mesh for the simulation, thus the models were conducted based on the fine mesh size (i.e. 0.2m x 0.4m), as illustrated in Figure 5.9



*Fig. 5. 8: Refined mesh was applied at the area of interest and the surround buildings. The cells size is  $0.2\text{ m} \times 0.4\text{ m}$  and the stretching ratio on the mesh resolution is 1.2. The total number of cells in the computational domain is 3,385,643 cells. 10 layers with  $0.2\text{ m}$  of cells were applied near wall surfaces.*

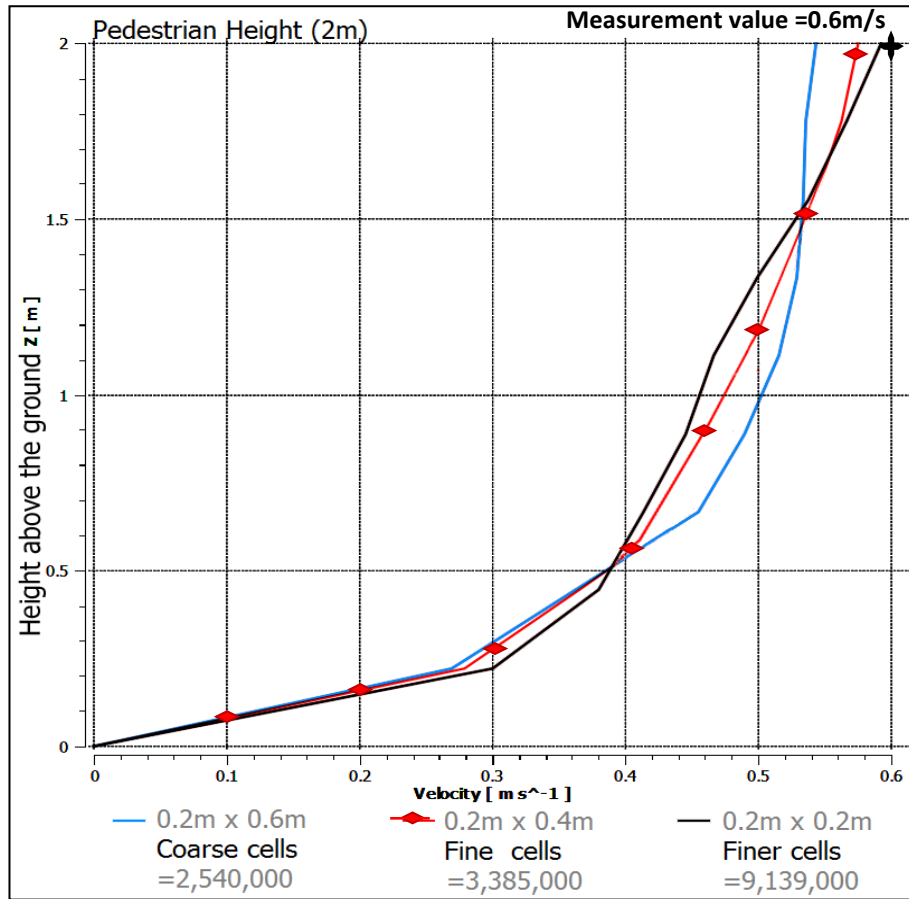


Fig. 5. 9: The current research dependency test of the coarse cells, fine cells and finer cells.

## 5.6. CFD Numerical Simulation Procedures (Phase 4)

In Phase 4, the objectives number 3, 5 and 6 in this research were addressed (refer to section 1.4), which were:

- To understand the effect of urban configurations on pedestrian level wind flow in urban street canyons (Chapter 4).
- To examine the effects of the optimisation of the building's height to street width aspect ratio from the base model (existing conditions) on the pedestrian wind flow and thermal comfort conditions (Chapter 7).
- To evaluate the effects of the optimisation of the urban canyon's configurations from an improved aspect ratio model (an optimum proposed scenario) on urban pedestrian microclimate (Chapter 8).

Thus, in Phase 4, numerical simulations were conducted using urban geometry information of the case study, data obtained from the meteorological station and CFD

modelling setting guidelines provided in Phase 1, Phase 2 and Phase 3, respectively (results are discussed in Chapters 7 and 8).

The simulations have been performed with the academic CFD code ANSYS-Fluent 13.0, 3D double precision, pressure based version and the steady RANS equations have been solved in combination with the realisable  $k-\varepsilon$  model base on the best CFD practice guidelines (refer to section 5.5.2). The numerical simulation method was used to examine the effect of the proposed asymmetrical urban street H/W aspect ratios scenarios on pedestrian level wind flow at the afternoon peak period in a mid-season, i.e. 15:00 hours in April 2013. Weather data from metrological data were used to statistically provide boundary conditions for the numerical model.

#### 5.6.1. Validation of CFD ANSYS-Fluent 13.0 Model

Field measurements and wind tunnel tests are the predominant methods used to validate CFD results (AIAA, 1998). According to Reiter (2008), “*wind tunnel tests give wind relevant results and stay a reference for new methods’ validity investigations*” (p: 1). However, the in situ-measurements method is easier to conduct and gives more accurate microclimatic data of the actual conditions, and commonly used for CFD validation process as well as for wind tunnel validation (Chung and Choo, 2011).

In order to validate the model, the case study area (high urban density zone) and the meteorological measurement data were used as input data for the CFD ANSYS-Fluent model. Field measurements for April 2013 were compared with the outcome of the simulation model at five different hours (i.e. 09:00; 12:00; 15:00; 18:00 and 21:00). The validation process was conducted based on the information of the technical studies obtained in Phase 3 (i.e. Technical Studies), using parameters such as the S2S radiation model, energy model, and realisable k-e turbulence model for the high urban density area (Case 1), using CFD ANSYS Fluent 13.0. The data input required for the validation including irradiance of the global radiation, irradiance of the diffuse radiation, air temperature, and wind speed as obtained from the meteorological station, as demonstrated in Table 5.3. The table also summarise the computational settings used in this current research as discussed in this chapter, including setting up the model domain, atmospheric boundary conditions, radiation model, ground surface conditions (i.e. material thermal properties) and building surface conditions.

Table 5. 3: Boundary conditions and initial setting of ANSYS-Fluent 13.0 modelling.

Location	Madinah (hot arid climate), 24.55N, 39.7E
Date/Time Simulated	At 15:00 (+2 GMT) on 1 <sup>st</sup> of April 2013
Model Domain	<ul style="list-style-type: none"> <li>- Computational domain dimensions: 5H on the laterals and the top of the cuboid, 5H upstream, 15H downstream.</li> <li>- Mesh size: 0.2m x 0.4m grid size, with 1.2 growth rate, and 10 layers of grids.</li> <li>- Hexahedral dominant mesh type with about 3,385,643 cells.</li> <li>- Realisable k-e models were activated with standard near wall treatment and full bouncy effect modelling.</li> <li>- Second order scheme method applied, while Coupled algorithm used to handle pressure-velocity coupling.</li> </ul>
Atmospheric Boundary Conditions	<p>Inlet boundary settings: user defined function UDF implemented in CFD ANSYS-Fluent 13.0 using equations number 1 through 4 for the upstream undisturbed wind-speed profile, kinetic energy, dissipation rate, and friction velocity, respectively, with initial wind speed of 4.7m/s at 10m above the ground. Aerodynamic roughness length of 0.5m was applied for a high density urban area.</p> <ul style="list-style-type: none"> <li>- Prevailing wind direction: South-Westerly direction (-112° angle of attack from the North) and approximately perpendicular to North-South oriented street (i.e. -22.5° street orientation from the North).</li> <li>- Initial Temperature: 29°C.</li> <li>- Outlet boundary: the Kinetic Energy and dissipation rate was specified by a profile of homogeneous wind profile of an empty domain, with zero value for the pressure.</li> <li>- Air property was applied with Boussinesq density of 1.225</li> </ul>
Radiation Model	<ul style="list-style-type: none"> <li>- Solar Load: Solar Calculator using Solar Ray Tracing Model</li> <li>- Surface to Surface (S2S) model was used with view factor.</li> <li>- Irradiance of global radiation: 781W/m<sup>2</sup></li> <li>- Irradiance of diffuse radiation: 194W/m<sup>2</sup></li> </ul>
Ground Surface Conditions	<p>Asphalt material property was applied to the ground surfaces.</p> <ul style="list-style-type: none"> <li>- Density: 2360 kg/m<sup>3</sup></li> <li>- Specific heat: 920 J/kg°C</li> <li>- Thermal conductivity: 1.3 W·K<sup>-1</sup></li> <li>- Internal emissivity: 0.93</li> </ul> <p>Roughness height was calculated based on equation number 5 of Ground Sand-Grain value. The roughness constant was specified to 5 in the user defined function UDF based on Blocken et al. (2007) recommendation.</p>
Building Surface Conditions	<p>Concrete material property was applied to the buildings surfaces.</p> <ul style="list-style-type: none"> <li>- Density: 1500 kg/m<sup>3</sup></li> <li>- Specific heat: 840 J/kg°C</li> <li>- Thermal conductivity: 1.7 W·K<sup>-1</sup></li> <li>- Internal emissivity: 0.92</li> </ul>

The outcomes were then compared with the field measurement data gathered in Phase 2. There are no trees and water features in the simulated area that may affect the relative humidity value. However, calculation of relative humidity was excluded due to its very low value in Madinah (i.e. 8.2%, as indicated from the field measurements), which can have minor impact on the surroundings (as no sort of water was included in



the model) (e.g. Ali-Toudart and Mayer, 2006). Future studies should consider relative humidity for more accurate results.

Since this simulation used the steady state RANS model instead of unsteady model, the simulation study was carried out on the 1<sup>st</sup> of April 2013 as it represents a mid-season (spring) based on averaging the data obtained from the airport meteorological station for between 1<sup>st</sup> of April to 12<sup>th</sup> of April. The model was simulated at 09:00, 12:00, 15:00, 18:00, and 21:00 hours for the validation purpose by comparing the results with the field measurements.

Table 5.4 shows the validation of the simulation results in the base model for the five chosen hours. The results indicated that incurred error margin between the CFD simulations and the field measurements ranges below 20% for wind speed simulation. Thus, the errors incurred for both wind speed and air temperature are within the acceptable error margin (i.e.  $\leq 20\%$ , as recommended by Willemsen and Wisse (2002)). The modelled wind velocity during the day recorded almost similar values compared to the field measurements (i.e. 0.6m/s) with error margin of 1% at 09:00 hours and a difference value almost equal to zero. Then followed by 7% of error at 12:00 hours with a small difference value of 0.04m/s, 8% at 15:00 hours with a difference value of 0.05m/s and 8% at 18:00 hours (difference of 0.05m/s). Thus, the simulation results of the wind velocity are in good agreement during the day with the field measurements.

While during the night at 21:00 hours the error recorded was 20%, which could be due to passing traffic and absence of the direct solar radiation. Thus, the model can be over predicting the wind speed by a difference value of 0.14m/s at night. However, the night time is not the research concern as more people use the outdoor spaces during the night when the air temperature is lower than the day hours.

*Table 5. 4: Data inputs and the simulated and measured air temperature ( $^{\circ}\text{C}$ ) and wind speed (m/s) differences at the Nazil Quba Street (leeward canyon). The results of wind velocity are within the acceptable error margin of 20% recommended by Willemsen and Wisse (2002).*

	Meteorological Data inputs for CFD Simulation				Outcome of Simulation		Field Measurements		Errors	
	irradiance of global radiation	irradiance of diffuse radiation	Air Temp	Wind Speed	Air Temp	Wind Speed	Air Temp	Wind Speed	Temp simulation error	Wind simulation error
09:00	430	115	24.9	2.7	28.6	0.396	27	0.4	6%	1%
12:00	877	241	30.9	3.9	33.5	0.56	31.8	0.6	5%	7%
15:00	781	194	29	4.7	35.3	0.65	33.7	0.6	5%	8%
18:00	188	102	31.3	4.7	31.8	0.65	32.3	0.6	2%	8%
21:00	0	0	27.5	2.9	29.6	0.56	30.3	0.7	2%	20%

The outcome of the wind velocity confirmed the ability of the CFD simulation (Fluent 13.0) in accurately simulating and predicting wind flow behaviour in outdoor urban thermal environment. Thus, owing to this capability, the software (Fluent 13.0) was adopted for the simulation of various strategies to enhance pedestrian microclimatic conditions. The existing situation of Quba Road has been replicated for the purpose of this simulation by applying the actual construction materials and ground surfaces, including concrete and asphalt, respectively, in the virtual CFD environment.

In a study of wind speed and thermal comfort of the environment surrounding a building in a case study in Hong Kong, Zhang et al. (2011) obtained the CFD results when the scaled residuals dropped below  $10^{-4}$ , as the study was performed by using the realisable k-e turbulent model and second-order upwind scheme. Thus, the results in the current study were obtained when the minimum scaled residuals converged below  $10^{-4}$ , as illustrated in in Figure 5.10 (the convergence diagrams obtained in this research can be found in the Figures between A5.1 to A5.31 in the Appendices).

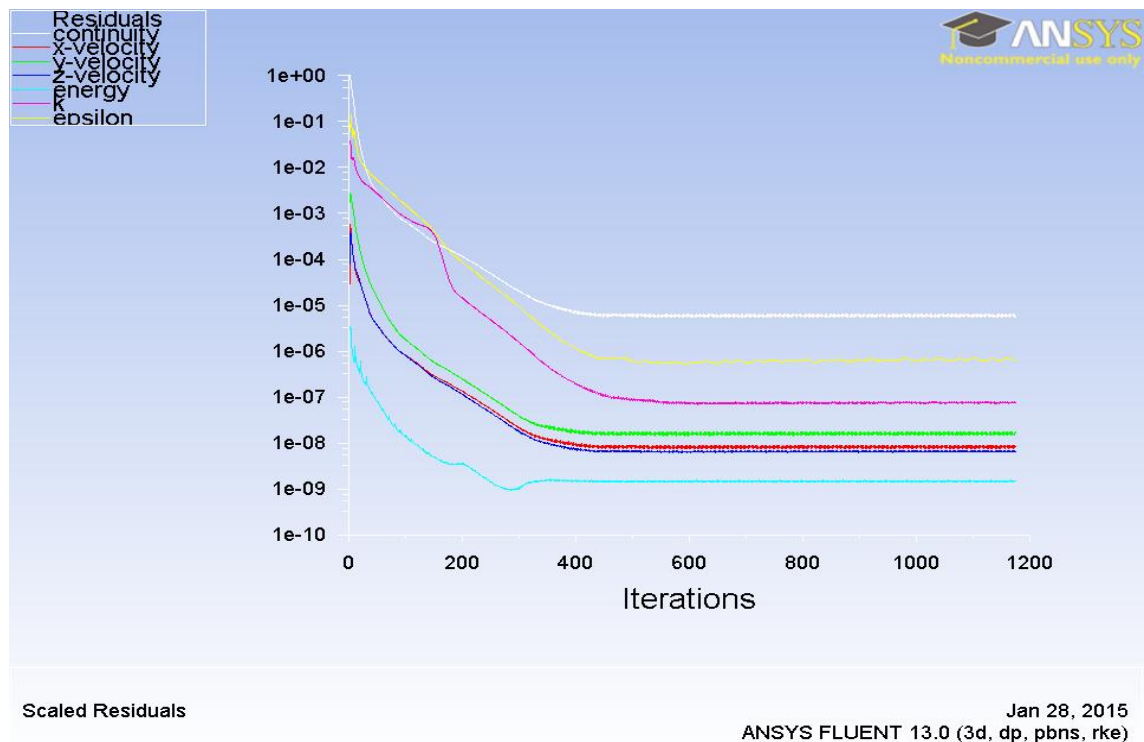


Fig. 5. 10: A typical example for convergence that was obtained within the current study.



### 5.6.2. Simulation of the Base Model (Existing Conditions)

The base model (referred here as S-1 or Scenario 1) is the replica of the existing situation in the study area within Quba Road. High urban density area was chosen as a base model for the numerical simulation studies of the existing conditions (as illustrated in Figure 5.2 and 5.11), to investigate the urban wind flow and pedestrian thermal comfort conditions. This base model (S-1) scenario was required to validate the simulation results with the in-situ measurements, and to be used as a yardstick to measure the performance of the other investigated scenarios through comparative analysis.

In this urban developed part of the route, the road's urban pattern consisted of three main rows of urban blocks and two parallel vehicular lanes (named as Tali'e Quba Road, i.e. windward canyon; and Nazil Quba Road, i.e. leeward canyon) with pedestrian paths on the sides of each canyon, as illustrated in Figure 5.11. The length and width of the urban area in the numerical simulation was 260mx178m, respectively. The measurements of wind velocity and air temperature were obtained within the interest area along the streets length of 120m and width of 12m.

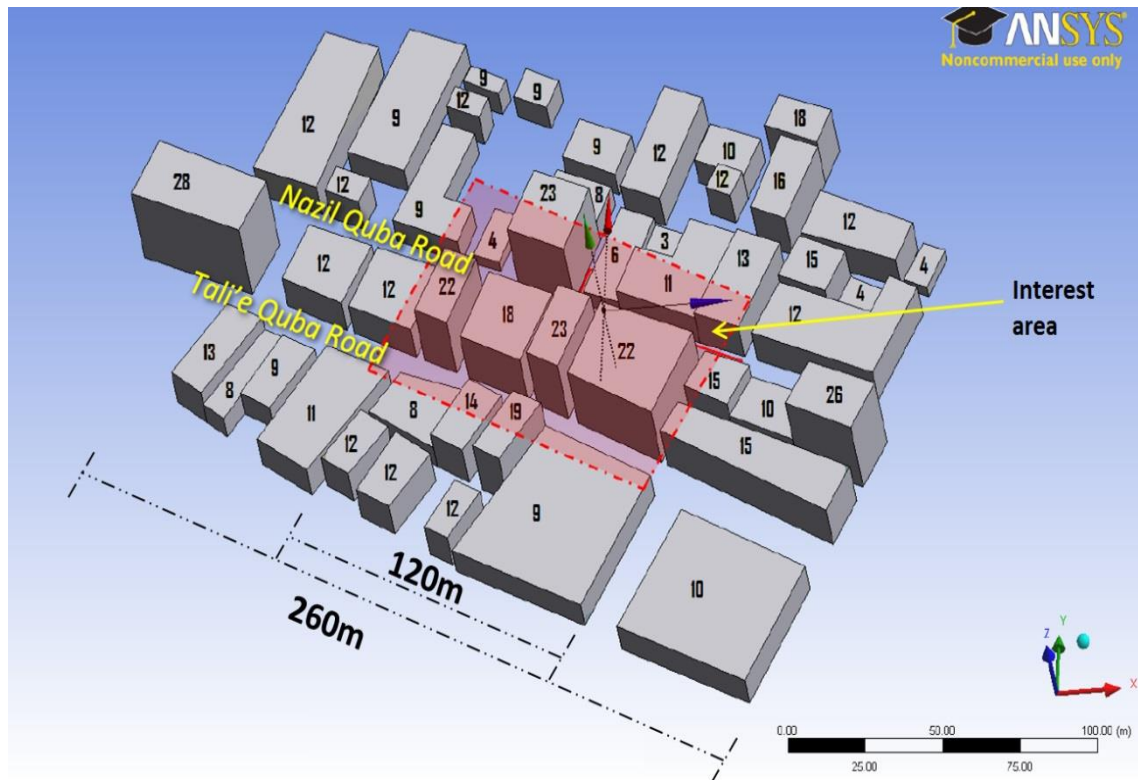


Fig. 5. 11: High urban density case (Base Model). Interest area of the study is 120 x 90m and the width of the Tali'e and Nazil Quba Roads is 12m.

The tallest building in the whole computational domain was 28m height as in the existing situation, and was situated outside the interest area, while building's height varied in the interest area from 4m to 23m, as illustrated in Figure 5.11. The study of the base model (S-1) analysed the air temperature and wind velocity measurements that were extracted from 15 points at each of the windward canyon (i.e. Tali'e Quba Road) and leeward canyon (i.e. Nazil Quba Road), particularly along the middles and the sides of the roads (at the left sides, i.e. near the leeward elevations, and at the right sides, i.e. near windward elevations), as illustrated in Figures 5.12, 5.13 and 5.14. Similar to the field measurements, the simulation results were extracted at the height of 2 metres above the ground level for the comparative purpose, which corresponds to the suggested pedestrian height in urban wind comfort studies (Blocken et al., 2009b).

Five cross-sections (E-1 through E-5) in the base model with variation of asymmetrical aspect ratios were analysed and compared with all the testing scenarios in this study, to find ways to improve the urban wind flow at the pedestrian level. Each cross-section had 3 measurement points on each canyon (i.e. total of 6 point per cross-section), as illustrated in Figures 5.12 and 5.13. The multi-asymmetrical aspect ratios ( $H_1/W - H_2/W - H_3/W$ ) for the three rows of the buildings of the five cross-sections (illustrated in Figure 5.12) were as follows:

- $H/W$  of 0.7 – 1.8 – 0.3 for E-1;
- $H/W$  of 1.2 – 1.5 – 1.9 for E-2;
- $H/W$  of 1.6 – 1.9 – 0.5 for E-3;
- $H/W$  of 0.8 – 1.8 – 0.9 for E-4; and
- $H/W$  of 0.8 – 1.8 – 1.1 for E-5

The variations in aspect ratios were based on variation in buildings height, while the street width was constant. Thus, the calculation of the multi-asymmetrical  $H_1/W - H_2/W - H_3/W$  aspect ratios were based on the following proposed equation 6 (adjusted from Qaid and Ossen, 2014), which starts from the windward side of the Tali'e Quba Road to the leeward side of the Nazil Quba Road. The equation (6) for the multi-asymmetrical aspect ratios is proposed here as:

$$\frac{H}{W} \text{ Ratio of } \frac{H_1}{W_1}; \frac{H_2}{(W_1+W_2)/2} \text{ and } \frac{H_3}{W_2} \quad (6)$$

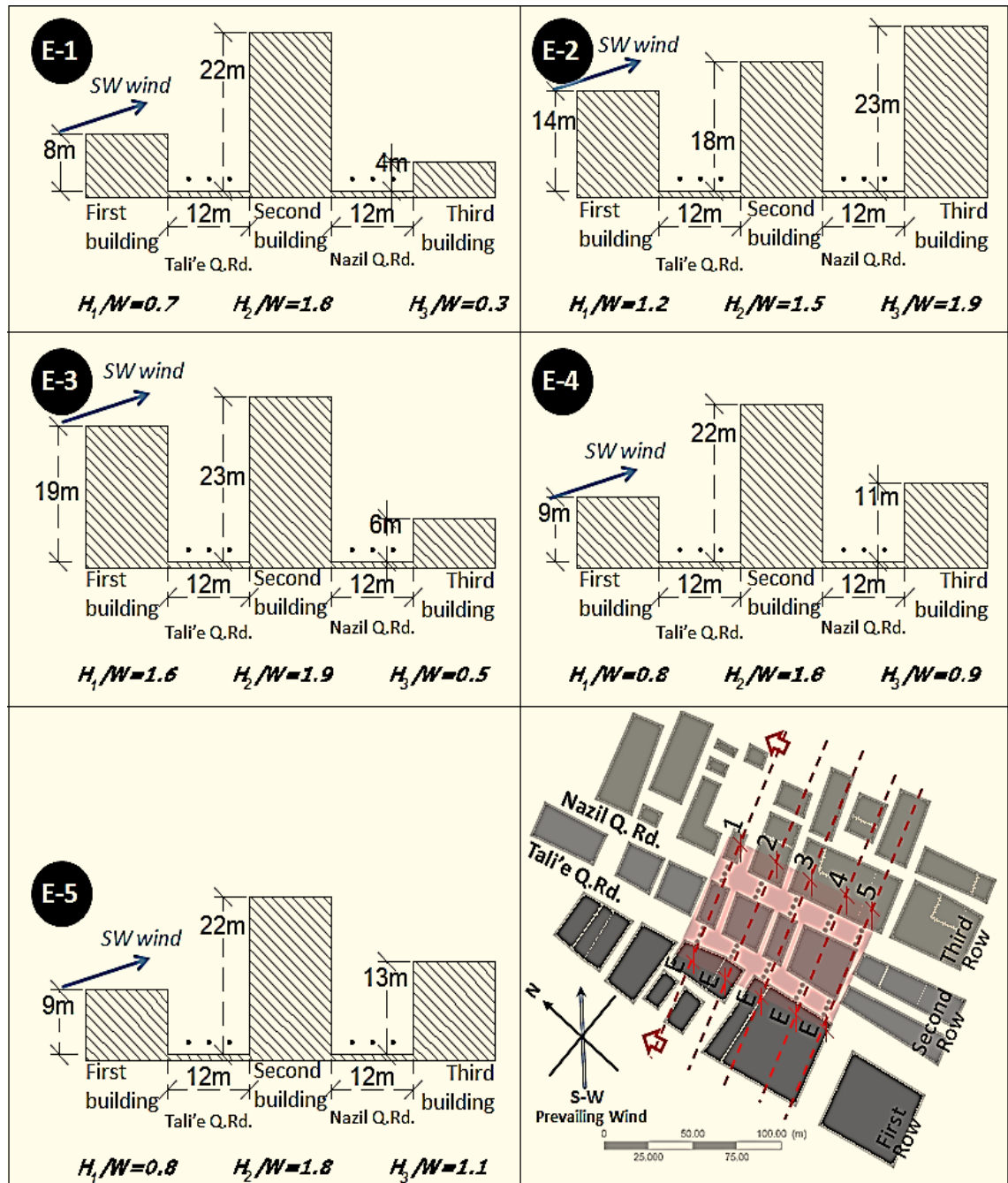


Fig. 5. 12: Asymmetric aspect ratios of the existing (E) case in the interest area, particularly along the five cross-sections of measurements points. Note that most of the numbers in  $H/W$  are rounded up.

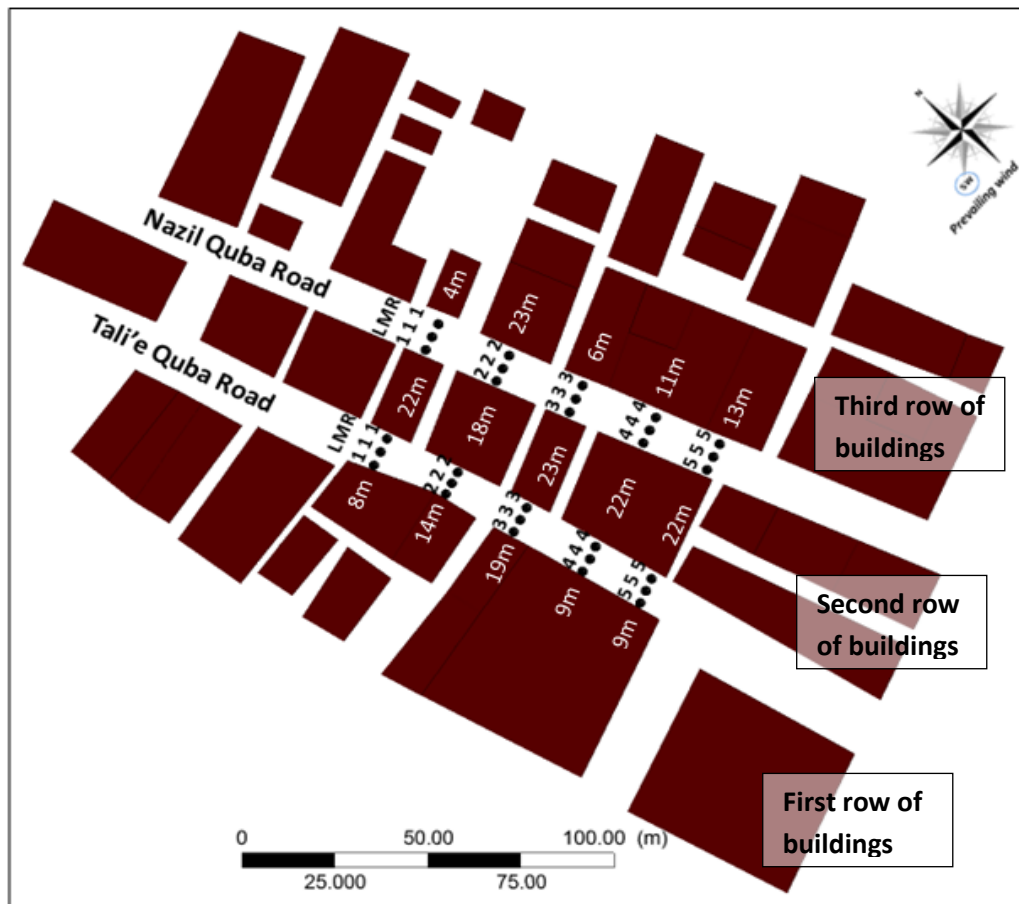


Fig. 5. 13: The figure shows 15 measurements points extracted for each of the two Quba canyons. Each canyon contains of three rows of measurements points, i.e. along the middle of the road, near leeward elevations (left) and near windward elevations (right).

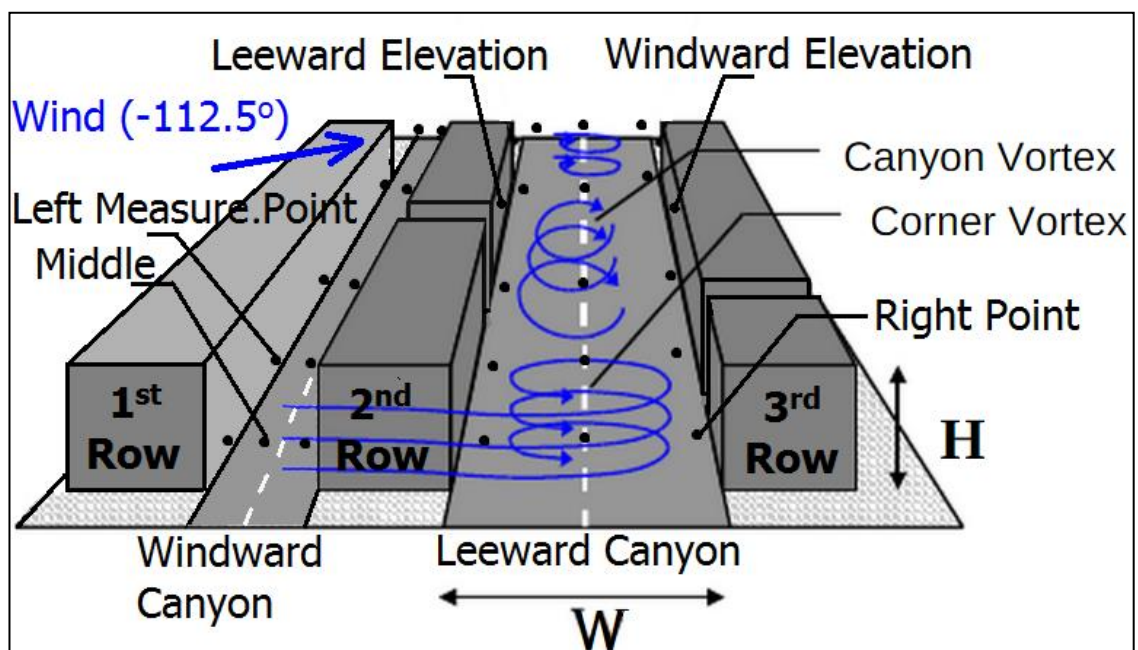


Fig. 5. 14: A simplified concept showing the locations of three rows of measurement points (left, middle and right; with 15 points in each canyon) between the three rows of buildings in the interest area.

### 5.6.3. Multi-Asymmetrical H/W Scenarios Based on Optimising the Base Case

The investigations of multi asymmetrical urban streets aspect ratios have not received much attention in the context of urban pedestrian thermal comfort (as asserted by Qaid and Ossen, 2014), particularly in hot arid regions. The main aim of this study was to examine the effects of the optimisation of the multi-asymmetrical aspect ratios to the existing urban configurations on the urban wind flow rate, seeking to find ways to improve the urban pedestrian microclimate conditions, particularly air velocity and air temperature, and pedestrian thermal comfort in hot arid climate of Quba Road canyons. To accomplish this aim, 15 scenarios (S-2 through S-16) were investigated and compared to the base model (S-1) based on modifying the buildings height.

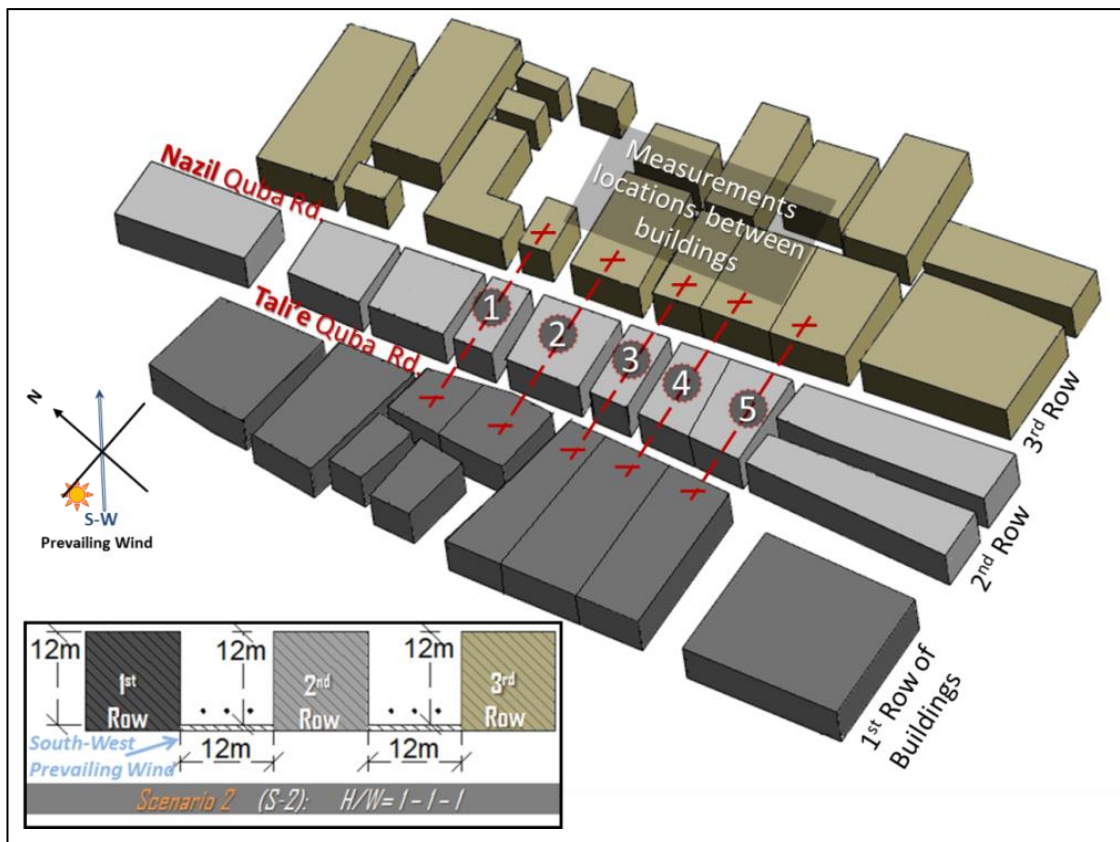


Fig. 5. 15: Symmetrical aspect ratio (S-2) scenario with five simulated locations of measurement points, showing unified buildings height of 12m for the three rows of buildings.

The second scenario (S-2 or Scenario 2) was a multi-symmetrical aspect ratios case, i.e. unified height of three rows of buildings to street width ratios ( $H_1/W - H_2/W - H_3/W$ ), as illustrated in Figure 5.15. The S-2 scenario was based on averaging the existing buildings height to street width aspect ratios, while it confirmed the recommended aspect ratio that can provide acceptable level of shading to canyons (Nakamura and Oke, 1988) for the approximately North-South street axis (with 22.5° anticlockwise orientation from the north). Thus, the buildings heights in the whole



computational domain in S-2 scenario were calculated to 12m for all the three rows of the buildings, while the widths of the two main Quba Roads were remained as in the existing case (i.e. 12m for each road), as illustrated in Figure 5.15. This S-2 scenario with multi-symmetrical aspect ratios (S-2) was proposed to find out whether symmetrical or unified buildings heights can achieve better wind velocities than the randomly varied buildings height in the base model (S-1) scenario. In addition, the land footprint and orientation of the urban street canyons were kept as in the existing situation, due to the local planning constraints (refer to Chapter 2). Thus, the symmetrical hypothetical aspect ratio for the three rows of buildings are  $H_1/W - H_2/W - H_3/W$  of  $1 - 1 - 1$  (i.e.  $H/W = 1$ ).

The S-3 through S-16 scenarios of multi-asymmetrical aspect ratios were proposed using the equation number 6 (mentioned above), based on optimising the heights of the second and the third rows of buildings from the proposed symmetrical aspect ratios (S-2), to satisfy the research aim of finding ways to enhance the pedestrian thermal comfort conditions. This is by increasing or decreasing number of floors (i.e. a height of 3m per floor) in each of the proposed aspect ratio scenarios. However, the simulation results of wind velocity and air temperature in the multi-asymmetrical aspect ratios scenarios (S-3 through S-16) were compared with base case S-1 scenario, but not with the hypothetical averaged height in the S-2 scenario. This is to evaluate their configuration effect on improving the microclimate of the existing conditions. The urban configuration properties for the proposed multi-asymmetrical aspect ratios scenarios are presented in Table 5.5. The strategy of increasing building The maximum buildings height of the proposed scenarios did not exceed 27m due to the local planning constraints (refer to the local planning and regulation section in Chapter 2).

The S-3 through S-12 scenarios of multi-asymmetrical aspect ratios were categorised into 3 groups based on variation of buildings height on both side of the canyons, which were: lower aspect ratios scenarios, medium aspect ratios scenarios and higher aspect ratios scenarios (e.g. Qaid and Ossen, 2014). S-13 through S-16 were categorised as leeward gradual increase in multi-asymmetrical aspect ratios, which were proposed based on Qaid and Ossen (2014), and were led by the results of the higher aspect ratios scenarios in current study, which were investigated to provide more options for urban street geometry configurations.

Thus, the specifications for the scenarios that were categorised as lower aspect ratios scenarios were:

- S-3 scenario with aspect ratios of 1 – 0.8 – 1.3; and
- S-4 scenario with interchanged aspect ratios of 1 – 1.3 – 0.8.

The second category was the medium aspect ratios scenarios, including three scenarios, which were:

- S-5 scenario with aspect ratios of 1 – 1.5 – 1.5;
- S-6 scenario with gradually increased aspect ratios of 1 – 1.3 – 1.8; and
- S-7 scenario with interchanged aspect ratios of 1 – 1.8 – 1.3.

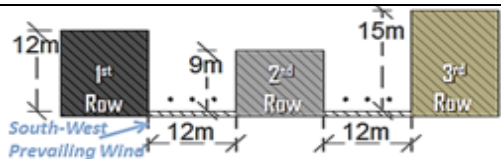
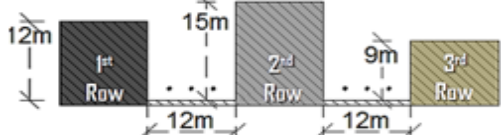
The third category was the high aspect ratio scenarios, including five cases, which were:

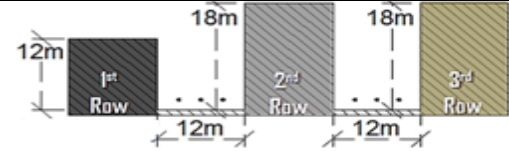
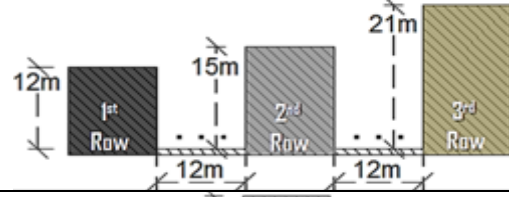
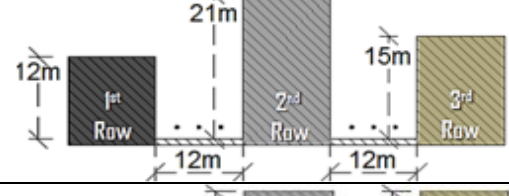

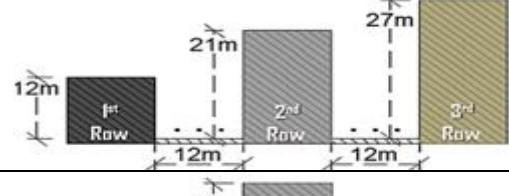
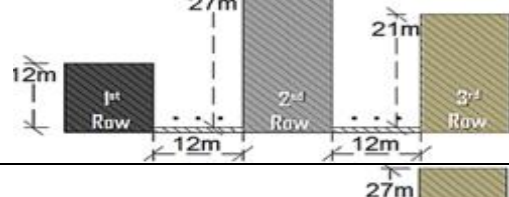
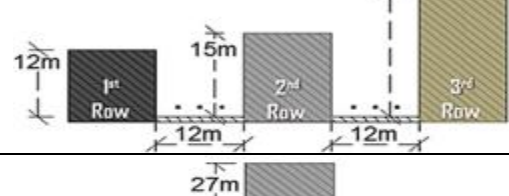
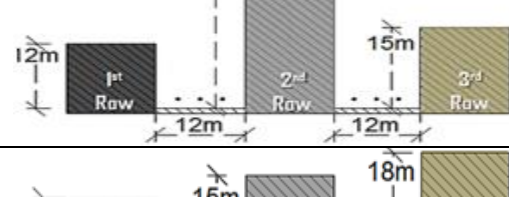
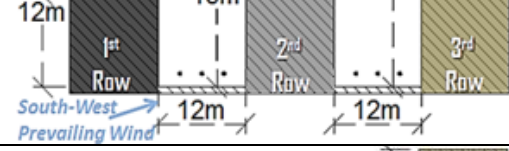
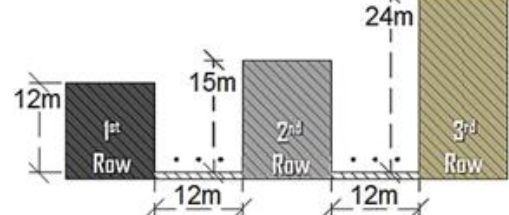
- S-8 scenario with aspect ratios of 1 – 2 – 2;
- S-9 scenario with gradually increased aspect ratios of 1 – 1.8 – 2.3;
- S-10 scenario with interchanged aspect ratios of 1 – 2.3 – 1.8;
- S-11 scenario with gradually increased aspect ratio of 1 – 1.3 – 2.3; and
- S-12 scenario with interchanged aspect ratio of 1 – 2.3 – 1.3.

The specifications for the leeward gradually increased aspect ratios scenarios (S-13 through S-16), which were:

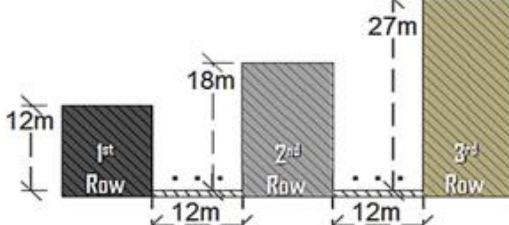
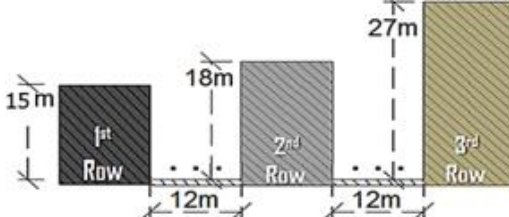
- S-13 scenario with aspect ratios of 1 – 1.3 – 1.5;
- S-14 scenario with aspect ratios of 1 – 1.3 – 2.0;
- S-15 scenario with aspect ratios of 1 – 1.5 – 2.3; and
- S-16 scenario with aspect ratios of 1.3 – 1.5 – 2.3 (note that the latter has higher aspect ratio on the first row of buildings).

Table 5. 5: Interchangeable multi-asymmetrical aspect ratios scenarios specifications for the second and third rows of buildings for S-3 through S-12, with the first row are constant as in S-2 scenario. Note that the numbers underlined in H/W are rounded up.

Scenario	Illustration	Aspect Ratio
Lower Aspect Ratios		H/W = 1 – <u>0.8</u> – <u>1.3</u>
		H/W = 1 – <u>1.3</u> – <u>0.8</u>

Intermediate aspect ratios	S-5		$H/W = 1 - 1.5 - 1.5$
	S-6		$H/W = 1 - \underline{1.3} - \underline{1.8}$
	S-7		$H/W = 1 - \underline{1.8} - \underline{1.3}$
Higher Aspect Ratios	S-8		$H/W = 1 - 2.0 - 2.0$
	S-9		$H/W = 1 - \underline{1.8} - \underline{2.3}$
	S-10		$H/W = 1 - \underline{2.3} - \underline{1.8}$
	S-11		$H/W = 1 - \underline{1.3} - \underline{2.3}$
	S-12		$H/W = 1 - \underline{2.3} - \underline{1.3}$
Leeward Gradual Increase in Aspect Ratios	S-13		$H/W = 1 - \underline{1.3} - \underline{1.5}$
	S-14		$H/W = 1 - \underline{1.3} - 2.0$



S-15		$H/W = 1 - 1.5 - \underline{2.3}$
S-16		$H/W = \underline{1.3} - 1.5 - \underline{2.3}$

The first row of buildings in S-3 through S15 (not including S-16), was specified with a unified building height of 12m (i.e. aspect ratio  $H_1/W$  of 1), which took into the account of the Nakamura and Oke (1988) recommendation. While in S-16, the first row of buildings had a height of 15m (i.e. aspect ratio  $H_1/W$  of 1.3), to measure its effects on wind velocity and air temperature in the adjacent canyon. The second and third rows of buildings for the scenarios between S-3 through S-12 were optimised with five interchangeable aspect ratios (e.g. Qaid and Ossen, 2014), while the scenarios between S-13 through S-16 were limited to gradually increased aspect ratios, as illustrated in Table 5.5.

#### 5.6.4.Scenarios Based on Optimising the Best Proposed Aspect Ratio Model

A best proposed aspect ratio model or an optimum H/W scenario in the current research was further investigated with 15 more scenarios (S-17 to S-31) to evaluate their effects on the urban wind flow rate and air temperature, seeking to find ways to improve the urban pedestrian microclimate (i.e. objective 6). These included scenarios on: time variations, different orientations of urban canyons with wind directions, increasing the number of buildings' rows, configuring new streets perpendicular to the existing canyons, removal of buildings, providing cantilevers, and changing material colours and changing the block patterns, as discussed in more details in the following subsections.

#### **5.6.4.1. Variations of Wind Flow at Night (S-17) and Noon (S-25) for the Best Proposed H/W Model**

In S-17 scenario and S-25 scenario, the effects of configuring the best asymmetrical aspect ratios strategy (H/W of 1–1.3–2.3) on the night time and noon wind flow were investigated, for the configuration illustrated in Figure 5.16. The initial study of pedestrian number in Quba Road during the night indicated that the number of users increased significantly just before the sun set to the mid night, as a result of lower air temperature and absence of solar radiation (refer to section 6.2.1). In addition, the number of pedestrian increases at noon due to the prayer time to perform prayers at adjacent mosque. Therefore, these investigations were important to study the night time and noon effect on wind flow. In addition, for a comparative purpose, another new scenarios called S-1 Night and S-1 Noon were tested to represent the night condition in the base model as in the existing situation at 21:00 hours and 12:00 hours, respectively (e.g. Rizk and Henze, 2010). While the wind speed profile at the inlet boundary condition is defined as 2.9m/s at 21:00 hours instead of the day time 4.7m/s (i.e. at 15:00 hours), and as 3.9m/s at noon, based on the city airport meteorological readings (refer to the validation section 5.6.1).

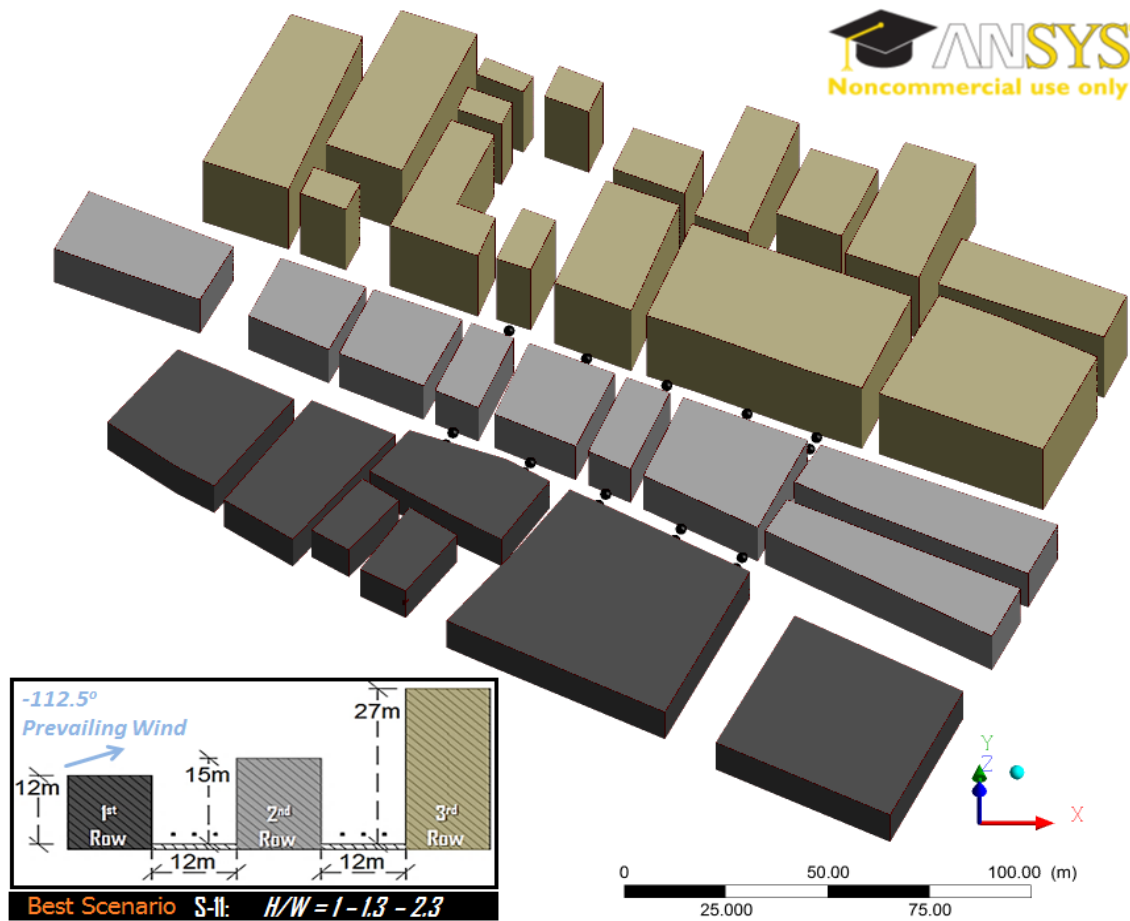


Fig. 5. 16: The best proposed multi-asymmetrical aspect ratios scenario (S-11) with five set of measurement locations for each of the two main canyons at the pedestrian level.

#### 5.6.4.2. Increasing the Number of Building's Rows (S-18, S-19)

The strategy of increasing the number of rows of buildings, in S-18 and S-19 scenarios, to the leeward area of the best proposed aspect ratio model was to study the variation of wind flow in the leeward urban areas (i.e. an area located beyond the third row of buildings), as illustrated in Figure 5.17. This is by increasing three more rows in the leeward with grid type buildings positions (S-18) and chess-board type buildings position (S-19). These two types of buildings position were designed based on the findings of Rizk and Henze (2010), where it was found that chess-board position style could improve the microclimate in their study compared to the grid position style, regardless the increase in aspect ratios. Thus, these scenarios aimed to find out the effect of increasing in aspect ratios on the urban microclimate in the leeward urban area.

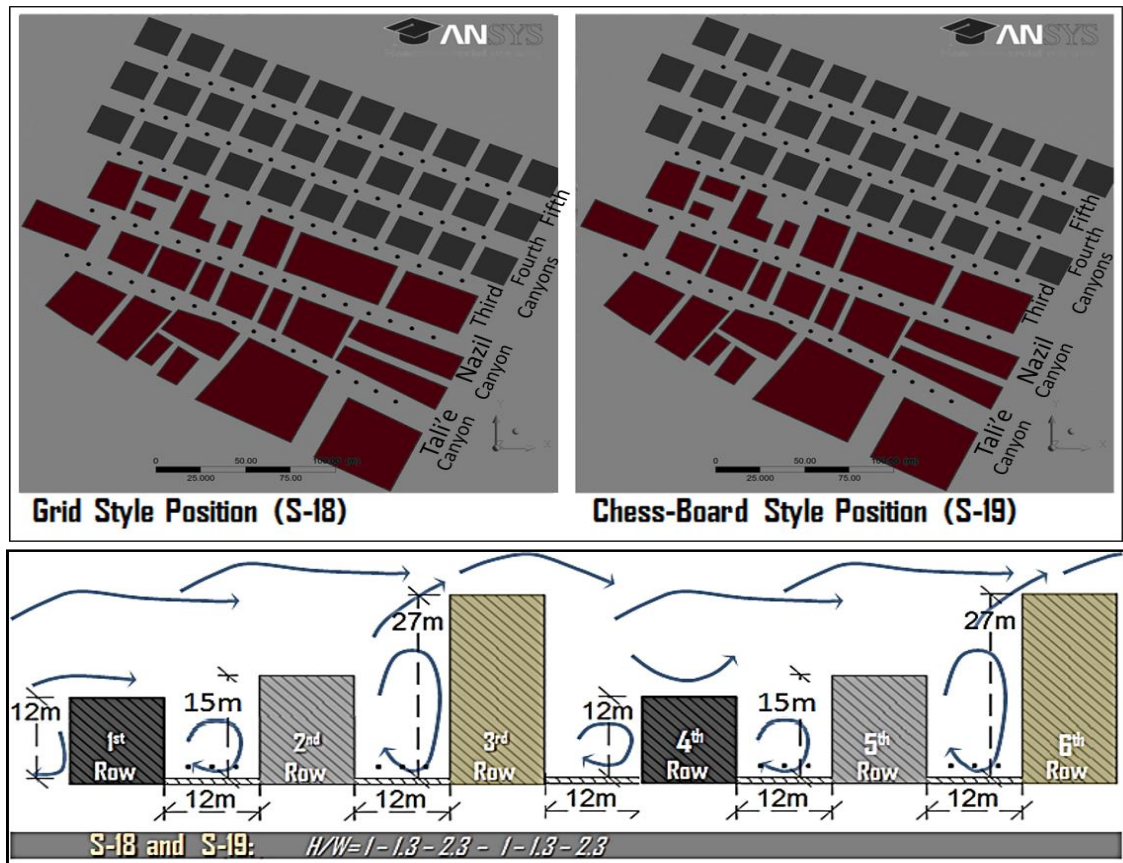


Fig. 5. 17: Increasing the number of rows of buildings on the best aspect ratio scenario from 3 rows to 6 rows. The last three rows are positioned as grid style in S-18, while as chess-board in S-19.

However, the aspect ratios of the three new rows (i.e. the fourth, fifth and the sixth rows of buildings) did not continue increasing in buildings' height after the maximum height of 27m of the third row of the buildings in the chosen proposed H/W model, but rather it alternated and started back from 12m, as shown in the cross-section in Figure 5.17. Thus, the first row and the fourth row shared the same height of 12m; the second row and the fifth row shared the height of 15m; and the third row and the sixth row shared the height of 27m. Thus, the multi asymmetrical aspect ratios in S-18 and S-19 scenarios were  $H_1/W-H_2/W-H_3/W-H_4/W-H_5/W-H_6/W$  of 1-1.3-2.3-1-1.3-2.3, with totally five canyons, as illustrated in Figure 5.17. The reason for the repetition of the gradual heights of the first three rows in the leeward area was due to the local planning regulations that limits the maximum height to 27m, while it follows Hang et al.'s (2015) recommendation on building height variations, seeking to produce downward wind flows in front of the taller buildings in the leeward area.

#### 5.6.4.3. Orientation of the Urban Canyon Geometry with Less Prevailing Wind Directions (S-20, S-21)

The three yearly prevailing wind directions in Madinah are mainly from South-West direction, followed by West direction (i.e. second level prevailing wind), then the North-West direction (i.e. third level prevailing wind). The best H/W model was based on South-Westerly prevailing wind direction with  $-112^\circ$  angle of attack to the urban canyon. Therefore, S-20 investigated the strategy of the orientation of the urban canyon with the westerly wind direction (i.e.  $-90^\circ$  angle of attack), while S-20 scenario investigated North-Westerly wind direction (i.e.  $-22^\circ$  angle of attack), as illustrated in Figure 5.18. The aim was to evaluate their effects on urban wind flow rate in the best proposed asymmetrical aspect ratio model.

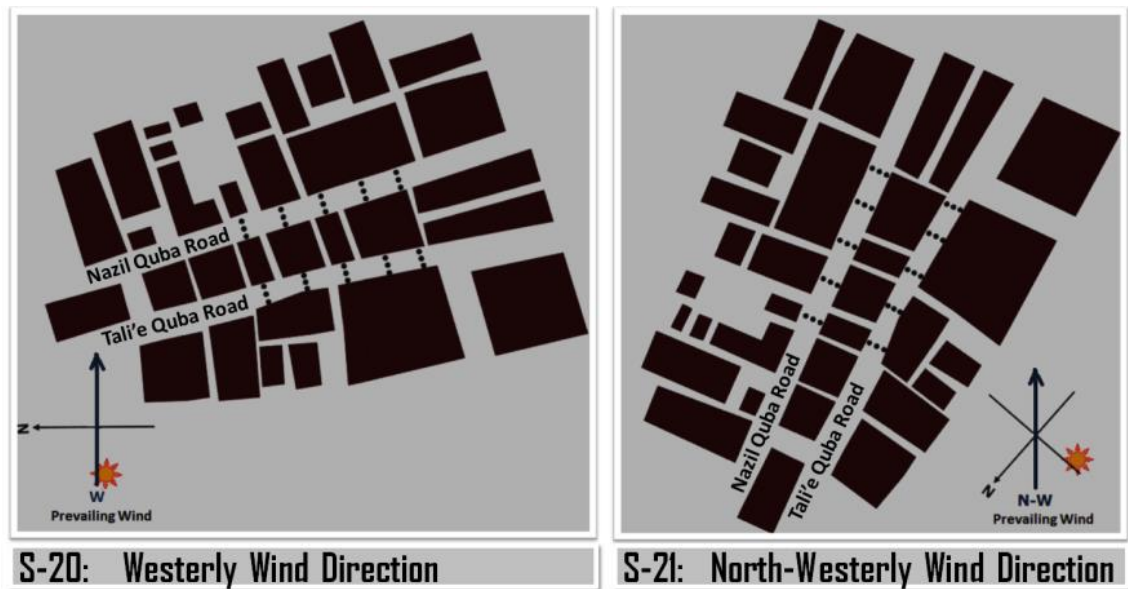


Fig. 5. 18: Orientation of urban canyon geometry with the Westerly second prevailing wind direction (S-20 scenario) and North-Westerly third prevailing wind direction (S-21 scenario).

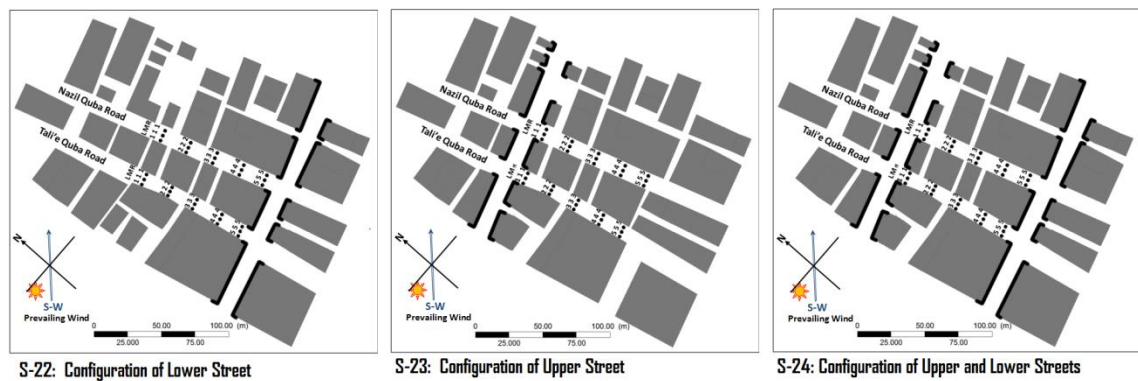
#### 5.6.4.4. Configuration of New Streets Perpendicular to the Quba Canyons (S-22, S-23, S-24)

The strategy of configuring new streets that were perpendicular to the North-South axis of Quba canyons while approximately parallel with the prevailing wind direction, was proposed in three scenarios (S-22 through S-24), as illustrated in Figure 5.19.

- The S-22 scenario investigated a street configuration located in the lower position of the interest area.

- The S-23 scenario investigated a street configuration located in the upper side of the interest area.
- The S-24 scenario investigated a configuration of two streets located in the upper and lower sides of the interest area.

Thus, these three scenarios (S-22 through S-24) were investigated seeking for better microclimatic enhancement strategy.



*Fig. 5. 19: Three scenarios on the configuration of new streets that are parallel with the main prevailing wind direction, while it is approximately perpendicular to the North-South axis of Quba Canyons.*

#### **5.6.4.5. Removal of Buildings (S-26) Forming Open Spaces for a Local Hub**

In the previous investigations of wind velocity and air temperature in S-11 scenario (the optimum aspect ratio strategy, refer to section 7.4.3), it was found the area behind a windward building of the third row, particularly near the simulated location number 4 in the Nazil Quba Road (leeward canyon), has a lower wind flow and higher air temperature results, compared to the existing situation. Therefore, scenario S-26 was proposed here to study the effect of removal of buildings on the variation of wind flow in the Nazil Quba Road (i.e. Leeward Canyon) as well as on the area behind the removed building, as illustrated in Figure 5.20. Thus, a passage between buildings parallel with the prevailing wind direction and an open space at the eastern side of the canyon were created to replace this removed building.



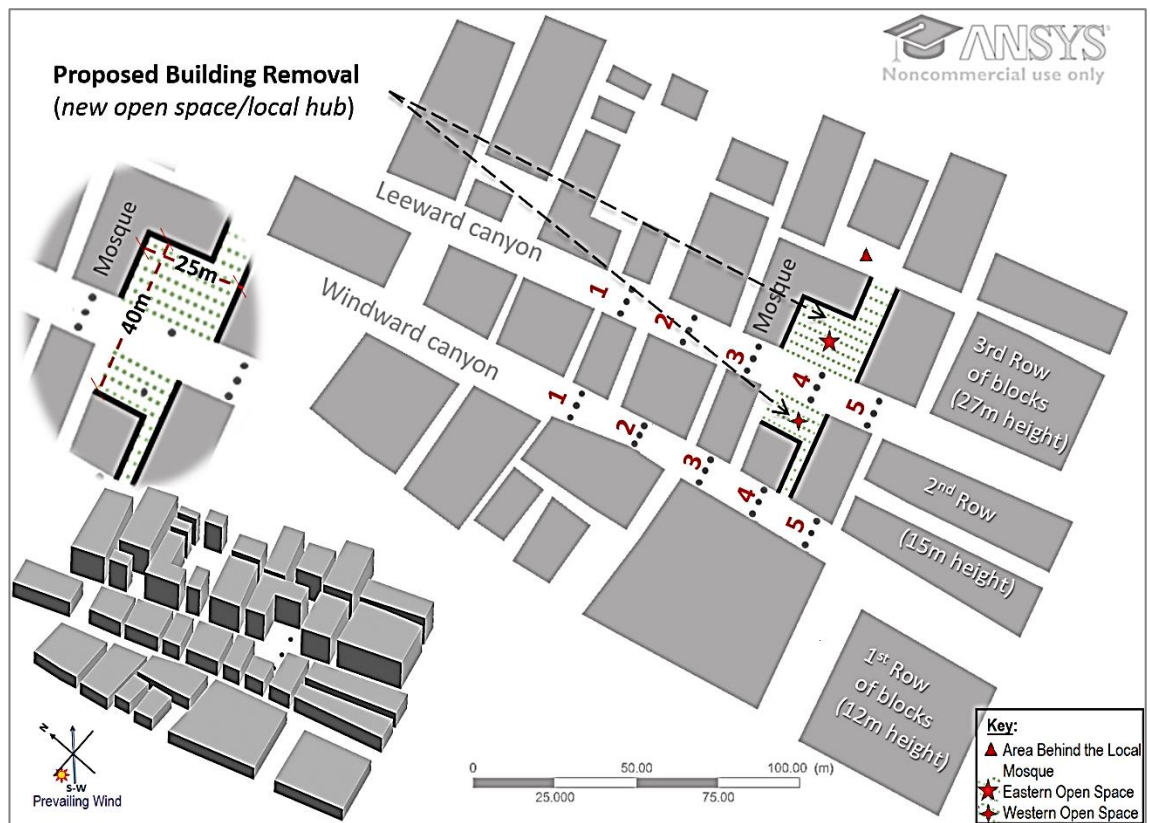


Fig. 5. 20: Scenario S-26 based on removing buildings and or creating open spaces and passages, particularly at simulation location number 4 in the leeward canyon (i.e. Nazil Quba Road).

In addition, in S-26 scenario, part of a leeward building at the location number 4 in the Nazil Quba Road (leeward canyon) was removed, to create a passage parallel with the prevailing wind direction, and an open space at the western side of the canyon. The integration of the two open spaces (at the eastern and western sides of the Nazil Quba Road or the leeward canyon), would form a local hub in this high urban density area.

An existing local mosque can be found on the third row of the buildings adjacent to the simulated locations number 3 and 4. An urban space location was recommended in a previous research by the author (Setaih, 2010), on the physical linkages between Quba and the Prophet mosques through proposing several nodes, that compromise of communal hubs with mosques and retail outlet based on acceptable walking distance in hot arid climate from one node to another, as illustrated in Figure 5.21.



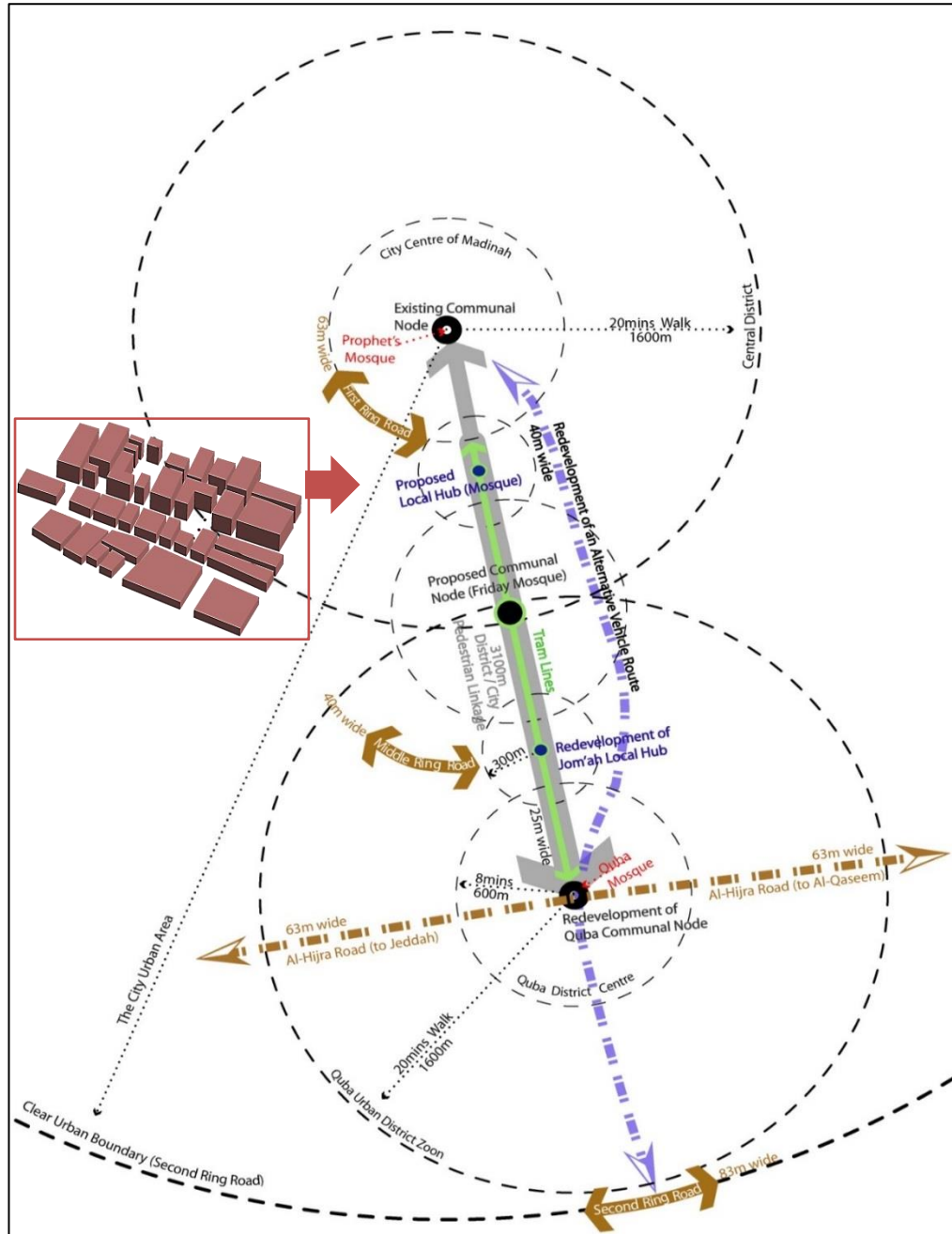


Fig. 5. 21: Conceptual diagram for proposed communal nodes and local hubs in Quba Road based on acceptable maximum walking time (in minutes) and distance (in metres). Adapted from Setaih (2010).

The urban street aspect ratio for locations 1, 2, 3 and 5 in S-26 (removal of buildings) scenario followed the  $H_1/W - H_2/W - H_3/W$  of 1 – 1.3 – 2.3 of the S-11 scenario (i.e. the optimum H/W strategy). While the aspect ratio for the proposed integrated urban open space at location 4 was changed to  $H_1/W - H_2/W$  of 1 – 1.3 in the windward canyon, and  $H_2/W - H_3/W$  of 0.4 – 0.7 in the leeward canyon. This was because the approximate width of the integrated open space in S-26 scenario was

increased to 40m, while the length was 25m in the eastern side of the leeward canyon and 20m in the western side.

#### 5.6.4.6. Protruding Upper Floors for Shading (S-27 and S-28)

The study aimed to evaluate the effects of shading by buildings' protruding upper floors, which narrows the streets openness to the sky (from 12m to 9m), on the urban pedestrian microclimate, particularly at 15:00 hours (i.e. S-27 scenario) and 12:00 hours (i.e. S-28 scenario). The effect on the wind velocity and air temperature were compared with the optimum multi-asymmetrical aspect ratios  $H/W$  of 1 – 1.3 – 2.3 in scenarios S-11 at 15:00 hours and S-25 at noon.

The heights of the three rows of the buildings in both of the protruding upper floors scenarios (S-27 and S-28) were 12m – 15m – 27m, which were the same as in S-11 and S-25 scenarios. While the width of the street openness to the sky was different, as it was calculated to 9m instead of 12m. This was due to an extension of 1.5m applied on the leeward and wind elevations in both of the Quba Road canyons in S-27 (protruding floors at 15:00 hours) and S-28 (protruding floors at noon), particularly the floors above the ground floor (i.e. above 3m from the ground), as illustrated in Figure 5.22.

Thus, the strategy of protruding upper floors for shading in S-27 (at 15:00 hours) and S-28 (at noon) has the multi-asymmetrical aspect ratios  $H/W$  specification of 1.3 – 1.7 – 3, based on optimising the street openness to the sky.

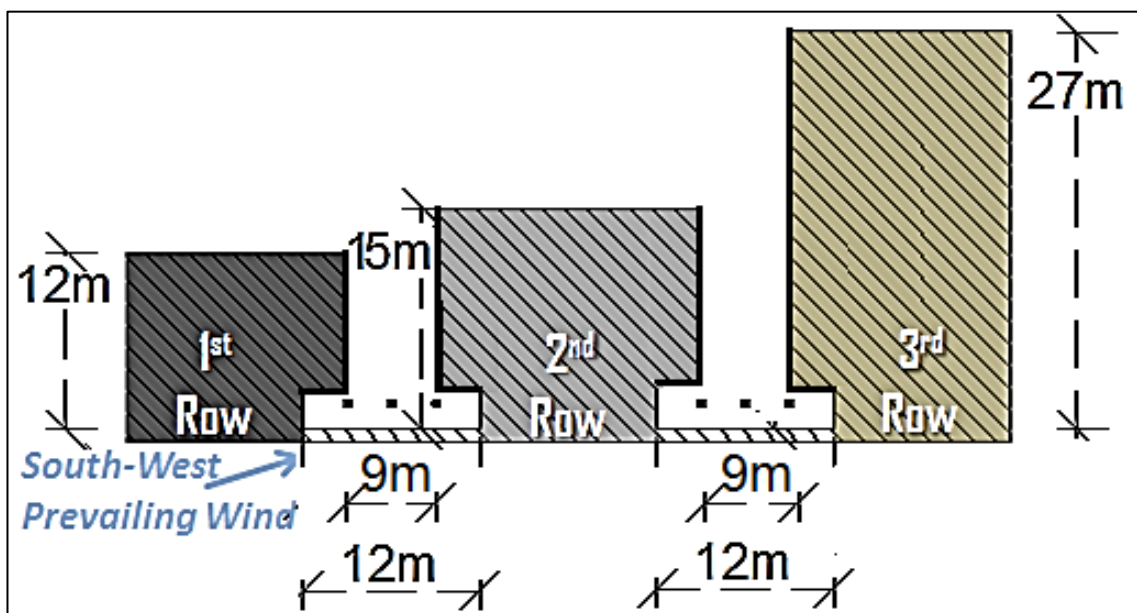


Fig. 5. 22: protruding upper floors scenario in S-27 and S-28 scenarios, with 9m street openness to the sky.



#### 5.6.4.7. Changes to Albedo Level for Surface Materials (S-29)

In the proposed scenarios in the current research, low albedo levels of asphalt and concrete material properties were applied to the ground and building surfaces, respectively. According to Ahranjani (2010), reducing the asphalt-paved area, and using higher solar reflectance (albedo) materials on buildings, can mitigate the heat stress in urban environments.

Therefore, S-29 scenario was proposed by changing the surface material properties from asphalt (i.e. for the ground) and concrete (i.e. for the buildings) to higher albedo levels of soil and white paint, respectively, to evaluate their effects on the variation of wind velocity and air temperature in the Quba Road canyons. Table 5.6 shows the specifications for soil and white paint surface materials used in this investigation, which were based on ASHRAE (2009) and a study by Qu (2011).

Table 5. 6: Material specifications based on ASHRAE (2009) and Qu (2011).

Material	Specific Heat J/(kg.°C)	Density kg/m <sup>3</sup>	Thermal Conductivity W·K <sup>-1</sup>	Emissivity	Albedo
Asphalt	920	2360	1.3	<b>0.93</b>	0.05-0.2
Concrete	840	1500	1.7	<b>0.92</b>	0.1-0.35
Soil	800	1600	0.75	<b>0.80</b>	0.14-0.37
White Paint	650	7000	6	<b>0.13</b>	0.6 – 1.0

#### 5.6.4.8. Changes to Block Patterns (S-30 and S-31)

In the previous investigations of wind velocity and air temperature for increasing the number of rows (from 3 to 6 rows) in the S-18 scenario (Grid Style building positions) and S-19 scenario (Chess-Board Style building positions), the first and second canyons (i.e. Tali'e and Nazil Quba Roads) had no further improvement in microclimate compared to the optimum aspect ratio model (i.e. S-11 with H/W of 1 – 1.3 – 2.3). This could be because of no changes were applied to the block pattern in the first three rows of the buildings in S-18 and S-19 scenarios.

Therefore, scenario S-30 (Grid Style building positions) and S-31 (Chess-Board Style building positions) were proposed to study the effect of changing the block

patterns of the first three rows of the buildings on the variation of wind flow in the Nazil Quba Road (i.e. Leeward Second Canyon) as well as on the area behind the first three rows, as illustrated in Figure 5.23. Three new rows of buildings were also proposed in the leeward area (i.e. beyond the third row) to compare the wind variation results in the canyons with the previously investigated scenarios of S-18 and S-19 (refer to section 5.6.4.2), based on buildings position style and shared multi-asymmetrical aspect ratios.

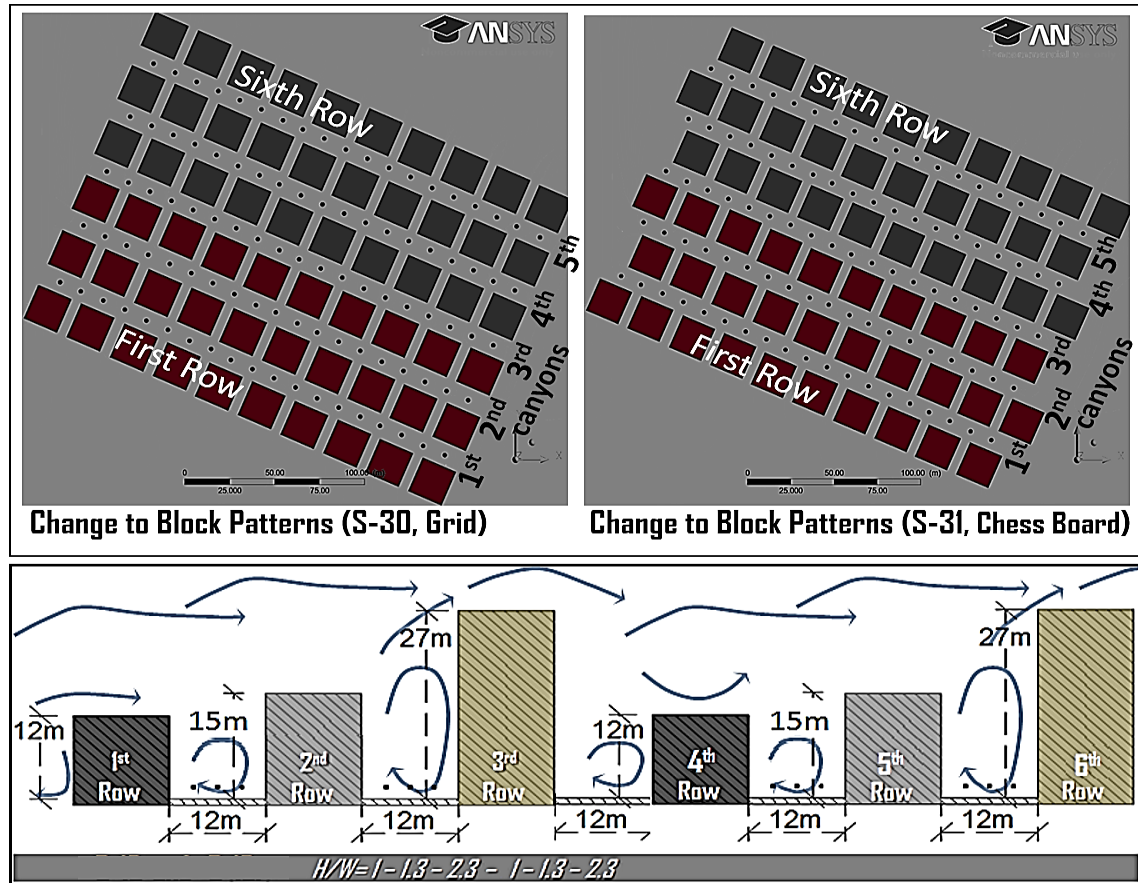


Fig. 5. 23: Changes to block patterns in S-30 with grid building position and S-31 with chess board building position, and increasing the number of rows to be total of 6 rows.

## 5.7. Calculation of PET Index and MRT Temperatures (Phase 5)

In Phase 5, the objectives number 4, 5 and 7 in this research were addressed (refer to section 1.4), which were evaluating the existing outdoor pedestrian thermal comfort conditions in the four climatic seasons of Madinah (discussed in Chapter 6), evaluating the outdoor pedestrian thermal comfort conditions in the proposed urban street aspect ratios models were conducted (discussed in Chapter 7), and to propose guidelines for planners for improving the wind flow and outdoor thermal comfort based on the case study of Quba Road (discussed in Chapter 8). Murakami (2006:109) has stated that “one of the final targets of environmental design is the evaluation of human

comfort". According to Erell et al. (2011) computer simulation and on-site measurement methods can provide the basic microclimatic measurements that can facilitate the calculation of human thermal comfort conditions outdoors, through the distribution of thermal comfort indices (e.g. PET, PMV, etc.).

The pedestrian thermal comfort was expressed by means of the physiologically equivalent temperature (PET) index (refer to section 3.5). PET was calculated using the RayMan model (Matzarakis et al., 2007), as illustrated in Figure 5.24. RayMan software simply takes inputs of the thermal comfort key factors (discussed in Chapter 3), and it is valid for hot and sunny climate in which values of MRT exceed 60°C at around noon (Abdel-Ghany et al., 2013; Matzarakis et al., 2007). PET index has been calibrated for hot arid regions, particularly in built up areas, with an upper limit of 31.3°C and lower limit of 21°C (Yahia and Johansson, 2013a). The factors that were necessary for calculating the PET index were: air temperature, mean radiant temperature, relative humidity, wind speed, pedestrian metabolic rate (i.e. activity level; 192.5 W for walking) and clothing insulation level (e.g. 0.59clo for summer clothing and 1.3clo for winter clothing). In the assessment process of the existing conditions, the required data were obtained in the field measurement process (Phase 2) for the four climatic seasons, except the Mean Radiant Temperature (MRT) data which were calculated based on the measured globe temperature.

**RayMan 1.3**

File Input Output Table Language ?

**Date and time**

Date (day.month.year)

Day of year

Local time (h:mm)

**Geographic data**

**Location:**

Geogr. longitude (°.'." E)

Geogr. latitude (°.'." N)

Altitude (m)

Timezone (UTC + h)

**Current data**

Air temperature Ta (°C)

Vapour pressure VP (hPa)

Rel. humidity RH (%)

Wind velocity v (m/s)

Cloud cover N (octas)

Global radiation G (W/m²)

Mean radiant temp. Tmrt (°C)

**Personal data**

Height (m)

Weight (kg)

Age (a)

Sex

**Clothing and activity**

Clothing (clo)

Activity (W)

**Thermal indices**

☐ PMV ☒ PET ☐ SET\*

Fig. 5. 24: Interface of RayMan software v. 1.3. to obtain PET thermal comfort values. The required six main inputs are numbered in this image from 1 to 6.

The MRT is defined as the uniform surface temperature of black enclosure with which an individual exchanges the same heat by radiation as the actual non-uniform environment (Gaitani et al., 2007; CIBSI, 2006b). MRT is a key factor in pedestrian thermal comfort, but is more complex than the air temperature as it affects the radiation mode of heat transfer, and thus it is a measure of radiation exchange of “*the average temperature of the surrounding surface elements*” (Szokolay, 2008:18; CIBSE, 2006a:8). Moreover, the difference between air temperature and MRT is that the latter has a greater influence on the body heat gain or loss to the environment, as our skin absorbs as much radiant energy as a matt black body, even though this can be decreased by reflective clothing (Streinu-Cercel et al., 2007).

In field based studies, the MRT equation (number 7) was given by ASHRAE (2009) with empirical coefficient recently refined by Thorsson et al. (2007b) based on globe temperature ( $T_g$ ) that is applicable for hot arid conditions (e.g. Johansson et al., 2014; Yahia and Johansson, 2013a):

$$MRT = \left[ (T_g + 273.15)^4 + (1.335 \times \frac{10^8 V^{0.71}}{\epsilon D^{0.4}}) \times (T_g - T_a) \right]^{\frac{1}{4}} - 273.15 \quad (7)$$

The MRT in the current research was estimated mathematically by determining globe temperature ( $T_g$  in  $^{\circ}C$ ; with globe emissivity,  $\epsilon$ , of 0.95 and globe diameter,  $D$ , of 25mm), ambient air temperature ( $T_a$  in  $^{\circ}C$ ) and air velocity ( $V$  in  $m/s$ ). The empirical derived parameter  $1.335 \times 10^8$  and the wind exponent ( $V^{0.71}$ ) together represent the globe's mean convection coefficient ( $1.335 \times 10^8 V^{0.71}$ ). According to Thorsson et al. (2007b), the likely error in estimating the MRT using Equation 7 is approximately  $\pm 3$  K.

However, in the numerical models, which was simulated at 15:00 hours during April (autumn season), the relative humidity was assumed equal to the field measurement value at 15:00 in April (i.e. 8.2%) in the high urban density area. This was because of no source of water exchange was available in the simulated models (i.e. water-proof surfaces, with no trees or water plants), and thus air humidity would not experience significant changes to thermal comfort (e.g. Ali-Toudert and Mayer, 2006), particularly in hot arid regions.

The MRT value was simplified in the simulation process in this research by assuming it to be  $1.7^{\circ}C$  higher than the simulated air temperature in the high urban density area in Quba Road, particularly at 15:00 in April. In previous studies by Zhang et al., 2011; Stavrakakis et al., 2010; Prianto and Depecker, 2003, the MRT was



simplified by assuming the MRT to be equalled to the air temperature, as the globe temperature reading is not available in the CFD Fluent 13.0 simulation code. However, in the current research, the MRT was calculated during the field measurement, and a difference value of 1.7°C is found at 15:00 compared to the air temperature in April (average measurement of 11 days, excluding the 10<sup>th</sup> of April 2013 due to over estimation of the globe temperature at this time, refer to Table A6.1 in the appendices). In addition, the difference value between the MRT and air temperature at 12:00 hours is found to be 11.1°C (average measurement of 12 days). Nevertheless, this method was used in the CFD numerical study only to obtain the PET values for the simulated models.

## 5.8. Summary

This chapter discussed the research methodology and procedures which were mainly quantitative methods. The main aim and objectives of the present study were accomplished using data obtained from preliminary studies (Phase 1), field measurements and meteorological data (Phase 2), and secondary data collection method through numerical simulation models (Phases 3 and 4, respectively). This chapter has also explained about the main modelling process and the basic CFD guidelines for using ANSYS Fluent 13.0 software. Equation 6 has been proposed for the multi-asymmetrical  $H_1/W - H_2/W - H_3/W$  aspect ratios scenario, which has been adjusted from Qaid and Ossen, 2014.

The pedestrian thermal comfort was expressed by means of the physiologically equivalent temperature (PET) index using RayMan software (Phase 5). The procedures for calculating the MRT has also been discussed. Thus, the outcome of this study would be divided into two parts. The first part will be the assessment of the urban microclimate and outdoor pedestrian thermal comfort conditions in the current three case studies along Quba Road, i.e. high urban density area (Case 1), intermediate urban density area (Case 2) and low urban density area (Case 3), using the field studies method (the results are presented in Chapter 6). The second part will be an enhancement approach to the pedestrian thermal comfort levels, using the numerical modelling tests of the urban street canyon modification based on modelling the high urban density area, i.e. Case 3 (the results are presented in Chapter 7 and 8).

# **CHAPTER 6: Field Measurements for the Assessment of Pedestrian Thermal Comfort**

## **Chapter Structure**

- 6.1. Introduction
- 6.2. The High Urban Density Area (Case 1)
- 6.3. The Intermediate Urban Density Area (Case 2)
- 6.4. The Low Urban Density Area (Case 3)
- 6.5. Comparison between the Three Urban Density Levels  
(Case 1, 2 and 3)
- 6.6. Summary

# Chapter 6:

## Field Measurements for the Assessment of Pedestrian Thermal Comfort

---

### 6.1. Introduction

This chapter focuses on conducting field measurements to explore the variations of the urban microclimate and pedestrian thermal comfort conditions over a year, in the residential and commercial urban canyon of Quba Road (i.e. Nazil Quba Road) in Madinah (i.e. objective 4 in section 1.4). The data are obtained for an approximately North-South street axis ( $-22.5^\circ$  from the north). Three areas are studied based on the built-up level, which are: the high urban density area (Case 1), the intermediate urban density area (Case 2), and the low urban density area (Case 3), as illustrated in Figure 6.1.

This chapter analyses the air temperature, air velocity, relative humidity, MRT (Mean Radiant Temperature), and PET index (Physiologically Equivalent Temperature).

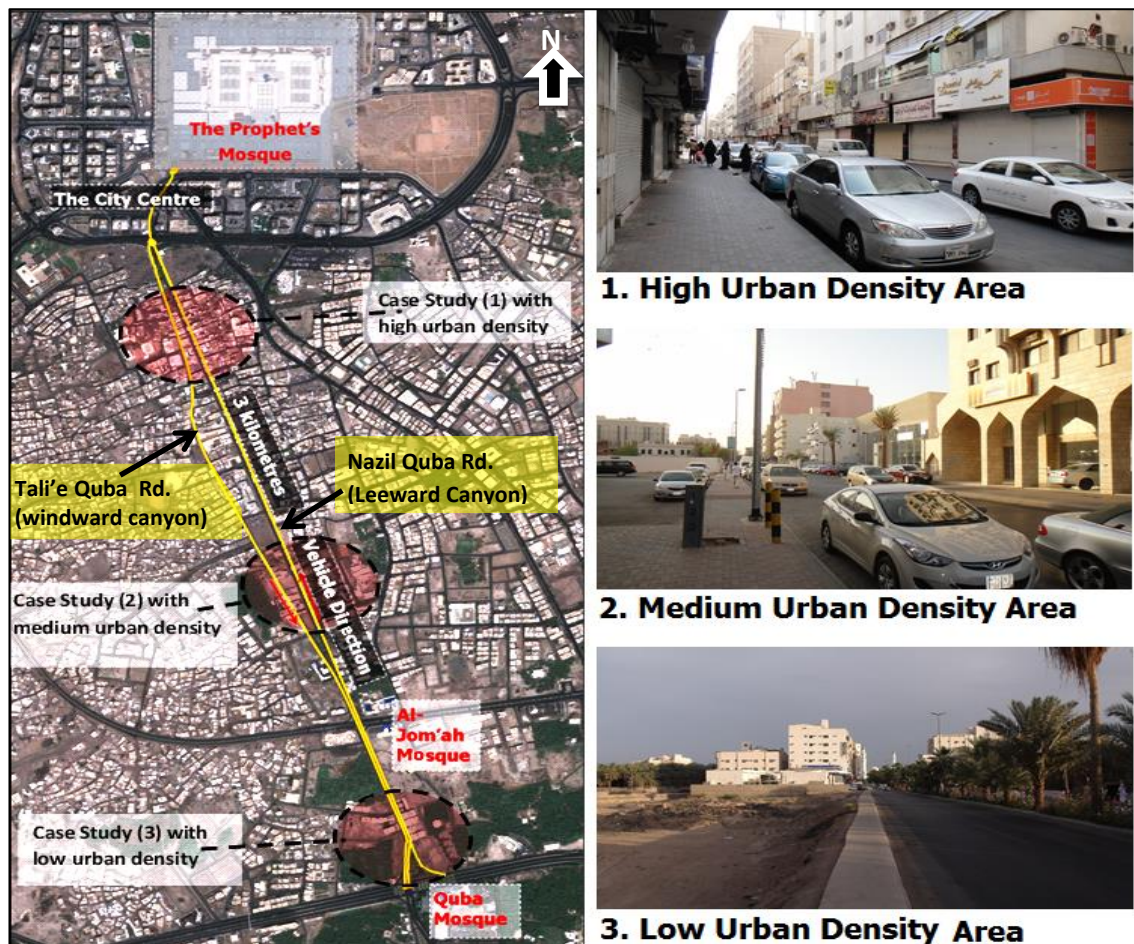


Fig. 6. 1: Measurements sites along Quba Road, characterised by different urban density zones.

## 6.2. The High Urban Density Area (Case 1)

The first field measurement area in the Nazil Quba Road (leeward canyon) was carried out in the high urban density area (Case 1), as illustrated in Figure 6.2. The number of shops in the Nazil Quba Road (leeward canyon) is significantly higher than the Tali'e Quba Road (windward canyon) with increased number of pedestrian. Four field measurement campaigns were carried out over a year, representing the four climatic seasons. This is to explore the variation in the microclimate and the outdoor thermal comfort conditions during 24 hours for the whole duration of the monitoring period. The four campaigns include:

- 14<sup>th</sup> to 25<sup>th</sup> of October 2012, in the autumn;
- 1<sup>st</sup> to 7<sup>th</sup> of January 2013, in the winter;
- 1<sup>st</sup> to 12<sup>th</sup> of April 2013, in the spring;
- 17<sup>th</sup> to 29<sup>th</sup> of June 2013, in the summer.



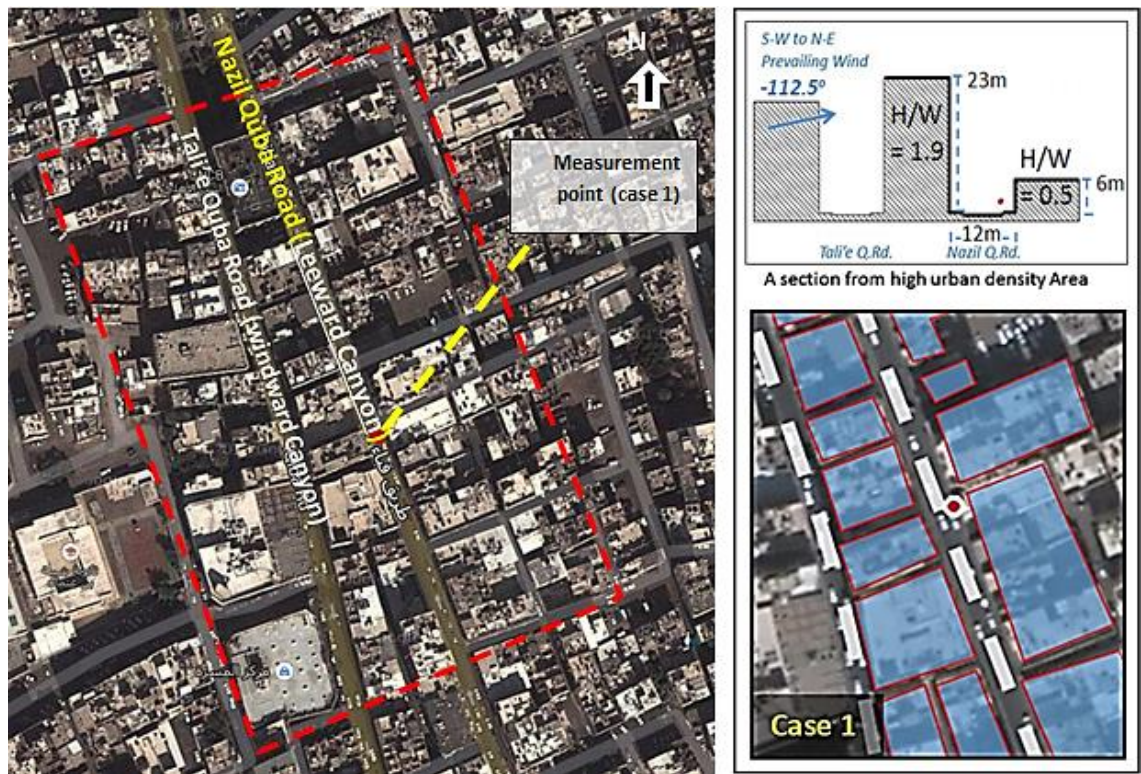


Fig. 6. 2: In-situ measurements point location in a high urban density area (Case1) in the Nazil Quba Road (i.e. leeward canyon).

The field measurement's instrument (Kestrel 4400 data logger) was positioned at 2m above the ground pavement (i.e. pedestrian height) between two asymmetrical building heights ( $H_1=23\text{m}$  and  $H_2=6\text{m}$ , and street width of 12m), with a distance of 2.5m from the lower windward elevation (or 9.5m from the higher leeward elevation). This is arguably less favourable asymmetrical aspect ratios ( $H_1/W$  and  $H_2/W$  of 1.9 and 0.5, respectively) in terms of wind velocity magnitude at the pedestrian level (e.g. Qaid and Ossen, 2014). Four microclimatic variables were obtained during the field measurements process, including: air temperature, globe temperature, wind velocity and relative humidity. The MRT (mean radiant temperature) was calculated using Equation 7 (refer to section 5.7) based on the field data of the globe temperature, wind velocity and air temperature. The hourly microclimatic results (i.e. 24 hours) were averaged from the whole duration of the monitoring period, and presented in the following subsections. The detailed hourly microclimatic data for the four climatic seasons are presented in A6.1 to A6.4 in the appendices.

### 6.2.1. Pedestrians Number (Case 1)

Figure 6.3 illustrates the number of pedestrians within the high urban density area (case 1), which was counted during the field measurements periods (except in summer and the night period of autumn), to provide an initial understanding of the

pedestrian usage pattern (i.e. in term of time of use). The number increases during the five daily prayer times, which is usually around the periods of 05:30, 12:30, 15:30, 18:00, and 20:30 hours. However, during the day time, the number of pedestrians decreases with the increase in air temperature outdoors, as a result of increase in solar radiation at the ground level. In contrast, due to low temperature in the evening and at the night, people occupy the Quba Road for walking and shopping activities, and others for transportation, i.e. driving between the city centre (including the Prophet's Mosque) and the south part of the City (including Quba Mosque).

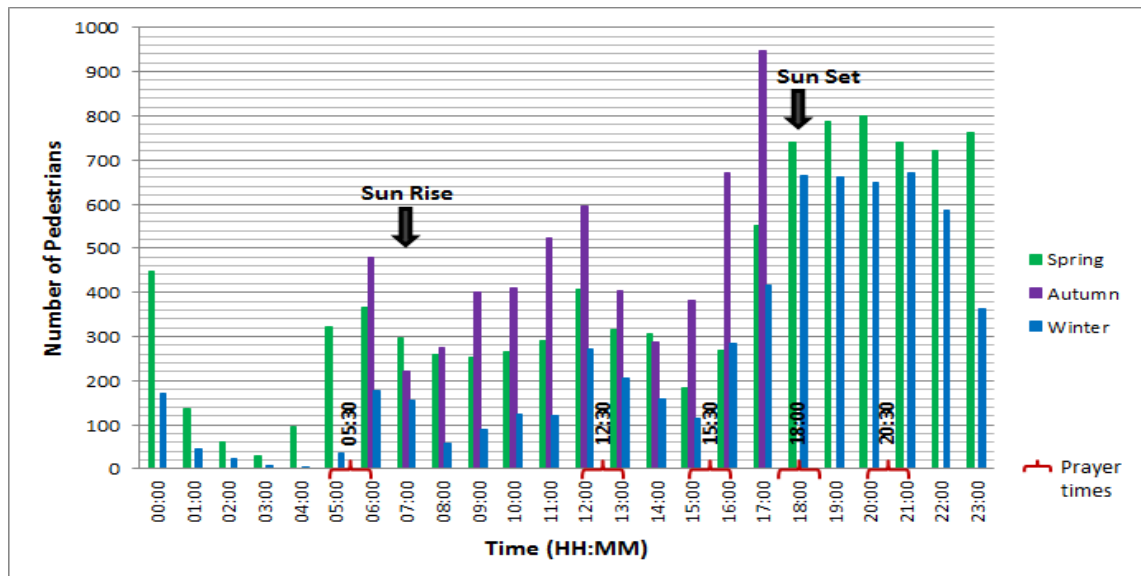


Fig. 6. 3: Number of pedestrians in high urban density area, during spring, autumn, and winter. Highlighted the 5 prayer times.

Although the Tali'e Quba Road (i.e. windward canyon) experiences less thermal stress than the leeward canyon (refer to simulation results in Chapter 7), the number of shops in the Nazil Quba Road (leeward canyon) is higher than the Tali'e Quba Road (windward canyon), thus increased number of pedestrian. This could be because of the Nazil Quba Road being the direct urban physical linkage between the two most visited sites in Madinah, namely the Prophet Mosque and Quba Mosque, with many mosques in between, which attract pedestrians during prayer time, while the Tali'e Quba Road lacks these religious venues.

Therefore, the number of pedestrians outdoors was significantly higher during prayer times. It is even higher during the evening hours, between 17:00 to 23:00, which is due to lower air temperatures and reduced mean radiant temperature (MRT). At the time of the measurements, autumn was the period when international visitors converged in Madinah to visit the Prophet's Mosque after performing the pilgrimage in Makkah.

### 6.2.2. Air Temperature

Figure 6.4 shows the hourly microclimatic results (i.e. 24 hours) that were averaged from the whole duration of the monitoring period in the high urban density area. The results indicate that the highest air temperature is experienced in summer, with an average daily value of 36.1°C (maximum value of 41°C and minimum 31°C), then followed by autumn with 32.8°C (max 36.6°C and min 28°C) and spring with an average daily value of 29.5°C (max 33.7°C and min 24.6°C). While winter having the lowest air temperature with an average daily value of 19.6°C (max 23.9°C and min 15.4°C).

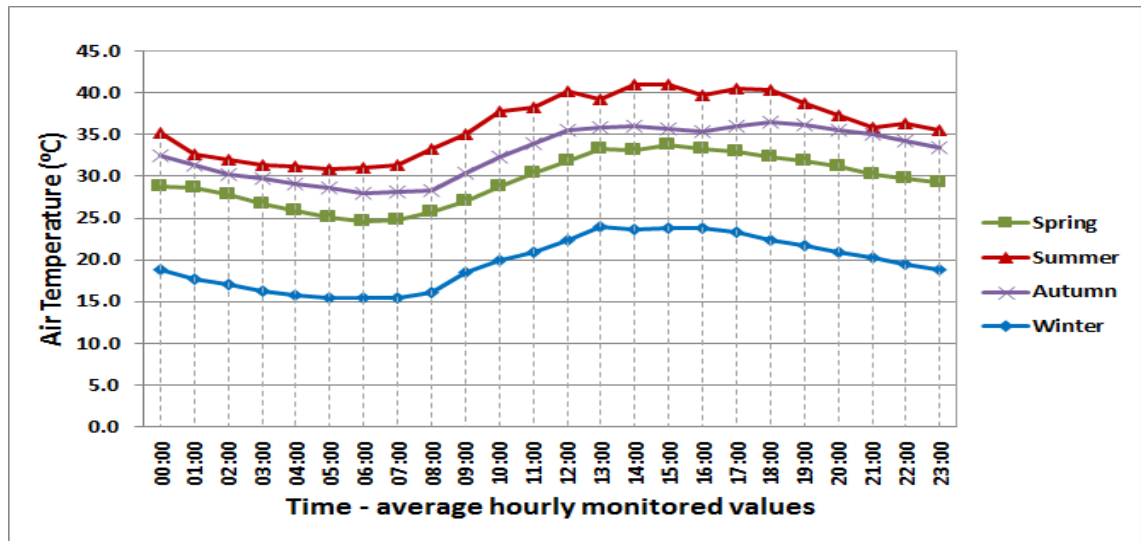


Fig. 6. 4: Air temperature pattern at a height of 2m above the ground for the four climatic seasons in the high urban density area (Case 1), based on average hourly values during the whole monitoring duration.

Figure 6.5 demonstrates the hourly pattern of air temperature in the high urban density area (Case 1) in Nazil Quba Road, particularly for the first 4 to 7 days in each of the monitored climatic seasons. The hourly microclimatic data for the whole monitoring periods are presented in A6.1 to A6.4 in the appendices.



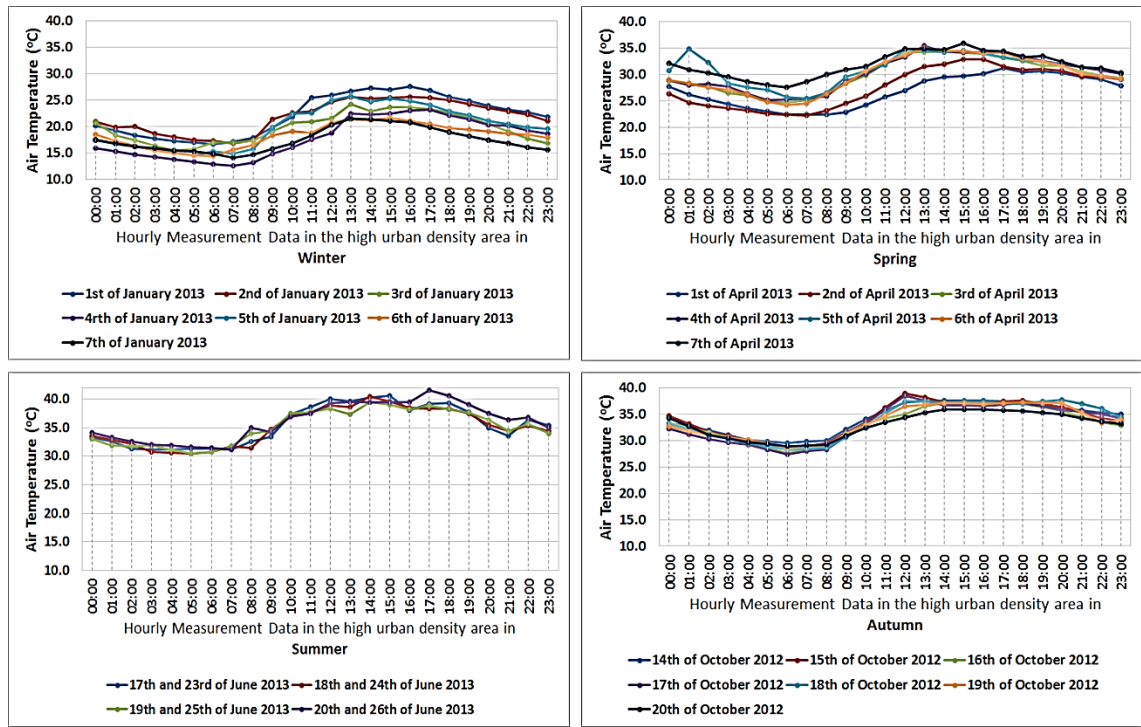


Fig. 6. 5: Some of the hourly air temperatures values (i.e.4 to 7 days ) representing the temperature pattern for the four climatic seasons in the high urban density area (Case 1) at 2m height above the ground.

The temperature pattern in spring, summer, autumn and winter are almost similar, which is in line with the previous studies (e.g. Johansson, 2006). The increase in air temperature begins immediately after the sunrise, and gradually decreases in the evening starting from the sunset hour (i.e. 18:00 in hot seasons and 17:00 in cold season) (e.g. Qaid and Ossen, 2014). The gradual decrease in air temperature during the night, in the high urban density area, is as a result of high thermal mass where heat is emitted from the adjacent buildings and other surrounding elements within the environment (e.g. Ali-Toudert et al., 2005; Rubio-Bellido et al., 2015).

In addition, in the cold season, the air temperature is highly influenced by the approaching air, as the daytime temperature remains low in deep canyons due to the lower sun elevation in winter and increased level of shading compared to the hot seasons, as illustrated in Figure 6.9 in the following section (6.2.3).

### 6.2.3. Mean Radiant Temperature (Case 1)

The MRT (mean radiant temperature) was estimated mathematically by determining the globe temperature, ambient air temperature and air velocity, based on the given equation by Thorsson et al. (2007) (refer to the equation number 7 in section

5.7). The hourly microclimatic results (i.e. 24 hours) were averaged from the whole duration of the monitoring period, as illustrated in Figure 6.6. The results demonstrates that high MRT values are experienced in summer with an average daily value of 36.3°C (max 42.8°C and min 31.3°C), followed by autumn with a value of 34.8°C (max 46.3°C and min 27.7°C) and then spring with a value of 31.5°C (max 44.1°C and min 24.1°C), respectively. With winter having the lowest average daily value of 23.4°C.

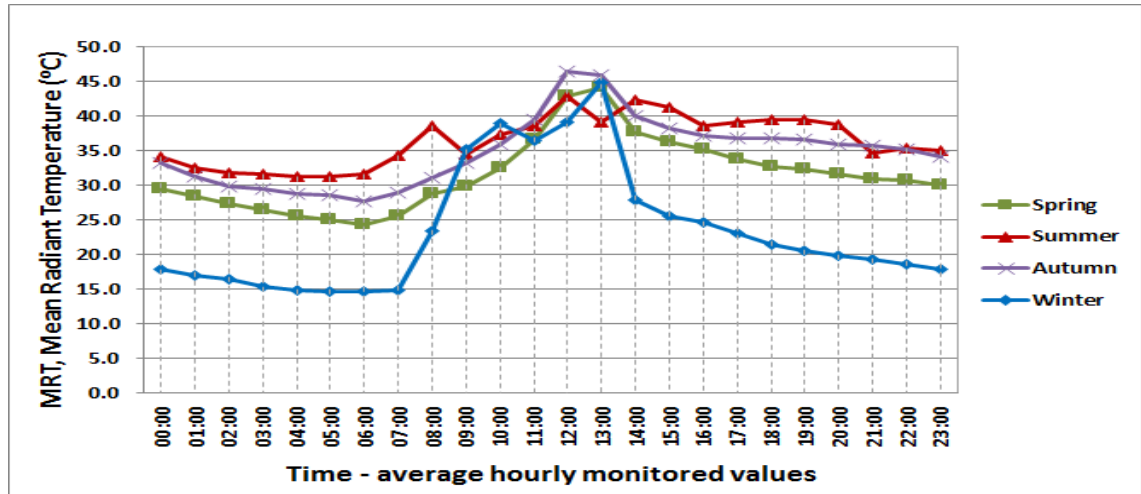


Fig. 6. 6: MRT pattern at a height of 2m above the ground for the four climatic seasons in the high urban density area (Case 1), based on average hourly values during the whole monitoring duration.

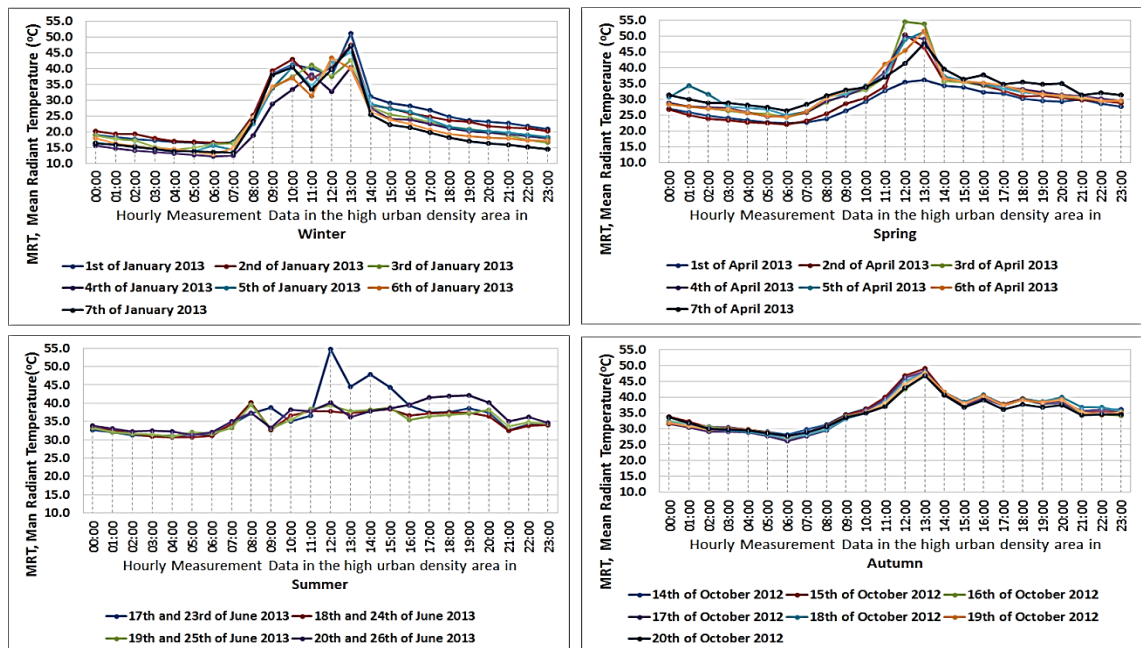


Fig. 6. 7: Some of the hourly MRT values (i.e.4 to 7 days ) representing the MRT pattern for the four climatic seasons in the high urban density area (Case 1) at 2m height above the ground.

The hourly microclimatic data for the whole monitoring periods are presented in A6.1 to A6.4 in the appendices. Figure 6.7 demonstrates the hourly pattern of the MRT in the high urban density area (Case 1) in Nazil Quba Road, particularly for the first 4 to

7 days in each of the monitored climatic seasons. The MRT in winter records the lowest average hourly value of 15°C at 07:00 hours just before the sun rise, and increases immediately to 23°C at 08:00 hours and peaks to 45°C at 13:00 hours.

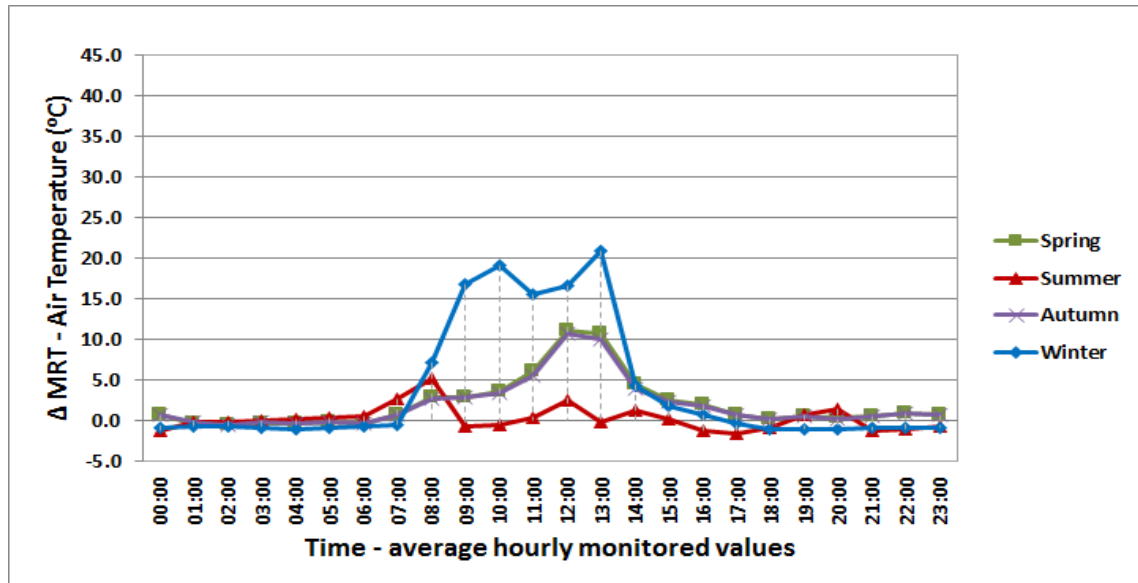


Fig. 6. 8: Difference in values between mean radiant temperature (MRT) and air temperature in the high urban density area (Case 1).

Figure 6.8 shows the difference in values between the MRT and air temperature in the high urban density area (Case 1). In summer, the MRT and air temperature are almost equal, resulting in uncomfortable thermal conditions (e.g. Ali-Toudert et al., 2005). During the spring and autumn seasons, the air temperature is lower than the MRT, with greater difference in values in the daytime (maximum difference of 11°C), resulting in better thermal conditions than summer.

Figure 6.9 shows the amount of shading in the Quba Road canyons (North-South axis) over a year. The level of shading in the existing situation was performed based on an hourly sun path at 09:00, 12:00 and 15:00 hours, using Ecotect software. The results of the difference between the MRT and air temperature emphasise the importance of shading in reducing the amount of the aggressive solar radiation in the canyons. Ali-Toudert and Mayer (2006) found that in a hot arid Algerian case study, the air temperature is more sensitive to the aspect ratio than the orientation, which is due to the shading effect from adjacent buildings.

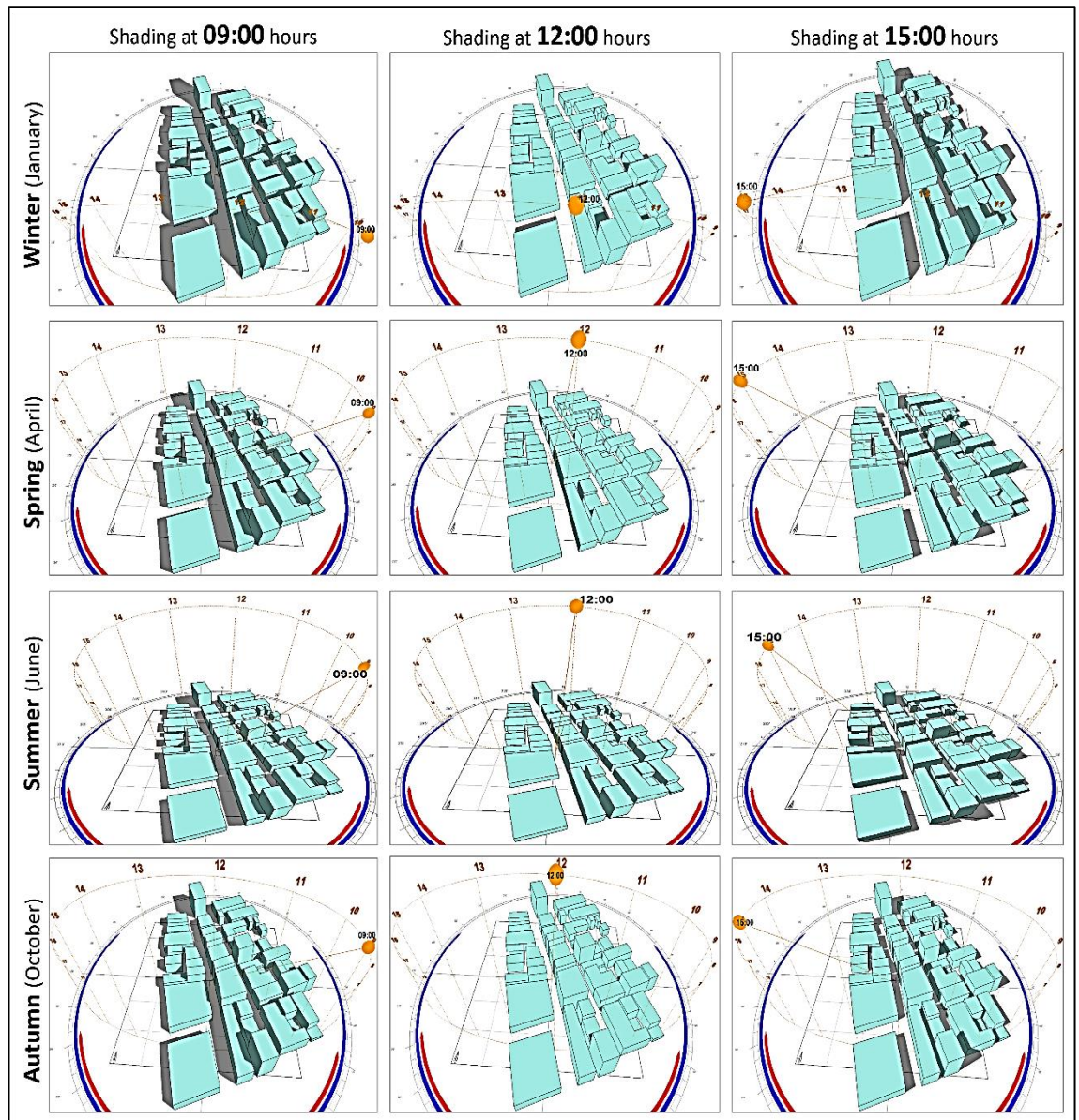


Fig. 6. 9: Amount of shading in the Quba Road canyons over a year at 09:00, 12:00 and 15:00 hours

Generally, the findings reveal that the north-south orientation of Quba Road canyons are in shade most of the morning and afternoon hours over a year. In addition, the taller buildings on the middle row of the urban area can provide higher amount of shading on the ground and building surfaces in the windward canyon (i.e. Tali'e Quba Road) at 09:00 hours, and in the leeward canyon (Nazil Quba Road) at 15:00 hours, due to the sun position in the east in the morning and the west in the afternoon, over a year (refer to section 7.2.1 in Chapter 7 for more information on shading at 15:00 hours). However, at noon, the ground and building surfaces in these North-South oriented canyons are exposed to solar radiation and lack of shading, due to the sun position in the south.



#### 6.2.4. Wind Speed and Directions (Case 1)

Wind speed and directions are important factors in enhancing the thermal comfort conditions in hot regions (Qaid and Ossen, 2014; Rizk and Henze, 2010). The wind speed measurement was conducted in the dense urban area (Case 1) along the Nazil Quba Road. The hourly wind speed results (i.e. 24 hours) were averaged from the whole duration of the monitoring period, as illustrated in Figure 6.10. The results indicate that the highest air speed is experienced in winter, with an average daily measurement of 1.4m/s, then followed by summer (0.7m/s) and spring (0.6m/s), respectively, with autumn having the lowest average wind speed (0.4m/s), at the pedestrian height (2m above the ground).

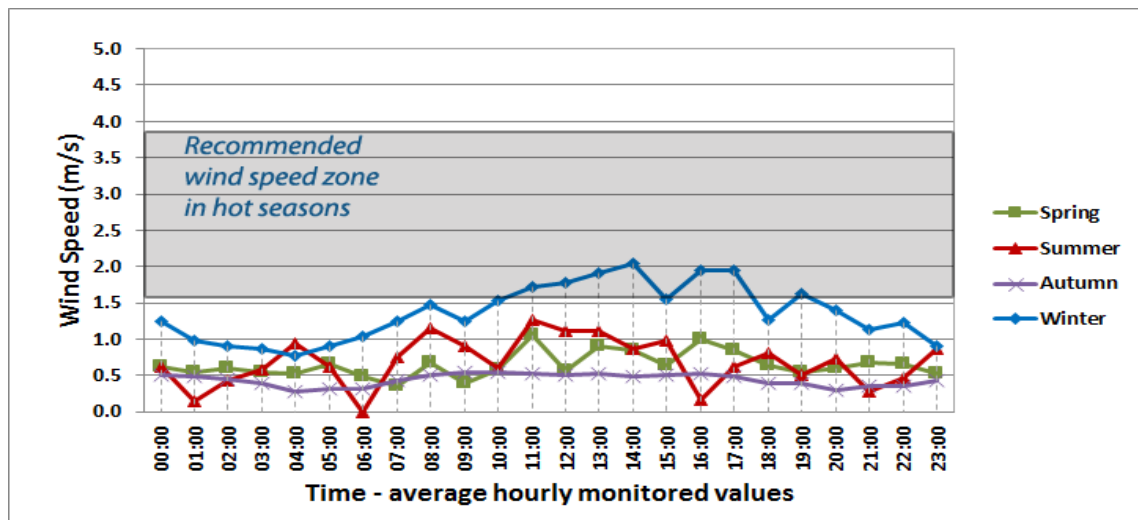


Fig. 6. 10: Wind speed values for the four climatic seasons in the high urban density area (Case 1). The figure highlights the recommended wind speed zone for pedestrians.

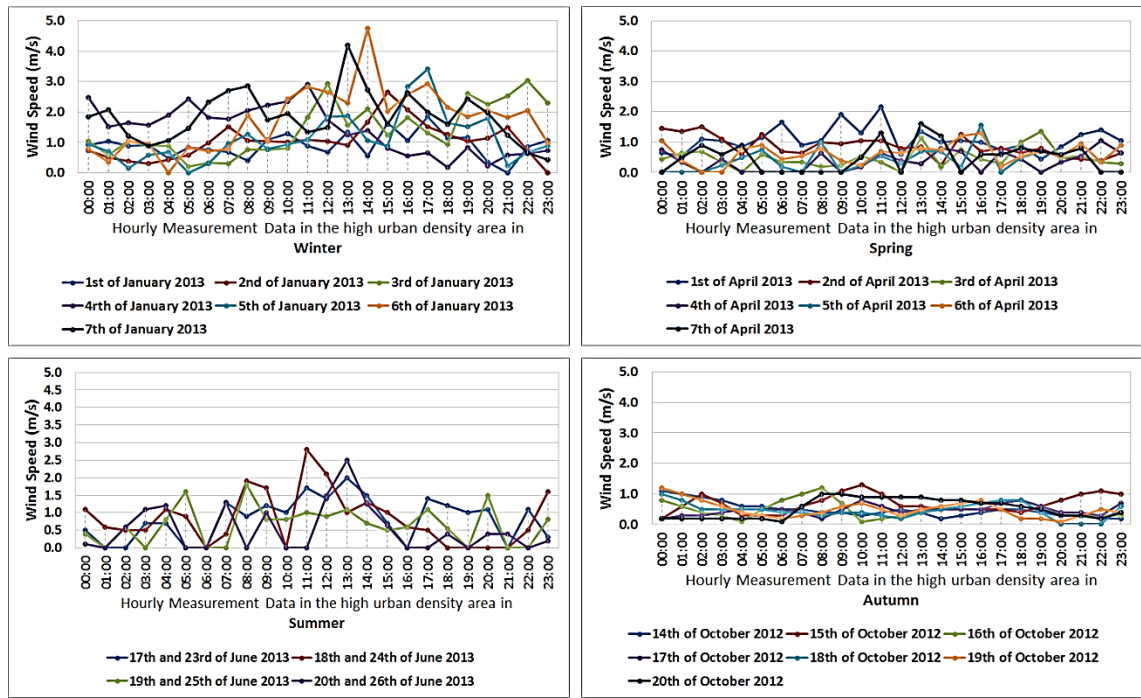


Fig. 6. 11: Some of the hourly wind speed values (i.e.4 to 7 days ) representing the speed pattern for the four climatic seasons in the high urban density area (Case 1) at 2m height above the ground.

Figure 6.11 demonstrates the hourly pattern of wind speed in the high urban density area (Case 1) in Nazil Quba Road, particularly for the first 4 to 7 days in each of the monitored climatic seasons. The hourly microclimatic data for the whole monitoring periods are presented in A6.1 to A6.4 in the appendices. Although the average wind speeds in Madinah is very low over a year, i.e. 3.2m/s summer at the city's airport (Iowa State University of Science and Technology, 2015), the speed pattern in all the four seasons in the high urban density area (Case 1) is somewhat different. For example, in winter, during the day hours of between 07:00 to 17:00 the average hourly wind speed increases in the range of 1.5 - 2m/s, whereas during the night time the wind remains within the range of 0.8 - 1.4m/s. Similarly, during the day hours wind speed slightly increases in the summer and spring seasons compared to the evening hours, but are lower than the winter season all day.

Rizk and Henze (2010) suggest the acceptable wind velocity range in hot arid climates to achieve thermal comfort for air temperatures that exceed 32°C in shade, with a lower limit threshold of 1.6m/s (based on ASHREA Standard 55, 2004), and upper limit of 3.8m/s (based on Beaufort Scale). However, the present wind speeds in the high urban density area (Case 1) in the hot seasons are below 1.6m/s, as the maximum wind speed does not exceed 1.3m/s. This might be as a result of the low approaching wind speed in Madinah, with an average lowest air speed of 2.5m/s recorded in winters and

average maximum of 3.5m/s recorded in summer at the city's airport (Iowa State University of Science and Technology, 2015).

In terms of wind directions, the city is exposed to a main prevailing South-Westerly wind, followed by the second prevailing Westerly direction, and the third prevailing North-Westerly direction over a year (Weather Underground, 2010). However, in urban areas, wind directions at the pedestrian level can be influenced by turbulences within the urban canyon as well as by any other moving objects (such as cars).

Therefore, the results of the wind direction in the high urban density (case 1) illustrate that, in autumn the prevailing direction is from North-East direction with wind speed range of 0.2-0.5m/s, as illustrated in Figure 6.12. In winter, the prevailing wind direction with speeds range of 1-1.9m/s is from the north-easterly direction, while for speeds between 2-2.9m/s is from south-westerly direction, as illustrated in Figure 6.13. In addition, the strongest wind speed amongst the measurements days in the spring season reached between 1-1.9m/s, approaching from the prevailing south westerly direction, followed by the speed of 0.6-0.7m/s from the same direction (Fig. 6.14). In this season, lower wind speeds of 0.2-0.3m/s were recorded from the directions of South South-Westerly and North North-Westerly. In the summer season, the prevailing wind direction was around North North-Westerly with wind speed reached within 1-3m/s (Fig. 6.15).



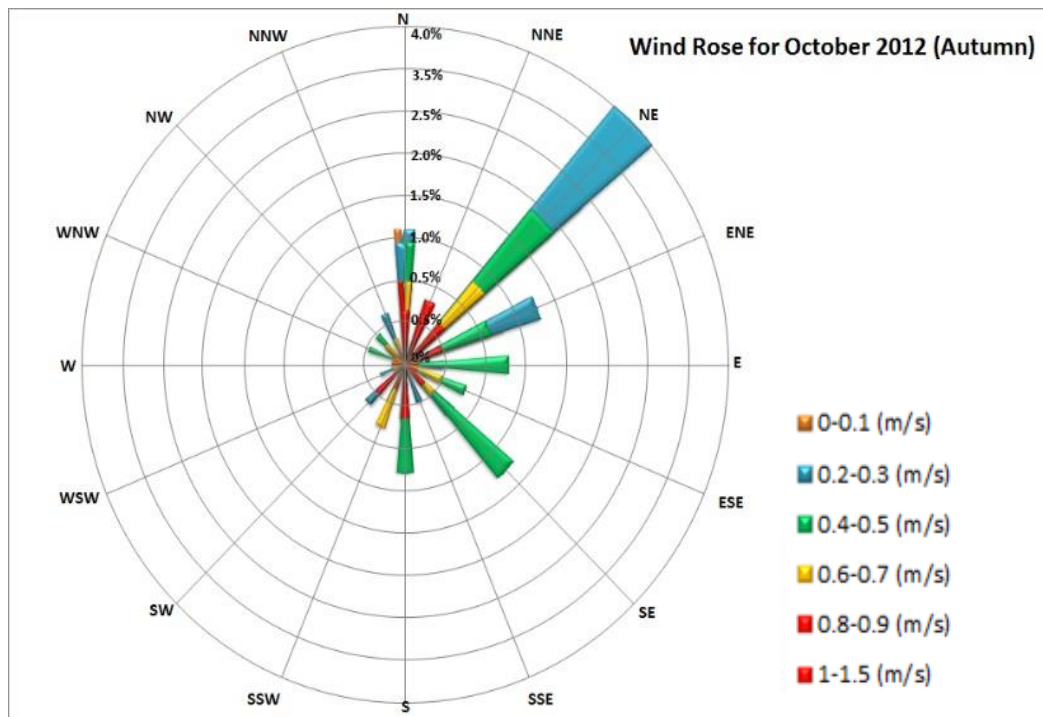


Fig. 6. 12: Wind rose for autumn season (October, 2012) in the high urban density area (Case 1).

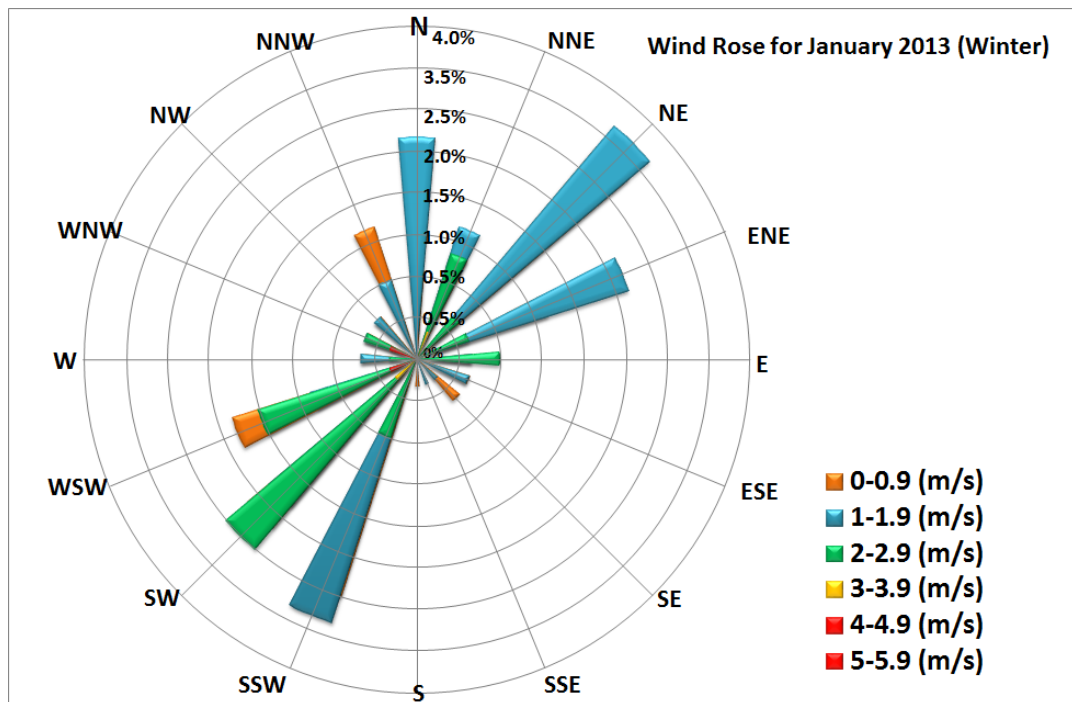


Fig. 6. 13: Wind rose for winter season (January, 2013) in the high urban density (Case 1).

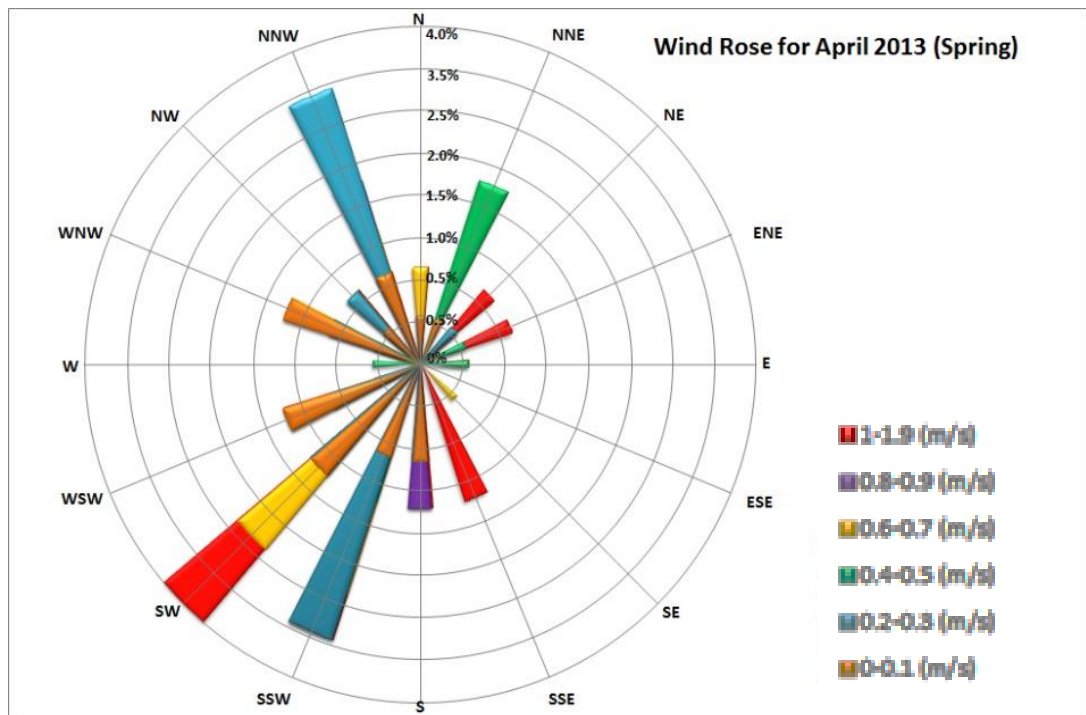


Fig. 6. 14: Wind rose for spring season (April, 2013) in the high urban density (Case 1).

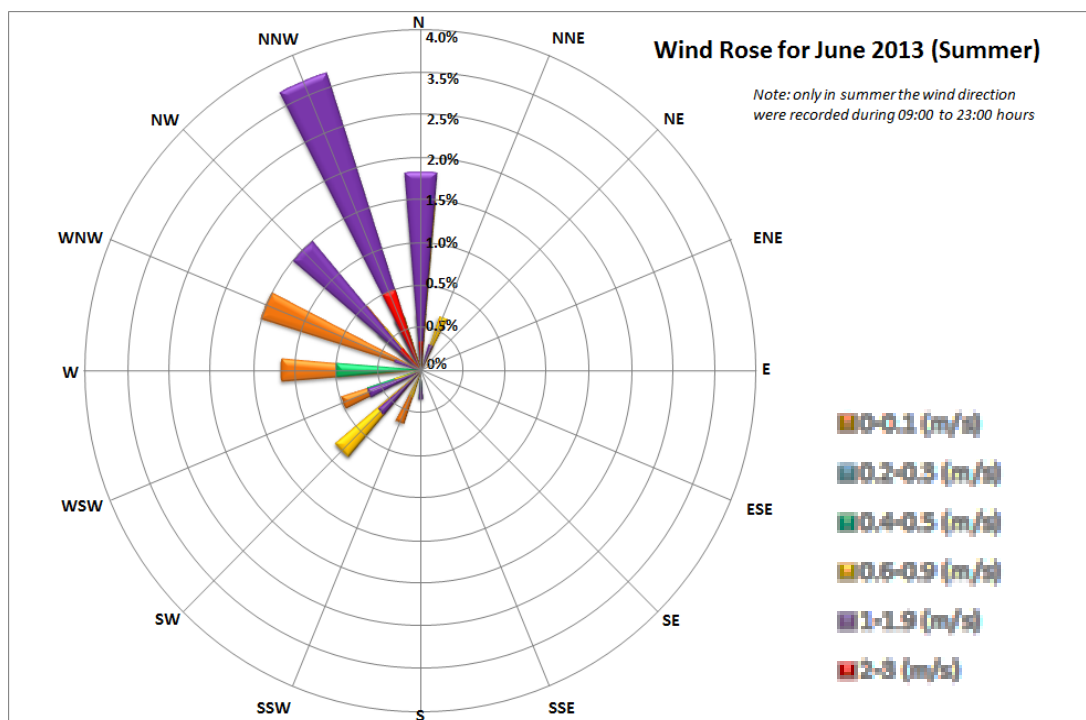


Fig. 6. 15: Wind rose for summer season (June, 2013) in the high urban density area (Case 1).

### 6.2.5. Relative Humidity (Case 1)

Relative humidity, which is the amount of water vapour in the air, is one of the factors influencing pedestrian thermal comfort conditions in outdoor urban environments. However, the relative humidity in Madinah is very low compared to coastal cities (e.g. Yanbu) in Al-Madinah province in Saudi Arabia.

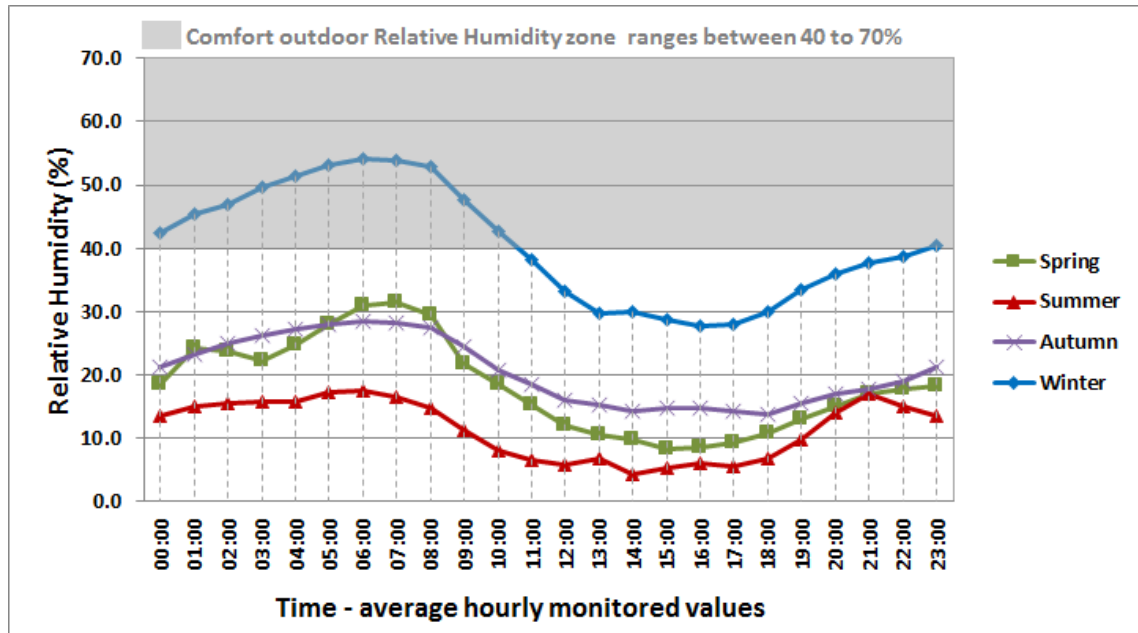


Fig. 6. 16: Comparison between the relative humidity values of the four climatic seasons in the high urban density area (Case 1).

Figures 6.16 and 6.17 illustrates the field measurement results of the relative humidity in the high urban density area (case 1) of Quba Road over a year, at the pedestrian level. The pattern of the relative humidity in summer, spring, autumn and winter are found to be almost similar. The results reveal that the relative humidity in winter is highest with an average daily measurement of 40.5%, followed by autumn (20.5%), then spring (18.3%), while summer recorded the lowest value (11.6%). However, the relative humidity values in the hot seasons fall far from the recommended comfort outdoor relative humidity range of 40% to 70% by Streinu-Cercel et al. (2007). In winter, the relative humidity in the period between 23:00 to 10:00 hours falls within the standard requirement, while from 11:00 hours to 22:00 hours are outside the standard comfort requirement.

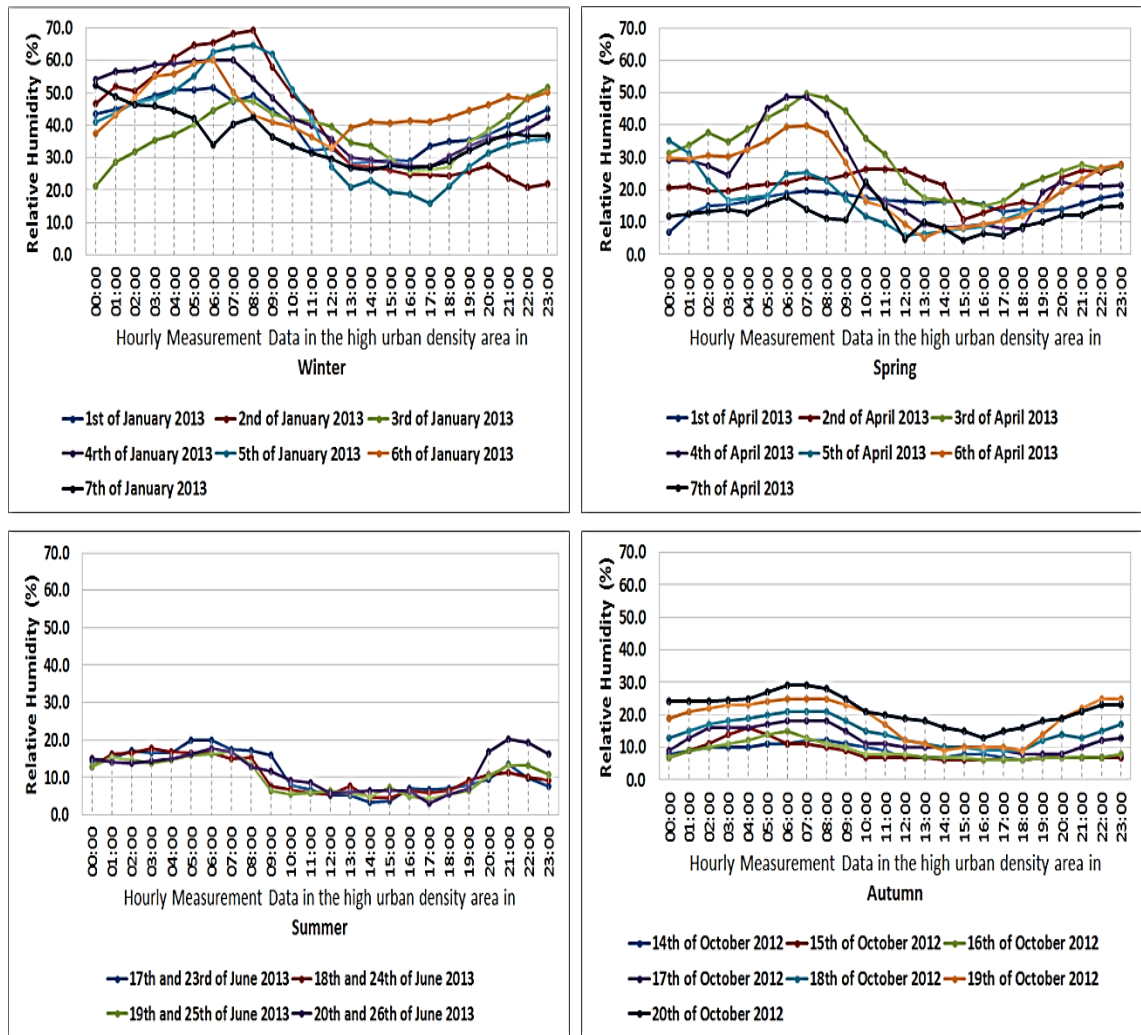


Fig. 6. 17: Some of the hourly relative humidity values (i.e.4 to 7 days ) representing the humidity pattern for the four climatic seasons in the high urban density area (Case 1) at 2m height above the ground..

### 6.2.6. Pedestrian's Thermal Comfort Conditions (Case 1)

In the present study, the pedestrian thermal comfort in the high urban density area (Case 1) was evaluated and analysed based on the physiologically equivalent temperature (PET) index (refer to section 3.5), which was calculated using RayMan model (Matzarakis et al., 2007). PET index has been calibrated for hot arid regions, particularly in built up areas, with upper limit of 31.3°C and lower limit of 21°C (Yahia and Johansson, 2013a).

The factors that are necessary for calculating the PET index are: air temperature, mean radiant temperature, relative humidity, wind speed, pedestrian metabolic rate (i.e. activity level; 192.5 W for walking) and clothing insulation level (e.g. 0.59clo for summer clothing and 1.3clo for winter clothing).

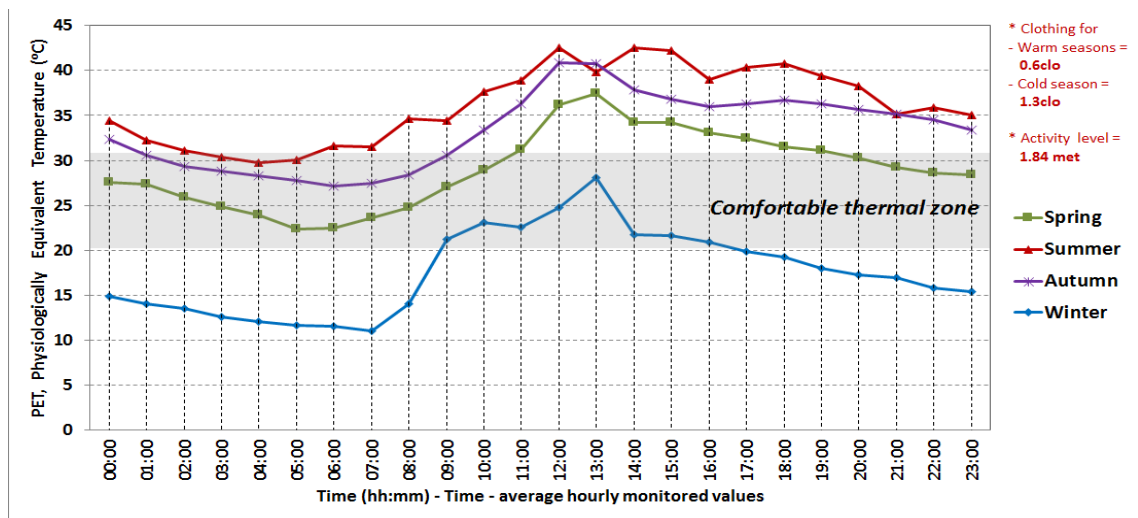


Fig. 6. 18: Comparison between the physiologically equivalent temperature (PET) index values of the four climatic seasons in the high urban density area (Case 1). The upper limit in summer and lower limit in winter comfort zone in hot arid areas are 31.3°C and 21°C, respectively.

Figure 6.18 demonstrates the PET temperature pattern over a year in the high urban density area (Case 1), which is similar in the three warm seasons of spring, summer and autumn, as well as the cold season of winter. The results indicate that the highest PET index temperature is obtainable in the summer season with an average daily value of 36.1°C (max 42.5°C and min 29.7°C), and then followed by autumn 33.4°C (max 40.9°C and min 27.1°C) and spring 29.0°C (max 37.4°C and min 22.4°C), respectively, while the winter season has the lowest average daily PET temperature value of 17.6°C (max 28.1°C and min 11.0°C).

The PET index values for winter have not satisfied the comfort lower limit requirement of 21°C (proposed by Yahia and Johansson, 2013a), particularly between 17:00 hours to 08:00 hours. The reason for winter having lower PET values (daily

average of 17.6°C) is as a result of the influence of shading in the high urban density area (Case 1) on most of the building and ground surfaces along the Quba Road, particularly in the early morning and the afternoon hours., due to lower sun elevation (refer to section 6.2.3).

The PET values decreased very slowly in the four climatic seasons during the night-time and roughly equalled the air temperature at mid-night (e.g. Ali-Toudert et al., 2005) due to the thermal mass (i.e. heat stored in buildings) and anthropogenic heat release. In the summer, the PET values between 02:00 hours to 06:00 hours are within the acceptable comfort zone for pedestrians (i.e. comfort threshold of 21°C to 31.3°C PET ), as illustrated in Figure 6.18. However, in this late night period, the number of users are significantly low (refer to section 6.2.1), as a result of closed shops and most residents are indoors.

In spring, this thermal comfort period extends, with a duration of 16 hours, between 19:00 hours (after the sunsets) to just before 11:00 hours to fall within the acceptable thermal comfort zone. Thus, the uncomfortable period between 11:00 hours through 18:00 hours in spring, are averaged to 33.8°C of PET, with the peak value of 37.4°C at 13:00 hours. Thus, the required average improvement difference in PET temperature to achieve thermal comfort during this uncomfortable period (i.e. between 11:00 to 18:00 hours) is 2.5°C PET, i.e. based on the upper limit of comfort threshold 31.3°C PET (given by Yahia and Johansson, 2013a), while for the peak value at 13:00 hours the required improvement difference is 6.1°C.

In autumn, the PET sensation index values between 01:00 and 09:00 have satisfied the upper comfort limit requirement of 31.3°C. The peak PET temperatures in spring, autumn and summer reach 37°C, 41°C, 43°C at 13:00, 13:00, and 14:00 hours, respectively.

It can be concluded that the PET temperatures in autumn and spring (i.e. mid-seasons) have lower thermal stress than the summer season, with spring having extended periods of comfort (i.e. duration of 17 hours) than the autumn season (i.e. duration of 9 hours). The current research aims to find ways to enhance the thermal comfort level in Quba Road within the high urban density area (refer to Chapter 7). Thus, it is feasible to investigate the spring season, to extend the use of outdoor space by shifting the thermal conditions from a range of thermal discomfort into a range of

critical thermal comfort as much as possible, passively without the introduction of any mechanical cooling system.

### **6.3. The Intermediate Urban Density Area (Case 2)**

The second field measurement area in the Nazil Quba Road (leeward canyon) was carried out in the intermediate urban density area (Case 2), as illustrated in Figure 6.19. This area is located around the middle length of the Nazil Quba Road, and about 1km away from Case 1 (i.e. the high urban density area) and Case 3 (i.e. the low urban density area). The microclimatic data in this second case were collected simultaneously with the first and the third field measurement areas, using Kestrel data loggers. Four field measurement campaigns were carried out over a year, representing the four climatic seasons in Madinah. This is in order to explore the variation in the microclimate and the outdoor pedestrian thermal comfort conditions during continuous 24 hours for the whole duration of the monitoring period.

However, in this intermediate urban density area (Case 2), the data for autumn and winter seasons were lost during the research, due to damage and theft of two measuring devices. Thus, the data obtained are for the following periods:

- 7<sup>th</sup> to 12<sup>th</sup> of April 2013, in spring;
- 17<sup>th</sup> to 22<sup>nd</sup> of June 2013, in summer.



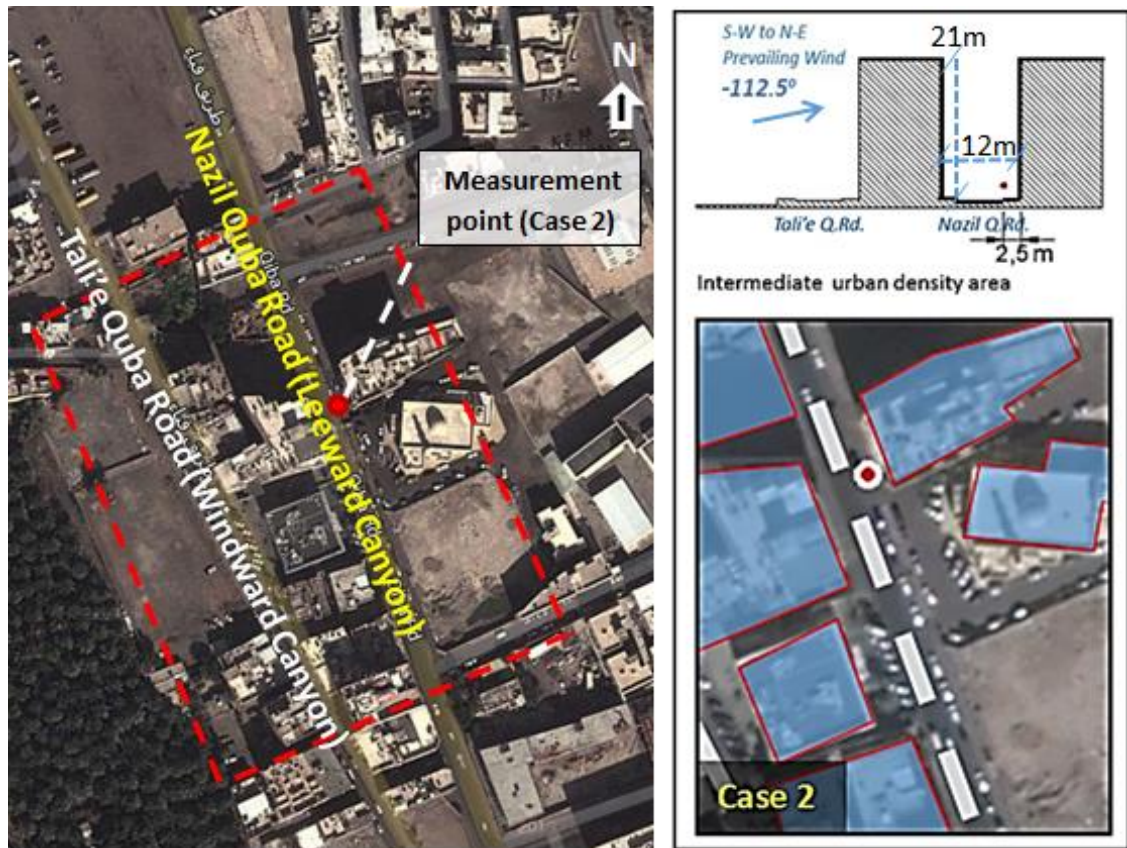


Fig. 6. 19: Measurement location for the intermediate urban density area (Case 2), between two symmetrical buildings (21m height), and distanced 2.5m from the windward elevation.

### 6.3.1. Air Temperature and Relative Humidity (Case 2)

Figure 6.20 illustrates the relationship between the air temperature and relative humidity in the intermediate urban density area (Case 2) based on average hourly data. The hourly microclimatic data for the whole monitoring periods in the intermediate urban density area are presented in A6.5 to A6.7 in the appendices. The results indicate an interrelationship between the air temperature values and relative humidity, as the latter parameter decreases with the increase in temperature values, and vice versa. The air temperature in summer is higher than spring, with a similar air temperature pattern for both of the hot seasons. The relative humidity is almost similar for the two seasons with spring being slightly higher than the summer season, with an average difference of 1.1%.

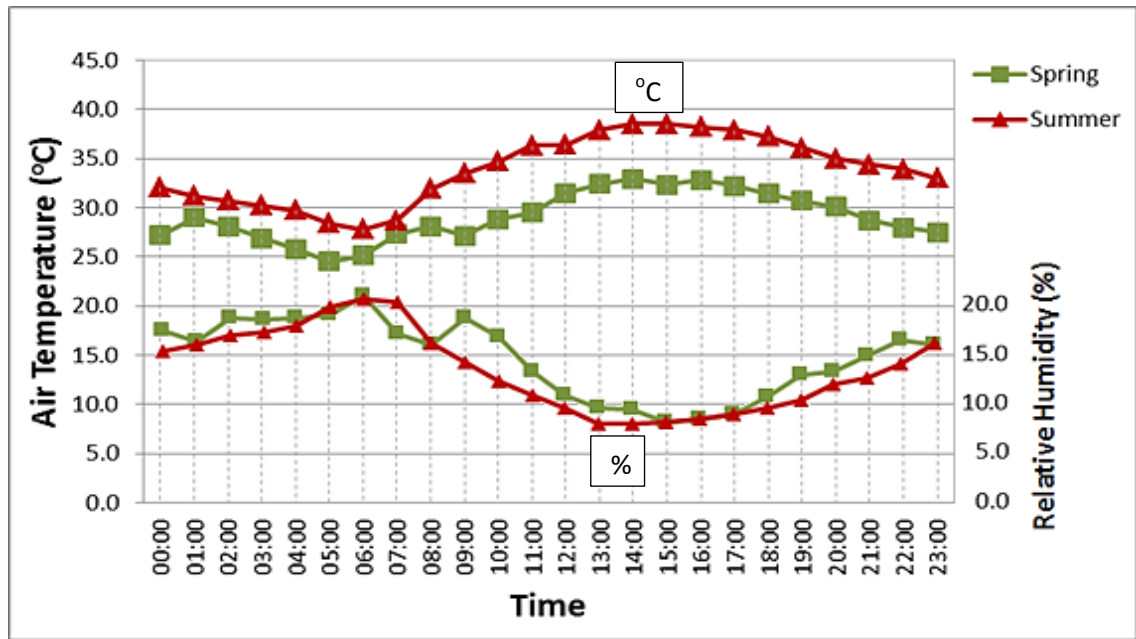


Fig. 6. 20: Comparison between the air temperature and relative humidity values for the spring and summer seasons in the intermediate urban density area (Case 2).

In summer, the average daily air temperature value is 33.8°C, while the relative humidity is found to be 14%. The outdoor air temperature in the summer peaks to about 38.5°C at 14:00 hours and later drops at the night time to early morning to reach minimum of 27.6°C at 06:00 (i.e. just before the sunrise time). The outdoor relative humidity in the summer peaks to 21% at 06:00 hours, and its lowest value of 8% is found at 14:00 hours.

This situation is similar for spring, but the temperatures are lower in this season as it peaks to about 32.9°C at 14:00 hours and drops to its minimum of 24.5°C at 05:00 hours. The relative humidity in spring peaks to 21.0% at 06:00 hours, and its lowest value of 10% is found to be at 14:00 hours. With the average daily air temperature value of 29.1°C, and relative humidity value of 15%.

### 6.3.2. Mean Radiant Temperature and Wind speed (Case 2)

The MRT was estimated mathematically by determining the globe temperature, ambient air temperature and air velocity, based on the given equation for the MRT by Thorsson et al. (2007) (refer to the equation number 7 in section 5.7). The hourly microclimatic data for the whole monitoring periods in the intermediate urban density area are presented in A6.5 to A6.7 in the appendices.

Figure 6.21 demonstrates that the MRT in the intermediate urban density (Case 2) is higher in the summer than the spring, with the average difference being 7.4°C. However, the MRT readings for most of the day times in the both seasons are very high, especially after 08:30 to the late evening hours. In comparison with the previously mentioned high urban density area (Case 1), it can be observed that the average difference for MRT temperatures in the summer season is 4.2°C higher than the MRT in the intermediate urban density, as well as in the spring season with a difference value of 1.6°C (refer to section 6.5 for the comparative analysis). The reason for these increased differences in MRT temperatures is relevant to the level of shading from buildings, as it is lower around the intermediate urban density than the high urban density area (e.g. Lin et al., 2010). Thus, this implies the importance of using shading devices to reduce the amount of the aggressive solar radiation in pedestrian spaces. The average MRT value in the intermediate urban density area is 40.5°C during the summer, and 33.1°C during

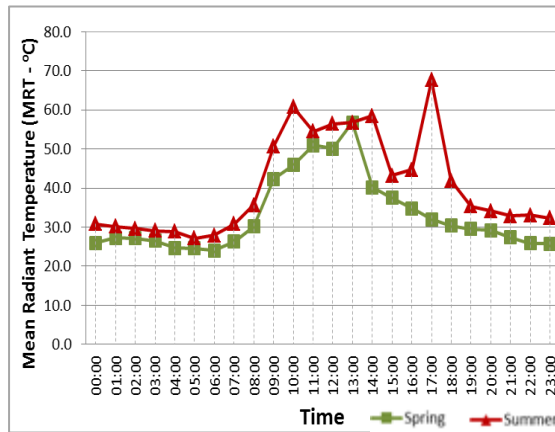


Fig. 6. 21: The MRT values in the spring and summer seasons in the intermediate urban density area (Case 2).  
spring.

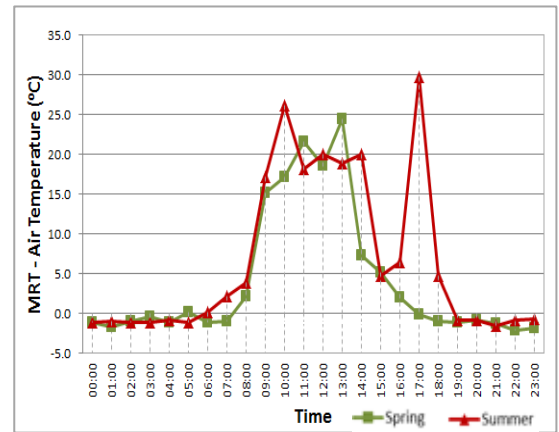


Fig. 6. 22: The difference in values between the MRT and air temperature in the intermediate urban density area (Case 2).

Figure 6.22 demonstrates the difference in the values between the MRT and air temperature during the spring and summer seasons. The difference value is greater in the daytime, with an average difference of 14.3°C in the summer and 12.6°C in the spring, while by night the MRT is about 1°C lower than the air temperature in the intermediate urban area (Case 2).

From the wind speed perspective, it is found that an increase in MRT temperature, cannot only influence the increase in air temperature, but also wind speed values. In other words, the wind speed increases with the increase in MRT value, due to the difference in static pressure from shaded areas to sunny areas, and vice versa. Thus,

due to the nature of the calm wind speed in Madinah and the relationship between the pattern of the MRT and wind speed in the findings, it can be suggested that several open spaces should be designed with partially sunny areas to allow for an increase in wind speed.

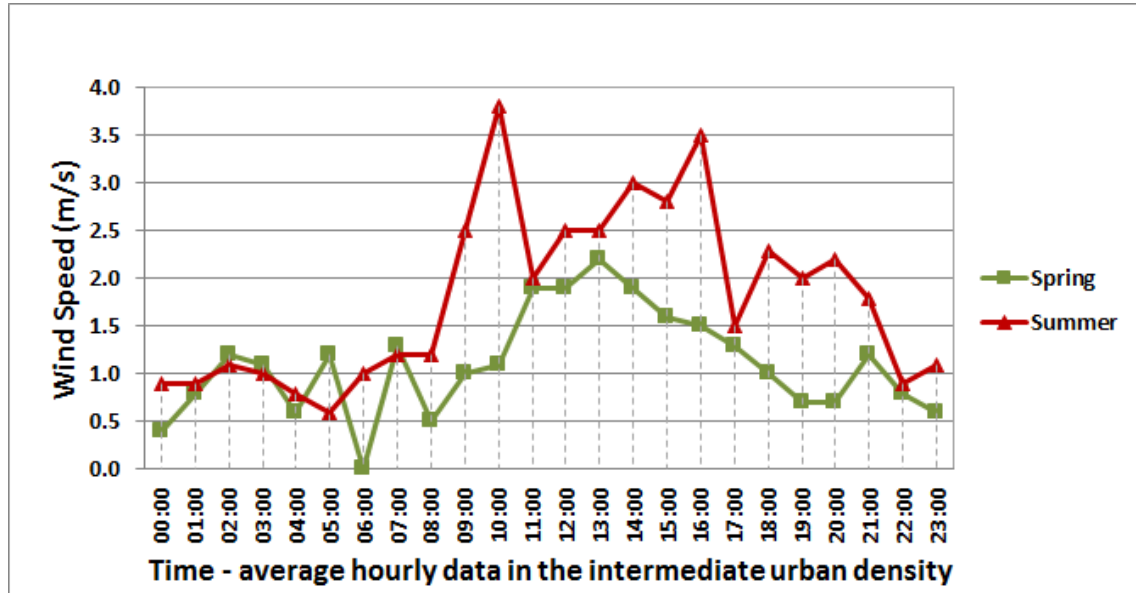


Fig. 6. 23: Comparison between the wind speed values of the spring and summer seasons in the intermediate urban density area (Case 2).

Figure 6.23 demonstrated that the wind speeds in the summer are higher than the spring. The wind speed pattern in the two seasons is somewhat similar, which is because the average wind speed in Madinah is always calm. In the summer, during the hours between 22:00 to 08:00 the air speeds are around 1m/s, however it increases significantly to between 2.5m/s – 3.8m/s during 09:00 to 16:00 hours. The average daily wind speed in this intermediate density is 1.8m/s and 1.1m/s for summer and spring, respectively which are slightly higher than Case 1 (i.e. high urban density area) as a result of reduced ground surface roughness value in Case 2 (e.g. Yahia and Johansson, 2013b).

### 6.3.3. Pedestrian's Thermal Comfort Conditions (Case 2)

The PET index temperature pattern is almost similar in both spring and summer, with the highest temperature reached in the summer season, an average daily value of 36.0°C, and followed by the spring with a value of 28.8°C, as illustrated in Figure 6.24. Yahia and Johansson (2013a) defined the lower thermal comfort limit for PET index in winter to 21°C and the upper limit in summer to 31.3°C. Thus, the PET index values for the summer season between 11:00 hours to just before 08:00 hours are within the neutral thermal sensation range. After 08:00 hours, the PET values increase significantly until 14:00 in the afternoon, and then decrease very slowly in the night-time, whereas most of the PET values in spring season have satisfied the comfort requirement, particularly between 16:00 to 09:00 hours (i.e. duration of 17 hours). The average PET value for the intermediate urban density area in the summer is 36°C and in spring is 28.8°C. In comparison to the high urban density area, it can be concluded that the intermediate urban density (Case 2) has the same average daily PET value as in higher urban density. However, in terms of urban heat island (UHI), the higher urban density area has a higher UHI effect than the intermediate density, with a difference air temperature value of 2°C found in summer, while there is almost zero difference in spring.

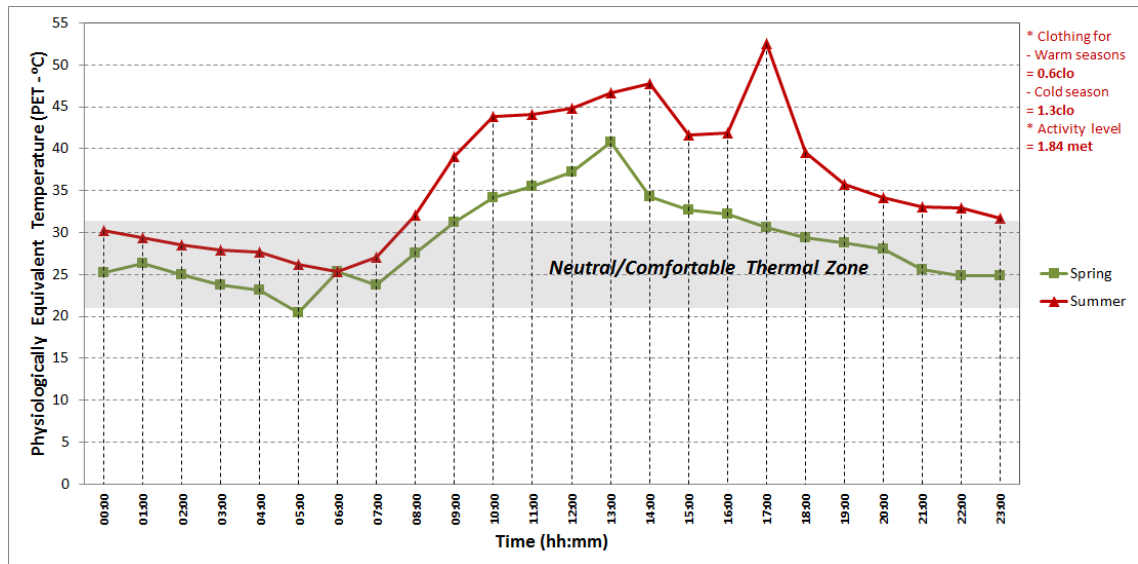


Fig. 6. 24: Comparison between the physiologically equivalent temperature (PET) index values of the spring and summer seasons in the intermediate urban density area (Case 2). The upper limit in summer and lower limit in winter comfort zone in hot arid areas are 31.3°C and 21°C, respectively.



#### 6.4. The Low Urban Density Area (Case 3)

The third location of the field measurement was carried out in the low urban density area (Case 3) in the Nazil Quba Road canyon, at about the southern edge of the road (Figure 6.25). This area is situated Quba Road, and about 1km away from Case 2 (i.e. the intermediate urban area), and the data logger was positioned between the Nazil and Tali'e Quba Road canyons (i.e. 15m away from the windward and leeward elevations), at 2m height above the ground. Four field measurement campaigns were carried out in order to explore the variation in the microclimate and the outdoor thermal comfort in the urban canyon over a year. However, in this low urban density area (Case 3), the data for autumn seasons were lost during the research, due to damage to the measuring device. Thus, the data obtained are for the following days, and for continuous periods of 24 hours:

- 1<sup>st</sup> to 7<sup>th</sup> of January 2013, in the winter;
- 1<sup>st</sup> to 12<sup>th</sup> of April 2013, in the spring;
- 17<sup>th</sup> to 22<sup>nd</sup> of June 2013, in the summer.

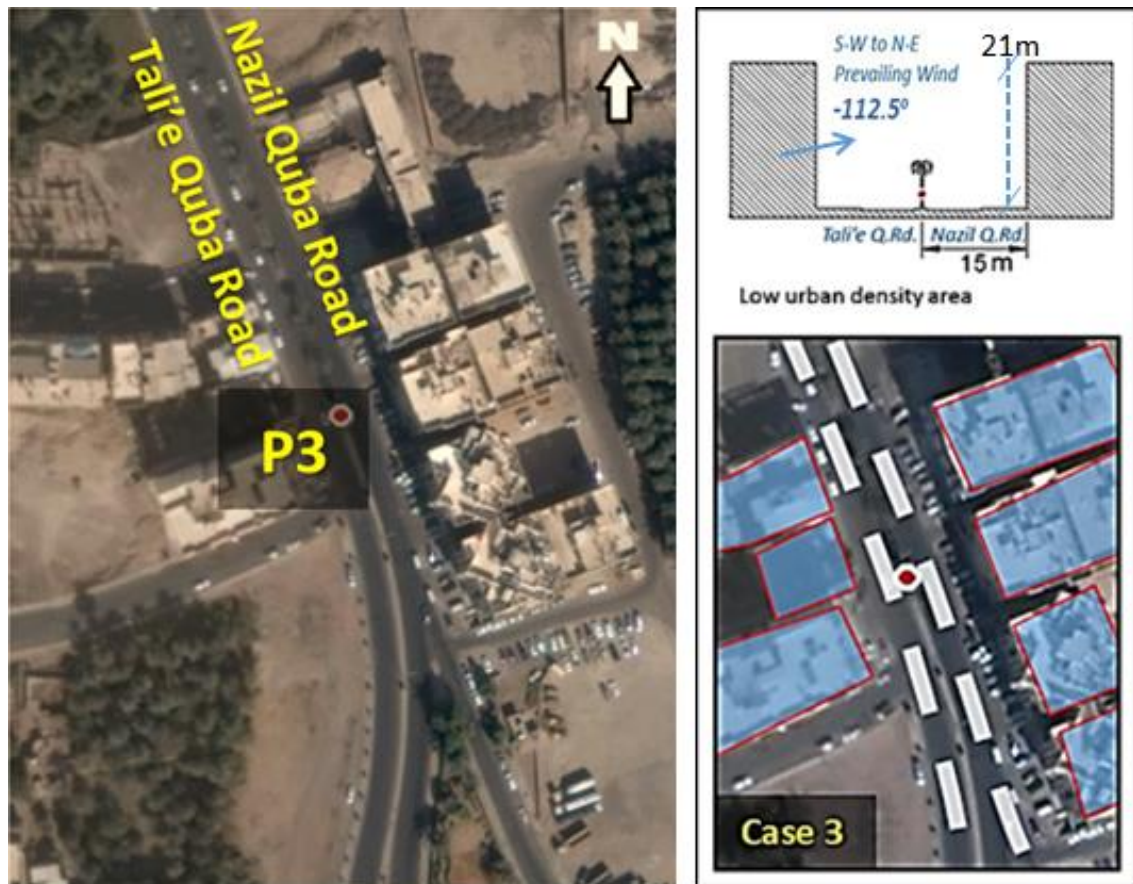


Fig. 6. 25: Field measurement location at the low urban density area (Case 3) along Quba Road.

#### 6.4.1. Air Temperature and Wind Speed (Case 3)

The air temperatures pattern in spring, summer, and winter are the same for the low urban density area (Case 3), as shown in Figure 6.26. The hourly microclimatic data for the whole monitoring periods in the low urban density area are presented in A6.8 to A6.11 in the appendices. The results indicate that the highest air temperature is experienced in the summer, with an average daily measurement of 33.6°C, then followed by spring (28°C), with winter reaching the lowest temperature (19.2°C). The configuration of lower urban street canyon's aspect ratios in the low urban density area (Case 3), with a wider street opening (i.e. 30m), leading to larger level of exposure to solar radiation, while in the dense urban area the street opening is lower (i.e. 12m of width), leading to larger shading level in the area (e.g. Ali-Toudert and Mayer, 2006 and 2007; Lin et al., 2010).

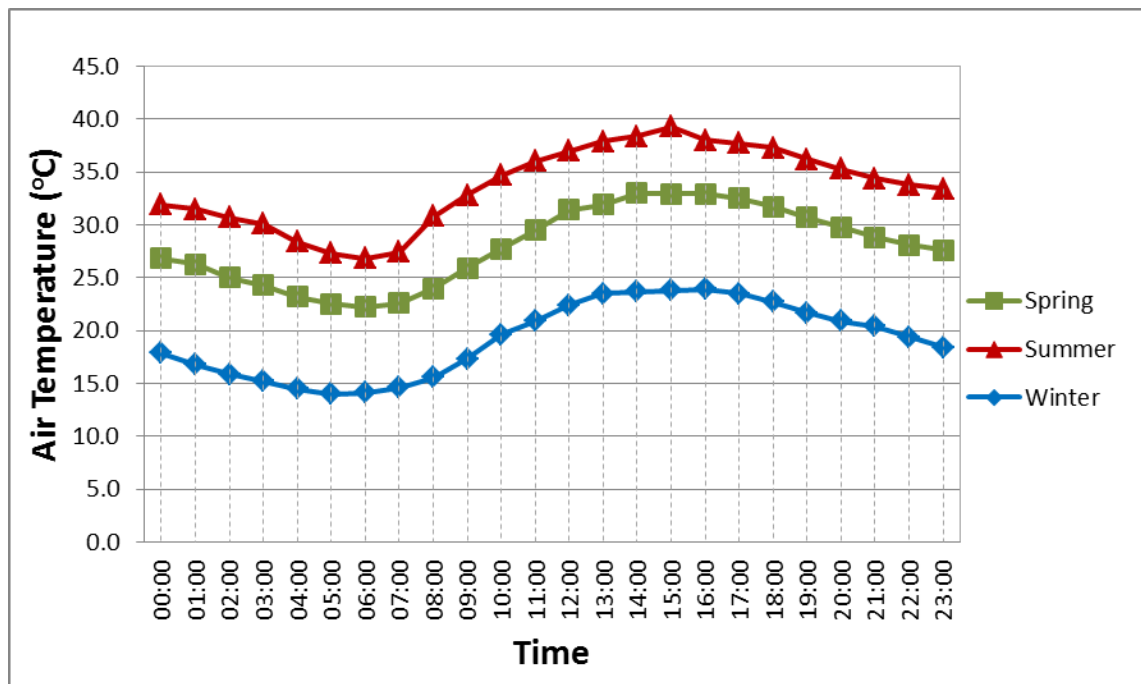


Fig. 6. 26: Comparison between the air temperature values of the spring, summer, and winter seasons in the low urban density area (Case 3), based on average hourly data.

The outdoor air temperature in the summer peaks to about 39°C in the afternoon (especially at 15:00), and later drops to about 27°C in the night time. This situation is similar for the spring, but the temperatures are lower in this season.



In addition, the heat during the night period can be released to the sky much more easily, without being trapped in the lower urban density compared to the higher urban density area (Case 1), which is due to the small amount of thermal mass elements or buildings and wider opening to the sky (e.g. Rubio-Bellido, 2015). Furthermore, the farms and vegetation are broadly provided in the lower dense area (Case 1), which supports providing the cooling effect by evaporation and evapotranspiration during the day, with maximum benefit of the effect in reducing air temperature at the night.

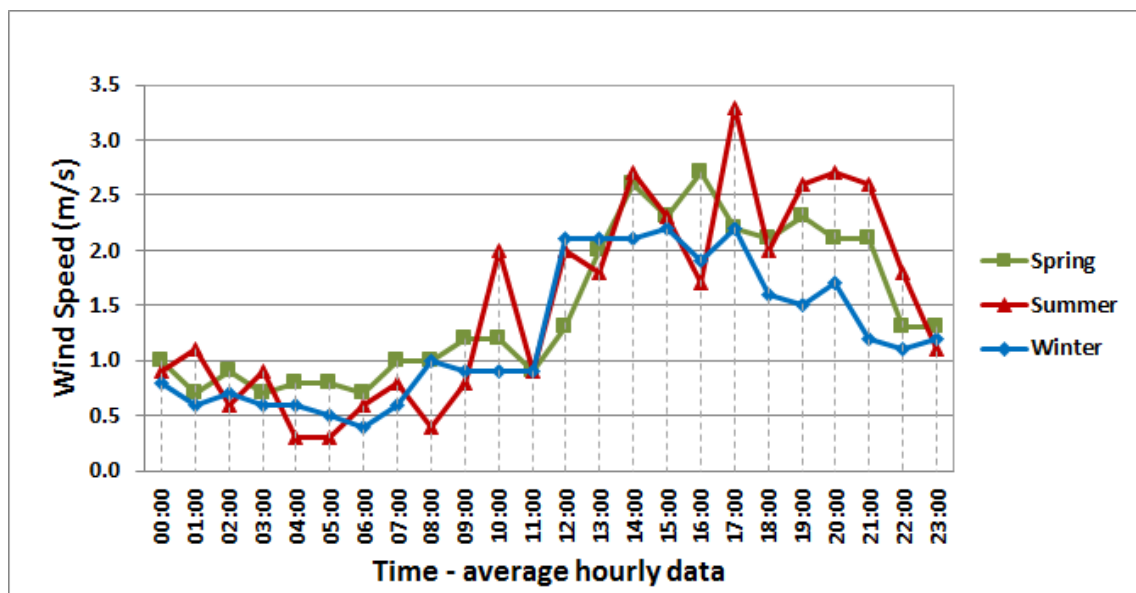


Fig. 6. 27: Comparison between the wind speed values of the spring, summer, and winter seasons in the low urban density area (Case 3), based on average hourly data.

In the three seasons, wind speed increases gradually above 1m/s after 08:30 hours in spring, at 10:00 hours in summer, and 11:00 hours in winter, then they gradually decrease starting from around the sunset, as illustrated in Figure 6.27. The peak wind speeds for summer, spring and winter are 3.3m/s, 2.7m/s, and 2.3 at 17:00 hours, 16:00 hours, and 15:00 hours, respectively. During the 00:00 hours to 08:00, the winds for all the three seasons do not exceed the speed of 1m/s. Rizk and Henze (2010) suggest the acceptable wind velocity range in hot arid climates to achieve thermal comfort for air temperatures that exceed 32°C in shade, with a lower limit threshold of 1.6m/s (based on ASHREA Standard 55, 2004), and upper limit of 3.8m/s (based on Beaufort Scale). In the hot seasons, the wind speeds in the low urban density are above the recommended lower limit of 1.6m/s between 12:00 hours to 22:00 hours in summer and between 13:00 hours to 21:00 hours in spring.



#### 6.4.2. Mean Radiant Temperature and Relative Humidity (Case 3)

The hourly microclimatic data for the whole monitoring periods in the low urban density area are presented in A6.8 to A6.11 in the appendices. Figure 6.28 demonstrates that the result pattern for the mean radiant temperature is similar for the summer, spring and winter seasons in the low urban density area (Case 3). The MRT is higher in the summer, with an average daily measurement of 38.9°C, followed by the spring (31.5°C), with winter being the lowest value (21.1°C). The MRT values for summer in the low urban density area (Case 3) increase significantly from 32°C at 09:00 to 51°C at 10:00 hours, and reduce from 59°C at 16:00 to 41°C at 17:00 (an hour before the sun set). This is due to high level of solar elevation in summer between this period (i.e. 10:00 to 16:00), with causing extreme heat stress (PET value of 41°C).

In the spring season, the MRT values increase gradually with the sun rise (i.e. at 06:00) from a value of 21°C to reach above 40°C between 13:00 to 16:00 hours. The MRT in winter peaks at 13:00 hours with temperature value of 41.7°C, while in the hot seasons, the MRT peaks at 16:00 hours in the summer with the value of 57.5°C, and at 14:00 hours in the spring with the value of 51.2°C.

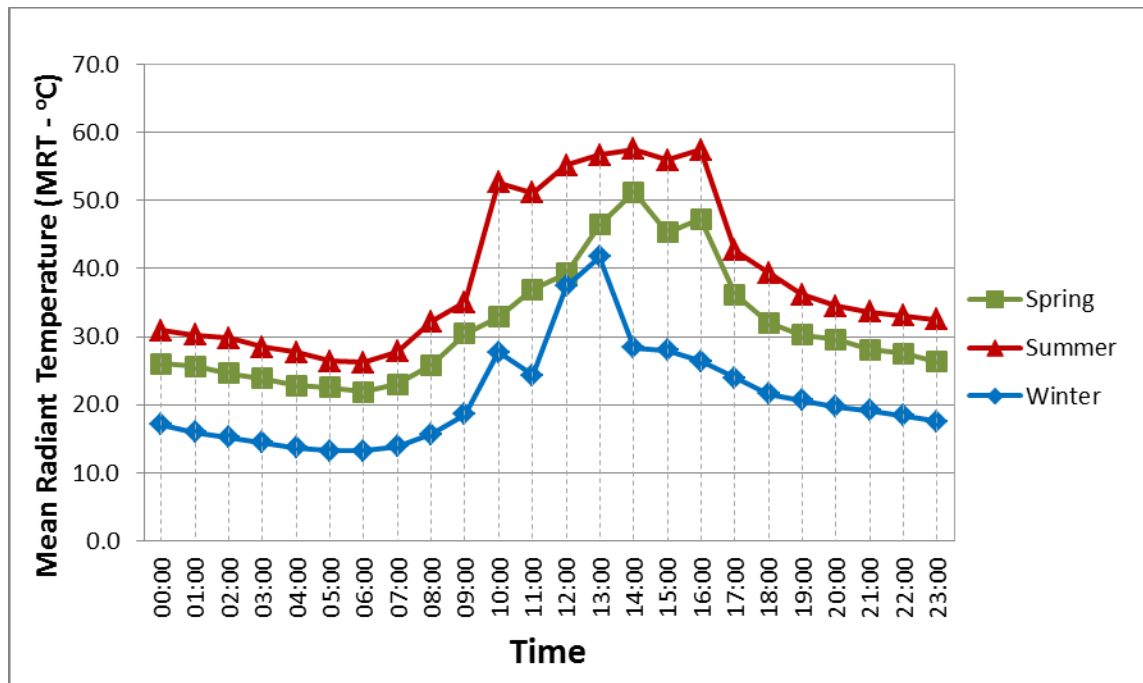


Fig. 6. 28: The MRT values of the spring, summer, and winter seasons in the low urban density area (Case 3).

Figure 6.29 demonstrates the pattern of the relative humidity in summer, spring and winter, with the three seasons having a similar pattern. Unlike the air temperature effect on humidity, it is found that the MRT has no significant effect on the relative humidity values during the night and evening hours, while relative humidity decreases in the afternoon when MRT is around its peak temperature. Summer obtained the lowest relative humidity percentage (14%), then followed by spring (23%), while winter has obtained the highest average daily value of 41%.

However, the relative humidity in the hot seasons measured fall short of the Streinu-Cercel et al. (2007) standard recommendation (40-70%). In winter, the relative humidity in the period between 23:00 throughout to 10:00 hours falls within the standard requirement, while after 10:00 hours in the morning to just before 23:00 hours at night are outside the standard comfort range. The peak in winter, spring and summer reached 60%, 39% and 23% at 06:00, 07:00 and 07:00 hours, respectively.

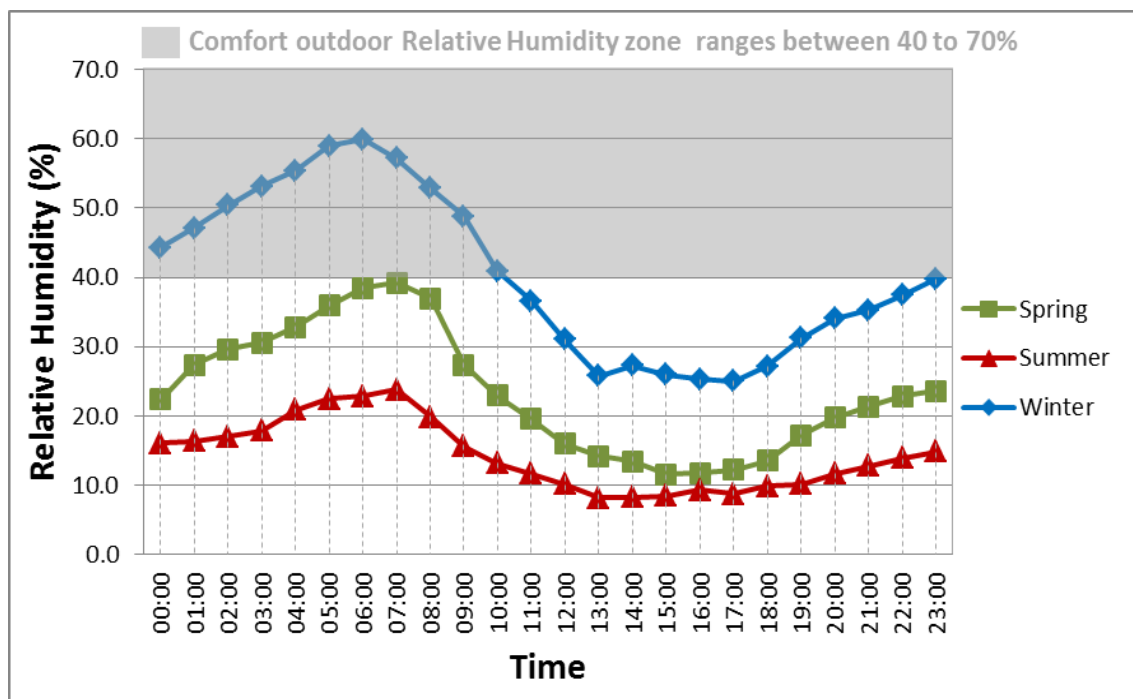


Fig. 6. 29: The relative humidity values of the spring, summer, and winter seasons in the low urban density area (Case 3).

Figure 6.30 demonstrates the difference in values between the MRT and air temperature. It is found that the difference in values in the summer is significantly high with 18°C greater in most of the daytime, particularly between 10:00 hours to 16:00, while at night they are almost equal. This is because of the low urban aspect ratio (H/W of 0.7) with wide openness to the sky (30m wide), leading to the intense solar radiation between this period (10:00 to 16:00 hours) to heat the urban wall surfaces and ground surfaces, as a result of lack in shading level. In winter, lower difference values of MRT compared to the air temperature are found between 18:00 to just before 8:00 hours. This situation is almost the same in the spring and summer seasons.

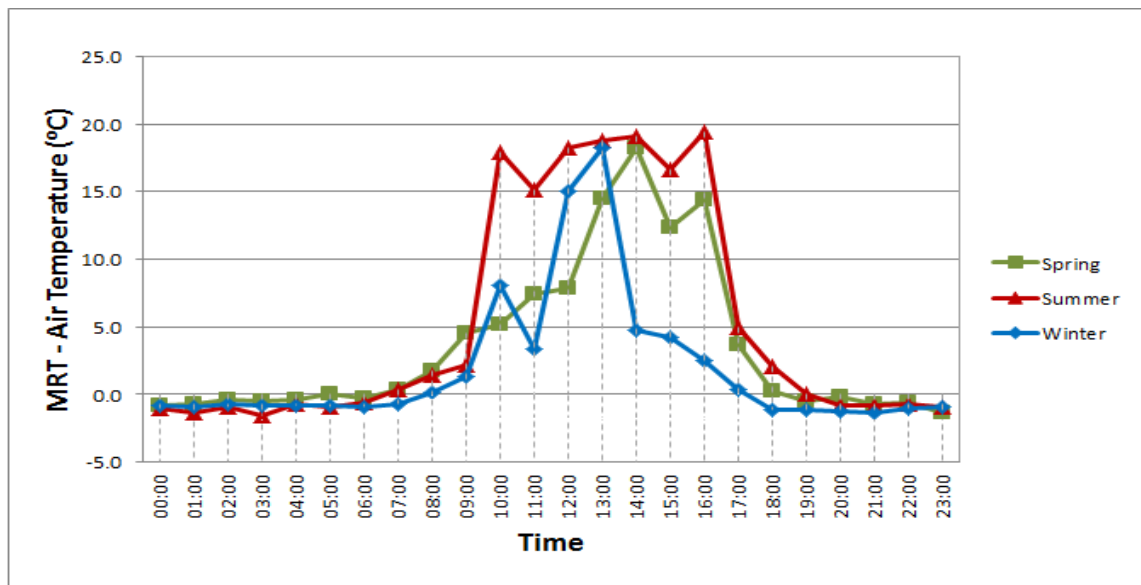


Fig. 6. 30: Difference between mean radiant temperature (MRT) and air temperature in the low urban density area (Case 3).

#### 6.4.3. Pedestrian's Thermal Comfort Conditions (Case 3)

In the current investigation, the pedestrian thermal comfort conditions of the low urban density (Case 3) has been evaluated and analysed for three different climate seasons, including winter, spring and summer.

The best season in Madinah is recognised by the locals to be the spring season, and this assertion has been proved in the findings of this study as can be observed from the thermal comfort PET temperature Figures 6.18, 6.24 and 6.31 (as well as the air temperature Figures 6.4, 6.20 and 6.26). as most of the PET values in the three different urban density cases during spring season are within the comfort zone (i.e. upper limit of

31.3°C and lower limit of 21°C), then followed by the autumn, with summer having the highest PET values.

Figure 6.31 indicates that the PET pattern is similar in all the three seasons of spring, summer and winter, with the highest PET index temperature in summer (average daily value of 35.4°C), and then followed by the spring season (26.8°C). The winter season has the lowest values, with an average daily measurement of 16.7°C. In spring, almost all the values of PET index falls between 17:00 to 11:00 (a duration of 17 hours) which satisfies the acceptable thermal comfort requirement of between 31.3°C (the upper limit) to 21.0°C (the lower limit), that was proposed by Yahia and Johansson (2013a).

In winter, with heavier clothing insulation (1.3 clo) and walking activity level (192.5 W or. 1.9 met), a person in the low urban density area (Case 3) feels extreme discomfort, particularly between 17:00 to 11:00 hours with an average PET value of 15°C, based on the lower limit of thermal comfort of 21°C PET proposed by Yahia and Johansson (2013a).

While in the summer season, with lighter clo value 0.6, the PET values exceeds the upper limit of tolerable thermal comfort condition (i.e. 31.5°C), starting from 09:00 hours to reach the extreme heat stress with PET temperature of above 41°C between 10:00 hours to 17:00 hours. However, PET decreases gradually afterwards to reach the comfort zone after 23:00 hours. The peak PET temperatures in the summer, spring, and winter reach 48°C, 39°C and 26°C at 15:00, 14:00 and 13:00 hours, respectively.

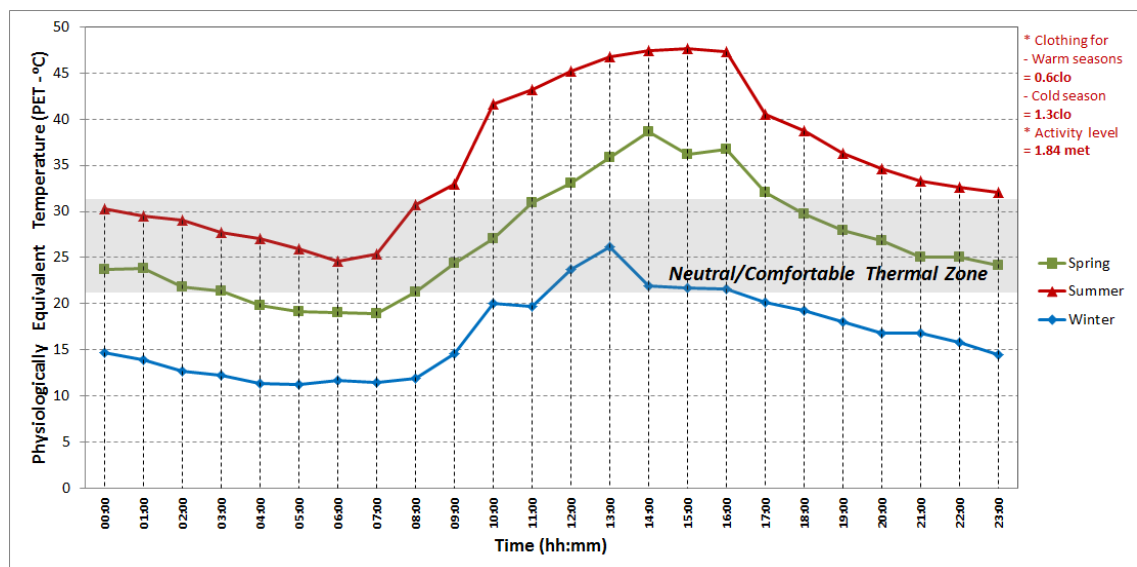


Fig. 6. 31: The PET index values in the low urban density area (Case 3).





### 6.5. Comparison between the Three Urban Density Levels (Case 1, 2, 3)

The urban density levels and characteristics of outdoor urban environments greatly impact the pedestrian thermal sensations because of their influence on wind speed and direction, air temperature, radiant temperature, and relative humidity. Thus, these parameters have been well considered in measuring and predicting pedestrian thermal comfort in the study areas.

The following subsections compare the three urban densities (Case 1, Case 2 and Case 3) based on the four climatic seasons, illustrated in Figure 6.32. However, some microclimatic data for the intermediate urban density and low urban density areas were lost during the research, due to damage and theft of two measuring devices, particularly during the autumn and winter in Case 2, and autumn in Case 3. Thus, only the high urban density area (Case 1) has a complete set of data for four climatic seasons. The hourly microclimatic data for the whole monitoring periods in the high, intermediate and low urban density areas are presented in A6.1 to A6.11 in the appendices.

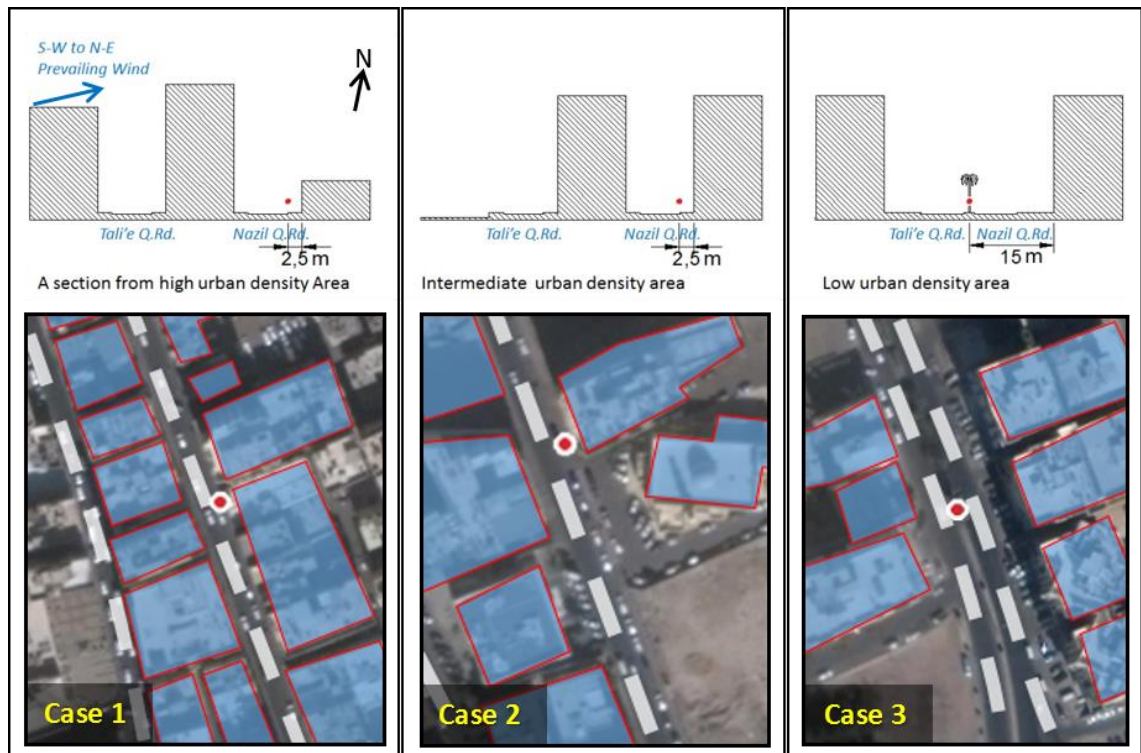


Fig. 6. 32: Field measurements locations for the three urban density cases, located at a height of 2m

### **6.5.1. Summer Results for the Three Urban Density Levels (Case 1, 2, 3)**

In the present study, the summer microclimatic data (i.e. air temperature, wind speed, relative humidity, mean radiant temperature) and the thermal comfort sensation results have been analysed for the three urban density types along the Nazil Quba Road. These analyses are conducted for high urban density (Case 1), intermediate urban density (Case 2), and low urban density (Case 3) areas. The field measurements were conducted for 24 hours and repeated over the monitoring period. The hourly microclimatic data for the whole monitoring periods in the high, intermediate and low urban density areas are presented in A6.1 to A6.11 in the appendices.

#### **6.5.1.1. Air Temperature in Summer (in Case 1, 2, 3)**

Figure 6.33 illustrates that the air temperature pattern in the three urban densities (Case 1, 2, 3), measured simultaneously during the summer season. The results indicate that the larger the urban density, the higher the air temperature is found. The air temperature pattern is similar for the three urban density levels, with the high urban density (Case 1) having the highest air temperature values with an average measurements of 36.1°C, followed by the intermediate urban density (Case 2) with an average measurement of 33.8°C, while the low urban density (Case 3) recorded the lowest at 33.6°C. Thus, the difference in air temperature value is 2°C higher than the temperatures in Case 2 and Case 3.

The increase in air temperature begins immediately after the sunrise, and decreases in the evening starting from the sunset hour (i.e. 18:00) (e.g. Qaid and Ossen, 2014). The increase in air temperature with the growth rate of urban density is as a result of high thermal mass emitted from the adjacent buildings and other surrounding elements within the environment (e.g. Ali-Toudert et al., 2005; Rubio-Bellido et al., 2015).

In other words, the reason for such higher temperatures when the built up density increases is because of the progressive modification of surface covers and structures which absorb more heat in high density of built up areas than the lower ones, which confirms the phenomena of Urban Heat Islands UHI, then it is released at night (e.g. Hu and Brunsell, 2015).

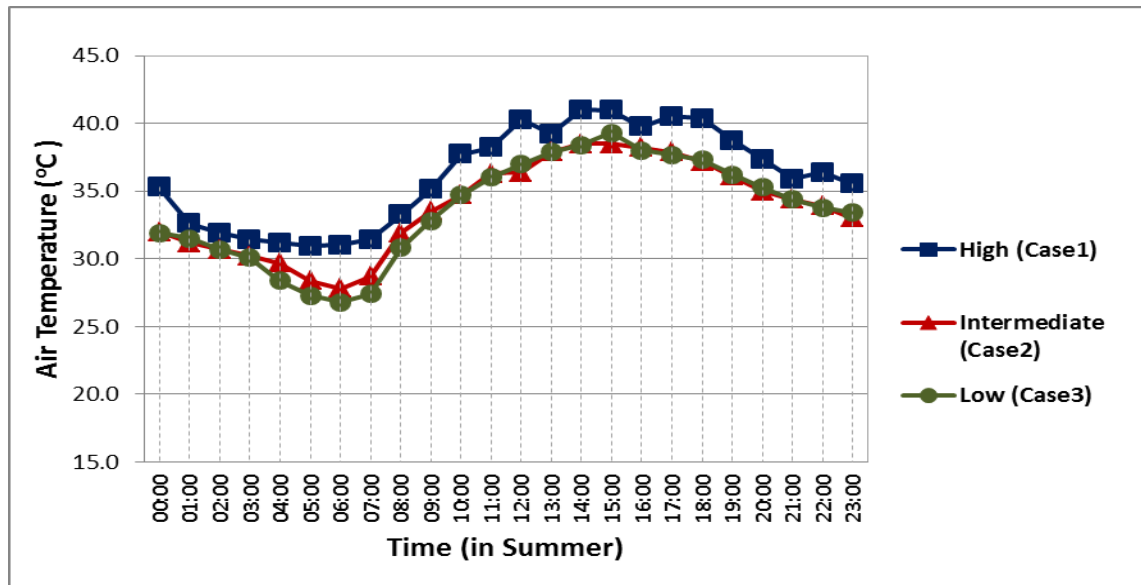


Fig. 6. 33: Comparison between the air temperature values of the high urban density (Case 1), intermediate density (Case 2) and low density (Case 3), measured simultaneously during the summer season.

The hourly microclimatic data for the whole monitoring periods in the high, intermediate and low urban density areas are presented in A6.1 to A6.11 in the appendices.

#### 6.5.1.2. Wind Speed in Summer (in Case 1, 2, 3)

Rizk and Henze (2010) suggest the acceptable wind velocity range in hot arid regions to achieve thermal comfort for air temperatures that exceed 32°C in shade, with a lower limit threshold of 1.6m/s (based on ASHREA Standard 55, 2004), and upper limit of 3.8m/s (based on Beaufort Scale). This suggested range of wind velocity will be used in this research as a required air velocity range for comfort in hot arid microclimates. However, it is acknowledged that it may not be possible for wind velocity alone to achieve thermal comfort, as there are other microclimatic factors (e.g. mean radiant temperature, relative humidity, etc.) that can have effects on pedestrian thermal comfort conditions.

In Figure 6.34, the results of the wind speed pattern indicate that the wind speeds in the three urban density areas, measured simultaneously during the monitoring periods, are not stable in the summer. It is found that the measured wind speed at the pedestrian height is greater in the intermediate urban density (Case 2) with an average daily measurement of 1.8m/s, which falls within the recommended wind speed (1.6 – 3.8m/s) by Rizk and Henze (2010), and then followed by the low urban density area (Case 3) 1.5m/s, while the high urban density (Case 1) has recorded the lowest value of 0.7m/s.

The wind speed is lower in the high urban density and the maximum wind speed does not exceed 1.3m/s, which is because of the ground surface roughness increases with increasing the density level, resulting in decrease in wind speed (e.g. Ali-Toudert et al., 2005). However, this assertion could not be justified in the case of the intermediate and low urban densities, because of the disparity in building heights. The lower density cases are high enough to get comfort (i.e. above the lower comfort threshold of 1.6m/s). The wind speed is higher in the intermediate urban density (with a maximum value reaches 3.8m/s) compared to the low urban density area (with a maximum value reaches 2.3m/s). This might be as a result of the low approaching wind speed in Madinah, with an average maximum of 3.5m/s recorded in summer at the city's airport (Iowa State University of Science and Technology, 2015).

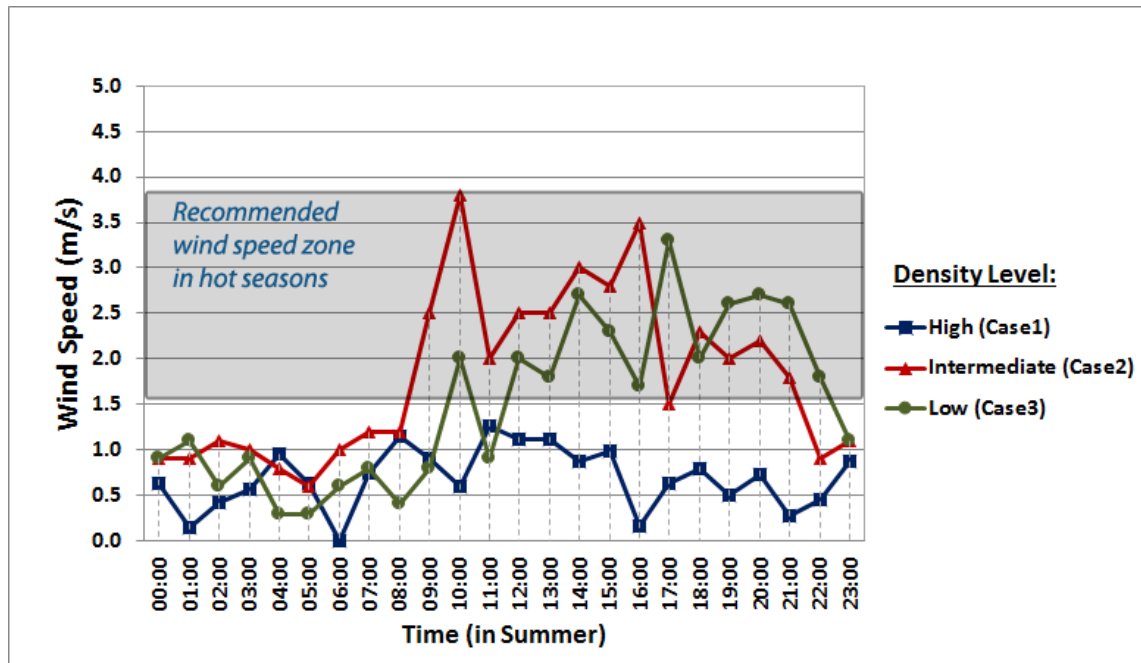


Fig. 6. 34: Comparison between the wind speed values of the high urban density (Case 1), intermediate density (Case 2) and low density (Case 3), measured simultaneously during the summer season.

### 6.5.1.3. Relative Humidity in Summer (in Case 1, 2, 3)

Figure 6.35 reflects the results of the relative humidity in the summer season for the three urban densities (Case 1, 2, and 3), measured simultaneously, along the Nazil Quba Road. It can be observed that the relative humidity is significantly influenced by the ambient air temperature, as it decreases immediately after the sun rises or with the increase of air temperature, and vice versa. The pattern of the relative humidity in the three urban densities during the summer season are similar, with the low urban density having the highest average measurement value of 14%, then followed by the intermediate density 13.5%, while the high urban density recorded the lowest 11.6%. The results are in line with the previous research of Yahia and Johansson (2013a). However, the relative humidity in all the three densities measured fall short of the Streinu-Cercel et al. (2007) standard recommendation (40-70%). In comparison with the airport metrological average daily humidity (14.1%), the low urban density and intermediate urban density are found to be almost identical in percentages, while in the high urban density it is found to be 2% lower than the airport.

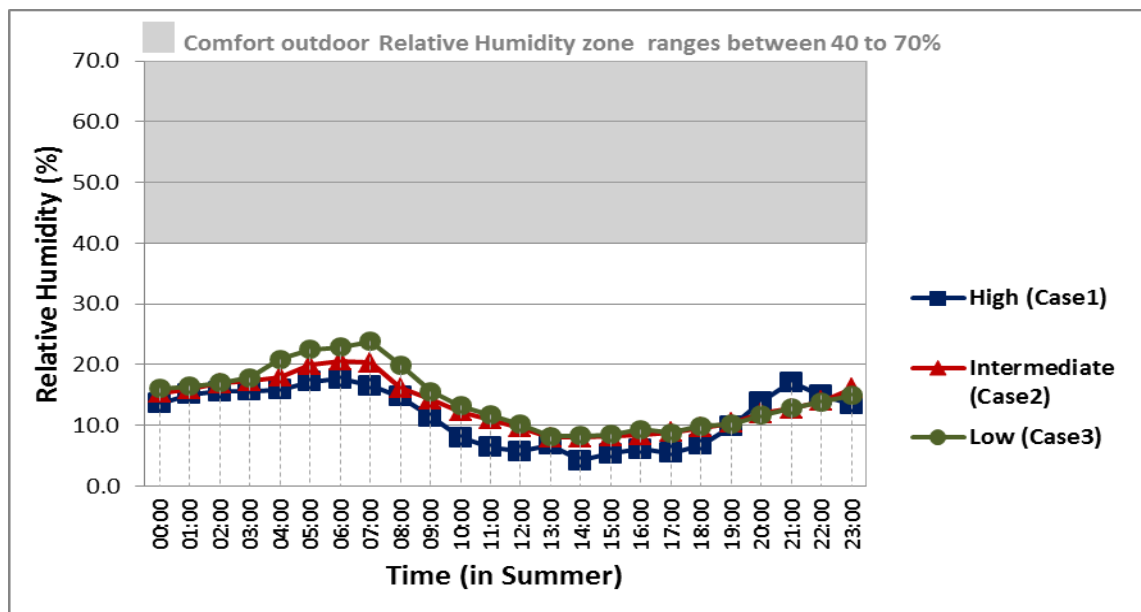


Fig. 6. 35: Comparison between the relative humidity values of the high urban density area, intermediate density area and low density area, measured simultaneously during the summer season.

#### 6.5.1.4. Mean Radiant Temperature (MRT) in Summer (in Case 1, 2, 3)

Figure 6.36 shows that the results pattern of MRT is similar for the low and intermediate urban densities, but differs for the high urban density, which could be due to different levels of shading effects provided by buildings. The MRT is found to be lowest in the high urban density (Case 1) with an average measurement value of 36.3°C, followed by the low urban density (Case 3) with the average measurement of 38.9°C, while the case of intermediate urban density (Case 2) recorded the highest values with average of 40.5°C.

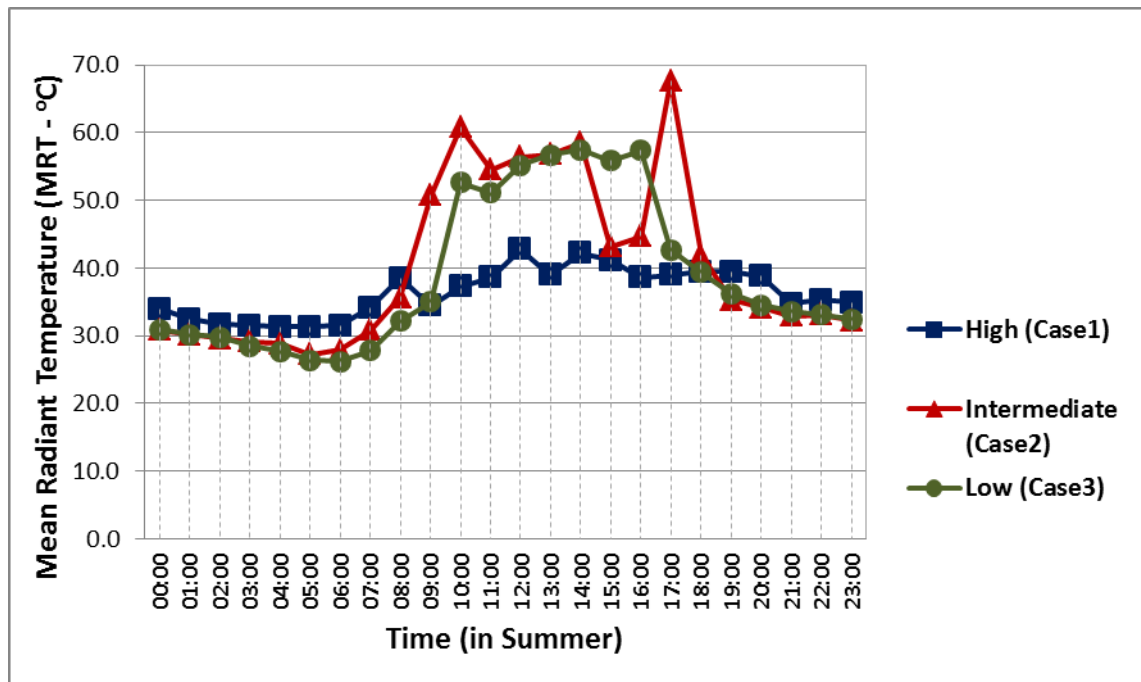


Fig. 6. 36: : Comparison between the MRT values of the high urban density (Case 1), intermediate density (Case 2) and low density (Case 3), measured simultaneously during the summer season.

There were similar findings in a study conducted in the hot arid region of Damascus in Syria (Yahia and Johansson, 2013b), which concluded that high urban density can protect pedestrians in summer by providing well shaded spaces compared to the low and intermediate urban densities. However, during the night times, the high urban density area retains the highest MRT values. This is because of heat from solar radiation is stored in the surrounding physical elements within the urban canyons (during the day) and is released during the night hours. In addition, higher urban density provides more shading than the low and intermediate densities, therefore it is recorded the lowest MRT value during the daytimes.

### 6.5.1.5. Pedestrian's Thermal Comfort Conditions in Summer (in Case 1, 2, 3)

The pedestrian thermal comfort of high urban density, intermediate and low urban densities for the summer has been calculated based on the data obtained from the measurements of the four main microclimatic parameters, including air temperature; relative humidity; mean radiant temperature; and air velocity. The thermal comfort sensation values were obtained based on Physiological Equivalent Temperature (PET), using RayMan software (refer to section 5.7 in the methodology chapter). The study also employed two personal factors including a summer clothing value of 0.6 clo and walking activity level with a value set to 192.5 W (i.e. 1.9 met or 106.94W/m<sup>2</sup>), which are required inputs in the calculation of PET index (Yahia and Johansson, 2013a).

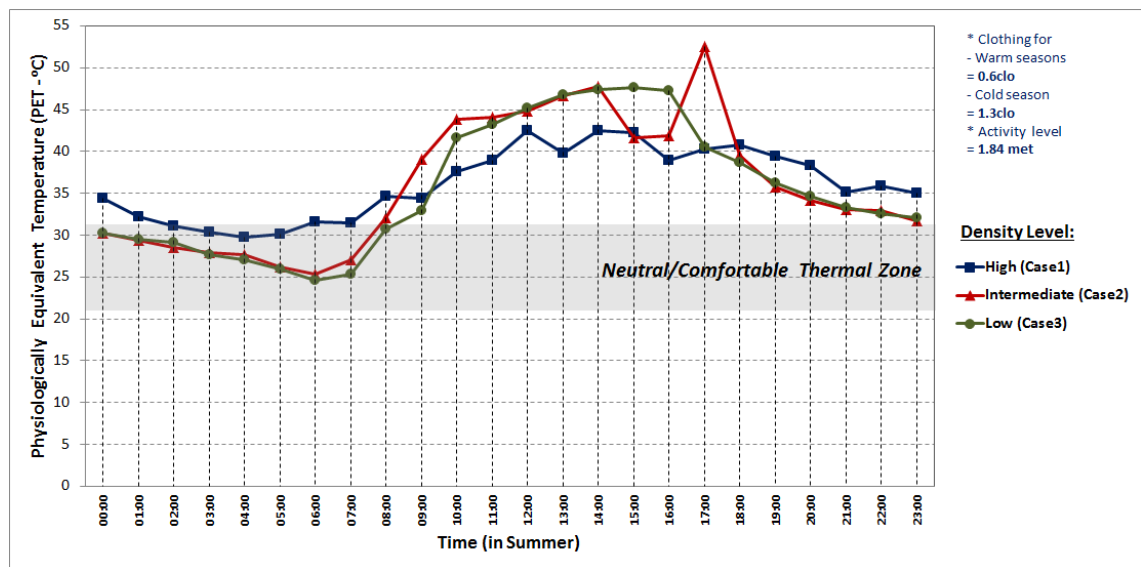


Fig. 6. 37: Comparison between the physiologically equivalent temperature (PET) index values of the high urban density (Case 1), intermediate density (Case 2) and low density (Case 3) during the summer season.

Figure 6.37 illustrates that the PET pattern in summer is somewhat similar in the three urban densities (Case 1, 2, 3), with the low urban density (Case 3) having the lowest average daily value of 35.4°C, followed by the intermediate urban density (Case 2) with an average daily value of 36.0°C, then the high urban density area (Case 1) with a value of 36.1°C. In comparison to the thermal comfort threshold in hot arid climates of between 21°C to 31.3°C PET, the overall PET result of the three urban densities in summer are found to be 4-5°C higher than the upper limit of comfort threshold. This difference in the value (4-5°C) will be considered in Chapter 7 for the assessment of the effects of modifications in the canyons' aspect ratios on the wind flow and thermal comfort conditions.



The results in Figure 6.37 also show that higher PET index temperatures are observed in the range between 9:00 hours to 18:00 hours for all the three urban densities, with averages of 39.8°C in the high urban density, 44.2°C in the intermediate urban density and 43.1°C in the low urban density. The reason for the high urban density recording the lowest average PET temperature in this specific day time hours (09:00 to 18:00) is due to the shading effects that are provided by larger number of buildings (e.g. Yahia and Johansson, 2013b). This agrees with Pearlmutter et al. (1999) that the heat gained by a human body within an urban street canyon of  $H/W = 1$  (deep canyon) is lower in comparison to a fully exposed location (shallow canyon) because of more shading within the canyon.

However, the pedestrian thermal sensation index indicates that most people would feel discomfort in the summer along the length of Quba Road (i.e. the three density cases), particularly after 07:00 hours to midnight (i.e. a duration of 17 hours). However, comfortable thermal values in summer in Case 1 (i.e. high urban density) are for only a short period between 02:00 to 06:00 (i.e. duration of 4 hours), with an average value equals the upper limit of comfort threshold of 31.3°C.

Extended periods of comfortable conditions in summer are found in the intermediate and low urban densities, particularly between midnight (00:00) to 08:00 hours in the morning, with PET temperature ranges between 25°C to 31.3°C, for a duration of 8 hours. During this period, the number of pedestrians is very low as no commercial activities are open along the Quba Road (refer to Figure 6.3 in section 6.2.1).

### **6.5.2. Spring Results for the Three Density Areas (Case 1, 2, 3)**

In the present section, the data of the four main microclimatic parameters during the spring season for the three urban densities of Nazil Quba Road were analysed and discussed. The measurements were conducted simultaneously for high urban density area (Case 1), intermediate urban density area (Case 2), and low urban density area (Case 3). The field measurements were conducted for 24 hours continuously over the monitoring period. The hourly microclimatic data for the whole monitoring periods in the high, intermediate and low urban density areas are presented in A6.1 to A6.11 in the appendices.

#### **6.5.2.1. Air Temperature during Spring (Case 1, 2, 3)**

Figure 6.38 demonstrates that the air temperature pattern for the three urban density levels, measured simultaneously during spring. With the high urban density (Case 1) having the highest air temperature values with average daily measurements of 29.5°C, followed by the intermediate urban density (Case 2) with an average daily value of 29.1°C, while the low urban density (Case 3) recorded the lowest average daily measurement of 28.0°C. The results also reflect that air temperature in spring begins to increase after sunrise (i.e. 06:00) in the three urban density areas, and starts to decline in the evening near sunset (i.e. 18:00). However, the decrease in air temperature is gradual in the evening in the three urban density areas, due to the thermal mass of the structures, which is higher in Case 1, with very small differences (of 0°C-0.5°C) between the values of the three cases during the hot day hours of between 09:00 to 18:00 (e.g. Rubio-Bellido et al., 2015).

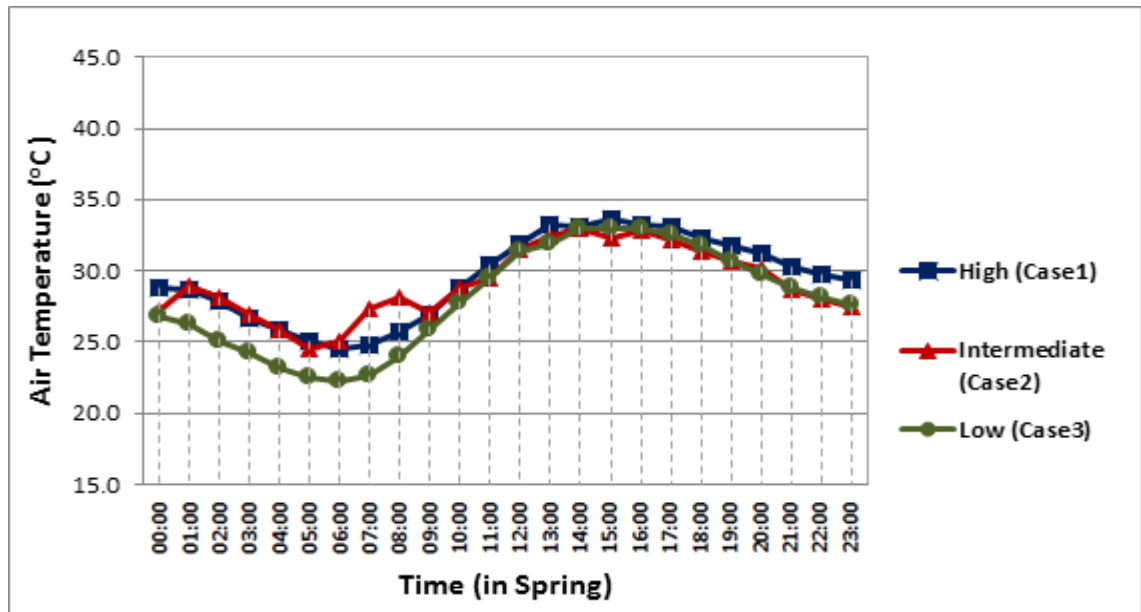


Fig. 6. 38: Comparison between the air temperature values of the high urban density (Case 1), intermediate density (Case 2) and low density (Case 3), measured simultaneously during the spring season.

Between the mid-night and the sunrise period, the low urban density area (Case 3) experiences of 3°C lower average difference in the air temperature values compared to the high urban density (Case 1), as the low urban density area has larger opening to the sky, thus allowing more heat to be released from wall surfaces to the sky. The air temperature values in the intermediate urban density (Case 2) in the evening are approximately equal to the values of low density area (Case 3), but it immediately increases about 2°C at 01:00 hours to equal the air temperature of the high urban density (Case 1). This raises the question of what causes this immediate increase after midnight in spring. In a previous study on the impact of increasing urban density on local climate in Melbourne, Australia, it was found that the intermediate urban density were almost equal to the high urban density areas during the night time in the spring season, particularly between 22:00 to 4:00, and about 1°C was higher than the low urban density area (Coutts et al., 2007). This validates the findings of the current research, where Case 2 was approximately equal to Case 1 after the midnight (highlighted above).

However, this does not answer the above mentioned question, but alternatively it indicates that the air temperature values actually decreased at about 2°C for the night time period of before 01:00. From this perspective, the effect of significant wind speeds that are blown over cooler green surfaces of the low urban density to the intermediate urban density during these critical hours of the night time until before 01:00 can justify the decrease in the temperature value (refer to wind graph in the following section).

#### 6.5.2.2. Wind Speed during Spring (Case 1, 2, 3)

In Figure 6.39, the results of the wind speed pattern indicate that the wind speeds in the three urban density areas, measured simultaneously during the monitoring periods, are not stable in the hot season of spring. The measured wind speed at the pedestrian level in the low urban density (Case 3) is found having the highest average value 1.5m/s, followed by the intermediate urban density (Case 2) with average measurement 1.1m/s, while the high urban density (Case 1) has recorded the lowest average value 0.65m/s. Wind speed in Case 2 peaks to 2.2m/s at 13:00, while Case 3 peaks to 2.7m/s at 16:00, with gradual decrease for the both cases until it reaches the midnight to calm in the range of between 0.5m/s to 1m/s. The wind speed is lower in the high urban density because the ground surface roughness increases with density, resulting in decrease in wind speed magnitude.

Rizk and Henze (2010) suggest the acceptable wind velocity range in hot arid climates to achieve thermal comfort for air temperatures that exceed 32°C in shade, with a lower limit threshold of 1.6m/s (based on ASHREA Standard 55, 2004), and upper limit of 3.8m/s (based on Beaufort Scale). However, wind speed in the high urban density area is not enough to get comfort. In the intermediate urban density area, a short period of between 11:00 hours to 15:00 hours falls within the required comfort standard, with extended period of comfort in the lower urban density area (i.e. between 13:00 hours to 21:00 hours). The hourly microclimatic data for the whole monitoring periods in the high, intermediate and low urban density areas are presented in A6.1 to A6.11 in the appendices.

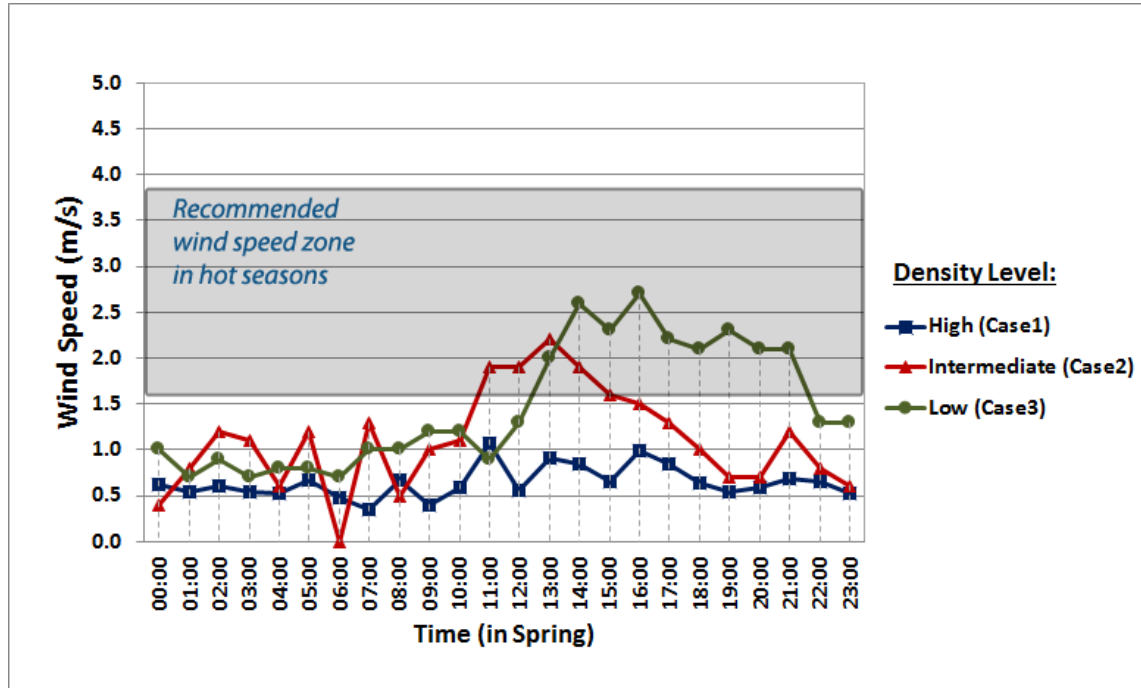


Fig. 6. 39: Comparison between the wind speed average hourly values of the high urban density (Case 1), intermediate density (Case 2) and low density (Case 3), measured simultaneously during the spring season.

### 6.5.2.3. Relative Humidity during Spring (Case 1, 2, 3)

Figure 6.40 reflects that the pattern of the relative humidity in the three urban densities during the spring season is similar, with the low urban density (Case 3) having the highest percentages with an average daily measurement of 23.4%, then unexpectedly followed by the high urban density (Case 1) with an average percentage of 18.3%, while the intermediate urban density (Case 2) recorded the lowest 14.6%. The hourly microclimatic data for the whole monitoring periods in the high, intermediate and low urban density areas are presented in A6.1 to A6.11 in the appendices.

The reason for the relative humidity in the intermediate density level being the lowest could be due to higher mean radiant temperature values that were recorded in this case during the day hours compared to other cases, as will be demonstrated in the following section. However, the relative humidity in all the three urban densities falls under the recommended standard (40-70%) by Streinu-Cercel et al. (2007).

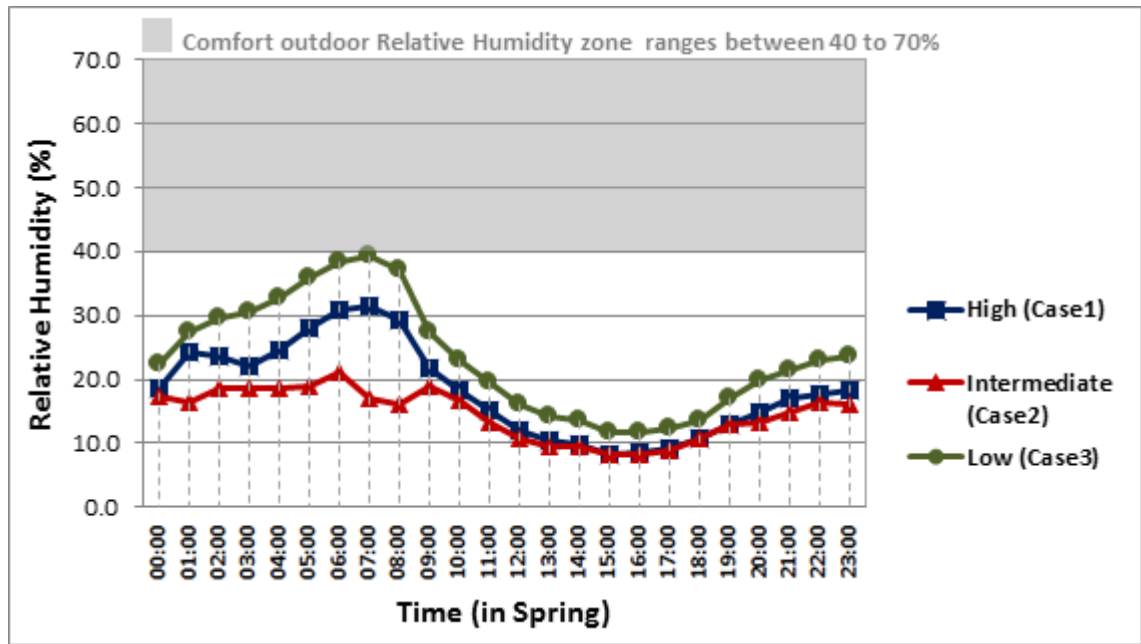


Fig. 6. 40: Comparison between the relative humidity average hourly values of the high urban density area, intermediate urban density and low urban density area, measured simultaneously during the spring season.

#### 6.5.2.4. Mean Radiant Temperature (MRT) during Spring (Case 1, 2, 3)

Figure 6.41 reflects that the MRT in the intermediate urban density area (Case 2) in spring has the highest average daily measurements value of 33.1°C, followed by both the high urban density (Case 1) and low urban density (Case 3) with an average value of 31.5°C for each. However, during the night times, the MRT in Case 1 (high urban density) retains the highest values than Case 2 and Case 3, which is normally a result of the thermal mass process with a difference value of 2°C at 23:00 hours. The hourly microclimatic data for the whole monitoring periods in the high, intermediate and low urban density areas are presented in A6.1 to A6.11 in the appendices.

The intermediate urban density (Case 2) in spring increases significantly from 30°C at 08:00 hours to 41°C at 09:00 hours, then decreases from the peak value of 58°C at 13:00 hours to 40°C at 14:00 hours, recording higher values in this period (09:00 to 13:00) than the high urban density and low urban density. This could be due to the adjacent large vacant plot allowing the solar radiation access to the canyon at the ground and pedestrian level, thus increasing the value of MRT by heating the wall surfaces.

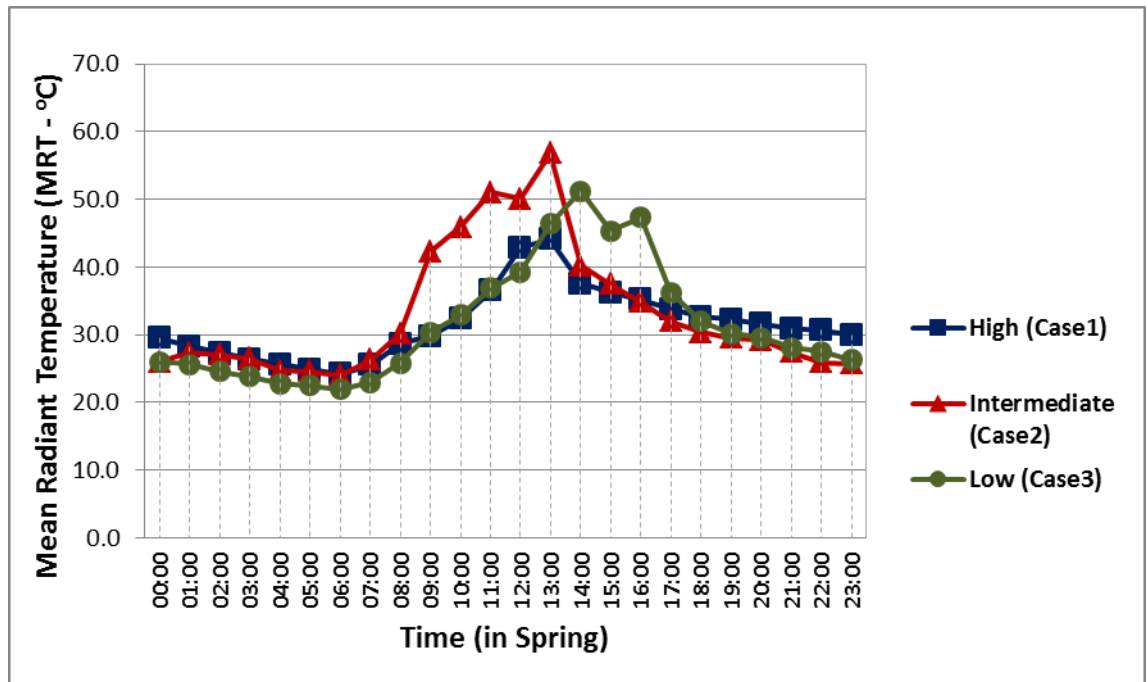


Fig. 6. 41: Comparison between the MRT average hourly values of the high urban density (Case 1), intermediate density (Case 2) and low density (Case 3) during the spring season.

#### 6.5.2.5. Pedestrian's Thermal Comfort Conditions during Spring (Case 1, 2, 3)

The provision of thermal comfort in outdoor pedestrian spaces can encourage pedestrians to spend more times outdoors (Ali-Toudert et al., 2005). The thermal comfort sensation values were obtained for the spring season using Physiological Equivalent Temperature (PET). The study also employed two personal factors including a summer clothing value of 0.6 clo and walking activity level with a value set to 192.5 W (i.e. 1.9 met or 106.94W/m<sup>2</sup>), which are required inputs in the calculation of PET index (Yahia and Johansson, 2013a). The PET pattern is similar in the three urban densities, as shown in Figure 6.42.

The outcome of the analysis shows that the highest PET index temperature is obtainable in the high urban density (Case 1) during the night hours, while the MRT in the intermediate urban density (Case 2) is the highest during the day hours. The overall average daily measurement of PET values in spring for Case 1, Case 2 and Case 3 are 29°C, 28.8°C, 26°C, respectively. This situation is in line with previous research conducted under hot arid conditions (e.g. Yahia and Johansson, 2013a).



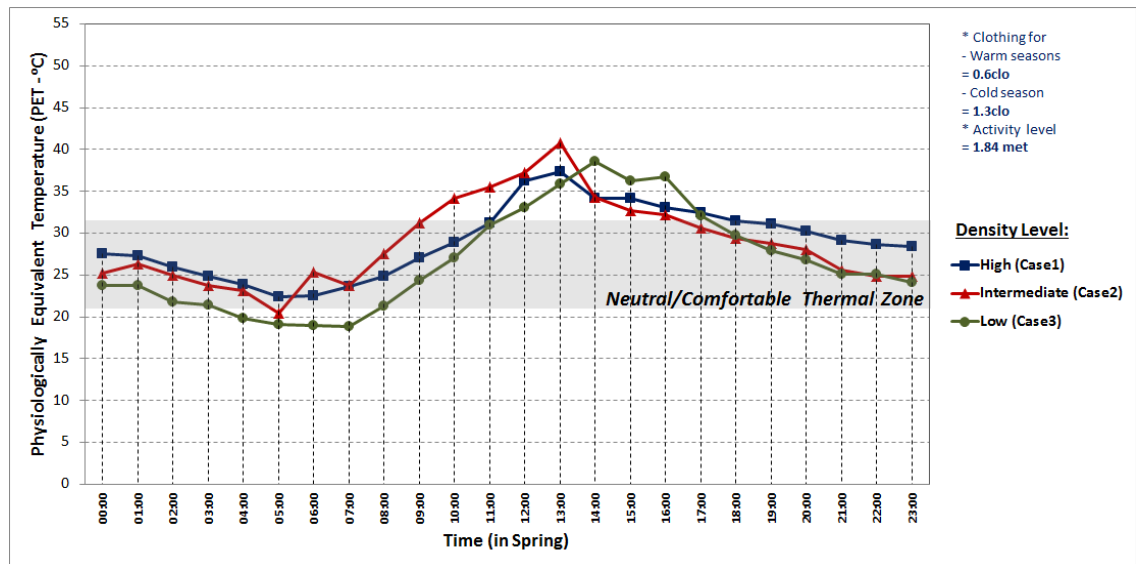


Fig. 6. 42: Comparison between the physiologically equivalent temperature (PET) index values of the high urban density (Case 1), intermediate density (Case 2) and low density (Case 3) during spring.

The acceptable hot season in Madinah is recognised by the locals, from a tolerable outdoor temperature sensation perspective, to be the spring season. This assertion has been proved in the findings of this study, as most of the PET values in the three different density cases during spring season are below the upper limit of the comfort zone (i.e. 31.3°C). However, the duration of when pedestrians may feel thermally uncomfortable occurs between 10:00 to 16:00 hours in all the three density cases, with average hourly temperature values of between 35°C to 40°C of PET (i.e. a difference of 4 to 9°C compared to the upper limit of tolerable thermal comfort). Thus, this period should be considered in this research when investigating the effect of different urban design scenarios (in Chapter 7) with the aim of extending the use of outdoor space by shifting the thermal conditions from a range of thermal discomfort into a range of critical thermal comfort as much as possible.

### **6.5.3. Winter Results for the High and Low Urban Density Areas (Case 1 and 3)**

In the present study, the winter data of the air temperature, wind speed, relative humidity and mean radiant temperature in the Nazil Quba Road have been measured and analysed. The pedestrian thermal comfort sensation conditions in winter were calculated based on PET index using RayMan software. The analyses were conducted for high urban density area (Case 1) and low urban density area (Case 3), while the data for the intermediate urban density (Case 2) were excluded from the analysis, due to damage of the data logger and loss of data. The field measurements were conducted for 24 hours continuously over the monitoring period. The hourly microclimatic data for the whole monitoring periods in the high and low urban density areas are presented in A6.1 to A6.5, and A6.9 to A6.11 in the appendices.

#### **6.5.3.1. Air Temperature during Winter (Case 1 and 3)**

In winter, the air temperatures in the high urban density area (Case 1) are following the same pattern as the low urban density area (Case 3) in Quba Road, as illustrated in Figure 6.43. The results for the high urban density and low urban density in winter area in line with a previous study of Johansson (2006). The air temperature found decreasing gradually at night between 17:00 to 05:00 hours from 24°C to 15°C in the high urban density and to 14°C in the low urban density area. The reason for the high urban density area having a slightly higher temperature (i.e. difference of 1°C) after the mid night is due to the effect of the thermal mass of adjacent buildings and heat trap by narrower openness to the sky. The overall average daily measurement of air temperature value for Case 1 and Case 3 in winter is as low as 19.6°C and 19.2°C, respectively.

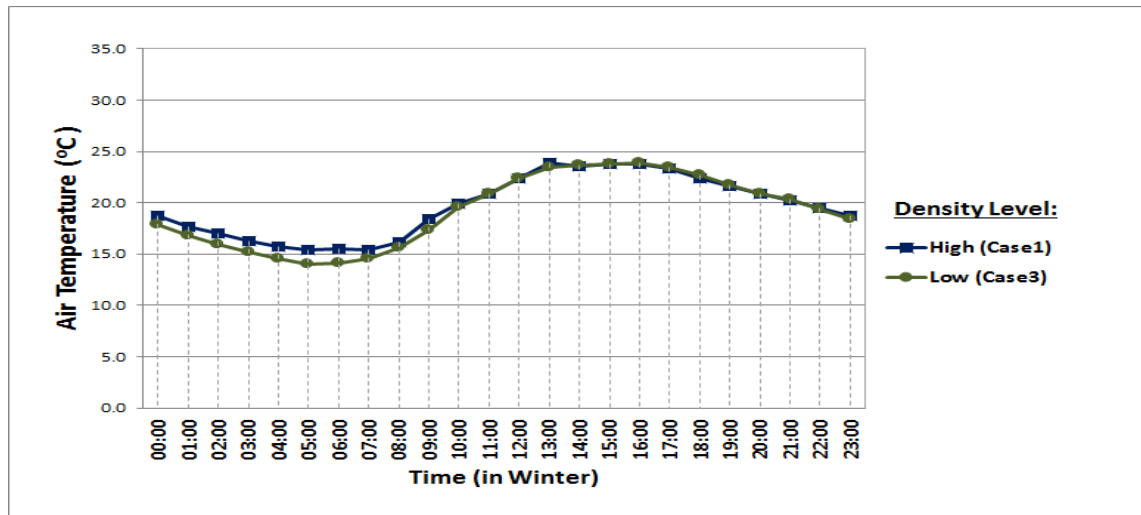


Fig. 6. 43: Air temperature values in areas of high urban density (Case 1) and low urban density (Case 3) during the winter season.

#### 6.5.3.2. Wind Speed during Winter (Case 1 and 3)

In Figure 6.44, the results indicate that the wind speeds pattern in the study areas (Case 1 and Case 3) for the measured period are not stable in winter, however it is somewhat following a similar pattern as the air temperature (refer to section 6.5.3.1). The average daily wind speed value for the high urban density (Case 1) and the low urban density (Case 3) is around to 1.3m/s. However, the wind speed in the low urban density (Case 3) between 12:00 to 23:00 is slightly higher than the high urban density area (Case 1), with an average hourly difference value of 0.1m/s during this period. In contrast, air speed is lower in Case 3 (i.e. the low urban density area) after the midnight to 11:00 hours with a difference value of 0.4m/s. The prevailing wind direction in the high urban density area (case 1) is from the north-easterly direction with speeds between 1-1.9m/s, and in the low urban density is from north westerly direction with speeds range of 0-0.9m/s. The hourly microclimatic data for the whole monitoring periods in the high and low urban density areas are presented in A6.1 to A6.5, and A6.9 to A6.11 in the appendices.

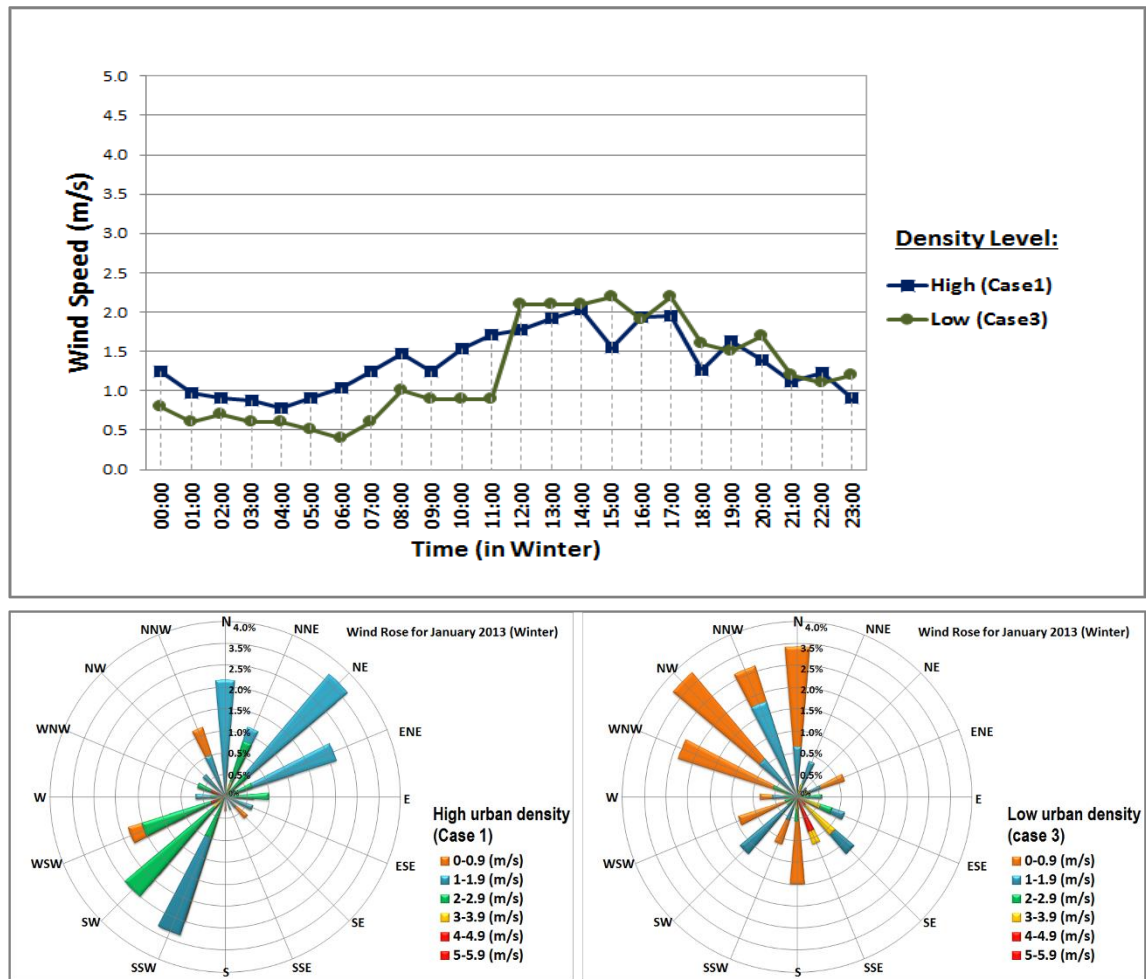


Fig. 6. 44: Wind speed values and wind directions in areas of high urban density (Case 1) and low urban density (Case 3) during the winter season.

### 6.5.3.3. Relative Humidity during Winter (Case 1 and 3)

In winter, the high urban density area (Case 1) is having lower relative humidity after the midnight and higher during the day hours compared to the low urban density area (Case 3), as illustrated in Figure 45. This is because the relative humidity is affected by the air temperature pattern, which is 1°C lower in Case 3 than Case 1 after the midnight. In contrast, relative humidity is higher in Case 3 during the late night between 23:00 to 10:00 hours. The average daily relative humidity values for Case 1 and Case 3 are identical and equalled to 40.5%. In addition, the relative humidity values in both the density cases measured satisfy the lower limit of recommended standard of 40%, particularly between 23:00 hours to 10:00 hours in the low urban density (Case 3) with a peak value of 60% and in the high urban density (Case 1) with a peak value of 52.5% just before the sunrise. The hourly microclimatic data for the whole monitoring periods in the high and low urban density areas are presented in A6.1 to A6.5, and A6.9 to A6.11 in the appendices.

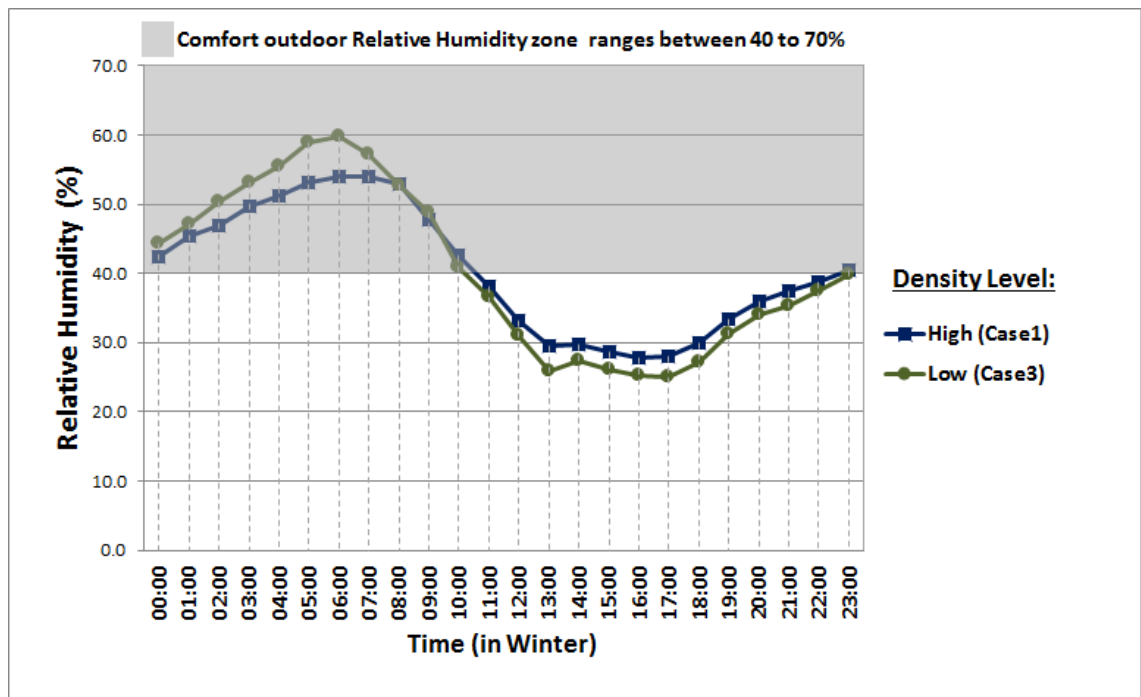


Fig. 6. 45: Relative humidity values in areas of high urban density (Case 1) and low urban density (Case 3) during the winter season.

#### 6.5.3.4. Mean Radiant Temperature (MRT) during Winter (in Case 1 and 3)

Mean radiant temperature during the winter season is very low compared to the hot seasons; however in Case 1 (high urban density area) the MRT values are slightly during the day hours than in Case 3 (i.e. low urban density area), as illustrated in Figure 6.46. This could be due to the low sun elevation in winter, and the radiative heat received to building surfaces are trapped in the narrower canyon (12m) compared to the low urban density with wider openness to the sky (30m). In winter, mean radiant temperature influences wind speed flow, as the wind increases in areas where radiant energy is increasing, and vice versa. The average MRT value in Case 1 and Case 3 are 23.4°C and 21.1°C, respectively. The hourly microclimatic data for the whole monitoring periods in the high and low urban density areas are presented in A6.1 to A6.5, and A6.9 to A6.11 in the appendices.

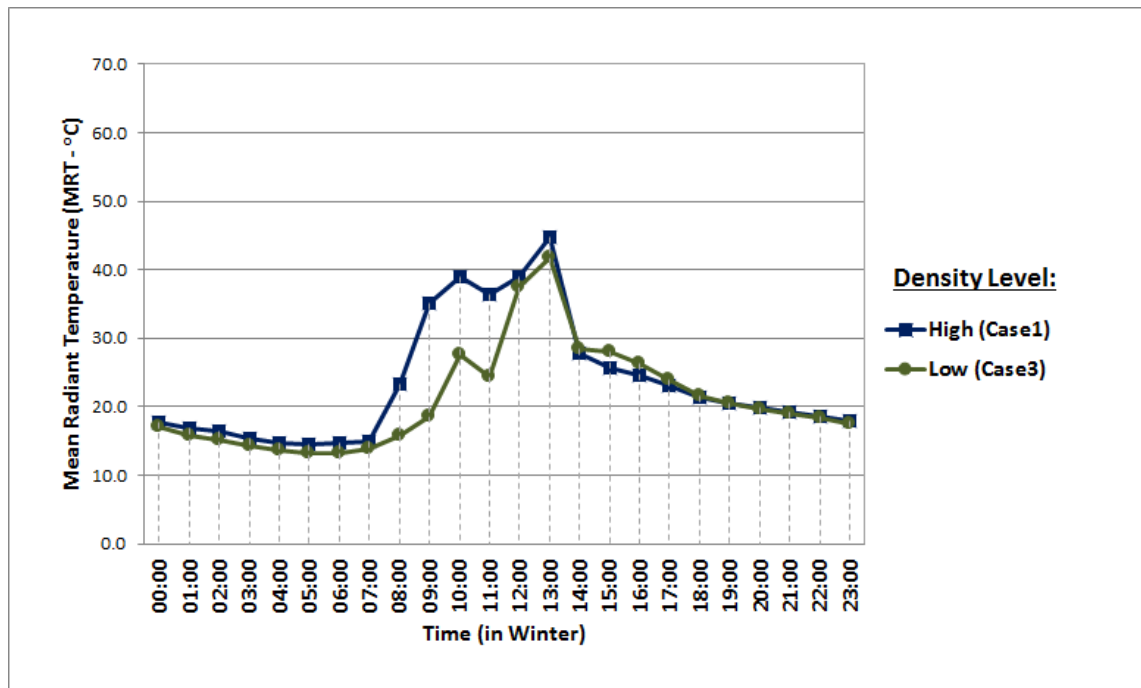


Fig. 6. 46: MRT values in areas of high urban density (Case 1) and low urban density (Case 3) during the winter season.

### 6.5.3.5. Pedestrian's Thermal Comfort Conditions during Winter (Case 1 and 3)

The pedestrian thermal comfort conditions in winter was calculated based on PET index temperature, using RayMan software. The PET values were obtained for the high urban density area (Case 1) and low urban density area (Case 3) in Quba Road, during 24 hours for the monitoring period in winter (1<sup>st</sup> to the 7<sup>th</sup> of January 2013), as illustrated in Figure 6.47. PET values were calculated for a walking activity (i.e. metabolic rate of 192.5 W or 1.9 met) and with winter clothing insulation rate of 1.3 clo value. Yahia and Johansson (2013a) identified the lower limit of thermal comfort threshold to 21°C.

The pedestrian thermal comfort conditions in Case 1 and Case 3 during winter are uncomfortable most of the time, with an average daily value for both of the cases is equal to 16.7°C and 17.6°C in PET, respectively. The results show that PET index value in the high urban density (Case 1) peaks to 28.2°C at 013:00 hours, whereas in the low urban density (Case 3) peaks to 26.2°C at 13:00 hours. The minimum value of 9.9°C is found at 07:00 in Case 1 and 11.2°C at 05:00 in Case 3.

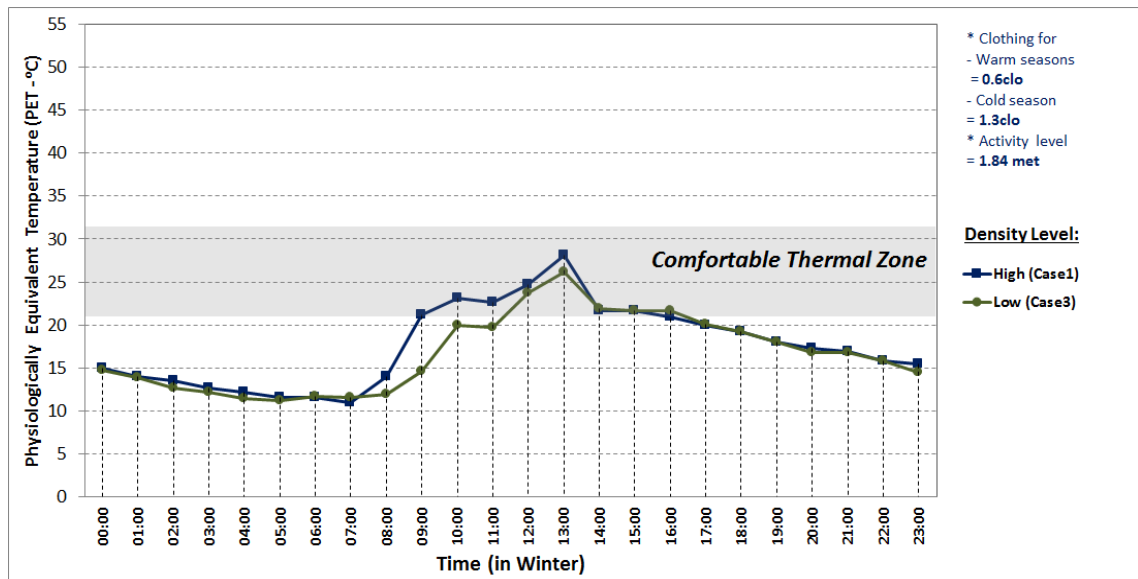


Fig. 6. 47: Comparison between the physiologically equivalent temperature (PET) index values of the high urban density (Case 1) and low urban density (Case 3) during the winter season. The upper limit in summer and lower limit in winter comfort zone in hot arid areas are 31.3°C and 21°C, respectively.



## 6.6. Summary

In this chapter, the analysis of air temperature, mean radiant temperature, relative humidity and wind speed under the four climatic seasons were investigated along Quba Road, particularly within the three selected cases based on the built up level, including the high urban density area (Case1), intermediate urban density (Case2) and low urban density (Case3). The data were obtained at a pedestrian height of 2m. The main objectives of this investigation were to evaluate the urban pedestrian microclimate levels in the Nazil Quba Road in Madinah, Saudi Arabia, and to assess the current outdoor pedestrian thermal comfort conditions.

The four climatic seasons of summer, spring, autumn and winter followed almost similar microclimatic pattern during the 24 hours. The number of pedestrians on the street was obtained in the high urban density area during January (in winter), April (in spring) and June (in summer), and an increase of Quba Road users were found within the five prayer times in Islam (i.e. at 05:00, 12:30, 15:30, 18:00 and 20:30 hours). The number increased significantly during late evening until the midnight, which was due to a decrease in the MRT values and PET values starting after 16:00 hours. Thus, there was an interrelationship between the number of users and PET comfort temperature.

In terms of air temperature, the comparison between the three different urban densities during the hot climatic seasons revealed that when urban density increases higher temperature values can be obtained during the 24 hours, as it increased directly after the sunrises and decreases after the sunsets. This situation is as a result of high thermal mass stored within the adjacent buildings and other surrounding elements within the environment and subsequently emitted during the night (e.g. Rubio-Bellido et al., 2015). However, the night thermal mass of the structures in the high urban density (Case 1) caused gradual decrease in air temperature in comparison to the intermediate urban density (Case 2) and low urban density (Case 3), particularly after the midnight.

The air temperature pattern in the four climatic seasons was similar in the high urban density area (Case 1). In the low urban density (Case 3), the air temperature patterns were lower than the high urban density area. This could be as a result of the heat during the night period can be released to the sky without being trapped between buildings compared to the higher urban density, which is due to the small amount of thermal mass elements or buildings. In addition, the farms and vegetation are broadly provided in the lower dense area, which support providing the cooling effect by

evaporation and evapotranspiration during the day, with maximum benefit of the effect in reducing air temperature at the night.

In terms of wind speeds, the comparison between the three different urban density cases during the hot climatic seasons indicated that wind speeds in the summer season is higher than the spring in Case 1, Case 2 and Case 3. In high urban density (Case 1), the highest wind speed was experienced in winter, followed by summer and then spring, while autumn had the lowest average air speed, as shown Table 6.1 below. The high urban density area experienced the lowest wind speeds at the measurement location and was not high enough to reach the recommended wind speed threshold (1.6m/s to 3.8m/s by Rizk and Henze, 2010) to get comfort in the hot seasons. In terms of wind directions, Madinah experiences three main wind directions, which are south-westerly, westerly and north westerly directions. In different urban density categories, however, wind direction values at pedestrian level (i.e. 2m height) can be influenced by the turbulences within the urban canyon as well as any other moving objects (such as cars). Therefore, the findings of the current high urban density (case 1) study illustrated that in autumn the prevailing direction was from North-East direction with prevailing speed of 0.2-0.5m/s. In addition, the strongest wind speed amongst the measurements days in spring season reached between 1-1.9m/s, approaching from the prevailing south westerly direction, followed by the speed of 0.6-0.7m/s from the same direction (Fig. 6.10). In the summer season, the prevailing wind speed direction was around North North-Westerly with wind speed reaching 1-3m/s.

In terms of relative humidity, the three different urban density cases during the hot climatic seasons indicated that the relative humidity in the four climatic seasons followed similar pattern. The results indicated that the relative humidity is significantly influenced by the ambient air temperature, as it decreases immediately after the sun rises with the increase of air temperature, and increases immediately when the air temperature falls after the sunset. The pattern of the relative humidity in the three urban densities during the spring season were similar, with the low urban density having the highest, then followed by the high density, while the intermediate urban density unexpectedly recorded the lowest, particularly during the early morning hours of between 00:00 to 8:00. The reason for the relative humidity in the intermediate density level being the lowest within this period could be due to the mean radiant temperature values that were recorded higher in this area. Thus, relative humidity is not only dependent on air temperature but also on the mean radiant temperature. Nevertheless,

relative humidity obtained was very low and does not satisfy the recommended standard of between 40% to 70% in the three cases during the hot seasons, however the relative humidity values in both the density cases measured satisfy the lower limit of recommended standard of 40%, particularly between 23:00 hours to 10:00 hours in low urban density (Case 3) with peak value of 60% and from 11:00 hours to 22:00 hours in high urban density (Case 1) with peak value of 52.5%.

In terms of the mean radiant temperature MRT, it was found that during the four climatic seasons the MRT in high urban density (Case 1) is the lowest during the day hours and the highest during the night, which is as a result of the thermal mass at night and day time shading effects by the near structures. The highest average value of MRT temperature in the three urban density cases was recorded in the summer, and then followed by autumn, then spring, while winter was the lowest, as summarised in Table 6.1.

In terms of PET thermal comfort index, the pedestrian thermal comfort in the three urban density cases and for the four different climatic seasons, has been evaluated and analysed. The study employed six different key factors of pedestrian thermal comfort, including two personal factors (activity level and clothing ratio), and four microclimatic variables (i.e. air temperature, mean radiant temperature, relative humidity, and air velocity). The thermal comfort sensation values were obtained using Physiological Equivalent Temperature (PET). The personal factors employed for the purpose of this study include a clothing value of 0.6 clo signifying warm seasons, 1.3 clo representing cold season; while activity level was set to 192.5 W or 1.9 met (which is walking activity level).

The best season in Madinah is recognised by the locals, from tolerable outdoor temperature sensation perspective, to be the spring season. This assertion has been proved in the findings of this study, as most of the PET values in the three different urban density cases during spring season are within the comfort zone (i.e. upper limit of 31.3°C and lower limit of 21°C), then followed by the autumn, with summer having the highest PET values. In the high urban density area during the spring season, the thermally uncomfortable period was found between 11:00 hours through 18:00 hours (an average measurement of 33.8°C PET), with maximum values of 37.4°C at 13:00 hours, and 34.2°C at 15:00 hours. Thus, the required average improvement difference in PET temperature to achieve thermal comfort during this uncomfortable period (i.e. between 11:00 to 18:00 hours) is 2.5°C PET, i.e. based on the upper limit of comfort

threshold 31.3°C PET (given by Yahia and Johansson, 2013a), while for the peak value at 13:00 hours and 15:00 hours the required improvement difference values are 6.1°C and 2.9°C, respectively.

Thus, it is feasible to investigate the spring season, to extend the use of outdoor space by shifting the thermal conditions from a range of thermal discomfort into a range

Climatic Season	Density Type	Air Temp. (°C)	MRT (°C)	Air Velocity (m/s)	Relative Humidity (%)	PET (°C)	Required PET difference to achieve comfort
-----------------	--------------	----------------	----------	--------------------	-----------------------	----------	--

of critical thermal comfort as much as possible, passively without the introduction of any mechanical cooling system (refer to Chapter 7).

*Table 6. 1: Average values of urban microclimate and PET thermal comfort conditions obtained at pedestrian height in different urban density and climatic seasons in the Nazil Quba Road, in Madinah.*

Sumer	High Urban Density (Case 1)	36.1	36.3	0.7	11.6	36.1	- 4.8°C
	Intermediate Urban Density (Case 2)	33.8	40.5	1.8	13.5	36	- 4.7°C
	Low Urban Density (Case 3)	33.6	38.9	1.5	14.4	35.4	- 4.1°C
	<b>Average</b>	<b>34.5</b>	<b>38.7</b>	<b>1.3</b>	<b>13.2</b>	<b>35.8</b>	<b>- 4.5°C</b>
Spring	High Urban Density (Case 1)	29.5	31.5	0.6	18.3	29	0
	Intermediate Urban Density (Case 2)	29.1	33.1	1.1	14.6	28.8	0
	Low Urban Density (Case 3)	28	31.5	1.5	23.4	26.8	0
	<b>Average</b>	<b>28.9</b>	<b>32</b>	<b>1.1</b>	<b>18.8</b>	<b>28.2</b>	<b>0</b>
Autumn	High Urban Density (Case 1)	32.8	34.8	0.4	20.5	33.4	- 2.1
Winter	High Urban Density (Case 1)	19.4	23.4	1.4	40.5	17.6	+ 3.4
	Low Urban Density (Case 3)	19.2	21.1	1.2	40.5	16.7	+ 4.3
	<b>Average</b>	<b>19.3</b>	<b>22.25</b>	<b>1.3</b>	<b>40.5</b>	<b>17.15</b>	<b>+ 3.85</b>

# **CHAPTER 7: The Effect of Asymmetrical Street Aspect Ratios on Urban Wind Flow and Pedestrian Thermal Comfort**

## **Chapter Structure**

- 7.1. Introduction
- 7.2. Base Case Scenario (S-1)
- 7.3. Symmetrical Aspect Ratios (S-2) Scenario
- 7.4. Multi-Asymmetrical Aspect Ratios Scenarios (S-3 to S-16)
- 7.5. Assessment of Pedestrian Thermal Comfort Conditions of the Best Aspect Ratios Model
- 7.6. Summary

# Chapter 7: The Effect of Asymmetrical Street Aspect Ratios on Urban Wind Flow and Pedestrian Thermal Comfort

---

## 7.1. Introduction

This chapter focuses on the numerical simulation of wind velocity and air temperature at the pedestrian level during spring (April), within the high urban density area of Quba Road in Madinah (refer to Chapter 2). Based on the findings of the field measurements (Chapter 6), the month of April (spring), having lower average daily air temperatures than October (autumn), was chosen as a primary period for performing the numerical simulation studies rather than in the summer peak period, to extend the use of outdoor space by shifting the thermal conditions from a range of thermal discomfort into a range of critical thermal comfort as much as possible.

The main objective of this study is to evaluate the effects of multiple asymmetrical aspect ratios on air velocity and air temperature, seeking to find ways to improve the urban pedestrian microclimate and thermal comfort conditions (refer to objective number 5). Thus, this chapter evaluates the base model as in the existing conditions and investigates different proposed urban street strategies including scenarios on:

- Base Model (S-1 scenario), to validate the use of the CFD simulation tool, to understand the existing microclimatic conditions, and to be used as a yardstick to measure the performance of the proposed scenarios through comparative analysis;
- Multiple symmetrical aspect street ratios (S-2), to find out whether unified building heights can achieve better wind velocities than the randomly varied building heights in the existing configuration;
- Multiple asymmetrical street aspect ratios with optimised building heights (S-3 to S-16 scenarios), to evaluate their effects on urban pedestrian microclimate in order to find ways to improve the urban wind flow, and thus pedestrian thermal comfort ;

CFD numerical simulation (Fluent 13.0 code) was applied for this purpose, while outdoor PET thermal sensation index was used to calculate the pedestrian thermal



comfort conditions from the data extracted from CFD model. The input data for the CFD numerical simulation and the meshing dependency test can be found in the methodology Chapter 5, which are summarised in the following Table 7.1. These settings were also applied to all the proposed scenarios in this study (except in the night time scenarios where the radiation model was not used and lower wind and temperature readings were applied). However, the relative humidity was excluded from the simulation, which is because of its low value of 8% and no source of water exchange is available in the simulated models (i.e. water-proof surfaces, with no trees or water plants), and thus relative humidity would not experience significant changes to thermal comfort (e.g. Ali-Toudert and Mayer, 2006), particularly in hot arid regions. Since this simulation used the steady state RANS model instead of unsteady model, the simulation study was carried out on the 1<sup>st</sup> of April 2013 as it represents a mid-season (spring) based on averaging the data obtained from the airport meteorological station for the 1<sup>st</sup> to 12<sup>th</sup> of April.

Table 7. 1: Boundary conditions and initial setting of ANSYS-Fluent 13.0 modelling.

Location	Madinah (hot arid climate), 24.55N, 39.7E
Date/Time Simulated	At 15:00 (+2 GMT) on 1 <sup>st</sup> of April 2013
<b>Model Domain:</b>	
<ul style="list-style-type: none"> <li>- Computational domain dimensions: 5H on the laterals and the top of the cuboid, 5H upstream, 15H downstream.</li> <li>- Mesh size: 0.2m x 0.4m grid size, with 1.2 growth rate, and 10 layers of grids.</li> <li>- Hexahedron dominant mesh type with about 3,385,643 cells.</li> <li>- Realisable k-epsilon models were activated with standard near wall treatment and full bouncy effect modelling.</li> <li>- Second order scheme method applied, while Coupled algorithm used to handle pressure-velocity coupling.</li> </ul>	
<ul style="list-style-type: none"> <li>- Setting of the Atmospheric Boundary Conditions: User defined function UDF implemented in CFD ANSYS-Fluent 13.0 using the following equations for the wind velocity (U), kinetic energy (k) turbulence dissipation rate (<math>\epsilon</math>), and friction velocity (<math>U^*</math>) at urban roughness length (<math>Z_0</math>) of 0.5m:</li> <li>- <math>U_{(z)} = \frac{U_{ABL}^*}{\kappa} \ln\left(\frac{z+z_0}{z_0}\right)</math>     <math>k_{(z)} = \frac{U_{ABL}^{*2}}{\sqrt{C_\mu}}</math>     <math>\epsilon_{(z)} = \frac{U_{ABL}^{*3}}{\kappa(z+z_0)}</math>     <math>U_{ABL}^* = \frac{\kappa U_z}{\ln\left(\frac{z+z_0}{z_0}\right)}</math></li> <li>- The velocity profile U at specified heights z, and roughness length <math>z_0</math> has been validated in COST (Franke et al., 2004) and Blocken et al. (2012), which takes into account the von Karman constant (<math>\kappa = 0.42</math>). A model empirical constant (<math>C_\mu=0.09</math>) (Blocken et al. 2007).</li> <li>- Initial wind speed of 4.7m/s at 10m above the ground was coded in UDF.</li> <li>- Prevailing wind direction: South-Westerly direction (-112.5o angle of attack from the North) and approximately perpendicular to North-South street axis (i.e. -22.5o orientation from North).</li> <li>- Initial Temperature: 29oC.</li> <li>- Outlet boundary: the Kinetic Energy and dissipation rate was specified by a profile of homogeneous wind profile of an empty domain, with zero value for the pressure.</li> <li>- Air property was applied with Boussinesq density of 1.225</li> </ul>	
<b>Radiation Model:</b>	
<ul style="list-style-type: none"> <li>- Solar Load: Solar Calculator using Solar Ray Tracing Model</li> <li>- Surface to Surface (S2S) model was used with view factor.</li> <li>- Irradiance of global radiation: 781W/m<sup>2</sup></li> <li>- Irradiance of diffuse radiation: 194W/m<sup>2</sup></li> </ul>	
<b>Ground Surface Conditions:</b> Asphalt material property was applied to the ground surfaces.	
Density: 2360 kg/m <sup>3</sup> ; Specific heat: 920 J/kg°C; Thermal conductivity: 1.3 W·K <sup>-1</sup> ; Internal emissivity:	

0.93

Roughness height was calculated based on Ground Sand-Grain equation  $k_{s,ABL}$  (Ramponi and Blocken, 2012):

$$k_{s,ABL} = \frac{9.793z_0}{C_s}$$

The roughness constant ( $C_s$ ) was specified to 5 in the user defined function UDF (Blocken et al. 2007).

**Buildings Conditions:** Concrete material property was applied to the buildings surfaces.

Density: 1500 kg/m<sup>3</sup>; Specific heat: 840 J/kg°C; Thermal conductivity: 1.7 W·K<sup>-1</sup>; Internal emissivity: 0.92

## 7.2. Base Case Scenario (S-1)

The base model (S-1 or Scenario 1) is the replica of the existing situation in the high urban density area within Quba Road (i.e. Case 1 in the field study chapter 6), which was required to validate the CFD simulation results with the field measurements (validated and discussed in Chapter 5, section 5.6.1), at location E-3 (discussed in the following subsections). The base model (S-1) was used as a yardstick to measure the performance of the other investigated scenarios through comparative analysis, with the aim to investigate the urban pedestrian microclimatic conditions and pedestrian thermal comfort levels in the high urban density area of Madinah.

In this urban developed part of the route, the road's urban pattern consisted of three main rows of urban blocks and two parallel vehicular lanes (named as Tali'e Quba Road, i.e. windward canyon; and Nazil Quba Road, i.e. leeward canyon) with pedestrian paths on the sides of each canyon, as illustrated in Figure 7.1. The length and width of the interest area in the numerical simulation was 120m x 90m, respectively. The measurements of wind velocity and air temperature were obtained within the interest area along the streets length of 120m and width of 12m. The tallest building in the whole computational domain was 28m height as in the existing situation, and was situated outside the interest area, while the height of the buildings varied in the interest area from 4m to 23m, as illustrated in Figure 7.1.

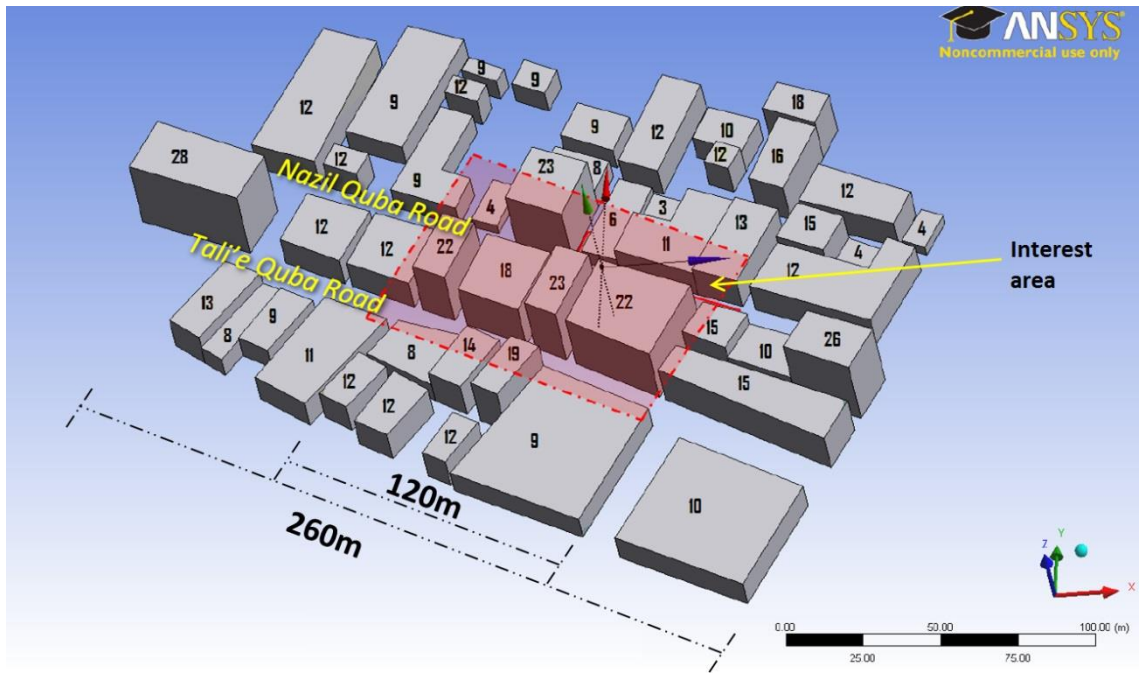


Fig. 7. 1: High urban density case (Base Model). Interest area of the study is 120 x 90m and the width of the Tali'e and Nazil Quba Roads is 12m.

Five cross-sections (E-1 through E-5) in the base model with variation of asymmetrical aspect ratios were analysed and compared with all the testing scenarios in this study (Figure 7.2), to find ways to improve the urban wind flow at the pedestrian level. The multi-asymmetrical aspect ratios ( $H_1/W - H_2/W - H_3/W$ ) for the three rows of the buildings of the five cross-sections were as follows:

- $H/W$  of 0.7 – 1.8 – 0.3 for E-1;
- $H/W$  of 1.2 – 1.5 – 1.9 for E-2;
- $H/W$  of 1.6 – 1.9 – 0.5 for E-3;
- $H/W$  of 0.8 – 1.8 – 0.9 for E-4; and
- $H/W$  of 0.8 – 1.8 – 1.1 for E-5

The base case (S-1 model) is related to the field study (from Chapter 6) at the third cross-section location, i.e. E-3 ( $H/W$  of 1.6 – 1.9 – 0.5).

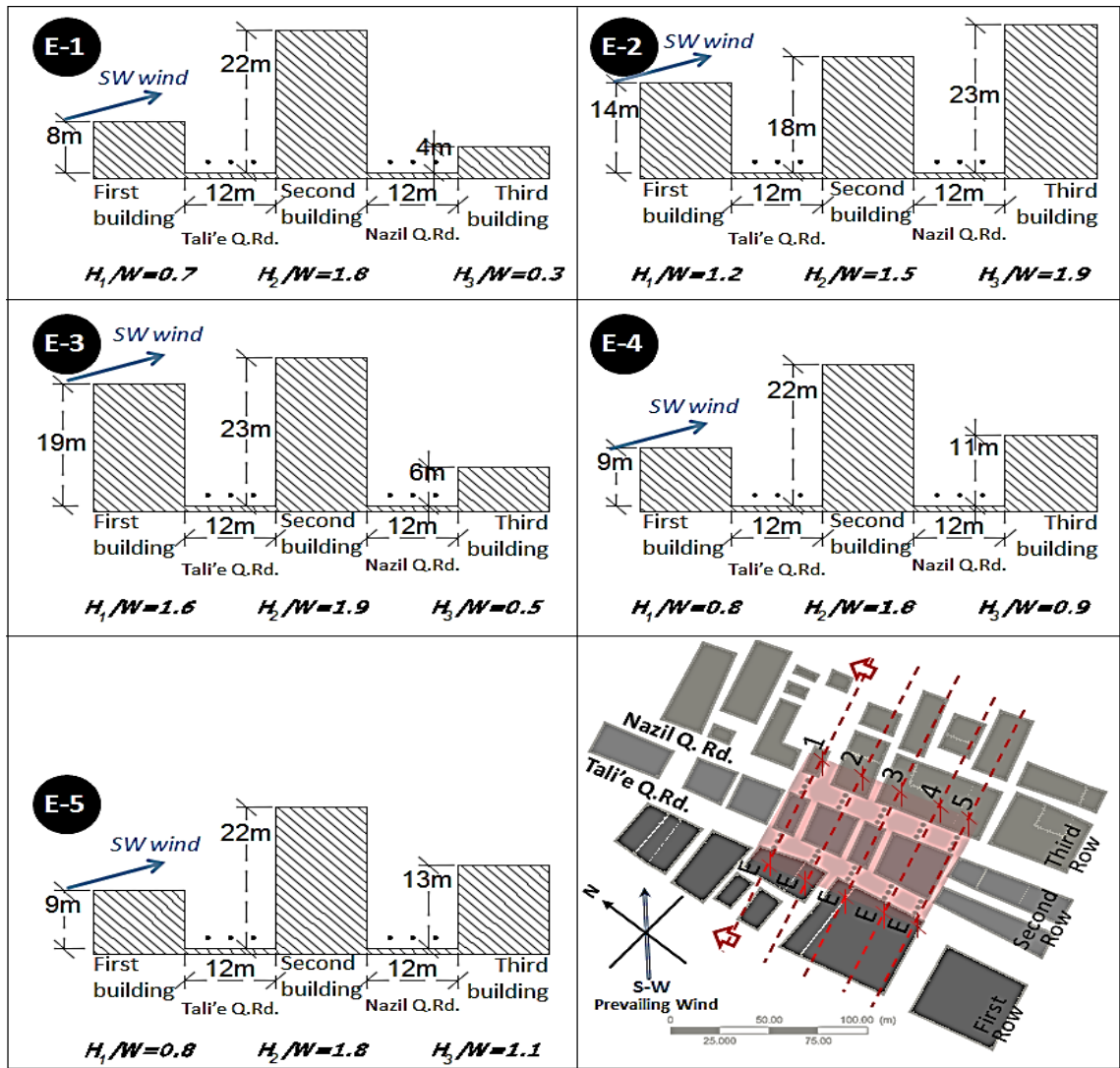


Fig. 7. 2: Asymmetric aspect ratios of the existing (E) case in the interest area, particularly along the five cross-sections of measurements points.

The simulated results were the wind velocity and air temperature measurements, obtained at the pedestrian level (2 metres above the ground). The results were extracted from 15 measurement points within each of the Quba Road canyons (i.e. windward and leeward canyons, respectively). In each canyon, five measurements locations between buildings are specified, with measurements located at the right side of the canyon (i.e. at windward elevation), on the middle of the canyon, and at the left side (i.e. at the leeward elevations), as illustrated previously in Figure 7.3. This representation has the advantage of giving a complete survey of the wind flow pattern and air temperature, and points out the differences between the edges and the centre of the two urban canyons.

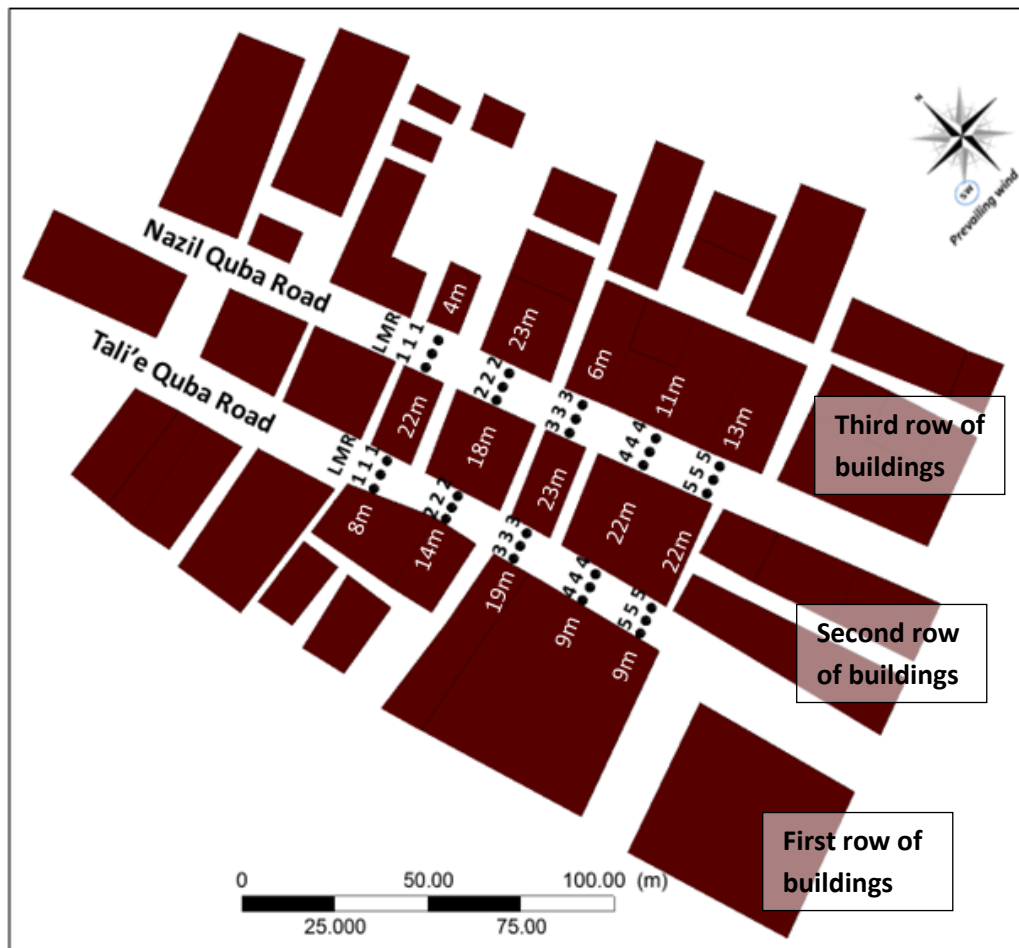


Fig. 7. 3: The figure shows 15 measurements points extracted for each of the two Quba canyons. Each canyon contains of three rows of measurements points, i.e. along the middle of the road, near leeward elevations (left) and near windward elevations (right).

### 7.2.1. Shading Level in Base Case (S-1)

In the previous chapter on the field study of Quba Road (Chapter 6), the results emphasised the importance of shading in reducing the amount of the aggressive solar radiation in pedestrian spaces. Similarly, Ali-Toudert and Mayer (2006) found that in a hot arid Algerian case study, the air temperature is more sensitive to the aspect ratio than the orientation, which is due to the shading effect from adjacent buildings.

Therefore, the level of shading in the base model (S-1) scenario was performed based on peak yearly sun path at 15:00 hours, using Ecotect Analysis software. Generally, the findings reveal that in the north-south orientation of Quba Road, the taller buildings with minimum of 18 metres in the interest area (i.e.  $H/W=1.5$ ) can provide more shading in the urban canyons. Therefore, the afternoon shading level in April in the leeward canyon (Nazil Quba Road) is higher and shaded all the year, as illustrated in Figure 7.4. However, in the windward canyon (Tali'e Quba Road), the shading level at 15:00 hours is lower in April, which obviously due to the presence of lower buildings height with minimum of 8 metres (i.e.  $H/W=0.7$ ).

While the focus of this research is on the leeward canyon, the current study excludes further investigations on shading, as the shading simulations indicate that it is adequately provided in the leeward canyon (Nazil Quba Road), as recommended by Nakamura and Oke (1988), which leads to studying possible urban configuration alteration to increase wind speed. Nevertheless, buildings height in the proposed investigations will follow the Nakamura and Oke (1988) recommendation on the minimum  $H/W$  of 1 (i.e. building height of 12) for shading, and the local planning constraints for maximum buildings height of 27m.



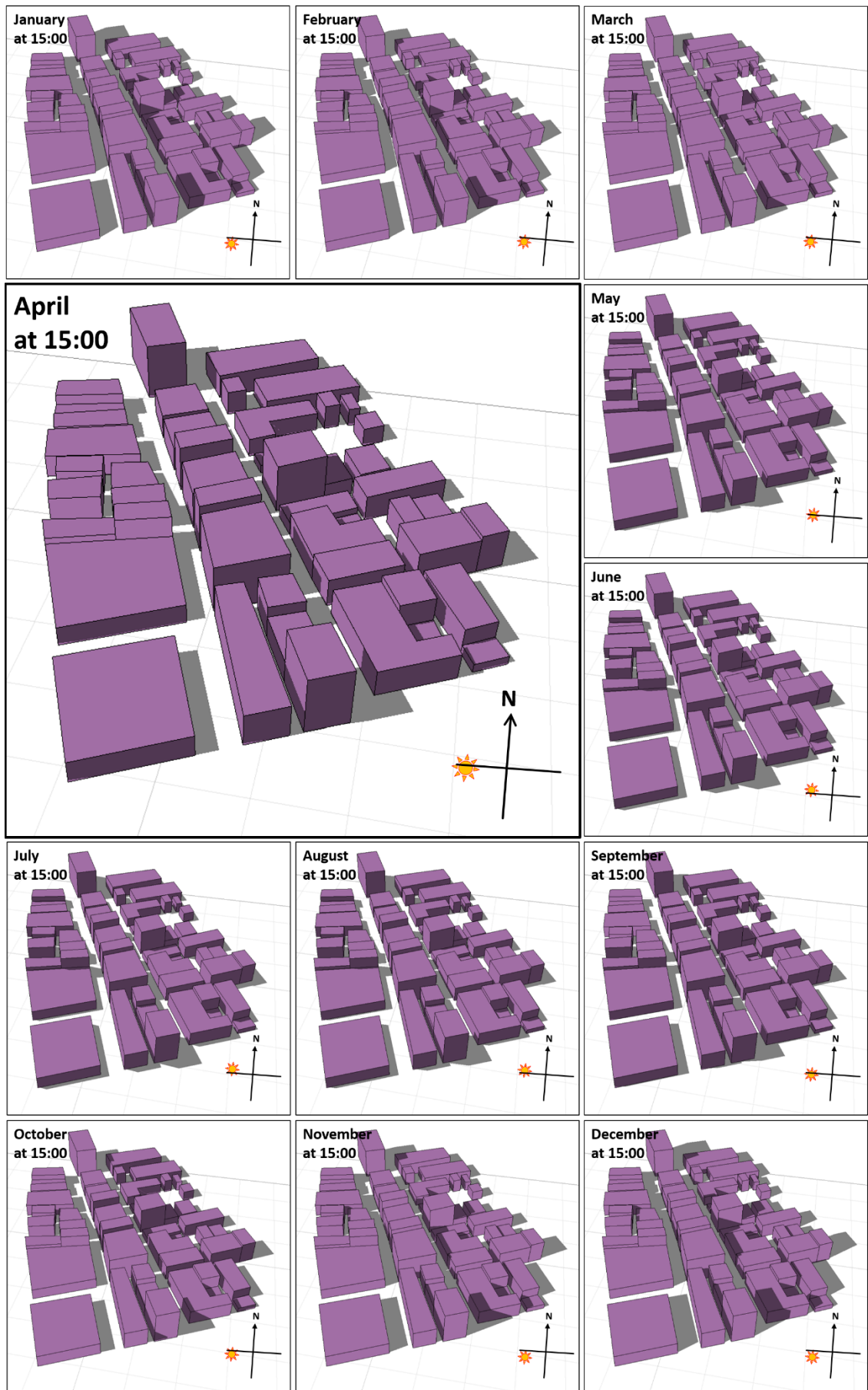


Fig. 7. 4: The level of shading in the base case (S-1) scenario based on yearly sun path at 15:00 hours. In April, the windward canyon (Tali'e Q. Rd.) has less shading than the leeward canyon (Nazil Q. Rd.).



### **7.2.2. Wind Velocity at the Pedestrian Level (S-1)**

Wind velocity is an important factor that can improve human thermal comfort conditions in outdoor thermal environments, as was observed in the previous chapter in the findings of the field measurements, and can be inferred in a previous research by Ali-Toudert and Mayer (2006). The simulation of wind flow in the current study of the base model (S-1) scenario shows results that are in line with previous research, including pedestrian level wind vortices at buildings' corners and the downwind vortices near ground level in the upstream area (e.g. Blocken and Carmeliet, 2004b), and the channel effect of narrow passages between buildings (Rizk and Henze, 2010), etc.

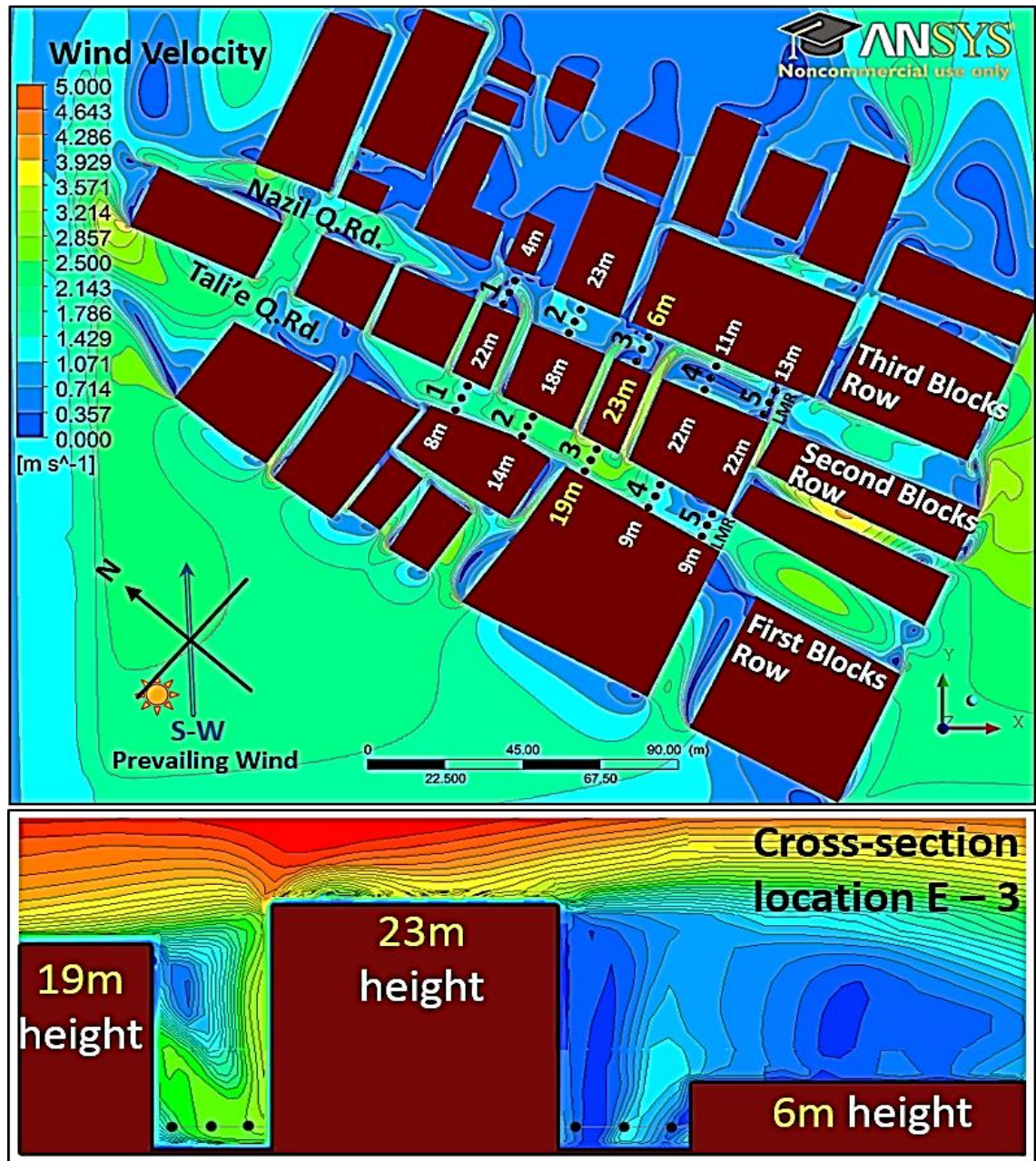


Fig. 7. 5: Contours of velocity magnitude (m/s) at pedestrian height for the base case (S- 1) of the high urban density area. Highlighting the 30 simulation points at the Left, Middle and Right (L,M,R) locations of the canyons. Vertical wind velocity within the canyon is presented for the E-3 cross-section location.

Figure 7.5 analyses the contour of velocity magnitudes (m/s) for the base case (S-1) scenario, while the approaching wind used as inlet boundary condition was 4.7m/s at the airport meteorological station at 15:00 hours in April. The figure highlights the E-3 location to compare the simulation results with the field measurements. It is found that wind velocities magnitude is generally very low at the pedestrian level with an average measurement value of 1.7m/s in the windward canyon (Tali'e Quba Road, i.e. between the first and the second rows of the buildings), and followed by approximately 0.7m/s in the leeward canyon (i.e. Nazil Quba Road). Similar wind flow pattern was found in the base case at night and noon time (refer to section 8.2.1 in Chapter 8). From the field

measurements results (Chapter 6), the average spring wind speed in the leeward canyon at location E-3 was 0.6m/s (i.e. at the right side of the canyon, hence the simulation model does show reasonable results.

This reduction of the wind velocities in the Quba Road canyons compared to the meteorological reading could be due to:

- The effect of higher ground roughness in urban areas compared to the airport area (e.g. Willemsen and Wisse, 2002);
- The difference in the measurement height above the ground;
- The prevailing wind flow direction is not parallel with the two Quba road canyons, as it is oriented about  $112.5^\circ$  anticlockwise from the canyons (e.g. Ali Toudert and Mayer, 2006).

The reason for recording higher wind velocity in the windward canyon compared to the leeward canyon (between the second and third rows of buildings, i.e. Nazil Quba Road.), is due to:

- The existence of taller buildings on the second row (height range between 18m to 23m, i.e. H/W of 1.5 to 1.9) (e.g. Lee et al., 2013).

The cross-section E-3 in Figure 7.5 shows that the location of taller buildings at the middle row acts as a wind catchment area in the windward canyon (Tali'e Quba Road) that deviate the incident wind flow down to pedestrian level where diverge at the ground stagnation point to form standing vortices (e.g. Blocken and Carmeliet, 2004b). However, the cross-section E-3 also show that taller buildings on the middle row prevent direct flow of air to the leeward canyon (Nazil Quba Road), as the wind velocity rate decreases from 1.7m/s to 0.7m/s at the pedestrian level, while lack of taller buildings on the third row (i.e. windward elevation in the leeward canyon) to form wind catchment area. This situation is also found in previous research at pedestrian heights (e.g. Lee et al., 2013). Therefore, from the comparison results of the different urban density levels in the field study (refer to Figure 6.39 in Chapter 6), the wind speed in the high urban density area (Case 1) recorded the lowest hourly values than the intermediate and low urban densities, with a difference measurement value of between 1m/s to 1.7m/s at 15:00 hours in April.

Figure 7.6 shows the wind flow pattern of the five cross-sections (E-1 through E-5; see Figures 7.2) in the windward canyon (Tali'e Quba Road). The measurement points are aligned in the middle of the road as well as at the right side, R (i.e. near the windward buildings surfaces) and left side, L (near the leeward buildings surfaces) of

this urban canyon. It is found that the wind velocity pattern is almost similar for the three sides of the measurements locations (L, M and R). The average measurements of wind velocity in the windward canyon for the three rows of measurement locations (right, middle and left) are as follows:

- The middle measurement location is having the highest average measurement wind velocity 1.9m/s,
- Then followed by the measurement points on the right (near the windward elevations) 1.7m/s,
- While at the left (near the leeward elevations) recorded the lowest values 1.6m/s.

Thus, the overall velocity value in this canyon is found to be 1.7m/s. The maximum wind velocity in this windward canyon is found at the third cross-section (E-3) for the right, middle and left locations, with a value of 2.7m/s, 2.7m/s and 2.0 m/s, respectively, with the average measurement value of 2.5m/s. This is because the windward elevation in the third cross-section (E-3) of the Tali'e Quba Road has the highest aspect ratio  $H_2/W$  of 1.9 (i.e. building height of 23m and street width of 12m) than the rest of the cross-sections. In addition, the flow is approaching from south-westerly direction, while blown over lower heights of the first row of the buildings, particularly at location E-4 with 9m height ( $H_1/W$  of 0.8), while facing taller elevations on the second row of buildings with 23m height ( $H_1/W$  of 1.9). Thus, the presence of the taller building has increased the opportunity of wind catchment area at E-3 in the Tali'e Quba Road.

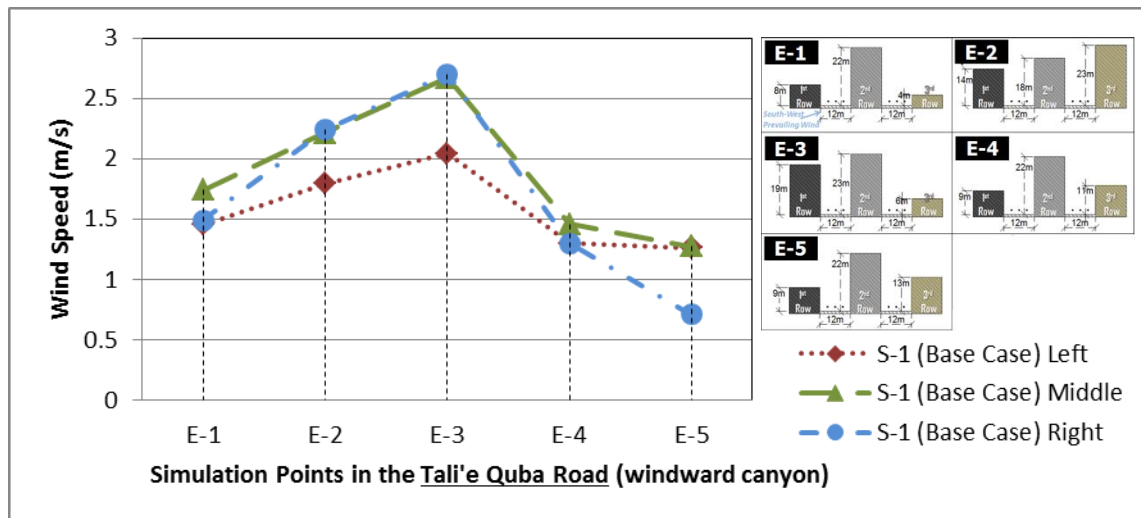


Fig. 7. 6: Wind speed for the base case (S-1) in the Tali'e Quba Road along five cross-sections.

On the other hand, Figure 7.7 shows the wind flow pattern of the five cross-sections locations in the leeward canyon (Nazil Quba Road). The measurement points are located at the middle and the sides of this canyon. It is found that the average measurement of the wind velocity in the leeward canyon for the three rows of the measurement points locations (right, middle and left) are as follows:

- The measurement points at the right (near the windward elevations) having the highest average measurement wind velocity value of approximately 0.7m/s,
- Then followed by the middle row of measurement locations 0.7m/s,
- While at the left (near the leeward elevations) recorded the lowest values 0.6m/s.

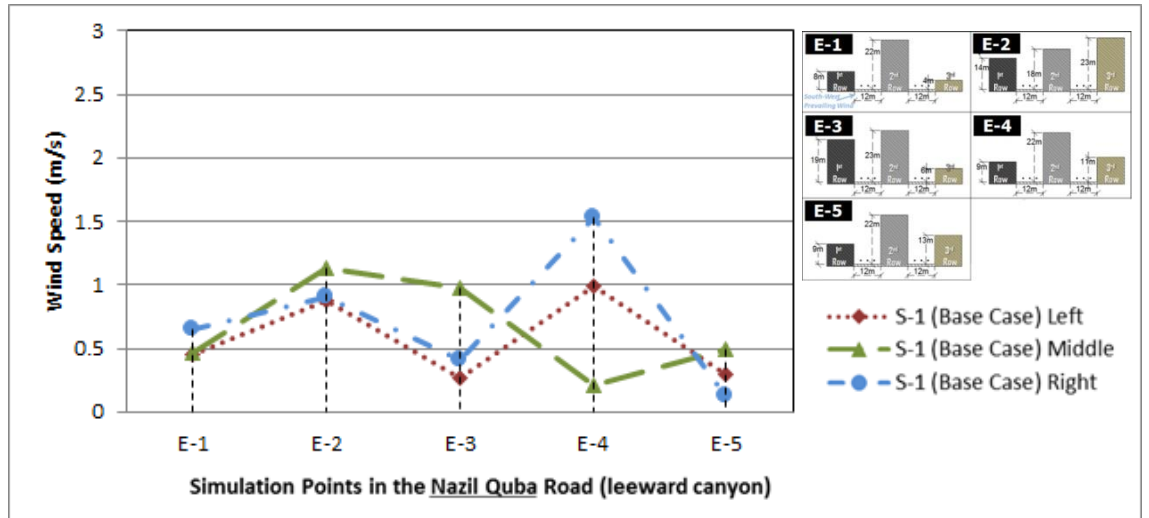


Fig. 7. 7: Wind speed for the base case (S-1) in the Nazil Quba Road along five cross-sections.

The simulated wind velocity result in S-1 scenario in E-3 location, at the right side of the Nazil Quba Road (i.e. leeward canyon), with a value of about 0.5m/s in Figure 7.7, corresponds to the field measurement point in Case 1 (i.e. the high urban density area) with an average value of 0.6m/s at 15:00 hours in Table A6.1 in the Appendices (also refer to the validation section 5.6.1 in Chapter 5). Thus, the simulation results of the wind velocity are in good agreement with the field measurements.

The overall wind velocity value in the leeward canyon is found to be 0.7m/s. The maximum wind velocity in the Nazil Quba Road (leeward canyon) is found at the fourth cross-section (E-4) at the location on right side of the canyon (near the windward elevation) with a value of 1.5m/s. However, the maximum wind velocity based on the

highest average wind velocity from the left, middle and right measurement locations is found at the second cross-section (E-2) with a value of 1m/s. This is because the windward elevation in the second cross-section (E-2) of the Nazil Quba Road has the highest aspect ratio  $H_3/W$  of 1.9 (i.e. building height of 23m and street width of 12m) compared to the rest of the cross-sections in the canyon. According to Blocken and Carmeliet (2004b), this increase in velocity is a result of standing vortices in front of tall buildings at pedestrian height.

Thus, the findings of the wind velocities in the base model (S-1) proves that the exiting urban configuration (i.e. buildings' height) has a negative impact on urban wind velocities, as taller buildings on the second row of buildings are blocking wind from reaching to the leeward canyon, while the third row of the buildings having lower buildings' height leading to lack of wind catchment opportunities in the canyon.

### 7.2.3. Air Temperature at the Pedestrian Level (S-1)

Figure 7.8 analyses the contour of air temperature in degrees ( $^{\circ}\text{C}$ ) for the base case (S-1) at the pedestrian level, while the specified air temperature as inlet boundary condition was  $29^{\circ}\text{C}$  at the airport metrological station. It is found that air temperature shows an opposite pattern to the wind velocity, as it reduces with the increase in wind speed and vice versa (e.g. Qaid and Ossen, 2014). On average, the air temperature at pedestrian height is found to be lower in the windward canyon (i.e. Tali'e Quba Road) with the average measurement value of  $34.0^{\circ}\text{C}$  and followed by  $36.1^{\circ}\text{C}$  in the leeward canyon (i.e. Nazil Quba Road), while the initial temperature used as inlet boundary condition was  $29^{\circ}\text{C}$  (airport meteorological station value). Similar air temperature pattern was found in the base case at night and noon time (refer to section 8.2.1 in Chapter 8).

This significant increase of air temperature in the Quba Road canyons compared to the airport temperature could be due to the effect of the heat stored in building in urban areas (including buildings and ground surface materials) which is causing thermal mass compared to the airport area, and the difference in the measurement height above the ground (e.g. Rubio-Bellido et al., 2015).





Fig. 7. 8: Contours of air temperature in degree ( $^{\circ}\text{C}$ ) at pedestrian height for the base case (S-1 scenario).

In addition, air temperature in the windward canyon (Tali'e Quba Road) is  $2.1^{\circ}\text{C}$  lower compared to the leeward canyon (Nazil Quba Road). Although at 15:00 hours in April (i.e. the simulation period) the windward canyon (i.e. Tali'e Quba Road) has a direct solar component, this temperature difference (i.e.  $2.1^{\circ}\text{C}$ ) between the canyons could be as a result of higher wind velocity values in the windward canyon compared to the leeward canyon (e.g. Qaid and Ossen, 2014). According to Qaid and Ossen (2014), introducing higher asymmetrical aspect ratio, i.e.  $H/W$  of  $0.8 - 2$ , improves wind velocity (e.g.  $1.1\text{m/s}$ ) in an urban canyon, thus reduces the air temperature (e.g. by  $4.7^{\circ}\text{C}$ ). This validates the findings of the current research, as it is apparent evidence that increased wind speed can reduce the thermal loads at pedestrian level. In addition, in the area behind the leeward canyon (Nazil Quba Road) where the 4 metres building height is located (i.e. at E-1), the area receives solar gain with calm wind speed, thus leading to higher temperatures at the pedestrian level with lack of convective heat transfer. Thus, wind movement and shading level are important factors in enhancing the air temperature at the pedestrian level.

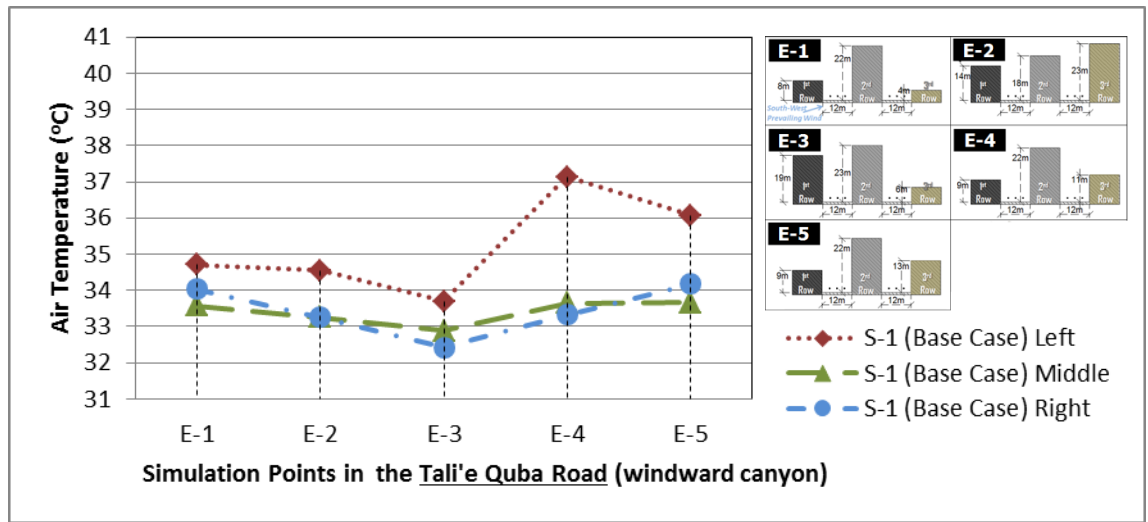


Fig. 7. 9: Air temperature for the base case (S-1) in the Tali'e Quba Road along five cross-sections.

Figure 7.9 shows the air temperature pattern in the Tali'e Quba Road (the windward canyon), which is almost similar for the three measurement sides (left, middle and right). It is found that:

- The middle measurements having the lowest average measurement air temperature value 33.4°C, as a result of the highest wind velocity value (1.9m/s) found along this measurement;
- Followed by the measurements at the right (near the windward elevations) 33.5°C,
- While at the left ones (near the leeward elevations) recorded the highest value 35.2°C, as a result of the lowest wind velocity value (1.6m/s) found at this measurement at the pedestrian height.

The minimum air temperature in the Tali'e Quba Road (windward canyon) is found at the position of the third cross-section (E-3) for the left, middle and right measurement locations with a value of 33.7°C, 32.88°C and 32.4°C, respectively. This is because the windward elevation of the third row of the buildings, particularly near the points in the third cross-section (E-3) in the Tali'e Quba Road, has the highest value of wind velocity compared to the rest of the measurement locations in the canyon, thus increasing the effect of heat mitigation by convective heat transfer (e.g. Hong and Lin, 2015).

In addition, the level of shading is larger at location E-3 during the simulation time (15:00 hours in April, spring season), as illustrated in Figure 7.4 in section 7.2.1,

which has also an effect on reducing the amount of air temperature compared to the rest of locations in the Tali'e Quba Road (windward canyon).

Figure 7.10 shows the air temperature pattern in the Nazil Quba Road (the leeward canyon) for the left, middle and right measurement locations. It is established that the air temperature pattern is almost similar for the three rows of the measurement points, with:

- The measurements at the right (near the windward elevations) having the lowest average measured air temperature 35.5°C,
- Then followed by the points on the middle row with average value 36.1°C,
- While at the left (near the leeward elevations) recorded the highest values 36.7°C.

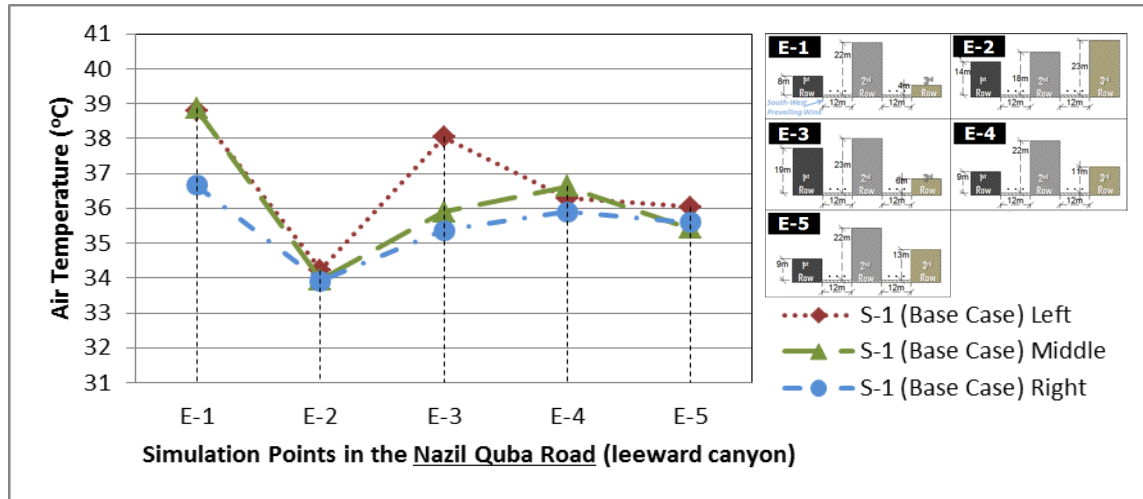


Fig. 7. 10: Air temperature for the base case (S-1) in the Nazil Quba Road along five cross-sections.

The simulated air temperature result in S-1 scenario in E-3 location, at the right side of the Nazil Quba Road (i.e. leeward canyon), with a value of 35.2°C in Figure 7.10, does not correspond to the field measurement point in Case 1 (i.e. the high urban density area) with an average value of 33.7°C at 15:00 hours in Table A6.1 in the Appendices. Thus, the model is over predicting the air temperature by a difference value of 1.5°C.

Nevertheless, the minimum air temperature (average measurement of 34.0°C) in the Nazil Quba Road (leeward canyon) is found at the position of the second cross-section (E-2) with the left, middle and right locations having a value of 34.2°C, 33.9°C and 33.9°C, respectively. This is due to the existence of the highest average measurement wind velocity (1m/s) in the Nazil Quba Road at this location of the second cross-section (E-2), as explained above in section 7.2.2. However, due to the low windward aspect ratios in the Nazil Quba Road (leeward canyon), the average wind

velocity at pedestrian level is found lower than the Tali'e Quba Road (windward canyon), leading to weak convective heat transfer, thus higher air temperature values (e.g. Hong and Lin, 2015; Pillai and Yoshie, 2012).

In addition, the third row of the buildings, particularly in the leeward canyon (i.e. the Nazil Quba Road) at locations of E-3, E-4 and E-5 has a wider windward elevation which limits the wind escape opportunity over the buildings, thus increasing air temperature values due to lack of convective heat transfer (e.g. Hong and Lin, 2015; Pillai and Yoshie, 2012). The highest air temperature value in the Nazil Quba Road is found at E-1 cross-section position, with the average measurement value of 38.1°C, as a result of the presence of a lower level of shading from an adjacent building (12m height) located on the second row of the buildings (outside the interest area) (e.g. Yahia, 2012; Lin et al., 2010), as illustrated in the Figure 7.4 in section 7.2.1 for April month at 15:00 hours. Moreover, the lack of standing vortex in front of the lowest aspect ratio ( $H_3/W=0.3$ , with building height of 4m) on the third row of the buildings has also led to increase in air temperature at this location (i.e. E-1 in the Nazil Quba Road). These results have been confirmed in a study by Qaid and Ossen (2014) on the effect of asymmetrical street aspect ratios on microclimates (but for North-East to South-West street orientation in hot humid regions) that areas with lower urban aspect ratio suffer from low air velocity and thus increased air temperature.

Thus, the findings of the air temperature in the base model (S-1) indicates that increasing of the buildings' height on the second row of the buildings, while the third row of the buildings having lower buildings' height, has a negative impact on wind speed and air temperature. As this configuration blocks wind from reaching to the leeward canyon, thus reducing convective heat transfer. Therefore, this lead to the need to carry on further investigations on the effect of optimisation in buildings on urban wind and pedestrian thermal comfort conditions, considering urban development planning and regulations as per chapter 2 section 2.3 and 2.4.

### 7.3. Symmetrical Aspect Ratios (S-2) Scenario

Objective number 5 of this research (refer to section 1.4) is to optimise the urban H/W (height-to-width) aspect ratios to the existing urban configurations on the urban pedestrian wind flow rate during the day. The S-2 (Scenario 2) is a proposed symmetrical aspect ratio model, i.e. unified height of the three rows of the buildings ( $H_1/W = H_2/W = H_3/W$ ). The local government redevelopment plan suggests demolishing the existing urban area, as this area has issues with the level of maintenance of the buildings, while is keeping the land footprints and main canyon axis direction due to the local planning constraints (refer to Chapter 2). The S-2 scenario hypothetically averages the existing buildings height to 12m (i.e. H/W of 1), while it confirms the recommended aspect ratio H/W of 1 suggested by Nakamura and Oke (1988) to provide the minimum acceptable level of shading in canyons. The width of the two main Quba Road canyons are remained as the existing condition (i.e. 12m for each canyon), as illustrated in Figure 7.11.

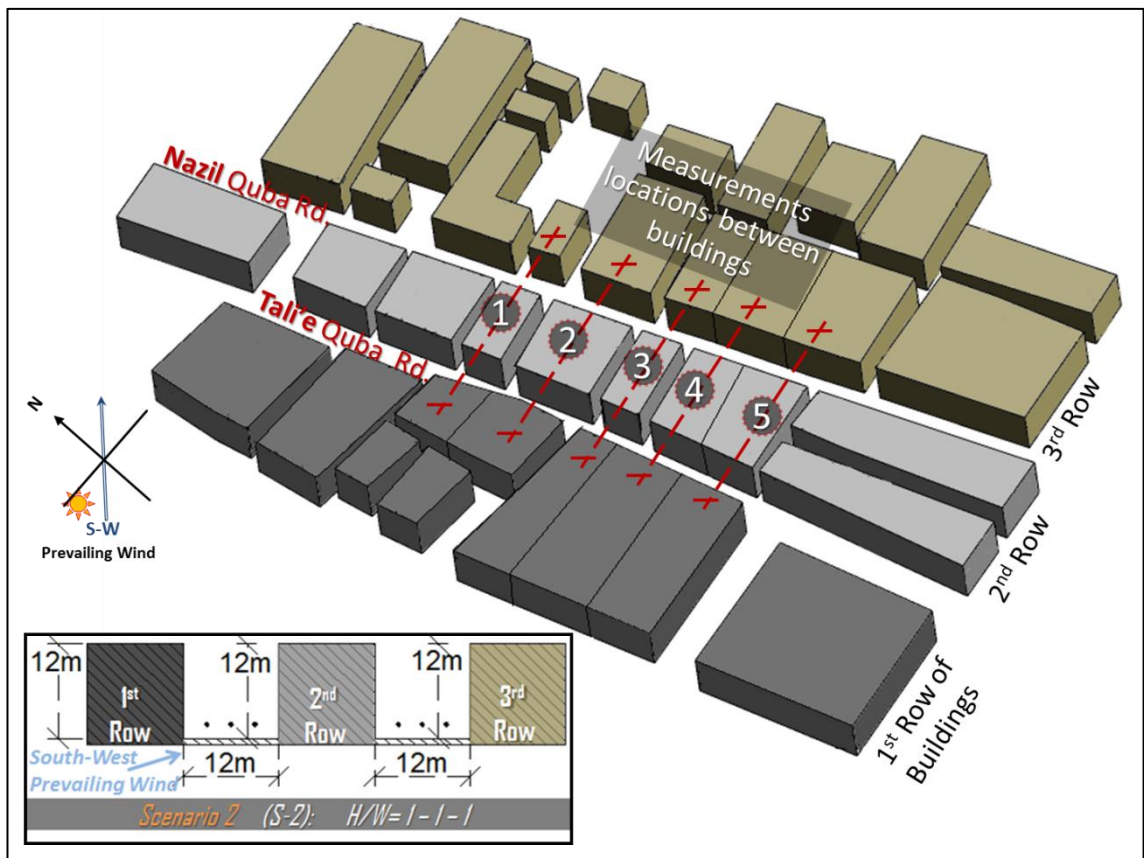


Fig. 7. 11: Symmetrical aspect ratio (S-2) model with unified buildings height of 12m (H/W of 1). The figure shows a cross-section that represents the five locations of the simulation measurements.



The study of S-2 scenario (symmetrical aspect ratio model) analyses the air temperature and wind velocity results that were measured from 15 locations at each of the Tali'e Quba Road (windward canyon) and Nazil Quba Road (leeward canyon), at the pedestrian height (2 metres above the ground). Figure 7.11 also shows a cross-section that represents the five locations (1 through 5) of the right, middle and left measurement points between the buildings within the interest area.

### **7.3.1. Wind Velocity at the Pedestrian Level (S-2)**

Figure 7.12 analyses the contour of velocity magnitudes (m/s) for the symmetrical aspect ratio scenario (S-2) at the pedestrian level. It is found that the overall wind velocities magnitude in S-2 model is slightly reduced within the windward canyon (Tali'e Quba Road) compared to the base model (i.e. S-1) from the average measurements 1.7m/s (i.e. in the base model) to 1.3m/s (i.e. -26.9%). However, in the leeward canyon (Nazil Quba Road), the wind velocity in S-2 is slightly improved from the average measurements 0.7m/s (i.e. in the base model) to 0.8m/s (i.e. 15.4%). The unified buildings height in S-2 model has led to a skimming wind flow regime over the arrays of the flat roofed buildings (e.g. Oke, 1988). This regime lowers the wind velocities at the pedestrian height.

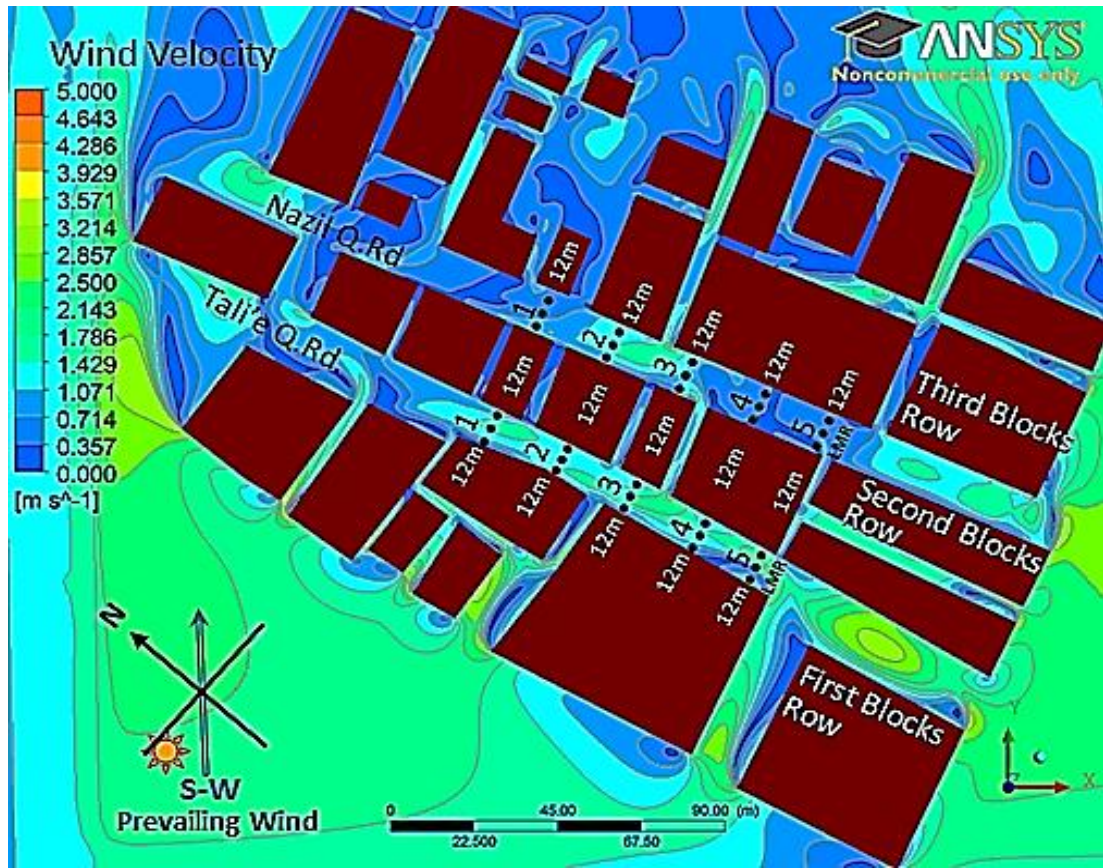


Fig. 7. 12: Contours of velocity magnitude (m/s) at pedestrian height for the symmetrical aspect ratio (S-2) of  $H_1/W - H_2/W - H_3/W = 1$ , showing measurement points locations.

According to Oke (1988), the skimming flow regime occurs with further increase in symmetrical  $H/W$  ratio, which is the case in many dense urban contexts, as the urban deep street becomes isolated from the above circulating air and a stable circulatory vortex is established in-canyon, thus influencing the microclimate conditions at street and pedestrian levels. Lee et al. (2013) explained that when the variation in buildings height is low or buildings are almost unified (i.e. symmetrical aspect ratio), low turbulence can be observed within the canyons, which can lead to a more stable wind flow at the pedestrian height.

In the S-2 model (symmetrical aspect ratio scenario), the wind velocity in the windward canyon (between the first two rows of the buildings, i.e. Tali'e Quba Road) is higher compared to the leeward canyon (between the second and third rows of the buildings, i.e. Nazil Quba Road). This result has been confirmed in previous investigations on symmetrical rows of buildings, including a study by Yuan and Ng (2012) and Hang et al. (2015). According to Hang et al. (2015), the wind speed in the urban area was accelerated in the windward canyon when the prevailing wind direction was approximately perpendicular to the canyon (i.e. -105 from north), while wind speed



was significantly decreased at the leeward canyons, as illustrated in Figure A7.1 in the appendices.

Figure 7.13 shows the wind flow pattern of the five measurements locations (1 through 5) between buildings in the Tali'e Quba Road (the windward canyon) in S-2 scenario, and compared with the base case (S-1) scenario at the pedestrian level. The simulation results in five measurements locations are extracted at the right side of the canyon (i.e. at windward elevation), on the middle of the canyon, and at the left side (i.e. at the leeward elevations), as illustrated previously in Figure 7.3. It is found that the wind velocity pattern in S-2 scenario is similar for the three rows of measurement points, with:

- The middle row having the highest average measurement wind velocity with a value of 1.5m/s,
- Followed by the points on the right row (at the windward elevations) with an average value of 1.4m/s,
- While the ones on the left (at the leeward elevations) recorded the lowest values with an average of 0.9m/s.

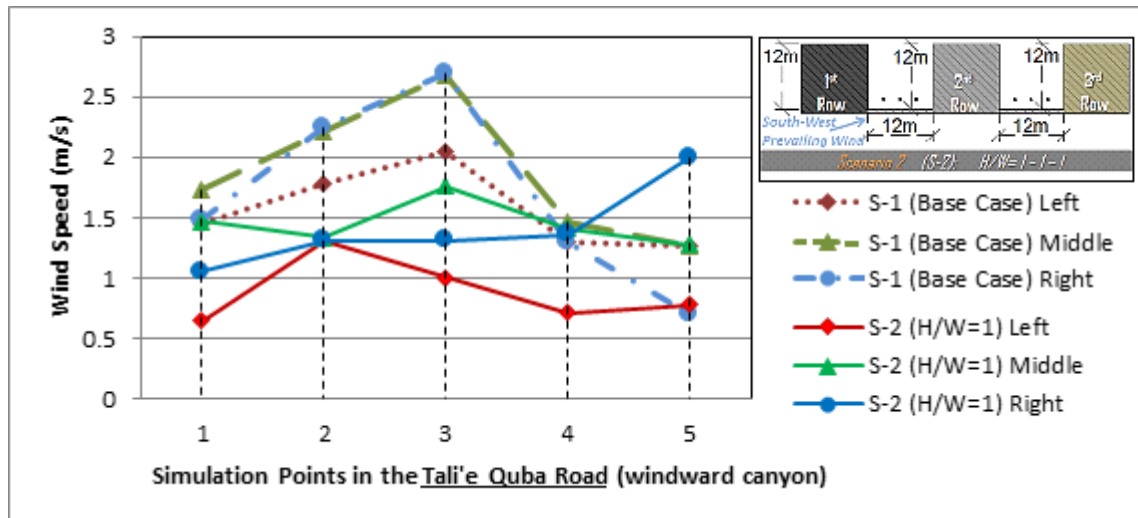


Fig. 7. 13: Wind speed in the Tali'e Quba Road for the multi-symmetrical aspect ratios (S-2) scenario at measurements locations, and compared with the base case S-1 scenario at the pedestrian level.

Thus, in the S-2 model, the average measurement of air velocity in the windward canyon (Tali'e Quba Road) is found to be 1.3m/s, which is 0.5m/s lower than the base model. The wind velocity values in this canon in the S-2 model is significantly worsened at the 3<sup>rd</sup> measurements location compared to the base model (S-1), with

difference values of -1.0m/s, -0.9m/s and -1.4m/s at the left, middle and right measurement points, respectively. This is because at the 3<sup>rd</sup> measurement location the base model (S-1) has the highest building height (23m) on the second row of the buildings that drags wind to the street level, which this opportunity in the unified low rise buildings model (S-2) is lacking.

Figure 7.14 shows the wind flow pattern of the five measurement points' locations in the Nazil Quba Road (leeward canyon) at the pedestrian level. It is established that the wind velocity pattern in S-2 scenario is almost similar, with:

- The middle measurement row having the highest average wind velocity with a value of 0.8m/s,
- Followed by the measurements at the right side of the road (at the windward elevations) with an average value of 0.8m/s,
- While the ones at the left side (at the leeward elevations) recorded the lowest values with an average measurement value of 0.7m/s.

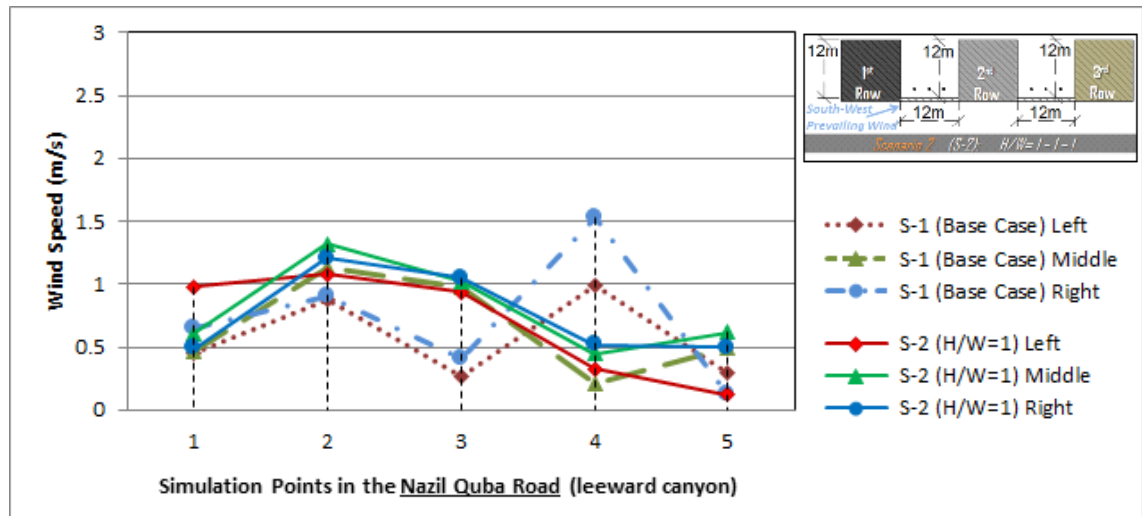


Fig. 7. 14: Wind speed in the Nazil Quba Road for the multi-symmetrical aspect ratios (S-2) scenario at measurements locations, and compared with the base case S-1 scenario at the pedestrian level.

Thus, in the S-2 model, the average measurement of air velocity in the leeward canyon (Nazil Quba Road) is found to be 0.8m/s, which is 0.1m/s higher than the base model. The maximum wind velocities in the Nazil Quba Road in S-2 scenario is found at the 2<sup>nd</sup> measurements location for the left, middle and right measurement points, with the values of 1.1m/s, 1.3m/s and 1.2m/s, respectively. This could be because of the width of the windward and leeward elevations of the adjacent buildings are just enough

to form undisturbed standing vortices in this location of the canyon (e.g. Blocken and Carmeliet, 2004b) as illustrated in the velocity contours in Figure. 7.12.

It is necessary in the current study to improve the wind velocity in the leeward canyon (Nazil Quba Road), due to the position of the canyon as a main commercial route in the Quba district, and as a straight urban physical linkage between the two most visited mosques in Madinah. According to Rizk and Henze (2010), to achieve the upper limit of tolerable thermal comfort in hot arid regions in mid-seasons where the air temperature ranges between 31 to 35°C, average measurement wind velocity should be greater than 2m/s. Although the symmetrical aspect ratio scenario (S-2) establishes minor improvement to the wind velocity (to 0.8m/s) at the pedestrian level in the leeward canyon compared to the base case, the main issue of low wind velocity remains as wind follows skimming flow regime over the buildings.

### 7.3.2. Air Temperature at the Pedestrian Level (S-2)

Air temperature is a critical factor in the calculation of thermal comfort in outdoor thermal environments. According to Ali-Toudert and Mayer (2006), in a hot arid Algerian case study, it appears that the air temperature is more sensitive to the urban aspect ratio than the orientation of the urban street canyon. As it was observed that the differences in air temperature between the same aspect ratio of both the orientations (E-W and N-S) are small.

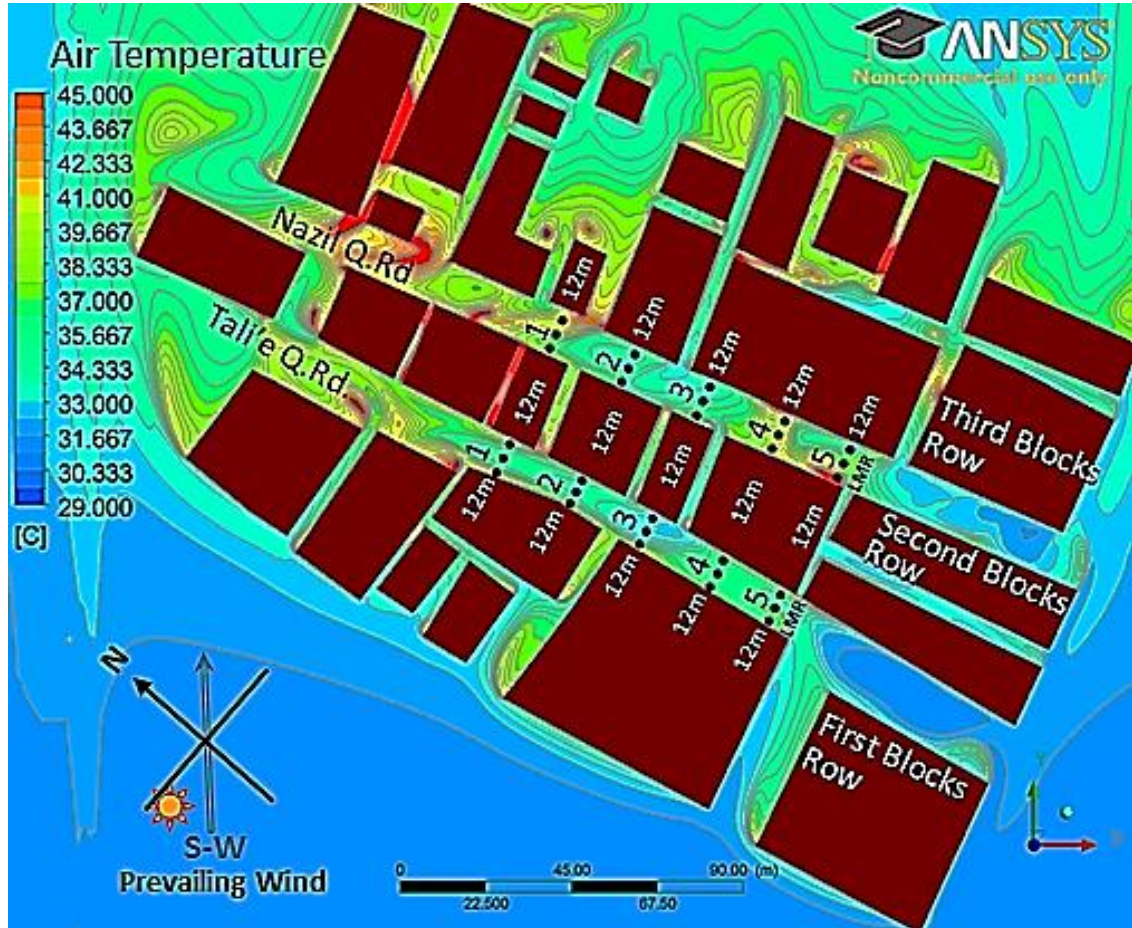
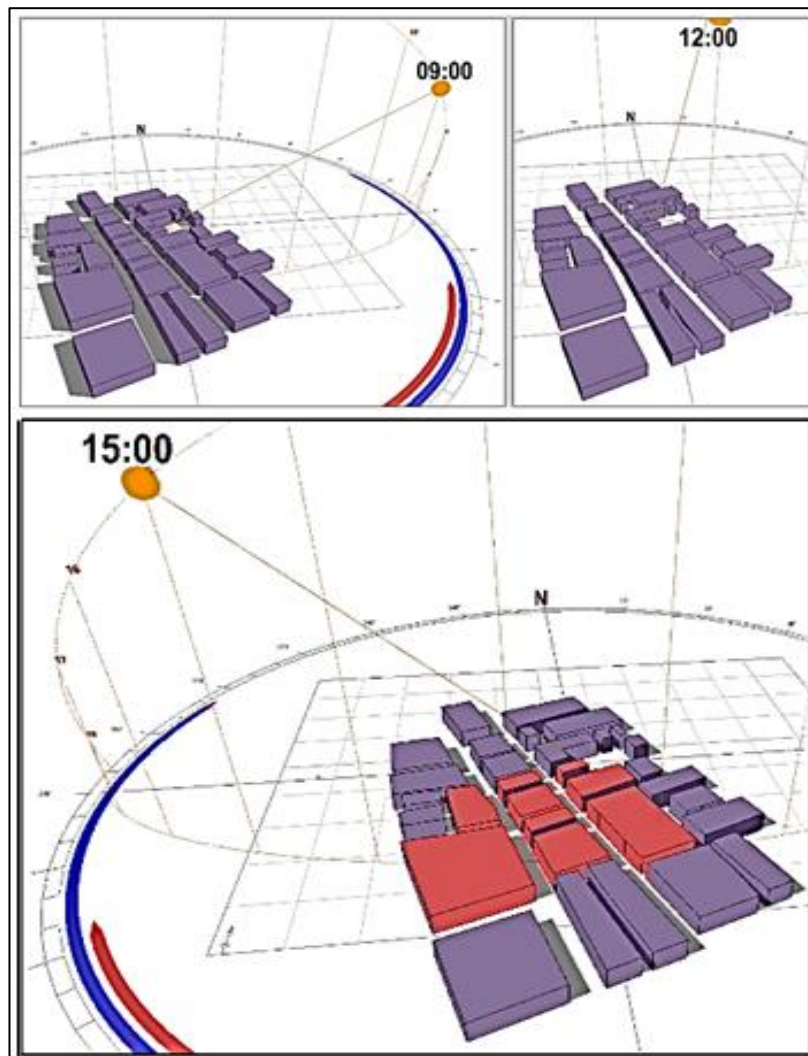


Fig. 7. 15: Contours of air temperature degree ( $^{\circ}\text{C}$ ) at pedestrian height for the symmetrical aspect ratio (S-2) of  $H_1/W - H_2/W - H_3/W = 1$ .

Figure 7.15 analyses the contours of air temperature in degrees ( $^{\circ}\text{C}$ ) for the symmetrical aspect ratio scenario (S-2) at the pedestrian height with uniform buildings height of 12m and aspect ratio  $H/W$  of 1. It is found that air temperature in S-2 scenario is higher than the base case (S-1) in both of the Quba Road canyons. Although changing the building heights to a symmetrical pattern (12m unified height) has increased the shading amount at locations E-1, E-4 and E-5 in the windward canyon, while the leeward canyon is approximately remained in shade at 15:00 hours (as illustrated in

Figure 7.16), the reason for increased air temperature could be due to a decrease in heat transfer by convection. The latter is as a result of lower wind velocity at the pedestrian level.

On average, the air temperature at the pedestrian height in S-2 model is found slightly reduced by  $1.6^{\circ}\text{C}$  in the windward canyon (Tali'e Quba Road) than the leeward canyon (Nazil Quba Road). The temperature in the windward canyon is predicted at an average measurement of  $36^{\circ}\text{C}$ , and at  $37.6^{\circ}\text{C}$  in the leeward canyon. This is as a result of higher wind velocity in the windward canyon compared to the leeward canyon. In addition, in the leeward canyon (i.e. the Nazil Quba Road) the measurement locations of E-4 and E-5 have wider windward and leeward elevations which limit the wind escape opportunity over the building, thus increasing air temperature values due to lack of convective heat transfer (e.g. Hong and Lin, 2015; Pillai and Yoshie, 2012).



*Fig. 7. 16: Shading level in the S-2 (symmetrical building height of 12m), in the morning, noon and afternoon periods in April. At the simulation time (15:00 hours) the canyons are in shade at the measurement locations.*



In Figure 7.16, the shading simulation indicates that shading is adequately provided at 15:00 hours in the windward and leeward canyons at the measurement locations (within the area of interest), as recommended by Nakamura and Oke (1988). Thus, based on this result, the current study excludes further investigations on shading for the scenarios that have higher building heights as which leads to studying possible urban configuration alteration to increase wind speed. Nevertheless, building heights in the proposed investigations will follow the Nakamura and Oke (1988) recommendation on the minimum H/W of 1 (i.e. building's height of 12) for shading, and the local planning constraints for maximum buildings height of 27m.

Figure 7.17 demonstrates the air temperature pattern of the five measurement points' locations (1 through 5) in the Tali'e Quba Road (the windward canyon). The measurement points are aligned in the middle of the canyon as well as at the right side (at the windward elevations) and the left side (at the leeward elevations).

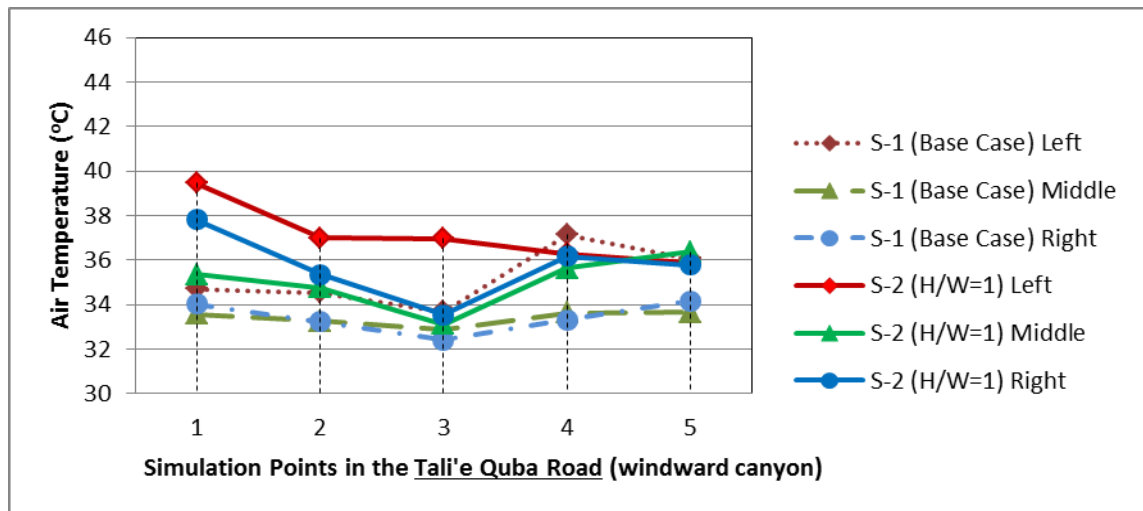


Fig. 7. 17: Air Temperature in the Tali'e Quba Road for the multi-symmetrical aspect ratios scenario (S-2) at measurements locations, and compared with the base case S-1 scenario at the pedestrian level.

It is found that the air temperature pattern is similar for the three measurements sides in S-2 scenario, with:

- The middle row having the lowest average air temperature with a value of 35.1°C,
- Followed by the points on the right row (near the windward elevations) with an average value of 35.7°C,

- While the ones on the left (near the leeward elevations) recorded the highest values with an average of 37.1°C.

The minimum average air temperature in the Tali'e Quba Road (windward canyon) is found at the 3<sup>rd</sup> measurements location with a value of 34.6°C, followed by the 2<sup>nd</sup> measurements location with a value of 35.7°C. This could be because of the narrow windward elevations of the second row of buildings near these two locations, thus allow heat to transfer by convection through the nearest passages, as it can also be observed in the base case S-1 scenario. The maximum air temperature value in the Tali'e Quba Road in S-2 scenario is found at the 1<sup>st</sup> measurements location, particularly for the left measurement point (at the leeward elevations) with a value of 39.5°C, where it has recorded the lowest wind speed in the canyon (0.7m/s), followed by the measurement point at the right side (at the windward elevation) with a value of 37.8°C, as illustrated above in Figure 7.17.

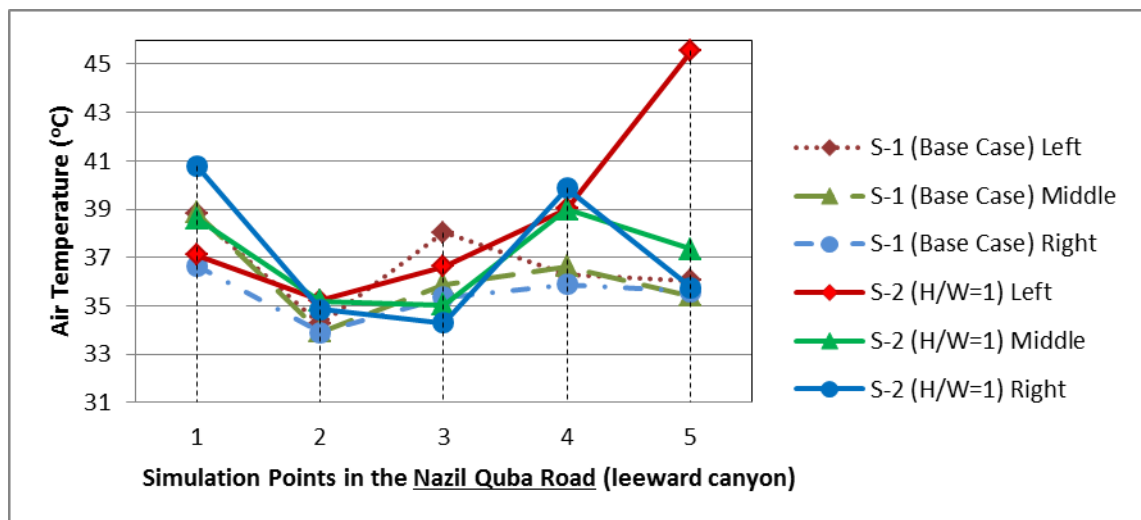


Fig. 7. 18: Air Temperature in the Nazil Quba Road for the multi-symmetrical aspect ratios scenario (S-2) at measurements locations, and compared with the base case S-1 scenario at the pedestrian level.

Figure 7.18 shows the air temperature pattern of the five measurement locations (1 through 5) in the Nazil Quba Road (the leeward canyon, between the second and the third rows of buildings) for the measurement points that are located at the middle and the sides of this canyon. It is established that the air temperature pattern is almost similar for the three rows of the measurement points, with the middle row having the lowest average air temperature of 37.0°C, followed by the points on the right row (near the windward elevations) with an average value of 37.1°C, while the ones on the left (near the leeward elevations) recorded the highest values with an average of 38.7°C.



The minimum air temperature in the Nazil Quba Road is found at the 2<sup>nd</sup> measurement location with an average value of 35.1°C. This is due to the width of the windward and leeward elevations of the adjacent buildings are just enough to form undisturbed standing vortices in this location of the canyon, thus increasing the opportunity for heat transfer by convection (e.g. Hong and Lin, 2015; Pillai and Yoshie, 2012), as illustrated above in contours images in Fig. 7.12 and 7.16. The maximum air temperature value in the Nazil Quba Road in S-2 scenario is found at the 5<sup>th</sup> measurement location, particularly for the left measurement point (at the leeward elevation) with a value of 45.5°C where it has the lowest wind speed in the canyon (0.1m/s).

According to Qaid and Ossen (2014) introducing higher asymmetrical aspect ratio, i.e.  $H/W$  of 0.8 – 2, improves wind velocity (e.g. 1.1m/s) in an urban canyon, thus reduces the air temperature (e.g. by 4.7°C). The following sections investigates the asymmetrical aspect ratios strategy, seeking for ways to improve the urban pedestrian microclimate.

#### 7.4. Multi-Asymmetrical Aspect Ratios Scenarios (S-3 to S-16)

This study aims to evaluate the effects of multi-asymmetrical street aspect ratios on urban pedestrian microclimate and outdoor thermal comfort, particularly in a low wind speed environment, through a case study of Quba Road, in order to find ways to improve the urban wind flow, and thus pedestrian thermal comfort conditions in the hot arid climate of Madinah. The study of multiple asymmetrical urban street aspect ratios (i.e. diverse buildings height to street width;  $H_1/W - H_2/W - H_3/W$ ), based on optimising the buildings' height to influence wind flow rate, has not received much attention in the context of urban pedestrian thermal comfort, particularly in low wind speed environments and in hot arid regions. Asymmetrical streets with tall buildings opposite low buildings in a canyon can create low exposure to solar radiation and create high wind velocities at ground level, which would enhance pedestrian thermal comfort (Qaid and Ossen, 2014; Emmanuel et al., 2007; Johansson and Emmanuel, 2006).

This section proposes 14 multi-asymmetrical urban streets aspect ratios models (i.e. S-3 through S-16), with each row of the buildings having unified buildings height, as illustrated in Table 7.2. The S-3 through S-16 scenarios of multi-asymmetrical aspect ratios are proposed using the equation number 6 (refer to section 5.6.2 in the Methodology Chapter). These scenarios (S-3 through S-16) are categorised into 4 groups based on variation of buildings height on both side of the windward and leeward canyons, which are: lower aspect ratios scenarios, medium aspect ratios scenarios and higher aspect ratios scenarios, and leeward gradual increase in multi-asymmetrical aspect ratios. The maximum buildings' height of the proposed scenarios does not exceed 27m due to the local planning constraints (refer to the local planning and regulation section in Chapter 2). The specifications for the scenarios that were categorised as lower aspect ratios scenarios were:

- S-3 scenario with aspect ratios of 1 – 0.8 – 1.3; and
- S-4 scenario with interchanged aspect ratios of 1 – 1.3 – 0.8.

The second category was the medium aspect ratios scenarios, including three scenarios, which were:

- S-5 scenario with aspect ratios of 1 – 1.5 – 1.5;
- S-6 scenario with gradually increased aspect ratios of 1 – 1.3 – 1.8; and
- S-7 scenario with interchanged aspect ratios of 1 – 1.8 – 1.3.

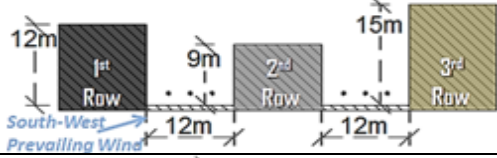
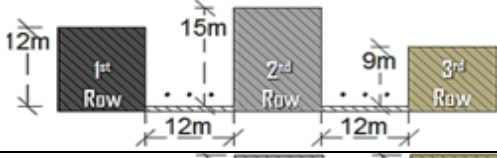
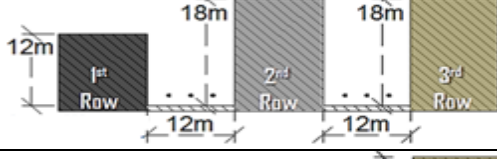
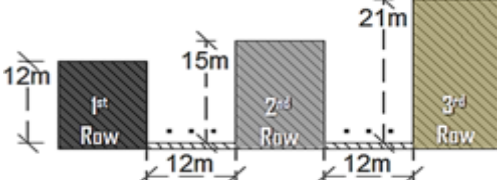
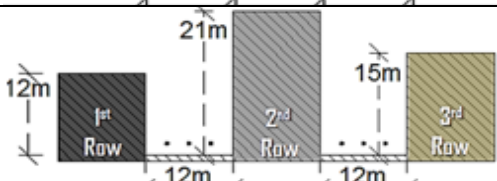
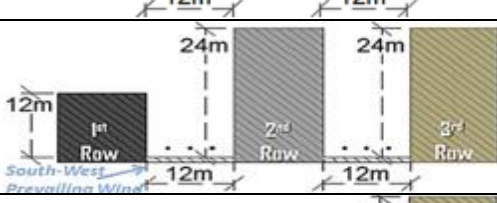
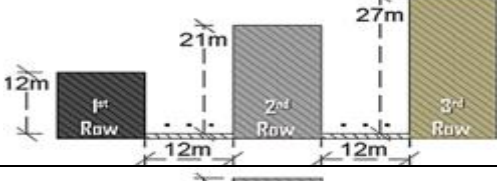
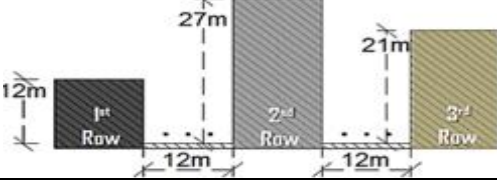
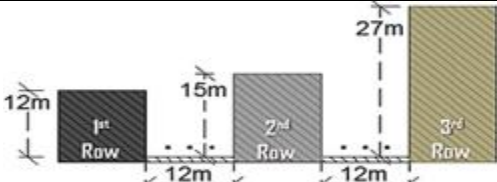
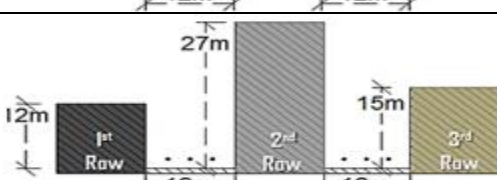
The third category was the high aspect ratio scenarios, including five cases, which were:

- S-8 scenario with aspect ratios of 1 – 2 – 2;
- S-9 scenario with gradually increased aspect ratios of 1 – 1.8 – 2.3;
- S-10 scenario with interchanged aspect ratios of 1 – 2.3 – 1.8;
- S-11 scenario with gradually increased aspect ratio of 1 – 1.3 – 2.3; and
- S-12 scenario with interchanged aspect ratio of 1 – 2.3 – 1.3.

The specifications for the leeward gradually increased aspect ratios scenarios (S-13 through S-16), which were:

- S-13 scenario with aspect ratios of 1 – 1.3 – 1.5;
- S-14 scenario with aspect ratios of 1 – 1.3 – 2.0;
- S-15 scenario with aspect ratios of 1 – 1.5 – 2.3; and
- S-16 scenario with aspect ratios of 1.3 – 1.5 – 2.3 (note that the latter has higher aspect ratio on the first row of buildings).

Table 7. 2: Interchangeable multi-asymmetrical aspect ratios scenarios specifications for the second and third rows of buildings for S-3 through S-12, with the first row are constant as in S-2 scenario. Note that the numbers underlined in H/W are rounded up.

Scenario	Illustration	Aspect Ratio
Lower Aspect Ratios	S-3 	H/W = 1 – <u>0.8</u> – <u>1.3</u>
	S-4 	H/W = 1 – <u>1.3</u> – <u>0.8</u>
Intermediate aspect ratios	S-5 	H/W = 1 – 1.5 – 1.5
	S-6 	H/W = 1 – <u>1.3</u> – <u>1.8</u>
	S-7 	H/W = 1 – <u>1.8</u> – <u>1.3</u>
Higher Aspect Ratios	S-8 	H/W = 1 – 2.0 – 2.0
	S-9 	H/W = 1 – <u>1.8</u> – <u>2.3</u>
	S-10 	H/W = 1 – <u>2.3</u> – <u>1.8</u>
	S-11 	H/W = 1 – <u>1.3</u> – <u>2.3</u>
	S-12 	H/W = 1 – <u>2.3</u> – <u>1.3</u>

<b>Leeward Gradual Increase in Aspect Ratios</b>	S-13		$H/W = 1 - \underline{1.3} - 1.5$
	S-14		$H/W = 1 - \underline{1.3} - 2.0$
	S-15		$H/W = 1 - 1.5 - \underline{2.3}$
	S-16		$H/W = \underline{1.3} - 1.5 - \underline{2.3}$

The first row of the buildings in S-3 through S15 (not including S-16), is kept constant as in S-2 scenario with the unified buildings height of 12m (i.e.  $H_l/W$  of 1), which is based on the Nakamura and Oke (1988) recommendation for the acceptable low aspect ratio that can provide acceptable levels of shading. In S-16 scenario, the first row of the buildings is increased to a height of 15m (i.e.  $H_l/W$  of 1.3), to measure its effects on wind velocity and air temperature in the adjacent canyon. The second and third rows of the buildings for the scenarios between S-3 through S-12 are optimised with five interchangeable aspect ratios (e.g. Qaid and Ossen, 2014), while the scenarios between S-13 through S-16 were limited to leeward gradually increased aspect ratios, as illustrated above in Table 7.2.

#### 7.4.1. Lower Multi-Asymmetrical Aspect Ratios Scenarios (S-3 and S-4)

S-3 and S-4 scenarios are categorised in this study as lower multi-asymmetrical aspect ratios models, which are based on lower buildings height, with the second and third rows in both of these scenarios having interchangeable aspect ratios, as illustrated in Figure 7.19. According to Qaid and Ossen (2014), the configuration of taller buildings opposite lower buildings in a canyon can create high wind velocities at the ground level. Thus, these scenarios aim to evaluate the effects of the lower multi-asymmetrical aspect ratios on urban pedestrian wind flow rate, compared to the base model (S-1), seeking for better microclimatic enhancement strategy.

The aspect ratios specifications for these proposed scenarios are as follows:

- S-3 scenario:  $H_1/W - H_2/W - H_3/W$  of 1–0.8–1.3
- S-4 scenario:  $H_1/W - H_2/W - H_3/W$  of 1–1.3–0.8.

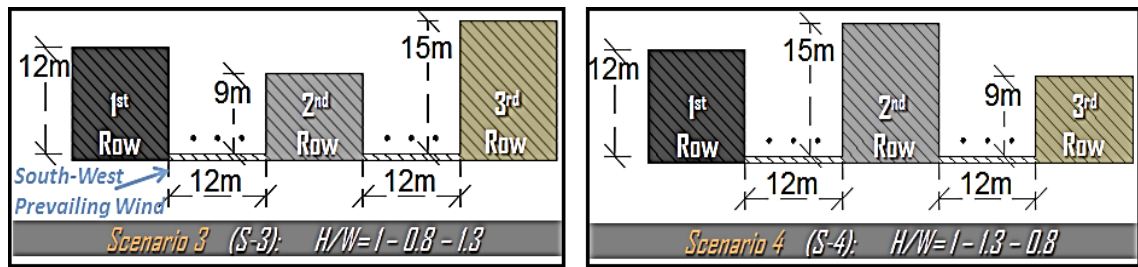


Fig. 7. 19: Low multi-asymmetrical aspect ratios (S-3 and S-4) scenarios showing a unified aspect ratio  $H_1/W$  of 1 on the first row of buildings, and unified interchangeable aspect ratios  $H_2/W$  and/or  $H_3/W$  of 0.8 and 1.3 for the second and third rows of buildings.

The buildings' height for the first row of buildings in the whole computational domain in these two scenarios is constantly unified with a height of 12m (as proposed in S-2 scenario), while the second row and the third row are tested with interchangeable heights of 9m and 15m, while the width of the two main Quba Roads are kept as the existing condition (i.e. 12m for each road), as illustrated in Figure 7.19. Thus, the building heights for the first, second and third rows of the buildings in S-3 scenario are 12m–9m–15m, and 12m–15m–9m in S-4 scenario.

The simulated results were the wind velocity and air temperature measurements, obtained at the pedestrian level. The results were extracted from 15 measurement points within each of the Tali'e and Nazil Quba Roads (i.e. windward and leeward canyons, respectively). In each canyon, five measurements locations between buildings are specified, with measurements located at the right side of the canyon (i.e. at windward elevation), along the middle of the canyon, and at the left side (i.e. at the leeward elevations), as illustrated previously in Figure 7.3.

#### 7.4.1.1. Wind Velocity at the Pedestrian Level (S-3, S-4)

Figure 7.20 analyses the contour of velocity magnitudes (m/s) for the low multi-asymmetrical aspect ratios scenarios in S-3 (with  $H/W$  of 1–0.8–1.3) and S-4 ( $H/W$  of 1–1.3–0.8), and compared with the base case (S-1) measurements at the pedestrian level. In S-3 scenario, the elevations on the second row of the buildings are lower ( $H_2 = 9\text{m}$ ) than the third row ( $H_3 = 15\text{m}$ ), while in S-4 are the reversed, but both are lower than building heights in the base case scenario (refer to Figure 7.2 in section 7.2).

In S-3 scenario ( $H/W = 1-0.8-1.3$ ), it is found that the overall wind magnitude is reduced within the windward canyon (Tali'e Quba Road) compared to S-1 (base model) from the average measurements 1.7m/s to 1.0m/s (i.e. -42%). It has increased in the leeward canyon (Nazil Quba Road) from the average measurement 0.7m/s to 1.6m/s (i.e. by 148%). This is because in the leeward canyon, the height of the leeward elevations (or the second row of the buildings) is significantly low ( $H_2=9\text{m}$ ) compared to the base case (S-1), i.e. more than half the existing height, which led to lower opportunity of wind catchment in the windward canyon, while allowing wind to flow over the second row of the buildings to the leeward canyon where the windward elevation in the latter canyon is higher ( $H_3/W$  of 1.3), thus higher wind drag to the pedestrian level.



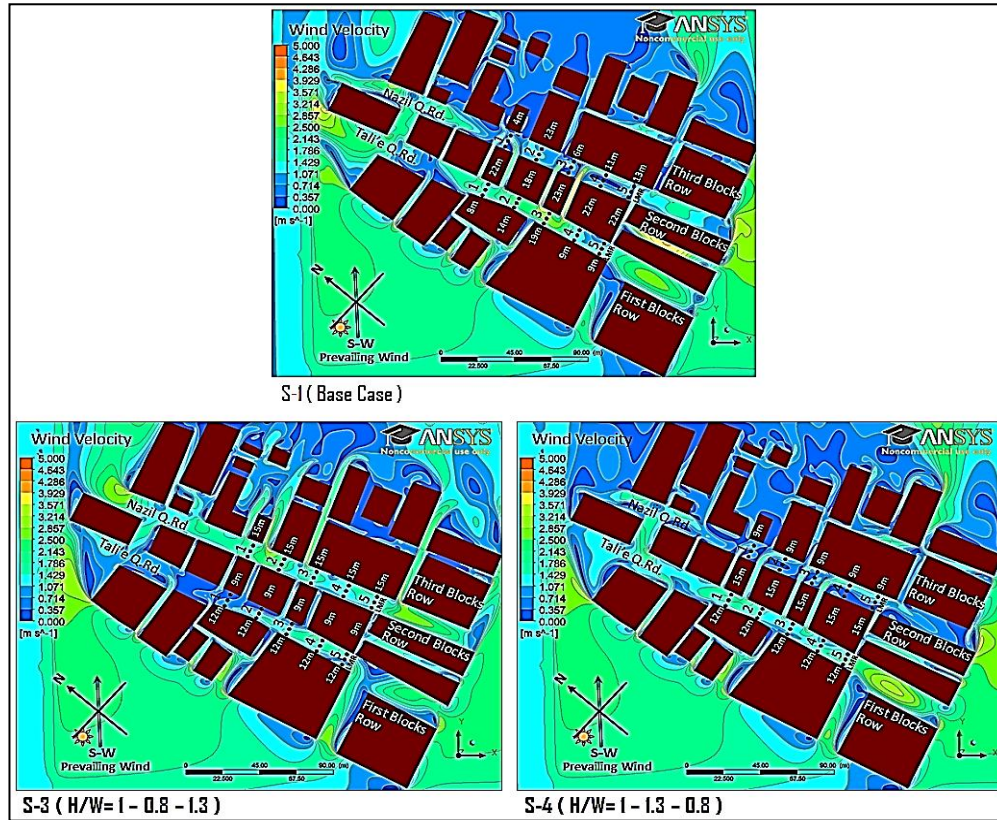


Fig. 7. 20: Contours of velocity magnitude (m/s) at pedestrian height (2m) for the low case aspect ratio scenarios of S-3 and S-4 and compared with the base case (S-1).

In S-4 scenario ( $H/W = 1-1.3-0.8$ ), where the elevations on the second row of the buildings are higher ( $H_2 = 15\text{m}$ ) than the third row ( $H_3 = 9\text{m}$ ) but both are lower than the base case scenario, it is found that the overall wind magnitude is slightly reduced within the windward canyon (between the first two rows of the buildings, i.e. Tali'e Quba Road) at the pedestrian level from the average measurements of  $1.7\text{m/s}$  to  $1.4\text{m/s}$  (i.e.  $-18.1\%$ ), followed by the leeward canyon (between the second and the third rows of buildings, i.e. Nazil Quba Road) from the average measurement  $0.7\text{m/s}$  to  $0.6\text{m/s}$  (i.e.  $-12.3\%$ ). This is consistent with findings from Lee et al. (2013), where the lower  $H/W$  and lower building heights leads to less turbulence and a more consistent and stable wind flow at the pedestrian level.

In Figure 7.21, it is found that wind magnitude in the windward canyon is lower in S-3 ( $H/W = 1-0.8-1.3$ ) than in S-4 ( $H/W = 1-1.3-0.8$ ), with a difference average measurement value of  $-0.4\text{m/s}$ . In contrast, it is found that in the leeward canyon the wind magnitude is higher in S-3 scenario than S-4, with a difference average measurement value of  $0.2\text{m/s}$ . The findings emphasise the importance of asymmetrical  $H/W$  aspect ratios in controlling wind velocities at the pedestrian level. However, the lower multi-asymmetrical aspect ratios scenarios (S-3 and S-4) are still not satisfactory for enhancing wind environment in Madinah, thus the thermal comfort. According to

Rizk and Henze (2010), to achieve the upper limit of tolerable thermal comfort in hot arid regions in mid-seasons, the average measurement wind velocity should be greater than 2m/s. In addition, S-3 scenario has achieved 148% improvement in wind velocity in the leeward canyon (to 1.61m/s), but it has worsened the windward canyon by 42%.

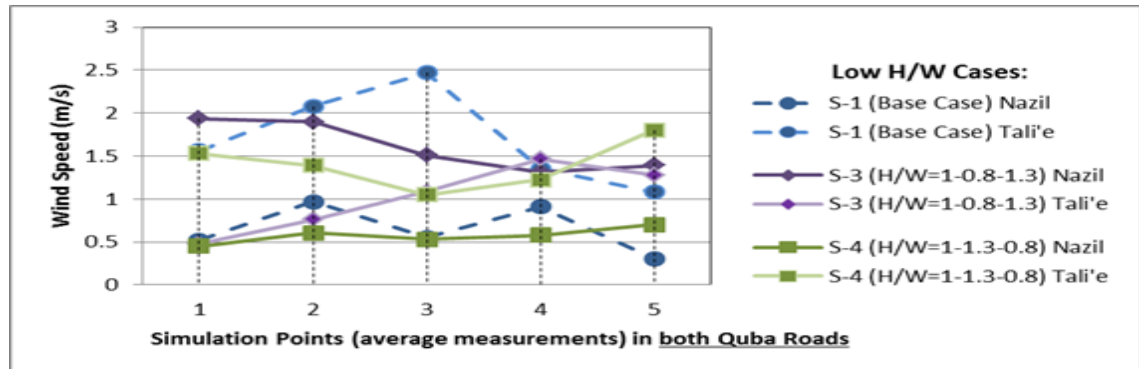


Fig. 7. 21: Overall wind velocity for the base case and the lower multi-asymmetrical H/W scenarios (S-3, S-4) in the Nazil and Tali'e Quba Roads (i.e. leeward and windward canyons, respectively).

The analysis for the locations at the left (the leeward walls), middle and the right (the windward walls) sides of the Tali'e and Nazil canyons wind speeds in the lower aspect ratio models can be found in the Appendices from A7.2 to A7.7.

#### 7.4.1.2. Air Temperature at the Pedestrian Level (S-3, S-4)

In Figure 7.22, it is found that the overall air temperature level in S-3 scenario (H/W of 1-0.8-1.3) is increased within the windward canyon (Tali'e Quba Road) at the pedestrian level compared to the base model (S-1), from an average of 34.0°C to 37.5°C (i.e. by 10%). It has decreased in the leeward canyon (Nazil Quba Road) from the average measurement 36.1°C to 33.3°C (i.e. by 8%). This is due to the proposed low aspect ratio ( $H_2/W$  of 0.8) on the second row of the buildings that led to a reduced air velocity magnitude, thus increased in air temperature in the windward canyon, while the aspect ratio is higher on the third row of buildings ( $H_3/W$  of 1.3) that led to an increase in wind velocity in the leeward canyon, thus decrease in air temperature.

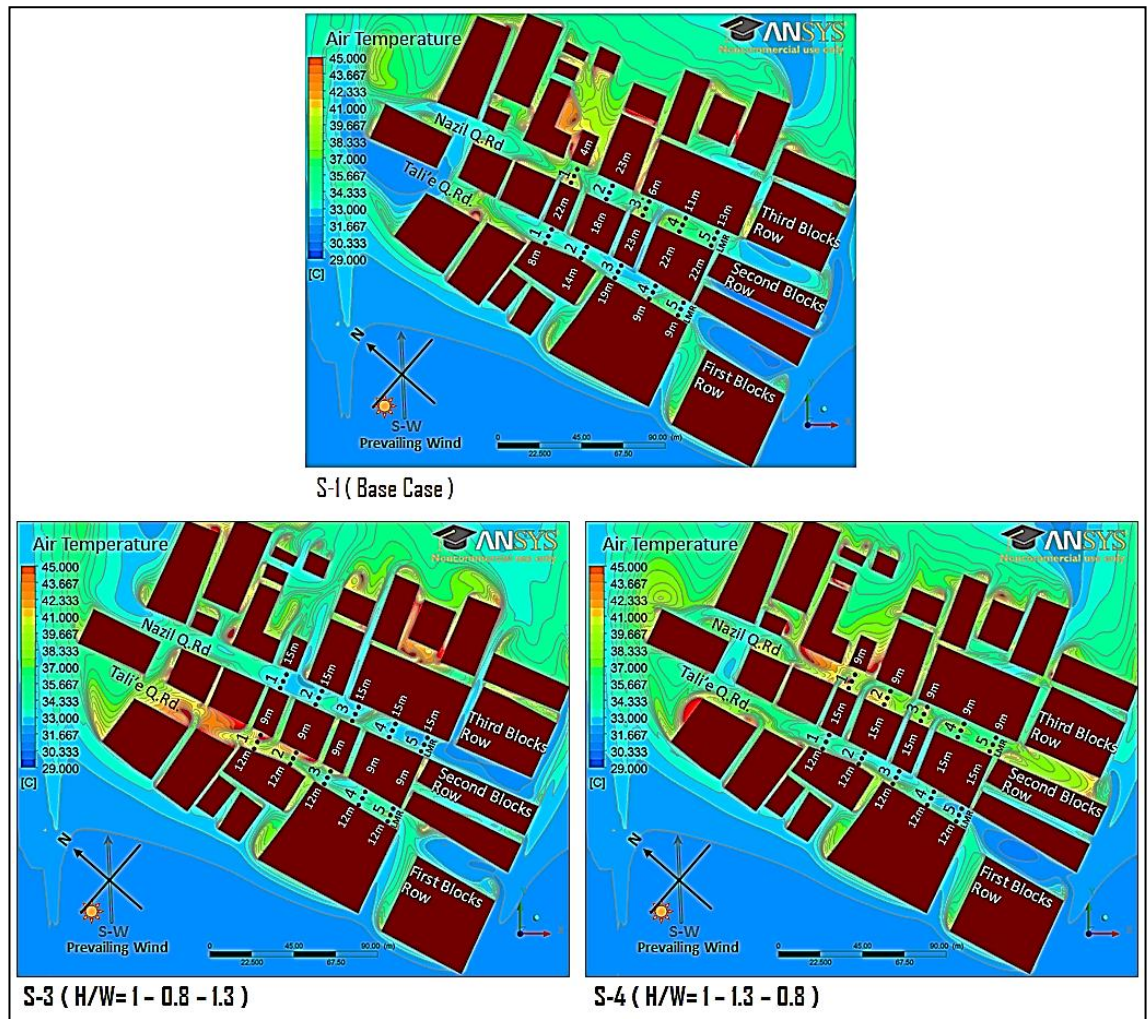


Fig. 7. 22: Contours of air temperature degrees ( $^{\circ}\text{C}$ ) at pedestrian height (2m) for the low case aspect ratio scenarios of S-3 and S-4 and compared with the base case (S-1) scenario.

On the other hand, in S-4 model compared to the base case scenario, it is found that the overall air temperature level is slightly increased within the windward canyon (Tali'e Quba Road) at the pedestrian level from the average measurements of  $34.0^{\circ}\text{C}$  to  $34.6^{\circ}\text{C}$  (i.e. by 2%); with a higher difference in the leeward canyon (Nazil Quba Road) from the average measurement of  $36.1^{\circ}\text{C}$  to  $38.2^{\circ}\text{C}$  (i.e. 6%). Although the leeward canyon is in shade during the simulation period (i.e. at 15:00 hours), the increase in air temperature by 6% is as a result of stable wind flow and less turbulence being generated at the pedestrian level.

Figure 7.23 shows the overall air temperature pattern for the five measurement locations (1 through 5) in each of the windward canyon (Tali'e Quba Road) and the leeward canyon (Nazil Quba Road) in S-3 and S-4 scenarios. It is found that the air temperature patterns in S-3 (with  $H/W$  of 1 – 0.8 – 1.3) and S-4 (with  $H/W$  of 1 – 1.3 –

0.8) are different compared to the base case scenario (S-1). The results shows that the leeward canyon (i.e. Nazil Quba Road) in S-3 having the lowest average air temperature, followed by the windward canyon (i.e. Tali Quba Road) in S-1, the windward canyon in S-4, the leeward canyon in S-1, the windward canyon in S-3, while the leeward canyon in S-4 recorded the lowest values.

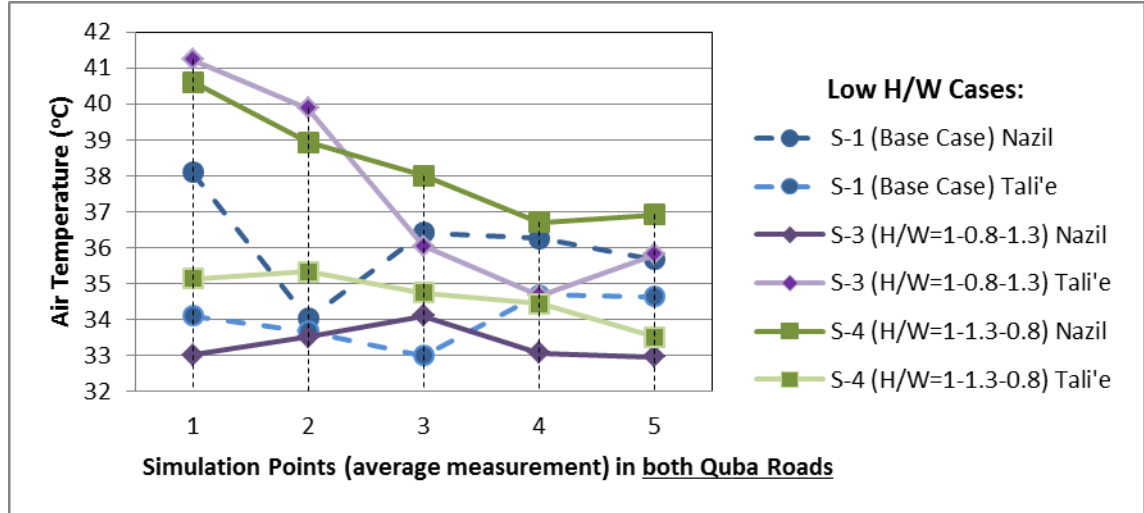


Fig. 7. 23: : Overall air temperature in the Nazil and Tali'e Quba roads for the low H/W multi-asymmetrical aspect ratios cases at five measurement locations, & compared with the base case (S-1).

The air temperature results for the locations at the left (the leeward walls), middle and the right (the windward walls) sides of the Tali'e and Nazil Quba canyons in the low aspect ratio models can be found in the Appendices from A7.8 to A7.13.

#### 7.4.2. Medium Multi-Asymmetrical Aspect Ratios Scenarios (S-5, S-6, S-7)

Due to unsatisfactory microclimatic results obtained from the lower multi-asymmetrical aspect ratios scenarios (investigated above), in terms of wind velocity and air temperature, three medium multi-asymmetrical aspect ratios scenarios (S-5, S-6 and S-7) are investigated, based on averaged building heights, as illustrated in Figure 7.24. The specifications of H/W for the 1<sup>st</sup>, 2<sup>nd</sup> and 3<sup>rd</sup> rows of the buildings are as follows:

- S-5 scenario with aspect ratios of 1 – 1.5 – 1.5;
- S-6 scenario with gradually increased aspect ratios of 1 – 1.3 – 1.8; and
- S-7 scenario with interchanged aspect ratios of 1 – 1.8 – 1.3.



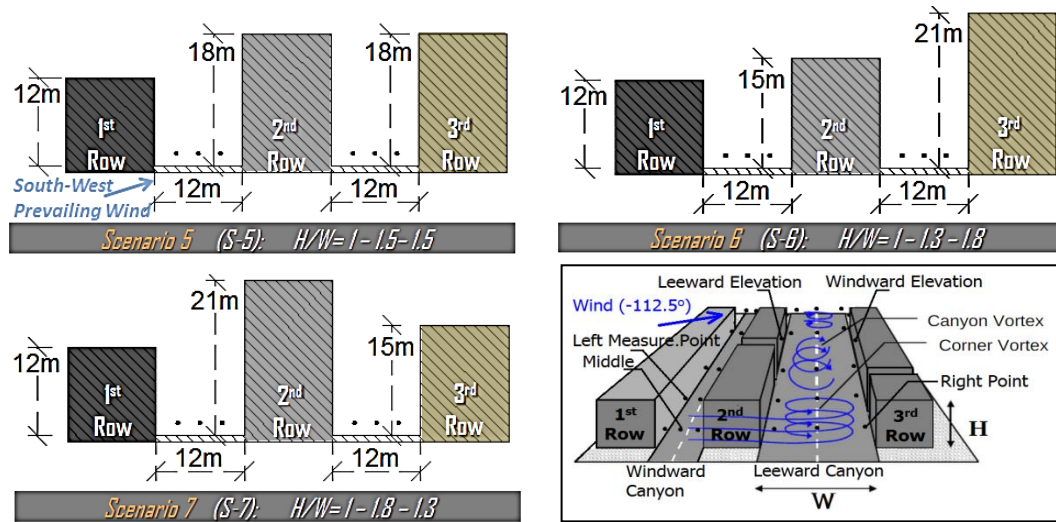


Fig. 7. 24: Medium multi-asymmetrical aspect ratios (S-5, S-6 and S-7) scenarios showing a unified aspect ratio  $H_1/W$  of 1 on the first row of buildings, and unified interchangeable aspect ratios  $H_2/W$  and/or  $H_3/W$  of 1.3, 1.5 and 1.8 for the second and third rows of buildings.

The buildings height for the first row of buildings in the whole computational domain in these three scenarios is unified with a height of 12m (as proposed in S-2 scenario in section 7.3), while the second row and the third row are tested with interchangeable heights of 18m in S-5 scenario, 15m and 21m in S-6 and S-7 scenarios, while the width of the two main Quba Road canyons is kept as in the existing condition (i.e. 12m), as illustrated in Figure 7.24. Thus, the building heights for the first, second and third rows of the buildings in S-5 scenario are: 12m–18m–18m; in S-6 are: 12m–15m–21m, and in S-7 scenario are: 12m–21m–15m.

These scenarios test findings from Qaid and Ossen (2014) of asymmetrical urban streets indicate that configuration of tall buildings opposite low buildings in a canyon can create high wind velocities at ground level. Results are then compared to the base case (S-1) to test impacts of wind velocity on pedestrian thermal comfort.

The simulated results were the wind velocity and air temperature measurements, obtained at the pedestrian level. The results were extracted from 15 measurement points within each of the Tali'e and Nazil Quba Roads (i.e. windward and leeward canyons, respectively). In each canyon, five measurements locations between buildings are specified, with measurements located at the right side of the canyon (i.e. at windward elevation), along the middle of the canyon, and at the left side (i.e. at the leeward elevations), as illustrated previously in Figure 7.3.

#### 7.4.2.1. Wind Velocity at the Pedestrian Level (S-5, S-6, S-7)

Figure 7.25 analyses the contour of velocity magnitudes (m/s) for the medium multi-asymmetrical aspect ratios scenarios in S-5 ( $H/W$  of 1–1.5–1.5), S-6 ( $H/W$  of 1–1.3–1.8) and S-7 ( $H/W$  of 1–1.8–1.3), and compared with the base model (S-1) at the pedestrian level (2m above the ground). Figure 7.26 shows the wind velocity pattern for the five measurement locations in both of the windward canyon (Tali'e Quba Road) and the leeward canyon (Nazil Quba Road).

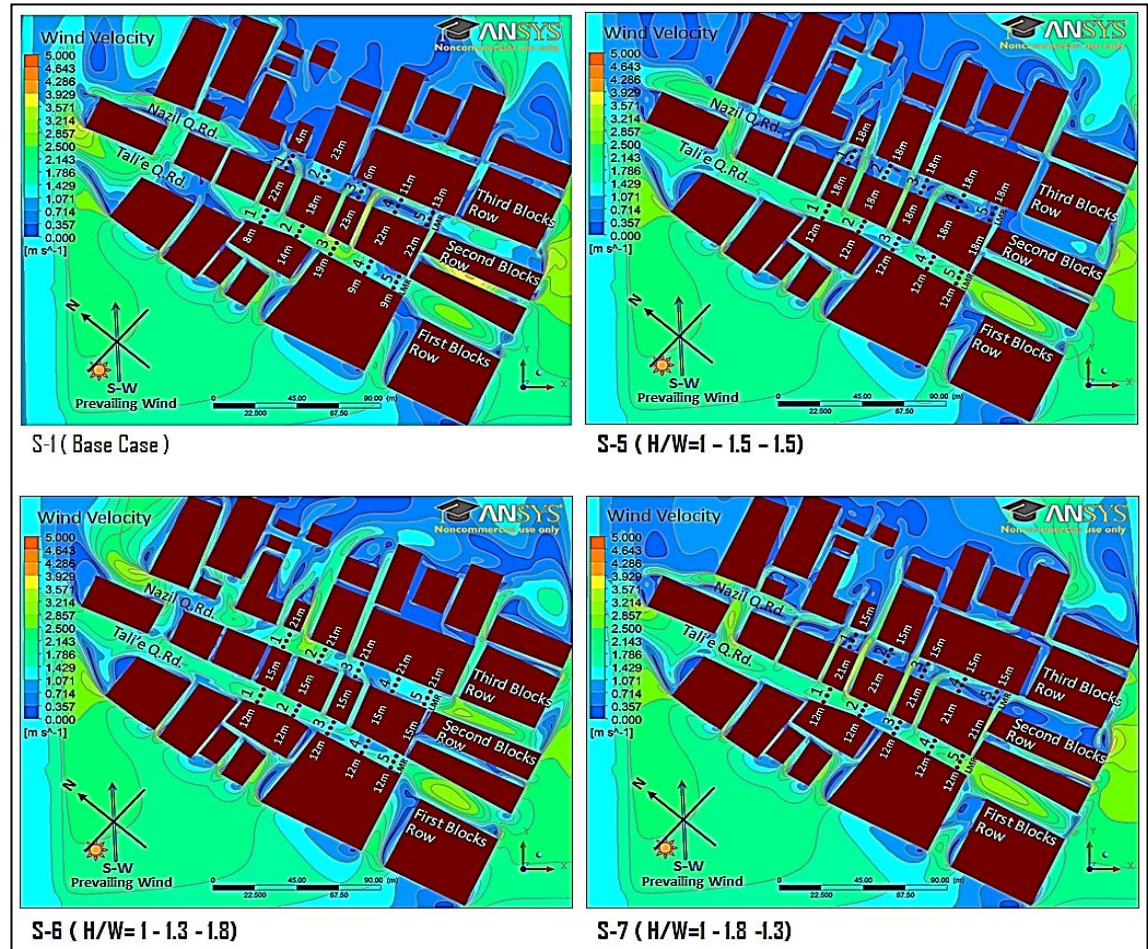


Fig. 7. 25: Contours of velocity magnitude (m/s) at pedestrian height (2m) for the medium case aspect ratio scenarios of S-5, S-6 and S-7 and compared with the base case (S-1) scenario.

In comparison with the base case (S-1), it is found that the overall wind magnitude in S-5 scenario ( $H/W$  of 1–1.5–1.5) is almost the same within the windward canyon (Tali'e Quba Road), with an average measurement of 1.7m/s. With a slight difference in wind velocity in the leeward canyon (Nazil Quba Road) from the average measurement of 0.7m/s to 0.6m/s (i.e. -13.8%). The latter case in S-5 scenario is due to the canyon's position between a symmetrical height of the second and third rows of buildings ( $H_2 = H_3 = 18\text{m}$ ). According to Qaid and Ossen (2014), symmetrical aspect ratios can have negative effect on urban pedestrian wind velocity, which is due to a lack

of wind catchment areas (i.e. higher windward elevations). Therefore, the winds that are flown over the second row of buildings has taken skimming flow regime, thus are significantly decreased within the symmetrical leeward canyon.

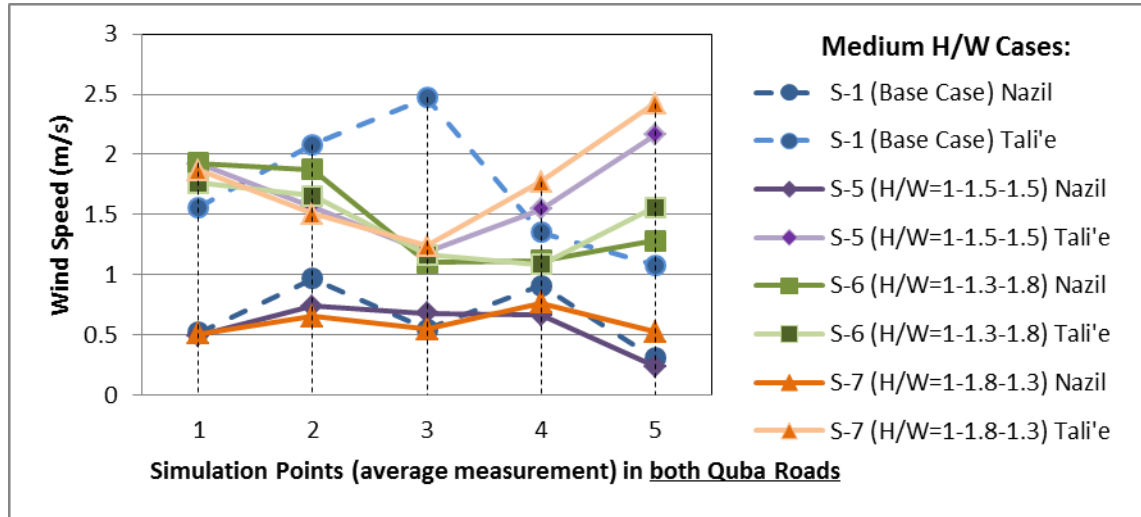


Fig. 7. 26: Overall wind speed in the Nazil and Tali'e Quba Roads for the medium type of  $H/W$  multi-asymmetrical aspect ratios cases at five measurement locations, & compared with the base case (S-1).

In S-6 scenario ( $H/W$  of 1–1.3–1.8), the configuration of the building heights follows a gradual increase with the wind direction, starting from the first row of the buildings (12m), followed by the second row (15m), then the third one (21m) to the third one. It is found that the overall wind magnitude in S-6 scenario is slightly decreased within the windward canyon (Tali'e Quba Road) at the pedestrian level compared to the base model (S-1), from the average measurement of 1.7m/s to 1.5m/s (i.e. -15.2%). While it the velocity magnitude is significantly improved in the leeward canyon (Nazil Quba Road) in S-6 scenario, from the average measurement of 0.7m/s to 1.5m/s (i.e. 124.6%). This is because of the second row of the buildings in S-6 scenario is having slightly lower heights (by 6m) compared to the base model, while allowing part of the wind flow to deviate over the building to the leeward canyon, where significantly higher windward elevations height (by 11m) are proposed on the third row in S-6.

In contrast, S-7 scenario ( $H/W$  of 1–1.8–1.3) shares somewhat similar urban height configurations, and the buildings height or aspect ratio on the middle row of the buildings is higher than the other two adjacent rows. Therefore, it is found that the



overall wind velocities within both of the windward and leeward canyons are almost similar to the base case S-1 scenario at the pedestrian level. The magnitude in this proposed scenario is slightly increased in the windward canyon from the average measurement 1.7m/s to 1.8m/s (i.e. 2.9%), while it is slightly decreased in the leeward canyon from the average measurement 0.7m/s to 0.6m/s (i.e. -7.7%).

These comparative analyses from the velocity contours of S-5, S-6 and S-7 against S-1 demonstrate that the S-6 scenario (H/W of 1–1.3–1.8), with leeward gradual increase in building heights, is the better option for the medium multi-asymmetrical aspect ratios category, to enhance the wind velocity in the leeward canyon, while having a slight decrease in the wind magnitude in the windward canyon. The wind speed results for the locations at the left (near the leeward walls), middle and the right (near the windward walls) sides of the Tali'e and Nazil canyons in the medium aspect ratio models can be found in the Appendices from A7.14 to A7.19.

#### **7.4.2.2. Air Temperature at the Pedestrian Level (S-5, S-6, S-7)**

Figure 7.27 analyses the contours of air temperature in degrees (°C) for the three medium multi-asymmetrical aspect ratios scenarios, i.e. S-5, S-6, and S-7, at the pedestrian level, and is compared with the base case S-1 scenario.

The comparative analysis indicates that the overall air temperature in S-5 scenario (H/W of 1–1.5–1.5) is slightly improved within the windward canyon (Tali'e Quba Road), from the average measurements of 34.0°C to 33.6°C (i.e. by 1%), while it is slightly worsened in the leeward canyon (Nazil Quba Road) from the average measurement of 36.1°C to 37.4°C (i.e. by 4%). The air temperature is decreased in the leeward canyon because it is surrounded by symmetrical buildings' height, which has led to lower wind turbulence being generated that is translated to stable wind flow, thus less convective heat transfer (e.g. Lee et al., 2013; Hong and Lin, 2015).

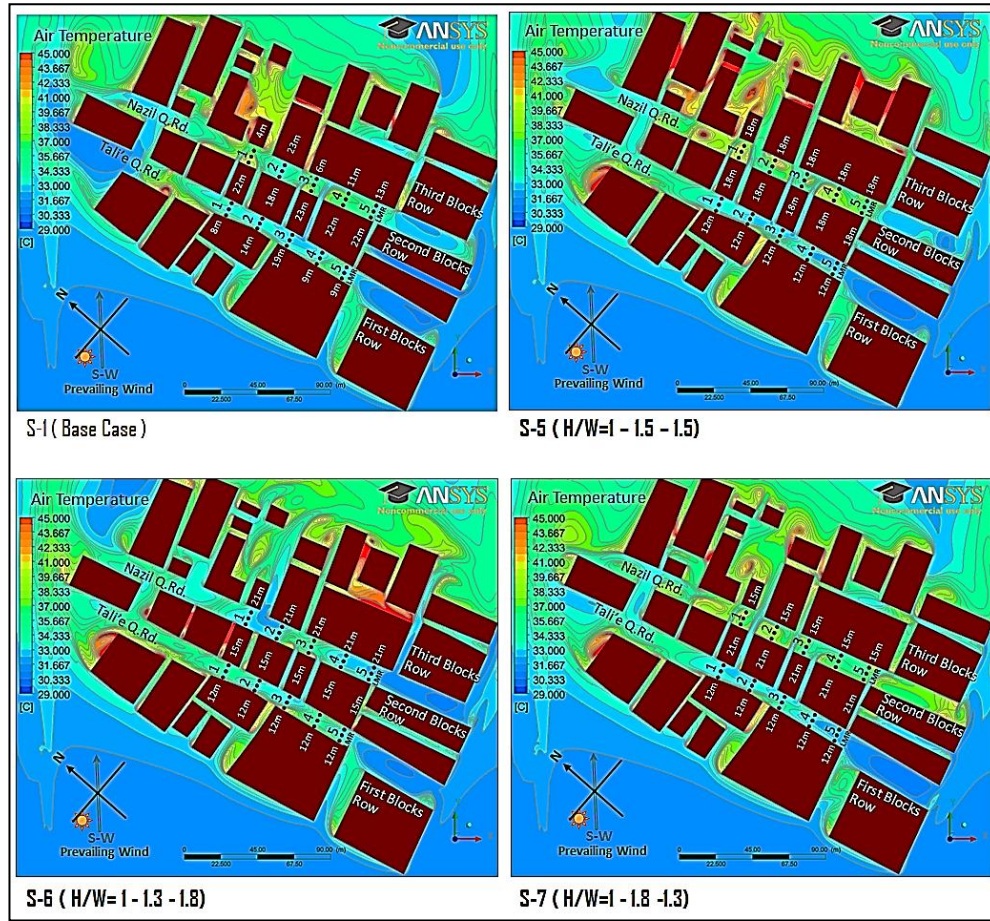


Fig. 7. 27: Contours of air temperature degrees ( $^{\circ}\text{C}$ ) at pedestrian height (2m) for the medium case aspect ratio scenarios of S-5, S-6 and S-7 and compared with the base case (S-1) scenario.

On the other hand, S-6 scenario (with  $H/W$  of 1–1.3–1.8), in comparison with the base case, indicates that the overall air temperature level is slightly worsened within the windward canyon at the pedestrian level from the average measurement  $34.03^{\circ}\text{C}$  to  $34.9^{\circ}\text{C}$  (i.e. 3%), while it is significantly improved in the leeward canyon from the average measurement  $36.1^{\circ}\text{C}$  to  $33.6^{\circ}\text{C}$  (i.e. by 7.0%). This is because of the S-6 model is proposed with a leeward gradual increase in the building heights, that obtained a significant increase in wind velocity at the pedestrian level (as discussed above).

Whereas in the S-7 scenario (with  $H/W$  of 1–1.8–1.3), it is found that air temperature in S-7 is slightly decreased in the windward canyon from the average measurement  $34.0^{\circ}\text{C}$  to  $33.4^{\circ}\text{C}$  (i.e. -1.9%), while it is slightly worsened in the leeward canyon from the average measurement  $36.1^{\circ}\text{C}$  to  $36.9^{\circ}\text{C}$  (i.e. 2.2%).

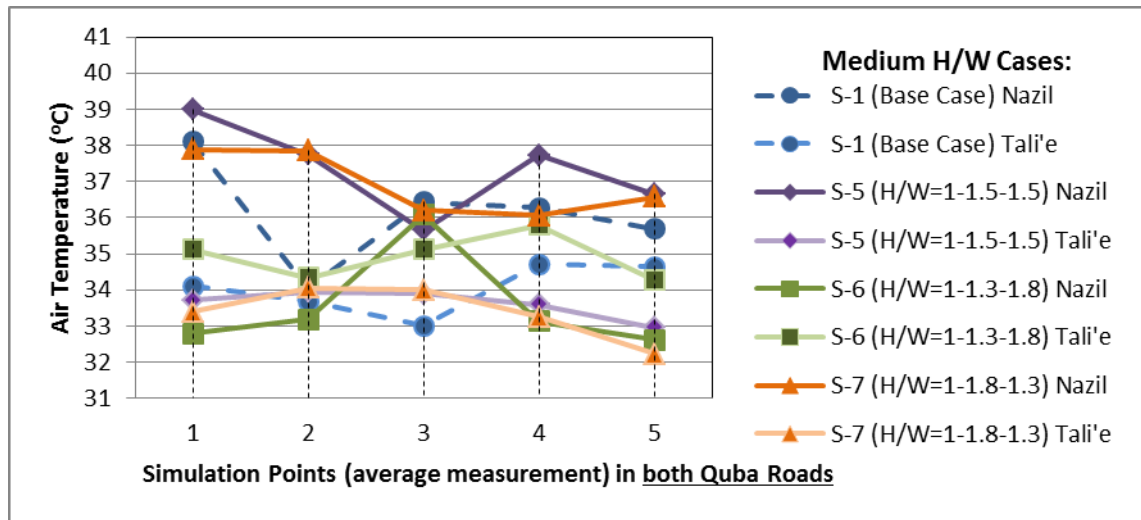


Fig. 7. 28: Overall air temperature in the Nazil and Tali'e Quba Road for the medium H/W multi-asymmetrical aspect ratios cases at five measurement locations, & compared with the base case (S-1).

Figure 7.28 shows air temperature pattern in the windward canyon and the leeward canyon for S-5, S-6 and S-7 scenarios. In the windward canyon (Tali'e Quba Road), S-7 has obtained the lowest temperature value followed by S-5, particularly at location 1, 4 and 5, as a result of higher air velocities. The average air temperature values in this canyon are 33.6°C, 34.9°C and 33.4°C for S-5, S-6 and S-7, respectively.

On the other hand, in the leeward canyon (Nazil Quba Road), the S-6 with aspect ratio H/W of 1-1.3-1.8 has the lowest air temperature values than S-1, S-5 and S-7 at all the five measured locations, whereas S-5 with aspect ratio H/W of 1-1.5-1.5 has the highest air temperature values at the 1<sup>st</sup>, 4<sup>th</sup> and 5<sup>th</sup> locations than the base case (S-1) scenario, and followed by the S-7 (H/W of 1-1.8-1.3). The average air temperature values from the five measurement points in this canyon are 37.4°C, 33.6°C and 36.9°C for S-5, S-6 and S-7, respectively. The air temperature results for the locations at the left (near the leeward walls), middle and the right (near the windward walls) sides of the Tali'e and Nazil canyons in the medium aspect ratio models can be found in the Appendices from A7.20 to A7.25.

### 7.4.3. Higher Multi-Asymmetrical Aspect Ratios Scenarios (S-8 through S-12)

Due to unsatisfactory microclimatic results obtained from the medium multi-asymmetrical aspect ratios scenarios (investigated above), in terms of wind velocity and air temperature, three higher multi-asymmetrical aspect ratios scenarios (S-8, S-9, S-10, S-11 and S-12) are investigated, based on higher building heights, as illustrated in Figure 7.29. Due to the local planning constraints, the maximum building heights of the proposed scenarios will not exceed 27m (refer to section 2.4 in the Case Study Chapter).

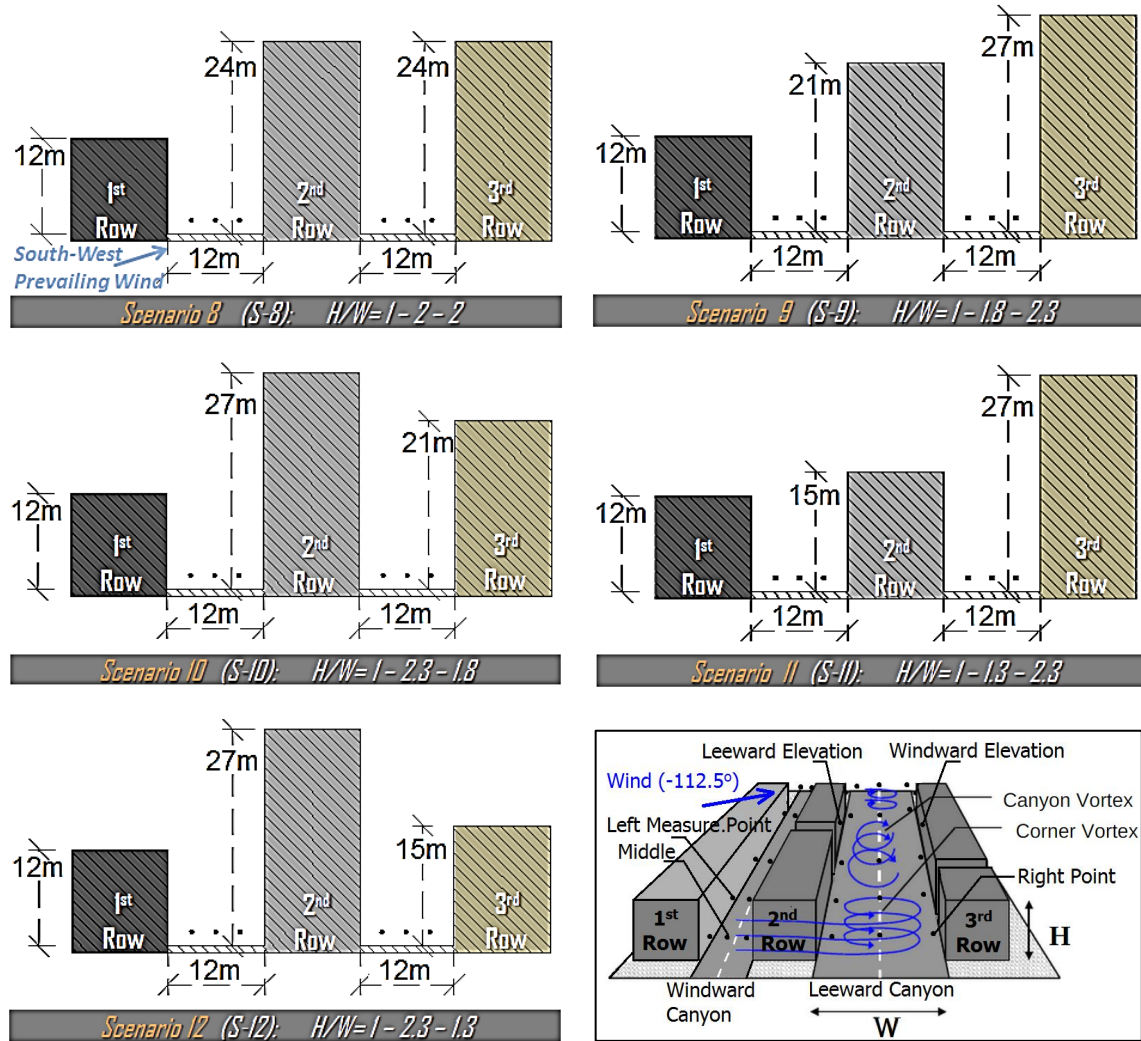


Fig. 7. 29: Five scenarios of higher multi-asymmetrical aspect ratios (S-8 to S-12), showing a unified aspect ratio  $H_1/W$  of 1 on the first row of buildings, and unified interchangeable aspect ratios  $H_2/W$  and/or  $H_3/W$  of 1.3, 1.5, 1.8, 2 and 2.3 for the second and third rows of buildings.

The specifications of aspect ratios in these scenarios for the first, second and third rows of the buildings are as follows:

- S-8 scenario with  $H/W$  aspect ratios of 1 – 2 – 2 (i.e. height of 12m – 24m – 24m );



- S-9 scenario with H/W aspect ratios of 1 – 1.8 – 2.3 (i.e. gradually increased heights of 12m – 21m – 27m );
- S-10 scenario with interchanged H/W aspect ratios of 1 – 2.3 – 1.8 (i.e. reversed heights to 12m – 27m – 21m );
- S-11 scenario with H/W aspect ratio of 1 – 1.3 – 2.3 (i.e. gradually increased heights of 12m – 15m – 27m ); and
- S-12 scenario with interchanged H/W aspect ratio of 1 – 2.3 – 1.3 (i.e. reversed heights to 12m – 27m – 15m).

The buildings height for the first row of buildings in the whole computational domain in these three scenarios is unified with a height of 12m (as proposed in S-2 scenario in section 7.3), while the second row and the third row are tested with interchangeable heights as specified above, while the width of the two main Quba Road canyons is kept as in the existing condition (i.e. 12m), as illustrated in Figure 7.29.

These scenarios test findings from Qaid and Ossen (2014) of asymmetrical urban streets indicating that configuration of tall buildings opposite low buildings in a canyon can create high wind velocities at ground level. Results are then compared to the base case (S-1) to test impacts of wind velocity on pedestrian thermal comfort. The simulated results were the wind velocity and air temperature measurements, obtained at the pedestrian level. The results were extracted from 15 measurement points within each of the Tali'e and Nazil Quba Roads (i.e. windward and leeward canyons, respectively). In each canyon, five measurements locations between buildings are specified, with measurements located at the right side of the canyon (i.e. at windward elevation), along the middle of the canyon, and at the left side (i.e. at the leeward elevations), as illustrated previously in Figure 7.3.

#### **7.4.3.1. Wind Velocity at the Pedestrian Level (S-8 through S-12)**

Figure 7.30 analyses the contours of velocity magnitudes (m/s) for the higher multi-asymmetrical aspect ratios scenarios (S-8, S-9, S-10, S-11 and S-12), and compared with the base model (S-1) at the pedestrian level.

In S-8 scenario (with  $H/W$  of 1–2–2), it is found that the overall wind velocities magnitude is slightly improved within the windward canyon (i.e. Tali'e Quba Road) compared to the S-1 scenario, from the average measurements of 1.71m/s to 2.0m/s (i.e. 14%). This is due to higher buildings elevations proposed on the second row of the

buildings (with unified height  $H_2$  of 24m). While in the leeward canyon (i.e. Nazil Quba Road), the wind magnitude is lessened in S-8 model compared to the existing conditions, from the average measurement of 0.7m/s to 0.5m/s (i.e. -23%). This is because the leeward canyon is situated between symmetrical buildings height of the second and the third rows of the buildings. Thus, leading reduced wind magnitude at the pedestrian level, due to skimming wind flow regime over the buildings, thus lower turbulence near the ground level.

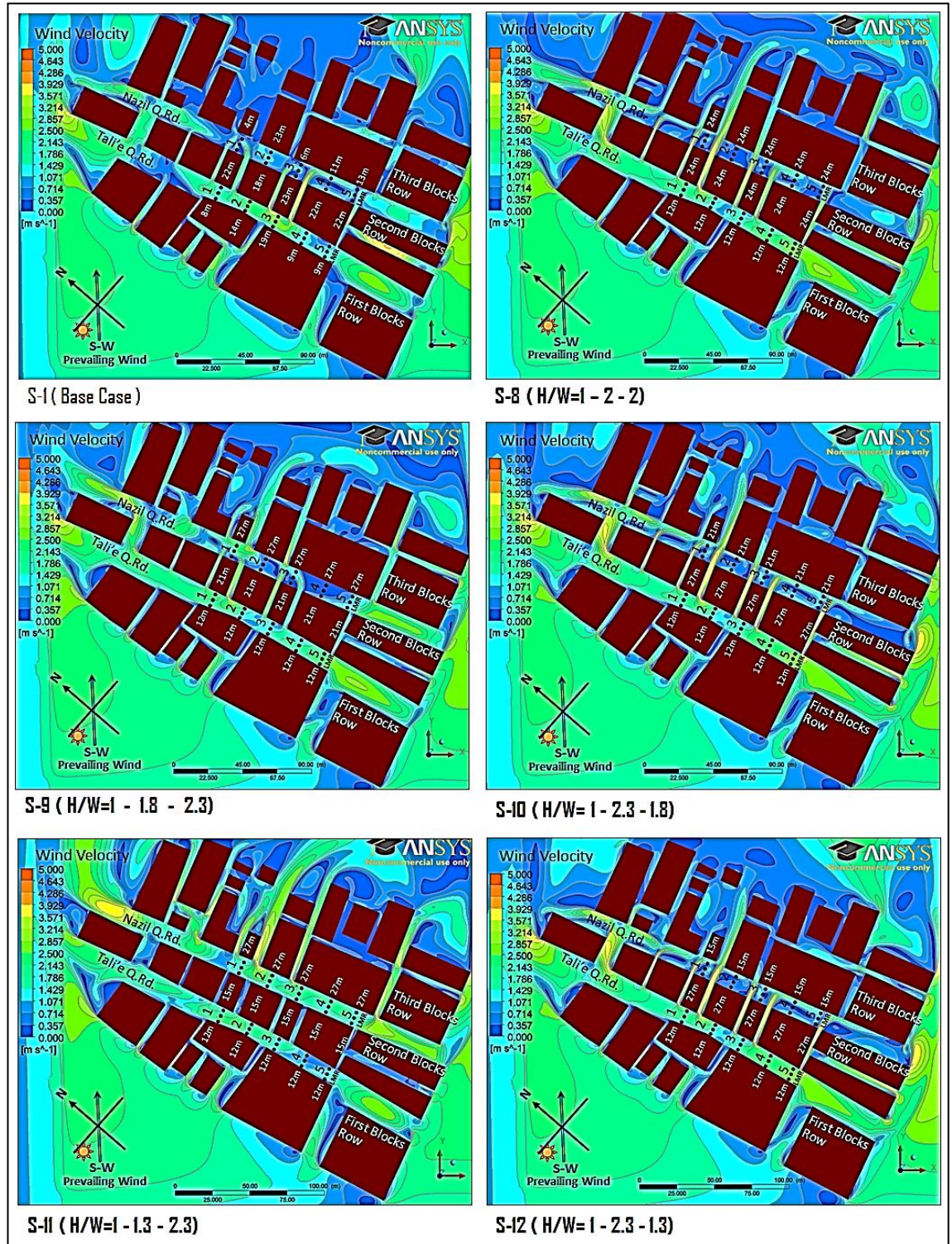


Fig. 7. 30: Contours of velocity magnitude (m/s) at pedestrian height (2m) for the high case aspect ratio scenarios of S-8, S-9, S-10, S-11 and S-12 and compared with the base case (S-1) scenario.

For the S-9 and S-11 scenarios compared to the base model (S-1), it is found that in the windward canyon (i.e. Tali'e Quba Road), the average measurement of the wind velocity in S-9 (with  $H/W$  of 1–1.8–2.3) is slightly improved from 1.7m/s to 1.8m/s (i.e. 6.4%), while in the S-11 scenario (with  $H/W$  of 1–1.3–2.3) the velocity is slightly decreased to 1.5m/s (i.e. -15.2%), as illustrated in Figures 7.30 and 7.31. This is because



the unified height of the windward elevations on the second row of the buildings in S-9 scenario ( $H_2 = 21\text{m}$ ) are approximately similar to the base case model (S-1), while are 6m lower in S-11 scenario ( $H_2 = 15\text{m}$ ).

In contrast, S-10 ( $H/W$  of 1–2.3–1.8) and S-12 ( $H/W$  of 1–2.3–1.3) share a strategy of higher buildings elevations on the second row of the buildings compared to the first and the third rows, which are similar to the configurations in the base model (S-1). It is found that in the windward canyon (i.e. Tali'e Quba Road), the average measurement of the wind velocity in S-10 (with  $H/W$  of 1–2.3–1.8) is slightly increased from 1.71m/s to 2.0m/s (i.e. 18%), and in the S-12 scenario (with  $H/W$  of 1–2.3–1.3) the wind magnitude is slightly increased to 2.0m/s (i.e. 16%), as illustrated in Figures 7.30 and 7.31. This is because the windward elevations on the second row of the buildings has higher buildings elevations on the second row of buildings in both S-10 scenario and S-12 scenario ( $H_2 = 27\text{m}$ ) compared to the base case ( $H_2 \approx 21$ ).

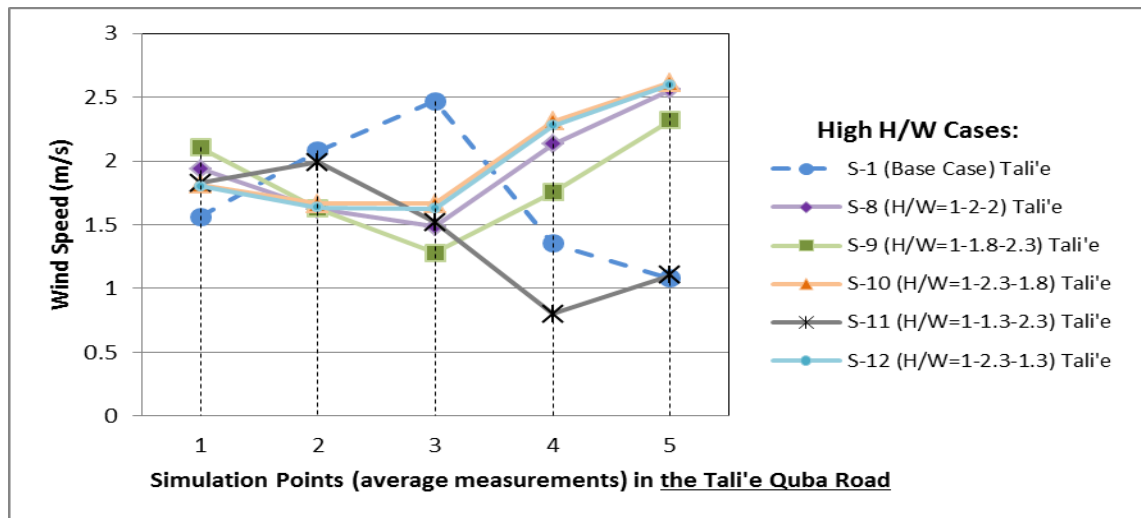


Fig. 7. 31: Overall wind speed within the Tali'e Quba Road for the high type of multi-asymmetrical aspect ratios cases at five average measurement locations, and compared with the base case (S-1).

On the other hand, it is found that in the leeward canyon (i.e. the Nazil Quba Road) the average measurement of wind velocity in S-9 ( $H/W$  of 1–1.8–2.3) is improved from 0.7m/s to 0.9m/s (i.e. 32%); with a significantly higher improvement difference in the S-11 scenario ( $H/W$  of 1–1.3–2.3) from the average measurement of 0.7m/s to 1.8m/s (i.e. 169%). This is because the leeward canyon in the S-11 scenario has lower leeward elevations on the second row of the buildings than the base model (S-1), allowing wind to flow over the buildings towards the leeward canyon (Nazil Quba Road), where 17m difference in windward elevations of this canyon was proposed

higher on the third row of the buildings (i.e.  $H_3 = 27\text{m}$ ); thus, greater wind drag towards the ground.

In S-10 and S-12, it is found that in the leeward canyon (i.e. the Nazil Quba Road), the wind velocity is slightly increased in S-10 from the average measurements of  $0.7\text{m/s}$  to  $0.8\text{m/s}$  (i.e. 21.5%) compared to the base model, and to  $0.74\text{m/s}$  in the S-12 scenario (i.e. 13.8%), as illustrated in Figure 7.32. This is because the leeward canyon in the S-10 scenario has slightly higher windward elevations on the third row of the buildings ( $H_3$  of  $21\text{m}$ ) compared to the base model, then followed by S-12 ( $H_3$  of  $15\text{m}$ ). The wind speed analysis for the locations at the left, middle and the right sides of the windward canyon and the leeward canyon in the high aspect ratio models can be found in the Appendices from A7.26 to A7.31.

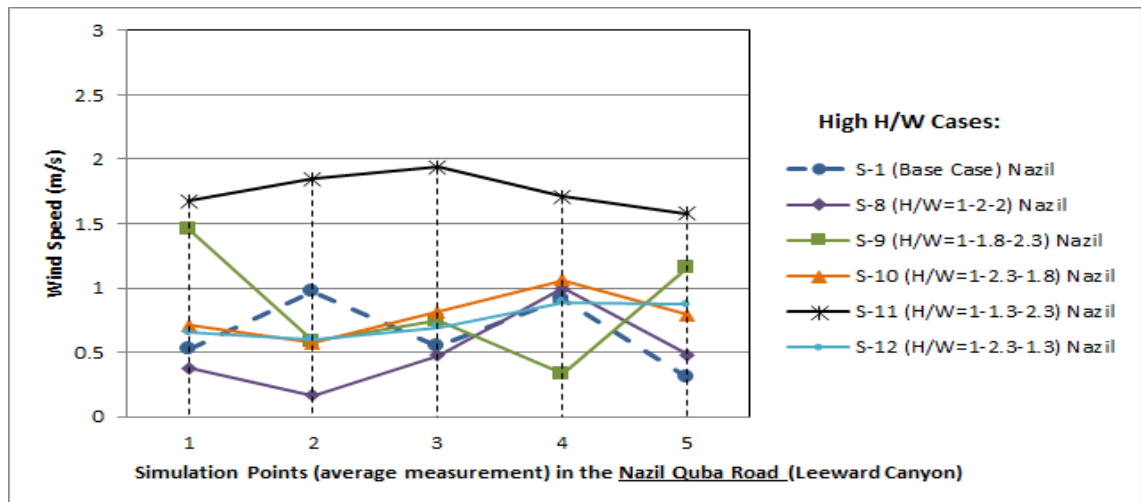


Fig. 7. 32: Overall wind speed within the Nazil Quba Road for the high type of multi-asymmetrical aspect ratios cases at five average measurement locations, and compared with the base case (S-1).

S-9 ( $H/W$  of 1–1.8–2.3) and S-11 ( $H/W$  of 1–1.3–2.3) scenarios share similar strategy of leeward gradual increase in building heights. This strategy is found to be effective on increasing the wind velocity in the leeward canyons. Thus, more scenarios should be investigated based on gradual increase in building heights with the prevailing wind direction, seeking for better wind flow results.

#### 7.4.3.2. Air Temperature at the Pedestrian Level (S-8 through S-12)

Figure 7.33 analyses the contours of air temperature for the higher multi-asymmetrical aspect ratios scenarios (S-8 through S-12), and compared with the base case. In S-8 scenario (with  $H/W$  of 1–2–2), the comparative analysis indicates that the overall air temperature is enhanced within the windward canyon (i.e. Tali'e Quba Road) from the average measurements of 34.0°C (i.e. in S-1) to 32.8°C (i.e. by 4%). This is due to higher wind velocities generated in this canyon as explained above. While in the leeward canyon (i.e. Nazil Quba Road), the air temperature is worsened from the average measurement of 36.1°C to 37.1°C (i.e. 3%), due to lower wind velocities in this canyon, thus lower heat transfer by convection (e.g. Hong and Lin, 2015).

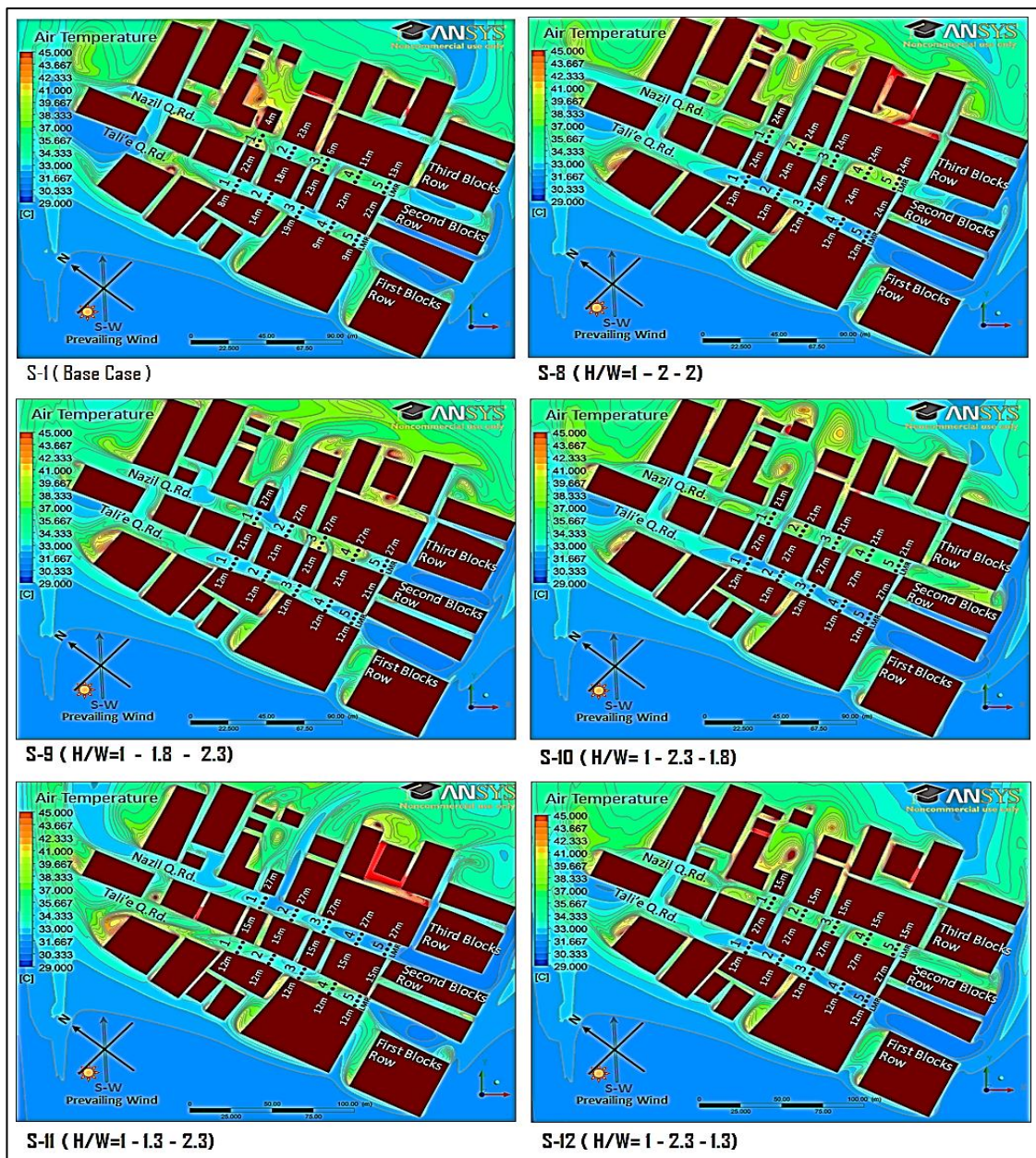


Fig. 7. 33: Contours of air temperature degrees (°C) magnitude at pedestrian height in five different high asymmetrical scenarios across five sections and extracted 30 points

For the S-9 and S-11 scenarios compared to the base model (S-1), it is found that in the windward canyon (i.e. Tali'e Quba Road), the average measurement of the air temperature in S-9 (with  $H/W$  of 1–1.8–2.3) is slightly improved from 34.0°C to 33.2°C (i.e. 3%), while in S-11 (with  $H/W$  of 1–1.3–2.3), the temperature is slightly increased to an average measurement of 34.6°C (i.e. 2%), as illustrated in Figure 7.34.

S-10 and S-12 scenarios share similar strategy of higher buildings elevations on the second row of buildings ( $H_2 = 27\text{m}$ ) than the first and third rows of buildings, which are similar configuration to the base case scenario ( $H_2 \approx 21\text{m}$ ). In the windward canyon (i.e. Tali'e Quba Road), the average measurement of the air temperature enhanced from 34.0°C to 32.5°C (i.e. by 5%) in the S-10 scenario ( $H/W$  of 1–2.3–1.8), and to a value of 32.5°C (i.e. 4%) in the S-12 scenario ( $H/W$  of 1–2.3–1.3), as illustrated in Figure 7.34.

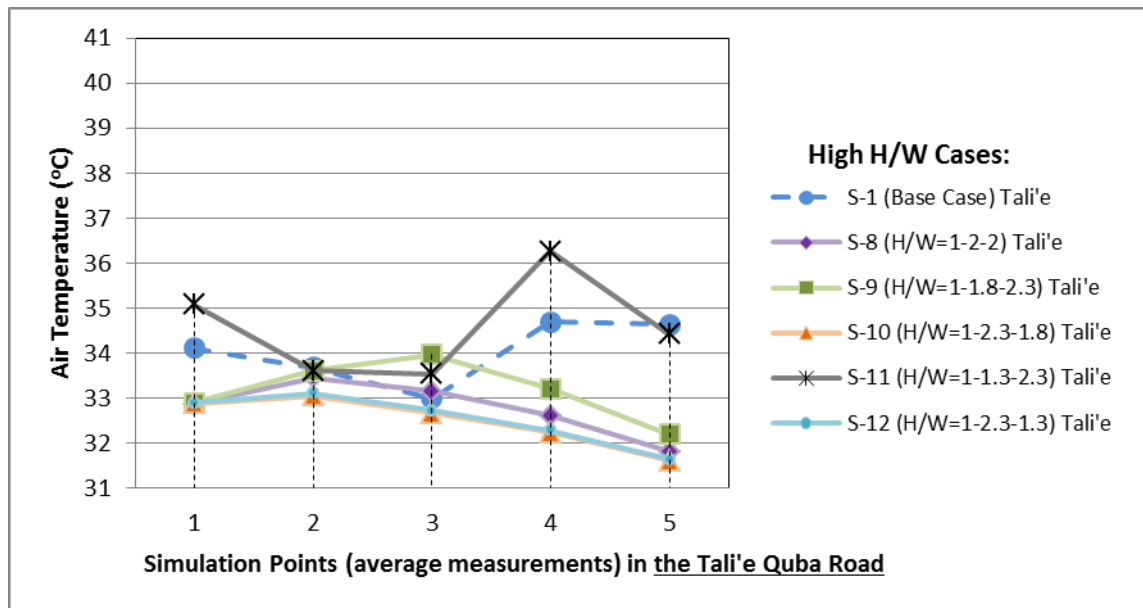


Fig. 7. 34: Air temperature in the Tali'e Quba Road for the higher type of  $H/W$  multi-asymmetrical aspect ratio cases at five average measurement locations, and compared with the base case (S-1).

On the other hand, Figure 7.35 shows that in the leeward canyon (i.e. the Nazil Quba Road), the average measurement of air temperature is slightly improved from 36.1°C to 35.4°C (i.e. 2%) in S-9 scenario (with  $H/W$  of 1–1.8–2.3), whereas it is significantly improved in the S-11 scenario (with  $H/W$  of 1–1.3–2.3) to 32.7°C (i.e. by 10%). This is because the leeward canyon in the S-11 scenario has a significant improvement in wind flow by 169% (i.e. from 0.7m/s to 1.8m/s) at the pedestrian level compared to the base case.



However, in S-10 (with  $H/W$  of 1–2.3–1.8) and S-12 (with  $H/W$  of 1–2.3–1.3), the air temperature is slightly worsened to an average measurement of 36.4°C (i.e. 0.8%), and 36.2°C (i.e. 0.4%), respectively in the leeward canyon (i.e. the Nazil Quba Road), as illustrated in Figure 7.35. This is due to the wind blockage ratio that is higher on the second row of the buildings ( $H_2 = 27\text{m}$ ) in S-10 and S-12 compared to the other buildings rows in these scenarios, thus resulting in stable wind flow and lesser convective heat transfer in the leeward canyon (e.g. Lee et al., 2013; Hong and Lin, 2015).

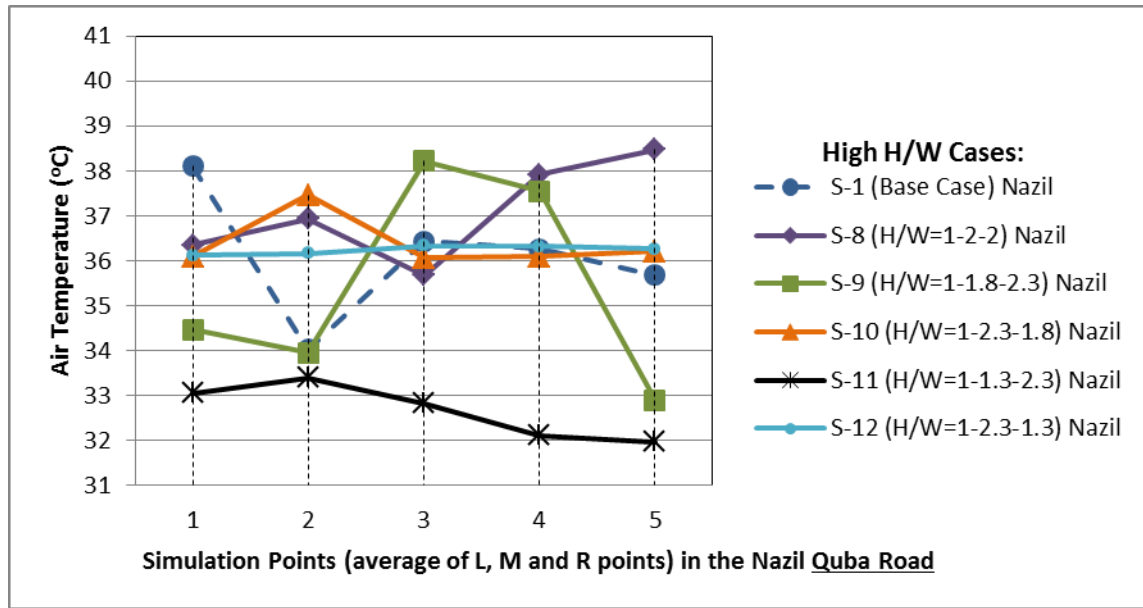


Fig. 7. 35: Air temperature in the Nazil Quba Road for the higher type of  $H/W$  multi-asymmetrical aspect ratio cases at five average measurement locations, and compared with the base case (S-1).

To sum up, S-9 and S-11 scenarios share similar strategy of gradual increase in building heights with the wind direction. This strategy is found to be effective on reducing the air temperature in the leeward canyons. S-11 scenario with  $H/W$  of 1 – 1.3 – 2.3 has reduced 3.4°C of air temperature (i.e. 10%) compared to the existing conditions (S-1). The findings emphasise a strong inverse relationship between the wind velocity magnitude and air temperature pattern. Although the shading level within the windward canyon in the scenarios between S-8 through S-12 (Taile Quba Road) are the same, the difference in air temperature values between these scenarios is dependent on the wind magnitude, controlled by variation building height or asymmetrical aspect ratios.

The air temperature analysis for the locations at the left, middle and the right sides of the windward canyon and leeward canyons in the high aspect ratio models can be found in the Appendices from A7.32 to A7.37.

#### **7.4.4. Leeward Gradual Increase in Asymmetrical Aspect Ratios (S-13 to S-16)**

Due to the significant of the leeward gradual increase in asymmetrical aspect ratios on improving the wind flow, air temperature and thermal comfort at the pedestrian, as were found in the S-6 ( $H/W$  of 1 – 1.3 – 1.8) and S-11 ( $H/W$  of 1 – 1.3 – 2.3) scenarios, this section tests four other scenarios (S-13 through S-16) that share similar strategy of gradual increase in  $H/W$  aspect ratios, as illustrated in Figure 7.36.

The specifications for the leeward gradually increased aspect ratios scenarios (S-13 through S-16), which were:

- S-13 scenario with aspect ratios of 1 – 1.3 – 1.5;
- S-14 scenario with aspect ratios of 1 – 1.3 – 2.0;
- S-15 scenario with aspect ratios of 1 – 1.5 – 2.3; and
- S-16 scenario with aspect ratios of 1.3 – 1.5 – 2.3 (note that the latter has higher aspect ratio on the first row of buildings).

The first row of buildings in S-3 through S15 (not including S-16), was kept constant as in S-2 scenario with the unified buildings height of 12m (i.e. aspect ratio  $H_l/W$  of 1), which took into the account of the Nakamura and Oke (1988) recommendation. While in S-16, the first row of buildings had a height of 15m (i.e. aspect ratio  $H_l/W$  of 1.3), to measure its effects on wind velocity and air temperature in the adjacent canyon. The second and third rows of buildings for the scenarios between S-3 through S-12 were optimised with five interchangeable aspect ratios (e.g. Qaid and Ossen, 2014), while the scenarios between S-13 through S-16 were limited to gradually increased aspect ratios, as illustrated in Figure 7.36.

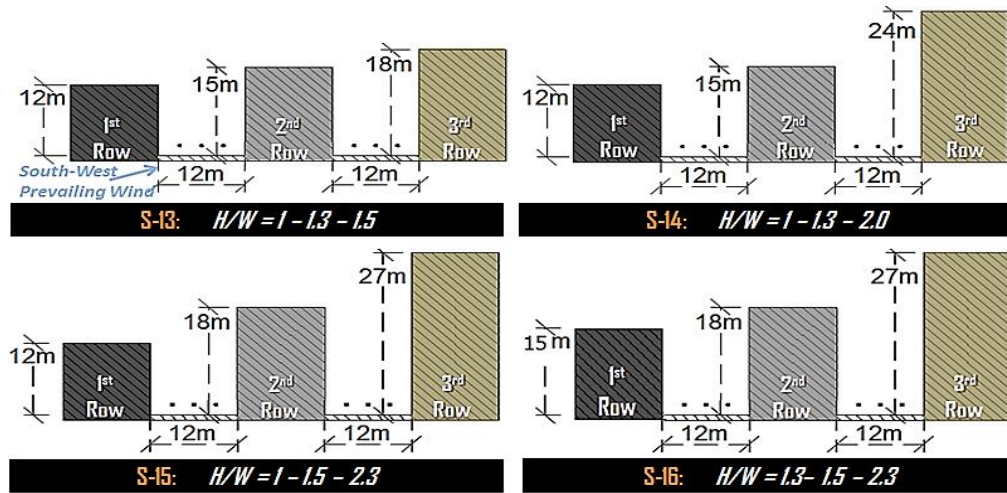
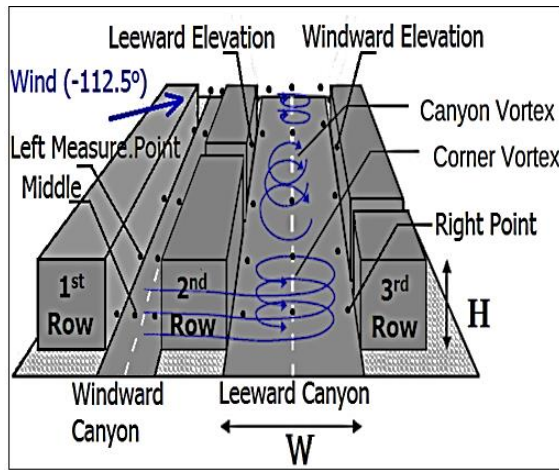


Fig. 7. 36: Leeward gradually increased multi-asymmetrical aspect ratios (S-13 to S-16). The building heights starts from 12m in S-13, S-14 and S-15, while it starts from 15m in S-16.

#### 7.4.4.1. Wind Velocity at the Pedestrian Level (S-13, S-14, S-15, S-16)

Figure 7.37 analyses the contours of velocity magnitudes (m/s) for the leeward gradual increase in multi-asymmetrical aspect ratios scenarios (S-13 through S-16), and compared with the base case (S-1), at the pedestrian level (2m above the ground).





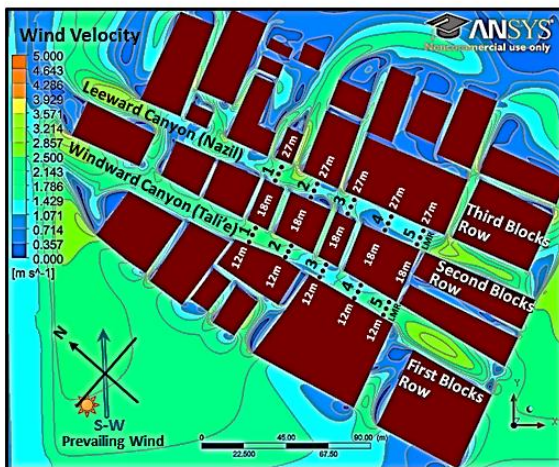
S-1 ( Base Case )



S-13 (  $H/W=1 - 1.3 - 1.5$  )



S-14 (  $H/W=1 - 1.3 - 2.0$  )



S-15 (  $H/W=1 - 1.5 - 2.3$  )



S-16 (  $H/W=1.3 - 1.5 - 2.3$  )

Fig. 7. 37: Contours of velocity magnitude at the pedestrian level for the cases of leeward gradual increase in aspect ratios on the three rows of buildings, & compared with the base case (S-1).

In the windward canyon (i.e. Tali'e Quba Road), it is found that the overall wind velocities magnitude in S-13 ( $H/W$  of 1–1.3–1.5) and S-14 ( $H/W$  of 1–1.3–2), compared to the base case S-1 scenario is slightly decreased, which is because both of the proposed scenarios have 6m lower elevations on the second low of the buildings than the base model. Thus, the wind velocity in this canyon is reduced from the average

measurement 1.7m/s to 1.5m/s in S-13 and in S-14 scenarios, as illustrated in Figures 7.37 and 7.38.

The overall wind velocity values in S-15 ( $H/W$  of 1–1.5–2.3) and S-16 ( $H/W$  of 1.3–1.5–2.3) are found to be approximately similar to the base case situation (1.7m/s) in the windward canyon (i.e. Tali'e Quba Road) at the measurement locations with an average value of 1.7m/s and 1.6m/s (i.e. -6.4%), respectively, as illustrated in Figures 7.39 and 7.40.

Figure 7.38 demonstrates that the wind velocity pattern in the windward canyon (i.e Tali Quba Road) is the same for all of these scenarios, but is different compared to the base case (S-1) scenario. With the base case S-1 scenario having the highest average measurements (1.7m/s), followed by S-15 scenario (1.7m/s), S-16 scenario (1.6m/s) and S-14 scenario (1.5m/s), while the S-13 scenario recorded the lowest value (1.5m/s). The urban roughness on the first row of the buildings in S-16 scenario ( $H_l = 15$ m) is 3m higher than S-15 scenario ( $H_l = 12$ m), which is the reason for the windward canyon in S-16 having less wind flow rate than S-15. The analysis for the locations at the left (near the leeward walls), middle and the right (near the windward walls) sides of the Tali'e Quba Road (i.e. windward canyon), in the leeward gradual increase in aspect ratio models, can be found in the Appendices from A7.38 to A7.40.

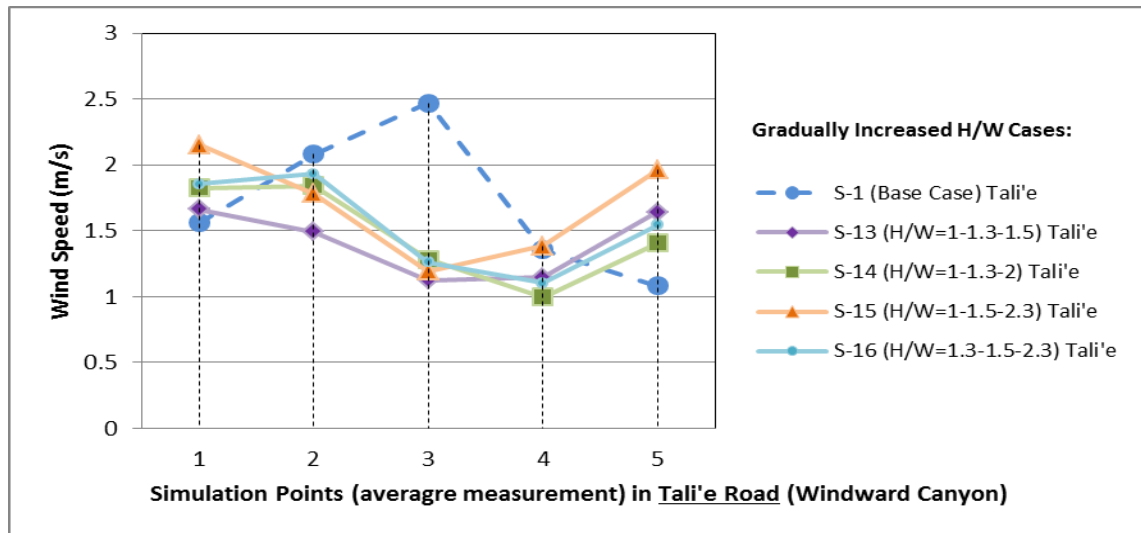


Fig. 7. 38: Overall wind speed within the Tali'e Quba Road for the leeward gradual increase in multi-asymmetrical aspect ratios cases at five measurement locations, & compared with the base case (S-1).

On the other hand, in the leeward canyon (i.e. the Nazil Quba Road), the average measurement of wind velocity is improved from 0.7m/s to 1.2m/s (i.e. 89.2%) in S-13 scenario ( $H/W$  of 1–1.3–1.5), to 1.8m/s (i.e. 146.2%) in S-14 scenario ( $H/W$  of 1–1.3–2), to 1.4m/s (i.e. 110.8%) in S-15 scenario, and to 1.5m/s (i.e. 135.4%) in S-16 scenario, as

illustrated in Figure 7.39. This is because the leeward canyon in these scenario has lower leeward elevations on the second row of buildings compared to the base case, which has allowed more wind to flow over the buildings towards the third row of buildings, where higher windward elevations are proposed, thus higher wind drag ratio to the ground level.

Figure 7.39 demonstrates that the wind velocity pattern in the leeward canyon (i.e. Nazil Quba Road) is somewhat similar for all of these scenarios. With S-14 scenario having the highest average measurement (1.6m/s), followed by S-16 scenario (1.53m/s), S-15 scenario (1.4m/s) and then S-13 scenario (1.2m/s), while the base case S-1 scenario recorded the lowest value (0.7m/s). The wind velocity analysis for the locations at the left (near the leeward walls), middle and the right (near the windward walls) sides of the Nazil Quba Road (i.e. leeward canyon), in the leeward gradual increase in aspect ratio models, can be found in the Appendices from A7.41 to A7.43.

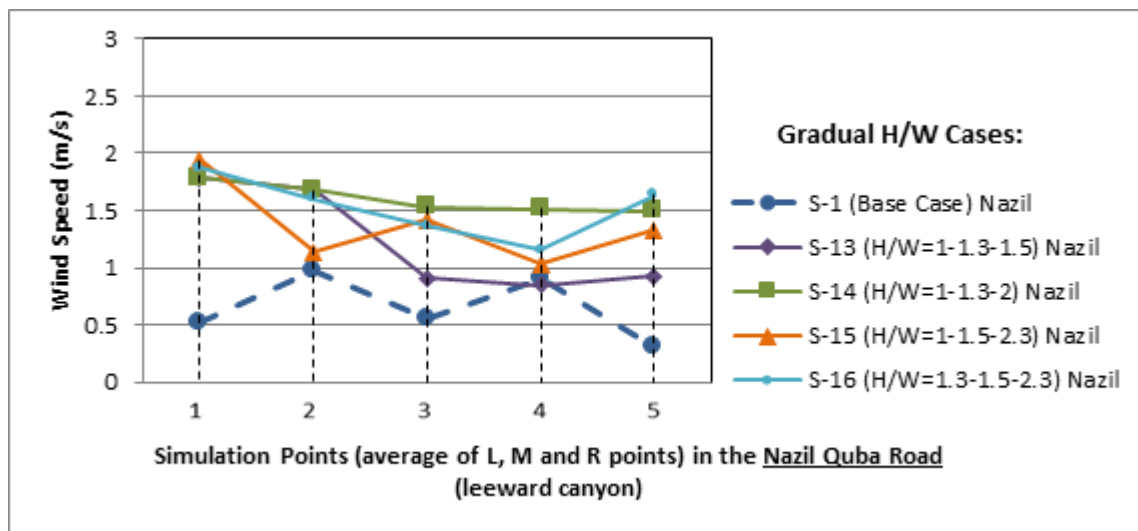


Fig. 7. 39: Overall wind speed within the Nazil Quba Road for the leeward gradual increase in multi-asymmetrical aspect ratios cases at five measurement locations, & compared with the base case (S-1).

Although S-14 has achieved an improvement of 146.2% in this category, it is 13% lower than previously simulated S-11 scenario ( $H/W$  of 1–1.3–2.3) in the higher aspect ratio category. Thus, under the local planning constraints (i.e. maximum building height and land footprint), S-11 strategy is recommended for Quba Road for improving the wind velocity at the pedestrian level.



#### 7.4.4.2. Air Temperature at the Pedestrian Level (S-13, S-14, S-15, S-16)

Figure 7.40 analyses the contours of air temperature in degrees ( $^{\circ}\text{C}$ ) for the leeward gradual increase in multi-asymmetrical aspect ratios scenarios (S-13 through S-16), and compared with the base case (S-1) results at the pedestrian level.

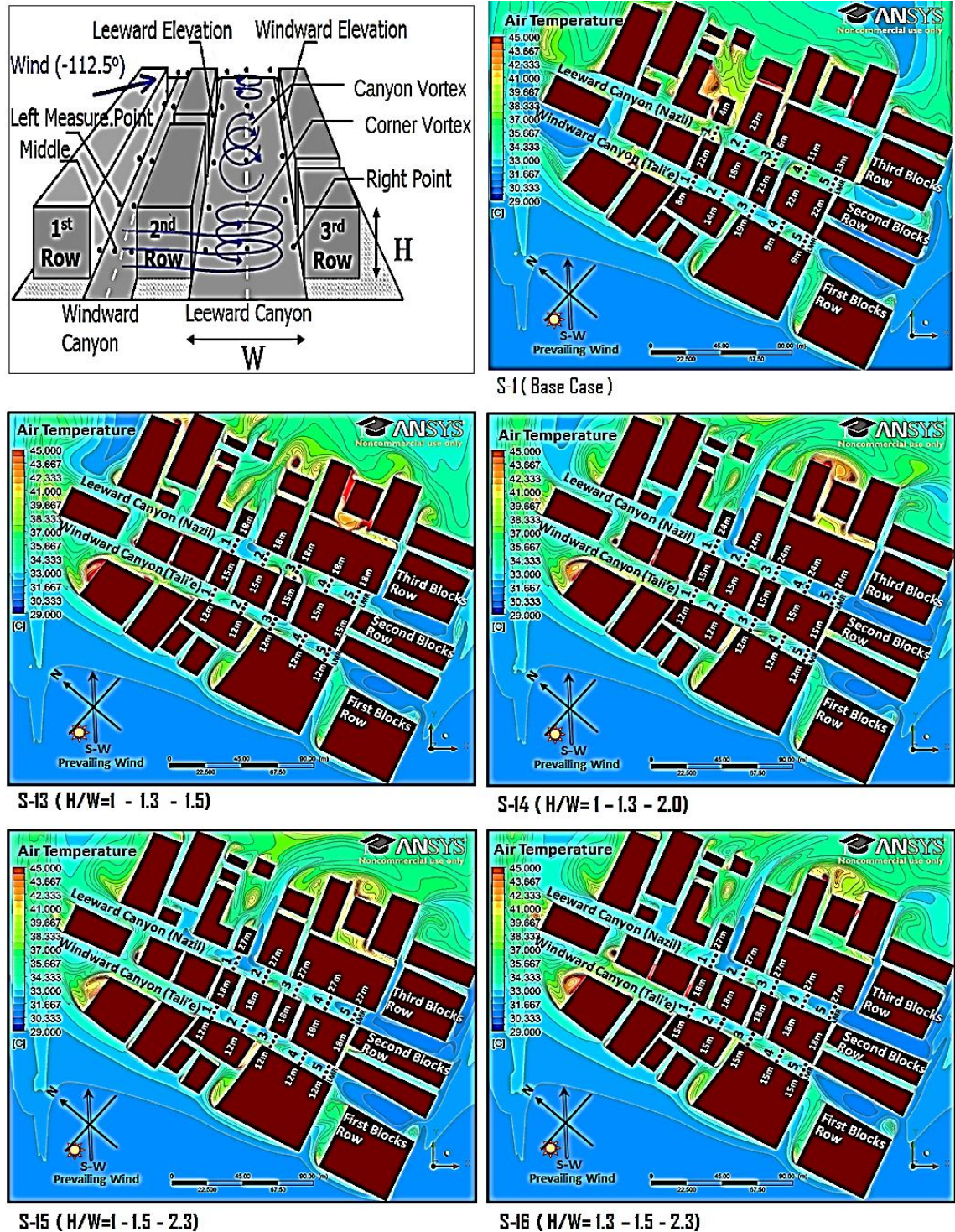


Fig. 7. 40: Contours of air temperature in degrees ( $^{\circ}\text{C}$ ) at the pedestrian level for the cases of leeward gradual increase in aspect ratios on the three rows of buildings, & compared with the base case (S-1).

In the windward canyon (i.e. Tali'e Quba Road), the comparative analysis indicates that the overall air temperature in S-13 scenario ( $H/W$  of 1–1.3–1.5) similar to the base case at the measurement locations with a value of  $34.0^{\circ}\text{C}$ , while in the S-14 scenario ( $H/W$  of 1–1.3–2) the temperature is slightly increased to  $34.1^{\circ}\text{C}$  (i.e. 0.3%), as illustrated in Figures 7.42 and 7.43. In the S-15 scenario ( $H/W$  of 1–1.5–2.3) and S-16 ( $H/W$  of 1.3–1.5–2.3) compared to the base case (S-1), the pedestrian level air temperature is slightly improved to an average measurement of  $33.6^{\circ}\text{C}$  (i.e. 1.4%) and  $33.7^{\circ}\text{C}$  (0.9%), respectively. Thus, it is observed that the configuration of these scenarios of the leeward gradual increase in multi-asymmetrical aspect ratios has minor improvement on the pedestrian air temperature level within the windward canyon compared to the existing conditions (S-1).

Figure 7.41 shows that the air temperature in the windward canyon (Tali'e Quba Road) follows the same temperature pattern in all of these scenarios, and is almost similar pattern to the base case (S-1) scenario. With S-15 scenario having the lowest average measurement ( $33.6^{\circ}\text{C}$ ), followed by S-16 scenario ( $33.7^{\circ}\text{C}$ ), S-13 scenario ( $34.0^{\circ}\text{C}$ ), and then the base case S-1 scenario ( $34.0^{\circ}\text{C}$ ), while S-14 scenario recorded the highest value ( $34.1^{\circ}\text{C}$ ).

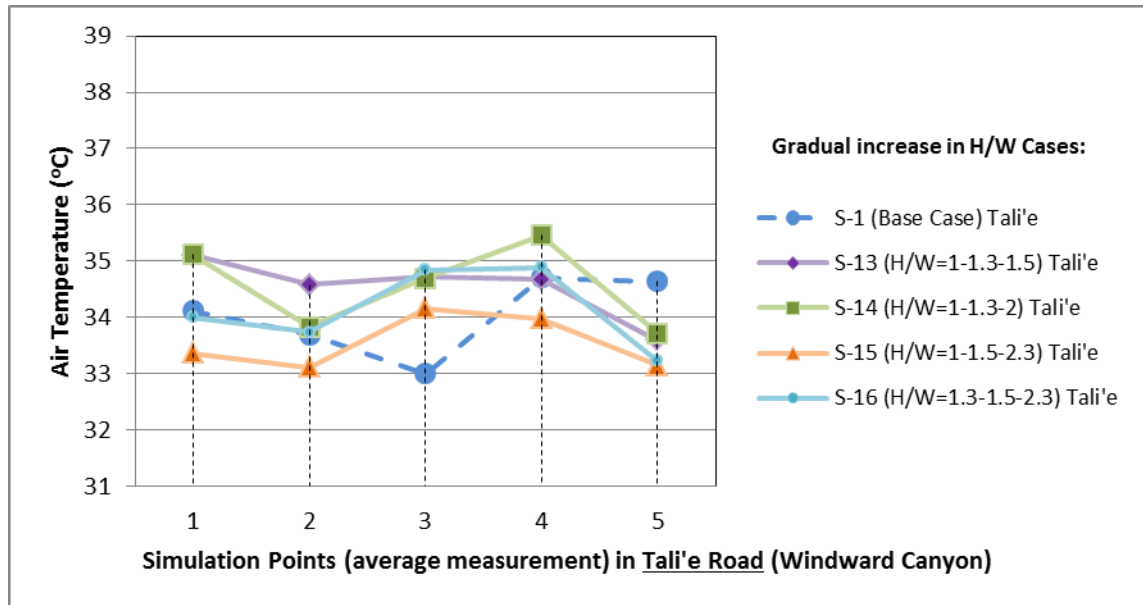


Fig. 7. 41: Overall air temperature within the Tali'e Quba Road for the leeward gradual increase in multi-asymmetrical aspect ratios cases at five measurement locations, & compared with the base case.

The analysis for the locations at the left, middle, and the right sides of the Tali'e Quba Road (i.e. windward canyon) can be found in the Appendices from A7.44 to A7.46.

On the other hand, Figure 7.42 demonstrates that in the leeward canyon (i.e. the Nazil Quba Road), the average measurement of air temperature is improved in most of these scenarios compared to the base model. The comparative analysis indicates that the overall air temperature within the leeward canyon (i.e. Nazil Quba Road) is improved from the average measurement of 36.1°C to 34.8°C (i.e. 4%) in S-13 ( $H/W$  of 1–1.3–1.5), 33.0°C (i.e. 9%) in the S-14 scenario ( $H/W$  of 1–1.3–2), 33.4°C (i.e. 8%) in S-15 ( $H/W$  of 1–1.5–2.3), and to 32.9°C (i.e. 9%) in S-16 ( $H/W$  of 1.3–1.5–2.3), as illustrated in Figures 7.42. It is found that the air temperature pattern in the leeward canyon (i.e. the Nazil Quba Road) is similar in the S-14, S-15 and S-16 scenarios as they have high windward elevations (above 24m), while is different in S-13 due to averaged windward elevations (18m), particularly on the third row of the buildings. The S-16 scenario is having the lowest average temperature measurement (32.9 °C), followed by S-14 scenario (33.0 °C), S-15 scenario (33.4 °C) and then S-13 (34.8 °C), while the base case S-1 scenario obtained the highest value (36.1 °C). The analysis for the locations at the left, middle, and the right sides of the canyons can be found in the Appendices from A7.47 to A7.49.

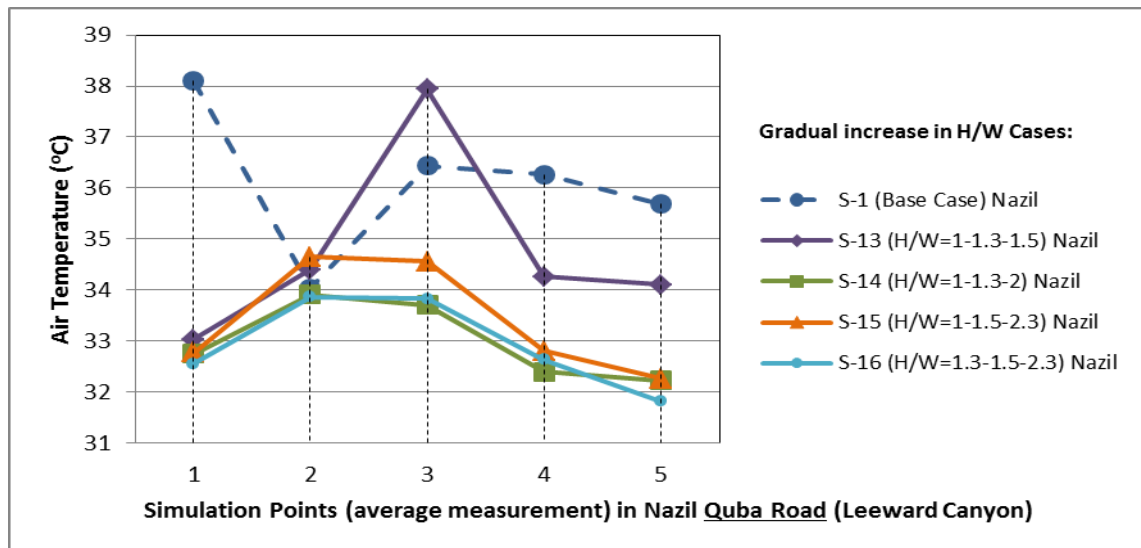


Fig. 7. 42: Overall air temperature within the Nazil Quba Road for the leeward gradual increase in multi-asymmetrical aspect ratios cases at five measurement locations, & compared with the base case.



Although S-16 and S-14 have achieved an improvement of 9% in this category, it is 1% lower than the previously simulated S-11 scenario ( $H/W$  of 1–1.3–2.3) in the higher aspect ratio category. Nevertheless, the results agree with the findings of Qaid and Ossen (2014:18) that “*the tall buildings of the asymmetrical street play an important role in enhancing wind velocity at street level [...] and have ability to enhance air flow and to release confined heat*”.

## 7.5. Assessment of Pedestrian Thermal Comfort Conditions of the Best Aspect Ratios Model

This section analysis pedestrian thermal comfort conditions for the base case and the proposed asymmetrical urban canyons’ aspect ratio models, based on data obtained from the CFD simulation. The pedestrian thermal comfort is expressed by means of the physiologically equivalent temperature (PET) index (refer to section 3.5). PET temperature was calculated using the RayMan model, proposed by Matzarakis et al., (2007). RayMan software simply takes inputs of the thermal comfort key factors (refer to section 5.7 in the Methodology Chapter). The main microclimatic factors that are used in the calculation of PET temperature for Quba Road are: the air temperature, wind velocity, mean radiant temperature MRT, and relative humidity. In addition, the following personal factors with their estimated values are also used in this calculation, which are: the human metabolic rate with a value of 1.9met for a walking activity level, and the summer clothing insulation value of 0.59clo (e.g. Yahia and Johansson, 2013a). PET index has been calibrated for hot arid regions by Yahia and Johansson (2013a), particularly in built up areas, with upper limit of 31.3°C and lower limit of 21°C.

The air temperature and wind velocity in the base model (S-1) were obtained from the CFD simulation results (as presented in the above sections). While, the relative humidity and the MRT values were excluded from the simulation for the simplification purpose due to the research time constraints, which may limit the accuracy of the predicted thermal comfort in the Base Model (S-1). Nevertheless, the relative humidity is assumed to be equalled to 8.2%, which was obtained from the field measurement data in April at 15:00 in the high urban density area (refer to Chapter 6). This assumption is based on a previous study by Ali-Toudert and Mayer (2006) on hot arid regions, due to no source of water exchange is available in the simulated models (i.e. water-proof surfaces, with no trees or water plants), and thus air humidity would not experience significant changes to thermal comfort.



The MRT was calculated during the field measurement in the current research, and a difference value of 1.7°C at 15:00 was found higher than the air temperature in April (average measurement of 11 days, refer to Table A6.1 in the appendices). Therefore, the MRT is assumed in the simulation process to be 1.7°C higher than the simulated air temperature in the proposed models.

### 7.5.1. PET Temperature at the Pedestrian Level in the Base Case (S-1)

Figure 7.43 shows the PET temperatures in the Tali'e Quba Road (the windward canyon) for the base case S-1 model at five simulated locations (E-1 to E-5), which are following almost similar pattern for the three measurement sides (left, middle and right) of the canyon. It is found that:

- The middle side of the canyon having the lowest average measurement of PET temperature of 32.8°C, as a result of the higher wind velocity value (1.9m/s) found along this measurement compared to the sides of the canyon;
- Followed by the measurements on the right (at the windward elevations) 32.9°C,
- While the ones at the left side of the canyon (near the leeward elevations) simulated the highest average measurement of 35.4°C, as a result of the lower wind velocity value (1.6m/s) found at this side of the canyon compared to the other sides, at the pedestrian height.

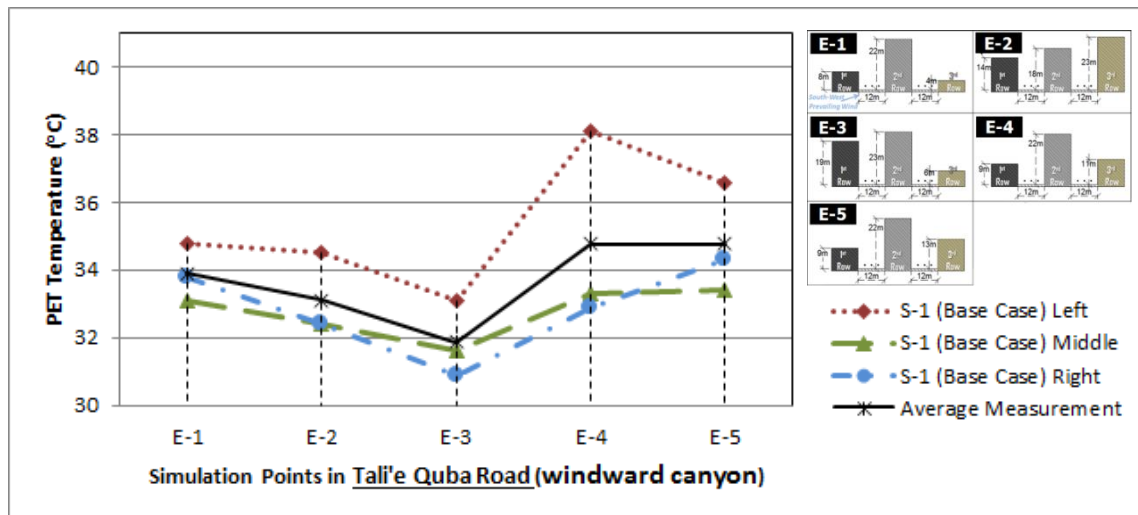


Fig. 7. 43: PET pattern for the windward canyon in the base case (S-1) scenario.

Figure 7.44 shows the PET temperature pattern in the Nazil Quba Road (the leeward canyon), which is almost similar for the three measurement sides (left, middle and right). It is found that:

- The right side of the leeward canyon (at the windward elevations) having the lowest average measurement of PET temperature 35.9°C,
- Then followed by the measurement on the middle with an average value of 36.7°C,

- While the ones at the left side of the leeward canyon (near the leeward elevations) obtained the highest PET values with an average measurement of 37.3°C.

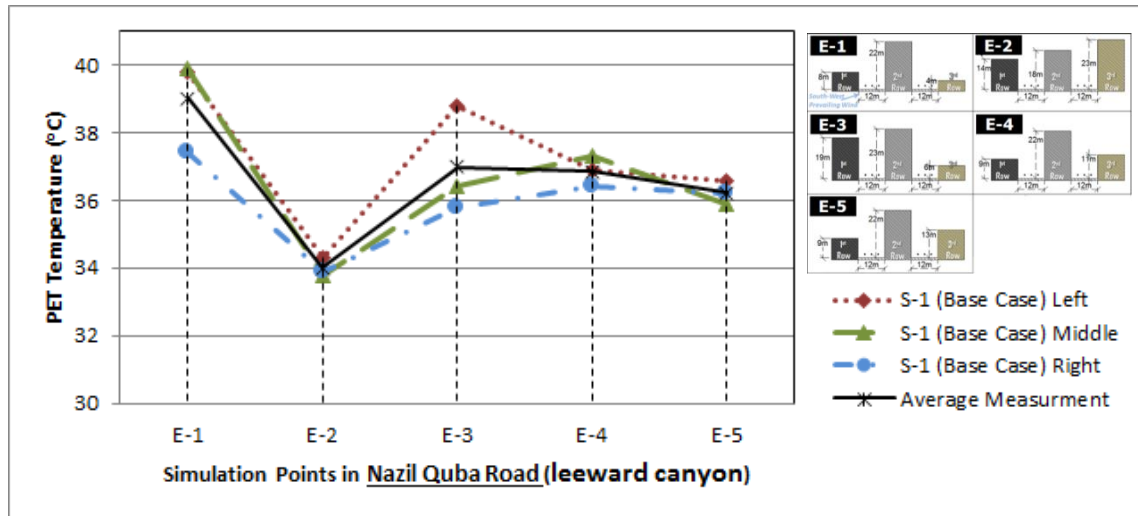


Fig. 7. 44: PET pattern for the leeward canyon in the base case (S-1) scenario.

### 7.5.2. PET Temperature at the Pedestrian Level in the Best Asymmetrical Aspect Ratio Model (S-11)

This section presents analyses the thermal comfort conditions in the leeward canyon (i.e. Nazil Quba Road) for the locations at the left (near the leeward walls), middle and the right (near the windward walls) sides of the canyon, particularly for the best aspect ratio scenario, and compared to the base case. The PET temperature values for the above investigated 16 scenarios (S-1 through to S-16) based on different street canyon aspect ratios, as demonstrated in Table 7.3.

The optimum scenario is selected based on the best level of improvement on microclimate and thermal comfort in the leeward canyon (i.e. Nazil Quba Road). The leeward canyon is an important route for pedestrians due to its position as the direct physical linkage between two most visited religious sites in Madinah, i.e. the prophet mosque and the Quba mosque, as well as due to its significant economic factors and existence of many mosques in between these two sites.

Table 7. 3: Level of improvement in thermal comfort PET temperature in the windward and leeward canyons for the proposed aspect ratio scenarios compared to the base case.

Tali'e Quba Road (Windward Canyon)							
Category	Specification	Air Temperature	Relative Humidity	Wind Velocity	MRT	PET	Improvement level in PET compared to the base case
		°C	%	m/s	°C	°C	°C
Base Case	S-1 (existing condition)	34.03	8.20	1.71	35.73	33.70	0
Symmetrical	S-2 (H/W=1-1-1)	35.97	8.20	1.25	37.67	36.50	2.8
low asymmetrical	S-3 (H/W=1-0.8-1.3)	37.53	8.20	1.01	39.23	38.50	4.8
	S-4 (H/W=1-1.3-0.8)	34.64	8.20	1.40	36.34	34.70	1
Medium Asymmetrical	S-5 (H/W=1-1.5-1.5)	33.61	8.20	1.68	35.31	33.10	-0.6
	S-6 (H/W=1-1.3-1.8)	34.93	8.20	1.45	36.63	35.10	1.4
	S-7 (H/W=1-1.8-1.3)	33.38	8.20	1.76	35.08	32.80	-0.9
High Asymmetrical	S-8 (H/W=1-2-2)	32.79	8.20	1.95	34.49	31.80	-1.9
	S-9 (H/W=1-1.8-2.3)	33.18	8.20	1.82	34.88	32.40	-1.3
	S-10 (H/W=1-2.3-1.8)	32.50	8.20	2.01	34.20	31.40	-2.3
	S-11 (H/W=1-1.3-2.3)	34.59	8.20	1.45	36.29	34.60	0.9
	S-12 (H/W=1-2.3-1.3)	32.54	8.20	1.99	34.24	31.40	-2.3
Gradual increase	S-13 (H/W=1-1.3-1.5)	34.50	8.20	1.41	36.20	34.50	0.8
	S-14 (H/W=1-1.3-2)	34.56	8.20	1.44	36.26	34.50	0.8
	S-15 (H/W=1-1.5-2.3)	33.55	8.20	1.70	35.25	33.00	-0.7
	S-16 (H/W=1.3-1.5-2.3)	34.14	8.20	1.54	35.84	33.90	0.2

Nazil Quba Road (Leeward Canyon)							
Category	Specification	Air Temperature	Relative Humidity	Wind Velocity	MRT	PET	Improvement level in PET compared to the base case
		°C	%	m/s	°C	°C	°C
Base Case	S-1 (existing condition)	36.10	8.20	0.65	37.80	36.7	0
Symmetrical	S-2 (H/W=1-1-1)	37.62	8.20	0.75	39.32	38.6	1.9
low asymmetrical	S-3 (H/W=1-0.8-1.3)	33.34	8.20	1.61	35.04	32.8	-3.9
	S-4 (H/W=1-1.3-0.8)	38.23	8.20	0.57	39.93	39.2	2.5
Medium Asymmetrical	S-5 (H/W=1-1.5-1.5)	37.35	8.20	0.56	39.05	38.2	1.5
	S-6 (H/W=1-1.3-1.8)	33.56	8.20	1.46	35.26	33.1	-3.6
	S-7 (H/W=1-1.8-1.3)	36.91	8.20	0.60	38.61	37.7	1
High Asymmetrical	S-8 (H/W=1-2-2)	37.07	8.20	0.50	38.77	37.8	1.1
	S-9 (H/W=1-1.8-2.3)	35.42	8.20	0.86	37.12	35.8	-0.9
	S-10 (H/W=1-2.3-1.8)	36.38	8.20	0.79	38.08	37	0.3
	S-11 (H/W=1-1.3-2.3)	32.67	8.20	1.75	34.37	31.8	-4.9
	S-12 (H/W=1-2.3-1.3)	36.24	8.20	0.74	37.94	36.9	0.2
Gradual increase	S-13 (H/W=1-1.3-1.5)	34.75	8.20	1.23	36.45	34.9	-1.8
	S-14 (H/W=1-1.3-2)	32.99	8.20	1.60	34.69	32.3	-4.4
	S-15 (H/W=1-1.5-2.3)	33.41	8.20	1.37	35.11	33	-3.7
	S-16 (H/W=1.3-1.5-2.3)	32.94	8.20	1.53	34.64	32.2	-4.5

Table 7.3 demonstrates the levels of improvement in the thermal comfort PET temperature for the proposed aspect ratio models in the windward and leeward canyons, and compared with the base case S-1 scenario, particularly at the pedestrian level. The best performance has the highest improvement level in PET temperature, air temperature and wind velocity. The S-11 scenario ( $H/W$  of 1–1.3–2.3) has obtained the optimum thermal performance in the current research, as it has significantly improved the PET temperature from the average measurement of:

- 36.7°C (i.e. the base case) to 31.8°C (i.e. enhanced by 13% or -4.9°C), particularly in the leeward canyon (i.e. Nazil Quba Road),
- While this configuration has almost no difference in PET temperature in the windward canyon (i.e. Tali'e Quba Road) with a value of 34.6°C compared to the base case S-1 model of the existing situation with a value of 33.7°C (i.e. PET temperature increased by 0.9°C).

Similarly, the other scenarios that share the strategy of gradual increase in aspect ratios have also enhanced the PET temperature in the leeward canyon (i.e. Nazil Quba Road), with a difference improvement values of:

- -4.5°C (i.e. 12%) in the S-16 scenario (with  $H/W$  of 1.3–1.5–2.3);
- -4.4°C (i.e. 12%) in the S-14 scenario (with  $H/W$  of 1–1.3–2), then followed by
- -3.7°C (i.e. 10%) in the S-15 scenario (with  $H/W$  of 1–1.5–2.3), then
- -3.6°C (i.e. 10%) in S-6 scenario (with  $H/W$  of 1–1.3–1.8).
- -1.8°C (i.e. 5%) in S-13 scenario (with  $H/W$  of 1–1.3–1.5).

On the other hand, the S-10 scenario ( $H/W$  of 1–2.3–1.8) and S-12 scenario ( $H/W$  of 1–2.3–1.3), with higher building heights on the middle row, can improve the PET temperature in the windward canyon by reducing 2.3°C in both scenarios from the average measurement of 33.7°C to 31.4°C, but do not improve the thermal sensation condition in the leeward canyon. Note that the leeward canyon is the direct link between the two most visited mosques in the city, and most of the local mosques and shops are aligned within the third row of the buildings, thus attracting more pedestrians and shoppers to use the leeward canyon (i.e. Nazil Quba Road). Therefore, it is important to improve the thermal comfort conditions in the leeward canyon to extend the use of the canyon (or the outdoor spaces).

Figure 7.45 shows the PET temperature pattern in the leeward canyon (Nazil Quba Road) for the five measurement locations (1 through 5) in the optimum aspect ratio configuration represented by S-11 scenario (with  $H/W$  of 1–1.3–1.5), and compared to the base case S-1 scenario (i.e. existing configurations). The PET temperature values calculated from the measurement locations at the left (near the leeward walls), middle and the right (near the windward walls) sides of the canyon.

It is found that the PET temperature pattern in the leeward canyon (i.e Nazil Quba Road) is almost similar for the three rows of measurement points in S-11 but different from the base model S-1 scenario. The middle side of the canyon having a lower average PET value of 31.1 °C, followed by the right side (near the windward elevations) with an average measurement value of 31.2°C, while the left side of the canyon (near the leeward elevations) obtained a higher value of 32.9 °C. The analysis for the windward canyon (Tali'e Quba Road) locations along the left (near the leeward walls), middle and the right (near the windward walls) sides of the canyon shows little effect of S-11 scenario on PET temperature, as illustrated in the Appendix A7.50.

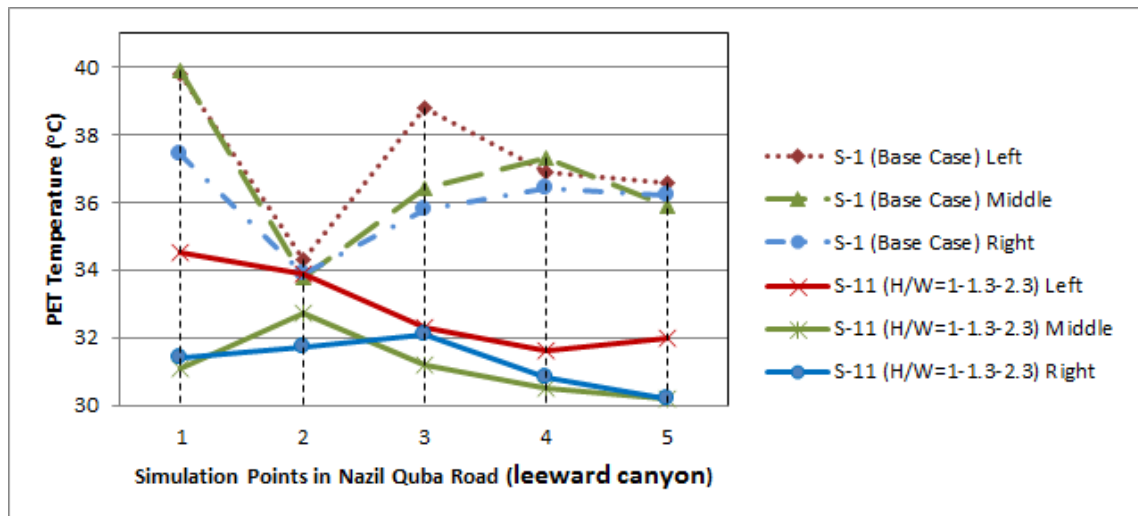


Fig. 7. 45: PET index temperature within the Nazil Quba Road for the best multi-asymmetrical aspect ratio scenario (S-11), at three sides of the canyon along five measurement locations, & compared with the base case.

In comparison to the base case S-1 model, it can be observed that there is a noticeable improvement in PET temperature values in S-11 scenario along the three sides of the leeward canyon (Nazil Quba Road). Thus, based on the simulation measurements of air temperature, wind velocity and thermal comfort improvement level, the optimum multiple asymmetrical aspect ratios scenario is found to be the scenario S-11 with  $H/W$  ratios of 1–1.3–2.3, with building heights of 12m-15m-27m. Thus, S-11 scenario is recommended for enhancing pedestrian microclimates (reduces the air



temperature by 3.4°C and increases wind velocity by 1.1m/s, i.e. 169.2% of improvement) in multiple street canyons and mitigating urban heat stress as it reduces thermal sensation level by 4.9°C in PET.

## 7.6. Summary

In this chapter, variations of building heights to street width H/W aspect ratios in each of three rows of buildings were tested on the base case, to predict their impact on enhancing urban pedestrian microclimatic conditions and pedestrian thermal comfort level. Wind velocity and air temperature analysis are compared to the performance of the multi-asymmetrical aspect ratios as well as multi-symmetrical aspect ratios of the three rows of buildings (with two urban street canyons).

Enhancement was achieved on the performance of pedestrian level wind velocity and air temperature in the leeward street canyon (i.e. Nazil Quba Road), with thermal comfort improvement percentage of 13% (i.e. -4.9°C in PET) from 36.7°C to 31.8°C PET. Yahia and Johansson (2013a) calibrated the PET index threshold for hot arid urban environments with the upper limit of 31.3°C and lower limit of 21°C. However, the obtained average PET temperature of 31.8°C in the leeward canyon in S-11 scenario (i.e. the optimum scenario) is slightly (i.e. 0.5°C PET) above the upper limit of the recommended thermal comfort threshold.

The specification of the proposed optimum aspect ratio scenario (S-11) was H/W of 1 – 1.3 – 2.3, with buildings height of 12m on the first row of buildings, followed gradual height of 15m on the second row, with the maximum height of 27m to be configured on the third row of buildings. The maximum building height of 27m is the constraint of the research based on the local planning and regulations for Quba urban areas.

However, it was found that, due to the approximately perpendicular prevailing wind direction to Quba Road canyons and the building heights on the middle row of the buildings are higher than the other rows in the existing configuration, these are blocking wind from reaching to the leeward canyon (i.e. Nazil Quba Road) at the pedestrian level. In addition, due to a low speed of approaching wind flow in Madinah (4.7m/s in April and 3.1m/s yearly average wind flow at the airport), the enhancement in the performance of wind velocity in the windward canyon (i.e. Tali'e Quba Road) is little in

S-11 scenario (H/W of 1 – 1.3 – 2.3). Nevertheless, the findings of the leeward canyon (i.e. Nazil Quba Road) revealed that a small incremental increase in wind velocity (e.g. 1.1m/s) can lead to a significant improvement in thermal comfort level (e.g. by  $-4.9^{\circ}\text{C}$ ).

Moreover, the lower and intermediate asymmetric street aspect ratios scenarios are incompatible with hot arid regions as they offer conflicting properties during the day times. Higher aspect ratios of asymmetrical street canyons, when facing the wind's direction or solar elevations, are better than symmetrical and low asymmetrical canyons height in enhancing wind flow pattern at a pedestrian level, and reducing exposure to solar radiation at ground level. Therefore, mitigating urban heat stress or enhancing thermal comfort conditions in asymmetrical streets is based on position of higher aspect ratios which capture winds or provide shades. In north-south orientation of urban canyons, intermediate aspect ratio of 1 – 1.3 – 1.8 in S-6 scenario reduces the afternoon peak thermal microclimate in a canyon between the second and the third rows of buildings yet the negative effects in a canyon between the first and second rows of buildings are greater than the positive effects in the followed canyon.

In addition, higher aspect ratios of 1 – 2.3 – 1.8 in S-10 scenario and 1 – 2.3 – 1.3 in S-12 scenario, with higher wall elevation on the middle row of the buildings than the side rows, can reduce  $1.5^{\circ}\text{C}$  of the air temperature conditions and enhance 17% of wind conditions (from 1.7m/s to 2m/s) in the windward canyon (between the first two rows of buildings, i.e. Tali'e Quba Road) and improve thermal comfort by  $2.3^{\circ}\text{C}$  PET. But in the leeward canyon, S-10 and S-12 have no improvement in microclimate and thermal comfort conditions. This is due to the similarity of building height configuration on the three rows of the buildings compared to the existing situation (i.e. the middle row of the buildings having higher height than the side rows).

Thus, S-11 scenario with H/W of 1 – 1.3 – 2.3 is recommended for enhancing pedestrian microclimates (reduces the air temperature by  $3.4^{\circ}\text{C}$  and increase 1.1m/s, i.e. 169.2% of wind velocity) in multiple street canyons and mitigating urban heat stress (reduces thermal sensation level by  $4.9^{\circ}\text{C}$  in PET).

Future studies are needed to test the effects of increasing buildings height to above 27m on wind flow, recommending planning policies change. This is to provide broader knowledge for official planners to consider when developing the city.

# **CHAPTER 8: Further Analysis and Design**

## **Implications (based on the Best Proposed H/W Model)**

### **Chapter Structure**

- 8.1. Introduction
- 8.2. Variation of Wind Flow at Night and Noon
- 8.3. Increasing the Number of Buildings' Rows
- 8.4. Orientation of Urban Canyon Geometry
- 8.5. Configuration of New Streets Perpendicular to Quba Canyons
- 8.6. Removal of Buildings
- 8.7. Protruding Upper Floors for Shading
- 8.8. Changes to Surface Albedo
- 8.9. Changes to Block Patterns
- 8.10. Implementation of the Research for Future Planning
- 8.11. Summary

# Chapter 8:

## Further Analysis and Design Implications (based on the Best Proposed H/W Model)

### 8.1. Introduction

This chapter further investigates a chosen multi-asymmetrical aspect ratios model based on its best performance level on enhancing urban microclimate and thermal comfort in Quba Road. Figure 8.1, illustrate the improved urban aspect ratio model, named here as the best proposed model represented in S-11 scenario with  $H/W$  of  $1 - 1.3 - 2.3$  (i.e. leeward gradual increase in building height ( $H$ ) of 12m – 15m – 27m with street width ( $W$ ) of 12m) (refer to section 7.4.3 in Chapter 7).

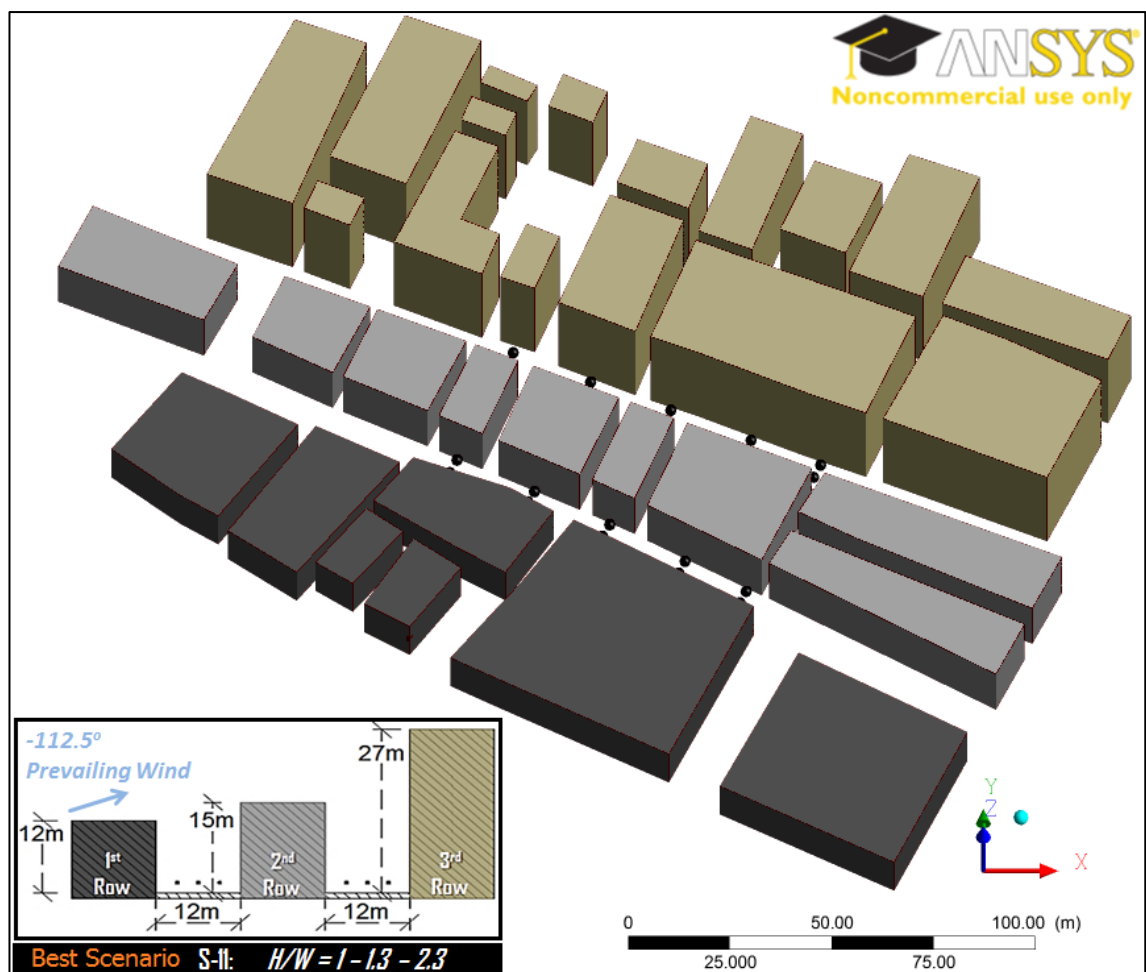


Fig. 8. 1: The best multi-asymmetrical aspect ratios scenario (S-11).

In this chapter, the S-11 model is further investigated with 8 more scenarios to evaluate their configuration effects on the urban wind flow rate, seeking to find ways to improve the urban pedestrian microclimate (i.e. objective 6 in section 1.4). These scenarios (S-17 through S-24), are as follows:

- S-17 scenario on evaluating the variation of wind flow at night for the best proposed H/W model, to find out its effects on the night time microclimate (e.g. Qaid and Ossen, 2014);
- S-18 and S-19 scenarios on increasing the number of buildings' rows (e.g. Lee et al., 2013; Rizk and Henze, 2010), to find out wind flow variation in the leeward area;
- S-20 and S-21 scenarios on orientation of urban canyons with different wind directions (e.g. Yuan and Ng, 2012), to find out their effects on wind flow rate in Quba Road; and
- S-22 through S-24 scenarios on configuring new streets perpendicular to the existing canyons (e.g. Golany, 1996), to find out whether they can further improve the wind flow in Quba Road.

The main focus here is on analysing the microclimate of the leeward canyon (i.e. Nazil Quba Road). The results of the windward canon are excluded as the findings of the multi-asymmetrical aspect ratios in S-11 model demonstrated minor improvement on the pedestrian microclimate compared to the existing conditions, while the level of improvement in the leeward canyon in the S-11 scenario is significant for air temperature ( $-4^{\circ}\text{C}$ ), wind speed ( $+1.1\text{m/s}$ ), and thermal comfort ( $-5^{\circ}\text{C}$ ).

## 8.2. Variation of Microclimate at Night (S-17) and at Noon (S-25) for the Best Proposed H/W Model

S-17Night and S-25Noon scenarios are proposed in this study to evaluate the effect of configuring the best proposed multi-asymmetrical aspect ratios (i.e. H/W of 1–1.3–2.3 in S-11 scenario) on the variation of wind flow and air temperature at night and noon, respectively. The field study in the current research indicated that the pedestrians number in the high urban density area of Quba Road increased significantly an hour before the sun set and decreased at the mid night (i.e. between 17:00 to 00:00 hours, refer to section 6.2.2), as illustrated in Figure 8.2. This was due to lower air temperature values with the absence of solar radiation. Although during the mid-day the air temperature reaches 32.0°C in the spring (to 40.0°C in the summer), the number of pedestrians are found to be increasing around the noon hour (i.e. 12pm), which is mostly to perform the noon prayer in the adjacent mosques. Therefore, it is crucial to investigate the effect of the proposed optimum model on microclimate pattern at night and noon periods.

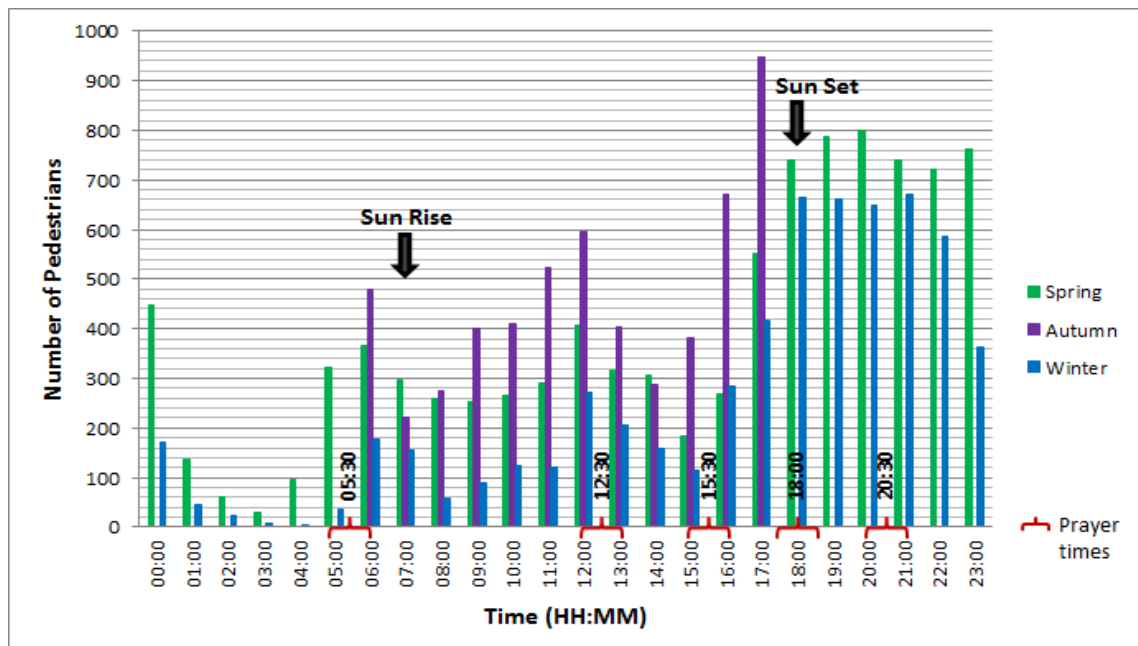


Fig. 8. 2: The number of pedestrians in a high urban density area in Quba Road, during spring, autumn, and winter seasons per 24 hours (except in autumn, between 06:00 to 17:00 hours). It shows increase of Quba road users within the five prayers time as well as during evening till 23:00 hours at night.

The results in S-17night (i.e. variation of wind flow at night) are compared with the existing situation at night (named as S-1 Night Scenario) at 21:00 hours in April (mid-season). The wind speed profile and the air temperature at the inlet boundary condition at 21:00 hours are defined as 2.9m/s and 27°C, respectively, instead of the day



time 4.7m/s and 29°C (i.e. at 15:00 hours in April, mid-season), based on the airport meteorological readings (refer to the validation section 5.6.1 in Chapter 5).

The results in S-25noon (i.e. variation of wind flow at noon) are compared with the existing conditions at noon (named as S-1 Noon Scenario) at 12:00 hours in April (mid-season). The wind speed profile and the air temperature at the inlet boundary condition are defined as 3.9m/s and 30.9°C, respectively. The study analyses the air temperature and wind velocity results that are obtained from 15 points within the leeward canyon (i.e. Nazil Quba Roads), particularly along the middle, at the right side (at windward elevations) and the left side (at the leeward elevations) of the canyons.

### 8.2.1. Wind Velocity at the Pedestrian Level (S-17Night and S-25Noon)

Figure 8.3 analyses the contours of wind velocity magnitudes (m/s) for the S-17Night scenario with the optimum H/W of 1-1.3-2.3, and compared with the existing conditions at 21:00pm (i.e. S-1 Night scenario) at the pedestrian level.

In comparison with the base case of the existing conditions at night model (S-1 Night Scenario), it is found that the wind magnitude in the leeward canyon (i.e. Nazil Quba Road) is improved in the S-17Night scenario with the optimum aspect ratios, from an average measurement of 0.4m/s (i.e. existing condition) to a value of 1.2m/s, (i.e. 183%). Thus, the optimum aspect H/W of 1-1.3-2.3 has a positive effect on enhancing wind velocity in the leeward canyon at night, while no major difference in the windward canyon, as illustrated in Figure 8.3.



Fig. 8. 3: Contours of velocity magnitude (m/s) at pedestrian height (2m) for S-17 that represents the night time (21:00pm) case based on the best H/W of (1-1.3-2.3), & compared with the night base case.

Similarly, the wind velocity in the leeward canyon (i.e. Nazil Quba Road) in S-25 Noon scenario has improved from an average measurement of 0.6m/s in the existing condition (i.e. S-1 Noon base case at 12:00pm) to a value of 1.5m/s, (i.e. 176%). Thus, the optimum aspect H/W of 1-1.3-2.3 has positive effect on enhancing wind velocity in the leeward canyon at noon, while no major difference in the windward canyon, as illustrated in Figure 8.5.

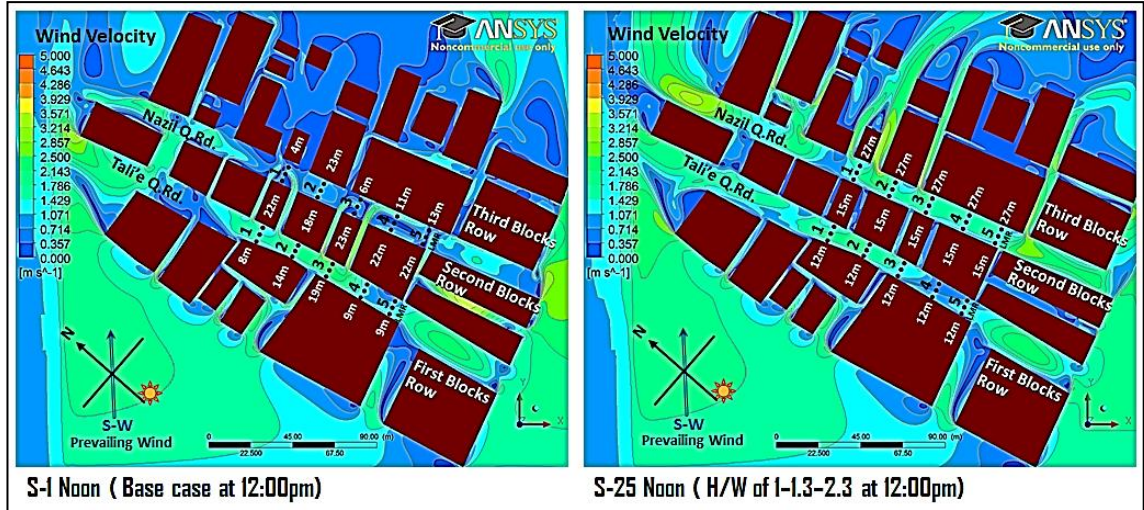


Fig. 8. 4: Contours of velocity magnitude (m/s) at pedestrian height (2m) for S-25Noon that represents the H/W of 1 – 1.3 – 2.3 at 12:00pm, & compared with the base case of the existing situation at noon.

This is because the leeward canyon in the S-17Night and S-25Noon scenarios (with optimum aspect ratios of  $H/W = 1 - 1.3 - 2.3$ ) has lower leeward elevations on the middle row of the buildings than the exiting configuration, allowing wind to flow over the buildings towards the leeward canyon (Nazil Quba Road), where the windward elevations are higher on the third row of the buildings (i.e.  $H_3 = 27\text{m}$ ) than the middle row; thus, greater wind drag towards the ground.

Figure 8.5 shows the wind velocity patterns at the pedestrian height in S-17Night scenario. The wind velocity is found to be higher in the middle of the leeward canyon (i.e. Nazil Quba Road) with an average measurement of 1.3m/s, followed by the measurements at the right side of the canyon (at the windward elevations) with an average value of 1.2m/s, while at the left side of the canyon (at the leeward elevations) has obtained the lowest wind velocity with an average measurement of 1.0m/s. The results for the windward canyon (i.e. Tali'e Quba Road) in S-17Night scenario are presented in the Figure A8.1 in the Appendices.

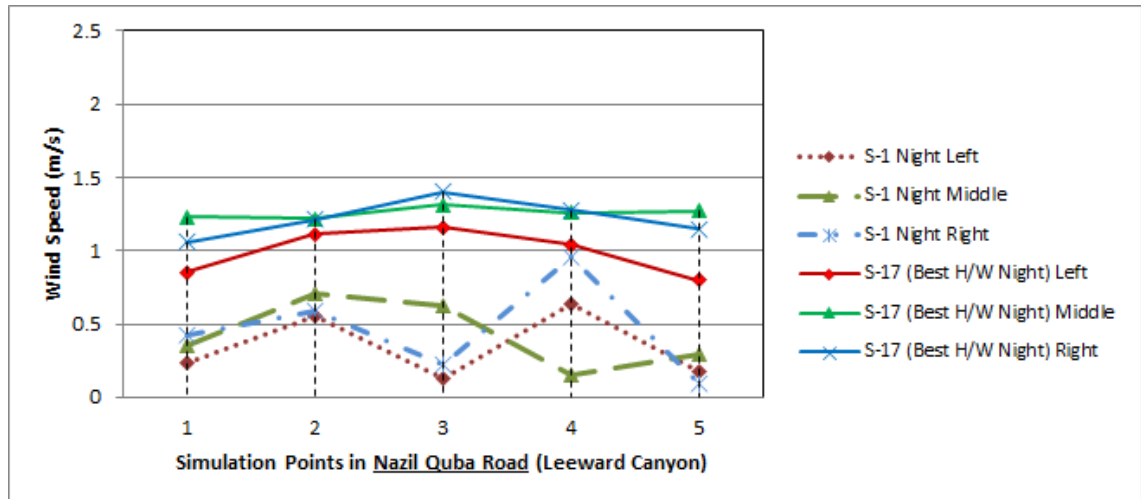


Fig. 8. 5: Wind velocity pattern at pedestrian height (2m) for S-17 that represents the night time (21:00pm) case with the best H/W of (1 – 1.3 – 2.3), and compared with the existing conditions during the night (S-1 Night), particularly for the Nazil Quba Road (leeward canyon) along five measurement locations.

Figure 8.6 shows the wind velocity patterns at the pedestrian height in S-25Noon scenario. The wind velocity is found to be higher in the middle of the leeward canyon (i.e. Nazil Quba Road) with an average measurement of 1.6m/s, followed by the measurements at the right side of the canyon (near the windward elevations) with an average measurement value of 1.6m/s, while at the left side of the canyon (near the leeward elevations) has obtained the lowest wind velocities with an average measurement of 1.3m/s.

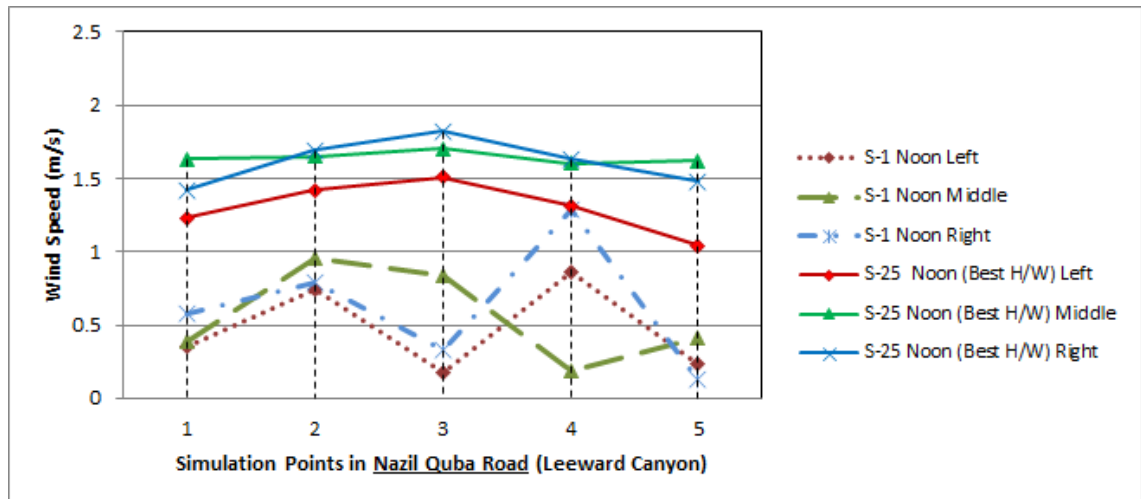


Fig. 8. 6: Wind velocity pattern at pedestrian height (2m) for S-25Noon that represents the results at noon (12:00pm) case with the optimum H/W of (1 – 1.3 – 2.3), and compared with the existing conditions during the mid-day (S-1 Noon), particularly for the Nazil Quba Road (leeward canyon).



### 8.2.2. Air Temperature at the Pedestrian Level (S-17Night and S-25Noon)

Figure 8.7 analyses the contours of air temperature for S-17Night scenario with the optimum H/W of 1-1.3-2.3, and compared with the existing conditions at 21:00pm (S-1 Night scenario) at the pedestrian level. The comparative study demonstrated that the air temperature in the leeward canyon (i.e. Nazil Quba Road) in the S-17 scenario is almost the same to the existing conditions at 21:00 hours (i.e. S-1 Night Scenario), with 0.03°C difference in temperature, as illustrated in Figure 8.8.

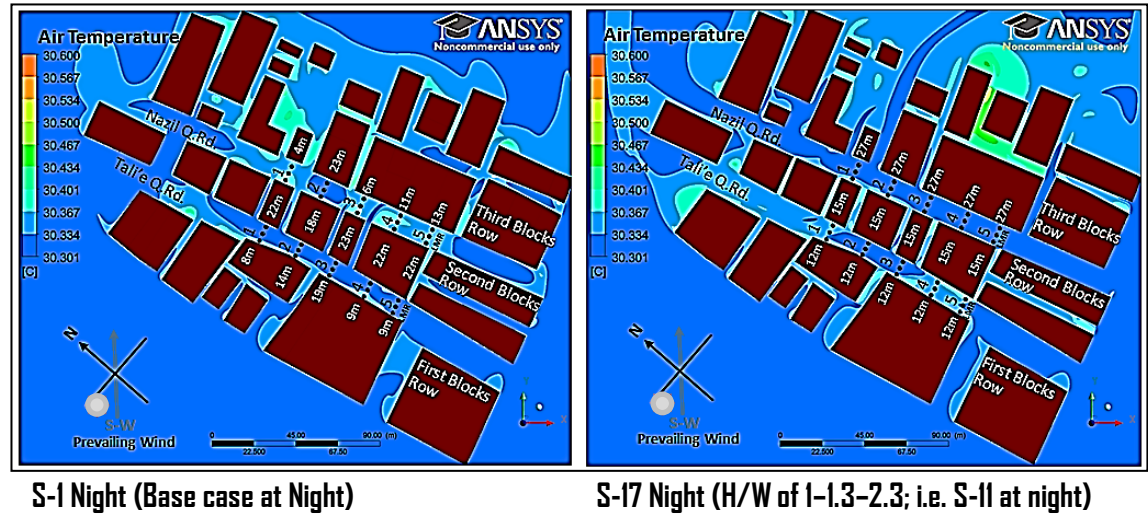


Fig. 8. 7: Contours of air temperature (°C) at pedestrian height (2m) for S-17 that represents the night time case (21:00pm) based on the optimum H/W of 1-1.3-2.3, & compared with the existing case at night.

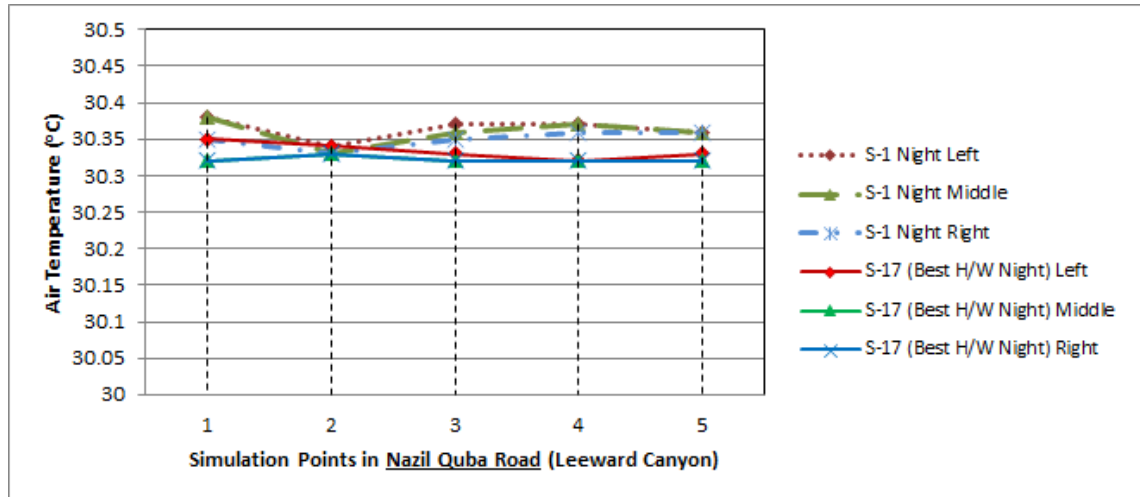


Fig. 8. 8: Air temperature at pedestrian height (2m) for S-17 that represents the night time case (21:00pm) based on the optimum H/W of 1-1.3-2.3, and compared with the S-1 Night (the existing case at night) in the leeward canyon.

A possible explanation for this could be that during the night there is no significant variation in air temperature from one measurement point to another, due to the absence of the major source of heat (i.e. the solar radiation) compared to the daytime scenarios, thus leading to minor improvement in temperature (e.g. Qaid and Ossen,

2014). The air temperature results for the windward canyon (i.e. Tali'e Quba Road), in the models of studying variation of wind flow at night, are presented in Figure A8.2 in the Appendices.

In S-25Noon scenario, the air temperature in the leeward canyon (i.e. Nazil Quba Road) has improved by  $-7.8^{\circ}\text{C}$  from an average measurement of  $45.4^{\circ}\text{C}$  found in the existing situation (i.e. S-1 Noon base case at 12:00pm) to a value of  $37.6^{\circ}\text{C}$ , (i.e. 17%), as illustrated in Figures 8.9 and 8.10. Thus, the optimum aspect H/W of 1-1.3-2.3 has positive effect on enhancing wind velocity in the leeward canyon at noon.

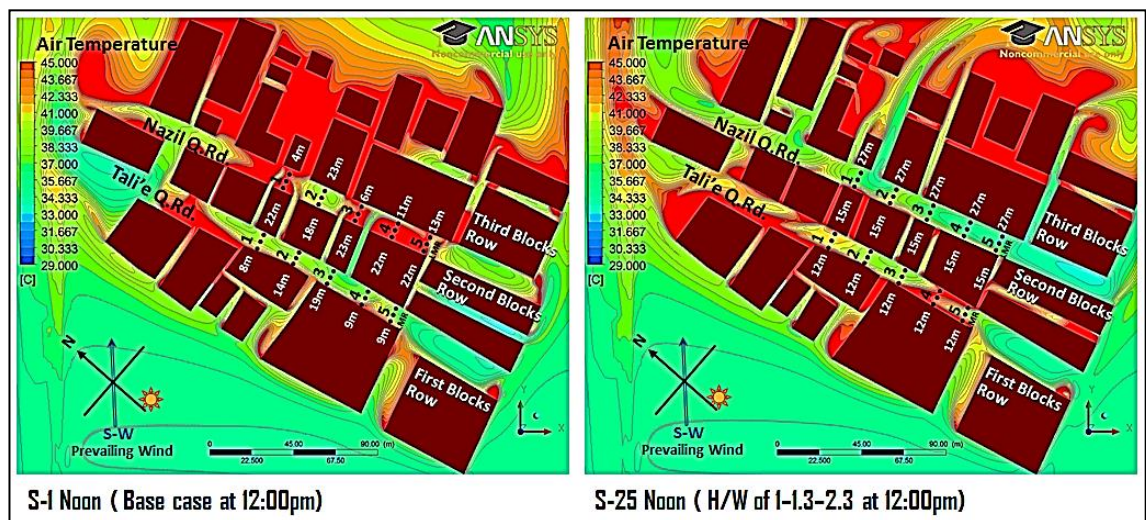


Fig. 8. 9: Contours of air temperature ( $^{\circ}\text{C}$ ) at pedestrian height (2m) for S-25Noon that represents the noon time case (12:00pm) based on the optimum H/W of 1-1.3-2.3, & compared with the existing case at noon.

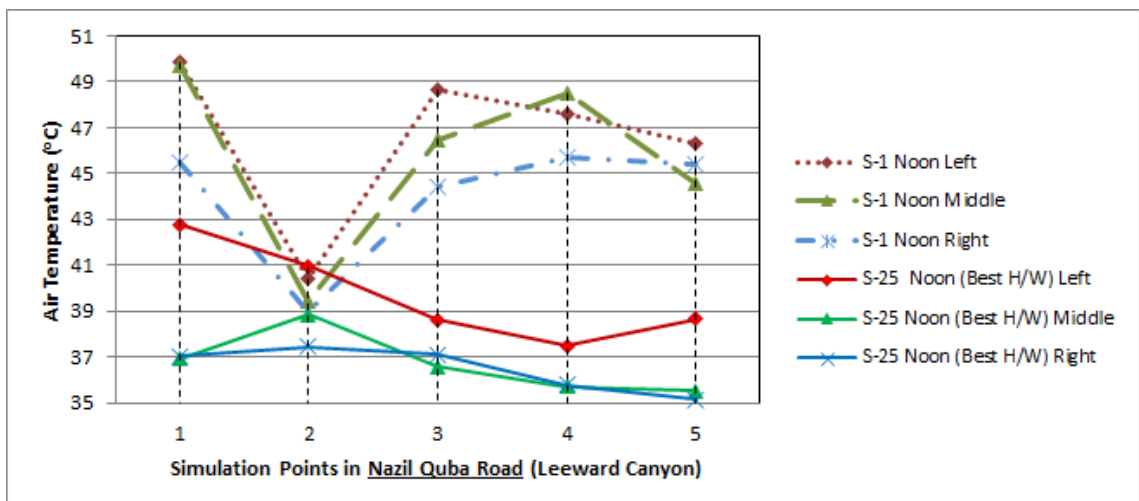


Fig. 8. 10: Air temperature in the leeward canyon for S-25Noon that represents the noon time case (12:00pm) based on the optimum H/W of 1-1.3-2.3, and compared with the S-1 Noon (existing case at noon).



The air temperature patterns in Figure 8.10 show that area at the right side of the leeward canyon (near the windward elevations) having the lowest values with an average measurement of 36.5°C, followed by the middle of the canyon with an average value of 36.7°C, while the area at the left side of the canyon (near the leeward elevations) has obtained the highest average measurement value of 39.7°C. In terms of thermal comfort conditions in S-25Noon scenario at 12:00pm, it is found that the optimum H/W of 1 – 1.3 – 2.3 can improve pedestrian thermal sensation in the leeward canyon (i.e. Nazil Quba Road) by -10°C in PET, from an average measurement PET value in the existing situation of 53°C to 43°C (i.e. 19%).

However, it is worth to mention that in the windward canyon (i.e. Tali'e Quba Road), the air temperature in S-25Noon scenario has increased by +2.55°C, from an average measurement of 39.7°C to a value of 42.3°C (i.e. 6%), as presented in Figure 8.11. This is unlike the findings that are found at 15:00 hours when the air temperature difference is found to be 0.6°C. In Terms of thermal comfort conditions in S-25Noon scenario at 12:00pm, it is found that the optimum H/W of 1 – 1.3 – 2.3 can worsen pedestrian thermal sensation in the windward canyon (i.e. Tali'e Quba Road) by +3°C in PET, from an average measurement PET value in the existing situation of 46°C to 46°C (i.e. 6%).

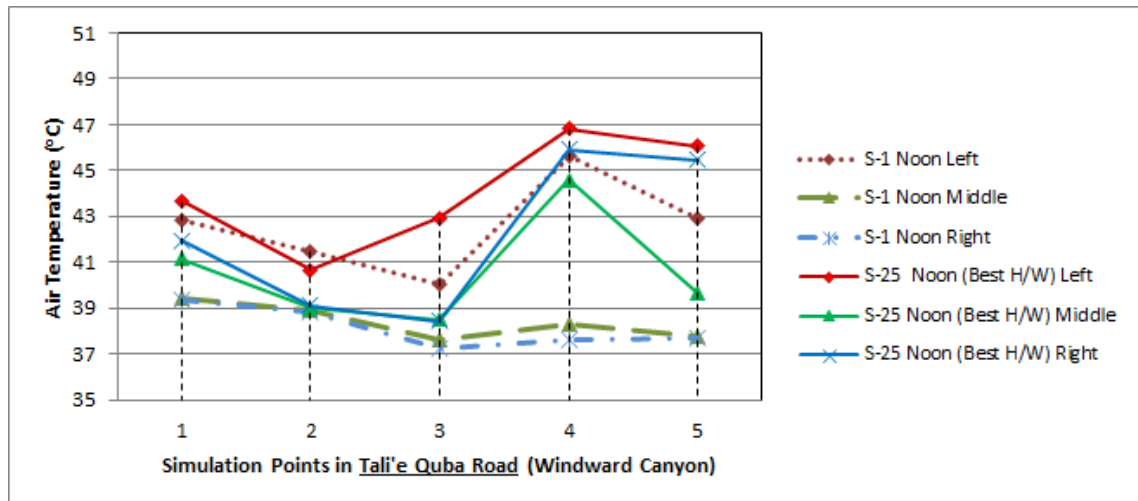


Fig. 8. 11: Air temperature in the windward canyon for S-25Noon that represents the noon time case (12:00pm) based on the optimum H/W of 1-1.3-2.3, and compared with the S-1 Noon (existing case at noon).

This could be as a result of higher level of exposure to solar radiation at 12:00 hours and lower wind velocity variations, particularly at the measurement locations 3 and 4 where wind flow is about 0.5 to 1.0 m/s lower than the existing situation, as a

result of a large building footprint size, leading to low opportunity for heat transfer by convection.

### 8.3. Increasing the Number of Buildings' Rows (S-18, S-19)

The study aims to evaluate the effects of configuring the best proposed multi-asymmetrical aspect ratio  $H/W$  of  $1 - 1.3 - 2.3$  (i.e. refer to S-11 scenario in section 7.4.3) on the microclimate conditions in the leeward urban area, beyond the third row of the buildings. Thus, three new rows of buildings are proposed in the leeward area (i.e. beyond the third row) in two scenarios (S-18 and S-19), based on buildings location style obtained from previous study by Rizk and Henze (2010), as illustrated in Figure 8.12, which are:

- S-18 scenario (Grid Style): to investigate the variation of microclimate in the leeward area for a grid style of buildings positions.
- S-19 scenario (Chess-Board Style): to investigate the variation of microclimate in the leeward area for a chess-board style of buildings position.

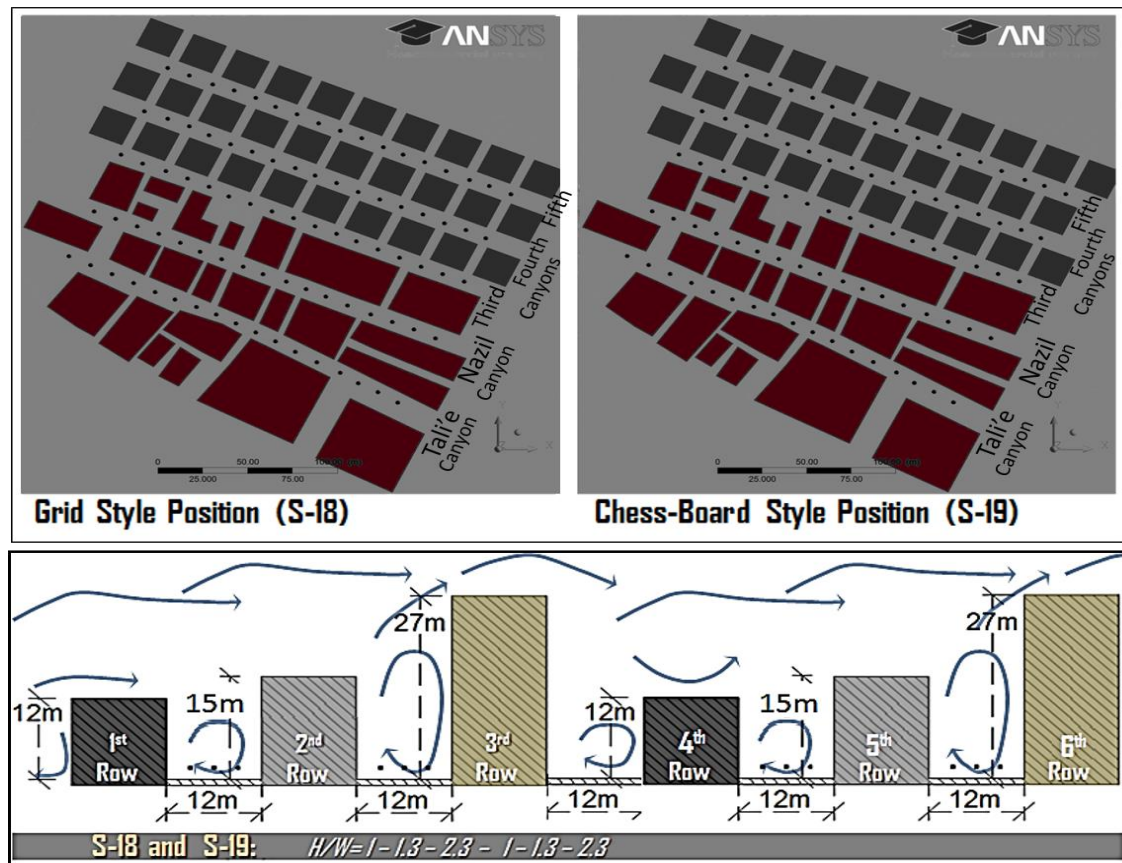


Fig. 8. 12: Increasing the number of rows of buildings to the leeward area in the best proposed aspect ratio scenario in this study. In S-18 scenario, the buildings in the new rows are positioned as grid style, while in S-19 scenario having a chess-board building position.

The buildings' heights of the three new rows in both of the S-18 (Grid Style) and S-19 (Chess-Board Style) are a duplicate of the first three rows, to share a multi-

asymmetrical aspect ratio  $H/W$  of 1–1.3–2.3 – 1–1.3–2.3. This is due to the local planning regulations that limits the maximum height to 27m, while it follows Hang et al.'s (2015) recommendation on building height variations, seeking to produce downward wind flows in front of the taller buildings.

The study of increasing the number of rows of buildings in the S-18 (Grid Style) and S-19 (Chess-Board Style) scenarios, analyses the air temperature and wind velocity results at 17 measurements points along the middle of each of the five urban canyons (the first two are the Tali'e and Nazil Quba Road canyons), as illustrated above in Figure 8.12. These scenarios (S-18 and S-19) test findings from Hang et al. (2015) of multiple urban streets, indicating that *“in the presence of building height variations, taller buildings produced stronger form drag than lower ones, producing downward helical flows in front of the taller buildings and upward helical flows behind them”*.

#### **8.3.1. Wind Velocity at the Pedestrian Level (S-18, S-19)**

Figure 8.13 shows the contours of wind velocity magnitudes (m/s) at the pedestrian level, for the increasing the number of building rows strategy in the S-18 (Grid Style) and S-19 (Chess-Board Style) scenarios, and compared with the base model of the best proposed aspect ratio (S-11 with  $H/W$  of 1-1.3-2.3).

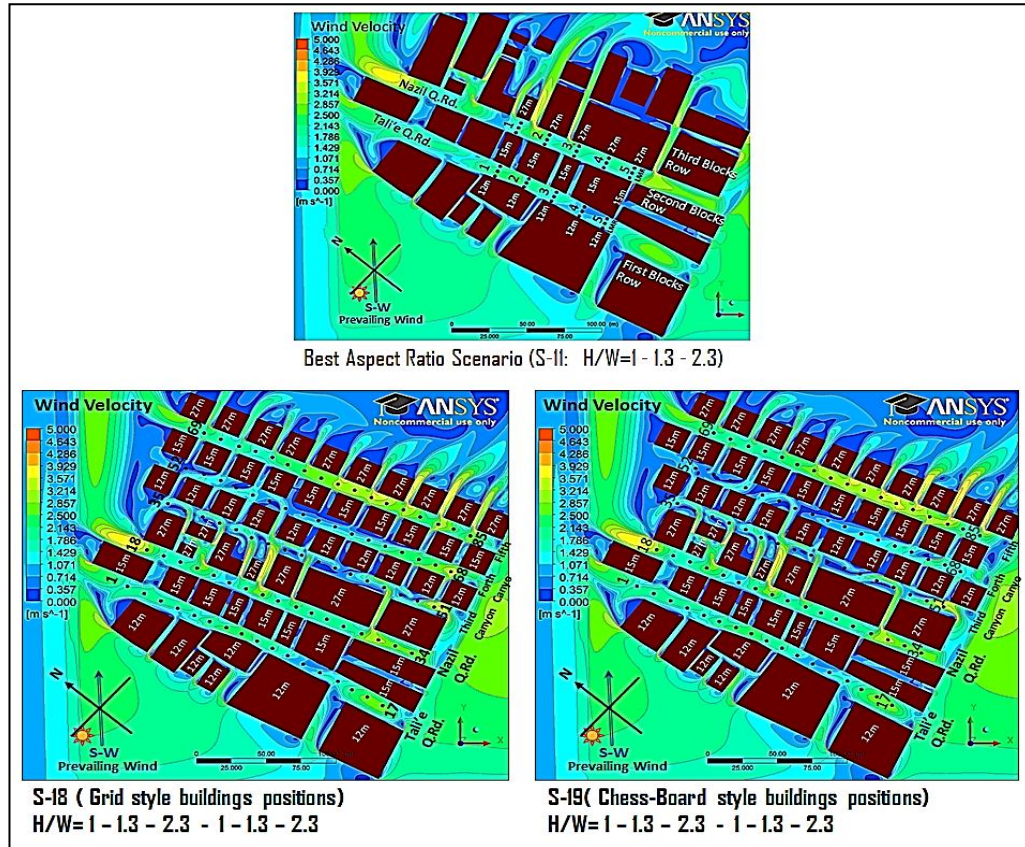


Fig. 8. 13: Contours of velocity magnitude (m/s) at pedestrian height for increase rows of buildings models in the S-18 scenario (Grid Style) and S-19 scenario (chess-board style).

In comparison between the S-18 (Grid Style) and S-19 (Chess-Board Style) with the base model (S-11), it is found that the wind magnitude in these scenarios for the windward canyon (i.e. Tali'e Quba Road) and the leeward canyon (i.e. Nazil Quba Road) are similar. This is because the first three rows of buildings in S-18 and S-19 share the same  $H/W$  as in the base model (S-11), thus no difference in pressure is created.

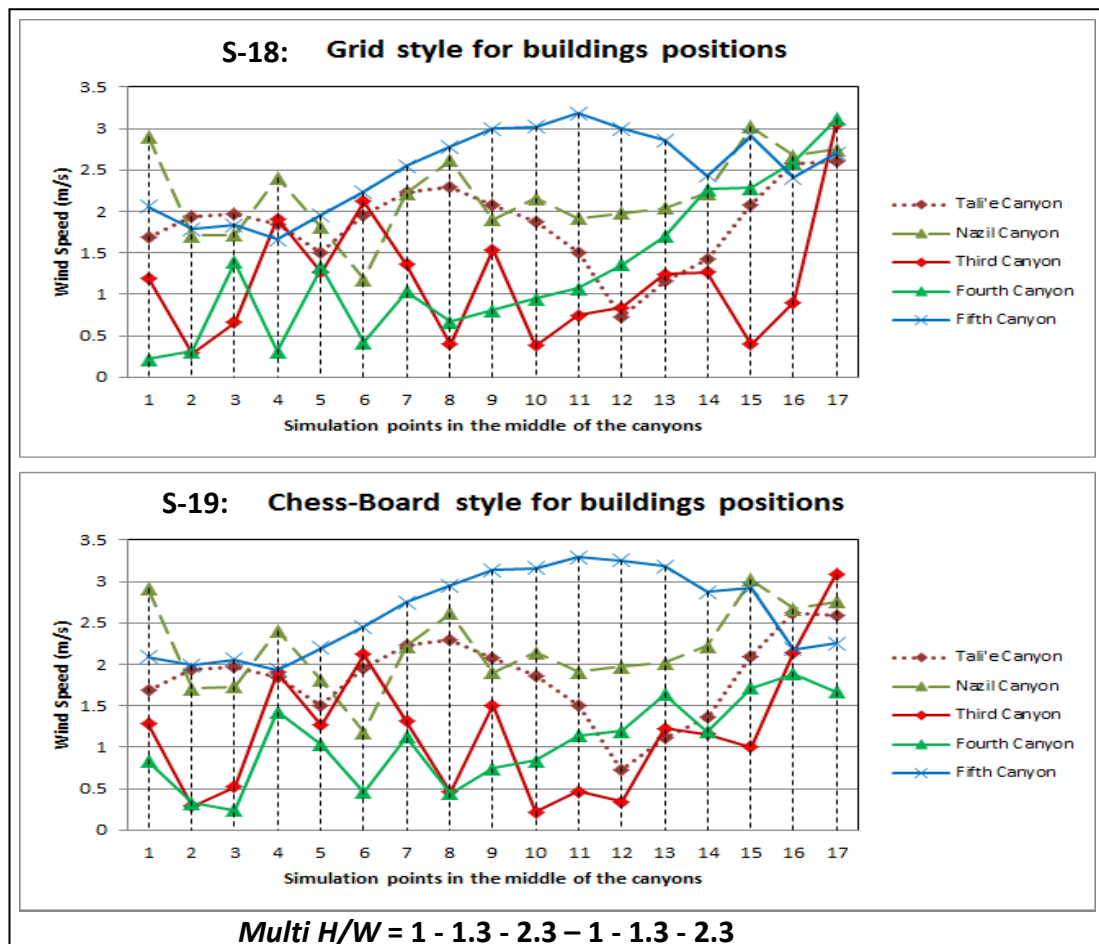


Fig. 8. 14: Wind velocity (m/s) pattern in five canyons for increased number of rows of buildings in S-18 (Grid style) and S-19 (Chess-Board style) scenarios.

Figure 8.14 shows that, in S-18 (Grid Style), the first canyon (the windward canyon, i.e. Tali'e Quba Road) has obtained an average wind velocity measurement of 1.9m/s along the middle of the canyon, with slightly higher velocity in the second canyon (the leeward canyon, i.e. Nail Quba Road) 2.2m/s. The same average wind velocity measurements are found in S-19 (Chess-Board Style) for the first and the second canyons. The followed canyon (i.e. third canyon) has obtained the lowest value in the S-18 (Grid Style) model, with an average measurement of 1.2m/s, then followed by the fourth canyon with a value of 1.3m/s. Similarly in the S-19 (Chess-Board Style) model, the third canyon obtained an average wind velocity of 1.2m/s, while in the fourth canyon it is slightly reduced to 1.1m/s.

An explanation for these results could be that:

- Their locations in the leeward area with low rise leeward building configurations.



- The third canyon has the highest leeward elevations (27m) and the lowest windward elevations (12m), thus higher wind blockage rate and lower turbulence generation at the pedestrian level.
- The fourth canyon has low leeward elevations (12m) and low windward elevations (15m), leading to low wind velocity.
- However, the chess-board building position style in S-19 has a higher difference value of 0.1m/s than the grid building position style, which is similar to the findings of Rizk and Henze (2010).

In addition, in comparison between the first canyon (i.e. Tali'e Quba Road) and the fourth canyon, which both share the same buildings height variation on the both sides of the canyon ( $H_1 = H_4 = 12\text{m}$ ; and  $H_2 = H_5 = 15\text{m}$ ), it is found that in the S-18 (Grid Style) scenario, the wind velocity in the fourth canyon is reduced from the average measurement of 1.9m/s (i.e. the first canyon's value) to a value of 1.3m/s (30%).

Unexpectedly, in comparison between the second canyon (i.e. Nazil Quba Road) and the fifth canyon, which both share the same buildings height variation on the both sides of the canyon ( $H_2 = H_5 = 15\text{m}$ ; and  $H_3 = H_6 = 27\text{m}$ ), it is found that in the S-18 (Grid Style) scenario, the wind velocity in the fifth canyon is slightly increased from the average measurement of 2.2m/s (i.e. the second canyon) to a value of 2.5m/s (i.e. 14%). This can be justified by a most recent study by Hang et al. (2015), as they found that the variations of building height can produce stronger downward flows drag in front of taller windward elevations, due to a higher static pressure level, than the lower windward elevations, as illustrated in Figure 8.15.

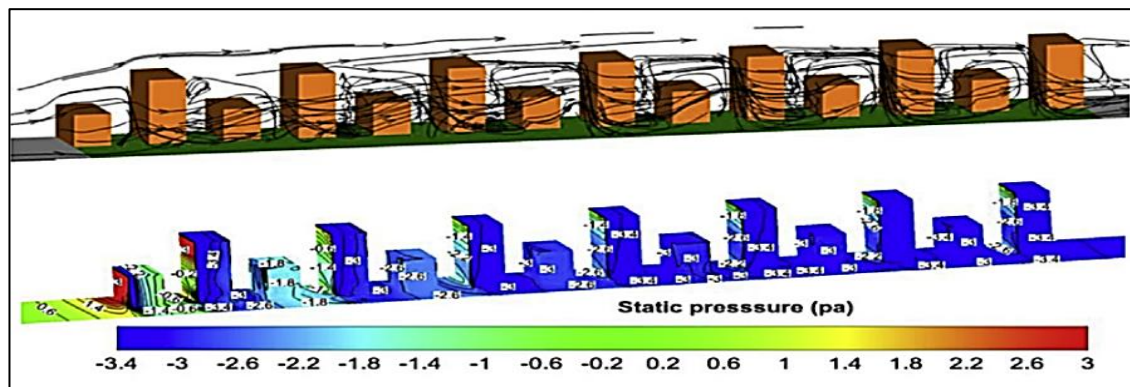


Fig. 8. 15: Wind flow streamline and pressure at wall surfaces for urban canyons with variation of building height. Source: Hang et al. (2015).

Regardless the variation in aspect ratio, these results also agree with Rizk and Henze (2010) that chess-board style positions of buildings can slightly increase wind speed in multiple street canyons than the grid style.

### 8.3.2. Air Temperature at the Pedestrian Level

Figure 8.16 shows the contours of air temperature at the pedestrian level, for the increasing the number of building rows strategy in the S-18 (Grid Style) and S-19 (Chess-Board Style) scenarios, and compared with the base model of the best proposed aspect ratio (S-11 with H/W of 1-1.3-2.3).

In comparison between the S-18 (Grid Style) and S-19 (Chess-Board Style) with the base model (S-11), it is found that the air temperatures in these scenarios for the windward canyon (the first canyon, i.e. Tali'e Quba Road) and the leeward canyon (the second canyon, i.e. Nazil Quba Road) are almost similar. This is because the first three rows of buildings in S-18 and S-19 share the same aspect ratios as in base model (S-11).

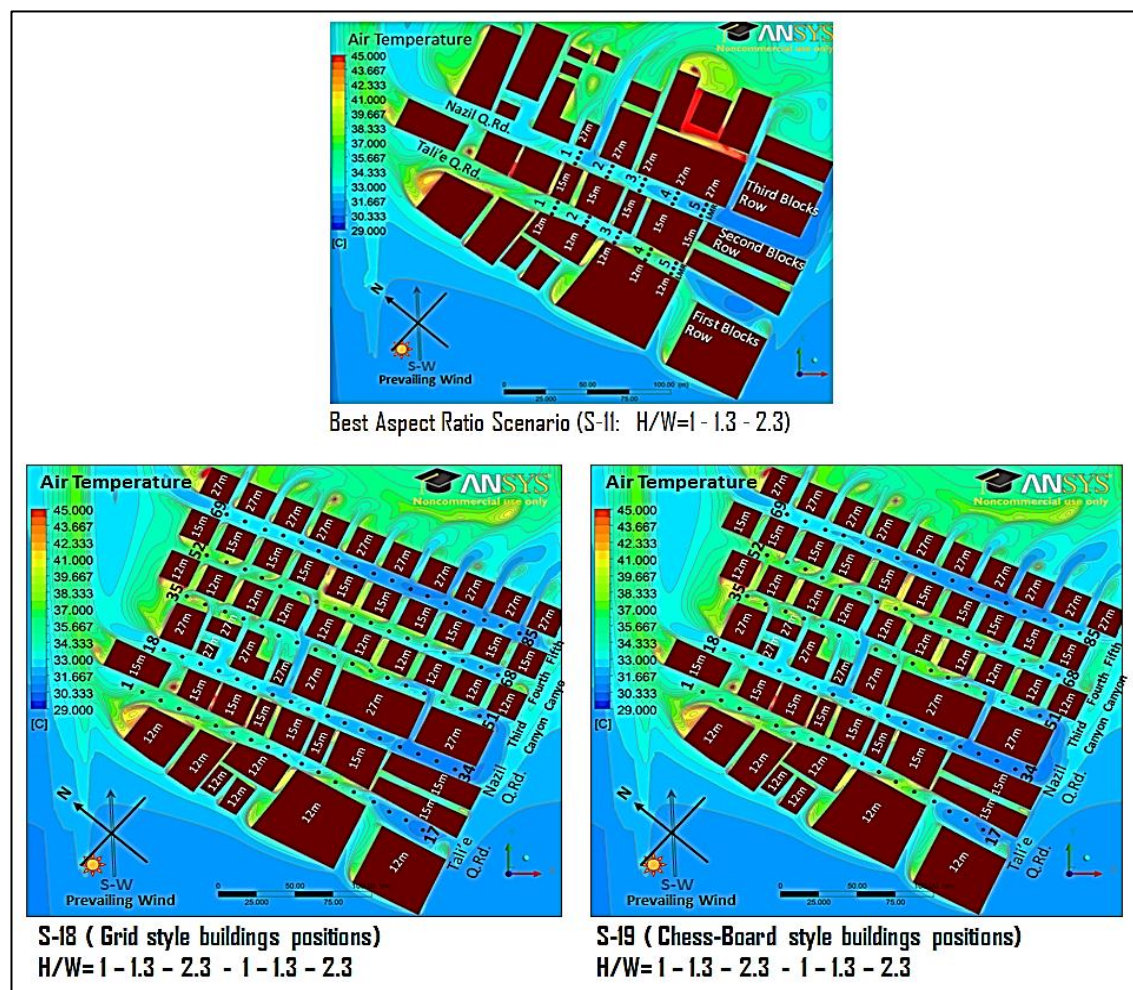


Fig. 8. 16: Contours of air temperature at pedestrian height for increase rows of buildings models in the S-18 scenario (Grid Style) and S-19 scenario (chess-board style).

Figure 8.17 shows that, in S-18 (Grid Style), the first canyon (the windward canyon, i.e. Tali'e Quba Road) has obtained an average air temperature measurement of 34.0°C along the middle of the canyon, with lower temperature in the second canyon (the leeward canyon, i.e. Nail Quba Road) 32.0°C. The same average air temperature results are found in S-19 (Chess-Board Style) for the first and the second canyons. The followed third canyon and fourth canyon have obtained a highest average measurement value of 35°C in the both of the S-18 (Grid Style) model and the S-19 (Chess-Board Style) model. This is because of the low wind speed area found in these two canyons (the third and the fourth canyons) than the other three canyons in the simulation (refer to section 8.3.1).

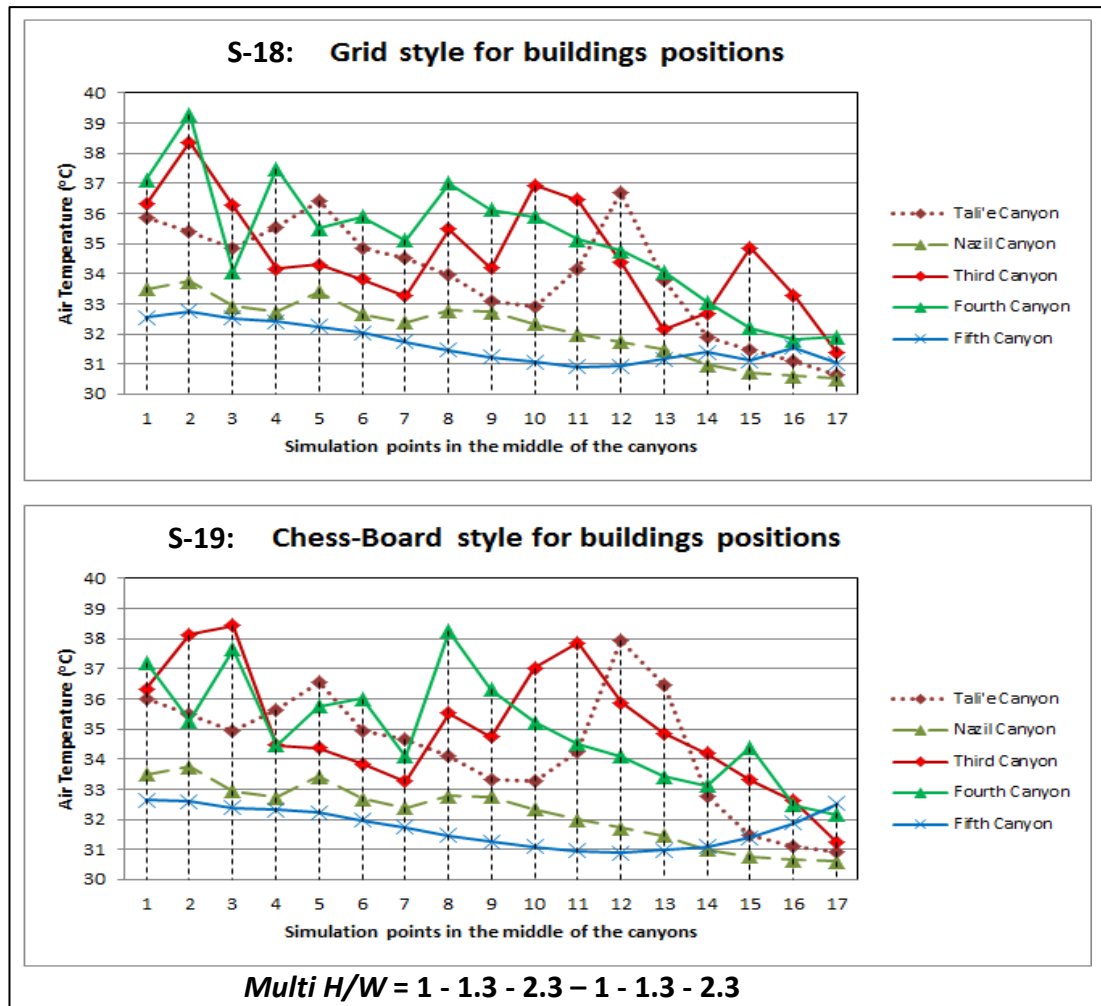


Fig. 8. 17: Air temperature pattern in five canyons for increased number of rows of buildings in S-18 (Grid style) and S-19 (Chess-Board style).

In addition, in comparison between the first canyon (i.e. Tali'e Quba Road) and the fourth canyon, which both share the same buildings height variation on the both sides of the canyon ( $H_1 = H_4 = 12\text{m}$ ; and  $H_2 = H_5 = 15\text{m}$ ), it is found that in both of the S-18 (Grid Style) scenario and the S-19 (Chess-Board Style), the air temperature in the

fourth canyon is obtained the highest value, as it is increased from the average measurement of 34°C (i.e. the first canyon's value) to a value of 35°C (i.e. 3%).

In comparison between the second canyon (i.e. Nazil Quba Road) and the fifth canyon, which both share the same buildings height variation on the both sides of the canyon ( $H_2 = H_5 = 15\text{m}$ ; and  $H_3 = H_6 = 27\text{m}$ ), it is found that in both of the S-18 (Grid Style) scenario and the S-19 scenario (Chess-Board Style), the wind velocity in the fifth canyon is obtained the lowest value, as it is slightly reduced from the average measurement of 32°C (i.e. the second canyon) to a value of 31.7°C (i.e. 1%).

#### 8.4. Orientation of the Urban Canyon Geometry (S-20, S-21)

This section aims to evaluate the effects of configuring the best proposed multi-asymmetrical aspect ratio  $H/W$  of  $1 - 1.3 - 2.3$  (i.e. refer to S-11 scenario in section 7.4.3), with the second and the third prevailing wind directions in Madinah, on the variation of the urban pedestrian microclimate conditions, as illustrated in Figure 8.18. The main prevailing wind direction, investigated in the best proposed  $H/W$  model, is the South-Westerly prevailing wind direction, with  $-112.5^\circ$  angle of attack from the north. The strategy of the orientation of the urban geometry are proposed in two scenarios (S-20 and S-21), which are:

- S-20 (W direction) scenario: investigates the orientation of the urban geometry with the Westerly second prevailing wind direction,  $-67.5^\circ$  angle of attack from the north.
- S-21 (NW direction) scenario: investigates the orientation of the urban geometry with the North-Westerly third prevailing wind direction,  $-22.5^\circ$  angle of attack from the north.

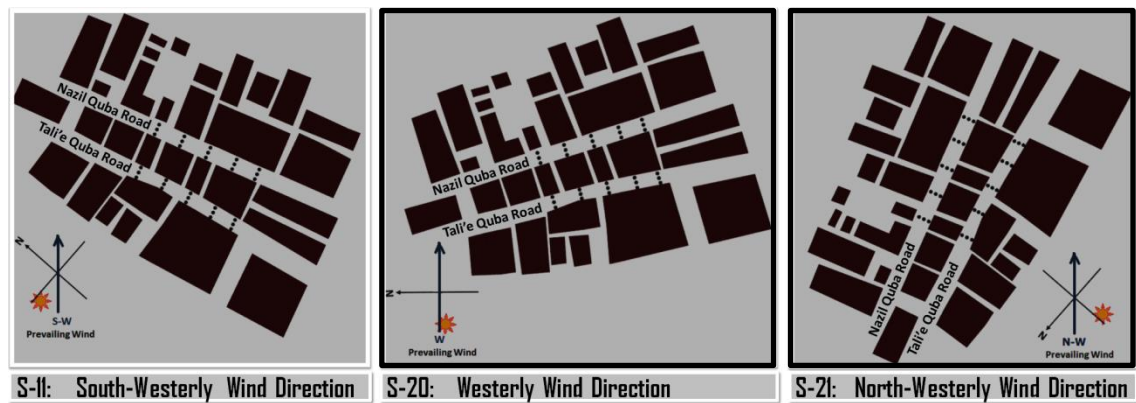


Fig. 8. 18: Orientation of urban canyon geometry with the Westerly second prevailing wind direction (S-20 scenario) and North-Westerly third prevailing wind direction (S-21 scenario), and compared to the South-Westerly main prevailing Wind Direction with the best aspect ratio scenario (S-11).

The study of the orientation of the urban canyon geometry scenarios analyses the air temperature and wind velocity results that are obtained from 15 measurement points locations within each of the windward canyon (i.e. Tali'e Quba Road) and the leeward canyon (i.e. Nazil Quba Roads), and averaged from the readings obtained in the middle, at the right and the left sides of the canyon.



#### 8.4.1. Wind Velocity at the Pedestrian Level (S-20, S-21)

Figure 8.19 shows the contours of wind velocity magnitudes (m/s) in the S-20 (W direction) and S-21 (NW direction) scenarios, and compared with the S-11 (SW direction) (direction).

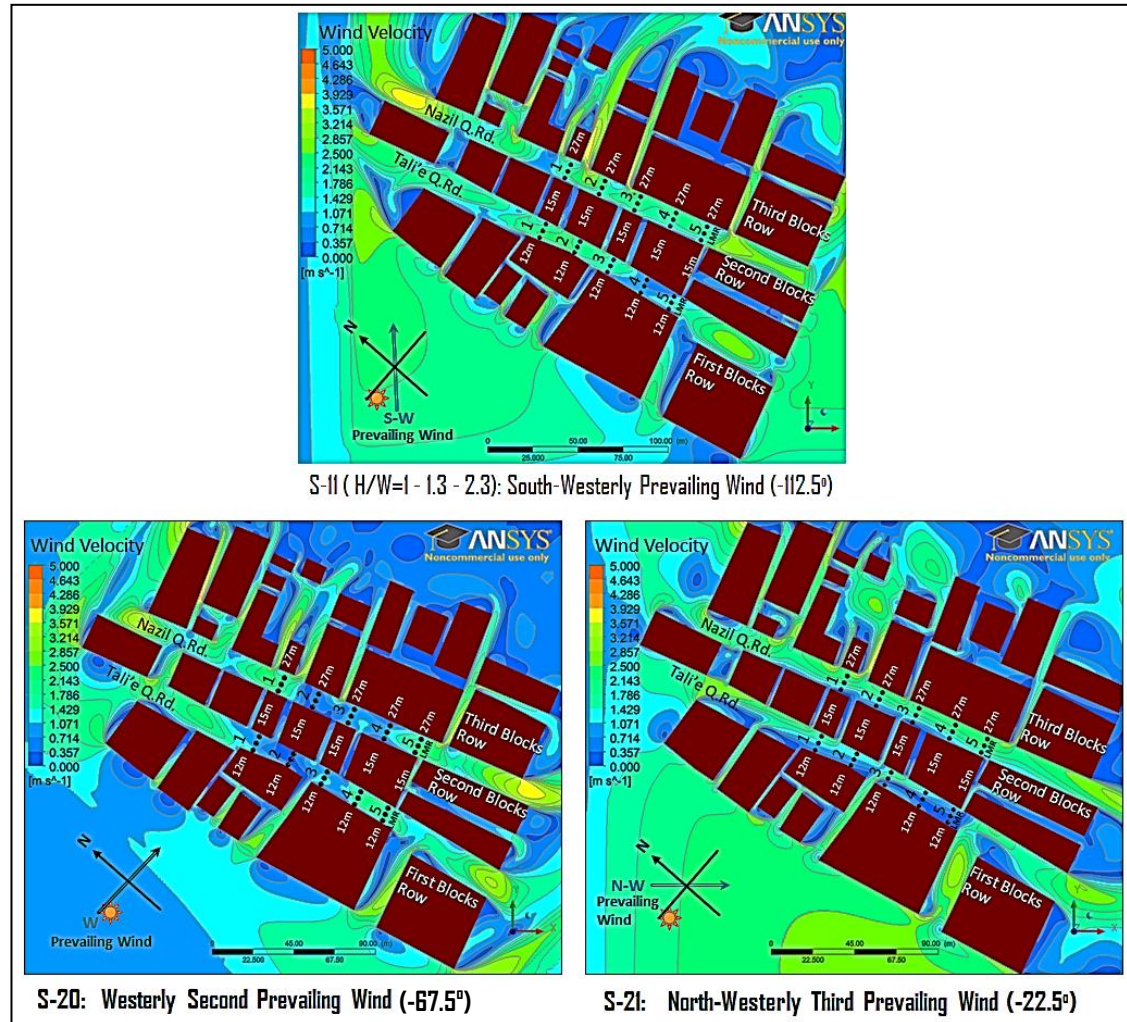


Fig. 8. 19: Contours of velocity magnitude (m/s) at pedestrian height (2m) in S-20 (W direction) and S-21 (NW direction), and compared with the best aspect ratio S-11 scenario (SW direction).

In comparison with the base model S-11 scenario (SW direction), in the windward canyon (i.e. Tali'e Quba Road), it is found that the velocity magnitude in the S-20 scenario (W direction, i.e. the second prevailing wind) is reduced from the average measurement of 1.5m/s to a value of 1.2m/s (i.e. 20%), as illustrated in Figures 8.19 and 8.20. With lower velocity values obtained in the S-21 scenario (NW direction, i.e. the third prevailing wind) from the average measurement value of 1.5m/s to a value of 0.9m/s (i.e. 40%), particularly at the pedestrian level. However, in S-21 (NW, third prevailing direction), the difference in the velocity magnitude is higher at the windward elevations of this canyon (i.e. windward canyon), with an average value of 1.4m/s compared to the leeward elevations (0.5m/s) and the middle of the canyon (0.8m/s).



On the other hand, in the leeward canyon (i.e. Nazil Quba Road), it is found that the overall wind magnitude is slightly reduced in the S-20 scenario (W direction) from the average measurement of 1.75m/s to a value of 1.20m/s (i.e. 31%). With slightly lower difference in S-21 scenario (NW direction) from the average measurement of 1.8m/s to 1.7m/s (4%), as illustrated in Figure 8.19 and 8.20. However, the lowest value that is found in S-20 (W direction), in the leeward canyon, compared to the other two prevailing winds (i.e. SW and NW) is found to be 85% higher than the existing conditions (0.7m/s), as illustrated in the Appendices from A8.9 to A8.14. Thus, the configuration of multi-asymmetrical aspect ratio with H/W of 1 – 1.3 – 2.3 is found to be positively effective in the leeward canyon (i.e. Nazil Quba Road) on improving wind flow at the pedestrian level for all the three prevailing wind directions in Madinah (SW, W, and NW directions).

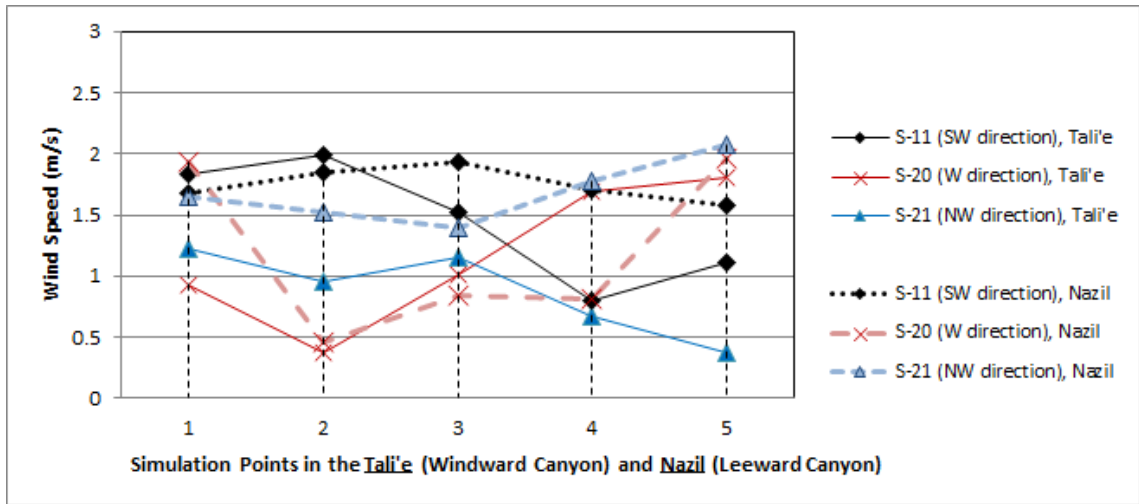


Fig. 8. 20: Wind speed at the pedestrian height (2m) in S-20 (W direction) and S-21 (NW direction), and compared with the best aspect ratio S-11 scenario (SW direction), with H/W of 1 – 1.3 – 2.3.

#### 8.4.2. Air Temperature at the Pedestrian Level (S-20, S-21)

Figure 8.21 shows the contours of air temperature in the S-20 (W direction) and S-21 (NW direction) scenarios, and compared with the base model S-11 scenario (SW direction) with the proposed aspect ratio H/W of 1 – 1.3 – 2.3.

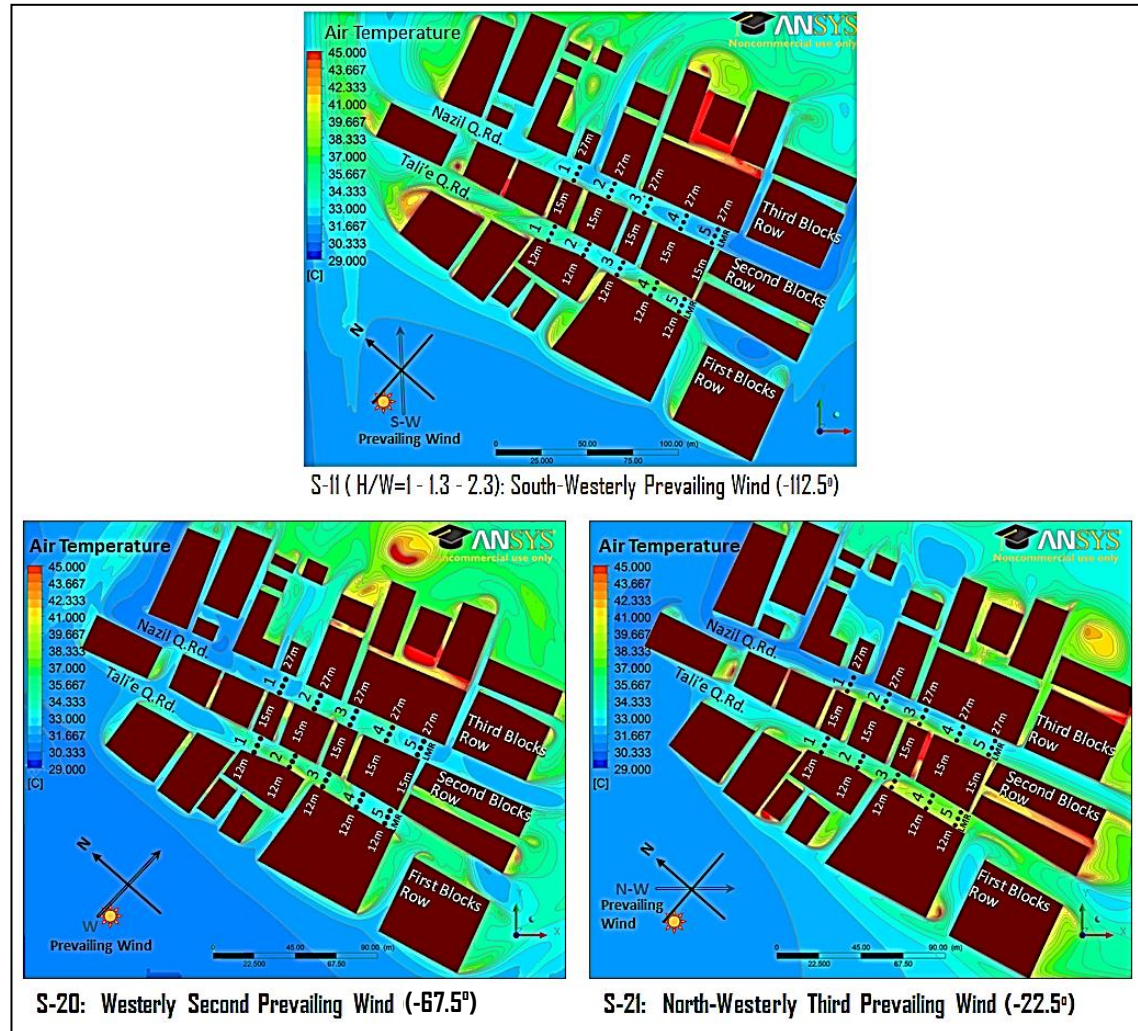


Fig. 8. 21: Contours of air temperature ( $^{\circ}\text{C}$ ) at the pedestrian level for the best aspect ratio with scenarios of Westerly prevailing wind direction (S-20) and North-Westerly prevailing wind (S-21), and compared with the best aspect ratio (S-11) scenario with South-Westerly wind direction.

In comparison with the base model S-11 scenario (SW direction), in the windward canyon (i.e. Tali'e Quba Road), it is found that the air temperature in the S-20 scenario (W direction, i.e. the second prevailing wind) is slightly increased from the average measurement of  $34.6^{\circ}\text{C}$  to a value of  $35.0^{\circ}\text{C}$  (i.e. 1%), as illustrated in Figures 8.21 and 8.22. With higher difference value obtained in the S-21 scenario (NW direction, i.e. the third prevailing wind) from the average measurement of  $34.6^{\circ}\text{C}$  to a value of  $37.1^{\circ}\text{C}$  (i.e. 7%), particularly at the pedestrian level. The latter case is as a result of lack of convective heat transfer in the canyon between the first two rows of the buildings.

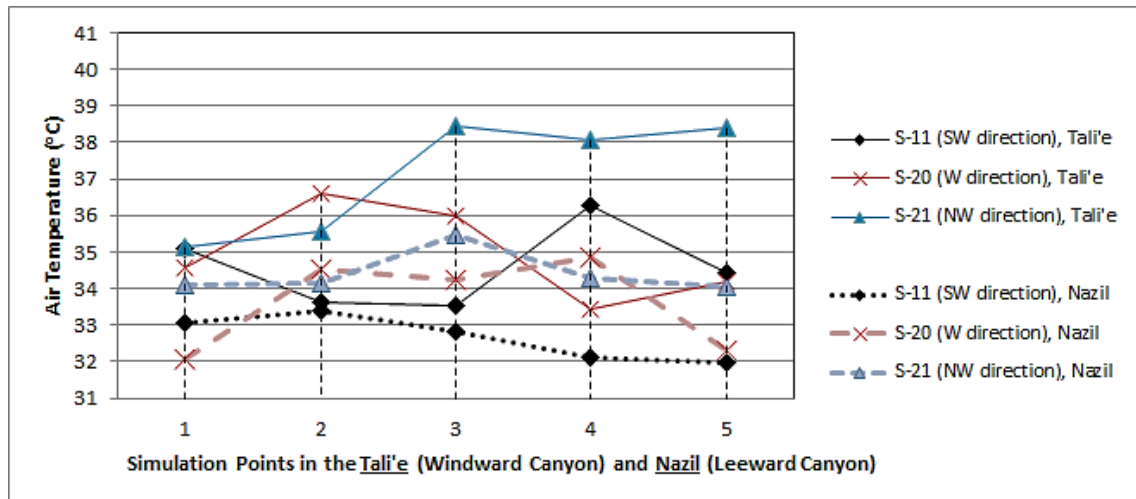


Fig. 8. 22: Air temperature in the Nazil Quba Road for the best aspect ratio with strategy ( $H/W$  of 1-1.3-2.3) in S-20 scenario with Westerly prevailing wind direction, and in S-21 scenario with North-Westerly prevailing wind, and compared to S-11 with South-Wester

On the other hand, in the leeward canyon (i.e. Nazil Quba Road), it is found that the overall air temperature is slightly increased in the S-20 scenario (W direction) from the average measurement of  $32.7^{\circ}\text{C}$  (i.e. SW direction) to a value of  $33.6^{\circ}\text{C}$  (i.e. 3%). With higher difference in S-21 scenario (NW direction) from the average measurement of  $32.7^{\circ}\text{C}$  to a value of  $34.4^{\circ}\text{C}$  (5%), as illustrated in Figure 8.21 and 8.22. The results for the locations at the left side (at the leeward elevations), middle, and the right side (at the windward elevations) of the Nazil Quba Road and the Tali'e Quba Road, can be found in the Appendices from A8.3 to A8.8.

### 8.5. Configuration of New Streets Perpendicular to the Quba Canyons (S-22, S-23, S-24)

According to Golany (1996), to support air movement into and within the urban areas, urban streets should be designed straight and parallel with the approaching wind. Hang et al. (2015) proved that parallel approaching wind induced higher wind velocity in urban areas at the pedestrian level than the oblique winds. However, there are no clear straight parallel streets with the prevailing wind in the existing urban area. Therefore, the strategy of configuring new streets that are perpendicular to the North-South axis of Quba canyons while approximately parallel with the prevailing wind direction, is proposed in three scenarios (S-22, S-23, S-24) in the current research, seeking for better microclimatic enhancement strategy, as illustrated in Figure 8.23. These scenarios are:

- The S-22 scenario (with a Lower Street Configuration): investigates a street configuration proposed in the lower side of the urban area, perpendicular to Quba Canyons.
- The S-23 scenario (with an Upper Street Configuration): investigates a street configuration located in the upper side of the urban area, perpendicular to Quba Canyons.
- The S-24 scenario (with an Upper and Lower Streets Configurations): investigates a configuration of two streets located in the upper and lower sides of the urban area, perpendicular to Quba Canyons.

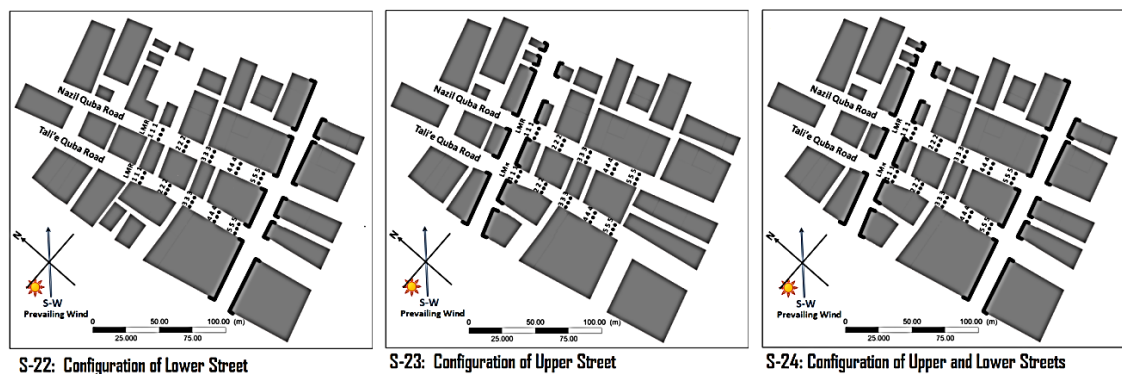


Fig. 8. 23: Three scenarios on the configuration of new streets that are parallel with the main prevailing wind direction, while it is approximately perpendicular to the North-South axis of Quba Canyons.

The study of the street configurations scenarios analyses the air temperature and wind velocity results that are obtained from 15 points within the leeward canyon (i.e.



Nazil Quba Roads), and averaged from the readings in the middle, at the right and the left sides of the canyon.

### 8.5.1. Wind Velocity at the Pedestrian Level (S-22, S-23, S-24)

Figure 8.24 analyses the contours of wind velocity magnitudes (m/s) for the configuration of new streets perpendicular to Quba Road canyons scenarios in S-22 (Lower Street), S-23 (Upper Street) and S-24 (Upper and Lower Streets) at the pedestrian level, and compared with the base model of the best proposed aspect ratio (S-11 with no new streets). Figure 8.20 shows the wind velocity pattern along the leeward canyon (Nazil Quba Road).

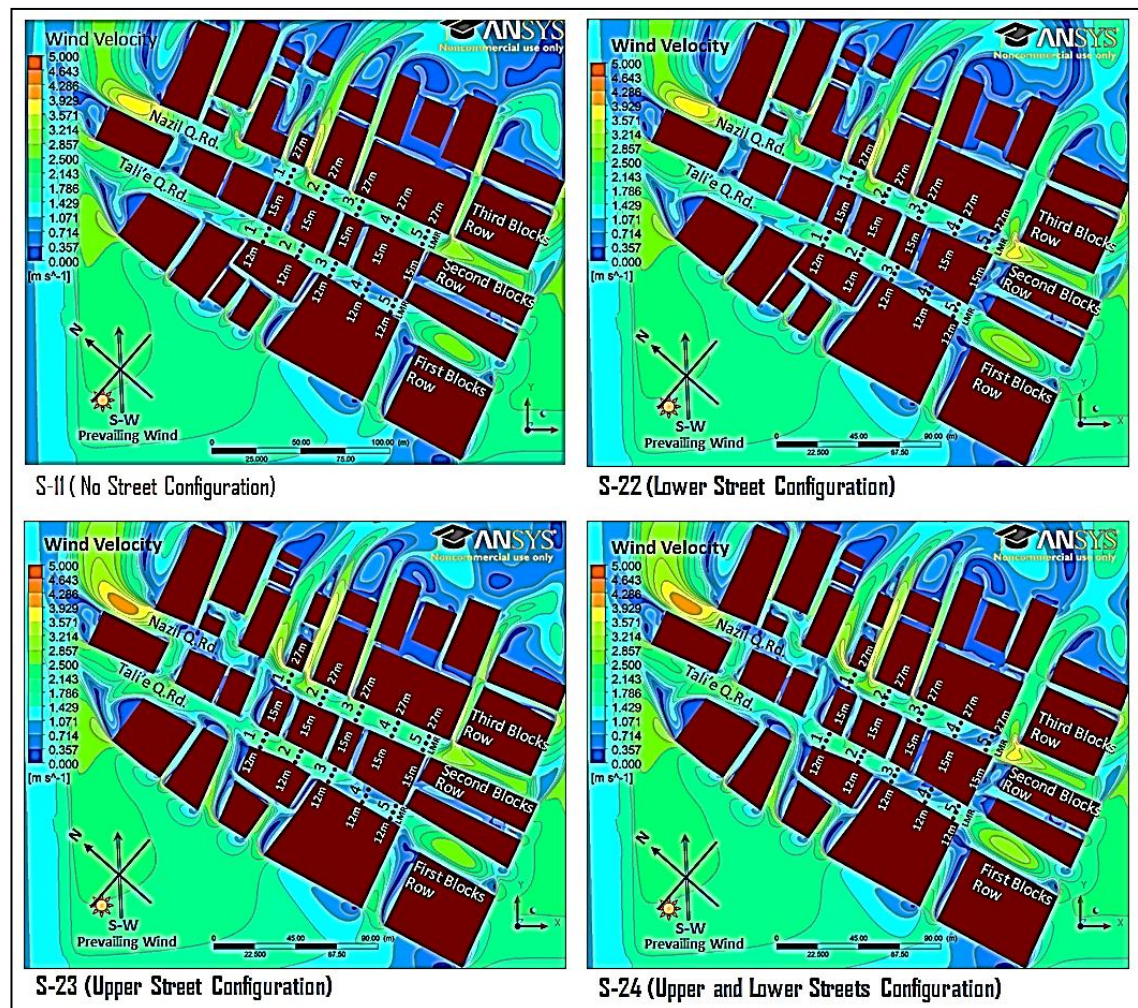


Fig. 8. 24: Contours of wind velocity (m/s) at the pedestrian level for the configuration of new streets perpendicular to Quba canyons strategy (S-22: Lower Street, S-23: Upper Street, S-24: Upper & Lower street configurations), and compared with the base model of best H/W scenario (S-11).

In comparison with the optimum aspect ratio model (S-11), it is found that the overall wind magnitude in the leeward canyon (i.e. Nazil Quba Road) is slightly

worsened in the S-22 scenario (Lower Street configuration) from the average measurement of 1.8m/s to 1.5m/s (i.e. 17%). With slightly lower difference in S-24 scenario (Upper and Lower Streets) from the average measurement of 1.8m/s to 1.5m/s (13%). While in the S-23 scenario (Upper Street configuration), it is found that the wind velocity magnitude in the leeward canyon is slightly improved from the average measurement of 1.8m/s to a value of 1.8m/s (i.e. 5%), as illustrated in Figure 8.25.

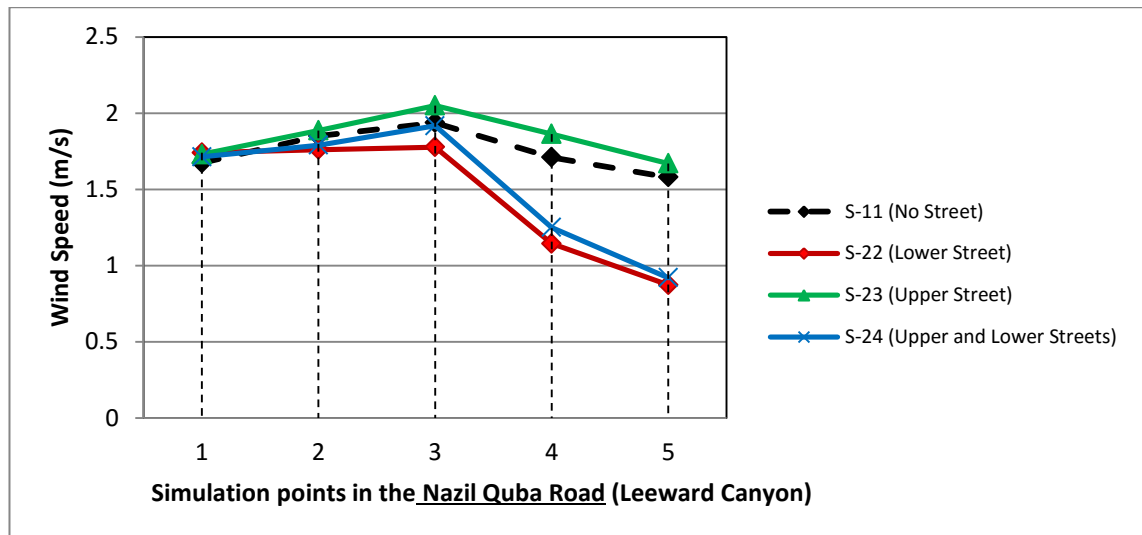


Fig. 8. 25: Wind speed pattern at the pedestrian level for the configuration of new streets perpendicular to Quba canyons strategy (S-22: Lower Street, S-23: Upper Street, S-24: Upper & Lower street configurations), and compared with the base model of best H/W scenario (S-11).

The outcome of these results indicates that configuration of new streets perpendicular to the existing Quba canyons has minor impact on improving wind velocity magnitude within the Quba Road canyons. This could be due to low approaching wind flow rate in Madinah (i.e. 4.7m/s at 15:00 hours in April). In addition, the orientation of Quba road canyons are not parallel with the wind direction, leading to reduced wind velocity in the canyons. Nevertheless, the results of the velocity contours validate the findings from Yuan and Ng (2012). It is found that parallel streets configuration with a prevailing wind direction can allow air flow to penetrate more deeply into the urban streets than those in the perpendicular streets to prevailing wind direction.



### 8.5.2. Air Temperature at the Pedestrian Level (S-22, S-23, S-24)

Figure 8.26 analyses the contours of air temperature in degrees ( $^{\circ}\text{C}$ ) at the pedestrian level (2m above the ground), for the configuration of new streets perpendicular to Quba Road canyons scenarios in S-22 (Lower Street), S-23 (Upper Street) and S-24 (Upper and Lower Streets), and compared with the base model of the best proposed aspect ratio (S-11 with no new streets). Figure 8.27 shows the air temperature pattern along the leeward canyon (Nazil Quba Road).

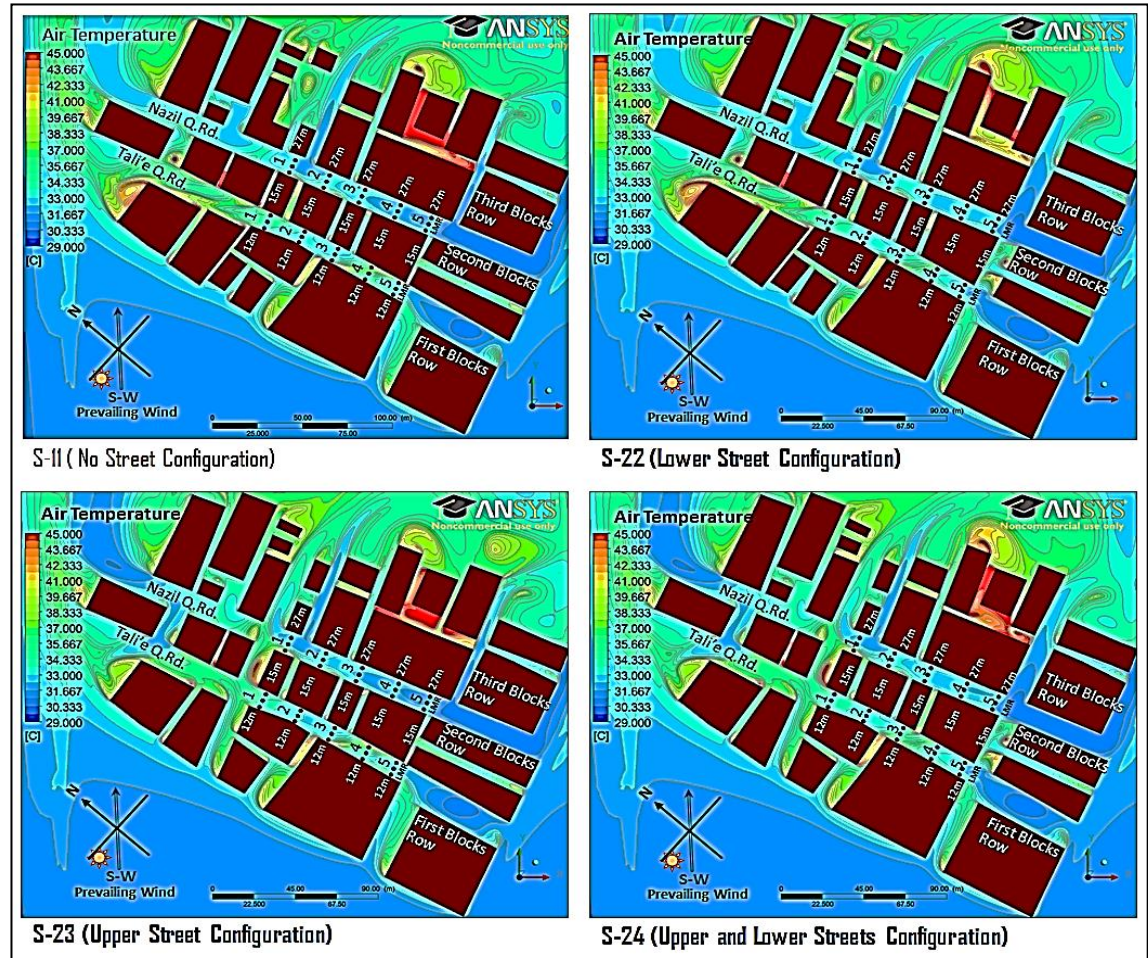


Fig. 8. 26: Contours of air temperature at the pedestrian level for the configuration of new streets perpendicular to Quba canyons strategy (S-22: Lower Street, S-23: Upper Street, S-24: Upper & Lower street configurations), and compared with the base model of best H/W scenario (S-11).

In comparison with the base model (S-11), it is found that the overall air temperature in the leeward canyon (i.e. Nazil Quba Road) is slightly increased in S-24 scenario (Upper and Lower Streets configuration) from the average measurement of  $32.7^{\circ}\text{C}$  to  $33.2^{\circ}\text{C}$  (2%). With slightly lower difference in the S-22 scenario (Lower Street) from the average measurement of  $32.7^{\circ}\text{C}$  to  $33.0^{\circ}\text{C}$  (i.e. 1%), and in the S-23

scenario (Upper Street) an average measurement of 32.8°C (i.e. 1%), as illustrated in Figure 8.27.

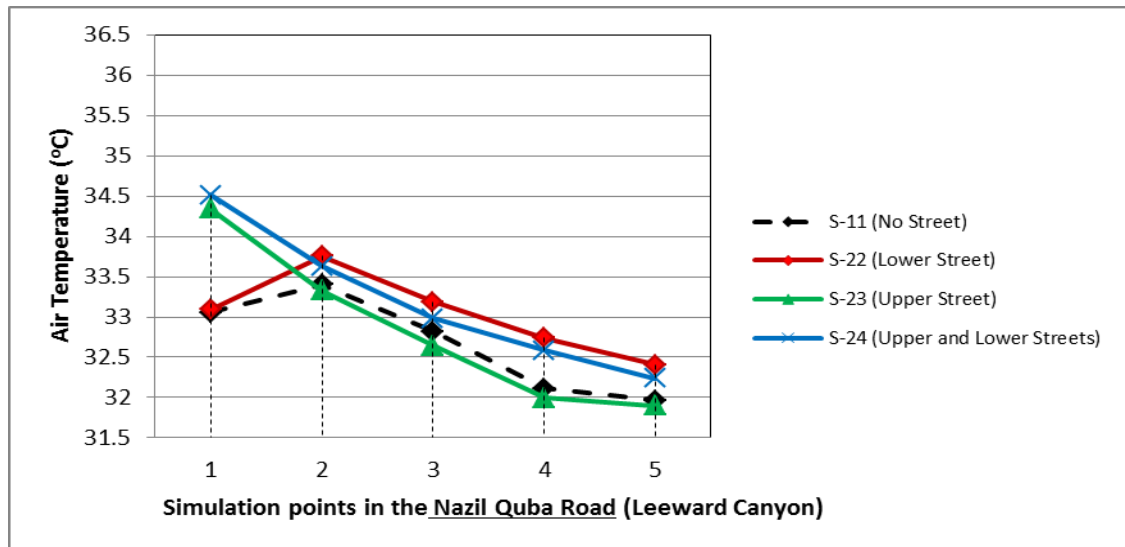


Fig. 8. 27: Air temperature pattern at the pedestrian level for the configuration of new streets perpendicular to Quba canyons strategy (S-22: Lower Street, S-23: Upper Street, S-24: Upper & Lower street configurations), and compared with the base model of best H/W scenario (S-11).

### 8.6. Removal of Buildings (S-26) Forming Open Spaces for a Local Hub

In the previous investigations of wind velocity and air temperature in S-11 scenario (the optimum aspect ratio strategy, refer to section 7.4.3), it was found that the configuration of H/W of 1 – 1.3 – 2.3 can improve the microclimate and thermal comfort in the leeward canyon (Nazil Quba Road). However, the area behind a windward building near the simulated location number 4 in the Nazil Quba Road (leeward canyon), has a lower wind flow and higher air temperature results, compared to the existing situation. Therefore, scenario S-26 is proposed here to study the effect of removal of buildings on the variation of wind flow in the Nazil Quba Road (i.e. Leeward Canyon) as well as on the area behind the removed building, as illustrated in Figure 8.28. Thus, a passage between buildings parallel with the prevailing wind direction and an open space at the eastern side of the canyon are created to replace this removed building.

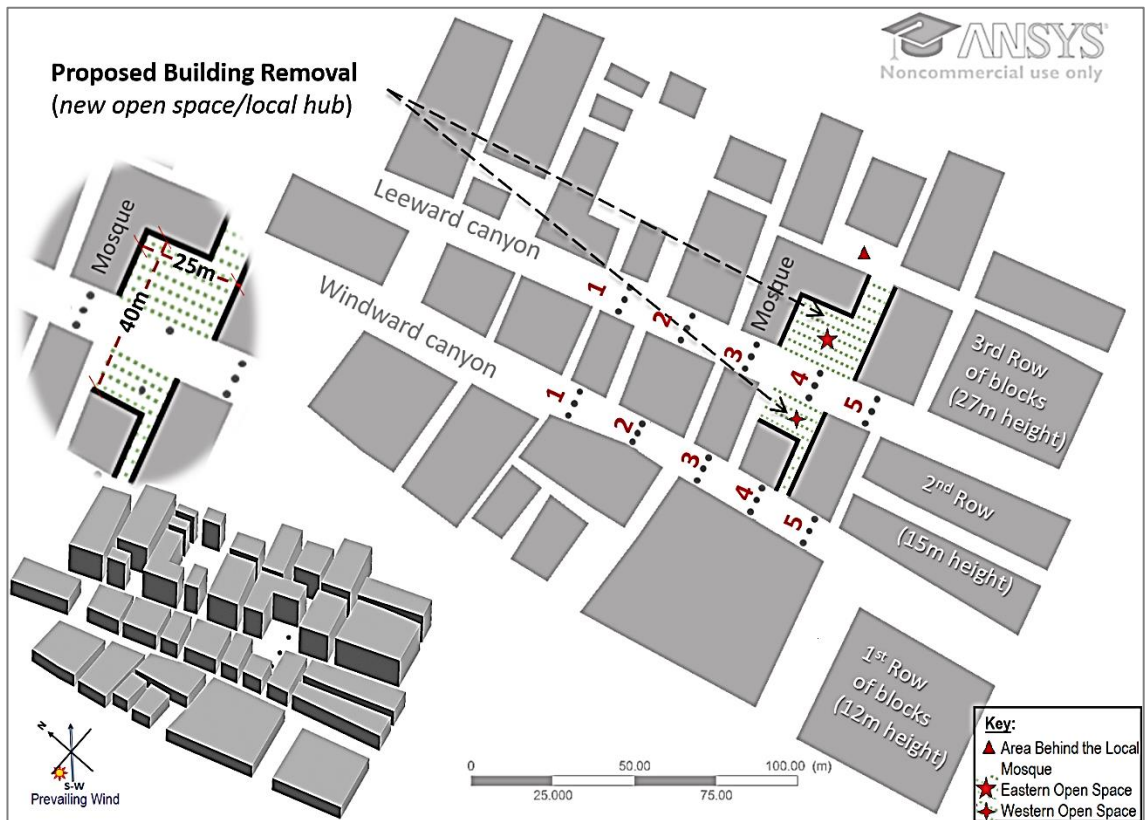


Fig. 8. 28: Scenario S-26 based on removing buildings and or creating open spaces and passages, particularly at simulation location number 4 in the leeward canyon (i.e. Nazil Quba Road).

In addition, in S-26 scenario, part of a leeward building at the location number 4 in the Nazil Quba Road (leeward canyon) is removed, to create a passage parallel with the prevailing wind direction, and an open space at the western side of the canyon. The

integration of the two open spaces (at the eastern and western sides of the Nazil Quba Road or the leeward canyon), will design a local hub in this high urban density area.

An existing local mosque can be found on the third row of the buildings adjacent to the simulated locations number 3 and 4. An urban space location was recommended in a previous research by the author (Setaih, 2010), on the physical linkages between Quba and the Prophet mosques through proposing several nodes, that comprise of communal hubs with mosques and retail outlet based on acceptable walking distance in hot arid climate from one node to another, as illustrated in Figure 8.29.



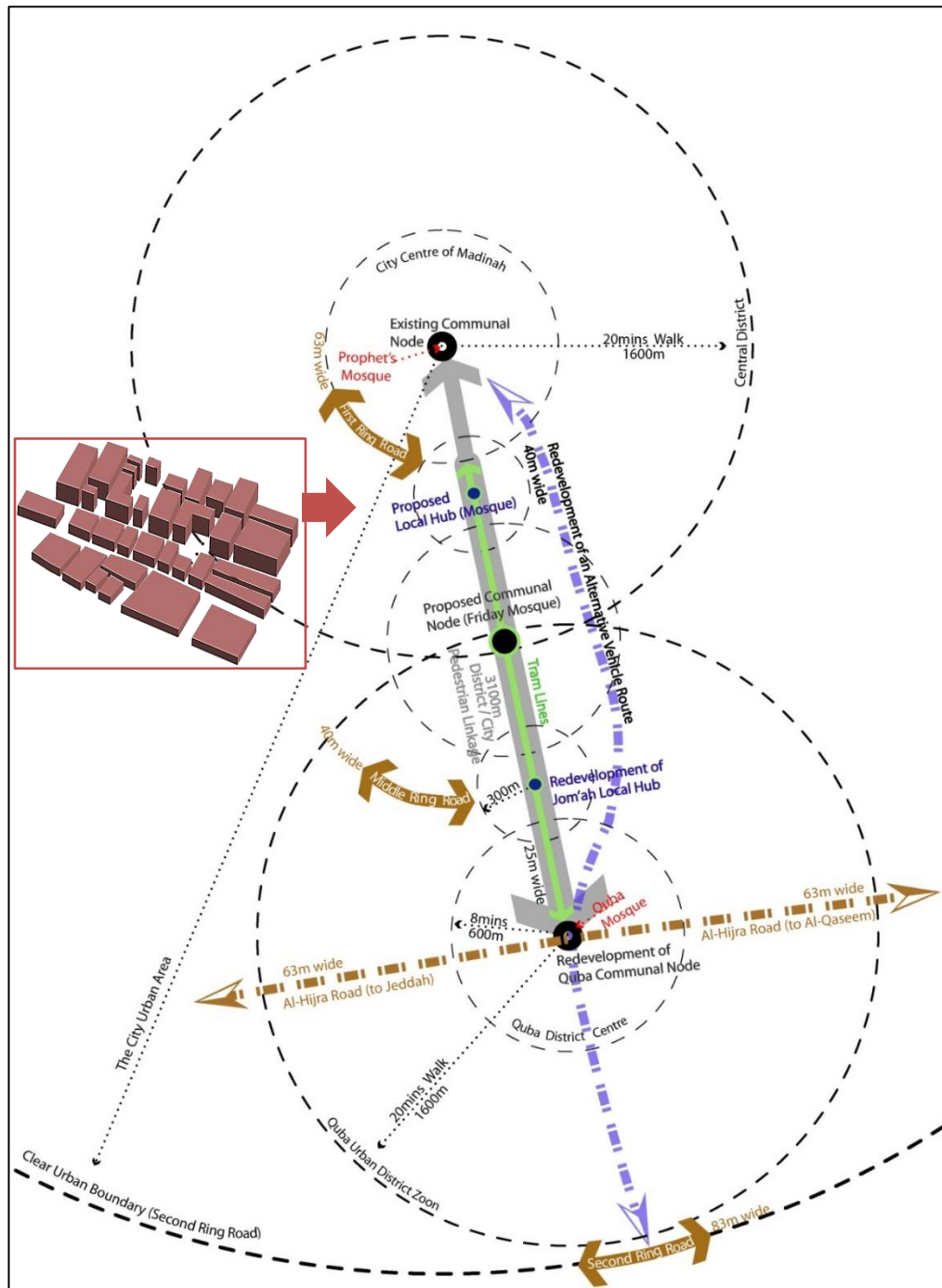


Fig. 8. 29: Conceptual diagram for proposed communal nodes and local hubs in Quba Road based on acceptable maximum walking time (in minutes) and distance (in metres). Adapted from Setaih (2010).

The urban street aspect ratio for locations 1, 2, 3 and 5 in S-26 (removal of buildings) scenario follows the  $H_1/W - H_2/W - H_3/W$  of 1 – 1.3 – 2.3 of the S-11 scenario (i.e. the optimum strategy). While the aspect ratio for the proposed integrated urban open space at location 4 is changed to  $H_1/W - H_2/W$  of 1 – 1.3 in the windward canyon, and  $H_2/W - H_3/W$  of 0.4 – 0.7 in the leeward canyon. This is because the approximate length of the integrated open space in S-26 scenario is 40m, while the width is 25m in the eastern side of the leeward canyon and 20m in the western side.

The study of the removal of buildings scenario (S-26) analyses the air temperature and wind velocity obtained from 15 measurement points locations within each of the windward canyon (i.e. Tali'e Quba Road) and the leeward canyon (i.e. Nazil Quba Roads), and averaged from the readings obtained in the middle, at the right and the left sides of the canyon. In addition, it analyses the microclimatic results in the area behind the local mosque, the eastern open space and the western open space from other 15 simulated locations in each of these areas.

#### 8.6.1. Wind Velocity at the Pedestrian Level (S-26: Removal of Buildings)

Figures 8.30 and 8.31 analyses the contours of wind velocity magnitudes (m/s) and velocity patterns, respectively, at the pedestrian level for the strategy of the removal of buildings in the Nazil Quba Road (leeward canyon), presented in scenario S-26, and compared with the optimum aspect ratio (S-11) scenario.



Fig. 8. 30: Contours of wind velocity (m/s) at the pedestrian level for the strategy of removal of buildings in S-26 scenario, and compared with the base model of the optimum H/W in S-11.



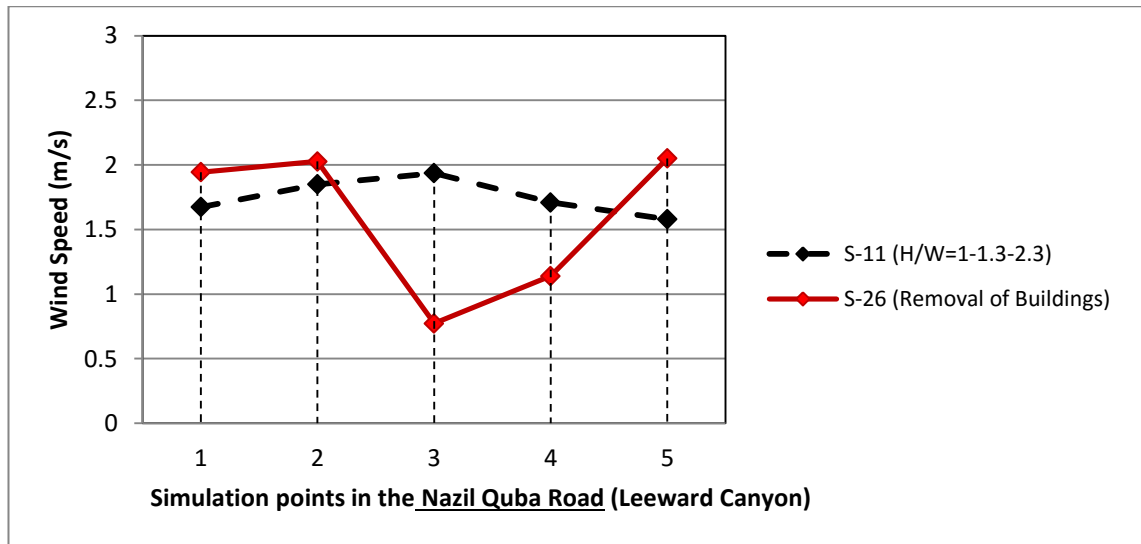


Fig. 8. 31: The wind velocity patterns at the pedestrian level for the strategy of removal of buildings in S-26 scenario, and compared with the base model of the optimum H/W in S-11 at five averaged simulated locations.

In comparison with the optimum aspect ratio model (S-11), wind velocity has improved in the area behind the local mosque building in S-26 scenario (i.e. removal of buildings) from 0.2m/s to 1.1m/s (i.e. 400%). This is due to the new passages at the simulated location 4, which are proposed parallel with the prevailing wind direction, allowing wind flow movement by channel effect and standing vortices (e.g. Rizk and Henze, 2010).

However, it is found that the overall wind magnitude in the leeward canyon (i.e. Nazil Quba Road) has slightly decreased in the S-26 scenario (i.e. removal of buildings) from the average measurement of 1.8m/s to 1.6m/s (i.e. -9%).

The wind velocity results in the eastern open space and the western open space are 1.0m/s and 0.4m/s, respectively. The latter has lower wind velocity due to its position next to a leeward elevation (15m height) of the Nazil Quba Road (leeward canyon) with no standing vortices compared to the eastern open space next to a windward elevation (27m height). Thus, the results implies that the eastern side of the Quba Road canyons is recommended for better ventilations when designing open spaces in the high urban density area.

### 8.6.2. Air Temperature at the Pedestrian Level (S-26: Removal of Buildings)

Figure 8.32 analyses the contours of air temperature in degrees ( $^{\circ}\text{C}$ ) at the pedestrian level for the strategy of the removal of buildings in the Nazil Quba Road (leeward canyon), presented in scenario S-26, and compared with the optimum aspect ratio (S-11) scenario. Figure 8.31 shows the air temperature pattern in the leeward canyon (Nazil Quba Road) along the five locations of averaged simulated results in the canyon.

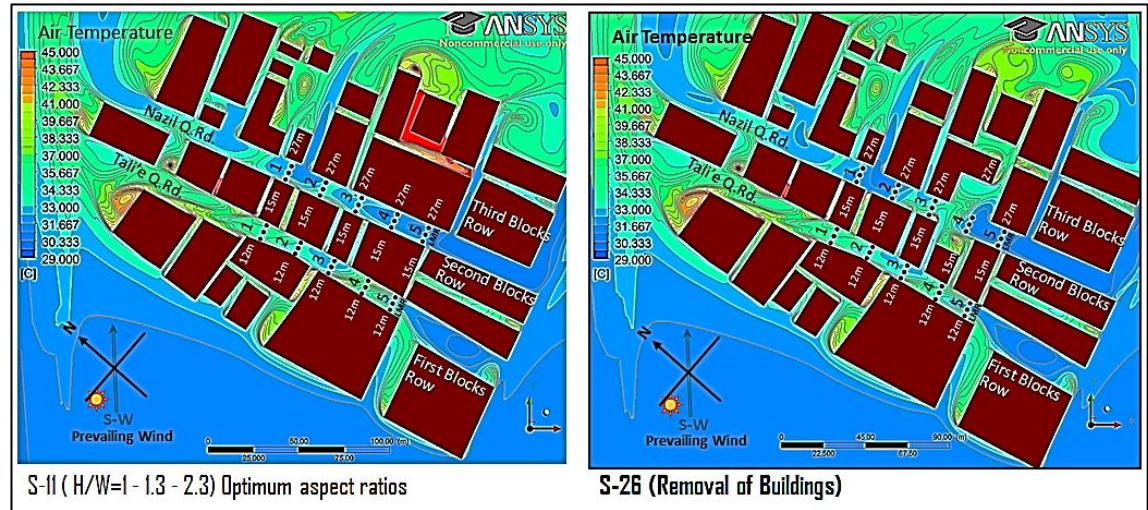


Fig. 8. 32: Contours of air temperature at the pedestrian level for the strategy of removal of buildings in S-26 scenario, and compared with the proposed model of the optimum H/W in S-11.

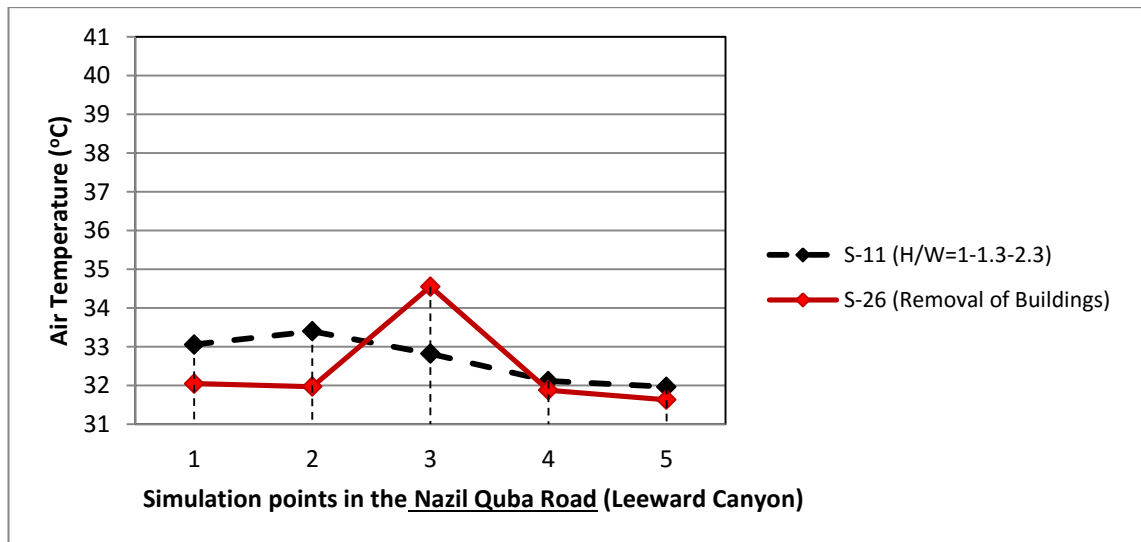


Fig. 8. 33: Air temperature pattern at the pedestrian level for the strategy of removal of buildings in S-26 scenario, and compared with the proposed model of the optimum H/W in S-11.

In comparison with the optimum aspect ratio model (S-11), the air temperature at the pedestrian height has improved in the area behind the local mosque building in S-26 scenario (i.e. removal of buildings) from 46°C to 36°C (i.e. 22%). Thus, the issue of trapped heat in the area behind the removed building (i.e. adjacent to the local mosque) is solved by providing opportunity of heat transfer by convection, which is through the new passages at simulated location 4 that are proposed parallel with the prevailing wind direction.

In addition, it is found that the overall air temperature in the leeward canyon (i.e. Nazil Quba Road) in the S-26 (i.e. removal of buildings) scenario is almost similar to the S-11 scenario, with a value of 32.4°C. However, the air temperature results in the eastern open space and the western open space are 34°C and 37°C, respectively. The latter has higher average air temperature value due to its position next to a leeward elevation (15m height) of the Nazil Quba Road (leeward canyon) with no standing vortices compared to the eastern open space next to a windward elevation (27m height), leading to lack of convective heat transfer. Thus, the results may recommend eastern side of the Quba Road canyons for open spaces for better air temperature and wind velocity results, and thus thermal comfort conditions.

### 8.7. Protruding Upper Floors for Shading (S-27 and S-28)

This section aims to evaluate the effects of shading by protruding upper floors in the buildings (i.e. cantilever effect), which narrows the streets openness to the sky (from 12m to 9m), on the urban pedestrian microclimate. The study was conducted particularly at 15:00 hours in S-27 scenario and 12:00 hours in S-28 scenario. The effect on the wind velocity and air temperature are compared here with the optimum multi-asymmetrical aspect ratios  $H/W$  of  $1 - 1.3 - 2.3$  in scenarios S-11 at 15:00 hours and S-25 at noon.

The heights of the three rows of the buildings in S-27 and S-28 are the same that are 12m – 15m – 27m, which are also the same as in S-11 and S-25 scenarios. While the width of the street openness to the sky is different, with the measurement of 9m instead of 12m. This is due to the application of 1.5m extensions on the leeward and wind elevations in both Quba Road canyons in S-27 and S-28, particularly the floors above the ground floor (i.e. above 3m from the ground), as illustrated in Figure 8.34.

Thus, the strategy of protruding upper floors for shading in S-27 (at 15:00 hours) and S-28 (at noon) has resulted in a new and higher multi-asymmetrical street aspect ratios  $H/W$  of  $1.3 - 1.7 - 3$ , based on optimising street openness to the sky.

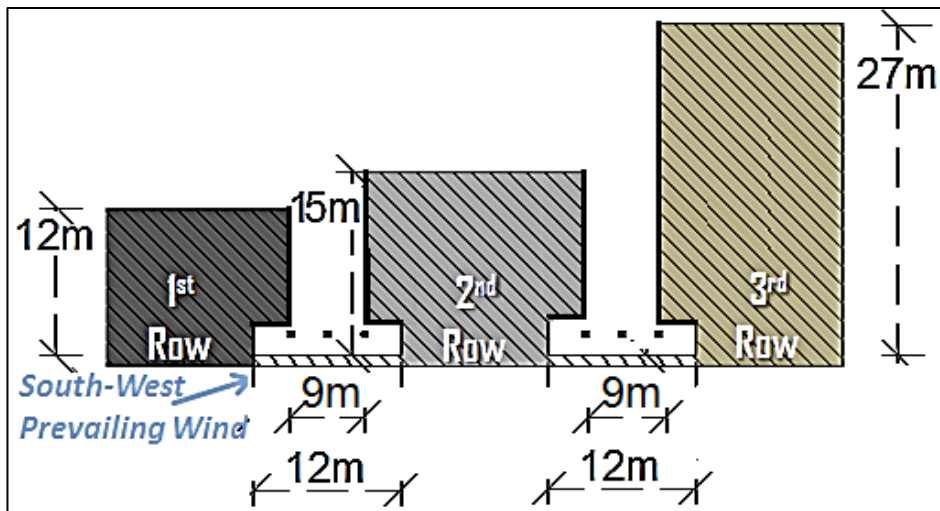


Fig. 8. 34: protruding upper floors scenario in S-27 and S-28 scenarios, with 9m street openness to the sky.

The study of the protruding upper floors for shading scenarios (S-27 and S-28) analyses the air temperature and wind velocity obtained from 15 measurement points within each of the windward canyon (i.e. Tali'e Quba Road) and the leeward canyon (i.e.

Nazil Quba Roads), and averaged from the readings obtained in the middle, at the right and the left sides of the canyon.

#### **8.7.1. Shading Level (S-27 and S-28)**

In the current study, the level of shading for the aspect ratio  $H/W$  of  $1.3 - 1.7 - 3$  with building heights of 12m, 15m and 27m was investigated for the protruding upper floors scenarios (S-27 and S-28), using Ecotect Analysis software. Figure 8.35 shows the shading level in the Quba Road canyons for the proposed aspect ratio of  $1.3 - 1.7 - 3$ . The simulation was performed based on hourly sun path in April. The findings reveal that due to the north-south axis orientation of Quba Road, the proposed building heights (12m – 15m – 27m) can provide high amount of shading in most of the day in the spring season. The Quba road canyons are found to be in full shade in the S-27 scenario at 15:00 hours, which is due to a low sun elevation at this time, as illustrated in Figure 8.35. However, the canyons are exposed to the solar radiation in S-28 scenario at 12:00 hours with almost no shading due to a higher level of the sun elevation at this period.

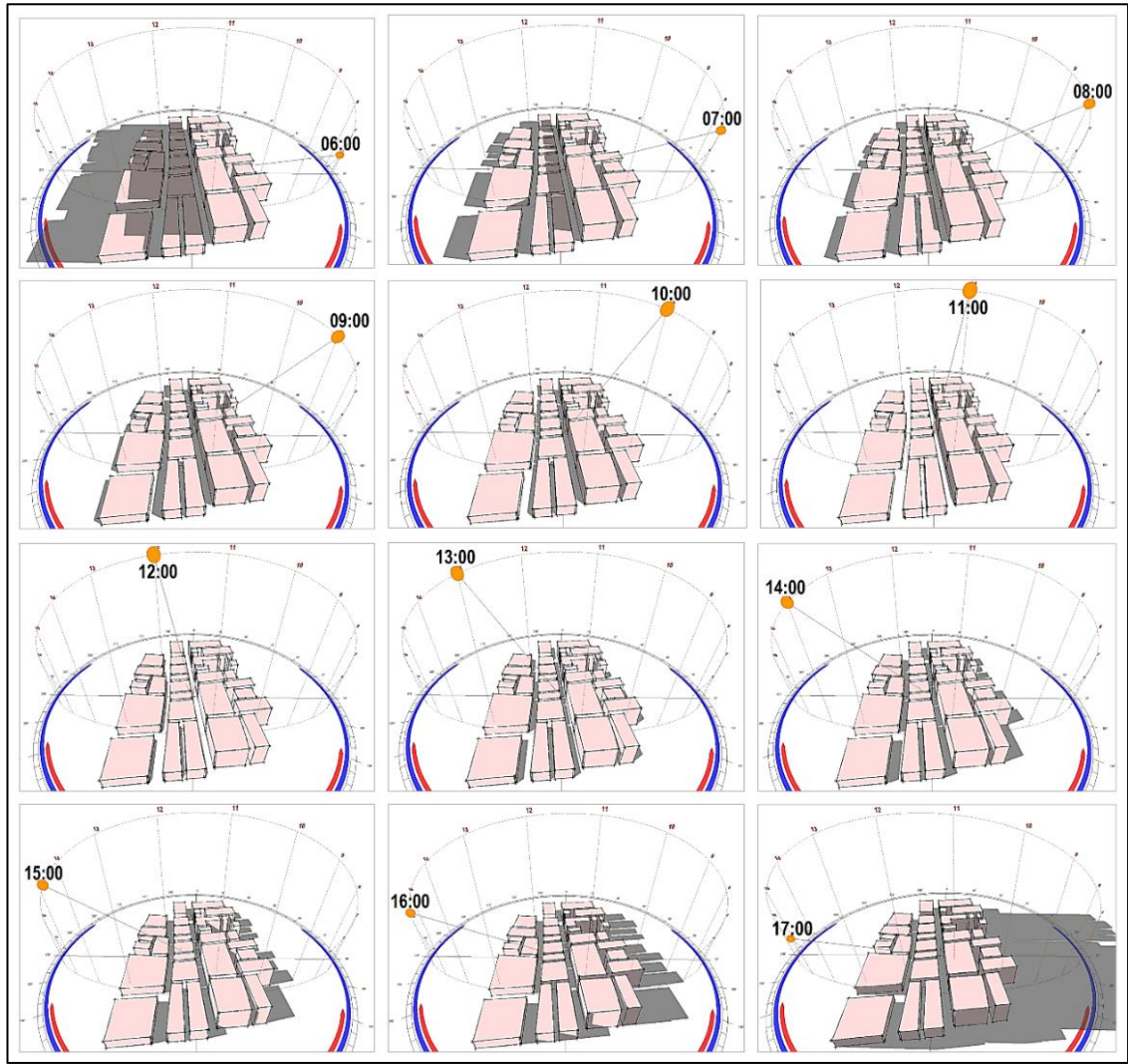


Fig. 8. 35: The level of shading during the day in April (simulation time in spring season) for the configuration of the protruding upper floors models, with building heights of 12m (first row), 15m (second row) and 27m (third row).

### 8.7.2. Wind Velocity at the Pedestrian Level (S-27 and S-28)

Figures 8.36 and 8.37 show the contours of wind velocity magnitudes (m/s) at the pedestrian level in the S-27 scenario (i.e. protruding floors at 15:00 hours) and S-28 scenario (i.e. protruding floors at 12:00 hours), respectively, and compared with the S-11 scenario and S-25 scenarios (i.e. H/W of 1 – 1.3 – 2.3 at 15:00 and 12:00 hours, respectively).





Fig. 8. 36: Velocity contours at the pedestrian level in the S-27 scenario (i.e. protruding floors) at 15:00 hours, and compared with the optimum aspect ratio scenario S-11 at 15:00 hours.

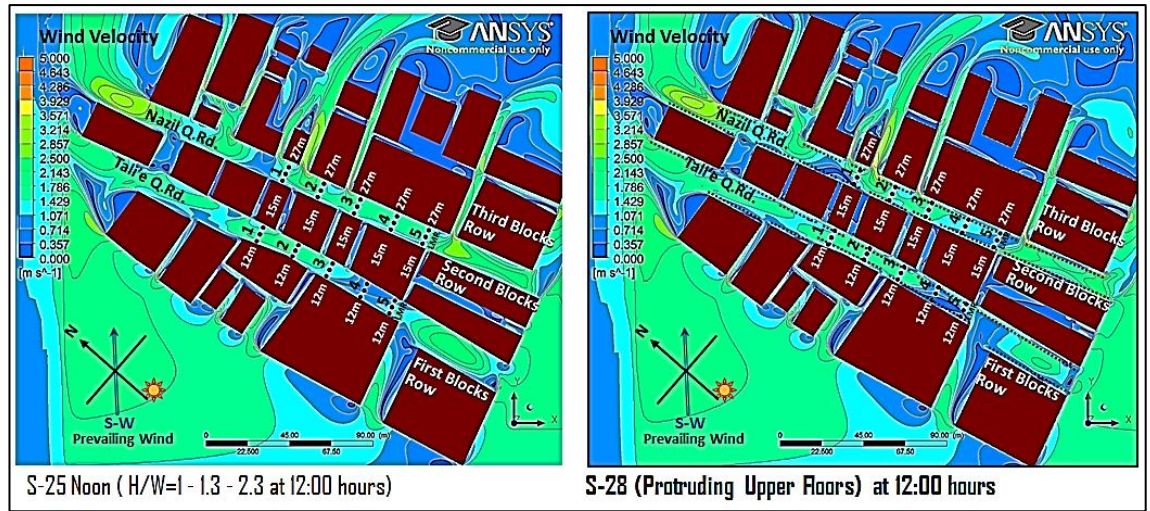


Fig. 8. 37: Velocity contours at the pedestrian level in the S-28 scenario (i.e. protruding floors, H/W of 1.3 - 1.7 - 3) at 12:00 hours, and compared with S-25 scenario (H/W of 1 - 1.3 - 2.3) at 12:00 hours.

It is found that the wind velocity magnitudes at the measurement locations in the leeward canyon (i.e. Nazil Quba Road), have a small difference in values, i.e. 0.2m/s, between the scenarios with protruding upper floors (i.e. S-27 and S-28) and the ones without protruding floors (i.e. S-11 and S-25). This is because these scenarios (S-27 and S-28; S-25 and S-11) share the same building heights of 12m - 15m - 27m for the three rows of buildings, while approaching wind is low. Similarly, the windward canyon (Tali'e Quba Road) has small changes to wind velocity in the protruding upper floors scenarios (S-27 and S-28) compared to the ones with no protruding elevations. The wind velocity values at the 15:00 hours (S-27 and S-11) is higher than at 12:00 hours (S-28 and S-25) scenarios, which is as a result of the approaching wind flow at the city airport is higher in the afternoon hours than the noon ones, i.e. 4.7m/s and 3.9m/s, respectively.

The comparative results in Figure 8.38 demonstrate that the overall wind magnitude in the leeward canyon (i.e. Nazil Quba Road) in S-11 at 15:00 hours (H/W = 1-1.3-2.3 with no protruding floors) obtained the highest average measurement value of 1.8m/s. Then followed by the S-27 at 15:00 hours (H/W of 1.3-1.7-3.0 with protruding floors), with an average measurement value of 1.5m/s, followed by S-25 at 12:00 hours (H/W of 1-1.3-2.3 with no protruding floors), with an average measurement value of 1.5m/s. While S-28 at 12:00 hours (H/W of 1.3-1.7-3 with no protruding floors) is having the lowest velocity values with an average measurement of 1.3m/s.

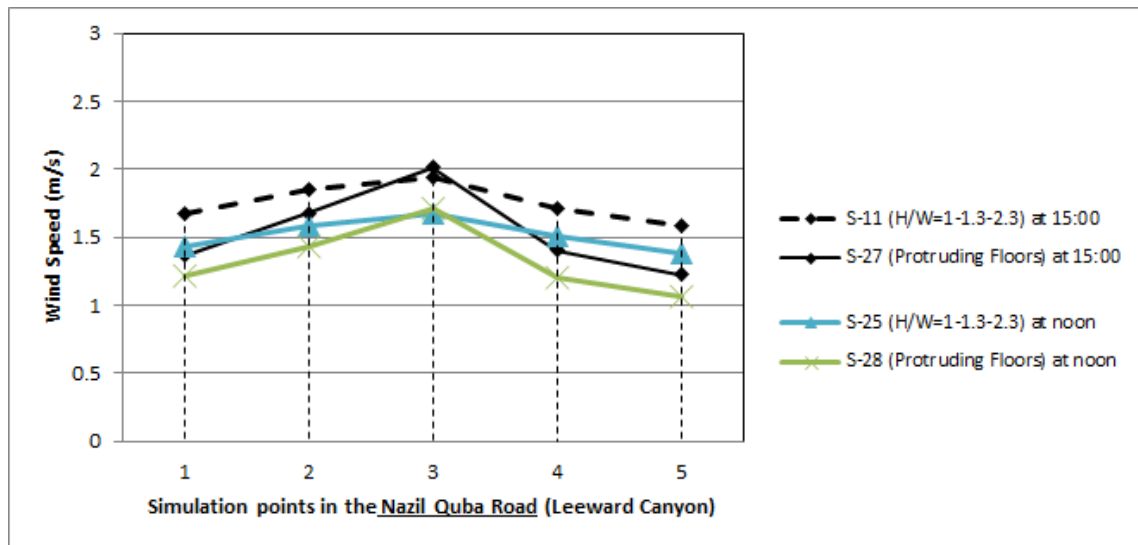


Fig. 8. 38: Wind velocity pattern at the pedestrian level in the leeward canyon for the S-27 scenario (i.e. protruding floors at 15:00 hours) and S-28 scenario (i.e. protruding floors at 12:00 hours), and compared with the S-11 and S-25 scenarios (i.e. H/W of 1 – 1.3 – 2.3 at 15:00hours and 12:00 hours, respectively).

Thus, the increase in urban street aspect ratios based on narrowing the openness to the sky is less effective, in terms of improving wind velocity, than the process of increasing the aspect ratios based on increasing building height.



### 8.7.3. Air Temperature at the Pedestrian Level (S-27 and S-28)

Figures 8.39 and 8.40 show the contours of air temperature at the pedestrian level in the S-27 scenario (i.e. protruding floors at 15:00 hours) and S-28 scenario (i.e. protruding floors at 12:00 hours), respectively, with the shared aspect ratios  $H/W$  of  $1.3 - 1.7 - 3$ . The results are compared with the S-11 scenario and S-25 scenario (i.e.  $H/W$  of  $1 - 1.3 - 2.3$  at 15:00 and 12:00 hours, respectively).

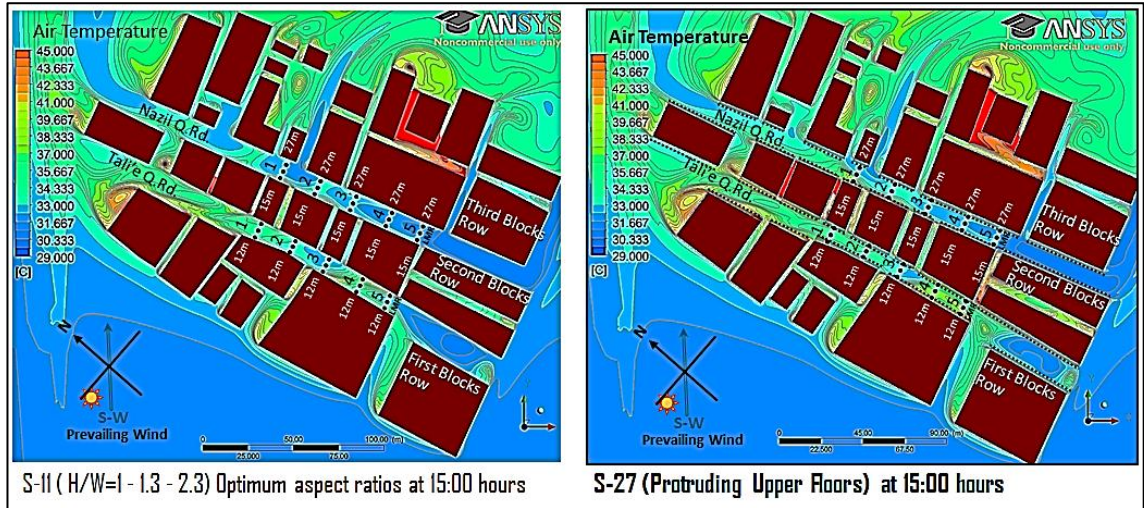


Fig. 8. 39: Air temperature contours at the pedestrian level in the S-27 scenario (i.e. protruding floors) at 15:00 hours, and compared with the optimum aspect ratio scenario S-11 at 15:00 hours.

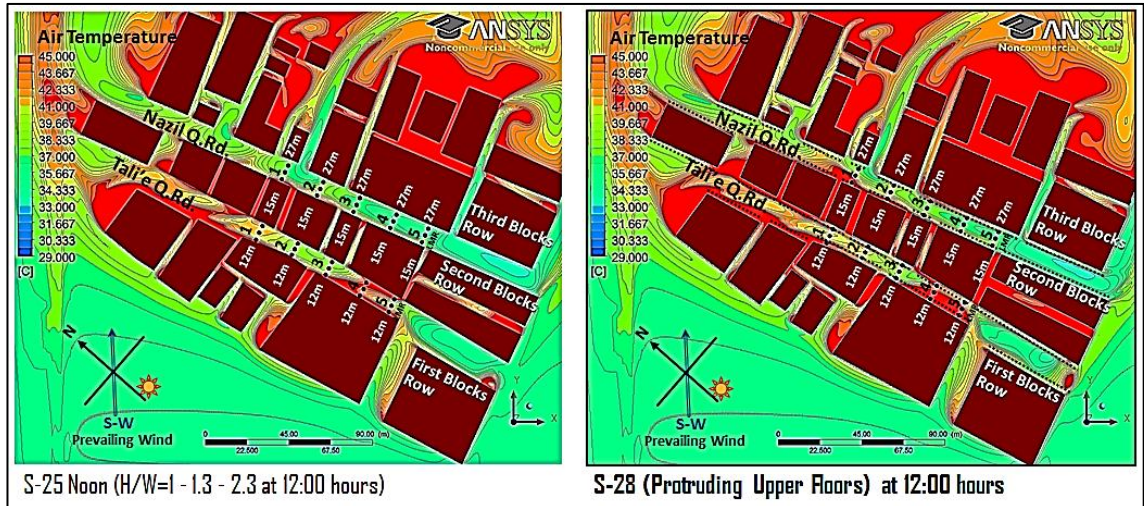


Fig. 8. 40: Air temperature contours at the pedestrian level in the S-28 scenario (i.e. protruding floors,  $H/W$  of  $1.3 - 1.7 - 3$ ) at 12:00 hours, and compared with S-25 scenario ( $H/W$  of  $1 - 1.3 - 2.3$ ) at 12:00 hours.

According to Johansson (2006), the deeper the street canyon (i.e. highly shaded street), which means higher aspect ratio of urban streets, the lower the air temperature. However, in the current study it is found that, at the 15:00 hours, the air temperature in

S-27 (with protruding upper floors, i.e. H/W of 1.3 - 1.7 - 3) has increased by a difference average measurement value of 1.1°C in the leeward canyon (i.e. Nazil Quba Road) compared to the scenario without the protruding upper floors (i.e. S-11 with H/W of 1 - 1.3 - 2.3). Similarly, at the 12:00 hours, the air temperature difference in S-28 (with the protruding upper floors) is having 2°C higher than the S-25 (without protruding floors). The possible explanation for this slight increase in air temperature could be due to the lower convective heat transfer at the pedestrian height, as a result of reduced wind speed in the canyon due to wind movement blockage caused by the protruding upper floors in S-28 and S-27 scenarios with narrower openness to the sky. The findings in Chapter 7 (section 7.2.3) also showed that air temperature followed an opposite pattern to the wind velocity, as it was reduced with the increase in wind speed and vice versa (e.g. Qaid and Ossen, 2014).

The comparative results in Figure 8.41 demonstrate that the overall air temperature at the measurement locations in the leeward canyon (i.e. Nazil Quba Road) in S-11 at 15:00 hours (H/W = 1-1.3-2.3 with no protruding floors) obtained the lowest average measurement value of 32.7°C, then followed by the S-27 scenario at 15:00 hours (H/W of 1.3-1.7-3.0 with the protruding floors), with an average measurement value of 33.8°C. The S-25 scenario at 12:00 hours (H/W of 1-1.3-2.3 with no protruding floors) is having an average measurement value of 37.6°C. While S-28 at 12:00 hours (H/W of 1.3-1.7-3 with protruding floors) is having the highest air temperature values with an average measurement of 39.6°C. The scenarios at 12:00 hours (S-25 and S-28) are having higher values than the ones at 15:00 hours (S-11 and S-27), which is due to the sun position in the south at noon with high level of solar radiation reaching to the north-south axis of Quba Road canyons, leading to a lack of shading, thus increase in air temperature, as illustrated in Figure 8.35 in the shading section 8.7.1.

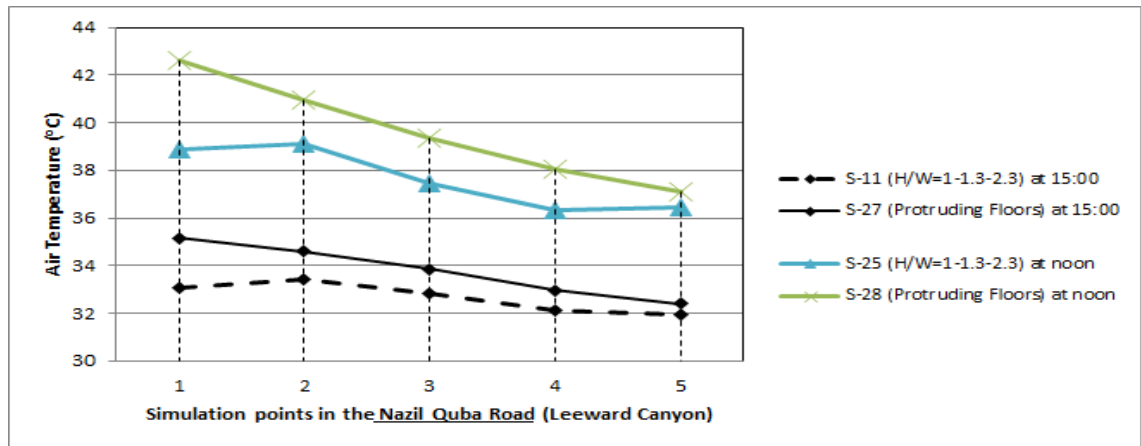


Fig. 8. 41: Air temperature pattern at the pedestrian level in the leeward canyon for the S-27 scenario (i.e. protruding floors at 15:00 hours) and S-28 scenario (i.e. protruding floors at 12:00 hours), and compared with the S-11 and S-25 scenarios (i.e. H/W of 1 – 1.3 – 2.3 at 15:00hours and 12:00 hours, respectively).

## 8.8. Changes to Albedo Level of Surface Materials (S-29)

In the previous proposed scenarios, asphalt and concrete materials with low albedo levels (as in the existing situations) were applied to the ground and building surfaces, respectively. According to Ahranjani (2010), reducing the asphalt-paved area, and using higher solar reflectance (albedo) materials on buildings, can mitigate the heat stress in urban environments.

In the present study, S-29 scenario is proposed by changing the surface material properties from asphalt (i.e. for the ground) and concrete (i.e. for the buildings) to higher albedo levels of soil and white paint, to evaluate their effects on the variation of wind velocity and air temperature in the Quba Road canyons. The material properties for the soil and white paint is based on a study by Qu (2011). The albedo level in this study changes from 0.1 to 0.6 (i.e. from dark surface to white paint) for the building surfaces. Thus, the emissivity of the white paint changes from 0.93 to a ratio of 0.13, compared to the material used in the optimum proposed scenario. While the soil emissivity changes from 0.92 to a value of 0.80 (refer to Table 5.6 in section 5.6.4.7 of the Methodology Chapter).

The study of the changes to albedo level (S-29) analyses the air temperature and wind velocity obtained from 15 measurement locations within each of the windward canyon (i.e. Tali'e Quba Road) and the leeward canyon (i.e. Nazil Quba Roads), and averaged from the readings obtained in the middle, at the right and the left sides of the canyon. The results are then compared with the optimum proposed model of S-11 scenario, as the both scenarios share the same H/W of 1 – 1.3 – 2.3, and the simulation run at 15:00 hours (April).



### 8.8.1. Wind Velocity at the Pedestrian Level (S-29)

Figure 8.42 shows the contours of wind velocity magnitudes (m/s) at the pedestrian level, for S-29 scenario on changing the albedo level of surface materials, and compared with the optimum model of the best proposed aspect ratio (S-11 with H/W of 1-1.3-2.3). The results of wind velocity in the increased albedo scenario (S-29) are similar to the lower albedo scenario in S-11 (i.e. optimum proposed aspect ratio model). Figure 8.43 shows that the wind velocity pattern at the simulated measurement points are the same, with an average measurement values of 1.8m/s. This indicate that increasing the albedo level of the building surfaces from 0.1 to 0.6 has no effect on the wind velocity at the pedestrian level at the simulation time (i.e. 15:00 hours).

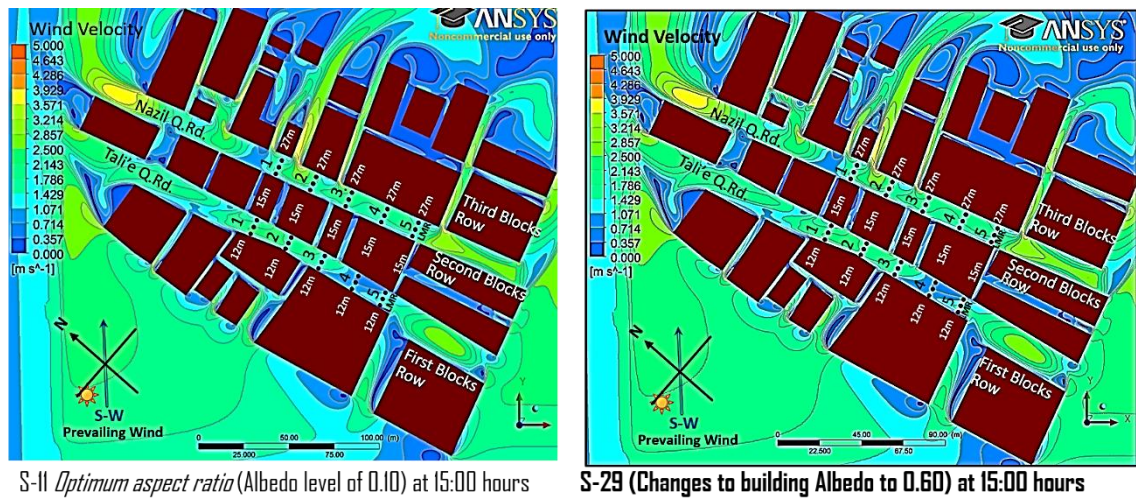


Fig. 8. 42: Velocity contours at the pedestrian level in the S-29 scenario (i.e. changing to a higher albedo level), and compared with the optimum aspect ratio scenario S-11 (lower albedo level) at 15:00 hours.

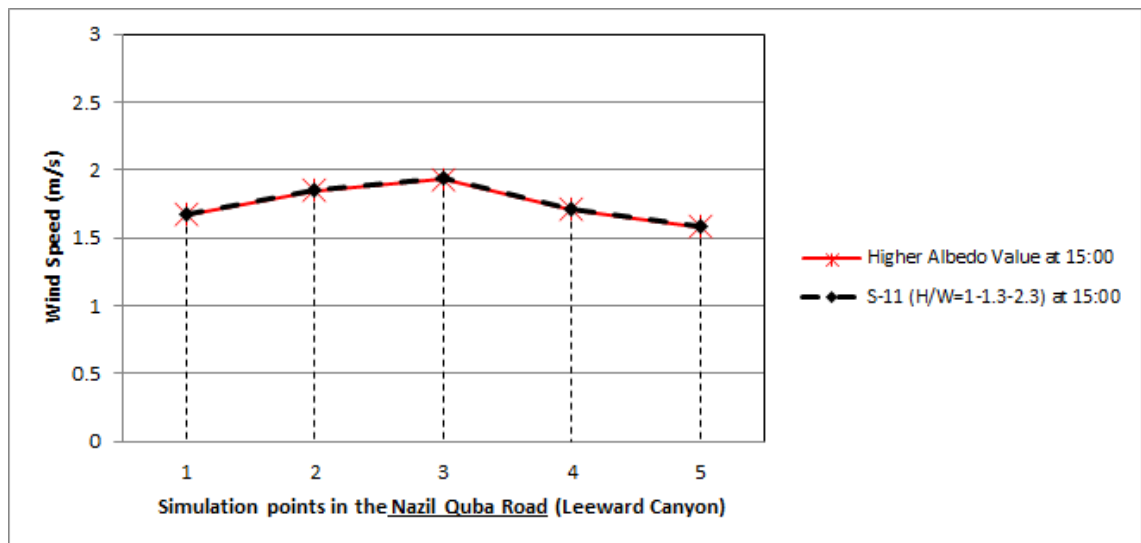


Fig. 8. 43: Wind velocity pattern at the pedestrian level in the leeward canyon for the S-29 scenario (i.e. changing to higher albedo level), compared to the S-11 (i.e. lower albedo) at 15:00 hours.

### 8.8.2. Air Temperature at the Pedestrian Level (S-29)

Figure 8.44 shows the contours of air temperature at the pedestrian level in the S-29 scenario with higher albedo level of surface materials, and compared with the optimum model of the best proposed aspect ratio (S-11 with H/W of 1-1.3-2.3) with lower albedo level at 15:00 hours. The results of air temperature velocity in S-29 (increased albedo level) has almost similar pattern compared to the lower albedo scenario (S-11) at the simulation time. Figure 8.45 shows a small difference in values at the measurement points between the two models, with an average measurement of 32.7°C found in the Nazil Quba Road (leeward canyon) in S-29 and S-11 scenarios. This indicate that increasing the albedo level of the building surfaces from 0.1 to 0.6 has no effect on the air temperature at the pedestrian level, particularly at the simulation time (i.e. 15:00 hours), when the two canyons are in shade.

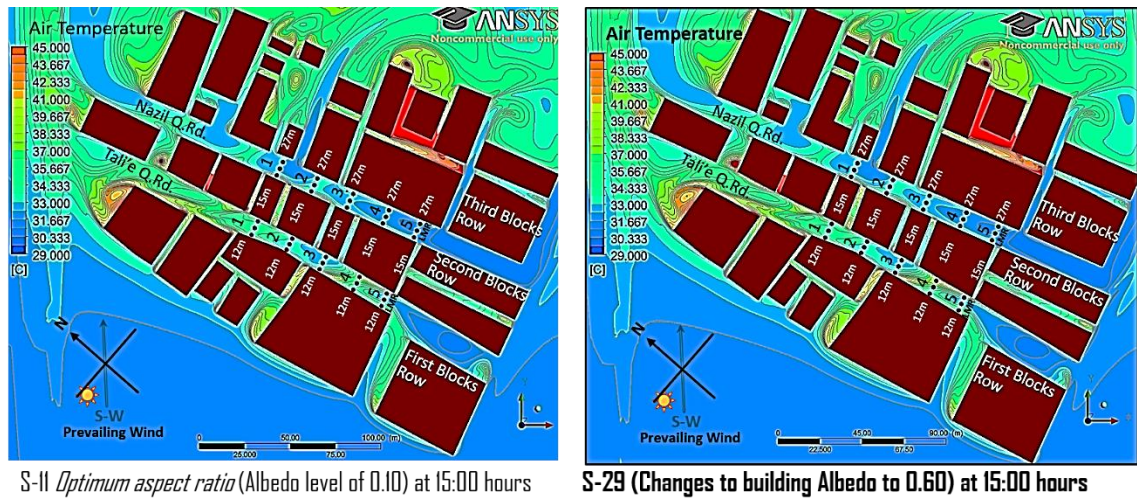


Fig. 8. 44: Air temperature contours at the pedestrian level in the S-29 scenario (i.e. higher albedo level), and compared with the optimum aspect ratio scenario S-11 (lower albedo level) at 15:00 hours.

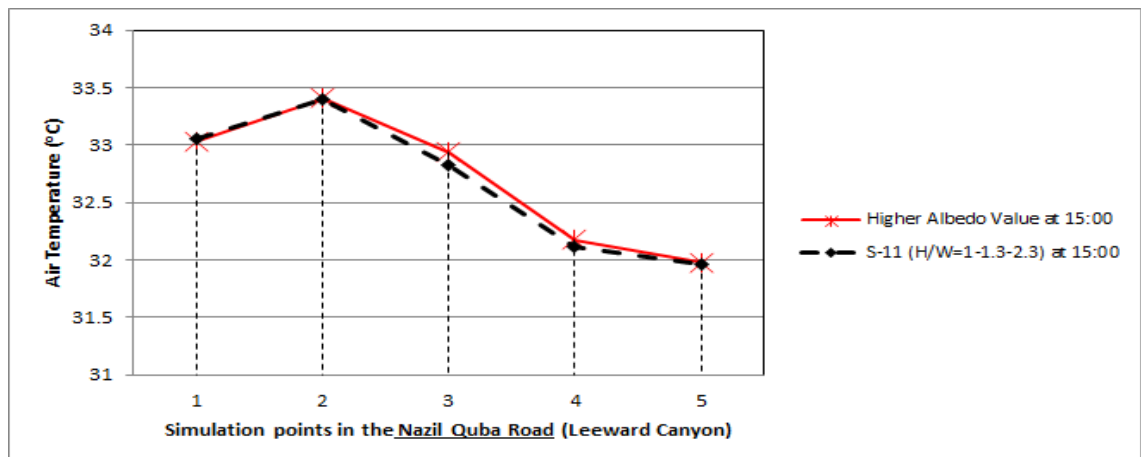


Fig. 8. 45: Air temperature pattern at the pedestrian level in the leeward canyon for the S-29 scenario (i.e. changing to higher albedo level), compared to the S-11 (i.e. lower albedo) at 15:00 hours.

### 8.9. Changes to Block Patterns (S-30 and S-31)

In the previous investigations of wind velocity and air temperature for increasing the number of rows (from 3 to 6 rows) in the S-18 scenario (Grid Style building positions) and S-19 scenario (Chess-Board Style building positions), it was found that the first and second canyons (i.e. Tali'e and Nazil Quba Roads) had no further improvement in microclimate compared to the optimum aspect ratio model (i.e. S-11 with H/W of 1 – 1.3 – 2.3). This could be because of no changes were applied to the block pattern in the first three rows of the buildings in S-18 and S-19 scenarios.

Therefore, scenario S-30 (Grid Style building positions) and S-31 (Chess-Board Style building positions) are proposed here to study the effect of changing the block pattern of the first three rows of the buildings (20m x 20m building footprint dimensions) on the variation of wind flow in the Nazil Quba Road (i.e. Leeward Second Canyon) as well as on the area behind the first three rows, as illustrated in Figure 8.45. Three new rows of buildings are proposed in the leeward area (i.e. beyond the third row) with similar block configurations of S-18 and S-19 for comparative purpose, based on buildings position style and shared multi-asymmetrical aspect ratios.

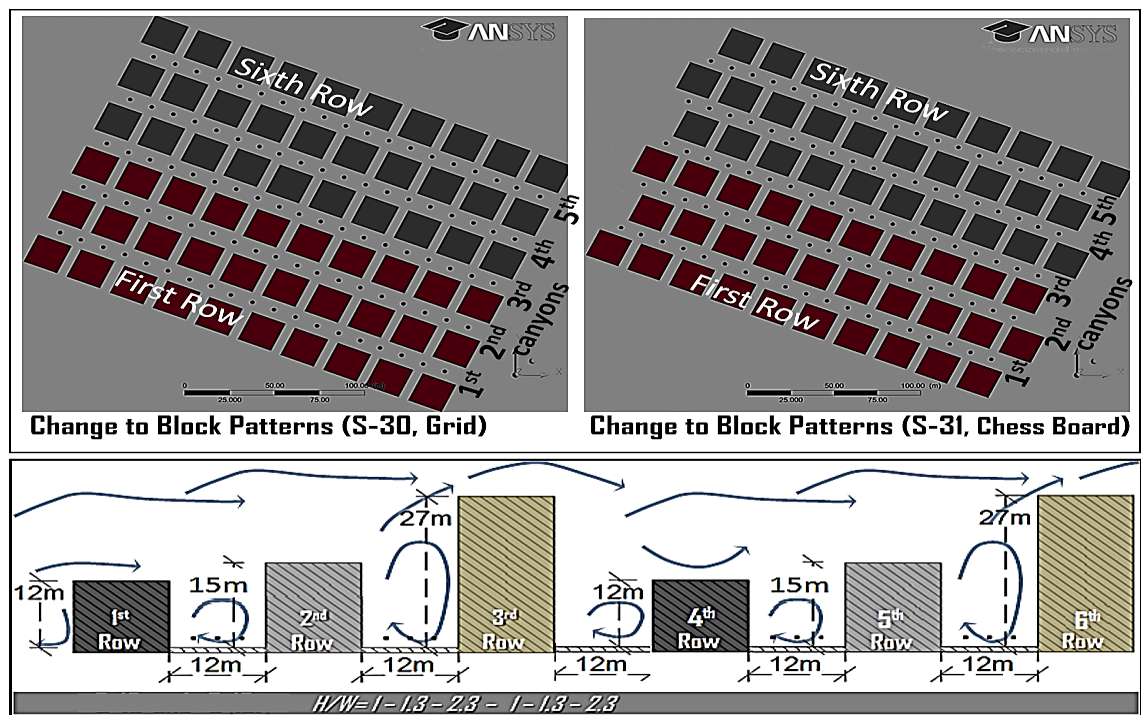


Fig. 8. 46: Changes to block patterns in S-30 with grid building position and S-31 with chess board building position, and increasing the number of rows to be total of 6 rows.



### 8.9.1. Wind Velocity at the Pedestrian Level (S-30, S-31)

Figure 8.47 shows the contours of wind velocity magnitudes (m/s) at the pedestrian level, for the scenarios on changing block patterns in S-30 (with grid style) and S-31 (with chess-board style), and compared with the previously investigated scenarios of increasing the number of building rows in the S-18 (Grid Style) and S-19 (Chess-Board Style).

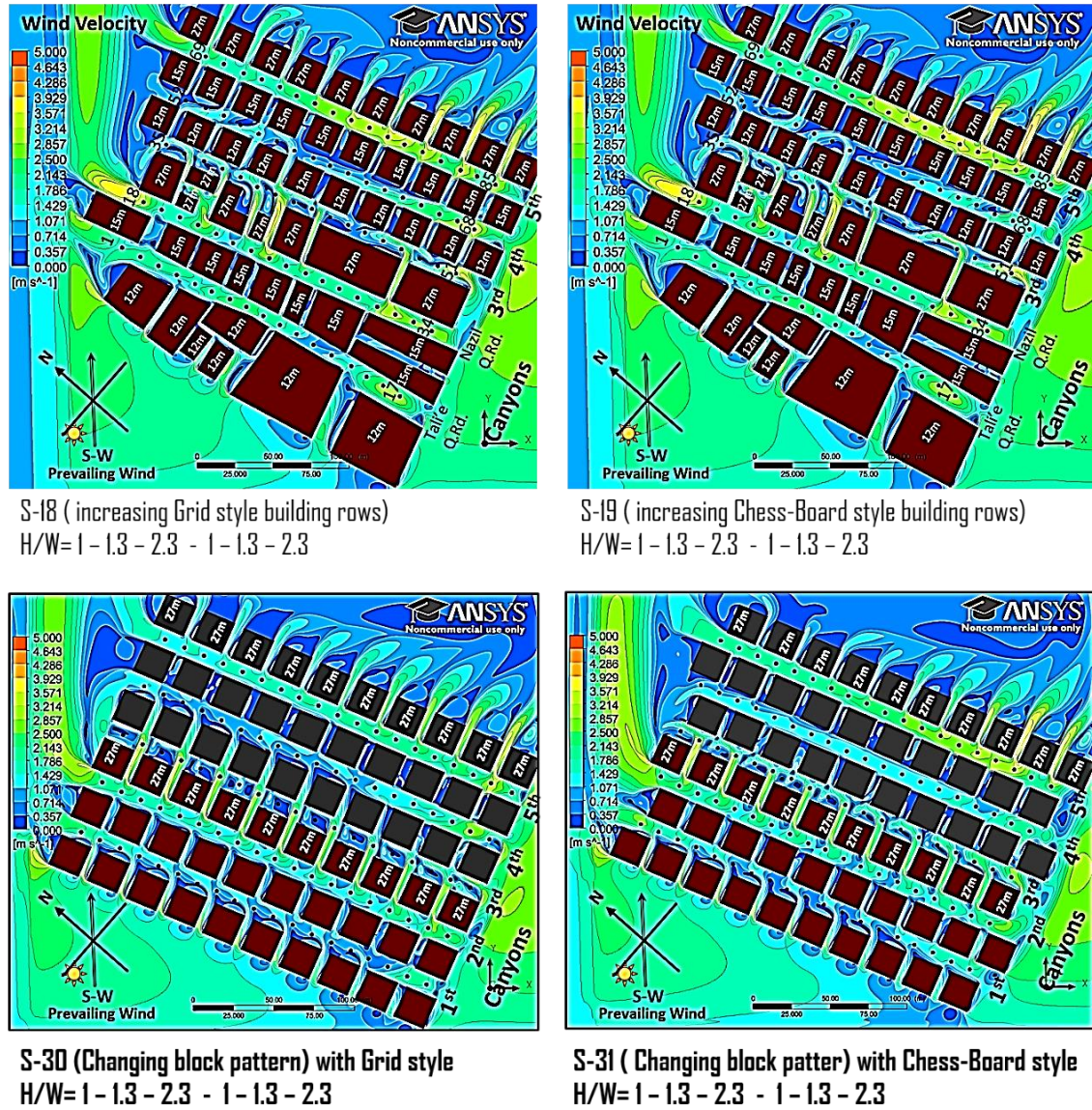


Fig. 8. 47: Wind velocity contour at the pedestrian level for the changing block patterns in S-30 and S-31 scenarios, compared with S-18 and S-19 that share the same aspect ratio configurations.

In comparison between the S-30 (Grid Style) and S-31 (Chess-Board Style), it is found that the chess-board block pattern can improve wind velocities in the leeward areas at the pedestrian height. It is also established that the average measurements of wind magnitude in S-30 scenario for each of the five canyons are 1m/s within the first

canyon (windward canyon), 1.7m/s in the second canyon, 1.3m/s in the third canyon, 1.1m/s in the fourth canyon, and 1.9m/s in the fifth canyon, as illustrated in Figure 8.48.

In S-31 with chess-board block style, the average measurement wind velocity at the pedestrian level is found to be slightly increased from the S-30 configuration, with a value of 1m/s in the first canyon, 1.7m/s in the second canyon, 1.5m/s in the third canyon, 1.3m/s in the fourth canyon, and 2.4m/s in the fifth canyon, as illustrated in Figure 8.49.

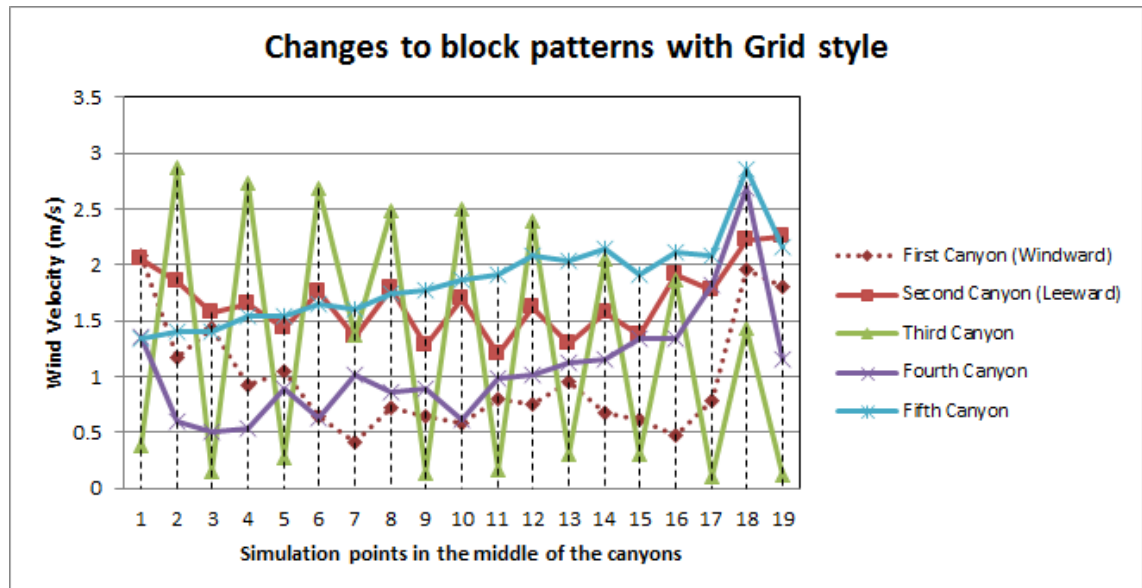


Fig. 8. 48: Wind velocity pattern at the pedestrian level for the changing block patterns in S-30 with grid style position of buildings.

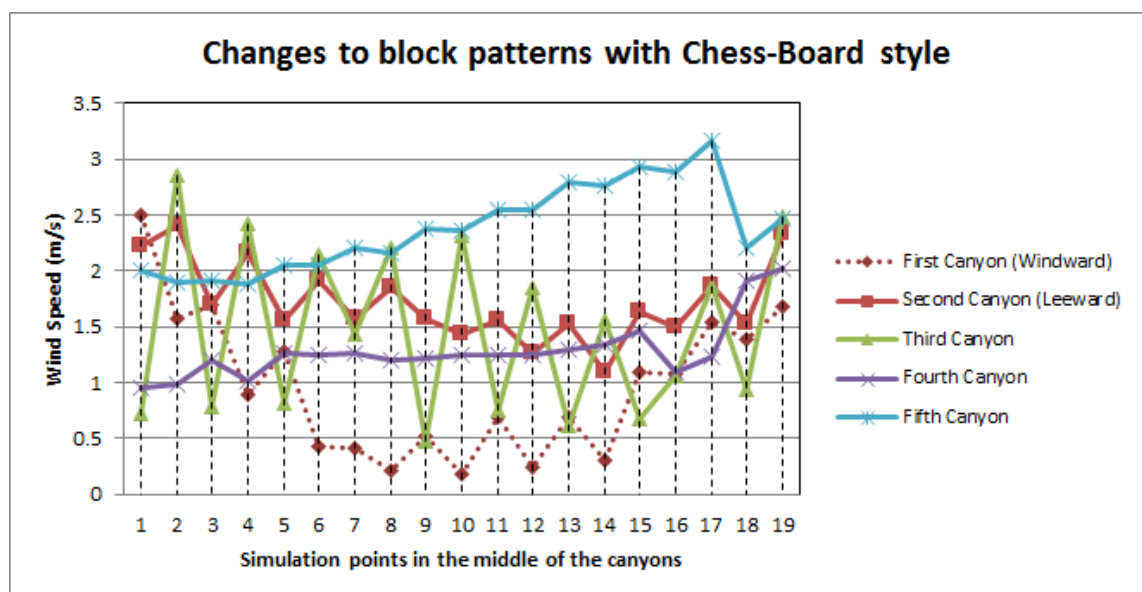
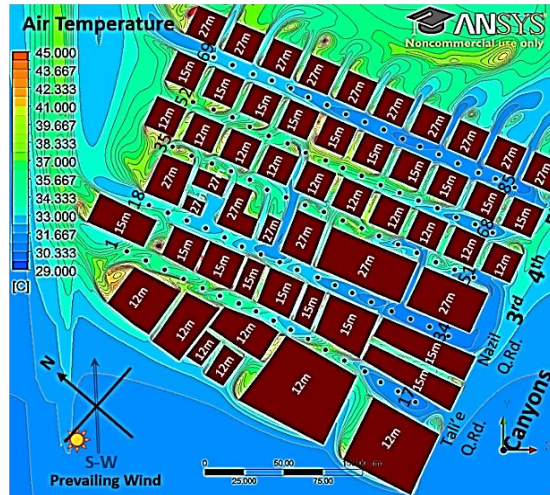


Fig. 8. 49: Wind velocity pattern at the pedestrian level for the changing block patterns in S-31 with chess-board style position of buildings.

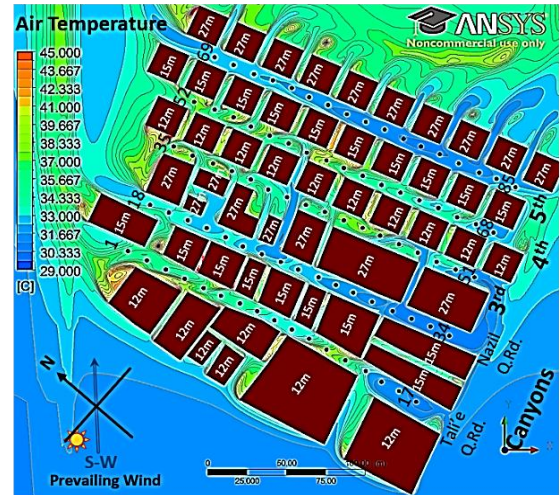


### 8.9.2. Air Temperature at the Pedestrian Level (S-30, S-31)

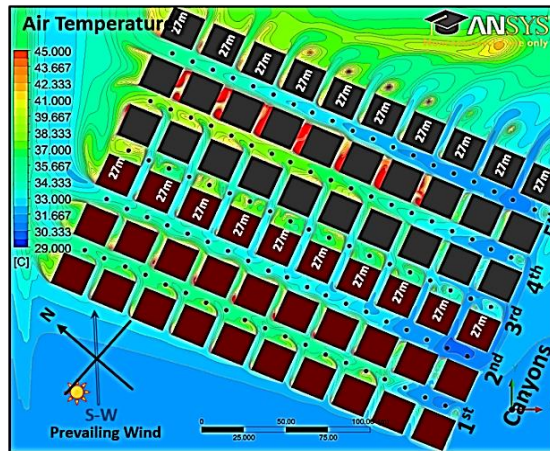
Figure 8.50 shows the contours of air temperature at the pedestrian level for the scenarios on changing block patterns in S-30 (with grid style) and S-31 (with chess-board style), and compared with the previously investigated scenarios of increasing the number of building rows in the S-18 (Grid Style) and S-19 (Chess-Board Style) scenarios.



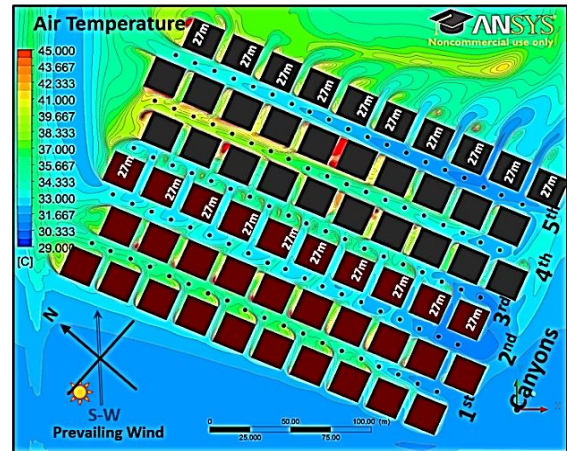
S-18 ( increasing Grid style building rows)  
H/W=1 - 1.3 - 2.3 - 1 - 1.3 - 2.3



S-19 ( increasing Chess-Board style building rows)  
H/W=1 - 1.3 - 2.3 - 1 - 1.3 - 2.3



S-30 (Changing block pattern) with Grid style  
H/W=1 - 1.3 - 2.3 - 1 - 1.3 - 2.3



S-31 ( Changing block patter) with Chess-Board style  
H/W=1 - 1.3 - 2.3 - 1 - 1.3 - 2.3

Fig. 8. 50: Air temperature contours at the pedestrian level for the changing block patterns in S-30 and S-31 scenarios, compared with S-18 and S-19 that share the same aspect ratio configurations.

It is found that the average measurements of air temperature in S-30 scenario within the five canyons are 35.6°C in the first canyon (windward canyon), 33.0°C in the second canyon, 34.8°C in the third canyon, 35.9°C in the fourth canyon, and 32.6°C in the fifth canyon, as illustrated in Figure 8.51. Comparing the results for the canyons



between the first three rows with the S-18 scenario, it can be observed that air temperature has increased in S-30 (change to block patterns to grid style) by a difference value of  $1.7^{\circ}\text{C}$  in the first canyon, and of  $0.8^{\circ}\text{C}$  within the second canyon. Thus, the changes to block patterns in S-30 scenario with grid building position style has no improvement on air temperature within the first three rows of the buildings. This could be due increase in solar access to the canyons when block patterns were reduced.

In S-31 with chess-board block style, the average measurement air temperature at the pedestrian level is obtained at a value of  $35.2^{\circ}\text{C}$  in the first canyon,  $32.7^{\circ}\text{C}$  in the second canyon,  $33.7^{\circ}\text{C}$  in the third canyon,  $36.1^{\circ}\text{C}$  in the fourth canyon, and  $32.1^{\circ}\text{C}$  in the fifth canyon, as illustrated in Figure 8.52. The air temperature measurements in S-30 (Grid style) is slightly higher than the S-31 scenario (Chess board style), which is in line with previous findings by Rizk and Henze (2010).

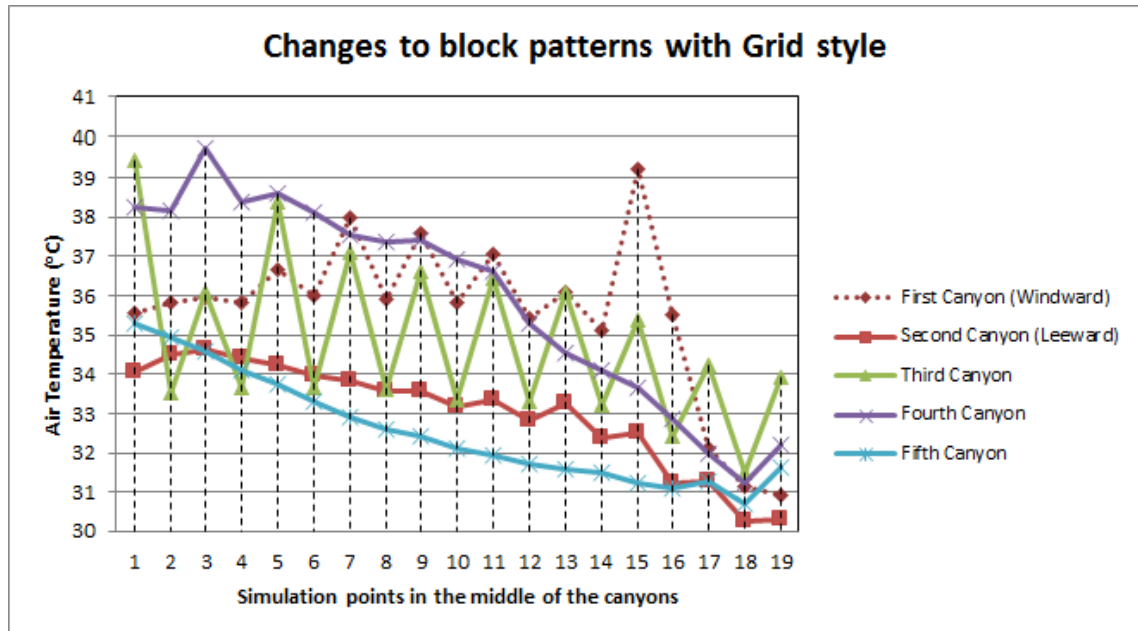


Fig. 8. 51: Air temperature pattern at the pedestrian level for the changing block patterns in S-30 with grid style position of buildings.

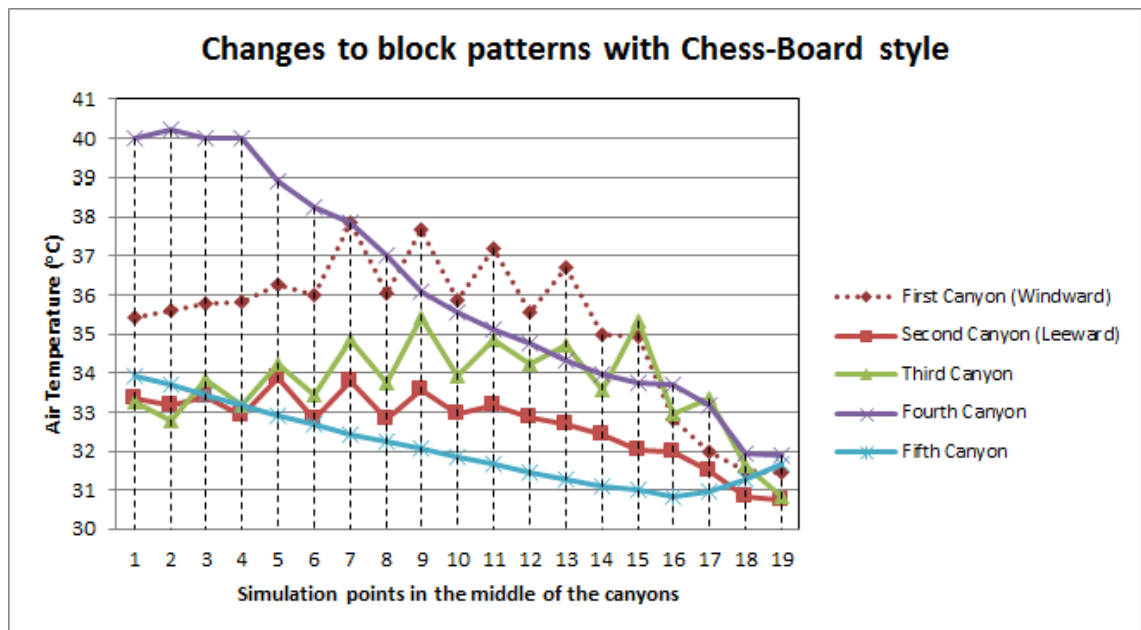


Fig. 8. 52: Air temperature pattern at the pedestrian level for the changing block patterns in S-31 with chess-board style position of buildings.

## 8.10. Implementation of the Research for Future Planning

The context of Madinah is experiencing major development, and the wind velocity in this city is found very low (yearly average of 3.1m/s at the airport). Therefore, this research investigated the possibility for improving wind velocity, thus enhancing pedestrian thermal comfort conditions, based on urban geometry configuration strategy (urban aspect ratios). The outcomes of this research are potentially significant for the redevelopment of Quba Road and for other pedestrian roads that share similar components and likely face similar issues. This section discusses the implementation of the research for future planning, focussing on the influence of multi-asymmetrical aspect ratios on urban pedestrian microclimate and thermal comfort conditions, and the wind variation in the leeward urban area. It also discusses the replicability of the proposed aspect ratios.

### 8.10.1. The Influence of Multi-Asymmetrical Aspect Ratios on Microclimate

For the redevelopment of Quba Road canyons, planners should consider the strategy of leeward gradual increase in urban canyon's aspect ratios, based on variations in building heights. This is because this strategy can increase wind catchment opportunities at the windward elevations, to drag wind downward at the ground and pedestrian levels. In this research, the appropriate specification for the asymmetrical aspect ratios of Quba Road is found to be  $H/W$  of 1 – 1.3 – 2.3, as illustrated in Figure 8. 42. With buildings height of 12m on the first row of the windward buildings, followed by an increased height of 15m on the second row, with the maximum height of 27m on the third row of buildings.

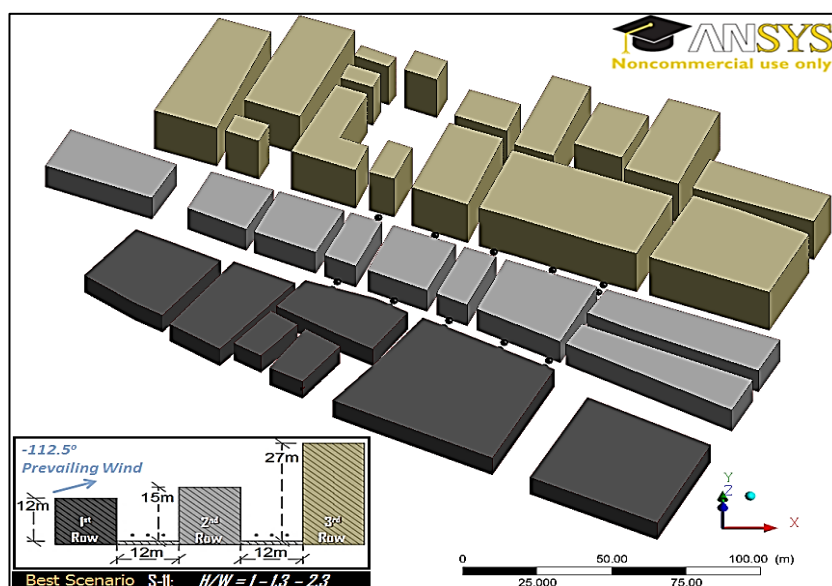


Fig. 8. 53: The best multi-asymmetrical aspect ratios scenario (S-11).

The findings of this research indicate that the strategy of the leeward gradual increase in asymmetrical aspect ratios, with  $H/W$  of 1 – 1.3 – 2.3, improves wind velocity magnitudes at the pedestrian level by 169.2% (i.e. from 0.65m/s to 1.75m/s), with a difference value of 1.1m/s compared to the existing conditions, and reduces ambient air temperatures by 3.4°C (as demonstrated in Table 8.1). Thus, this strategy is recommended for enhancing urban pedestrian microclimates in low wind speed environments.

However, future studies are needed to test the effects of increasing buildings height to above 27m on wind flow, recommending planning policies change. This is to provide broader knowledge for official planners to consider when developing the city.

#### **8.10.2. The Influence of Multi-Asymmetrical Aspect Ratios on Thermal Comfort**

The best performance has the highest improvement level in PET temperature, air temperature and wind velocity, is found in  $H/W$  of 1–1.3–2.3 (i.e. S-11 scenario), as it has improved from an average measurement of 36.7°C to 31.8°C PET (i.e. enhanced by 13%), as demonstrated in Table 8.1. Thus, the research predicts that possible changes to the configuration of the urban fabric can decrease heat stress for pedestrians by 4.9°C (PET).

Lower asymmetrical aspect ratios are not recommended in low wind speed environments, such as in Madinah (average yearly wind 3.1m/s at the airport), as they lead to a skimming wind flow regime over rows of low rise buildings, thus reduced wind velocities at the pedestrian level. Table 8.1 provides a summary of the different aspect ratio configuration results, based on the lower, intermediate and higher variation of buildings height, predicted by the CFD simulation in this research.

The other scenarios that share similar strategy of gradual increase in aspect ratios have also significantly enhanced the PET temperature in the leeward canyon, which are:

- S-16 scenario, with  $H/W$  of 1.3–1.5–2.3, enhances PET by -4.5°C (i.e. 12%).
- S-14 scenario, with  $H/W$  of 1–1.3–2, enhances PET by -4.4°C (i.e. 12%).
- S-15 scenario, with  $H/W$  of 1–1.5–2.3, enhances PET by -3.7°C (i.e. 10%).
- S-6 scenario, with  $H/W$  of 1–1.3–1.8, enhances PET by -3.6°C (i.e. 10%).
- S-13 scenario, with  $H/W$  of 1–1.3–1.5, enhances PET by -1.8°C (i.e. 5%).

PET index has been calibrated for a hot arid climate in built up areas by Yahia and Johansson (2013a), with an upper limit of 31.3°C and lower limit of 21°C. However, these estimated PET values for hot arid urban areas are proposed for Damascus, which is not necessarily transferable to Madinah. Nevertheless, the estimated upper PET thermal comfort limit of 31.3°C and lower limit of 21°C have been used as a reference in this study since no other reference values calibrated for Madinah.

Table 8. 1: Proposed level of thermal comfort performance in the current research based on the Urban Street Canyon H/W Simulation Analysis Compared to the Base Case.

Nazil Quba Road (Leeward Canyon)									
Category	Specification	Air Temperature	Relative Humidity	Wind Velocity	MRT	PET	Improvement level in PET compared to the base case		Level of thermal comfort performance
		°C	%	m/s	°C	°C	°C	(%)	code number
Base Case	S-1 (existing condition)	36.10	8.20	0.65	37.80	36.7	0	0%	1
Symmetrical	S-2 (H/W=1-1-1)	37.62	8.20	0.75	39.32	38.6	1.9	-5%	1**
low asymmetrical	S-3 (H/W=1-0.8-1.3)	33.34	8.20	1.61	35.04	32.8	-3.9	11%	3
	S-4 (H/W=1-1.3-0.8)	38.23	8.20	0.57	39.93	39.2	2.5	-7%	1**
Medium Asymmetrical	S-5 (H/W=1-1.5-1.5)	37.35	8.20	0.56	39.05	38.2	1.5	-4%	1**
	S-6 (H/W=1-1.3-1.8)	33.56	8.20	1.46	35.26	33.1	-3.6	10%	3
	S-7 (H/W=1-1.8-1.3)	36.91	8.20	0.60	38.61	37.7	1	-3%	1*
High Asymmetrical	S-8 (H/W=1-2-2)	37.07	8.20	0.50	38.77	37.8	1.1	-3%	1*
	S-9 (H/W=1-1.8-2.3)	35.42	8.20	0.86	37.12	35.8	-0.9	2%	2
	S-10 (H/W=1-2.3-1.8)	36.38	8.20	0.79	38.08	37	0.3	-1%	1*
	S-11 (H/W=1-1.3-2.3)	32.67	8.20	1.75	34.37	31.8	-4.9	13%	4
	S-12 (H/W=1-2.3-1.3)	36.24	8.20	0.74	37.94	36.9	0.2	-1%	1
Gradual increase	S-13 (H/W=1-1.3-1.5)	34.75	8.20	1.23	36.45	34.9	-1.8	5%	2
	S-14 (H/W=1-1.3-2)	32.99	8.20	1.60	34.69	32.3	-4.4	12%	3
	S-15 (H/W=1-1.5-2.3)	33.41	8.20	1.37	35.11	33	-3.7	10%	3
	S-16 (H/W=1.3-1.5-2.3)	32.94	8.20	1.53	34.64	32.2	-4.5	12%	3

Level of thermal comfort performance	code number	Improvement level in PET compared to the base case
worse performance	1**	≤ -5%
insignificant worse performance	1*	-4% to -1%
no improvement	1	0%
insignificant improvement	2	1% to 4%
significant improvement	3	5% to 12%
best performance	4	≥ 13%

### 8.10.3. The Influence of Increasing the Number of Buildings on Wind Flow in the Leeward Urban Areas

Increasing the number of building rows in the leeward area should duplicate the height and aspect ratios of the first three rows of the buildings, to allow wind velocity to sustain increase. Thus, the aspect ratios with the increased number to six rows of buildings should be  $H/W = 1 - 1.3 - 2.3 - 1 - 1.3 - 2.3$ , as illustrated in Figure 8.43.

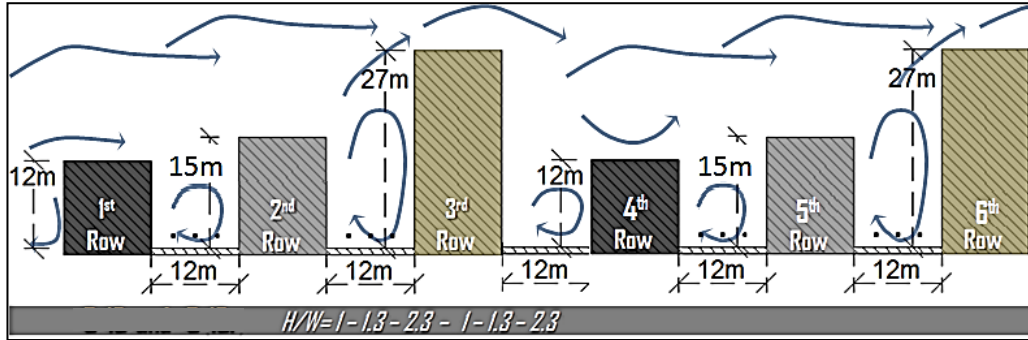


Fig. 8. 54: Proposed implementation aspect ratios for three to six rows of buildings.

The strategy of having the first row and the fourth row of buildings to share the same height of 12m; then gradually increased in the second row and the fifth row of buildings with the height of 15m; while the third row and the sixth row of buildings share the highest elevations of 27m, has shown a 20% improvement in wind velocity at the fifth canyon compared to the second canyon with equivalent windward elevations. This improvement is as a result of the lower pressure zone in between the third row of buildings and the fifth row of buildings leading wind flow to divert from the higher pressure above the third row of buildings downward and toward the sixth row of buildings, where the latter has the higher wind catchment elevations. Thus, it can be concluded that the configuration of the multi-asymmetrical aspect ratio of S-11 ( $H/W$  of 1-1.3-2.3) scenario can improve the wind velocity in the leeward area, particularly if the aspect ratios in the leeward area of the three new rows (i.e. the fourth, fifth and the sixth rows of buildings) have not continue growing gradually from S-11 scenario, but rather after the maximum height of 27m (i.e. the height of the third row in S-11) it should alternate and start back from 12m (i.e. the height of the first row of buildings in S-11 scenario).



#### 8.10.4. The Replicability of the Proposed Asymmetrical Aspect Ratios

The outcomes of this research are potentially significant for the redevelopment of Quba Road and for other pedestrian roads that share similar components and likely face similar issues. However, the study highlighted the effect of the asymmetrical aspect ratios on the urban pedestrian microclimate, based on the existing land footprint and the North-South axis orientation of the urban street canyons, and the maximum height investigated does not exceed 27m, due to the local planning constants.

In this research, the effects of different prevailing wind direction on wind velocity within the proposed street canyon aspect ratio ( $H/W$  of 1 – 1.3 – 2.3) were investigated, and the results were discussed in section 8.4. This includes the South-Westerly (SW) main prevailing wind direction (i.e. S-11 scenario), the Westerly (W) second prevailing wind direction, and the North-Westerly (NW) third prevailing wind directions

This proposed aspect ratio can improve wind velocity at the pedestrian level with all the three prevailing wind directions (SW, W and NW) compared to the existing configuration. However, the street axis is oriented  $-22.5^\circ$  from the north. Thus, wind direction is approximately perpendicular to the canyon in the SW (i.e.  $-112.5^\circ$ ) and W (i.e.  $-67.5^\circ$ ) models, while it is approximately parallel with the NW (i.e.  $-22.5^\circ$ ) model. The SW oriented model obtained the highest wind magnitude for the proposed aspect ratio with a value improved from 0.7m/s to 1.8m/s (i.e. 169%), followed by the NW oriented model, with a value of 1.68m/s (159%), then the W oriented model 1.20m/s (85%).

The configuration of multi-asymmetrical aspect ratio with  $H/W$  of 1 – 1.3 – 2.3 can be replicated in Madinah in areas that share similar street axis of North-South orientation. This is because of the prevailing wind flow direction is approximately perpendicular to the urban canyons. However, in East-West orientation of urban canyons, where the prevailing wind direction is parallel with the canyons, the wind speed can be found higher than the North-South orientation (e.g. Hang et al., 2015). A hypothetical scenario of parallel wind direction with the urban canyon (wind flow from the south) was tested to find out its effects on wind flow at the pedestrian level, as reflected in Appendices from A8.9 to A8.14. Although this is not necessarily applicable to the actual case of wind directions in Quba Road area, but it can provide guidance on East-West canyons orientation in Madinah. The results show increase in the wind velocities for the canyon between the second and the third rows of buildings (i.e. the

Nazil), from the average measurement value of 0.7m/s to 1.8m/s (173.8%) compared to the existing conditions with south-westerly prevailing wind direction.

### 8.11. Summary

In this chapter, further investigations (S-17 through S-24 scenarios) were conducted on the chosen multi-asymmetrical aspect ratios model (S-11 scenario, with  $H/W$  of 1 – 1.3 – 2.3), based on its best performance level on enhancing urban microclimate and thermal comfort in Quba Road, to evaluate their configuration effects on the urban wind flow rate, seeking to find better ways to improve the urban pedestrian microclimate. These scenarios were:

- A scenario on evaluating the variation of wind flow at night (i.e. S-17) for the best proposed  $H/W$  model, to find out its effects on the night time microclimate (e.g. Qaid and Ossen, 2014);
- Two scenarios on increasing the number of buildings' rows with grid building style position (S-18) and chess-board style (S-19) (e.g. Lee et al., 2013; Rizk and Henze, 2010), to find out wind flow variation in the leeward area;
- Two scenarios on orientation of urban canyons with different wind directions (e.g. Yuan and Ng, 2012), including westerly direction (S-20) and north westerly direction (S-21), to find out their effects on wind flow rate in Quba Road; and
- Three scenarios on configuring new streets perpendicular to the existing canyons (e.g. Golany, 1996), including lower street configuration (S-22), upper street configuration (S-23), and upper and lower streets (S-24), to find out whether they can further improve the wind flow in Quba Road.

In the study of the variation of wind flow at night (S-17 scenario), it was found that the wind magnitude in the leeward canyon (i.e. Nazil Quba Road) was improved from an average measurement of 0.4m/s (i.e. existing condition) to a value of 1.2m/s, (i.e. 183%). Thus, the configuration of leeward gradual increase in aspect ratio  $H/W$  of 1 – 1.3 – 2.3 (with building heights of 12m – 15m – 27m), has positive effect on wind velocity during the day and night.

In the study of the variation of wind flow in the leeward area, it was found that by increasing the number of buildings rows in the leeward area to a maximum of 6 rows, with duplicating the height and aspect ratios of the first rows of the buildings, wind

velocity was continued to increase, particularly at the fifth canyon, where higher windward elevations were proposed.

In the study of the orientation of the urban canyon geometry, it was found that in the leeward canyon, the overall wind magnitude was slightly reduced in with the westerly wind direction (S-20 scenario), from the average measurement of 1.8m/s to a value of 1.2m/s (i.e. 31%). With slightly lower difference in the north-westerly wind direction model (S-21 scenario), from the average measurement of 1.8m/s to 1.7m/s (4%).

In the study of the configuration of new streets perpendicular to the Quba canyons, it was found that the overall wind magnitude in the leeward canyon (i.e. Nazil Quba Road) was slightly decreased in the S-22 scenario with the configuration of the Lower Street from the average measurement of 1.8m/s to 1.5m/s (i.e. 17%). With slightly lower difference in S-24 scenario with the configuration of the Upper and Lower Streets from the average measurement of 1.8m/s to 1.5m/s (13%). While in the S-23 scenario with the configuration of the Upper Street, it is found that the wind velocity magnitude in the leeward canyon at the measurement locations has similar average measurement value of 1.8m/s compared to the optimum model (S-11).

## **CHAPTER 9: Conclusions and Recommendations for Future Work**

### **Chapter Structure**

9.1. Introduction

9.2. Main Conclusions

9.3. Limitations of This Research and Implications for  
Future Research

9.4. Recommendations

# Chapter 9:

## Conclusions and Recommendations for Future Work

---

### 9.1. Introduction

The main driver that underpins this research is an opportunity to improve pedestrian thermal comfort in the central part of the hot arid city of Madinah. As the city develops and current street patterns are kept, a study of the possibility of manipulating the asymmetrical aspect ratio of building heights to improve low wind velocities is presented. The conclusions on enhancement of outdoor pedestrian thermal comfort conditions and the proposed future work in the field are outlined in this chapter.

### 9.2. Main Conclusions

This research evaluated the urban pedestrian microclimate and thermal comfort in the main commercial street (Quba Road) in the hot arid climate of Madinah, and evaluated the effect of optimising the existing urban configurations on urban wind flow and pedestrian thermal comfort. The general conclusions drawn from each of the research objectives are as follows:

**Objective 1** (Understanding the context of the case study area and the climatic characteristics - Chapter 2)

Chapter 2 discussed the characteristics of Madinah, including its geographical, economic, and religious importance. The climate in Madinah, the city development plans and local planning and regulations constraints were also discussed. Key issues that were considered were:

- The city experiences low wind velocities and extremely hot arid climate.
- The redevelopment plans of Madinah were discussed, highlighting the potential for conducting this research on Quba Road.
- The local planning and regulations were reviewed and the planning constraints were discussed and linked to the simulation chapters (Chapter 7 and 8). The maximum buildings height of 27 metres and maintaining the existing urban

street footprint were highlighted for the modelling constraints in the current research.

- Three locations were selected for the investigations based on their urban density, which were: the high urban density area (Case 1), intermediate urban density area (Case 2) and low urban density area (Case 3).
- Quba Road canyons (N-S axis with -22.5° orientation from north) are characterized by low wind flow rates (average yearly of 3.1m/s), and high air temperature during the day (average maximum of 36.1°C to 45.8°C), as a result of the approximately perpendicular prevailing wind direction (from south-westerly direction) to the urban canyons with approximately -112° angle of attack, and large building length exposed to extreme solar radiation that increases air temperature at ground level by thermal mass of buildings.

**Objective 2** (Understanding the outdoor thermal comfort interaction factors and the pedestrian thermal comfort criteria for hot arid regions - Chapter 3):

In Chapter 3, a study of the literature provided information regarding the outdoor pedestrian microclimate and thermal comfort. The following was outlined:

- It highlighted some of the main factors leading to urban discomfort (e.g. removing vegetation, lack of shading devices, anthropogenic heat release, etc.).
- It reviewed the previous field studies on outdoor thermal comfort and relevant thermal comfort criteria that is applicable for hot arid climates. Physiological Equivalent Temperature (PET) index was selected for the prediction of thermal comfort conditions in a hot arid region, with upper thermal comfort limit of 31.3°C and lower limit of 21°C.
- It is acknowledged here that temperatures in peak summer season fall out of tolerable and critical thermal comfort ranges (21°C – 31.3°C PET). Therefore, applying any possible urban mitigation measures would rationally aim at improving thermal conditions in intermediate seasons (spring and autumn), where there is a possibility of finding passive means to reduce sensations of near critical thermal comfort conditions.

In addition, the knowledge gap based on the literature review was identified, including:



- Lack of field studies on urban microclimate and outdoor thermal comfort in Saudi Arabia, while no such research has been conducted in Madinah.
- Lack of field studies conducted under the four climatic seasons, particularly in hot arid regions, continuously for periods of 24 hours.

**Objective 3** (Understanding the effects of urban street canyon's configuration on urban wind flow - Chapter 4):

In Chapter 4, the importance of enhancing outdoor pedestrian microclimate and thermal comfort for the usability and attractiveness of public places was discussed and the strategies for urban heat mitigation in urban canyon were reviewed, including:

- Urban street aspect ratios ( $H/W$ ) with variation in buildings height found effective in improving wind speed.
- Orientation of urban streets with prevailing wind directions were found important in controlling wind speed and direction in urban areas at the pedestrian level.

This chapter also reviewed the previous numerical simulation studies on urban pedestrian microclimates and outdoor thermal comfort. To achieve the research aim of finding ways to mitigate heat stress through urban geometry design, highlighting that CFD (computational fluid dynamics) numerical simulation is appropriate for this task.

In addition, the knowledge gap based on the literature review was identified, including:

- The majority of previous studies on thermal comfort have focused on symmetrical aspect ratios rather than asymmetrical ones, thus limit the available knowledge on asymmetrical canyon studies, which are more representative of actual urban areas.
- The study of multiple asymmetrical urban street aspect ratios (i.e. diverse buildings height to street width;  $H_1/W - H_2/W - H_3/W$ ), based on optimising the buildings' height to influence wind flow rate, has not received much attention in the context of urban pedestrian thermal comfort, particularly in low wind speed environments and in hot arid regions.

**Objective 4** (Assessment of the current outdoor thermal comfort in different urban density along Quba Road in Madinah – Chapter 6):

In chapter 6, the analysis of air temperature, mean radiant temperature, relative humidity and wind speed under the four climatic seasons were investigated along Quba Road, particularly within the three selected case studies based on the built up level (i.e. high, intermediate and low urban density areas).

**1) In terms of number of pedestrians, findings were as follows:**

- The number of pedestrians on the street was monitored in the high urban density area during January (in winter), April (in spring) and June (in summer), and an increase of Quba road users were found within the five prayers time (i.e. at 05:00, 12:30, 15:30, 18:00 and 20:30 hours).
- The number increased significantly during late evening until the midnight, which was due to the decrease in MRT values and PET values starting after 16:00 hours. Thus, there is an interrelationship between the number of users and PET comfort temperature.

**2) In terms of air temperature:**

- Comparison between the three different urban densities during the hot climatic seasons revealed that the urban heat island effect (UHI) was higher within the higher urban density areas compared to the low and intermediate urban densities.
- The air temperature patterns in the case studies were similar for the four climatic seasons.
- Heat trap in a deep canyon (street width of 12m) in the high urban density area is higher than in the low urban density area (Case 3), as the latter case has a larger opening to the sky (30m street wide).

**3) In terms of wind speeds and direction:**

- In high urban density (Case 1), the highest air speed is experienced in winter, with an average daily measurement of 1.4m/s, then followed by summer (0.7m/s)

and spring (0.6m/s), respectively, with autumn having the lowest average air speed (0.4m/s), at the pedestrian height.

- Madinah experiences three main wind directions, which are westerly, south-westerly and north westerly directions. However, in built up areas, wind directions can be affected by rough surfaces and moving objects. In autumn, the prevailing direction was from North-East direction with prevailing speed of 0.2-0.5m/s. In winter, the prevailing wind direction with speeds range of 2-2.9m/s was from around south-westerly. In spring, winds reached between 1-1.9m/s, approaching from the prevailing south westerly direction. In summer, the prevailing wind speed direction was around North North-Westerly with wind speed reaching 1-3m/s.

#### **4) In terms of PET thermal comfort index:**

- The best season in Madinah is recognised by the locals, from a tolerable outdoor temperature sensation perspective, to be the spring season, as shown by the fact that most of the PET values in the three different urban density cases during spring season are within the comfort zone (i.e. between 21°C and 31.3°C), then followed by the autumn, while summer having the highest PET values.
- However, the duration of extremely thermal discomfort conditions in spring occurred between 9:00 to 16:00 in the intermediate urban density area, 11:00 to 18:00 in the high urban density, and between 11:00 to 17:00 hours in the low urban density case.
- In the high urban density area, the required average improvement difference in PET temperature to achieve thermal comfort during the uncomfortable period of between 11:00 to 18:00 hours, is 2.5°C PET, i.e. based on the upper limit of comfort threshold 31.3°C PET, while for the peak at 13:00 hours the required improvement difference is 6.1°C.

**Objective 5** (Studying the effects of multi-asymmetrical street aspect ratios on wind flow and thermal comfort - Chapter 7):

In chapter 7, the high urban density area with the three rows of the buildings and the two canyons of Quba Road were simulated using CFD numerical modelling. The effects of variations of building heights to street width  $H/W$  aspect ratios for the three rows of the buildings on urban wind flow were tested on the base case (i.e. the existing situations). Findings can be summarised as follows:

- The simulation results of wind velocity in S-1 scenario in E-3 location, at the right side of the Nazil Quba Road (i.e. leeward canyon), with a value of about 0.5m/s (refer to Figure 7.7), corresponds to the field measurement point in Case 1 (i.e. the high urban density area) with an average value of 0.6m/s at 15:00 hours (refer to Table A6.1 in the Appendices). Thus, the simulation results of the wind velocity are in good agreement with the field measurements.
- The findings of the wind velocities in the base model (S-1) proves that the existing urban configuration (i.e. higher elevations on the middle row of the buildings than side rows) has a negative impact on urban wind velocities in the leeward canyon through blocking the air movement.
- Using the strategy of a leeward gradual increase in the building heights, with multi-asymmetrical aspect ratios  $H/W$  of 1 – 1.3 – 2.3 (i.e. scenario S-11), improves wind velocity magnitudes at the pedestrian level by 169% (i.e. from approximately 0.7m/s to 1.8m/s), decreases ambient air temperature by 3.4°C, and decreases heat stress for pedestrians by 4.9°C PET (i.e. 13%, reduced from 36.7°C to 31.8°C in PET).
- The findings revealed that small incremental increase in wind velocity (e.g. from 0.7m/s to 1.8m/s) can lead to a significant improvement in thermal comfort level.

The other scenarios that share similar strategy of gradual increase in multi-asymmetrical aspect ratios have also enhanced the PET temperature in the leeward canyon, and the findings can be summarised as follows:

- S-16 scenario, with  $H/W$  of 1.3–1.5–2.3, enhances PET by 4.5°C
- S-14 scenario, with  $H/W$  of 1–1.3–2, enhances PET by 4.4°C
- S-15 scenario, with  $H/W$  of 1–1.5–2.3, enhances PET by 3.7°C
- S-6 scenario, with  $H/W$  of 1–1.3–1.8, enhances PET by 3.6°C
- S-13 scenario (with  $H/W$  of 1–1.3–1.5), enhances PET by 1.8°C.

**Objective 6** (Further investigations on a proposed aspect ratio model - Chapter 8)

In chapter 8, further investigations were conducted on the chosen multi-asymmetrical aspect ratios model (S-11 scenario, with H/W of 1 – 1.3 – 2.3), based on its best performance level on enhancing urban microclimate and thermal comfort in Quba Road, to evaluate their configuration effects on the urban wind flow rate, seeking to find better ways to improve the urban pedestrian microclimate.

- A scenario on evaluating the variation of wind flow at night (i.e. S-17) for the best proposed H/W model, to find out its effects on the night time microclimate. It was found that the wind magnitude in the leeward canyon (i.e. Nazil Quba Road) was improved from an average measurement of 0.4m/s (i.e. existing condition) to a value of 1.2m/s, (i.e. 183%).
- Two scenarios were tested on the variation of pedestrian wind velocities in the leeward direction, through increasing the number of buildings' rows with grid building style position (S-18) and chess-board style (S-19). It was found that by increasing the number of buildings rows in the leeward area to a maximum of 6 rows, with duplicating the height and aspect ratios of the first three rows of the buildings, wind velocity continued to increase with a 20% improvement in wind velocity at the fifth canyon compared to the second canyon that has equivalent windward elevations (27m height).
- Two scenarios were tested on orientation of urban canyons with other prevailing wind directions, including westerly direction (S-20) and north westerly direction (S-21). It was found that in the leeward canyon, the overall wind magnitude was slightly reduced in the westerly wind direction model (S-20), from the average measurement of 1.8m/s to a value of 1.2m/s (i.e. 31%). There was a lower difference in the north-westerly wind direction model (S-21 scenario), from the average measurement of 1.8m/s to 1.7m/s (4%).
- Three scenarios were tested on configuring new streets perpendicular to the existing canyons, including lower street configuration (S-22), upper street configuration (S-23), and upper and lower streets (S-24), to find out whether they could further improve the wind flow in Quba Road. It was found that the overall wind magnitude in the leeward canyon (i.e. Nazil Quba Road) was slightly decreased in the S-22 scenario with the configuration of the Lower Street from the average measurement of 1.8m/s to 1.5m/s (i.e. 17%). There was a slightly lower difference in S-24 scenario with the configuration of the Upper

and Lower Streets from the average measurement of approximately 1.8m/s to 1.5m/s (13%), while in the S-23 scenario with the configuration of the Upper Street, it was found that the wind velocity magnitude in the leeward canyon has no effect on improving wind velocity at the measurement locations, with an average measurement value of 1.8m/s.

- The study also established that the eastern side of the Quba Road canyons is recommended for better ventilations when designing open spaces in the high urban density area, due to the gradual increase in the building heights in the leeward direction.

**Objective 7** (Guidelines for future planning and implementation of the research – Chapter 8):

For the redevelopment of Quba Road canyons, planners should consider the following:

- Configuring variations in buildings' height, with the improved asymmetrical aspect ratios of H/W of 1 – 1.3 – 2.3. This is with buildings height of 12m on the first row of buildings, followed gradual height of 15m on the second row, with the maximum height of 27m to be configured on the third row of buildings. This configuration can increase wind speed in the leeward canyon by 169%, with a difference value of 1.1m/s compared to the existing conditions. This small increase in wind speed can improve the pedestrian thermal comfort level by reducing 4.9°C of PET temperature.
- The strategy of having the first row and the fourth row of buildings to share the same height of 12m; then gradually increased in the second row and the fifth row of buildings with the height of 15m; while the third row and the sixth row of buildings sharing the highest elevations of 27m, has shown a 20% improvement in wind velocity at the fifth canyon compared to the second canyon with equivalent windward elevations.

Generally, other investigated scenarios such as protruding upper floors, changing Albedos, and changing block patterns have negligible effects on thermal comfort and wind velocity at the pedestrian levels. This is due to the low approaching wind speed in the study area. Although 4.9°C was attained in PET, however it is difficult to achieve acceptable thermal comfort level during the hot seasons of the year.



### **9.3. Limitations of This Research and Implications for Future Research**

The major limitations in this research are the local planning and regulation constraints for the maximum buildings height as well as the large footprints for buildings. This research analysed the effect of optimisation of buildings height (aspect ratios) based on these constraints. Therefore, in future studies, increasing the buildings height above 27m could be recommended to further enhance the wind environments, thus the outdoor pedestrian thermal comfort levels. In addition, further studies are required to include more variations in buildings forms and footprints (particularly by reducing the size of the current large footprints found in this research). Future research could also consider different orientations of urban street canyon with the prevailing wind directions, as this current research is limited to north-south axis orientation while approximately perpendicular to the prevailing wind directions.

The other limitations of this research are due to limitations in computing time and resource, the steady state CFD RANS numerical simulation were applied instead of the unsteady method, thus only one day (the average reading of a hot April month found in the weather file) of the spring season was analysed and this may not represent the whole spring season months. Moreover, thermal comfort analysis using CFD FLUENT was not possible due to the limitations of the software in certain thermal comfort boundary conditions (e.g. setting humidity, mean radiant temperature, etc.). Therefore, in future studies, the simulation research method could be different to address the limitations in computing time and resource.

Furthermore, the simulation study of outdoor thermal comfort in the current research is limited to the base model of high urban density area with no source of water or vegetation, thus future studies could consider testing the implementation of these urban interventions to find out their contribution in mitigating the urban heat stress.

#### **9.4. Recommendations**

This study focused on the optimisation of urban street aspect ratio as a heat mitigation strategy, and it is established that this strategy can enhance 169% of wind speed, 3.4°C of air temperature and thus 4.9°C in thermal comfort conditions at the pedestrian level in the study area. However, there are many other mitigation parameters that have not been investigated in this research due to time limitation. Therefore, the following urban interventions are recommended for future studies:

- Vegetation to control the effects of; wind flow, radiation and shading, pollution concentration level, and humidity and moisture in the surrounding air.
- Water features to control the effects of evaporative cooling as heat mitigation technique in hot climates.

Future studies are needed to test the effects of increasing buildings height to above 27m on wind flow, recommending planning policies change. This is to provide broader knowledge for official planners to consider when developing the city.

## References

- Abdel-Ghany, A.M., Al-Helal, I.M. and Shady, M.R. (2013) 'Human Thermal Comfort and Heat Stress in an Outdoor Urban Arid Environment: A Case Study', *Advances in Meteorology*, 2013, pp. 1-7.
- Abohela, I., Hamza, N. and Dudek, S. (2013) 'Effect of Roof Shape, Wind Direction, Building Height and Urban Configuration on the Energy Yield and Positioning of Roof Mounted Wind Turbines', *Renewable Energy*, 50(0), pp. 1106-1118.
- Ahmed, K.S. (2003) 'Comfort in Urban Spaces: Defining the Boundaries of Outdoor Thermal Comfort for the Tropical Urban Environments', *Energy and Buildings*, 35(1), pp. 103-110.
- Ahmed-Ouameur, F., Potvin, A. (2007) 'Microclimates and Thermal Comfort in Outdoor Pedestrian Spaces, a Dynamic Approach Assessing Thermal Transients and Adaptability of the Users.' *Conference Proceedings of the American Solar Energy Society (ASES)*, SOLAR, 17-12 July, Cleaveland, Ohio.
- Ahranjani, P.M. (2010) *Systematic Simulation Method to Quantify and Control Pedestrian Comfort and Exposure during Urban Heat Island*. Concordia University [Online]. Available at: [http://spectrum.library.concordia.ca/7040/1/Aranjani\\_PhD\\_S2011.pdf](http://spectrum.library.concordia.ca/7040/1/Aranjani_PhD_S2011.pdf).
- AIAA (1998) *Guide for the Verification and Validation of Computational Fluid Dynamics Simulation*. AIAA.
- Aihua, M., Jie, L., Yi, L., Xiaonan, L. and Ruomei, W. (2011) 'A Multi-disciplinary Strategy for Computer-Aided Clothing Thermal Engineering Design', *ELSEVIER Computer-Aided Design*, 43, pp. 1854-1869.
- Akbari, H., Davis, S., Dorsano, S., Huang, Y.J. and Winnett, S. (1992) *Cooling Our Communities: A Guidebook on Tree Planting and Light-Colored Surfacing*. U.S. Environmental Protection Agency Office of Policy: Analysis Climate Change Division. Available at: <http://escholarship.org/uc/item/98z8p10x#page-195>.
- Al-Ajmia, F.F., Loveday, D.L., Bedwell, K.H. and Havenith, G. (2008) 'Thermal Insulation and Clothing Area Factors of Typical Arabian Gulf Clothing Ensembles for Males and Females: Measurements Using Thermal Manikins', *Applied Ergonomics*, 39(3), pp. 407-414.
- Al-Ibrahim, M.H. (1990) 'The Criticism of Modern Architecture in Saudi Arabia', *Journal of King Saud University*, 2, pp. 63-80.
- Alexandri, E. and Jones, P. (2008) 'Temperature Decreases in an Urban Canyon due to Green Walls and Green Roofs in Diverse Climates', *Building and Environment*, 43(4), pp. 480-493.

- Ali-Toudert, F. (2005) *Dependence of Outdoor Thermal Comfort on Street Design in Hot and Dry Climate*. Freiburg University [Online]. Available at: <https://www.meteo.uni-freiburg.de/forschung/publikationen/berichte/report15.pdf>.
- Ali-Toudert, F., Djenane, M., Bensalem, R. and Mayer, H. (2005) 'Outdoor Thermal Comfort in the Old Desert City of Beni-Isguen, Algeria', *Journal of Climate Research*, 28, pp. 243-256.
- Ali-Toudert, F. and Mayer, H. (2006) 'Numerical Study on the Effects of Aspect Ratio and Orientation of an Urban Street Canyon on Outdoor Thermal Comfort in Hot and Dry Climate', *Building and Environment*, 41(2), pp. 94-108.
- Ali-Toudert, F. and Mayer, H. (2007) 'Effects of Asymmetry, Galleries, Overhanging Façades and Vegetation on Thermal Comfort in Urban Street Canyons', *Solar Energy*, 81(6), pp. 742-754.
- Aljawabra, F. and Nikolopoulou, M. (2010) 'Influence of Hot Arid Climate on the Use of Outdoor Urban Spaces and Thermal Comfort: Do Cultural and Social Backgrounds Matter?', *Intelligent Buildings International*, 2, pp. 198-217.
- Al Madinah Regional Municipality (2011) 'Madinah's Geographical Background'. 27 October 2011. Madinah: Al Madinah Regional Municipality. Available at: <http://www.amana-md.gov.sa/sites/en/AboutAlmadinah/GeographicalGlance/Pages/Home.aspx>.
- Al-Sallal, K.A. and Al-Rais, L. (2011) 'Outdoor Airflow Analysis and Potential for Passive Cooling in the Traditional Urban Context of Dubai', *Renewable Energy*, 36(9), pp. 2494-2501.
- Al-Sallal, K.A. and Al-Rais, L. (2012) 'Outdoor Airflow Analysis and Potential for Passive Cooling in the Modern Urban Context of Dubai', *Renewable Energy*, 38(1), pp. 40-49.
- Arnfield, A.J. (2003) 'Two Decades of Urban Climate Research: A Review of Turbulence, Exchanges of Energy and Water, and the Urban Heat Island', *International Journal of Climatology*, 23(1), pp. 1-26.
- ASCE (1996) 'Wind-Tunnel Studies of Buildings and Structures', *Journal of Aerospace Engineering, American Society of Civil Engineers (ASCE)*, 9(1), pp. 19-36.
- ASHRAE (1985) 'Handbook of Fundamentals: An Instrument of Service Prepared for the Profession Containing Technical Information' *American Society of Heating, Refrigerating and Air Conditioning Engineers*. SI Edition.
- ASHRAE (2004) *ASHRAE Standard 55*. American Society of Heating, Refrigerating and Air-Conditioning Engineers.
- ASHRAE (2009) *ASHRAE Handbook, Fundamentals*. Inch-Pound edn. Atlanta: American Society of Heating, Refrigerating and Air-Conditioning Engineers.

- ASHRAE (2013) *Thermal Environmental Conditions for Human Occupancy*. ANSI/ASHRAE Standard 55-2013 edn. Atlanta: American Society of Heating, Refrigerating and Air-Conditioning Engineers.
- Auliciems, A. and Szokolay, S.V. (2007) *Thermal Comfort* (PLEA Note 3: Passive and Low Energy Architecture International: Design Tools and Techniques). [Online]. Available at: <http://plea-arch.org/wp-content/uploads/PLEA-NOTE-3-THERMAL-COMFORT.pdf>.
- Bartzis, J.G., Vlachogiannis, D. and Sfetsos, A. (2004) 'Thematic Area 5: Best Practice Advice for Environmental Flows', *The QNET-CFD Network Newsletter*, 2(4), pp. 34-39.
- Berger, X. (1988) 'The Pumping Effect of Clothing', *International Journal of Ambient Energy*, 9(1), pp. 37-46.
- Błażejczyk, K., Broede, P., Fiala, D., Havenith, G., Holmér, I., Jendritzky, G., Kampmann, B. and Kunert, A. (2010) 'Principles of the New Universal Thermal Climate Index (UTCI) and its Application to Bioclimatic Research in European Scale', *Miscellanea Geographica*, 14, pp. 91-102.
- Blocken, B. and Carmeliet, J. (2004a) 'A Review of Wind-Driven Rain Research in Building Science', *Journal of Wind Engineering and Industrial Aerodynamics*, 92(13), pp. 1079-1130.
- Blocken, B. and Carmeliet, J. (2004b) 'Pedestrian Wind Environment around Buildings: Literature Review and Practical Examples', *Journal of Thermal Envelope and Building Science*, 28(2), pp. 107-159.
- Blocken, B., Roels, S. and Carmeliet, J. (2004) 'Modification of Pedestrian Wind Comfort in the Silvertop Tower Passages by an Automatic Control System', *Journal of Wind Engineering and Industrial Aerodynamics*, 92(10), pp. 849-873.
- Blocken, B., Stathopoulos, T. and Carmeliet, J. (2007) 'CFD Simulation of the Atmospheric Boundary Layer: Wall Function Problems', *Atmospheric Environment*, 41(2), pp. 238-252.
- Blocken, B. and Carmeliet, J. (2008) 'Pedestrian Wind Conditions at Outdoor Platforms in a High-Rise Apartment Building: Generic Sub-Configuration Validation, Wind Comfort Assessment and Uncertainty Issues', *Wind and Structures*, 11(1), pp. 51-70.
- Blocken, B., Defraeye, T., Derome, D. and Carmeliet, J. (2009a) 'High-Resolution CFD Simulations for Forced Convective Heat Transfer Coefficients at the Facade of a Low-Rise Building', *Building and Environment*, 44(12), pp. 2396-2412.
- Blocken, B., Stathopoulos, T., Carmeliet, J. and Hensen, J. (2009b) 'Application of CFD in Building Performance Simulation for the Outdoor Environment', *11<sup>th</sup> International IBPSA Conference: Building Simulation*. Scotland: Glasgow, 27-30 July. pp. 489-496.
- Blocken, B. and Persoon, J. (2009) 'Pedestrian wind comfort around a large football stadium in an urban environment: CFD simulation, validation and application of the

new Dutch wind nuisance standard', *Journal of Wind Engineering and Industrial Aerodynamics*, 97(5–6), pp. 255-270.

Blocken, B., Janssen, W.D. and van Hooff, T. (2012) 'CFD simulation for pedestrian wind comfort and wind safety in urban areas: General decision framework and case study for the Eindhoven University campus', *Environmental Modelling & Software*, 30(0), pp. 15-34.

Brown, R.D. and Gillespie, T.J. (1995) *Microclimate Landscape Design: Creating Thermal Comfort and Energy Efficiency*. New York: John Wiley & Sons.

Brown, R. (2010) *Design with Microclimate: The Secret to Comfortable Outdoor Space*. Island Press.

Bottema, M. (2000) 'A Method for Optimisation of Wind Discomfort Criteria', *Building and Environment*, 35(1), pp. 1-18.

Bottillo, S., De Lieto Vollaro, A., Galli, G. and Vallati, A. (2014) 'Fluid Dynamic and Heat Transfer Parameters in an Urban Canyon', *Solar Energy*, 99(0), pp. 1-10.

Bourbia, F., and Boucheriba, F. (2010) 'Impact of Street Design on Urban Microclimate for Semi Arid Climate (Constantine).' *Renewable Energy*, Vol. 35, pp. 343-347.

Bourbia, F. and Awbi, H.B. (2004a) 'Building Cluster and Shading in Urban Canyon for Hot Dry Climate: Part 1: Air and Surface Temperature Measurements', *Renewable Energy*, 29(2), pp. 249-262.

Bourbia, F. and Awbi, H.B. (2004b) 'Building Cluster and Shading in Urban Canyon for Hot Dry Climate: Part 2: Shading Simulations', *Renewable Energy*, 29(2), pp. 291-301.

Bouyer, J., Vinet, J., Delpech, P. and Carré, S. (2007) 'Thermal Comfort Assessment in Semi-Outdoor Environments: Application to Comfort Study in Stadia', *Journal of Wind Engineering and Industrial Aerodynamics*, 95(9–11), pp. 963-976.

Bröde, P., Krüger, E., Rossi, F. and Fiala, D. (2012) 'Predicting Urban Outdoor Thermal Comfort by the Universal Thermal Climate Index UTCI—A Case Study in Southern Brazil', *International Journal of Biometeorology*, 56(3), pp. 471-480.

Bruse, M. (2009) 'Analysing Human Outdoor Thermal Comfort and Open Space Usage with the Multi-Agent System BOTworld', *the Seventh International Conference on Urban Climate*. Yokohama, Japan. pp. 1-4. Available at:  
[http://www.ide.titech.ac.jp/~icuc7/extended\\_abstracts/pdf/382880-3-090514011206-002.pdf](http://www.ide.titech.ac.jp/~icuc7/extended_abstracts/pdf/382880-3-090514011206-002.pdf).

Campos-Arriaga, L. (2009) *Wind Energy in the Built Environment: a Design Analysis Using CFD and Wind Tunnel Modelling Approach*. PhD Thesis, University of Nottingham, Available online at: <http://etheses.nottingham.ac.uk/806/>.

Carmona, M., Heath, T., Oc, T., and Tiesdell, S. (2003). 'Public Places Urban Spaces: The Dimensions of Urban Design.' *Architectural Press*, Oxford, England.



Catalano, P. and Amato, M. (2003) 'An Evaluation of RANS Turbulence Modelling for Aerodynamic Applications', *Aerospace Science and Technology*, 7(7), pp. 493-509.

Chalfoun, N.V. (2001) *Thermal Comfort Assessment of Outdoor Spaces Using MRT and Fish-Eye Lens Photography of Architectural Scale Models: a Case Study of the "Arts Oasis" Plaza at the University of Arizona, USA*. Brazil: Florianopolis. PLEA: Conference on Passive and Low Energy Architecture.

Chen, H., Ooka, R. and Kato, S. (2008) 'Study on Optimum Design Method for Pleasant Outdoor Thermal Environment Using Genetic Algorithms (GA) and Coupled Simulation of Convection, Radiation and Conduction', *Building and Environment*, 43, pp. 18-30.

Chen, H., Ooka, R., Huang, H. and Tsuchiya, T. (2009a) 'Study on Mitigation Measures for Outdoor Thermal Environment on Present Urban Blocks in Tokyo Using Coupled Simulation', *Building and Environment*, 44(11), pp. 2290-2299.

Chen, L. and Ng, E. (2012) 'Outdoor thermal comfort and outdoor activities: A review of research in the past decade', *Cities*, 29(2), pp. 118-125.

Cheng, V. and Ng, E. (2006) 'Thermal Comfort in Urban Open Spaces for Hong Kong', *Architectural Science Review*, 49(3), pp. 236-242.

Cheng, V., Ng, E. and Givoni, B. (2007) 'Outdoor Thermal Comfort for Hong Kong People: A Longitudinal Study', *PLEA 2007: Proceedings of the 24<sup>th</sup> Passive and Low Energy Architecture*. Singapore.

Chung, D.H.J. and Choo, M-L.L. (2011) 'Computational Fluid Dynamics for Urban Design: The Prospects for Greater Integration', *International Journal of Architectural Computing*, 9(1), pp. 33-54.

CIBSE (2006a) 'CIBSE Knowledge Series - KS6: Comfort', *Chartered Institution of Building Services Engineers*.

CIBSE (2006b) 'Environmental Design: CIBSE Guide A', *Chartered Institution of Building Services Engineers*.

Clarke, J.F., Ching, J.K.S. and Godwitch, J.M. (1982) *An Experimental Study of Turbulence in an Urban Environment*. U.S Environmental Protection Agency, Research Triangle Park.

Coronel, J.F. and Álvarez, S. (2001) 'Experimental Work and Analysis of Confined Urban Spaces', *Solar Energy*, 70(3), pp. 263-273.

De Lieto Vollaro, A., De Simone, G., Romagnoli, R., Vallati, A. and Bottillo, S. (2014) 'Numerical Study of Urban Canyon Microclimate Related to Geometrical Parameters', *Sustainability*, 6(11), p. 7894-7905.

De Schiller, S. and Evans, J.M. (2000) 'Urban Climate and Compact Cities in Developing Countries', in Jenks, M. and Burgess, R. (eds.) *Compact Cities: Sustainable*

- Urban Forms for Developing Countries*. Spon Press. Available at: [http://istoeidade.weebly.com/uploads/3/0/2/0/3020261/compact\\_cities.pdf](http://istoeidade.weebly.com/uploads/3/0/2/0/3020261/compact_cities.pdf) (Accessed: 30.12.2013).
- Defraeye, T., Blocken, B. and Carmeliet, J. (2010) 'CFD analysis of Convective Heat Transfer at the Surfaces of a Cube Immersed in a Turbulent Boundary Layer', *International Journal of Heat and Mass Transfer*, 53(1–3), pp. 297-308.
- DePaul, F.T. and Sheih, C.M. (1986) 'Measurements of Wind Velocities in a Street Canyon', *Atmospheric Environment* (1967), 20(3), pp. 455-459.
- Djamila, H., Chu, C.-M. and Kumaresan, S. (2014) 'Effect of Humidity on thermal comfort in the Humid Tropics', *Journal of building Construction and Planning Research*, 2, pp. 109-117.
- Djenane, M., Farhi, A., Benzerzour, M. and Musy, M. (2008) 'Microclimatic Behaviour of Urban Forms in Hot Dry Regions. Towards a Definition of Adapted Indicators', *PLEA 2008 - 25<sup>th</sup> Conference on Passive and Low Energy Architecture*. Dublin, 22-24 October.
- Eben Saleh, M.A. (1997) 'Privacy and Communal Socialization: The Role of Space in the Security of Traditional and Contemporary Neighborhoods in Saudi Arabia', *Habitat International*, 21(2), pp. 167-184.
- Elnahas, M.M. (2003) 'The Effects of Urban Configuration on Urban Air Temperatures', *Architectural Science Review*, 46, pp. 135-138.
- Emmanuel, R. (2005) *An Urban Approach to Climate-Sensitive Design Strategies for the Tropics*. London: Spon Press.
- Emmanuel, R. and Johansson, E. (2006) 'Influence of Urban Morphology and Sea Breeze on Hot Humid Microclimate: the Case of Colombo, Sri Lanka', *Climate Research*, 30, pp. 189-200.
- Emmanuel, R., Rosenlund, H. and Johansson, E. (2007) 'Urban Shading—A Design Option for the Tropics? A Study in Colombo, Sri Lanka', *International Journal of Climatology*, 27(14), pp. 1995-2004.
- Erell, E. (2005) *Predicting Air Temperatures in City Streets on the Basis of Measured Reference Data*. PhD Thesis, University of Adelaide, Available online at: <http://digital.library.adelaide.edu.au/dspace/handle/2440/58698/>.
- Erell, E. and Williamson, T. (2007) 'Intra-Urban Differences in Canopy Layer Air Temperature at a Mid-Latitude City', *International Journal of Climatology*, 27, pp. 1243-1255.
- Erell, E., Pearlmutter, D. and Williamson, T. (2011) *Urban Microclimate: Designing the Spaces between Buildings*. London: Earthscan.

- Fahmy, M., Sharples, S. and Yahiya, M. (2010) 'LAI Based Trees Selection for Mid Latitude Urban Developments: A Microclimatic Study in Cairo, Egypt', *Building and Environment*, 45(2), pp. 345-357.
- Fanger, P.O. (1970) *Thermal Comfort: Analysis and Application in Environment Engineering*. Copenhagen: Danish Technical Press.
- Fintikakis, N., Gaitani, N., Santamouris, M., Assimakopoulos, M., Assimakopoulos, D.N., Fintikaki, M., Albanis, G., Papadimitriou, K., Chryssochoides, E., Katopodi, K. and Doumas, P. (2011) 'Bioclimatic Design of Open Public Spaces in the Historic Centre of Tirana, Albania', *Sustainable Cities and Society*, 1(1), pp. 54-62.
- Franke, J., Hirsch, C., Jensen, A.G., Krus, H.W., Schatzmann, M., Westbury, P.S., Miles, S.D., Wisse, J.A. and Wright, N.G. (2004) 'Recommendations on the Use of CFD in Wind Engineering', In: van Beeck, J.P.A.J. (Ed.), *COST Action C14, Impact of Wind and Storm on City Life Built Environment*. Proceedings of the International Conference on urban Wind Engineering and Building Aerodynamics, 5-7 May. von Karman Institute, Sint-Genesius-Rode, Belgium.
- Franke, J. (2006) 'Recommendations of the COST Action C14 on the Use of CFD in Predicting Pedestrian Wind Environment', *The Fourth International Symposium on Computational Wind Engineering (CWE2006)*. Japan: Yokohama. pp. 529-532.
- Franke, J., Hellsten, A., Schlunzen, H. and Carissimo, B. (2007) 'Best Practice Guideline for the CFD Simulation of Flows in the Urban Environment', *COST Action 732: Quality Assurance and Improvement of Microscale Meteorological Models*, pp. 1-52.
- Fujii, S., Cha, H., Kagi, N., Miyamura, H. and Kim, Y. (2005) 'Effects on Air Pollutant Removal by Plant Absorption and Adsorption', *Building and Environment*, 40, pp. 105-112.
- Furbo, E., Harju, J. and Nilsson, H. (2009) *Evaluation of Turbulence Models for Prediction of Flow Separation at a Smooth Surface*. Report in Scientific Computing Advanced Course, Project 9.
- Gagge, A.P. (1981) 'Rational Temperature Indices of Thermal Comfort', *ELSEVIER: Studies in Environmental Science*, 10, pp. 79-98.
- Gagge, A.P., Fobelets, A.P. and Berglund, L.G. (1986) 'A Standard Predictive Index of Human Responses to the Thermal Environment', *ASHRAE Transactions*, 92, pp. 709-731.
- Gaitani, N., Mihalakakou, G., Santamouris, M. (2007) 'On the Use of Bioclimatic Architecture Principles in Order to Improve Thermal Comfort Situations in Outdoor Spaces.' *Building and Environment*, Vol. 42, pp. 317-324.
- Georgakis, C. and Santamouris, M. (2006) 'Experimental Investigation of Air Flow and Temperature Distribution in Deep Urban Canyons for Natural Ventilation Purposes', *Energy and Buildings*, 38(4), pp. 367-376.

- Giridharan, R., Lau, S.S.Y., Ganesan, S. and Givoni, B. (2007) 'Urban Design Factors Influencing Heat Island Intensity in High-Rise High-Density Environments of Hong Kong', *ELSEVIER: Building and Environment*, 42(10), pp. 3669-3684.
- Givoni, B. (1998) *Climate Considerations in Building and Urban Design*. United States: New York: John Wiley & Sons Inc.
- Givoni, B., Noguchi, M., Saaroni, H., Pochter, O., Yaacov, Y., Feller, N. and Becker, S. (2003) 'Outdoor Comfort Research Issues', *ELSEVIER: Energy and Buildings*, 35, pp. 77-86.
- Givoni, B. (2010) 'Thermal Comfort Issues and Implications in High-Density Cities', in Ng, E. (ed.) *Designing High-Density Cities: For Social & Environmental Sustainability*. UK: London: Earthscan.
- Glover, N., Guillas, S. and Malki-Epshtein, L. (2011) *Statistical Calibration of CFD Modelling for Street Canyon Flows*. Sydney, 14-16 November. 12th Conference of International Building Performance Simulation Association.
- Golany, G.S. (1996) 'Urban Design Morphology and Thermal Performance', *Atmospheric Environment*, 30(3), pp. 455-465.
- Golany, G.S. (1995) *Ethics & Urban Design: Culture, Form, & Environment*. USA: John Wiley & Sons, Inc.
- Gómez, M.A., Feijoo, M.A.Á., Comesaña, R., Eguía, P., Míguez, J.L. and Porteiro, J. (2012) 'CFD Simulation of a Concrete Cubicle to Analyze the Thermal Effect of Phase Change Materials in Buildings', *Energies*, 5, pp. 2093-2111.
- Gousseau, P., Blocken, B. and van Heijst, G.J.F. (2013) 'Quality Assessment of Large-Eddy Simulation of Wind Flow around a High-rise Building: Validation and Solution Verification', *Computers & Fluids*, 79(0), pp. 120-133.
- Gut, P. and Ackerknecht, D. (1993) *Climate Responsive Building: Appropriate Building Construction in Tropical and Subtropical Regions*. 1st edn. Switzerland: SKAT, Swiss Centre for Development Cooperation in Technology and Management.
- Hang, J., Wang, Q., Chen, X., Sandberg, M., Zhu, W., Buccolieri, R. and Di Sabatino, S. (2015) 'City Breathability in Medium Density Urban-Like Geometries Evaluated Through the Pollutant Transport Rate and the Net Escape Velocity', *Building and Environment*, 94, Part 1, pp. 166-182.
- Hanqie Production (2010) *Madinah City Profile*. Available at: <http://infoshasmira.blogspot.co.uk/2010/11/madinah-city-profile.html> (Accessed: 25/03/2013).
- Hataya, N., Mochida, A., Iwata, T., Tabata, Y., Yoshino, H. and Tominaga, Y. (2006) 'Development of the Simulation Method for Thermal Environment and Pollutant Diffusion in Street Canyons with Subgrid Scale Obstacles', *The Fourth International*

*Symposium on Computational Wind Engineering (CWE2006)*. Japan: Yokohama. pp. 553-556.

He, J. and Song, C.C.S. (1999) 'Evaluation of Pedestrian Winds in Urban Area by Numerical Approach', *Journal of Wind Engineering and Industrial Aerodynamics*, 81(1-3), pp. 295-309.

He, J., Hoyano, A. (2010) 'Measurement and Evaluation of the Summer Microclimate in the Semi-Enclosed Space under a Membrane Structure.' *Building and Environment*, Vol. 45, pp. 230-242.

Holm, D. and Engelbrecht, F.A. (2005) 'Practical Choice of Thermal Comfort Scale and Range in Naturally Ventilated Buildings in South Africa', *Journal of the South African Institution of Civil Engineering*, 47, pp. 9-14.

Hong, B. and Lin, B. (2015) 'Numerical studies of the outdoor wind environment and thermal comfort at pedestrian level in housing blocks with different building layout patterns and trees arrangement', *Renewable Energy*, 73(0), pp. 18-27.

Honjo, T. (2009) 'Thermal Comfort in Outdoor Environment', *Global Environmental Research*, 13(1), pp. 43-47.

Höppe, P. (1999) 'The Physiological Equivalent Temperature - a Universal Index for the Biometeorological Assessment of the Thermal Environment', *Springer Publication: International Journal of Biometeorology*.

Höppe, P. (2002) 'Different Aspects of Assessing Indoor and Outdoor Thermal Comfort', *Elsevier Science Journal of Energy and Buildings*, 34, pp. 661-665.

HSE (2012) 'Health and Safety Executive', *Thermal Comfort*. Available at: <http://www.hse.gov.uk/temperature/thermal/index.htm> (Accessed: 20.11.12).

Hu, L. and Brunzell, N.A. (2015) 'A New Perspective to Assess the Urban Heat Island through Remotely Sensed Atmospheric Profiles', *Remote Sensing of Environment*, 158(0), pp. 393-406.

Humphreys, M.A. (1979) 'The Influence of Season and Ambient Temperature on Human Clothing Behaviour', in Fanger, P.O. and Valbjorn, O. (eds.) *Indoor Climate*. Copenhagen: Danish Building Research.

Humphreys, M.A., Nicol, J.F. and Raja, I.A. (2007) 'Field Studies of Indoor Thermal Comfort and the Progress of the Adaptive Approach', *Journal of Advances on Building Energy Research*, 1, pp. 55-88.

Hussain, M. and Lee, B.E. (1980) 'A wind tunnel study of the mean pressure forces acting on large groups of low-rise buildings', *Journal of Wind Engineering and Industrial Aerodynamics*, 6(3-4), pp. 207-225.

Hwang, R.-L. and Lin, T.-P. (2007) 'Thermal Comfort Requirements of Occupants of Semi-Outdoor and Outdoor Environments in Hot Humid Regions', *Architectural Science Review*, 50(4), pp. 357-364.

Iqbal, O. (2013) 'Madinah and Umrah', *Scribd*, pp. 1-12 [Online]. Available at: <http://www.scribd.com/doc/121753678/Madinah-and-Umrah> (Accessed: 25/03/2013).

Iowa State University of Science and Technology (2015) [OEMA] *Madinah International Airport: Wind Roses*. Available at: [http://mesonet.agron.iastate.edu/sites/windrose.phtml?station=OEMA&network=SA\\_A\\_SOS](http://mesonet.agron.iastate.edu/sites/windrose.phtml?station=OEMA&network=SA_A_SOS) (Accessed: 10.2.2015).

Islam, S. (2011) 'A Study on Zoning Regulations' Impact on Thermal Comfort Conditions in Non-Conditioned Apartment Buildings in Dhaka City'. PhD Thesis, Texas A&M University. Available at: <http://repository.tamu.edu/bitstream/handle/1969.1/ETD-TAMU-2011-12-10702/ISLAM-DISSERTATION.pdf?sequence=2>

Jacobs, J. (1993) *The Death and Life of Great American Cities*. USA: New York: Random House, Inc.

Janssen, W.D., Blocken, B. and van Hooff, T. (2013) 'Pedestrian Wind Comfort around Buildings: Comparison of Wind Comfort Criteria Based on Whole-Flow field Data for a Complex Case Study', *Journal of Building and Environment*, 59(0), pp. 547-562.

Jeong, S.J. and Andrews, M.J. (2002) 'Application of the  $k-\epsilon$  Turbulence Model to the High Reynolds Number Skimming Flow Field of an Urban Street Canyon', *Atmospheric Environment*, 36(7), pp. 1137-1145.

Johansson, E. (2006) 'Influence of Urban Geometry on Outdoor Thermal Comfort in a Hot Dry Climate: A study in Fez, Morocco', *Building and Environment*, 41(10), pp. 1326-1338.

Johansson, E. and Emmanuel, R. (2006) 'The Influence of Urban Design on Outdoor Thermal Comfort in the Hot, Humid City of Colombo, Sri Lanka', *International Journal of Biometeorology*, 51(2), pp. 119-133.

Johansson, E., Thorsson, S., Emmanuel, R. and Krüger, E. (2014) 'Instruments and Methods in Outdoor Thermal Comfort Studies – The Need for Standardization', *Urban Climate*, 10, pp. 346-366.

Kim, J.-J. and Baik, J.-J. (2001) 'Urban Street-Canyon Flows with Bottom Heating', *Atmospheric Environment*, 35(20), pp. 3395-3404.

Klemm, K. (2007) 'Application of Numerical Simulation in Assessment of Microclimatic Condition in Urban Areas', *Proceedings of Building Simulation*. Beijing, China, September. IBPSA.

Kotzen, B. (2003) 'An Investigation of Shade under Six Different Tree Species of the Negev Desert towards their Potential Use for Enhancing Micro-climatic Conditions in



Landscape Architectural Development', *Journal of Arid Environments*, 55(2), pp. 231-274.

Krüger, E.L., Minella, F.O. and Rasia, F. (2011) 'Impact of Urban Geometry on Outdoor Thermal Comfort and Air Quality from Field Measurements in Curitiba, Brazil', *Building and Environment*, 46, pp. 621-634.

Lam, C.-Y. 'Climate Changes Brought About by Urban Living', in Ng, E. (ed.) *Designing High-Density Cities: for Social & Environmental Sustainability*. London: UK: Earthscan, pp. 55-61.

Lawson, T.V. and Penwarden, A.D. (1975) 'The Effects of Wind on People in the Vicinity of Buildings', *Proceedings of 4<sup>th</sup> International Conference on Wind Effects on Buildings and Structures*. Cambridge University Press, Heathrow. pp. 605-622.

Leduc, G., Thellir, F., Lacarriere, B., Monchoux, F. and Bonnis-Sassi, M. (2006) 'Regulation of a Human Thermal Environment by Inverse Method', *Journal of Applied Thermal Engineering*, 26, pp. 2176-2183.

Lee, R.X., Jusuf, S.K. and Wong, N.H. (2013) 'The Study of Height Variation on Outdoor Ventilation for Singapore's High-Rise Residential Housing Estates', *International Journal of Low-Carbon Technologies*.

Lee, R.-X. and Wong, N.-H. (2014) 'A Parametric Study of Gross Building Coverage Ratio (GBCR) Variation on Outdoor Ventilation in Singapore's High-rise Residential Estates', *Journal of Civil Engineering and Science*, 3(2), pp. 92-116.

Lenzhölzer, S. (2010) *Designing Atmospheres: Research and Design for Thermal Comfort in Dutch Urban Squares*. PhD thesis. Wageningen University [Online]. Available at: <http://edepot.wur.nl/139053>.

Lenzhölzer, S., Koh J. (2010) 'Immersed in Microclimatic Space: Microclimate Experience and Perception of Spatial Configuration in Dutch Squares.' *Landscape and Urban Planning*, Vol. 95, pp. 1-15.

Lin, T. (2009) 'Thermal Perception, Adaptation and Attendance in a Public Square in Hot and Humid Regions', *Journal of Building and Environment*, 44(10), pp. 2017-26.

Lin, T.-P., Matzarakis, A. and Hwang, R.-L. (2010) 'Shading Effect on Long-Term Outdoor Thermal Comfort', *Building and Environment*, 45(1), pp. 213-221.

Litschke, T. and Kuttler, W. (2008) 'On the Reduction of Urban Particle Concentration by Vegetation - a Review', *Meteorologische Zeitschrift*, 17, pp. 229-240.

Mahmoud, A.H.A. (2011) 'Analysis of the Microclimatic and Human Comfort Conditions in an Urban Park in Hot and Arid Regions', *Building and Environment*, 46(12), pp. 2641-2656.

Masnavi, M., Laghai, H.-A. and Ghobadi, N. (2012) 'Eco Design and the Optimization of Passive Cooling Ventilation for Energy Saving in the Buildings: A Framework for

Prediction of Wind Environment and Natural Ventilation in Different Neighborhood Patterns', in Matsumoto, M., Umeda, Y., Masui, K. and Fukushima, S. (eds.) *Design for Innovative Value Towards a Sustainable Society*. Springer Netherlands, pp. 177-182.

Martins, T., Adolphe, L. and KRAUSE, C. (2012) 'Microclimate Effects of Urban Geometry on Outdoor Thermal Comfort in the Brazilian Tropical Semi-arid Climate', *28th Conference, Opportunities, Limits & Needs Towards an Environmentally Responsible Architecture*. Perú. PLEA2012, pp. 1-6. Available at: <http://www.plea2012.pe/pdfs/T01-20120111-0010.pdf>.

Matzarakis, A. and Mayer, H. (1996) 'Another Kind of Environmental Stress: Thermal Stress', *WHO Collaborating Centre for Air Quality Management and Air Pollution Control* (Newsletters no. 18), pp. 7-10. [Online] Available at: [http://www.urbanclimate.net/matzarakis/papers/who\\_heat.pdf](http://www.urbanclimate.net/matzarakis/papers/who_heat.pdf).

Matzarakis, A. (2007) 'Assessment Method for Climate and Tourism Based on Daily Data', in Matzarakis, A., De Freitas, C.R. and Scott, D. (eds.) *Developments in Tourism Climatology*. German Meteorological Society.

Matzarakis, A., Rutz, F. and Mayer, H. (2007) 'Modelling Radiation Fluxes in Simple and Complex Environments - Application of the RayMan Model', *International Journal of Biometeorology*, 51(4), pp. 323-334.

Mayer, H. and Höppe, P. (1987) 'Thermal Comfort of Man in Different Urban Environments', *Journal of Theoretical and Applied Climatology*, 38, pp. 43-49.

McGregor, G. (2012) 'Special issue: Universal Thermal Comfort Index (UTCI)', *International Journal of Biometeorology*, 56(3), pp. 419-419.

Mirzaei, P.A. and Haghighat, F. (2010) 'Approaches to Study Urban Heat Island – Abilities and Limitations', *Building and Environment*, 45(10), pp. 2192-2201.

MMM Group Limited and Moriyama & Teshima Architects (2012a) *Comprehensive Plan: Comprehensive Plan for Madinah* (1).

MMM Group Limited and Moriyama & Teshima Architects (2012b) *Environment Plan: Comprehensive Plan for Madinah*, (14), pp. 1-392.

MMM Group Limited and Moriyama & Teshima Architects (2012c) *Transport Plan: Comprehensive Plan for Madinah* (9), pp. 1-392.

MMM Group Limited and Moriyama & Teshima Architects (2012d) *Urban Design & Architectural Guidelines: Comprehensive Plan for Madinah* (13), pp. 1-454.

MMM Group Limited and Moriyama & Teshima Architects (2012e) *Urban Development Regulations: Comprehensive Plan for Madinah*, (16), pp. 1-210.

MMM Group Limited and Moriyama & Teshima Architects (2012f) *Population and Employment Plan: Comprehensive Plan for Madinah* (2), pp. 1-170.

- MMM Group Limited and Moriyama & Teshima Architects (2012g) *Major Investment Projects: Comprehensive Plan for Madinah*, (19), pp. 1-122.
- Mochida, A., Yoshino, H., Miyauchi, S. and Mitamura, T. (2006) 'Total Analysis of Cooling Effects of Cross-Ventilation Affected by Microclimate around a Building', *Solar Energy*, 80(4), pp. 371-382.
- Mochida, A. and Lun, Y.F. (2006) *Prediction of Wind Environment and Thermal Comfort at Pedestrian Level in Urban Area*. Yokohama: The Fourth International Symposium on Computational Wind Engineering (CWE2006), pp. 33-59.
- Montazeri, H. and Blocken, B. (2013) 'CFD simulation of wind-induced pressure coefficients on buildings with and without balconies: Validation and sensitivity analysis', *Building and Environment*, 60(0), pp. 137-149.
- Murakami, S. (2006) 'Environmental Design of Outdoor Climate Based on CFD', *Journal of Fluid Dynamics Research*, 38, pp. 108-126.
- Nakamura, Y. and Oke, T.R. (1988) 'Wind, Temperature and Stability Conditions in an East-West Oriented Urban Canyon', *Atmospheric Environment*, 22, pp. 2691-2700.
- Nasir, R.A., Ahmad, S.S. and Ahmed, A.Z. (2012) 'Psychological Adaptation of Outdoor Thermal Comfort in Shaded Green Spaces in Malaysia', *Social and Behavioral Sciences*, 68, pp. 865-878.
- Ndetto, E. and Matzarakis, A. (2014) 'Urban Atmospheric Environment and Human Biometeorological Studies in Dar es Salaam, Tanzania', *Air Quality, Atmosphere & Health*, pp. 1-17.
- Ng, E. and Cheng, V. (2012) 'Urban human thermal comfort in hot and humid Hong Kong', *Energy and Buildings*, 55(0), pp. 51-65.
- Nicol, F., Wilson, E., Ueberjahn-Tritta, A., Nanayakkara, L. and Kessler, M. (2006) 'Comfort in Outdoor Spaces in Manchester and Lewes, UK', *Proceedings of the Fourth Windsor Conference: Comfort and Energy Use in Buildings: Getting it right*. London. Network for Comfort and Energy Use in Buildings. Available at: <http://nceub.commoncense.info/uploads/66Nicol.pdf>.
- Nicol, F., Humphreys, M. and Roaf, S. (2012) *Adaptive Thermal Comfort*. Kent, Great Britain: Routledge.
- Nielsen (ed), P.V., Allard, F., Awbi, H.B., Davidson, L. and Schälin, A. (2007) *Computational Fluid Dynamics in Ventilation Design*. Brussels: REHVA Guide Book 10. RHEVA (Federation of European Heating and Air-Conditioning Association).
- Nikolopoulou, M., Baker, N. and Steemers, K. (2001) 'Thermal Comfort in Outdoor Urban Spaces: Understanding the Human Parameter', *Solar Energy*, 70(3), pp. 227-235.
- Nikolopoulou, M., Lykoudis, S., Kikira, M., Kofoed, N., Gaardsted, M., Scudo, G., Dessi, V., Rogora, A. and et al. (2004) *Designing Open Spaces in the Urban*

*Environment: a Bioclimatic Approach*. Greece: Centre for Renewable Energy Sources (CRES).

Nikolopoulou, M. and Lykoudis, S. (2006) 'Thermal Comfort in Outdoor Urban Spaces: Analysis Across Different European Countries', *Building and Environment*, 41(11), pp. 1455-1470.

Nikolopoulou, M., Lykoudis, S. (2007) 'Use of Outdoor Spaces and Microclimate in a Mediterranean Urban Area.' *Building and Environment*, Vol. 42, pp. 3691-3707.

Nishimura, N., Nomura, T., Iyota, H. and Kimoto, S. (1998) 'Novel Water Facilities for Creation of Comfortable Urban Micrometeorology', *Solar Energy*, 64(4-6), pp. 197-207.

Oguro, M., Murakami, S., Morikawa, Y., Mochida, A., Ashie, Y., Ooka, R., Yoshida, S. and Ono, K. (2002) 'A Study on Design Methodology for Outdoor Thermal Environment Based on CFD Analyses', *AIJ Journal of Technology and Design*, 16, pp. 185-190 (in Japanese).

Oliveira, S. and Andrade, H. (2007) 'An Initial Assessment of the Bioclimatic Comfort in an Outdoor Public Space in Lisbon', *International Journal of Biometeorology*, 52(1), pp. 69-84.

Oke, T.R. (1988) 'Street Design and Urban Canopy Layer Climate', *Energy and Buildings*, 11, pp. 103-113.

Oke, T.R. (1999) 'Observing Urban Weather and Climate Using 'Standard' Stations', *Biometeorology and Urban Climatology at the Turn of the Millennium*. Selected Papers from the Conference ICB-ICUC '99 (Sydney, 8-12 November, 1999), WCASP-50, WMO/TD-No. 1026, pp. 443-448.

Parsons, K. (2003) *Human Thermal Environments: The Effect of Hot, Moderate and Cold Environments on Human Health, Comfort and Performance*. 2<sup>nd</sup> edn. Simultaneously Published in the USA and Canada: Taylor & Francis Inc.

Parsons, K. (2006) 'Heat Stress Standard ISO 7243 and its Global Application', *Industrial Health*, 44, pp. 368-379.

Pearlmutter, D. (1998) 'Street Canyon Geometry and Microclimate: Designing for Urban Comfort under Arid Conditions', *Environmentally Friendly Cities and Proceedings of PLEA*. Portugal. James & James Publishers Ltd, pp. 163-166. Available at: <http://www.bgu.ac.il/CDAUP/plea/plea-paper.html>.

Pearlmutter, D., Berliner, P. and Shaviv, E. (2007) 'Integrated Modeling of Pedestrian Energy Exchange and Thermal Comfort in Urban Street Canyons', *Building and Environment*, 42(6), pp. 2396-2409.

Pentz, M. and Shott, M. (eds.) (1988) *Handling Experimental Data*. Edited by Francis Aprahamian. Milton Keynes and Philadelphia: Open University Press.

- Pickup, J. and de Dear, R.J. (1999) 'An Outdoor Thermal Comfort Index (OUT\_SET\*) - Part 1- The Model and its Assumptions', *The 15th International Congress of Biometeorology and International Conference on Urban Climatology*. Sydney.
- Poreh, M. (1996) 'Investigation of Heat Islands Using Small Scale Models', *Atmospheric Environment*, 30(3), pp. 467-474.
- Potter, J. and de Dear, R.J. (2000) 'Field Study to Calibrate Outdoor Thermal Comfort Index', in de Dear, K., Oke and Auliciems (ed.) *Biometeorology and Urban Climatology at the Turn of the Millennium*. Geneva: World Meteorological Organization (WMO), pp. 315-320.
- Prek, M. (2006) 'Thermodynamical Analysis of Human Thermal Comfort', *Journal of Energy*, 31, pp. 732-734.
- Prianto, E. and Depecker, P. (2003) 'Optimization of Architectural Design Elements in Tropical Humid Region with Thermal Comfort Approach', *Energy and Buildings*, 35(3), pp. 273-280.
- Priyadarsini, R., Hien, W.N. and Wai David, C.K. (2008) 'Microclimatic Modeling of the Urban Thermal Environment of Singapore to Mitigate Urban Heat Island', *Solar Energy*, 82(8), pp. 727-745.
- Qaid, A. and Ossen, D. (2014) 'Effect of asymmetrical street aspect ratios on microclimates in hot, humid regions', *International Journal of Biometeorology*, pp. 1-21.
- QU, Y. (2011) *Three-Dimensional Modeling of Radiative and Convective Exchanges in the Urban Atmosphere*. PhD thesis. University of Paris-Est [Online]. Available at: <http://ceria.enpc.fr/fich/yongfengthesisfinal.pdf>.
- Radhi, H., Fikry, F. and Sharples, S. (2013) 'Impacts of Urbanisation on the Thermal Behaviour of New Built up Environments: A Scoping Study of the Urban Heat Island in Bahrain', *Landscape and Urban Planning*, 113, pp. 47-61.
- Radhi, H., Sharples, S. and Assem, E. (2015) 'Impact of Urban Heat Islands on the Thermal Comfort and Cooling Energy Demand of Artificial Islands—A Case Study of AMWAJ Islands in Bahrain', *Sustainable Cities and Society*.
- Ramponi, R. and Blocken, B. (2012) 'CFD simulation of Cross-Ventilation for a Generic Isolated Building: Impact of Computational Parameters', *Building and Environment*, 53(0), pp. 34-48.
- Reiter, S. (2008) 'Validation Process for CFD Simulations of Wind Around Buildings', *Proceedings of the European Built Environment CAE Conference*. London, UK. pp. 1-18. Available at: <http://orbi.ulg.ac.be/bitstream/2268/20400/1/EBE-Reiter.pdf>.
- Richards, P.J., Mallison, G.D., McMillan, D. and Li, Y.F. (2002) 'Pedestrian Level Wind Speeds in Downtown Auckland', *Wind and Structures*, 5(2-4), pp. 151-164.

- Rizk, A.A. and Henze, G.P. (2010) 'Improved Airflow around Multiple Rows of Buildings in Hot Arid Climates', *Energy and Buildings*, 42(10), pp. 1711-1718.
- Robinette, G.O. (1972) *Plants, People, and Environmental Quality: A Study of Plants and their Environmental Functions*. U.S.: Washington: National Government Publication.
- Robinson, N.H. (2004) *The Planting Design Handbook*. Ashgate Publishing Limited. Available at: <file:///tower4/home24/a8903901/Downloads/Planting%20Design%20Handbook.pdf>.
- Robitu, M., Musy, M., Inard, C. and Groleau, D. (2006) 'Modeling the Influence of Vegetation and Water Pond on Urban Microclimate', *Solar Energy*, 80(4), pp. 435-447.
- Rubio-Bellido, C., Pulido-Arcas, J. and Cabeza-Lainez, J. (2015) 'Adaptation Strategies and Resilience to Climate Change of Historic Dwellings', *Sustainability*, 7(4), pp. 3695-3713.
- Saneinejad, S., Moonen, P., Defraeye, T., Derome, D. and Carmeliet, J. (2012) 'Coupled CFD, Radiation and Porous Media Transport Model for Evaluating Evaporative Cooling in an Urban Environment', *Journal of Wind Engineering and Industrial Aerodynamics*, 104–106(0), pp. 455-463.
- Santamouris, M., Papanikolaou, N., Koronakis, I., Livada, I. and Asimakopoulos, D. (1999) 'Thermal and Air Flow Characteristics in a Deep Pedestrian Canyon Under Hot Weather Conditions', *Atmospheric Environment*, 33(27), pp. 4503-4521.
- Santamouris, M. (2001) 'Appropriate Materials for the Urban Environment', in Santamouris, M. (ed.) *Energy and Climate in the Urban Built Environment*. London: James & James, pp. 160-180.
- Santiago, J.L., Dejoan, A., Martilli, A., Martin, F. and Pinelli, A. (2010) 'Comparison between Large-Eddy Simulation and Reynolds-Averaged Navier-Stokes Computations for the MUST Field Experiment. Part I: Study of the Flow for an Incident Wind Directed Perpendicularly to the Front Array of Containers', *Boundary-Layer Meteorology*, 135(1), pp. 109-132.
- Sengupta, K., Mashayek, F. and Jacobs, G. (2008) 'Direct Numerical Simulation of Turbulent Flows Using Spectral Method', *46th AIAA Aerospace Sciences Meeting and Exhibit*. Reno, Nevada, 7-10 January. American Institute of Aeronautics and Astronautics.
- Setaih, K. (2010) *Urban Design in a Religious context: Physical Linkages between Historic Buildings: A Case study of Quba and the Prophet's Mosque in Madinah, K.S.A.* Master of Art (MA) in Urban Design thesis. Newcastle University, UK.
- Setaih, K., Hamza, N. and Townshend, T. (2013a) 'Assessment of Outdoor Thermal Comfort in Urban Microclimate in Hot Arid Areas', *Proceedings of BS2013: 13th Conference of International Building Performance Simulation Association*. Chambéry, France, 26-28 of August. pp. 3153-3160.



- Setaih, K., Hamza, N. and Townshend, T. (2013b) 'Use of CFD Simulation in Urban Design for Outdoor Thermal Comfort in Hot and Dry Climates: A Review', *International PostGraduate Research Conference (IPGRC)*. April 2013. pp. 1069-1076.
- Setaih, K., Hamza, N. and Townshend, T. (2013c) 'Crafting and Assessing Urban Environments Using Computational Fluid Dynamics', *7<sup>th</sup> International Conference of the Arab Society for Computer Aided Architectural Design (Proceedings of ASCAAD)*. Saudi Arabia: Jeddah. ASCAAD, pp. 315-322. Available at: [http://www.researchgate.net/publication/262497974\\_Crafting\\_and\\_Assessing\\_Urban\\_Environments\\_Using\\_Computational\\_Fluid\\_Dynamics](http://www.researchgate.net/publication/262497974_Crafting_and_Assessing_Urban_Environments_Using_Computational_Fluid_Dynamics).
- Setaih, K., Hamza, N., Mohammed, M.A., Dudek, S. and Townshend, T. (2014) 'CFD Modeling as a Tool for Assessing Outdoor Thermal Comfort Conditions in Urban Settings in Hot Arid Climates', *Journal of Information Technology in Construction (ITcon)*, 19, pp. 248-269.
- Shahidan, M.F., Mustafa, K.M.S. and Saleh, E. (2007) 'Effects of tree Canopies on Solar Radiation Filtration in a Tropical Microclimatic Environment', *PLEA2007 Conference*. Singapore. Available at: <http://plea-arch.org/ARCHIVE/2007/html/pdf/P0282.pdf>.
- Shahidan, M.F. and Jones, P. (2008) '179: Plant Canopy Design in Modifying Urban Thermal Environment: Theory and Guidelines', *25<sup>th</sup> Conference on Passive and Low Energy Architecture*. Ireland: Dublin. PLEA2008. Available at: [http://architecture.ucd.ie/Paul/PLEA2008/content/papers/oral/PLEA\\_FinalPaper\\_ref\\_179.pdf](http://architecture.ucd.ie/Paul/PLEA2008/content/papers/oral/PLEA_FinalPaper_ref_179.pdf).
- Shahidan, M.F., Jones, P.J., Gwilliam, J. and Salleh, E. (2012) 'An Evaluation of Outdoor and Building Environment Cooling Achieved through Combination Modification of Trees with Ground Materials', *Building and Environment*, 58(0), pp. 245-257.
- Shashua-Bar, L., Pearlmutter, D. and Erell, E. (2009) 'The Cooling Efficiency of Urban Landscape Strategies in a Hot Dry Climate', *Landscape and Urban Planning*, 92(3-4), pp. 179-186.
- Shishegar, N. (2013) 'Street Design and Urban Microclimate: Analyzing the Effects of Street Geometry and Orientation on Airflow and Solar Access in Urban Canyons', *Journal of Clean Energy Technologies*, 1(1), pp. 52-56.
- Spagnolo, J. and de Dear, R. (2003a) 'A Field Study of Thermal Comfort in Outdoor and Semi-Outdoor Environments in Subtropical Sydney Australia', *Building and Environment*, 38(5), pp. 721-738.
- Spagnolo, J. and de Dear, R.J. (2003b) 'A Human Thermal Climatology of Subtropical Sydney', *International Journal of Climatology*, 23, pp. 1383-1395.
- Spalart, P.R. (2009) 'Detached-Eddy Simulation', *Annual Review of Fluid Mechanics*, 41(1), pp. 181-202.

Stankovic, S., Campbell, N. and Harries, A. (2009) *Urban Wind Energy*. London: Earthscan.

Stathopoulos, T. and Baskaran, B.A. (1996) 'Computer Simulation of Wind Environmental Conditions around Buildings', *Engineering Structures*, 18(11), pp. 876-885.

Stathopoulos, T. (2006) 'Pedestrian Level Winds and Outdoor Human Comfort', *Journal of Wind Engineering and Industrial Aerodynamics*, 94(11), pp. 769-780.

Stavrakakis, G.M., Zervas, P.L., Sarimveis, H. and Markatos, N.C. (2010) 'Development of a Computational Tool to Quantify Architectural-Design Effects on Thermal Comfort in Naturally Ventilated Rural Houses', *Building and Environment*, 45(1), pp. 65-80.

Stavrakakis, G.M., Tzanaki, E., Genetzaki, V.I., Anagnostakis, G., Galetakis, G. and Grigorakis, E. (2012) 'A Computational Methodology for Effective Bioclimatic-Design Applications in the Urban Environment', *Sustainable Cities and Society*, 4(0), pp. 41-57.

Streinu-Cercel, A., Costoiu, S., Marza, M., Petrescu, A. and Marza, M. (2007) 'Extensions for Establishing Decision in the Management of the Medical National System from the Point of View of the Quality and Efficiency: Models for the Indices of Thermal Comfort', *International Conference on Advancements of Medicine and Health Care Through Technology*. Romania, September 2007.

Pillai, S.S. and Yoshie, R. (2012) 'Experimental and numerical studies on convective heat transfer from various urban canopy configurations', *Journal of Wind Engineering and Industrial Aerodynamics*, 104–106(0), pp. 447-454.

Sun Design. (Undated) *Sun design sunrooms*. Retrieved from <http://www.sundesign.com>.

Swaid, H., Bar-El, M. and Hoffman, M.E. (1993) 'A Bioclimatic Design Methodology for Urban Outdoor Spaces', *Theoretical and Applied Climatology*, 48(1), pp. 49-61.

Szokolay, S.V. (2008) *Introduction to Architectural Science : The Basis of Sustainable Design*. Taylor & Francis. Available at: <http://NCL.ebib.com/patron/FullRecord.aspx?p=349479> (Accessed: 1 June 2011).

Takakura, S., Suyama, Y. and Aoyama, M. (1993) 'Numerical Simulation of Flowfield around Buildings in an Urban Area', *Journal of Wind Engineering and Industrial Aerodynamics*, 46–47(0), pp. 765-771.

Thani, S.K.S.O., Mohamad, N.H.N. and Abdullah, S.M.S. (2013) 'The Influence of Urban Landscape Morphology on the Temperature Distribution of Hot-Humid Urban Centre', *Procedia - Social and Behavioral Sciences*, 85(0), pp. 356-367.

The Saudi Network. (Undated.). *Madinah City Profile*. Retrieved from <http://www.thesaudi.net/saudi-arabia/madinah/Madinah%20City%20-%20Saudi%20Arabia.htm>.

- Thom, E.C. (1998) *Methods for the Human-Biometerological Assessment of Climate and Air Hygiene for Urban and Regional Planning*. The Discomfort Index. Weatherwise 12:57-60VDI. Part I: Climate. VDI Guideline 3787. Part 2, Berlin: Beuth, 1959.
- Thorsson, S., Lindqvist, M. and Lindqvist, S. (2004) 'Thermal bioclimatic conditions and patterns of behaviour in an urban park in Göteborg, Sweden', *International Journal of Biometeorology*, 48(3), pp. 149-156.
- Thorsson, S., Honjo, T., Lindberg, F., Eliasson, I. and Lim, E.-M. (2007) 'Thermal Comfort and Outdoor Activity in Japanese Urban Public Places', *Journal of Environment and Behavior*, 39(5), pp. 660-684.
- Thorsson, S., Lindberg, F., Eliasson, I. and Holmer, B. (2007b) 'Different Methods for Estimating the Mean Radiant Temperature in an Outdoor Urban Setting', *International Journal of Climatology*, 27(14), pp. 1983-1993.
- Todhunter, P.E. (1990) 'Microclimatic Variations Attributable to Urban-Canyon Asymmetry and Orientation', *Physical Geography*, 11(2), pp. 131-141.
- Tominaga, Y., Yoshie, R., Mochida, A., Kataoka, H., Harimoto, K. and Nozu, T. (2005) 'Cross Comparisons of CFD Prediction for Wind Environment at Pedestrian Level around Buildings - Part 2: Comparison of Results for Flowfield around Building Complex in Actual Urban Area', *The Sixth Asia-Pacific Conference on Wind Engineering (APCWE-VI)*. Korea: Seoul, 12-14 September. pp. 2661-2670.
- Tominaga, Y., Mochida, A., Yoshie, R., Kataoka, H., Nozu, T., Yoshikawa, M. and Shirasawa, T. (2008) 'AIJ Guidelines for Practical Applications of CFD to Pedestrian Wind Environment around Buildings', *Journal of Wind Engineering and Industrial Aerodynamics*, 96, pp. 1749-1761.
- Traum, M.J., Griffith, P., Thomas, E.L. and Peters, W.A. (2008) 'Latent Heat Fluxes Through Soft Materials With Microtruss Architectures', *ASME: Journal of Heat Transfer*, 130(4), pp. 042403-1 - 042403-11.
- van Hooff, T. and Blocken, B. (2010) 'Coupled urban wind flow and indoor natural ventilation modelling on a high-resolution grid: A case study for the Amsterdam Arena stadium', *Environmental Modelling & Software*, 25(1), pp. 51-65.
- Vanos, J., Warland, J., Gillespie, T. and Kenny, N. (2010) 'Review of the Physiology of Human Thermal Comfort while Exercising in Urban Landscapes and Implications for Bioclimatic Design', *International Journal of Biometeorology*, 54(4), pp. 319-334.
- Vasilikou, C. and Nikolopoulou, M. (2014) 'Degrees of Environmental Diversity for Pedestrian Thermal Comfort in the Urban Continuum: A New Methodological Approach', in Edgerton, E., Romice, O. and Thwaites, K. (eds.) *Bridging the Boundaries: Human Experience in the Natural and Built Environment and Implications for Research, Policy, and Practice*. Advances in People-Environment Studies: Volume 5: HOGREFE.

Watson, S. and Studdert, D. (2006) 'Markets as Sites for Social Interaction: Spaces of Diversity'. England: The Policy Press: published for The Joseph Rowntree Foundation, pp. 1-53. Available at: <http://www.jrf.org.uk/sites/files/jrf/1940-markets-social-interaction.pdf>.

Weather Underground. (2010). *Weather history and data archive*. Retrieved from <http://www.wunderground.com/history>.

Wei, Y. (2014) *Outdoor Thermal Comfort in Urban Spaces in Singapore*. National University of Singapore [Online]. Available at: <http://www.scholarbank.nus.edu.sg/handle/10635/49354>.

Wieringa, J. (1992) 'Updating the Davenport Roughness Classification', *Journal of Wind Engineering and Industrial Aerodynamics*, 41(1-3), pp. 357-368.

Willemsen, E. and Wisse, J.A. (2002) 'Accuracy of Assessment of Wind Speed in the Built Environment', *ELSEVIER Publications: Journal of Wind Engineering and Industrial Aerodynamics*, 90(10), pp. 1183-1190.

Wise, A.F.E. (1970) 'Wind Effects Due to Groups of Buildings', London. Royal Society Symposium Architectural Aerodynamics.

Wohlwill, J.F. (1975) 'Behavioral Response and Adaptation to Environmental Stimulation', in Damon, A. (ed.) *Physiological Anthropology*. Cambridge: Harvard University Press, pp. 295-334.

Wong, N.H. and Khoo, S.S. (2003) 'Thermal Comfort in Classrooms in the Tropics', *Energy and Buildings*, 35(4), pp. 337-351.

Worpole, K. and Knox, K. (2007) *The Social Value of Public Spaces*. England: The Joseph Rowntree Foundation. [Online]. Available at: <http://www.jrf.org.uk/sites/files/jrf/2050-public-space-community.pdf>.

Xi, T., Li, Q., Mochida, A. and Meng, Q. (2012) 'Study on the Outdoor Thermal Environment and Thermal Comfort around Campus Clusters in Subtropical Urban Areas', *Building and Environment*, 52(0), pp. 162-170.

Yahia, M.W. (2012) *Microclimate and Thermal Comfort of Urban Spaces in Hot Dry Damascus: influence of Urban Design and Planning Regulations*. PhD thesis. Lund University.

Yahia, M.W. and Johansson, E. (2013a) 'Evaluating the Behaviour of Different Thermal Indices by Investigating Various Outdoor Urban Environments in the Hot Dry City of Damascus, Syria', *International Journal of Biometeorology*, pp. 1-16.

Yahia, M.W. and Johansson, E. (2013b) 'Influence of Urban Planning Regulations on the Microclimate in a Hot Dry Climate: The Example of Damascus, Syria', *Journal of Housing and the Built Environment*, 28(1), pp. 51-65.

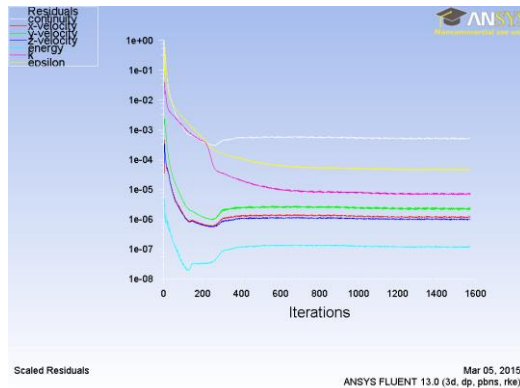
- Yang, F., Lau, S.S.Y. and Qian, F. (2010) 'Summertime Heat Island Intensities in Three High-Rise Housing Quarters in Inner-City Shanghai China: Building Layout, Density and Greenery', *ELSEVIER: Building and Environment*, 45(1), pp. 115-134.
- Yoshie, R., Mochida, A., Tominaga, Y., Kataoka, H., Harimoto, K., Nozu, T. and Shirasawa, T. (2007) 'Cooperative Project for CFD Prediction of Pedestrian Wind Environment in the Architectural Institute of Japan', *Journal of Wind Engineering and Industrial Aerodynamics*, 95, pp. 1551-1578.
- Yuan, C. and Ng, E. (2012) 'Building Porosity for Better Urban Ventilation in High-Density Cities – A Computational Parametric Study', *Building and Environment*, 50(0), pp. 176-189.
- Zhang, G., Zheng, C., Yang, W.M., Zhang, Q. and Moschandreas, D.J. (2007) 'Thermal Comfort Investigation of Naturally Ventilated Classrooms in a Subtropical Region', *Indoor and Built Environment*, 16(2), pp. 148-158.
- Zhang, W., Qi, J. and Li, X. (2009) 'CFD Simulation for Urban Environment Planning', *Management and Service Science, 2009. MASS '09. International Conference on*. 20-22 Sept. 2009. pp. 1-4. Available at:  
<http://ieeexplore.ieee.org/stamp/stamp.jsp?tp=&arnumber=5301625>.
- Zhang, W., Mak, C.M., Ai, Z.T. and Siu, W.M. (2011) 'A Study of the Ventilation and Thermal Comfort of the Environment Surrounding a New University Building under Construction', *Indoor and Built Environment*.
- Zoras, S., Tsermentselis, A., Kosmopoulos, P. and Dimoudi, A. (2014) 'Evaluation of the Application of Cool Materials in Urban Spaces: A Case Study in the Center of Florina', *Sustainable Cities and Society*, 13(0), pp. 223-229.

# Appendices

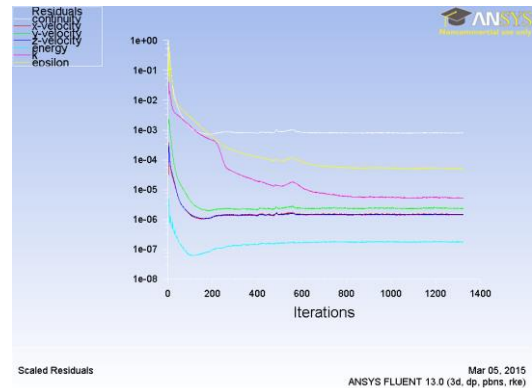
---



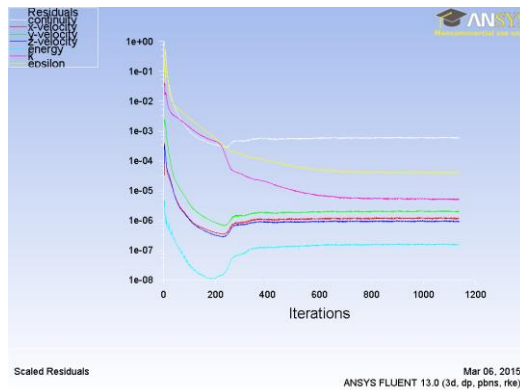
## A5: Appendices for Chapter 5 (from A5.1 to A5.24)



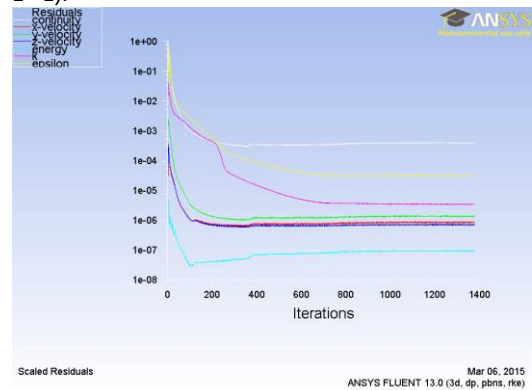
A5. 1: Convergence obtained for S-1 model (Base Case).



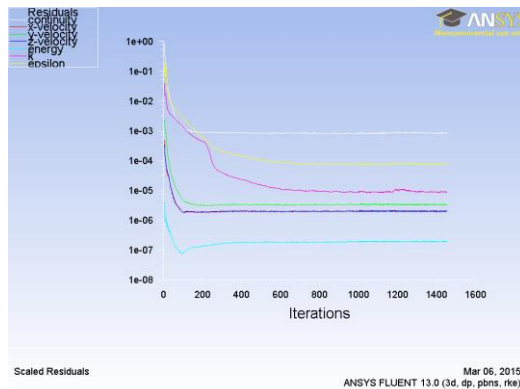
A5. 2: Convergence obtained for S-2 model (H/W of 1 - 1).



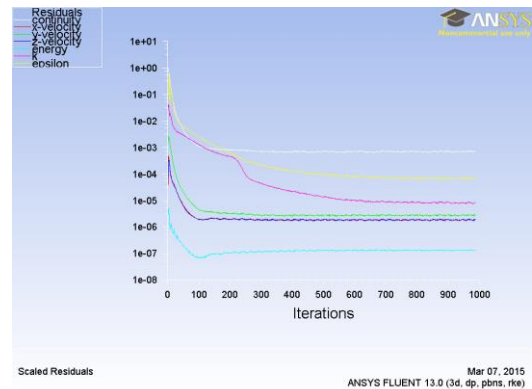
A5. 3: Convergence obtained for S-3 model (H/W=1-0.8-1.3).



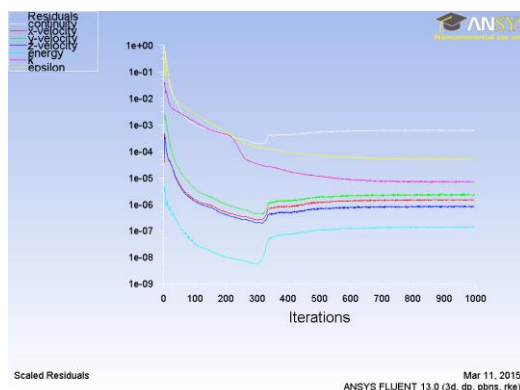
A5. 4: Convergence obtained for S-4 model (H/W=1-1.3-0.8).



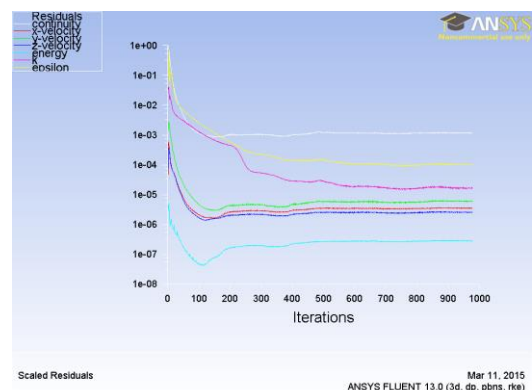
A5. 5: Convergence obtained for S-5 model (H/W=1-1.5-1.5).



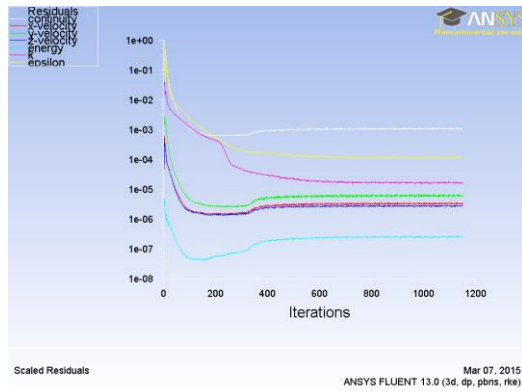
A5. 6: Convergence obtained for S-6 model (H/W=1-1.3-1.8).



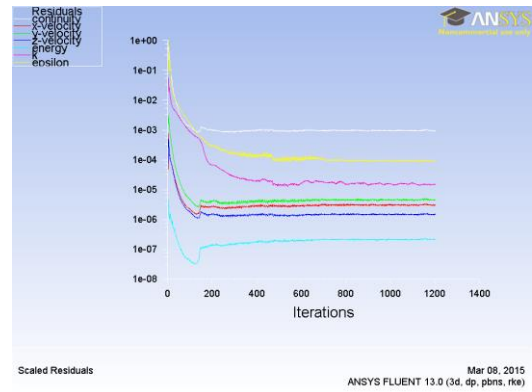
A5. 7: Convergence obtained for S-7 model (H/W=1-1.8-1.3).



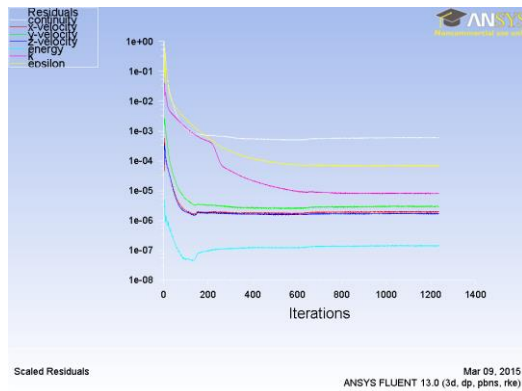
A5. 8: Convergence obtained for S-8 model (H/W=1-2-2).



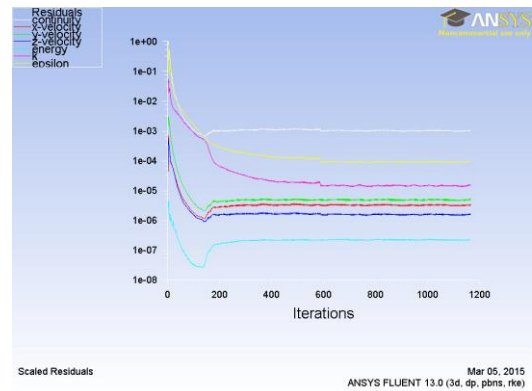
A5. 9: Convergence obtained for S-9 model ( $H/W=1.8-2.3$ ).



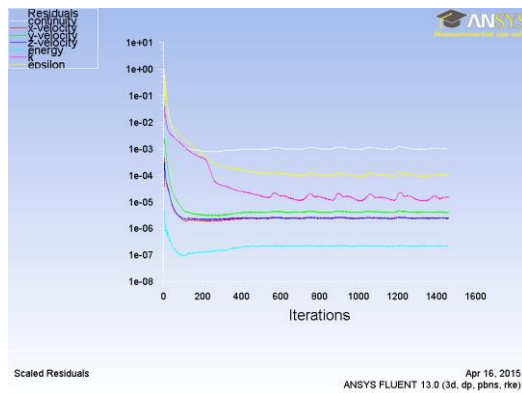
A5. 10: Convergence obtained for S-10 model ( $H/W=1.2-1.8$ ).



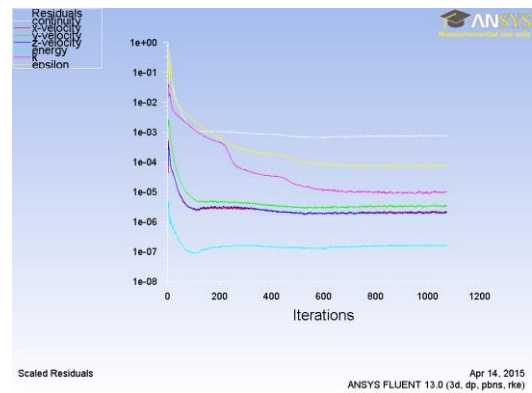
A5. 11: Convergence obtained for S-11 model ( $H/W=1.3-2.3$ ).



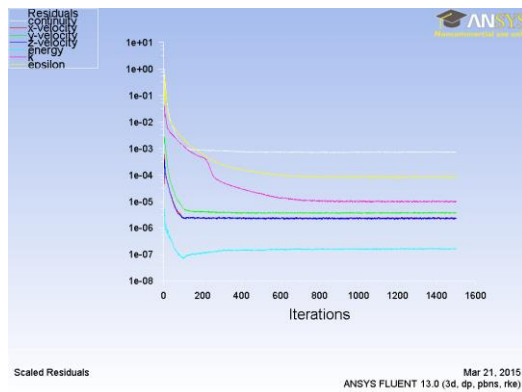
A5. 12: Convergence obtained for S-12 model ( $H/W=1.2-1.3$ ).



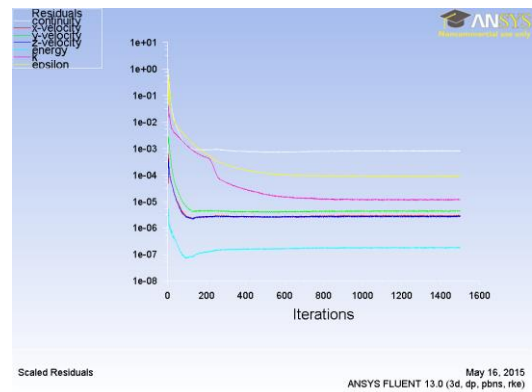
A5. 13: Convergence obtained for S-13 model ( $H/W=1.3-1.5$ ).



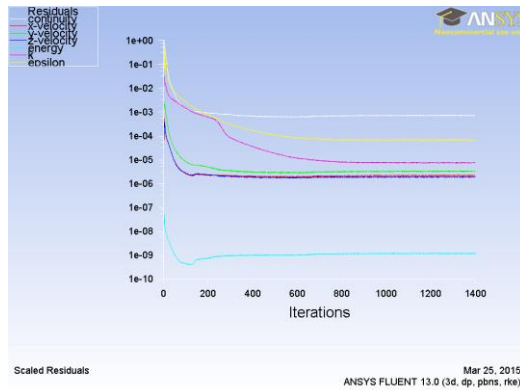
A5. 14: Convergence obtained for S-14 model ( $H/W=1.3-2$ ).



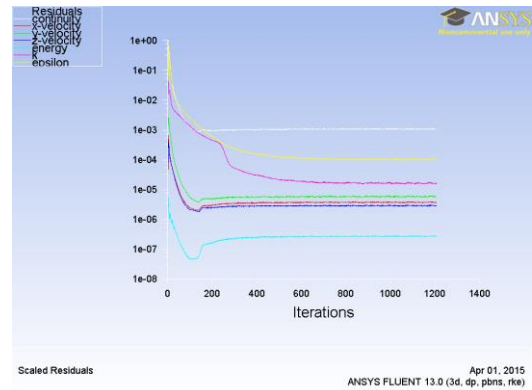
A5. 15: Convergence obtained for S-15 model ( $H/W=1.5-2.3$ ).



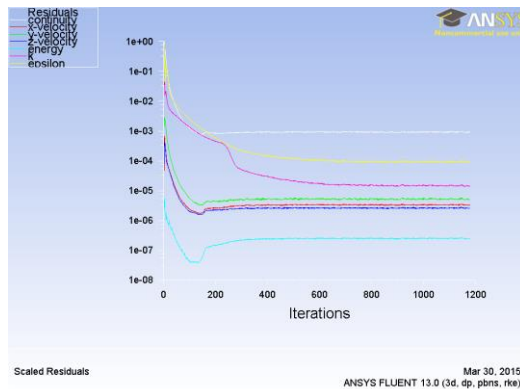
A5. 16: Convergence obtained for S-16 model ( $H/W=1.3-1.5-2.3$ ).



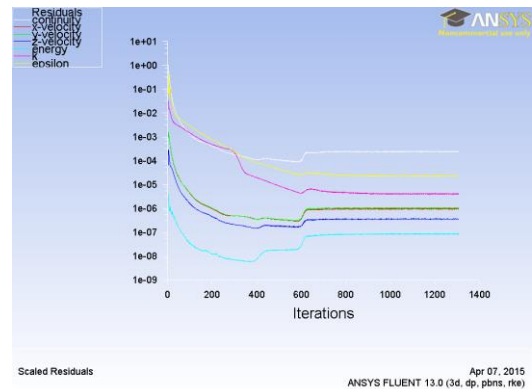
A5. 17: Convergence obtained for S-17 model (microclimate at night for  $H/W=1.3-1.5-2.3$ ).



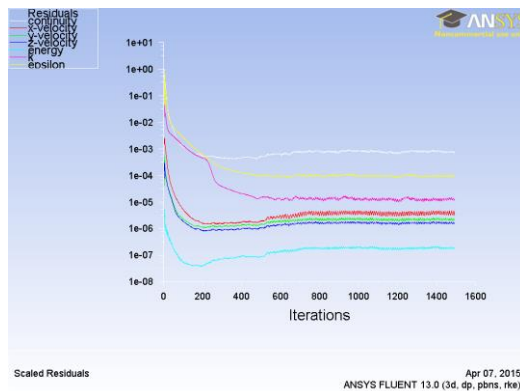
A5. 18: Convergence obtained for S-18 model (leeward increase in building' rows with grid position).



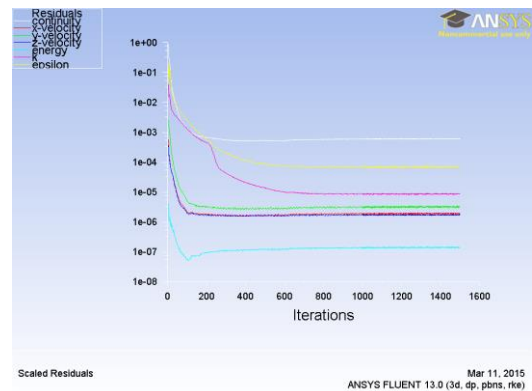
A5. 19: Convergence obtained for S-19 model (leeward increase in building's rows with chess-board position).



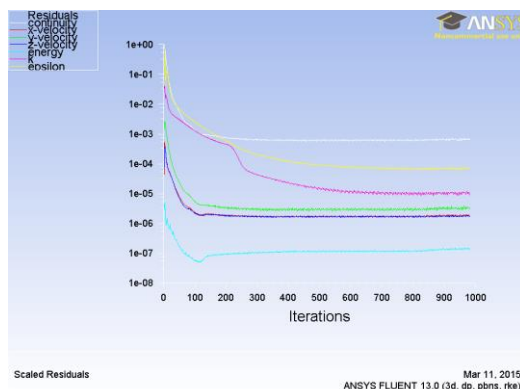
A5. 20: Convergence obtained for S-20 model (Westerly wind direction).



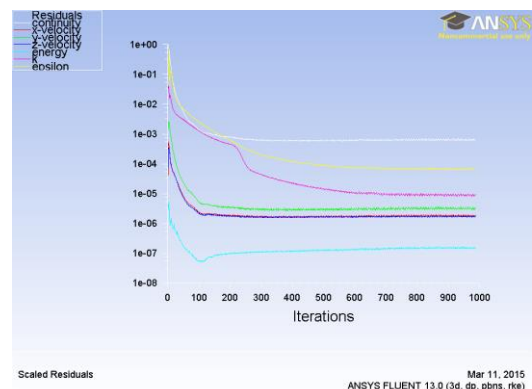
A5. 21: Convergence obtained for S-21 model (North-Westerly wind direction).



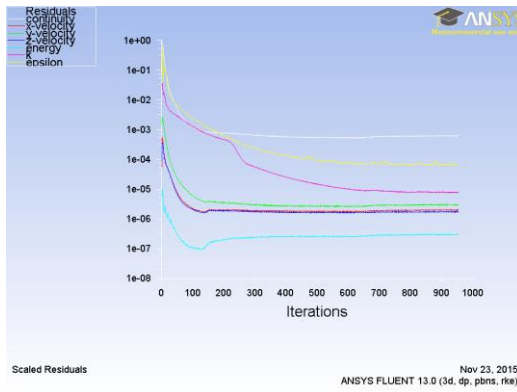
A5. 22: Convergence obtained for S-22 model (Lower Street).



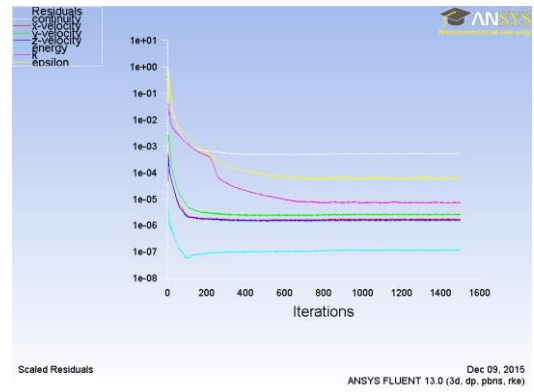
A5. 23: Convergence obtained for S-23 model (Upper Street).



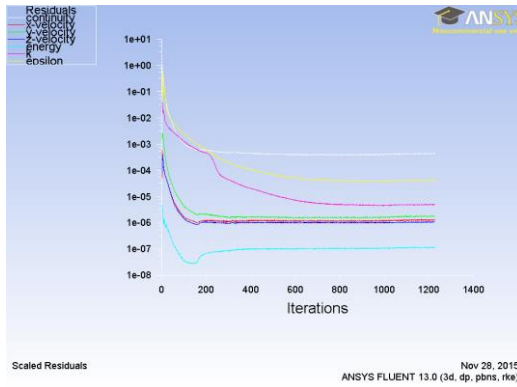
A5. 24: Convergence obtained for S-24 model (Upper and Lower Streets).



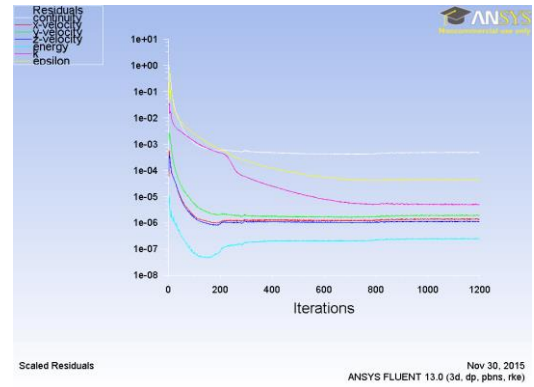
**A5. 25: Convergence obtained for S-25 model (Optimum H/W at Noon).**



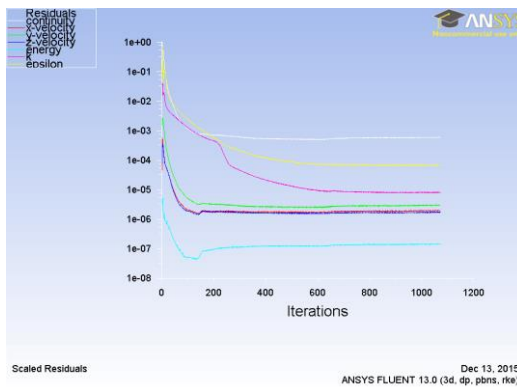
**A5. 26: Convergence obtained for S-26 model (removal of buildings)**



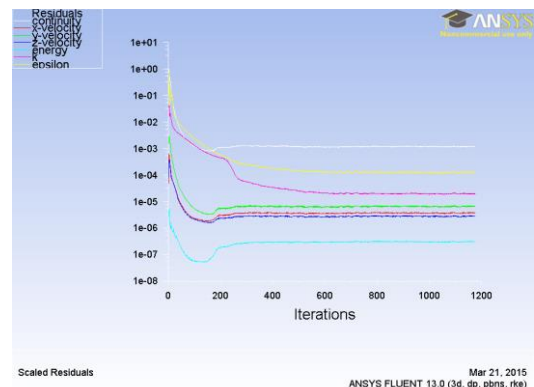
**A5. 27: Convergence obtained for S-27 model (Protruding floors at 15:00 hours).**



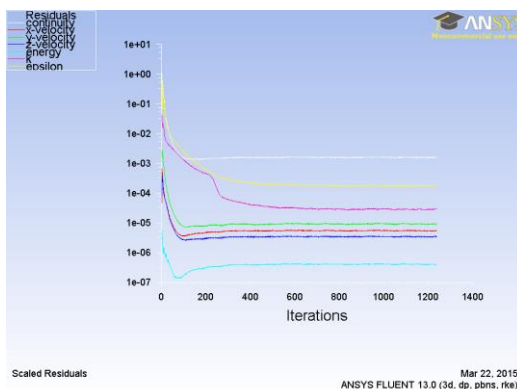
**A5. 28: Convergence obtained for S-28 model (Protruding floors at Noon).**



**A5. 29: Convergence obtained for S-29 model (Changes to albedo at 15:00 hours).**



**A5. 30: Convergence obtained for S-30 model (Changes to Block Patterns, Grid Style).**



**A5. 31: Convergence obtained for S-31 model (Changes to Block Patterns, Chess-Board Style).**



**A6: Appendices for Chapter 6 (From A6.1 to A6.5) for the hourly and average hourly monitored microclimatic data over a year in the high urban density area (Case 1).**

A6. 1: Average hourly Microclimatic data monitored in the high urban density area (Case 1).

Time HH:MM		October 2012 (Autumn)						January 2013 (Winter)						April 2013 (Spring)						June 2013 (Summer)					
		V	Ta	RH	Tg	MRT	PET	V	Ta	RH	Tg	MRT	PET	V	Ta	RH	Tg	MRT	PET	V	Ta	RH	Tg	MRT	PET
		m/s	°C	%	°C	°C	°C	m/s	°C	%	°C	°C	°C	m/s	°C	%	°C	°C	°C	m/s	°C	%	°C	°C	°C
00:00		0.5	32.5	21.2	33.1	33.2	32.3	1.8	22.4	33.1	33.6	39.0	24.7	0.6	28.8	18.6	29.4	29.5	27.6	0.6	35.3	13.6	34.2	34.0	34.4
01:00		0.5	31.4	23.3	31.2	31.2	30.6	1.9	23.9	29.6	35.1	45.0	28.2	0.5	28.7	24.2	28.4	28.3	27.3	0.2	32.6	15.1	32.5	32.5	32.2
02:00		0.4	30.3	25.1	29.9	29.8	29.3	2.0	23.6	29.9	26.3	27.9	21.7	0.6	27.8	23.7	27.4	27.3	25.9	0.4	31.9	15.6	31.8	31.7	31.1
03:00		0.4	29.7	26.3	29.5	29.5	28.8	1.6	23.8	28.7	25.0	25.6	21.6	0.5	26.7	22.2	26.4	26.4	24.9	0.6	31.4	15.7	31.5	31.5	30.4
04:00		0.3	29.1	27.3	28.8	28.8	28.3	1.9	23.8	27.8	24.3	24.6	20.9	0.5	25.9	24.6	25.6	25.6	23.9	1.0	31.2	15.8	31.3	31.3	29.7
05:00		0.3	28.6	28.0	28.5	28.5	27.8	1.9	23.3	28.0	23.1	23.0	19.9	0.7	25.0	28.0	24.9	24.9	22.4	0.6	31.0	17.2	31.2	31.2	30.1
06:00		0.3	28.0	28.4	27.7	27.7	27.1	1.3	22.4	30.0	21.7	21.4	19.2	0.5	24.6	31.0	24.3	24.2	22.5	0.0	31.0	17.6	31.5	31.5	31.6
07:00		0.4	28.2	28.2	28.8	28.9	27.5	1.6	21.7	33.4	21.0	20.6	18.0	0.4	24.8	31.5	25.4	25.5	23.6	0.8	31.4	16.6	33.6	34.2	31.5
08:00		0.5	28.3	27.5	30.6	31.1	28.4	1.4	20.9	36.0	20.2	19.8	17.2	0.7	25.8	29.4	28.0	28.7	24.8	1.2	33.3	14.7	37.2	38.5	34.6
09:00		0.6	30.3	24.4	32.7	33.2	30.6	1.1	20.2	37.6	19.6	19.3	16.9	0.4	27.0	21.8	29.4	29.8	27.0	0.9	35.1	11.4	34.6	34.4	34.4
10:00		0.5	32.3	20.8	35.2	35.8	33.4	1.2	19.5	38.7	18.8	18.5	15.8	0.6	28.8	18.4	31.7	32.4	28.9	0.6	37.7	8.1	37.4	37.3	37.6
11:00		0.5	33.9	18.6	38.5	39.4	36.3	0.9	18.7	40.5	18.1	17.8	15.4	1.1	30.4	15.3	34.9	36.5	31.2	1.3	38.2	6.4	38.5	38.6	38.9
12:00		0.5	35.5	16.0	44.6	46.3	40.9	1.3	18.1	41.5	17.4	17.1	13.9	0.6	31.8	11.9	41.0	42.9	36.2	1.1	40.3	5.7	42.2	42.8	42.5
13:00		0.5	35.8	15.3	44.2	45.8	40.8	1.1	17.3	45.9	16.7	16.5	13.4	0.9	33.3	10.6	41.7	44.1	37.4	1.1	39.2	6.7	39.0	39.0	39.8
14:00		0.5	36.0	14.2	39.4	40.0	37.9	1.0	16.7	46.8	16.2	16.0	12.9	0.9	33.2	9.7	36.6	37.6	34.2	0.9	41.0	4.2	42.0	42.2	42.5
15:00		0.5	35.7	14.7	37.7	38.1	36.8	0.9	16.0	49.3	15.3	15.0	12.2	0.6	33.7	8.2	35.8	36.2	34.2	1.0	41.0	5.4	41.2	41.2	42.2
16:00		0.5	35.3	14.8	36.8	37.1	36.0	0.9	15.5	50.4	14.6	14.3	11.5	1.0	33.3	8.6	34.8	35.2	33.1	0.2	39.8	6.1	38.7	38.6	39.0
17:00		0.5	36.0	14.4	36.6	36.7	36.3	1.0	15.1	51.8	14.4	14.1	10.9	0.8	33.0	9.3	33.6	33.8	32.4	0.6	40.5	5.5	39.3	39.0	40.3
18:00		0.4	36.6	13.7	36.8	36.8	36.7	1.2	15.2	51.6	14.7	14.4	10.6	0.6	32.3	10.8	32.6	32.6	31.5	0.8	40.4	6.8	39.7	39.5	40.8
19:00		0.4	36.1	15.6	36.5	36.6	36.3	1.5	15.0	52.9	14.6	14.4	9.9	0.5	31.8	12.9	32.2	32.3	31.1	0.5	38.8	9.8	39.4	39.5	39.4
20:00		0.3	35.6	16.9	35.9	35.9	35.7	1.8	15.7	52.0	20.4	23.2	12.9	0.6	31.2	15.0	31.5	31.6	30.3	0.7	37.4	13.9	38.5	38.8	38.3
21:00		0.4	35.0	17.9	35.5	35.6	35.1	1.3	17.8	46.6	30.1	35.1	20.3	0.7	30.3	17.0	30.7	30.9	29.2	0.3	35.9	17.1	34.8	34.7	35.2
22:00		0.4	34.3	18.9	35.1	35.2	34.5	1.6	19.2	41.6	32.7	39.0	22.3	0.7	29.7	17.8	30.5	30.7	28.6	0.5	36.4	15.0	35.5	35.3	35.9
23:00		0.4	33.4	21.3	34.0	34.1	33.4	1.8	19.9	38.1	30.3	35.5	21.1	0.5	29.3	18.4	29.9	30.0	28.4	0.9	35.5	13.5	35.0	34.9	35.0
AVERAGE		0.4	32.8	20.5	34.5	34.8	33.4	1.4	19.4	40.1	22.0	23.2	17.1	0.6	29.5	18.3	31.1	31.5	29.0	0.7	36.1	11.6	36.3	36.3	36.1

**A6. 2: Detailed hourly microclimatic data in the high urban density area (October)**

<b>Field measurements for Autumn (14th to 25th of October 2012) in the High Urban Density Area (Case 1)</b>							
Date	Time	Winds. (m/s)	Ta (°C)	RH (%)	Tg (°C)	MRT (°C)	Wind Direction
<b>14th of October 2012</b>							
14.10.12	00:00	1.1	33.2	8.0	32.6	32.4	ENE
14.10.12	01:00	1.0	32.6	9.0	31.9	31.7	NE
14.10.12	02:00	0.9	31.9	10.0	31.0	30.7	NNE
14.10.12	03:00	0.8	31.0	10.0	30.5	30.4	S
14.10.12	04:00	0.6	30.1	10.0	29.9	29.9	SW
14.10.12	05:00	0.6	29.8	11.0	29.3	29.2	S
14.10.12	06:00	0.5	29.5	11.0	28.5	28.3	S
14.10.12	07:00	0.5	29.8	12.0	29.7	29.7	SE
14.10.12	08:00	0.4	30.0	12.0	31.2	31.4	ESE
14.10.12	09:00	0.4	32.0	11.0	34.1	34.5	SE
14.10.12	10:00	0.3	34.0	10.0	36.0	36.3	W
14.10.12	11:00	0.4	35.6	9.0	38.4	38.9	SE
14.10.12	12:00	0.5	37.2	7.0	43.8	45.0	SE
14.10.12	13:00	0.4	37.4	7.0	46.5	47.9	E
14.10.12	14:00	0.2	37.5	7.0	41.2	41.6	NE
14.10.12	15:00	0.3	37.5	8.0	38.2	38.3	NE
14.10.12	16:00	0.4	37.5	8.0	40.2	40.6	NE
14.10.12	17:00	0.5	37.3	7.0	37.6	37.7	NE
14.10.12	18:00	0.5	37.1	6.0	38.9	39.3	ENE
14.10.12	19:00	0.4	36.6	7.0	37.8	38.0	S
14.10.12	20:00	0.3	36.1	7.0	38.3	38.6	WSW
14.10.12	21:00	0.3	35.7	7.0	35.7	35.7	S
14.10.12	22:00	0.2	35.2	7.0	36.1	36.2	S
14.10.12	23:00	0.2	34.9	7.0	36.1	36.2	SSW
<b>15th of October 2012</b>							
15.10.12	00:00	0.2	34.6	7.0	34.0	33.9	SW
15.10.12	01:00	0.6	33.1	9.0	32.4	32.2	SSW
15.10.12	02:00	1.0	31.6	11.0	30.7	30.4	S
15.10.12	03:00	0.7	30.8	14.0	30.3	30.2	ESE
15.10.12	04:00	0.3	29.9	16.0	29.7	29.7	NE
15.10.12	05:00	0.3	29.1	14.0	28.6	28.5	N
15.10.12	06:00	0.3	28.3	11.0	27.3	27.1	WNW
15.10.12	07:00	0.6	28.9	11.0	28.8	28.8	NNW
15.10.12	08:00	0.8	29.4	10.0	30.6	31.0	N
15.10.12	09:00	1.1	31.4	9.0	33.5	34.3	NNE
15.10.12	10:00	1.3	33.4	7.0	35.4	36.2	ENE
15.10.12	11:00	1.0	36.2	7.0	39.0	39.9	ESE
15.10.12	12:00	0.6	38.9	7.0	45.5	46.9	SE
15.10.12	13:00	0.6	38.1	7.0	47.2	49.1	SSE
15.10.12	14:00	0.5	37.2	6.0	40.9	41.6	SE
15.10.12	15:00	0.5	37.1	6.0	37.8	37.9	ESE
15.10.12	16:00	0.5	37.0	6.0	39.7	40.2	E
15.10.12	17:00	0.5	37.3	6.0	37.6	37.7	E
15.10.12	18:00	0.4	37.5	6.0	39.3	39.6	E
15.10.12	19:00	0.6	36.9	7.0	38.1	38.4	NE
15.10.12	20:00	0.8	36.3	7.0	38.5	39.1	N
15.10.12	21:00	1.0	35.3	7.0	35.3	35.3	N
15.10.12	22:00	1.1	34.2	7.0	35.1	35.4	N
15.10.12	23:00	1.0	33.7	7.0	34.9	35.3	WNW



Date	Time	Winds. (m/s)	Ta (°C)	RH (%)	Tg (°C)	MRT (°C)	Wind Direction
<b>16th of October 2012</b>							
16.10.12	00:00	0.8	33.2	7.0	32.6	32.4	W
16.10.12	01:00	0.6	32.4	9.0	31.7	31.5	W
16.10.12	02:00	0.4	31.5	10.0	30.6	30.4	WSW
16.10.12	03:00	0.3	30.5	11.0	30.0	29.9	NNW
16.10.12	04:00	0.1	29.5	12.0	29.3	29.3	ENE
16.10.12	05:00	0.5	28.6	14.0	28.1	28.0	ENE
16.10.12	06:00	0.8	27.7	15.0	26.7	26.4	ENE
16.10.12	07:00	1.0	28.4	13.0	28.3	28.3	NNE
16.10.12	08:00	1.2	29.0	11.0	30.2	30.7	N
16.10.12	09:00	0.7	31.1	10.0	33.2	33.7	N
16.10.12	10:00	0.1	33.1	8.0	35.1	35.2	N
16.10.12	11:00	0.2	34.1	8.0	36.9	37.2	NNW
16.10.12	12:00	0.3	35.0	8.0	41.6	42.5	NNW
16.10.12	13:00	0.4	36.5	7.0	45.6	47.0	NW
16.10.12	14:00	0.5	37.1	7.0	40.8	41.5	NW
16.10.12	15:00	0.6	37.0	7.0	37.7	37.9	NW
16.10.12	16:00	0.7	36.8	6.0	39.5	40.2	NW
16.10.12	17:00	0.8	36.9	6.0	37.2	37.3	NW
16.10.12	18:00	0.8	36.9	6.0	38.7	39.2	SW
16.10.12	19:00	0.6	36.3	7.0	37.5	37.8	WNW
16.10.12	20:00	0.3	35.6	7.0	37.8	38.1	N
16.10.12	21:00	0.3	34.5	7.0	34.5	34.5	N
16.10.12	22:00	0.3	33.4	7.0	34.3	34.4	N
16.10.12	23:00	0.3	32.8	8.0	34.0	34.2	NNE
<b>17th of October 2012</b>							
17.10.12	00:00	0.2	32.2	9.0	31.6	31.5	NE
17.10.12	01:00	0.3	31.2	13.0	30.5	30.4	SSE
17.10.12	02:00	0.3	30.2	16.0	29.3	29.2	SSW
17.10.12	03:00	0.4	29.7	16.0	29.2	29.1	S
17.10.12	04:00	0.5	29.1	16.0	28.9	28.9	S
17.10.12	05:00	0.5	28.3	17.0	27.8	27.7	ESE
17.10.12	06:00	0.5	27.4	18.0	26.4	26.2	NE
17.10.12	07:00	0.4	27.9	18.0	27.8	27.8	SE
17.10.12	08:00	0.2	28.3	18.0	29.5	29.6	SW
17.10.12	09:00	0.5	30.7	15.0	32.8	33.2	ESE
17.10.12	10:00	0.8	33.1	11.0	35.1	35.7	NNE
17.10.12	11:00	0.6	35.8	11.0	38.6	39.2	NE
17.10.12	12:00	0.4	38.4	10.0	45.0	46.0	ENE
17.10.12	13:00	0.5	37.5	10.0	46.6	48.2	N
17.10.12	14:00	0.5	36.6	10.0	40.3	41.0	NW
17.10.12	15:00	0.5	36.6	10.0	37.3	37.4	WNW
17.10.12	16:00	0.5	36.5	10.0	39.2	39.7	W
17.10.12	17:00	0.7	36.8	9.0	37.1	37.2	WSW
17.10.12	18:00	0.8	37.0	8.0	38.8	39.3	SW
17.10.12	19:00	0.6	36.4	8.0	37.6	37.9	SSE
17.10.12	20:00	0.4	35.7	8.0	37.9	38.3	ESE
17.10.12	21:00	0.4	35.4	10.0	35.4	35.4	NE
17.10.12	22:00	0.3	35.0	12.0	35.9	36.0	N
17.10.12	23:00	0.7	34.1	13.0	35.3	35.6	N

Date	Time	Winds. (m/s)	Ta (°C)	RH (%)	Tg (°C)	MRT (°C)	Wind Direction
<b>18th of October 2012</b>							
18.10.12	00:00	1.0	33.1	13.0	32.5	32.3	NNE
18.10.12	01:00	0.8	32.1	15.0	31.4	31.2	NNE
18.10.12	02:00	0.5	31.0	17.0	30.1	29.9	NNE
18.10.12	03:00	0.5	30.2	18.0	29.7	29.6	N
18.10.12	04:00	0.5	29.4	19.0	29.2	29.2	N
18.10.12	05:00	0.5	28.9	20.0	28.4	28.3	N
18.10.12	06:00	0.4	28.3	21.0	27.3	27.1	NNE
18.10.12	07:00	0.4	28.4	21.0	28.3	28.3	NE
18.10.12	08:00	0.3	28.5	21.0	29.7	29.9	ENE
18.10.12	09:00	0.4	30.6	18.0	32.7	33.1	NE
18.10.12	10:00	0.4	32.7	15.0	34.7	35.0	NE
18.10.12	11:00	0.3	35.1	14.0	37.9	38.3	SE
18.10.12	12:00	0.2	37.4	12.0	44.0	44.6	SW
18.10.12	13:00	0.4	37.3	11.0	46.4	47.8	SE
18.10.12	14:00	0.5	37.2	10.0	40.9	41.6	E
18.10.12	15:00	0.6	37.3	10.0	38.0	38.2	ENE
18.10.12	16:00	0.7	37.3	9.0	40.0	40.7	NE
18.10.12	17:00	0.8	37.1	9.0	37.4	37.5	SE
18.10.12	18:00	0.8	36.9	9.0	38.7	39.2	SSW
18.10.12	19:00	0.4	37.3	12.0	38.5	38.7	SE
18.10.12	20:00	0.0	37.7	14.0	39.9	39.9	E
18.10.12	21:00	0.0	36.9	13.0	36.9	36.9	NE
18.10.12	22:00	0.0	36.0	15.0	36.9	36.9	N
18.10.12	23:00	0.6	34.3	17.0	35.5	35.8	N
<b>19th of October 2012</b>							
19.10.12	00:00	1.2	32.6	19.0	32.0	31.8	NNE
19.10.12	01:00	1.0	31.8	21.0	31.1	30.9	N
19.10.12	02:00	0.8	31.0	22.0	30.1	29.8	NNE
19.10.12	03:00	0.6	30.6	23.0	30.1	30.0	NE
19.10.12	04:00	0.4	30.1	23.0	29.9	29.9	NE
19.10.12	05:00	0.3	29.4	24.0	28.9	28.8	NE
19.10.12	06:00	0.2	28.6	25.0	27.6	27.5	ENE
19.10.12	07:00	0.3	28.9	25.0	28.8	28.8	ENE
19.10.12	08:00	0.4	29.2	25.0	30.4	30.6	ENE
19.10.12	09:00	0.6	31.0	23.0	33.1	33.6	NE
19.10.12	10:00	0.7	32.8	21.0	34.8	35.3	N
19.10.12	11:00	0.5	34.7	17.0	37.5	38.1	WNW
19.10.12	12:00	0.3	36.5	12.0	43.1	44.0	SW
19.10.12	13:00	0.5	36.8	11.0	45.9	47.5	SSW
19.10.12	14:00	0.6	37.1	9.0	40.8	41.6	SSW
19.10.12	15:00	0.7	37.0	10.0	37.7	37.9	SSW
19.10.12	16:00	0.8	36.9	10.0	39.6	40.3	S
19.10.12	17:00	0.5	37.1	10.0	37.4	37.5	S
19.10.12	18:00	0.2	37.2	9.0	39.0	39.2	SSW
19.10.12	19:00	0.2	37.1	14.0	38.3	38.4	N
19.10.12	20:00	0.1	37.0	19.0	39.2	39.3	N
19.10.12	21:00	0.3	35.2	22.0	35.2	35.2	N
19.10.12	22:00	0.5	33.3	25.0	34.2	34.4	NNE
19.10.12	23:00	0.4	33.8	25.0	35.0	35.2	N

Date	Time	Winds. (m/s)	Ta (°C)	RH (%)	Tg (°C)	MRT (°C)	Wind Direction
<b>20th of October 2012</b>							
20.10.12	00:00	0.2	34.2	24.0	33.6	33.5	N
20.10.12	01:00	0.2	32.6	24.0	31.9	31.8	NE
20.10.12	02:00	0.2	31.0	24.0	30.1	30.0	E
20.10.12	03:00	0.2	30.4	24.5	29.9	29.8	S
20.10.12	04:00	0.2	29.7	25.0	29.5	29.5	WSW
20.10.12	05:00	0.2	29.3	27.0	28.8	28.7	NNW
20.10.12	06:00	0.1	28.9	29.0	27.9	27.8	NE
20.10.12	07:00	0.6	29.0	29.0	28.9	28.9	ESE
20.10.12	08:00	1.0	29.1	28.0	30.3	30.7	S
20.10.12	09:00	1.0	30.8	25.0	32.9	33.6	SE
20.10.12	10:00	0.9	32.4	21.0	34.4	35.0	E
20.10.12	11:00	0.9	33.4	20.0	36.2	37.0	NE
20.10.12	12:00	0.9	34.4	19.0	41.0	42.9	NNE
20.10.12	13:00	0.9	35.2	18.0	44.3	46.8	NE
20.10.12	14:00	0.8	35.9	16.0	39.6	40.6	NE
20.10.12	15:00	0.8	35.9	15.0	36.6	36.8	NE
20.10.12	16:00	0.7	35.8	13.0	38.5	39.2	NE
20.10.12	17:00	0.7	35.7	15.0	36.0	36.1	NE
20.10.12	18:00	0.6	35.6	16.0	37.4	37.8	E
20.10.12	19:00	0.5	35.3	18.0	36.5	36.7	ENE
20.10.12	20:00	0.3	34.9	19.0	37.1	37.4	NE
20.10.12	21:00	0.3	34.2	21.0	34.2	34.2	NE
20.10.12	22:00	0.2	33.5	23.0	34.4	34.5	NE
20.10.12	23:00	0.4	33.1	23.0	34.3	34.5	NE
<b>21st of October 2012</b>							
21.10.12	00:00	0.5	32.6	23.0	32.0	31.9	NE
21.10.12	01:00	0.4	31.7	31.0	31.0	30.9	E
21.10.12	02:00	0.2	30.7	38.0	29.8	29.7	SSE
21.10.12	03:00	0.2	30.2	39.0	29.7	29.6	NE
21.10.12	04:00	0.1	29.7	40.0	29.5	29.5	NW
21.10.12	05:00	0.1	29.5	39.0	29.0	29.0	NE
21.10.12	06:00	0.1	29.2	38.0	28.2	28.1	NE
21.10.12	07:00	0.4	29.3	31.0	29.2	29.2	NE
21.10.12	08:00	0.7	29.3	23.0	30.5	30.8	NE
21.10.12	09:00	0.5	31.7	22.0	33.8	34.2	NE
21.10.12	10:00	0.3	34.1	21.0	36.1	36.4	NNE
21.10.12	11:00	0.6	35.3	16.0	38.1	38.7	ESE
21.10.12	12:00	0.9	36.4	11.0	43.0	44.9	SSW
21.10.12	13:00	0.8	36.5	12.0	45.6	47.9	S
21.10.12	14:00	0.6	36.6	12.0	40.3	41.1	S
21.10.12	15:00	0.4	35.8	17.0	36.5	36.6	S
21.10.12	16:00	0.2	35.0	21.0	37.7	38.0	S
21.10.12	17:00	0.2	36.2	19.0	36.5	36.5	SE
21.10.12	18:00	0.2	37.4	16.0	39.2	39.4	ESE
21.10.12	19:00	0.2	36.8	18.0	38.0	38.1	NE
21.10.12	20:00	0.1	36.1	19.0	38.3	38.4	N
21.10.12	21:00	0.6	35.4	23.0	35.4	35.4	N
21.10.12	22:00	1.1	34.7	26.0	35.6	35.9	NNW
21.10.12	23:00	0.6	29.5	42.0	30.7	31.0	NNW

Date	Time	Winds. (m/s)	Ta (°C)	RH (%)	Tg (°C)	MRT (°C)	Wind Direction
<b>22nd of October 2012</b>							
22.10.12	00:00	0.1	24.2	58.0	23.6	23.6	NNW
22.10.12	01:00	0.2	23.5	56.0	22.8	22.7	NE
22.10.12	02:00	0.3	22.8	54.0	21.9	21.8	ESE
22.10.12	03:00	0.2	23.2	52.0	22.7	22.6	SE
22.10.12	04:00	0.1	23.6	50.0	23.4	23.4	SSE
22.10.12	05:00	0.1	23.2	52.0	22.7	22.7	ESE
22.10.12	06:00	0.1	22.8	53.0	21.8	21.7	ENE
22.10.12	07:00	0.2	23.1	55.0	23.0	23.0	NE
22.10.12	08:00	0.2	23.4	56.0	24.6	24.7	NE
22.10.12	09:00	0.1	25.6	50.0	27.7	27.8	NNE
22.10.12	10:00	0.0	27.7	43.0	29.7	29.7	N
22.10.12	11:00	0.4	28.9	40.0	31.7	32.2	N
22.10.12	12:00	0.8	30.0	37.0	36.6	38.4	SW
22.10.12	13:00	0.7	30.9	33.0	40.0	42.2	N
22.10.12	14:00	0.5	31.7	29.0	35.4	36.1	NE
22.10.12	15:00	0.5	31.9	28.0	32.6	32.7	NNE
22.10.12	16:00	0.4	32.1	27.0	34.8	35.3	NNE
22.10.12	17:00	0.3	33.8	25.0	34.1	34.1	NNE
22.10.12	18:00	0.2	35.4	23.0	37.2	37.4	NNE
22.10.12	19:00	0.2	35.6	23.0	36.8	36.9	NE
22.10.12	20:00	0.1	35.7	22.0	37.9	38.0	ENE
22.10.12	21:00	0.1	36.1	22.0	36.1	36.1	ENE
22.10.12	22:00	0.0	36.4	22.0	37.3	37.3	ENE
22.10.12	23:00	0.1	35.6	24.0	36.8	36.9	NE
<b>23rd of October 2012</b>							
23.10.12	00:00	0.1	34.7	25.0	34.1	34.1	NE
23.10.12	01:00	0.1	32.7	28.0	32.0	32.0	NE
23.10.12	02:00	0.1	30.6	30.0	29.7	29.6	NE
23.10.12	03:00	0.1	30.0	33.0	29.5	29.5	NE
23.10.12	04:00	0.1	29.3	35.0	29.1	29.1	NE
23.10.12	05:00	0.1	28.7	35.0	28.2	28.2	NE
23.10.12	06:00	0.1	28.1	35.0	27.1	27.0	NE
23.10.12	07:00	0.1	28.0	38.0	27.9	27.9	NE
23.10.12	08:00	0.1	27.8	40.0	29.0	29.1	NE
23.10.12	09:00	0.1	29.1	36.0	31.2	31.3	NE
23.10.12	10:00	0.1	30.3	32.0	32.3	32.4	NW
23.10.12	11:00	0.1	31.4	30.0	34.2	34.4	E
23.10.12	12:00	0.1	32.5	27.0	39.1	39.5	E
23.10.12	13:00	0.1	33.0	27.0	42.1	42.6	NE
23.10.12	14:00	0.1	33.5	26.0	37.2	37.4	NE
23.10.12	15:00	0.3	31.1	28.0	31.8	31.9	NE
23.10.12	16:00	0.5	28.6	30.0	31.3	31.9	NE
23.10.12	17:00	0.3	30.7	29.0	31.0	31.0	NE
23.10.12	18:00	0.0	32.8	27.0	34.6	34.6	N
23.10.12	19:00	0.3	34.2	26.0	35.4	35.6	ENE
23.10.12	20:00	0.5	35.6	24.0	37.8	38.2	SE
23.10.12	21:00	0.4	35.7	24.0	35.7	35.7	E
23.10.12	22:00	0.2	35.8	23.0	36.7	36.8	ENE
23.10.12	23:00	0.5	34.6	25.0	35.8	36.0	SE

Date	Time	Winds. (m/s)	Ta (°C)	RH (%)	Tg (°C)	MRT (°C)	Wind Direction
<b>24th of October 2012</b>							
24.10.12	00:00	0.7	33.4	27.0	32.8	32.6	S
24.10.12	01:00	0.6	32.1	29.0	31.4	31.2	S
24.10.12	02:00	0.5	30.8	31.0	29.9	29.7	S
24.10.12	03:00	0.4	30.1	36.0	29.6	29.5	S
24.10.12	04:00	0.3	29.3	41.0	29.1	29.1	SSW
24.10.12	05:00	0.4	28.9	42.0	28.4	28.3	SSW
24.10.12	06:00	0.4	28.4	43.0	27.4	27.2	WNW
24.10.12	07:00	0.4	27.9	43.0	27.8	27.8	N
24.10.12	08:00	0.4	27.4	43.0	28.6	28.8	N
24.10.12	09:00	1.0	29.8	34.0	31.9	32.6	NE
24.10.12	10:00	1.5	32.2	25.0	34.2	35.1	ENE
24.10.12	11:00	1.1	34.0	20.0	36.8	37.8	SE
24.10.12	12:00	0.7	35.8	15.0	42.4	44.0	SSW
24.10.12	13:00	0.8	36.2	13.5	45.3	47.6	S
24.10.12	14:00	0.8	36.6	12.0	40.3	41.3	SE
24.10.12	15:00	0.7	36.3	12.5	37.0	37.2	SE
24.10.12	16:00	0.6	35.9	13.0	38.6	39.2	SE
24.10.12	17:00	0.4	36.9	15.5	37.2	37.3	SE
24.10.12	18:00	0.2	37.9	18.0	39.7	39.9	SE
24.10.12	19:00	0.4	35.8	25.0	37.0	37.2	E
24.10.12	20:00	0.5	33.7	32.0	35.9	36.3	ENE
24.10.12	21:00	0.4	33.2	33.0	33.2	33.2	NE
24.10.12	22:00	0.2	32.6	34.0	33.5	33.6	N
24.10.12	23:00	0.1	32.4	34.0	33.6	33.7	NE
<b>25th of October 2012</b>							
25.10.12	00:00	0.0	32.2	34.0	31.6	31.6	ENE
25.10.12	01:00	0.1	31.3	36.0	30.6	30.6	ENE
25.10.12	02:00	0.1	30.4	38.0	29.5	29.4	ENE
25.10.12	03:00	0.2	30.0	39.0	29.5	29.4	ENE
25.10.12	04:00	0.2	29.5	40.0	29.3	29.3	ENE
25.10.12	05:00	0.2	29.1	41.0	28.6	28.5	ENE
25.10.12	06:00	0.2	28.6	42.0	27.6	27.5	ENE
25.10.12	07:00	0.3	28.5	42.5	28.4	28.4	ENE
25.10.12	08:00	0.3	28.4	43.0	29.6	29.8	NE
25.10.12	09:00	0.2	30.1	39.5	32.2	32.4	NE
25.10.12	10:00	0.1	31.8	36.0	33.8	33.9	NNE
25.10.12	11:00	0.3	32.7	31.5	35.5	35.9	N
25.10.12	12:00	0.4	33.5	27.0	40.1	41.2	N
25.10.12	13:00	0.3	34.1	26.5	43.2	44.4	NE
25.10.12	14:00	0.2	34.7	26.0	38.4	38.8	NE
25.10.12	15:00	0.2	34.7	25.0	35.4	35.5	NE
25.10.12	16:00	0.2	34.6	24.0	37.3	37.6	E
25.10.12	17:00	0.2	35.9	22.0	36.2	36.2	E
25.10.12	18:00	0.1	37.2	20.0	39.0	39.1	ENE
25.10.12	19:00	0.2	35.1	22.5	36.3	36.4	NE
25.10.12	20:00	0.2	33.0	25.0	35.2	35.4	NE
25.10.12	21:00	0.2	32.4	25.5	32.4	32.4	NE
25.10.12	22:00	0.2	31.7	26.0	32.6	32.7	ENE
25.10.12	23:00	0.2	31.7	30.0	32.9	33.0	SE



**A6. 3: Detailed hourly microclimatic data in the high urban density area (Winter)**

<b>Field measurements for Winter (1st to 7th of January 2013) in the High Urban Density Area (Case 1)</b>							
Date	Time	Winds. (m/s)	Ta (°C)	RH (%)	Tg (°C)	MRT (°C)	Wind Direction
<b>1st of January 2013</b>							
01/01/2013	00:00	0.9	20.2	43.5	19.4	19.1	SSW
01/01/2013	01:00	1.0	19.3	44.9	18.7	18.4	SSW
01/01/2013	02:00	0.9	18.4	47.0	17.8	17.6	SW
01/01/2013	03:00	0.9	17.8	49.3	17.3	17.1	SSW
01/01/2013	04:00	0.5	17.3	50.9	16.8	16.6	WSW
01/01/2013	05:00	0.8	17.0	50.9	16.7	16.5	SSW
01/01/2013	06:00	0.8	16.6	51.7	16.3	16.1	SW
01/01/2013	07:00	0.7	17.1	47.3	16.8	16.7	ESE
01/01/2013	08:00	0.4	17.9	49.3	24.0	25.2	SW
01/01/2013	09:00	1.1	19.9	44.5	33.6	38.4	SSW
01/01/2013	10:00	1.3	21.8	40.8	35.8	41.2	ESE
01/01/2013	11:00	0.9	25.4	32.3	36.6	39.9	ENE
01/01/2013	12:00	0.7	25.9	32.8	35.3	37.6	SW
01/01/2013	13:00	1.3	26.7	28.5	44.6	51.0	SSW
01/01/2013	14:00	0.6	27.4	28.5	30.4	31.1	SSW
01/01/2013	15:00	1.7	27.0	29.4	28.4	29.1	NE
01/01/2013	16:00	1.1	27.7	29.2	28.0	28.1	ENE
01/01/2013	17:00	1.8	26.9	33.5	26.8	26.8	NE
01/01/2013	18:00	1.1	25.6	35.0	25.0	24.7	NE
01/01/2013	19:00	1.2	24.9	35.5	24.0	23.6	NNE
01/01/2013	20:00	0.4	24.0	37.1	23.2	23.1	NE
01/01/2013	21:00	0.0	23.3	39.8	22.6	22.6	NE
01/01/2013	22:00	0.8	22.8	42.2	22.1	21.8	NE
01/01/2013	23:00	1.1	21.8	45.0	21.1	20.8	NNE
<b>2nd of January 2013</b>							
02/01/2013	00:00	0.7	20.9	46.9	20.3	20.1	NE
02/01/2013	01:00	0.5	19.9	52.0	19.4	19.3	NE
02/01/2013	02:00	0.4	20.0	50.7	19.4	19.2	SSW
02/01/2013	03:00	0.3	18.7	55.6	18.0	17.9	N
02/01/2013	04:00	0.4	18.1	60.8	17.3	17.1	SW
02/01/2013	05:00	0.6	17.4	64.6	17.0	16.8	NW
02/01/2013	06:00	1.0	17.2	65.6	16.7	16.4	WNW
02/01/2013	07:00	1.5	16.8	68.1	16.5	16.4	WSW
02/01/2013	08:00	1.1	17.5	69.2	23.1	25.2	SW
02/01/2013	09:00	1.0	21.3	58.0	34.7	39.1	SW
02/01/2013	10:00	1.0	22.6	49.5	38.0	42.8	ENE
02/01/2013	11:00	1.1	22.9	43.8	33.1	36.6	NE
02/01/2013	12:00	1.0	24.7	34.0	36.5	40.4	SSE
02/01/2013	13:00	0.9	25.7	27.5	42.6	47.3	SE
02/01/2013	14:00	1.7	25.3	27.4	27.3	28.3	ENE
02/01/2013	15:00	2.7	25.5	26.0	26.6	27.4	NNE
02/01/2013	16:00	2.1	25.6	24.9	25.7	25.8	NNE
02/01/2013	17:00	1.5	25.5	24.7	24.9	24.6	NE
02/01/2013	18:00	1.3	25.0	24.4	24.0	23.5	ENE
02/01/2013	19:00	1.0	24.3	25.8	23.4	23.1	NE
02/01/2013	20:00	1.1	23.6	27.8	22.3	21.8	NE
02/01/2013	21:00	1.5	23.0	23.6	21.9	21.4	ENE
02/01/2013	22:00	0.7	22.2	21.0	21.3	21.0	NE
02/01/2013	23:00	0.0	21.0	21.8	20.2	20.1	NE



Date	Time	Winds. (m/s)	Ta (°C)	RH (%)	Tg (°C)	MRT (°C)	Wind Direction
<b>3rd of January 2013</b>							
03/01/2013	00:00	1.0	20.7	21.3	19.4	18.8	NE
03/01/2013	01:00	0.6	18.4	28.6	17.9	17.7	WNW
03/01/2013	02:00	1.1	17.4	31.7	17.3	17.3	NE
03/01/2013	03:00	0.9	16.3	35.5	15.5	15.1	ENE
03/01/2013	04:00	0.9	15.4	37.3	14.6	14.3	ESE
03/01/2013	05:00	0.2	15.8	40.3	15.0	14.8	WSW
03/01/2013	06:00	0.3	16.9	44.7	16.3	16.1	SE
03/01/2013	07:00	0.3	16.9	47.9	16.5	16.4	SSW
03/01/2013	08:00	0.8	17.3	47.6	22.5	24.1	S
03/01/2013	09:00	0.8	19.1	43.6	30.6	33.8	SSW
03/01/2013	10:00	0.8	20.7	41.8	33.8	37.4	E
03/01/2013	11:00	1.8	20.9	41.4	34.4	41.0	ESE
03/01/2013	12:00	2.9	21.5	39.5	30.8	37.5	SSW
03/01/2013	13:00	1.6	24.2	34.8	37.1	42.7	E
03/01/2013	14:00	2.1	23.0	33.6	26.0	27.8	SW
03/01/2013	15:00	1.2	23.6	29.7	24.8	25.3	E
03/01/2013	16:00	1.8	23.7	25.9	24.2	24.5	SSW
03/01/2013	17:00	1.3	23.3	26.3	23.2	23.2	SSW
03/01/2013	18:00	0.9	22.7	27.4	21.9	21.6	NW
03/01/2013	19:00	2.6	21.7	34.7	21.3	20.9	SW
03/01/2013	20:00	2.3	20.5	38.5	20.1	19.8	WSW
03/01/2013	21:00	2.5	19.2	42.9	18.9	18.7	NW
03/01/2013	22:00	3.0	17.7	48.6	17.5	17.3	SW
03/01/2013	23:00	2.3	16.8	51.8	16.6	16.4	SW
<b>4rth of January 2013</b>							
04/01/2013	00:00	2.5	16.0	54.3	15.8	15.6	SW
04/01/2013	01:00	1.5	15.3	56.5	14.9	14.6	SSW
04/01/2013	02:00	1.7	14.7	56.9	14.2	13.9	SSW
04/01/2013	03:00	1.6	14.2	58.6	13.8	13.6	NNE
04/01/2013	04:00	1.9	13.8	59.2	13.4	13.1	SSW
04/01/2013	05:00	2.4	13.3	59.7	12.9	12.6	SSW
04/01/2013	06:00	1.8	13.0	60.1	12.5	12.2	SW
04/01/2013	07:00	1.8	12.6	60.1	12.5	12.4	N
04/01/2013	08:00	2.0	13.2	54.5	16.6	18.7	ENE
04/01/2013	09:00	2.2	14.8	48.4	23.4	28.9	SW
04/01/2013	10:00	2.3	16.1	42.1	26.6	33.3	SW
04/01/2013	11:00	2.9	17.6	39.9	29.6	38.1	WSW
04/01/2013	12:00	1.7	18.9	35.6	28.0	32.6	SW
04/01/2013	13:00	1.2	22.5	30.0	35.5	40.3	SW
04/01/2013	14:00	1.4	22.3	29.5	25.8	27.3	ENE
04/01/2013	15:00	0.8	22.5	28.3	23.6	24.0	SSW
04/01/2013	16:00	0.6	23.1	27.5	23.7	23.9	E
04/01/2013	17:00	0.6	23.2	27.2	22.6	22.4	WSW
04/01/2013	18:00	0.2	22.1	30.3	21.3	21.2	ENE
04/01/2013	19:00	0.8	21.3	33.7	20.5	20.2	ENE
04/01/2013	20:00	0.2	20.3	35.9	19.8	19.7	NNE
04/01/2013	21:00	0.6	20.2	36.6	19.4	19.2	NE
04/01/2013	22:00	0.6	19.3	39.0	18.7	18.5	NE
04/01/2013	23:00	0.7	18.6	42.3	18.1	17.9	NNE

Date	Time	Winds. (m/s)	Ta (°C)	RH (%)	Tg (°C)	MRT (°C)	Wind Direction
<b>5th of January 2013</b>							
05/01/2013	00:00	0.9	17.6	41.2	16.9	16.6	WSW
05/01/2013	01:00	0.7	16.7	44.0	16.1	15.9	WSW
05/01/2013	02:00	0.2	16.2	47.0	15.8	15.7	WSW
05/01/2013	03:00	0.6	15.7	48.0	14.9	14.7	WSW
05/01/2013	04:00	0.7	15.0	50.7	14.1	13.8	SW
05/01/2013	05:00	0.0	14.5	55.1	13.8	13.8	SW
05/01/2013	06:00	0.3	15.4	62.5	15.6	15.6	ENE
05/01/2013	07:00	1.0	14.9	63.9	14.5	14.3	N
05/01/2013	08:00	1.3	15.8	64.8	20.3	22.3	SW
05/01/2013	09:00	0.8	19.8	61.8	30.7	33.8	NNW
05/01/2013	10:00	0.9	22.4	51.1	36.2	40.4	SW
05/01/2013	11:00	1.1	22.7	42.3	31.4	34.5	SSW
05/01/2013	12:00	1.8	25.0	27.3	36.3	41.8	NNW
05/01/2013	13:00	1.9	25.8	20.7	38.8	45.1	SE
05/01/2013	14:00	1.1	24.8	23.0	27.7	28.7	WSW
05/01/2013	15:00	0.9	25.4	19.5	26.7	27.1	SSW
05/01/2013	16:00	2.8	24.8	18.7	25.6	26.2	E
05/01/2013	17:00	3.4	24.1	15.9	24.0	23.9	NNE
05/01/2013	18:00	1.6	22.9	21.3	22.1	21.6	WSW
05/01/2013	19:00	1.5	22.1	27.2	21.1	20.6	WSW
05/01/2013	20:00	1.8	21.1	31.5	20.5	20.1	N
05/01/2013	21:00	0.2	20.5	34.1	19.9	19.8	NNE
05/01/2013	22:00	0.7	19.9	35.5	19.2	19.0	NNW
05/01/2013	23:00	0.9	19.6	35.8	18.7	18.3	NNE
<b>6th of January 2013</b>							
06/01/2013	00:00	0.8	18.6	37.6	18.1	18.0	NNW
06/01/2013	01:00	0.4	17.3	43.1	16.5	16.3	W
06/01/2013	02:00	1.0	16.4	48.3	15.7	15.4	W
06/01/2013	03:00	1.0	15.5	55.2	14.9	14.6	NNW
06/01/2013	04:00	0.0	15.0	55.9	14.5	14.5	WNW
06/01/2013	05:00	0.8	14.5	59.0	13.8	13.5	W
06/01/2013	06:00	0.7	14.4	60.3	13.3	12.9	NNW
06/01/2013	07:00	0.8	15.7	50.3	14.9	14.6	NNW
06/01/2013	08:00	1.9	16.5	43.2	21.5	24.5	SSW
06/01/2013	09:00	1.0	18.4	41.0	30.2	34.2	ENE
06/01/2013	10:00	2.4	19.2	39.5	30.1	37.0	NE
06/01/2013	11:00	2.8	18.8	36.5	26.0	31.2	NNE
06/01/2013	12:00	2.7	20.7	33.1	34.5	43.3	E
06/01/2013	13:00	2.3	21.3	39.2	33.0	39.9	NW
06/01/2013	14:00	4.7	21.2	41.0	23.6	26.3	WSW
06/01/2013	15:00	2.0	21.7	40.7	23.1	23.9	SW
06/01/2013	16:00	2.6	21.1	41.3	21.8	22.3	WSW
06/01/2013	17:00	2.9	20.5	41.1	20.6	20.6	W
06/01/2013	18:00	2.1	19.8	42.3	19.4	19.2	WSW
06/01/2013	19:00	1.9	19.4	44.7	18.9	18.6	W
06/01/2013	20:00	2.0	19.2	46.3	18.6	18.2	WNW
06/01/2013	21:00	1.8	18.6	48.7	18.2	17.9	WNW
06/01/2013	22:00	2.1	18.5	48.1	17.7	17.2	WNW
06/01/2013	23:00	1.0	17.9	50.1	17.4	17.2	N

Date	Time	Winds. (m/s)	Ta (°C)	RH (%)	Tg (°C)	MRT (°C)	Wind Direction
<b>7th of January 2013</b>							
07/01/2013	00:00	1.8	17.4	52.3	16.8	16.4	N
07/01/2013	01:00	2.1	16.8	48.7	16.3	15.9	WSW
07/01/2013	02:00	1.2	16.2	46.5	15.5	15.2	N
07/01/2013	03:00	0.9	15.9	46.0	14.9	14.5	N
07/01/2013	04:00	1.1	15.5	44.5	14.3	13.8	NE
07/01/2013	05:00	1.5	15.3	42.0	14.3	13.8	NNE
07/01/2013	06:00	2.3	14.9	34.1	14.2	13.6	NE
07/01/2013	07:00	2.7	14.2	40.2	13.7	13.3	ENE
07/01/2013	08:00	2.9	14.7	42.3	19.5	23.3	E
07/01/2013	09:00	1.7	15.8	36.6	30.5	37.8	SW
07/01/2013	10:00	1.9	16.8	33.5	32.4	40.5	NE
07/01/2013	11:00	1.3	18.3	31.5	28.8	33.3	NNE
07/01/2013	12:00	1.5	20.3	29.7	33.9	39.8	ENE
07/01/2013	13:00	4.2	21.5	26.8	35.1	46.9	WNW
07/01/2013	14:00	2.7	21.4	26.1	23.7	25.4	SW
07/01/2013	15:00	1.6	21.0	27.5	21.8	22.2	NNW
07/01/2013	16:00	2.6	20.8	27.1	21.1	21.3	SSW
07/01/2013	17:00	2.0	19.9	27.1	19.8	19.7	SW
07/01/2013	18:00	1.6	19.0	29.2	18.4	18.0	N
07/01/2013	19:00	2.4	18.2	32.1	17.6	17.1	WSW
07/01/2013	20:00	2.0	17.5	34.9	16.8	16.3	NNE
07/01/2013	21:00	1.2	16.8	37.4	16.1	15.8	N
07/01/2013	22:00	0.6	16.1	36.7	15.3	15.1	N
07/01/2013	23:00	0.4	15.6	36.7	14.7	14.5	NE

A6. 4: Detailed hourly microclimatic data in the high urban density area (spring)

Field measurements for Spring (1st to 12th of April 2013) in the High Urban Density Area (Case 1)							
Date	Time	Winds. (m/s)	Ta (°C)	RH (%)	Tg (°C)	MRT (°C)	Wind Direction
1st of April 2013							
01/04/2013	00:00	0.7	27.7	7.0	27.2	27.1	N
01/04/2013	01:00	0.6	26.1	12.4	26.1	26.0	E
01/04/2013	02:00	1.1	25.3	14.9	25.0	24.9	NE
01/04/2013	03:00	1.1	24.4	15.4	24.2	24.1	ENE
01/04/2013	04:00	0.9	23.6	16.4	23.5	23.4	SW
01/04/2013	05:00	1.2	23.0	17.7	22.8	22.7	NE
01/04/2013	06:00	1.7	22.3	18.9	22.5	22.5	SSE
01/04/2013	07:00	0.9	22.4	19.5	22.6	22.7	S
01/04/2013	08:00	1.1	22.4	19.4	23.5	23.9	SSE
01/04/2013	09:00	1.9	22.9	18.7	25.1	26.3	SW
01/04/2013	10:00	1.3	24.2	17.6	27.9	29.4	S
01/04/2013	11:00	2.2	25.7	16.9	30.2	32.8	ENE
01/04/2013	12:00	0.6	27.0	16.5	33.9	35.4	SW
01/04/2013	13:00	1.4	28.7	16.2	34.1	36.2	SSE
01/04/2013	14:00	1.0	29.5	16.6	33.2	34.4	WSW
01/04/2013	15:00	1.1	29.7	16.6	32.8	33.9	SW
01/04/2013	16:00	1.0	30.1	15.4	31.8	32.3	S
01/04/2013	17:00	0.8	31.2	13.4	31.7	31.8	NE
01/04/2013	18:00	0.9	30.4	14.1	30.3	30.3	S
01/04/2013	19:00	0.5	30.6	13.5	29.8	29.6	SW
01/04/2013	20:00	0.9	30.3	14.0	29.6	29.3	SW
01/04/2013	21:00	1.3	29.5	15.8	29.9	30.0	S
01/04/2013	22:00	1.4	29.1	17.7	28.8	28.7	SW
01/04/2013	23:00	1.1	27.9	18.7	27.8	27.8	SW
2nd of April 2013							
02/04/2013	00:00	1.5	26.4	20.6	26.8	26.9	N
02/04/2013	01:00	1.4	24.7	21.0	24.9	25.0	E
02/04/2013	02:00	1.5	24.0	19.6	23.9	23.9	SSW
02/04/2013	03:00	1.1	23.5	19.7	23.4	23.4	SSW
02/04/2013	04:00	0.6	23.1	21.2	22.9	22.8	SE
02/04/2013	05:00	1.3	22.5	21.8	22.5	22.4	SSW
02/04/2013	06:00	0.7	22.3	22.0	22.2	22.2	NNE
02/04/2013	07:00	0.7	22.2	23.7	23.0	23.2	SW
02/04/2013	08:00	1.0	23.2	23.2	24.8	25.4	SW
02/04/2013	09:00	1.0	24.4	24.6	27.6	28.6	SW
02/04/2013	10:00	1.1	25.9	26.3	29.3	30.5	SW
02/04/2013	11:00	1.1	28.0	26.3	32.6	34.2	SSW
02/04/2013	12:00	0.8	29.9	26.1	46.4	50.5	SSW
02/04/2013	13:00	0.9	31.4	23.4	43.3	46.5	S
02/04/2013	14:00	0.3	31.9	21.4	35.4	35.8	NNW
02/04/2013	15:00	1.3	32.8	10.8	35.3	36.2	SW
02/04/2013	16:00	0.7	32.8	13.0	34.0	34.3	SSW
02/04/2013	17:00	0.8	31.5	15.2	32.4	32.7	NNW
02/04/2013	18:00	0.7	30.9	16.2	31.0	31.0	NNW
02/04/2013	19:00	0.8	31.0	15.4	31.1	31.1	NE
02/04/2013	20:00	0.5	30.7	23.9	30.5	30.4	WSW
02/04/2013	21:00	0.5	29.7	25.9	29.8	29.8	N
02/04/2013	22:00	0.4	29.6	25.8	29.6	29.5	NNE
02/04/2013	23:00	0.7	29.0	27.9	29.0	29.0	NNW

Date	Time	Winds. (m/s)	Ta (°C)	RH (%)	Tg (°C)	MRT (°C)	Wind Direction
<b>3rd of April 2013</b>							
03/04/2013	00:00	0.5	28.8	31.5	28.5	28.4	NE
03/04/2013	01:00	0.7	28.1	33.9	27.9	27.8	SSW
03/04/2013	02:00	0.7	27.7	37.7	27.4	27.3	SSW
03/04/2013	03:00	0.4	26.4	34.8	26.4	26.3	SW
03/04/2013	04:00	0.0	26.0	38.6	25.8	25.8	WSW
03/04/2013	05:00	0.6	24.9	42.3	25.3	25.4	SW
03/04/2013	06:00	0.4	24.7	45.6	24.5	24.4	SW
03/04/2013	07:00	0.4	25.1	49.7	25.9	26.0	SSW
03/04/2013	08:00	0.2	26.2	48.2	28.9	29.1	SSW
03/04/2013	09:00	0.3	28.3	44.3	31.3	31.7	SSW
03/04/2013	10:00	0.6	29.8	35.8	32.4	32.9	SSW
03/04/2013	11:00	0.4	32.1	31.1	36.5	37.2	NNW
03/04/2013	12:00	0.0	34.2	22.4	54.6	54.6	WNW
03/04/2013	13:00	1.2	34.2	17.4	49.3	54.0	WSW
03/04/2013	14:00	0.2	34.3	16.8	35.7	35.8	SW
03/04/2013	15:00	0.8	34.0	16.4	35.3	35.6	WSW
03/04/2013	16:00	0.5	33.8	15.1	34.4	34.5	WNW
03/04/2013	17:00	0.3	33.2	16.4	33.9	34.0	WNW
03/04/2013	18:00	1.0	32.5	20.9	32.6	32.7	NNW
03/04/2013	19:00	1.4	31.7	23.7	31.9	31.9	WNW
03/04/2013	20:00	0.5	31.6	25.8	31.1	31.0	SW
03/04/2013	21:00	0.6	30.6	27.8	30.5	30.4	NNW
03/04/2013	22:00	0.4	29.8	26.4	29.9	29.9	WSW
03/04/2013	23:00	0.3	29.4	27.5	29.5	29.5	NNW
<b>4th of April 2013</b>							
04/04/2013	00:00	0.8	28.8	29.1	28.8	28.8	N
04/04/2013	01:00	0.4	28.0	29.1	27.7	27.7	NNW
04/04/2013	02:00	0.0	28.1	27.3	27.6	27.6	S
04/04/2013	03:00	0.5	27.6	24.6	27.4	27.4	S
04/04/2013	04:00	0.0	26.3	33.6	25.9	25.9	SW
04/04/2013	05:00	0.0	25.1	45.1	24.7	24.7	S
04/04/2013	06:00	0.0	25.3	48.5	24.9	24.9	SSW
04/04/2013	07:00	0.0	25.4	48.5	25.9	25.9	SW
04/04/2013	08:00	0.7	25.8	43.4	28.9	29.6	SSW
04/04/2013	09:00	0.0	28.7	32.7	31.2	31.2	SW
04/04/2013	10:00	0.2	30.1	21.5	33.5	33.9	NW
04/04/2013	11:00	0.7	32.1	16.1	37.5	38.8	WNW
04/04/2013	12:00	0.4	33.2	13.3	47.8	50.0	NNE
04/04/2013	13:00	0.3	35.4	9.5	47.6	49.1	S
04/04/2013	14:00	0.8	34.1	8.4	36.4	37.0	NNW
04/04/2013	15:00	0.7	34.2	8.6	35.6	36.0	SW
04/04/2013	16:00	0.0	34.1	9.2	34.7	34.7	WNW
04/04/2013	17:00	0.7	34.1	7.8	34.1	34.0	SSW
04/04/2013	18:00	0.5	33.5	8.1	33.3	33.2	NW
04/04/2013	19:00	0.0	32.6	19.1	32.4	32.4	NW
04/04/2013	20:00	0.4	31.9	22.4	31.6	31.5	NW
04/04/2013	21:00	0.6	31.3	21.2	31.1	31.1	W
04/04/2013	22:00	1.1	30.7	20.9	30.5	30.4	WSW
04/04/2013	23:00	0.7	30.1	21.5	29.8	29.7	WSW



5th of April 2013							
05/04/2013	00:00	0.0	30.7	35.4	30.7	30.7	NNW
05/04/2013	01:00	0.0	34.8	31.2	34.3	34.3	WSW
05/04/2013	02:00	0.0	32.2	22.9	31.7	31.7	N
05/04/2013	03:00	0.3	28.3	16.7	27.9	27.8	NE
05/04/2013	04:00	0.5	27.5	17.4	27.3	27.3	NNE
05/04/2013	05:00	0.8	27.0	18.3	26.9	26.8	S
05/04/2013	06:00	0.2	25.7	25.0	25.2	25.1	WNW
05/04/2013	07:00	0.0	25.5	25.2	26.2	26.1	WSW
05/04/2013	08:00	1.0	26.5	23.0	29.6	30.7	SSW
05/04/2013	09:00	0.0	29.5	17.2	31.9	31.9	SSW
05/04/2013	10:00	0.3	30.7	12.0	34.1	34.5	SSW
05/04/2013	11:00	0.6	31.8	9.9	36.3	37.3	WSW
05/04/2013	12:00	0.3	34.8	5.7	47.4	48.9	SSW
05/04/2013	13:00	0.7	34.5	6.6	48.4	51.4	NNW
05/04/2013	14:00	0.7	34.2	7.2	36.8	37.4	SW
05/04/2013	15:00	0.2	34.6	7.8	35.8	35.9	NNW
05/04/2013	16:00	1.6	33.8	8.6	34.7	35.0	NW
05/04/2013	17:00	0.0	33.3	10.7	33.5	33.5	WNW
05/04/2013	18:00	0.5	32.7	13.0	32.4	32.3	NNW
05/04/2013	19:00	0.7	32.3	15.6	31.8	31.7	NW
05/04/2013	20:00	0.6	31.6	19.7	31.3	31.2	NW
05/04/2013	21:00	1.0	30.1	23.2	30.5	30.6	N
05/04/2013	22:00	0.4	29.7	26.6	29.6	29.6	NNW
05/04/2013	23:00	0.9	29.2	27.9	29.4	29.5	NW
6th of April 2013							
06/04/2013	00:00	1.1	28.9	29.9	28.6	28.5	NNW
06/04/2013	01:00	0.4	28.2	29.5	27.8	27.7	NNE
06/04/2013	02:00	0.0	27.6	30.6	27.2	27.2	NNW
06/04/2013	03:00	0.0	27.0	30.4	26.9	26.9	NNE
06/04/2013	04:00	0.8	26.1	32.4	25.8	25.6	SSW
06/04/2013	05:00	0.9	24.8	35.4	24.8	24.7	SSW
06/04/2013	06:00	0.5	24.2	39.4	24.4	24.4	SSW
06/04/2013	07:00	0.6	24.5	40.0	25.8	26.1	SSW
06/04/2013	08:00	0.8	26.3	37.4	29.5	30.5	WSW
06/04/2013	09:00	0.4	28.2	28.5	32.1	32.7	ENE
06/04/2013	10:00	0.3	30.7	16.5	33.7	34.0	S
06/04/2013	11:00	0.7	32.3	14.8	39.5	41.3	WSW
06/04/2013	12:00	0.7	33.5	9.5	43.3	45.4	WNW
06/04/2013	13:00	0.8	34.9	5.3	48.4	51.6	WNW
06/04/2013	14:00	0.8	34.5	7.8	36.2	36.7	S
06/04/2013	15:00	1.2	34.3	8.4	35.4	35.8	SSW
06/04/2013	16:00	1.3	34.0	9.3	34.9	35.3	NW
06/04/2013	17:00	0.2	34.0	10.3	34.5	34.6	SSW
06/04/2013	18:00	0.6	32.9	12.0	32.8	32.8	WNW
06/04/2013	19:00	0.7	32.3	15.6	31.8	31.7	WNW
06/04/2013	20:00	0.6	31.6	19.7	31.3	31.2	SW
06/04/2013	21:00	1.0	30.1	23.2	30.5	30.6	NNW
06/04/2013	22:00	0.4	29.7	26.6	29.6	29.6	WSW
06/04/2013	23:00	0.9	29.2	27.9	29.4	29.5	NNW



7th of April 2013							
07/04/2013	00:00	0.0	32.0	11.8	31.4	31.4	N
07/04/2013	01:00	0.5	30.8	12.6	30.1	30.0	***
07/04/2013	02:00	0.9	30.2	13.2	29.3	29.0	***
07/04/2013	03:00	0.6	29.5	13.9	29.0	28.9	***
07/04/2013	04:00	0.9	28.6	13.0	28.4	28.3	***
07/04/2013	05:00	0.0	28.0	15.8	27.5	27.5	***
07/04/2013	06:00	0.0	27.5	17.7	26.5	26.5	***
07/04/2013	07:00	0.0	28.5	14.0	28.4	28.4	***
07/04/2013	08:00	0.0	30.0	11.3	31.2	31.2	***
07/04/2013	09:00	0.0	30.9	10.9	33.0	33.0	***
07/04/2013	10:00	0.5	31.4	22.3	33.4	33.8	***
07/04/2013	11:00	1.3	33.3	14.5	36.1	37.2	***
07/04/2013	12:00	0.0	34.8	4.8	41.4	41.4	***
07/04/2013	13:00	1.6	34.8	10.1	43.9	47.7	***
07/04/2013	14:00	1.2	34.6	8.0	38.3	39.6	***
07/04/2013	15:00	0.0	35.8	4.3	36.5	36.5	***
07/04/2013	16:00	0.6	34.5	6.7	37.2	37.8	***
07/04/2013	17:00	0.6	34.4	5.7	34.7	34.8	***
07/04/2013	18:00	0.8	33.3	8.8	35.1	35.6	***
07/04/2013	19:00	0.7	33.4	10.1	34.6	34.9	***
07/04/2013	20:00	0.6	32.4	12.3	34.6	35.1	***
07/04/2013	21:00	0.8	31.3	12.3	31.3	31.3	***
07/04/2013	22:00	0.0	31.1	14.5	32.0	32.0	***
07/04/2013	23:00	0.0	30.3	15.2	31.5	31.5	***
8th of April 2013							
08/04/2013	00:00	0.7	29.7	15.6	29.7	29.7	***
***	01:00	***	***	***	***		***
***	02:00	***	***	***	***		***
***	03:00	***	***	***	***		***
***	04:00	***	***	***	***		***
***	05:00	***	***	***	***		***
***	06:00	***	***	***	***		***
***	07:00	***	***	***	***		***
***	08:00	***	***	***	***		***
08/04/2013	09:00	0.7	27.3	28.9	28.1	28.3	***
08/04/2013	10:00	0.5	31.4	22.3	33.4	33.8	***
08/04/2013	11:00	1.3	33.3	14.5	36.1	37.2	***
08/04/2013	12:00	0.4	34.0	9.4	39.3	40.2	***
08/04/2013	13:00	1.6	34.8	10.1	43.9	47.7	***
08/04/2013	14:00	1.2	34.6	8.0	38.3	39.6	***
08/04/2013	15:00	0.4	35.4	6.1	36.0	36.1	***
08/04/2013	16:00	1.0	35.1	6.6	35.6	35.8	***
08/04/2013	17:00	1.8	35.5	7.3	34.7	34.3	***
08/04/2013	18:00	1.5	34.5	13.5	34.7	34.8	***
08/04/2013	19:00	0.0	32.5	13.2	34.3	34.3	***
08/04/2013	20:00	0.0	32.2	11.3	32.8	32.8	***
08/04/2013	21:00	0.8	31.0	16.8	31.5	31.6	***
08/04/2013	22:00	0.4	30.2	17.2	31.9	32.2	***
08/04/2013	23:00	0.4	29.9	14.8	31.6	31.9	***

Date	Time	Winds. (m/s)	Ta (°C)	RH (%)	Tg (°C)	MRT (°C)	Wind Direction
<b>9th of April 2013</b>							
09/04/2013	00:00	0.4	29.8	13.8	31.6	31.9	***
***	01:00	***	***	***	***		***
***	02:00	***	***	***	***		***
***	03:00	***	***	***	***		***
***	04:00	***	***	***	***		***
***	05:00	***	***	***	***		***
***	06:00	***	***	***	***		***
***	07:00	***	***	***	***		***
***	08:00	***	***	***	***		***
09/04/2013	09:00	0.5	28.5	15.8	30.5	30.9	***
09/04/2013	10:00	0.5	29.4	13.5	32.6	33.3	***
09/04/2013	11:00	0.6	31.6	11.4	34.9	35.7	***
09/04/2013	12:00	1.6	31.9	7.9	36.1	38.0	***
09/04/2013	13:00	0.0	33.6	3.8	36.3	36.3	***
09/04/2013	14:00	1.7	33.0	6.7	35.5	36.7	***
09/04/2013	15:00	1.1	33.5	4.9	35.1	35.7	***
09/04/2013	16:00	2.4	32.7	4.6	35.2	36.7	***
09/04/2013	17:00	2.1	32.8	9.7	33.0	33.1	***
09/04/2013	18:00	0.4	30.8	7.9	32.8	33.2	***
09/04/2013	19:00	0.0	29.5	12.1	32.1	32.1	***
09/04/2013	20:00	0.4	28.8	13.0	30.6	30.9	***
09/04/2013	21:00	0.7	27.3	15.5	31.0	32.0	***
09/04/2013	22:00	1.1	27.2	16.5	29.9	30.9	***
09/04/2013	23:00	0.6	27.6	17.6	29.3	29.7	***
<b>10th of April 2013</b>							
10/04/2013	00:00	0.5	27.1	12.9	31.2	32.1	***
***	01:00	***	***	***	***		***
***	02:00	***	***	***	***		***
***	03:00	***	***	***	***		***
***	04:00	***	***	***	***		***
***	05:00	***	***	***	***		***
***	06:00	***	***	***	***		***
***	07:00	***	***	***	***		***
***	08:00	***	***	***	***		***
10/04/2013	09:00	0.0	23.2	18.1	26.7	26.7	***
10/04/2013	10:00	1.1	24.9	14.9	28.2	29.4	***
10/04/2013	11:00	1.3	25.7	13.7	33.0	35.9	***
10/04/2013	12:00	0.7	26.0	13.8	32.9	34.7	***
10/04/2013	13:00	1.7	29.3	10.2	38.9	43.3	***
10/04/2013	14:00	0.5	32.1	5.3	42.3	44.2	***
10/04/2013	15:00	0.5	32.1	5.3	42.3	44.2	***
10/04/2013	16:00	0.6	31.2	6.1	35.6	36.6	***
10/04/2013	17:00	1.3	30.0	5.8	33.9	35.5	***
10/04/2013	18:00	0.0	30.7	5.1	30.1	30.1	***
10/04/2013	19:00	0.9	30.3	4.9	31.0	31.2	***
10/04/2013	20:00	1.3	29.4	5.0	29.7	29.8	***
10/04/2013	21:00	0.7	28.9	6.7	29.5	29.7	***
10/04/2013	22:00	1.1	27.6	6.9	30.9	32.1	***
10/04/2013	23:00	0.0	28.4	7.4	30.1	30.1	***

Date	Time	Winds. (m/s)	Ta (°C)	RH (%)	Tg (°C)	MRT (°C)	Wind Direction
<b>11th of April 2013</b>							
11/04/2013	00:00	1.5	26.8	8.2	29.5	30.8	***
***	01:00	***	***	***	***		***
***	02:00	***	***	***	***		***
***	03:00	***	***	***	***		***
***	04:00	***	***	***	***		***
***	05:00	***	***	***	***		***
***	06:00	***	***	***	***		***
***	07:00	***	***	***	***		***
***	08:00	***	***	***	***		***
11/04/2013	09:00	0.0	25.1	11.6	27.3	27.3	***
11/04/2013	10:00	0.0	26.8	12.2	29.0	29.0	***
11/04/2013	11:00	2.3	27.4	9.5	31.9	34.6	***
11/04/2013	12:00	1.3	29.5	9.1	32.9	34.3	***
11/04/2013	13:00	0.0	32.4	9.3	32.6	32.6	***
11/04/2013	14:00	1.0	30.6	7.5	36.1	37.9	***
11/04/2013	15:00	0.6	32.5	6.9	34.2	34.6	***
11/04/2013	16:00	1.6	32.5	6.6	33.3	33.7	***
11/04/2013	17:00	1.6	32.5	6.6	33.3	33.7	***
11/04/2013	18:00	0.9	31.4	6.9	31.9	32.1	***
11/04/2013	19:00	0.9	31.4	6.9	31.9	32.1	***
11/04/2013	20:00	0.8	31.3	6.6	31.6	31.7	***
11/04/2013	21:00	0.0	31.0	7.5	30.2	30.2	***
11/04/2013	22:00	0.5	31.2	7.1	31.0	31.0	***
11/04/2013	23:00	0.0	29.8	7.4	29.4	29.4	***
<b>12th of April 2013</b>							
12/04/2013	00:00	0.0	29.0	7.9	28.7	28.7	***
***	01:00	***	***	***	***		***
***	02:00	***	***	***	***		***
***	03:00	***	***	***	***		***
***	04:00	***	***	***	***		***
***	05:00	***	***	***	***		***
***	06:00	***	***	***	***		***
***	07:00	***	***	***	***		***
***	08:00	***	***	***	***		***
12/04/2013	09:00	0.0	26.9	10.4	27.7	27.7	***
12/04/2013	10:00	0.8	30.4	6.4	33.6	34.5	***
12/04/2013	11:00	0.5	31.2	5.4	34.8	35.5	***
12/04/2013	12:00	0.0	33.3	4.8	36.0	36.0	***
12/04/2013	13:00	0.9	35.6	5.3	33.6	33.0	***
12/04/2013	14:00	0.9	34.7	3.2	34.9	35.0	***
12/04/2013	15:00	0.0	35.7	2.5	34.9	34.9	***
12/04/2013	16:00	0.7	34.6	2.6	35.8	36.1	***
12/04/2013	17:00	0.0	34.1	3.0	34.1	34.1	***
12/04/2013	18:00	0.0	34.5	2.8	34.1	34.1	***
12/04/2013	19:00	0.0	34.0	5.5	33.9	33.9	***
12/04/2013	20:00	0.7	33.1	6.6	33.8	34.0	***
12/04/2013	21:00	0.5	32.5	8.7	33.2	33.3	***
12/04/2013	22:00	0.8	31.0	6.9	32.0	32.3	***
12/04/2013	23:00	0.8	31.0	6.9	32.0	32.3	***

A6. 5: Detailed hourly microclimatic data in the high urban density area (summer)

Field measurements for Summer (17th to 20th and 23rd to 29th of June 2013) in the High Urban Density Area (Case 1)							
Date	Time	Winds. (m/s)	Ta (°C)	RH (%)	Tg (°C)	MRT (°C)	Wind Direction
17th and 23rd of June 2013							
17/06/2013	00:00	0.5	33.3	14.4	32.8	32.7	***
17/06/2013	01:00	0.0	32.6	14.9	32.1	32.1	***
17/06/2013	02:00	0.0	31.3	17.1	31.2	31.2	***
17/06/2013	03:00	0.7	31.1	16.6	31.1	31.1	***
17/06/2013	04:00	0.7	31.1	16.6	31.1	31.1	***
17/06/2013	05:00	0.0	31.3	19.8	31.4	31.4	***
17/06/2013	06:00	0.0	31.3	19.8	31.4	31.4	***
17/06/2013	07:00	1.3	31.1	17.4	33.3	34.2	***
17/06/2013	08:00	0.9	32.6	17.2	36.1	37.2	***
17/06/2013	09:00	1.2	33.4	15.8	37.4	38.9	NW
23/06/2013	10:00	1.0	37.3	8.0	35.6	35.0	NW
23/06/2013	11:00	1.7	38.6	6.8	37.3	36.7	NNW
23/06/2013	12:00	1.4	40.0	5.3	50.8	54.6	N
23/06/2013	13:00	2.0	39.5	5.2	42.8	44.4	NW
23/06/2013	14:00	1.5	40.3	3.4	45.7	47.8	S
23/06/2013	15:00	0.7	40.5	3.8	43.6	44.3	NNE
23/06/2013	16:00	0.0	38.0	7.1	39.3	39.3	SW
23/06/2013	17:00	1.4	39.1	6.8	37.9	37.4	NNW
23/06/2013	18:00	1.2	39.3	7.2	38.1	37.7	WSW
23/06/2013	19:00	1.0	37.8	8.0	38.4	38.6	SW
23/06/2013	20:00	1.1	34.9	9.5	36.7	37.3	NW
23/06/2013	21:00	0.0	33.5	13.5	32.6	32.6	WSW
23/06/2013	22:00	1.1	36.4	9.7	34.8	34.2	WSW
23/06/2013	23:00	0.3	35.4	7.8	34.2	34.0	NW
18th and 24th of June 2013							
18/06/2013	00:00	1.1	33.6	12.8	33.4	33.3	***
18/06/2013	01:00	0.6	32.8	16.2	32.7	32.7	***
18/06/2013	02:00	0.5	32.1	16.7	31.8	31.7	***
18/06/2013	03:00	0.5	30.8	17.7	30.9	30.9	***
18/06/2013	04:00	1.1	30.6	16.9	30.7	30.7	***
18/06/2013	05:00	0.9	30.5	16.7	30.6	30.6	***
18/06/2013	06:00	0.0	30.7	16.5	31.1	31.1	***
18/06/2013	07:00	0.4	31.7	14.9	34.0	34.4	***
18/06/2013	08:00	1.9	31.5	15.4	37.3	40.2	***
24/06/2013	09:00	1.7	34.7	7.6	33.3	32.6	N
24/06/2013	10:00	0.0	37.1	6.7	36.6	36.6	NNW
24/06/2013	11:00	2.8	37.8	5.7	37.8	37.8	N
24/06/2013	12:00	2.1	38.8	5.5	38.2	37.9	NNW
24/06/2013	13:00	1.0	38.6	7.7	37.6	37.3	NNW
24/06/2013	14:00	1.3	40.4	4.5	38.6	37.9	SW
24/06/2013	15:00	1.0	39.6	4.5	38.7	38.4	N
24/06/2013	16:00	0.6	38.4	6.6	36.9	36.6	N
24/06/2013	17:00	0.5	38.3	5.8	37.4	37.2	NNW
24/06/2013	18:00	0.0	38.3	6.4	37.4	37.4	W
24/06/2013	19:00	0.0	37.4	9.1	37.5	37.5	NNE
24/06/2013	20:00	0.0	35.5	10.8	36.4	36.4	N
24/06/2013	21:00	0.0	34.4	11.4	32.5	32.5	WSW
24/06/2013	22:00	0.5	35.4	10.2	34.2	34.0	S
24/06/2013	23:00	1.6	34.4	9.3	34.1	34.0	N

Date	Time	Winds. (m/s)	Ta (°C)	RH (%)	Tg (°C)	MRT (°C)	Wind Direction
<b>19th and 25th of June 2013</b>							
19/06/2013	00:00	0.4	33.0	13.0	33.2	33.3	***
19/06/2013	01:00	0.0	31.9	15.3	32.0	32.0	***
19/06/2013	02:00	0.6	31.7	14.6	31.7	31.7	***
19/06/2013	03:00	0.0	31.8	13.9	31.5	31.5	***
19/06/2013	04:00	0.8	31.1	14.8	31.0	31.0	***
19/06/2013	05:00	1.6	30.4	16.0	31.5	32.0	***
19/06/2013	06:00	0.0	30.7	16.4	31.6	31.6	***
19/06/2013	07:00	0.0	31.7	17.0	33.2	33.2	***
19/06/2013	08:00	1.8	33.9	13.4	37.7	39.5	***
25/06/2013	09:00	0.8	34.4	6.4	33.3	33.0	SSW
25/06/2013	10:00	0.8	37.5	5.6	35.9	35.5	NNW
25/06/2013	11:00	1.0	37.7	5.7	38.2	38.4	NW
25/06/2013	12:00	0.9	38.3	6.4	39.1	39.3	N
25/06/2013	13:00	1.1	37.3	5.9	37.6	37.7	NNW
25/06/2013	14:00	0.7	39.4	5.0	38.4	38.2	SW
25/06/2013	15:00	0.5	39.0	7.3	38.8	38.8	NNW
25/06/2013	16:00	0.6	38.1	4.9	35.9	35.4	N
25/06/2013	17:00	1.1	38.8	4.4	37.0	36.4	NNE
25/06/2013	18:00	0.6	38.2	5.5	37.2	36.8	W
25/06/2013	19:00	0.0	37.6	6.6	37.3	37.3	SW
25/06/2013	20:00	1.5	36.3	10.5	37.6	38.2	NW
25/06/2013	21:00	0.0	34.4	13.3	33.6	33.6	W
25/06/2013	22:00	0.0	35.7	13.2	34.8	34.8	SW
25/06/2013	23:00	0.8	34.0	10.7	34.4	34.5	N
<b>20th and 26th of June 2013</b>							
20/06/2013	00:00	0.1	34.0	15.1	33.9	33.9	***
20/06/2013	01:00	0.0	33.2	14.0	33.1	33.1	***
20/06/2013	02:00	0.6	32.6	13.9	32.3	32.2	***
20/06/2013	03:00	1.1	32.0	14.5	32.4	32.5	***
20/06/2013	04:00	1.2	31.9	15.0	32.2	32.3	***
20/06/2013	05:00	0.0	31.6	16.4	31.3	31.3	***
20/06/2013	06:00	0.0	31.4	17.8	32.0	32.0	***
20/06/2013	07:00	1.3	31.2	17.0	33.9	35.0	***
20/06/2013	08:00	0.0	35.0	12.8	37.5	37.5	***
26/06/2013	09:00	1.0	34.3	11.6	33.5	33.2	N
26/06/2013	10:00	0.0	36.9	9.1	38.2	38.2	NW
26/06/2013	11:00	0.0	37.5	8.6	37.8	37.8	WNW
26/06/2013	12:00	1.5	39.3	5.8	39.9	40.2	NNW
26/06/2013	13:00	2.5	39.4	6.1	37.4	36.2	NNW
26/06/2013	14:00	1.3	39.4	6.3	38.5	37.8	SW
26/06/2013	15:00	0.6	39.4	6.4	39.0	38.7	N
26/06/2013	16:00	0.0	39.4	6.5	39.5	39.5	NW
26/06/2013	17:00	0.0	41.5	3.2	41.5	41.5	WNW
26/06/2013	18:00	0.4	40.6	5.6	41.7	41.9	WSW
26/06/2013	19:00	0.0	39.0	7.2	42.1	42.1	WNW
26/06/2013	20:00	0.4	37.4	17.0	39.7	40.1	W
26/06/2013	21:00	0.4	36.3	20.2	35.3	35.1	WSW
26/06/2013	22:00	0.0	36.8	19.3	36.2	36.2	WNW
26/06/2013	23:00	0.2	34.9	16.2	34.7	34.7	NNW



Date	Time	Winds. (m/s)	Ta (°C)	RH (%)	Tg (°C)	MRT (°C)	Wind Direction
<b>27th of June 2013</b>							
27/06/2013	00:00	0.5	33.3	14.4	32.8	32.7	***
27/06/2013	01:00	***	***	***	***	***	***
27/06/2013	02:00	***	***	***	***	***	***
27/06/2013	03:00	***	***	***	***	***	***
27/06/2013	04:00	***	***	***	***	***	***
27/06/2013	05:00	***	***	***	***	***	***
27/06/2013	06:00	***	***	***	***	***	***
27/06/2013	07:00	***	***	***	***	***	***
27/06/2013	08:00	***	***	***	***	***	***
27/06/2013	09:00	0.0	35.5	15.8	34.1	34.1	NW
27/06/2013	10:00	***	***	***	***	***	WNW
27/06/2013	11:00	0.8	39.4	5.4	41.2	41.7	NNE
27/06/2013	12:00	0.7	42.3	5.1	41.9	41.8	SW
27/06/2013	13:00	0.8	41.8	5.5	39.0	38.2	SW
27/06/2013	14:00	0.0	43.9	3.9	45.2	45.2	N
27/06/2013	15:00	0.0	42.7	4.5	43.6	43.6	SSW
27/06/2013	16:00	0.0	42.1	5.3	39.3	39.3	WSW
27/06/2013	17:00	0.0	40.4	7.2	39.4	39.4	W
27/06/2013	18:00	***	***	***	***	***	NW
27/06/2013	19:00	1.0	39.3	16.1	39.3	39.3	NNW
27/06/2013	20:00	0.0	38.5	18.4	39.1	39.1	SSW
27/06/2013	21:00	0.5	37.2	21.3	35.9	35.6	W
27/06/2013	22:00	***	***	***	***	***	WSW
27/06/2013	23:00	1.4	37.1	15.9	37.8	38.1	WNW
<b>28th of June 2013</b>							
28/06/2013	00:00	1.4	37.1	15.9	37.8	38.1	***
28/06/2013	01:00	***	***	***	***	***	***
28/06/2013	02:00	***	***	***	***	***	***
28/06/2013	03:00	***	***	***	***	***	***
28/06/2013	04:00	***	***	***	***	***	***
28/06/2013	05:00	***	***	***	***	***	***
28/06/2013	06:00	***	***	***	***	***	***
28/06/2013	07:00	***	***	***	***	***	***
28/06/2013	08:00	***	***	***	***	***	***
28/06/2013	09:00	0.6	35.6	15.9	35.2	35.1	SW
28/06/2013	10:00	0.4	38.2	12.2	37.7	37.6	W
28/06/2013	11:00	***	***	***	***	***	SW
28/06/2013	12:00	0.0	41.3	5.4	44.3	44.3	WNW
28/06/2013	13:00	0.0	38.1	6.6	39.4	39.4	W
28/06/2013	14:00	***	***	***	***	***	NNW
28/06/2013	15:00	***	***	***	***	***	WSW
28/06/2013	16:00	0.0	42.2	5.3	40.3	40.3	W
28/06/2013	17:00	1.0	43.0	5.8	41.4	40.9	WSW
28/06/2013	18:00	0.7	41.8	9.5	41.0	40.8	N
28/06/2013	19:00	0.9	39.0	16.3	40.5	40.9	NNW
28/06/2013	20:00	0.6	39.1	18.7	39.4	39.5	WSW
28/06/2013	21:00	1.0	37.6	24.8	35.1	34.3	NNW
28/06/2013	22:00	0.7	37.6	22.4	37.3	37.2	NW
28/06/2013	23:00	1.2	37.8	22.3	37.1	36.8	N



Date	Time	Winds. (m/s)	Ta (°C)	RH (%)	Tg (°C)	MRT (°C)	Wind Direction
<b>29th of June 2013</b>							
29/06/2013	00:00	0.5	33.3	14.4	37.0	37.7	***
29/06/2013	01:00	***	***	***	***	***	***
29/06/2013	02:00	***	***	***	***	***	***
29/06/2013	03:00	***	***	***	***	***	***
29/06/2013	04:00	***	***	***	***	***	***
29/06/2013	05:00	***	***	***	***	***	***
29/06/2013	06:00	***	***	***	***	***	***
29/06/2013	07:00	***	***	***	***	***	***
29/06/2013	08:00	***	***	***	***	***	***
29/06/2013	09:00	1.0	37.8	9.0	36.4	35.9	NNW
29/06/2013	10:00	1.4	39.4	6.7	40.4	40.8	N
29/06/2013	11:00	***	***	***	***	***	W
29/06/2013	12:00	1.2	41.9	6.4	41.0	40.7	NNW
29/06/2013	13:00	0.4	39.8	10.2	39.4	39.3	NW
29/06/2013	14:00	***	***	***	***	***	WNW
29/06/2013	15:00	2.7	43.0	6.7	41.2	40.1	NNW
29/06/2013	16:00	0.0	40.1	6.9	39.7	39.7	SW
29/06/2013	17:00	0.4	42.6	5.0	40.6	40.3	NW
29/06/2013	18:00	1.7	41.9	5.4	40.4	39.7	NNW
29/06/2013	19:00	0.6	41.2	5.6	40.6	40.5	N
29/06/2013	20:00	1.5	39.8	12.6	40.8	41.2	NW
29/06/2013	21:00	0.0	37.9	15.1	38.6	38.6	WNW
29/06/2013	22:00	***	***	***	***	***	W
29/06/2013	23:00	0.8	39.2	9.5	37.5	37.0	NW

**Appendices for Chapter 6 (A6.6 to A6.8) for the hourly and average monitored microclimatic data over a year in the intermediate urban density area (Case 2).**

**A6. 6: Average hourly microclimatic data monitored in the intermediate urban density area (Case2)**

Time HH:MM	October 2012 (Autumn)						January 2013 (Winter)						April 2013 (Spring)						June 2013 (Summer)					
	V m/s	Ta °C	RH %	Tg °C	MRT °C	PET °C	V m/s	Ta °C	RH %	Tg °C	MRT °C	PET °C	V m/s	Ta °C	RH %	Tg °C	MRT °C	PET °C	V m/s	Ta °C	RH %	Tg °C	MRT °C	PET °C
00:00	-	-	-	-	-	-	-	-	-	-	-	-	0.4	27.2	17.4	26.2	26.0	25.2	0.9	32.0	15.3	31.1	30.8	30.3
01:00	-	-	-	-	-	-	-	-	-	-	-	-	0.8	29.0	16.3	27.7	27.3	26.3	0.9	31.2	16.0	30.5	30.2	29.4
02:00	-	-	-	-	-	-	-	-	-	-	-	-	1.2	28.1	18.7	27.4	27.1	25.0	1.1	30.7	16.9	29.9	29.6	28.5
03:00	-	-	-	-	-	-	-	-	-	-	-	-	1.1	26.9	18.5	26.6	26.5	23.7	1.0	30.2	17.3	29.4	29.1	27.9
04:00	-	-	-	-	-	-	-	-	-	-	-	-	0.6	25.8	18.7	24.9	24.7	23.1	0.8	29.7	18.0	29.1	28.9	27.7
05:00	-	-	-	-	-	-	-	-	-	-	-	-	1.2	24.5	19.0	24.6	24.6	20.5	0.6	28.4	19.9	27.5	27.2	26.2
06:00	-	-	-	-	-	-	-	-	-	-	-	-	0.0	25.1	21.0	24.0	24.0	25.3	1.0	27.8	20.6	27.9	27.9	25.4
07:00	-	-	-	-	-	-	-	-	-	-	-	-	1.3	27.3	17.1	26.6	26.3	23.7	1.2	28.7	20.3	30.2	30.8	27.1
08:00	-	-	-	-	-	-	-	-	-	-	-	-	0.5	28.1	16.0	29.8	30.2	27.6	1.2	31.9	16.2	34.7	35.7	32.1
09:00	-	-	-	-	-	-	-	-	-	-	-	-	1.0	27.1	18.8	38.7	42.3	31.2	2.5	33.5	14.3	44.5	50.7	39.1
10:00	-	-	-	-	-	-	-	-	-	-	-	-	1.1	28.8	16.8	41.6	45.9	34.2	3.8	34.7	12.3	50.0	60.8	43.8
11:00	-	-	-	-	-	-	-	-	-	-	-	-	1.9	29.5	13.2	44.2	51.0	35.5	2.0	36.3	10.9	48.7	54.5	44.1
12:00	-	-	-	-	-	-	-	-	-	-	-	-	1.9	31.5	10.8	44.2	50.1	37.2	2.5	36.4	9.6	49.4	56.4	44.8
13:00	-	-	-	-	-	-	-	-	-	-	-	-	2.2	32.4	9.6	48.9	56.8	40.8	2.5	37.9	8.0	50.2	56.8	46.6
14:00	-	-	-	-	-	-	-	-	-	-	-	-	1.9	32.9	9.4	37.8	40.2	34.3	3.0	38.5	8.0	51.0	58.5	47.8
15:00	-	-	-	-	-	-	-	-	-	-	-	-	1.6	32.3	8.2	35.9	37.5	32.7	2.8	38.5	8.2	41.4	43.2	41.6
16:00	-	-	-	-	-	-	-	-	-	-	-	-	1.5	32.8	8.4	34.2	34.8	32.2	3.5	38.2	8.4	41.9	44.7	41.9
17:00	-	-	-	-	-	-	-	-	-	-	-	-	1.3	32.2	9.0	32.1	32.0	30.6	1.5	37.9	8.9	60.0	67.6	52.6
18:00	-	-	-	-	-	-	-	-	-	-	-	-	1.0	31.4	10.7	30.7	30.4	29.4	2.3	37.2	9.6	40.2	41.9	39.6
19:00	-	-	-	-	-	-	-	-	-	-	-	-	0.7	30.7	12.9	29.8	29.5	28.8	2.0	36.1	10.4	35.6	35.3	35.8
20:00	-	-	-	-	-	-	-	-	-	-	-	-	0.7	30.1	13.2	29.4	29.2	28.1	2.2	35.0	12.0	34.5	34.2	34.2
21:00	-	-	-	-	-	-	-	-	-	-	-	-	1.2	28.7	14.8	27.8	27.4	25.6	1.8	34.4	12.7	33.4	32.9	33.1
22:00	-	-	-	-	-	-	-	-	-	-	-	-	0.8	28.0	16.5	26.4	25.9	24.9	0.9	33.9	14.0	33.3	33.1	32.9
23:00	-	-	-	-	-	-	-	-	-	-	-	-	0.6	27.5	16.0	26.1	25.7	24.8	1.1	33.0	16.1	32.5	32.3	31.7
AVERAGE	-	-	-	-	-	-	-	-	-	-	-	-	1.1	29.1	14.6	31.9	33.1	28.8	1.8	33.8	13.5	38.2	40.5	36.0

**A6. 7: Detailed hourly microclimatic data in the intermediate urban density area (spring).**

<b>Field measurements for Spring (1st to 15th of April 2013) in the intermediate Urban Density Area (Case 2)</b>							
Date	Time	Winds. (m/s)	Ta (°C)	RH (%)	Tg (°C)	MRT (°C)	Wind Direction
<b>7th of April 2013</b>							
07/04/2013	00:00	0.7	29.1	16.6	28.6	28.5	***
07/04/2013	01:00	0.8	29.0	16.3	27.7	27.3	***
07/04/2013	02:00	1.2	28.1	18.7	27.4	27.1	***
07/04/2013	03:00	1.1	26.9	18.5	26.6	26.5	***
07/04/2013	04:00	0.6	25.8	18.7	24.9	24.7	***
07/04/2013	05:00	1.2	24.5	19.0	24.6	24.6	***
07/04/2013	06:00	0.0	25.1	21.0	24.0	24.0	***
07/04/2013	07:00	1.3	27.3	17.1	26.6	26.3	***
07/04/2013	08:00	0.5	28.1	16.0	29.8	30.2	***
07/04/2013	09:00	0.8	28.5	12.9	40.1	43.2	***
07/04/2013	10:00	0.8	29.8	10.3	44.0	47.6	***
07/04/2013	11:00	2.2	32.1	7.6	47.3	54.9	***
07/04/2013	12:00	1.9	34.2	5.0	48.9	55.4	***
07/04/2013	13:00	3.3	34.2	5.3	46.6	54.9	***
07/04/2013	14:00	2.7	35.4	5.0	46.4	52.8	***
07/04/2013	15:00	2.3	34.5	5.3	36.5	37.7	***
07/04/2013	16:00	1.5	34.1	8.4	35.4	36.0	***
07/04/2013	17:00	0.6	33.7	8.0	34.0	34.1	***
07/04/2013	18:00	0.9	31.9	11.4	30.7	30.3	***
07/04/2013	19:00	0.0	31.4	13.1	29.9	29.9	***
07/04/2013	20:00	0.8	30.6	14.3	29.7	29.4	***
07/04/2013	21:00	2.0	29.9	15.7	28.8	28.2	***
07/04/2013	22:00	1.6	28.7	16.7	26.9	26.0	***
07/04/2013	23:00	0.9	28.5	17.6	27.4	27.0	***
<b>8th and 7th of April 2013</b>							
08/04/2013	00:00	0.0	28.2	19.1	28.0	28.0	***
07/04/2013	01:00	0.8	29.0	16.3	27.7	27.3	***
07/04/2013	02:00	1.2	28.1	18.7	27.4	27.1	***
07/04/2013	03:00	1.1	26.9	18.5	26.6	26.5	***
07/04/2013	04:00	0.6	25.8	18.7	24.9	24.7	***
07/04/2013	05:00	1.2	24.5	19.0	24.6	24.6	***
07/04/2013	06:00	0.0	25.1	21.0	24.0	24.0	***
07/04/2013	07:00	1.3	27.3	17.1	26.6	26.3	***
07/04/2013	08:00	0.5	28.1	16.0	29.8	30.2	***
08/04/2013	09:00	0.7	28.2	30.2	38.9	41.5	***
08/04/2013	10:00	0.7	30.3	26.5	41.4	44.1	***
08/04/2013	11:00	1.2	31.5	14.1	44.8	49.3	***
08/04/2013	12:00	3.3	32.9	13.2	37.9	41.6	***
08/04/2013	13:00	3.4	34.2	9.7	68.2	86.4	***
08/04/2013	14:00	2.7	34.3	9.0	37.2	39.1	***
08/04/2013	15:00	2.3	34.4	6.9	37.3	39.0	***
08/04/2013	16:00	1.7	34.4	7.8	35.2	35.6	***
08/04/2013	17:00	3.4	33.6	8.4	34.1	34.5	***
08/04/2013	18:00	3.1	32.2	18.1	32.2	32.2	***
08/04/2013	19:00	0.5	31.5	17.7	30.5	30.3	***
08/04/2013	20:00	1.1	30.9	14.1	29.7	29.3	***
08/04/2013	21:00	1.0	29.6	20.7	28.8	28.5	***
08/04/2013	22:00	0.8	28.5	21.6	28.5	28.5	***
08/04/2013	23:00	0.3	28.1	19.2	27.2	27.1	***

Date	Time	Winds. (m/s)	Ta (°C)	RH (%)	Tg (°C)	MRT (°C)	Wind Direction
<b>9th and 7th of April 2013</b>							
09/04/2013	00:00	0.3	28.1	19.2	27.2	27.1	***
07/04/2013	01:00	0.8	29.0	16.3	27.7	27.3	***
07/04/2013	02:00	1.2	28.1	18.7	27.4	27.1	***
07/04/2013	03:00	1.1	26.9	18.5	26.6	26.5	***
07/04/2013	04:00	0.6	25.8	18.7	24.9	24.7	***
07/04/2013	05:00	1.2	24.5	19.0	24.6	24.6	***
07/04/2013	06:00	0.0	25.1	21.0	24.0	24.0	***
07/04/2013	07:00	1.3	27.3	17.1	26.6	26.3	***
07/04/2013	08:00	0.5	28.1	16.0	29.8	30.2	***
09/04/2013	09:00	1.1	27.7	21.8	38.7	42.4	***
09/04/2013	10:00	2.1	27.9	20.7	41.0	47.7	***
09/04/2013	11:00	2.8	28.0	17.9	43.7	53.2	***
09/04/2013	12:00	0.5	33.7	12.5	43.8	45.7	***
09/04/2013	13:00	0.5	33.7	12.5	43.8	45.7	***
09/04/2013	14:00	3.9	32.4	11.9	36.2	39.4	***
09/04/2013	15:00	3.2	31.6	7.7	34.9	37.4	***
09/04/2013	16:00	2.2	31.1	9.8	33.9	35.5	***
09/04/2013	17:00	0.5	30.1	15.1	30.8	30.9	***
09/04/2013	18:00	0.0	28.9	12.5	28.3	28.3	***
09/04/2013	19:00	1.1	27.5	18.1	27.0	26.8	***
09/04/2013	20:00	0.6	25.9	20.4	25.5	25.4	***
09/04/2013	21:00	0.7	25.8	20.7	25.2	25.0	***
09/04/2013	22:00	1.0	25.1	25.4	23.8	23.3	***
09/04/2013	23:00	1.1	25.1	23.8	24.0	23.6	***
<b>10th and 7th of April 2013</b>							
10/04/2013	00:00	0.3	24.9	22.2	24.2	24.1	***
07/04/2013	01:00	0.8	29.0	16.3	27.7	27.3	***
07/04/2013	02:00	1.2	28.1	18.7	27.4	27.1	***
07/04/2013	03:00	1.1	26.9	18.5	26.6	26.5	***
07/04/2013	04:00	0.6	25.8	18.7	24.9	24.7	***
07/04/2013	05:00	1.2	24.5	19.0	24.6	24.6	***
07/04/2013	06:00	0.0	25.1	21.0	24.0	24.0	***
07/04/2013	07:00	1.3	27.3	17.1	26.6	26.3	***
07/04/2013	08:00	0.5	28.1	16.0	29.8	30.2	***
10/04/2013	09:00	0.6	22.4	22.8	35.4	38.3	***
10/04/2013	10:00	1.4	24.4	19.8	36.1	40.9	***
10/04/2013	11:00	1.5	23.2	20.3	36.8	42.5	***
10/04/2013	12:00	2.0	26.4	14.7	42.3	50.0	***
10/04/2013	13:00	2.5	26.7	13.3	40.1	47.9	***
10/04/2013	14:00	1.3	28.1	12.0	31.0	32.2	***
10/04/2013	15:00	0.7	28.5	10.9	30.2	30.7	***
10/04/2013	16:00	1.5	30.2	10.0	29.6	29.3	***
10/04/2013	17:00	1.4	29.5	8.7	29.4	29.4	***
10/04/2013	18:00	1.1	29.6	7.6	28.8	28.5	***
10/04/2013	19:00	2.0	29.1	6.8	28.5	28.2	***
10/04/2013	20:00	1.4	28.7	7.5	28.3	28.1	***
10/04/2013	21:00	0.6	27.7	8.8	26.8	26.6	***
10/04/2013	22:00	0.5	27.3	10.3	26.1	25.8	***
10/04/2013	23:00	0.6	26.8	11.0	24.2	23.5	***

Date	Time	Winds. (m/s)	Ta (°C)	RH (%)	Tg (°C)	MRT (°C)	Wind Direction
<b>11th and 7th of April 2013</b>							
11/04/2013	00:00	0.6	26.3	12.7	24.4	23.9	***
07/04/2013	01:00	0.8	29.0	16.3	27.7	27.3	***
07/04/2013	02:00	1.2	28.1	18.7	27.4	27.1	***
07/04/2013	03:00	1.1	26.9	18.5	26.6	26.5	***
07/04/2013	04:00	0.6	25.8	18.7	24.9	24.7	***
07/04/2013	05:00	1.2	24.5	19.0	24.6	24.6	***
07/04/2013	06:00	0.0	25.1	21.0	24.0	24.0	***
07/04/2013	07:00	1.3	27.3	17.1	26.6	26.3	***
07/04/2013	08:00	0.5	28.1	16.0	29.8	30.2	***
11/04/2013	09:00	1.4	24.7	15.9	36.9	41.8	***
11/04/2013	10:00	0.7	27.6	14.9	40.5	43.6	***
11/04/2013	11:00	2.3	28.1	12.8	39.0	45.1	***
11/04/2013	12:00	2.3	28.1	12.8	39.0	45.1	***
11/04/2013	13:00	0.9	30.6	11.0	45.8	49.9	***
11/04/2013	14:00	0.0	31.7	13.0	37.8	37.8	***
11/04/2013	15:00	1.1	30.7	9.8	35.8	37.6	***
11/04/2013	16:00	1.7	31.6	9.3	33.5	34.4	***
11/04/2013	17:00	0.4	30.9	9.2	30.8	30.8	***
11/04/2013	18:00	0.4	31.3	9.8	30.2	30.0	***
11/04/2013	19:00	0.0	32.2	12.3	32.0	32.0	***
11/04/2013	20:00	0.0	32.2	12.3	32.0	32.0	***
11/04/2013	21:00	0.7	29.3	11.8	27.9	27.5	***
11/04/2013	22:00	0.4	28.3	13.4	24.0	23.2	***
11/04/2013	23:00	0.4	26.9	13.7	24.9	24.5	***
<b>12th and 7th of April 2013</b>							
12/04/2013	00:00	0.7	26.3	14.8	24.5	24.0	***
07/04/2013	01:00	0.8	29.0	16.3	27.7	27.3	***
07/04/2013	02:00	1.2	28.1	18.7	27.4	27.1	***
07/04/2013	03:00	1.1	26.9	18.5	26.6	26.5	***
07/04/2013	04:00	0.6	25.8	18.7	24.9	24.7	***
07/04/2013	05:00	1.2	24.5	19.0	24.6	24.6	***
07/04/2013	06:00	0.0	25.1	21.0	24.0	24.0	***
07/04/2013	07:00	1.3	27.3	17.1	26.6	26.3	***
07/04/2013	08:00	0.5	28.1	16.0	29.8	30.2	***
12/04/2013	09:00	1.3	31.3	9.1	42.4	46.4	***
12/04/2013	10:00	1.1	32.9	8.7	46.6	50.9	***
12/04/2013	11:00	1.4	33.8	6.6	53.5	60.2	***
12/04/2013	12:00	1.4	33.8	6.6	53.5	60.2	***
12/04/2013	13:00	2.3	35.1	5.5	48.9	55.9	***
12/04/2013	14:00	0.5	35.6	5.7	38.0	38.5	***
12/04/2013	15:00	0.0	34.3	8.6	40.8	40.8	***
12/04/2013	16:00	0.4	35.5	4.8	37.5	37.8	***
12/04/2013	17:00	1.2	35.2	4.5	33.2	32.4	***
12/04/2013	18:00	0.7	34.6	4.5	34.0	33.8	***
12/04/2013	19:00	0.3	32.4	9.6	30.7	30.4	***
12/04/2013	20:00	0.5	32.2	10.6	31.2	31.0	***
12/04/2013	21:00	2.1	30.1	11.3	29.2	28.7	***
12/04/2013	22:00	0.4	29.9	11.6	29.1	29.0	***
12/04/2013	23:00	0.4	29.3	10.9	28.6	28.5	***



**A6. 8: Detailed hourly microclimatic data in the intermediate urban density area (summer).**

Field measurements for Summer (17th to 22nd of June 2013) in the intermediate Urban Density Area (Case 2)							
Date	Time	Winds. (m/s)	Ta (°C)	RH (%)	Tg (°C)	MRT (°C)	Wind Direction
17th of June 2013							
17/06/2013	00:00	0.9	31.5	14.4	30.9	30.7	***
17/06/2013	01:00	0.9	30.9	15.7	29.9	29.6	***
17/06/2013	02:00	1.6	30.3	17.6	29.8	29.6	***
17/06/2013	03:00	0.7	30.1	17.9	29.4	29.2	***
17/06/2013	04:00	0.7	30.1	17.9	29.4	29.2	***
17/06/2013	05:00	0.9	28.0	20.0	27.6	27.5	***
17/06/2013	06:00	1.2	27.8	20.1	27.8	27.8	***
17/06/2013	07:00	1.6	28.9	20.5	30.9	31.9	***
17/06/2013	08:00	1.3	31.6	16.4	34.3	35.4	***
17/06/2013	09:00	3.1	32.2	19.8	41.6	47.9	ENE
17/06/2013	10:00	1.3	33.7	16.5	44.6	48.5	NE
17/06/2013	11:00	1.9	34.6	13.6	50.1	56.9	NNW
17/06/2013	12:00	2.5	35.5	8.6	49.3	56.7	NNE
17/06/2013	13:00	2.6	38.5	3.8	50.1	56.5	WSW
17/06/2013	14:00	3.2	39.4	4.7	52.4	60.4	WNW
17/06/2013	15:00	1.8	39.2	5.3	42.0	43.3	NNE
17/06/2013	16:00	2.8	38.4	5.8	41.2	43.0	SSW
17/06/2013	17:00	2.1	37.7	6.0	45.6	49.5	W
17/06/2013	18:00	0.9	37.2	7.8	39.5	40.2	WSW
17/06/2013	19:00	3.1	35.5	10.0	35.1	34.8	SW
17/06/2013	20:00	1.7	35.0	12.0	34.2	33.8	SSW
17/06/2013	21:00	2.0	34.2	12.4	33.5	33.1	SW
17/06/2013	22:00	3.4	33.0	17.0	32.8	32.6	SW
17/06/2013	23:00	1.6	32.1	20.2	31.8	31.7	SSW
18th of June 2013							
18/06/2013	00:00	1.0	31.9	18.3	30.9	30.6	***
18/06/2013	01:00	0.0	30.9	17.9	30.4	30.4	***
18/06/2013	02:00	0.7	30.5	18.2	29.7	29.5	***
18/06/2013	03:00	1.9	29.8	18.7	29.1	28.7	***
18/06/2013	04:00	1.1	29.7	18.1	28.9	28.6	***
18/06/2013	05:00	1.1	28.5	19.8	27.4	27.0	***
18/06/2013	06:00	1.4	28.1	20.0	27.8	27.7	***
18/06/2013	07:00	0.7	28.5	19.3	30.3	30.8	***
18/06/2013	08:00	1.3	31.6	16.4	34.3	35.4	***
18/06/2013	09:00	0.0	33.3	16.3	43.0	43.0	ENE
18/06/2013	10:00	4.0	34.8	11.4	48.9	59.3	N
18/06/2013	11:00	2.5	35.8	10.1	47.2	53.5	WSW
18/06/2013	12:00	4.0	36.7	9.5	49.4	58.8	SW
18/06/2013	13:00	1.8	38.2	8.9	50.5	55.7	WSW
18/06/2013	14:00	4.6	37.5	9.1	48.1	56.9	SW
18/06/2013	15:00	2.1	38.4	9.4	39.9	40.7	WSW
18/06/2013	16:00	3.9	38.5	8.5	40.4	42.0	SW
18/06/2013	17:00	2.2	37.1	9.9	68.6	81.3	WSW
18/06/2013	18:00	2.7	36.2	9.8	40.4	43.0	WSW
18/06/2013	19:00	1.6	35.6	9.3	35.1	34.9	SSW
18/06/2013	20:00	3.2	34.1	12.0	33.7	33.4	WSW
18/06/2013	21:00	1.6	33.6	12.9	32.7	32.3	WSW
18/06/2013	22:00	1.5	32.7	13.3	31.9	31.5	WSW
18/06/2013	23:00	1.4	32.2	13.5	31.4	31.1	WSW



Date	Time	Winds. (m/s)	Ta (°C)	RH (%)	Tg (°C)	MRT (°C)	Wind Direction
<b>19th of June 2013</b>							
19/06/2013	00:00	1.3	31.7	13.7	31.0	30.7	***
19/06/2013	01:00	1.2	30.8	16.0	30.2	30.0	***
19/06/2013	02:00	0.9	30.3	17.0	29.3	29.0	***
19/06/2013	03:00	0.6	30.1	16.8	29.3	29.1	***
19/06/2013	04:00	0.8	29.0	18.1	28.5	28.3	***
19/06/2013	05:00	0.4	28.3	20.0	27.1	26.9	***
19/06/2013	06:00	0.5	27.5	20.0	27.8	27.9	***
19/06/2013	07:00	0.8	28.8	20.5	29.8	30.1	***
19/06/2013	08:00	0.5	31.9	16.5	34.5	35.0	***
19/06/2013	09:00	1.3	33.0	13.5	44.4	48.5	ENE
19/06/2013	10:00	3.4	34.7	12.2	48.2	57.2	SW
19/06/2013	11:00	4.7	35.8	11.4	47.8	57.9	NNE
19/06/2013	12:00	3.1	35.7	11.6	48.6	56.7	NE
19/06/2013	13:00	1.4	37.4	11.1	50.0	54.5	NNE
19/06/2013	14:00	2.6	38.0	10.0	50.2	56.9	SSW
19/06/2013	15:00	5.1	37.2	9.5	41.5	45.7	W
19/06/2013	16:00	3.6	37.7	9.6	40.8	43.2	W
19/06/2013	17:00	1.6	37.6	10.5	68.8	78.9	NNW
19/06/2013	18:00	3.1	36.5	10.9	40.4	43.1	WSW
19/06/2013	19:00	1.9	35.7	11.9	35.0	34.6	WSW
19/06/2013	20:00	1.9	34.5	12.3	34.1	33.9	WSW
19/06/2013	21:00	1.7	33.9	13.6	33.2	32.9	WSW
19/06/2013	22:00	0.0	33.3	15.5	32.6	32.6	S
19/06/2013	23:00	0.3	33.1	15.2	32.1	31.9	SSW
<b>20th of June 2013</b>							
20/06/2013	00:00	0.5	32.8	14.8	31.5	31.2	***
20/06/2013	01:00	1.4	32.2	14.3	31.4	31.1	***
20/06/2013	02:00	1.1	31.7	14.7	30.7	30.3	***
20/06/2013	03:00	0.8	30.9	15.8	29.8	29.5	***
20/06/2013	04:00	0.4	29.9	18.0	29.6	29.5	***
20/06/2013	05:00	0.0	28.9	19.7	27.8	27.8	***
20/06/2013	06:00	1.0	27.8	22.2	28.1	28.2	***
20/06/2013	07:00	1.7	28.5	20.9	29.9	30.6	***
20/06/2013	08:00	1.6	32.6	15.6	35.5	36.8	***
20/06/2013	09:00	2.1	33.7	13.8	46.0	52.0	NW
20/06/2013	10:00	4.0	34.5	11.8	45.3	53.6	WSW
20/06/2013	11:00	0.6	38.9	10.6	49.8	52.0	W
20/06/2013	12:00	2.3	36.7	11.2	47.6	52.8	NW
20/06/2013	13:00	1.4	36.9	10.8	45.6	50.2	NNW
20/06/2013	14:00	2.6	36.8	11.0	46.6	51.5	NW
20/06/2013	15:00	5.1	37.2	10.2	43.1	46.8	N
20/06/2013	16:00	6.2	37.5	9.5	39.7	42.2	ENE
20/06/2013	17:00	0.7	38.8	10.0	68.0	73.4	S
20/06/2013	18:00	1.2	37.7	10.4	39.5	40.1	N
20/06/2013	19:00	2.3	35.9	11.9	35.6	35.4	WSW
20/06/2013	20:00	2.7	35.1	12.2	34.7	34.4	SW
20/06/2013	21:00	2.2	34.4	12.5	33.9	33.6	WSW
20/06/2013	22:00	0.7	33.9	13.3	33.2	33.0	SW
20/06/2013	23:00	1.6	33.1	13.8	32.5	32.2	WSW

Date	Time	Winds. (m/s)	Ta (°C)	RH (%)	Tg (°C)	MRT (°C)	Wind Direction
<b>21st of June 2013</b>							
21/06/2013	00:00	***	***	***	***	***	***
21/06/2013	01:00	***	***	***	***	***	***
21/06/2013	02:00	***	***	***	***	***	***
21/06/2013	03:00	***	***	***	***	***	***
21/06/2013	04:00	***	***	***	***	***	***
21/06/2013	05:00	***	***	***	***	***	***
21/06/2013	06:00	***	***	***	***	***	***
21/06/2013	07:00	***	***	***	***	***	***
21/06/2013	08:00	***	***	***	***	***	***
21/06/2013	09:00	6.2	33.7	10.7	43.2	53.3	ENE
21/06/2013	10:00	6.0	35.1	10.5	67.7	93.2	NNE
21/06/2013	11:00	0.7	36.0	9.4	46.4	48.8	NE
21/06/2013	12:00	1.7	36.2	8.7	48.2	53.2	NE
21/06/2013	13:00	3.0	37.5	8.1	48.9	55.9	NNE
21/06/2013	14:00	0.6	38.9	7.7	51.4	53.8	NNW
21/06/2013	15:00	3.4	38.7	8.6	40.8	42.4	ENE
21/06/2013	16:00	2.0	38.5	8.4	41.2	42.6	WSW
21/06/2013	17:00	1.0	38.4	8.3	49.1	52.2	N
21/06/2013	18:00	2.6	37.8	8.9	41.2	43.3	W
21/06/2013	19:00	1.0	36.7	9.9	36.1	35.9	WNW
21/06/2013	20:00	3.1	35.4	11.4	34.9	34.5	WSW
21/06/2013	21:00	2.8	34.9	12.4	34.2	33.7	SW
21/06/2013	22:00	0.6	34.2	13.5	33.7	33.6	SW
21/06/2013	23:00	0.0	33.8	14.4	33.2	33.2	WSW
<b>22nd of June 2013</b>							
22/06/2013	00:00	***	***	***	***	***	***
22/06/2013	01:00	***	***	***	***	***	***
22/06/2013	02:00	***	***	***	***	***	***
22/06/2013	03:00	***	***	***	***	***	***
22/06/2013	04:00	***	***	***	***	***	***
22/06/2013	05:00	***	***	***	***	***	***
22/06/2013	06:00	***	***	***	***	***	***
22/06/2013	07:00	***	***	***	***	***	***
22/06/2013	08:00	***	***	***	***	***	***
22/06/2013	09:00	2.2	34.8	11.5	48.8	55.7	E
22/06/2013	10:00	4.0	35.2	11.6	45.2	53.0	NNE
22/06/2013	11:00	1.8	36.5	10.1	50.8	56.8	E
22/06/2013	12:00	1.2	37.7	9.4	51.4	55.7	NE
22/06/2013	13:00	3.6	38.0	8.2	51.7	60.9	E
22/06/2013	14:00	4.0	38.8	8.3	53.1	63.3	SW
22/06/2013	15:00	1.5	39.2	8.4	42.6	44.0	ENE
22/06/2013	16:00	2.5	38.8	8.6	48.2	53.3	SW
22/06/2013	17:00	***	***	***	***	***	SW
22/06/2013	18:00	3.0	37.9	9.5	40.4	42.1	WNW
22/06/2013	19:00	1.8	37.2	9.3	36.6	36.3	WSW
22/06/2013	20:00	0.7	36.1	11.8	35.6		WSW
22/06/2013	21:00	0.7	35.2	12.5	33.1		NNW
22/06/2013	22:00	0.0	35.3	10.9	34.2		SW
22/06/2013	23:00	***	***	***	***	***	S

**Appendices for Chapter 6 (A6.9 to A6.12) for the hourly and averaged hourly monitored microclimatic data over a year in the low urban density area (Case 3).**

**A6. 9: Average microclimatic data monitored in the low urban density area (Case3).**

Time HH:MM		October 2012 (Autumn)						January 2013 (Winter)						April 2013 (Spring)						June 2013 (Summer)					
		V m/s	Ta °C	RH %	Tg °C	MRT °C	PET °C	V m/s	Ta °C	RH %	Tg °C	MRT °C	PET °C	V m/s	Ta °C	RH %	Tg °C	MRT °C	PET °C	V m/s	Ta °C	RH %	Tg °C	MRT °C	PET °C
00:00	-	-	-	-	-	-	-	0.8	17.9	44.3	17.3	17.1	14.7	1.0	26.8	22.4	26.2	26.0	23.7	0.9	31.9	16.1	31.1	30.9	30.3
01:00	-	-	-	-	-	-	-	0.6	16.8	47.1	16.1	15.9	13.9	0.7	26.3	27.4	25.7	25.6	23.8	1.1	31.5	16.4	30.6	30.2	29.5
02:00	-	-	-	-	-	-	-	0.7	15.9	50.4	15.4	15.2	12.7	0.9	25.0	29.6	24.7	24.6	21.8	0.6	30.7	17.0	30.0	29.8	29.1
03:00	-	-	-	-	-	-	-	0.6	15.2	53.1	14.6	14.4	12.2	0.7	24.3	30.6	23.9	23.8	21.4	0.9	30.1	17.9	28.9	28.5	27.7
04:00	-	-	-	-	-	-	-	0.6	14.5	55.4	13.9	13.7	11.4	0.8	23.2	32.8	22.9	22.8	19.8	0.3	28.4	20.9	27.8	27.7	27.1
05:00	-	-	-	-	-	-	-	0.5	14.0	59.0	13.3	13.2	11.2	0.8	22.5	35.9	22.5	22.5	19.1	0.3	27.3	22.5	26.5	26.4	25.9
06:00	-	-	-	-	-	-	-	0.4	14.1	59.9	13.4	13.2	11.7	0.7	22.2	38.5	21.9	21.9	19.0	0.6	26.8	22.9	26.4	26.2	24.6
07:00	-	-	-	-	-	-	-	0.6	14.6	57.2	14.0	13.9	11.5	1.0	22.6	39.2	22.9	23.0	18.9	0.8	27.4	23.8	27.7	27.8	25.4
08:00	-	-	-	-	-	-	-	1.0	15.6	52.8	15.7	15.7	11.9	1.0	24.0	37.0	25.4	25.8	21.3	0.4	30.8	19.9	32.0	32.2	30.7
09:00	-	-	-	-	-	-	-	0.9	17.3	48.8	18.2	18.6	14.6	1.2	25.9	27.4	29.1	30.4	24.4	0.8	32.8	15.6	34.5	35.0	33.0
10:00	-	-	-	-	-	-	-	0.9	19.6	40.9	25.7	27.7	20.0	1.2	27.7	23.0	31.5	32.9	27.1	2.0	34.7	13.2	46.9	52.6	41.6
11:00	-	-	-	-	-	-	-	0.9	20.9	36.6	23.4	24.3	19.7	0.9	29.5	19.6	35.2	36.9	31.0	0.9	36.0	11.7	47.9	51.1	43.2
12:00	-	-	-	-	-	-	-	2.1	22.4	31.0	32.0	37.4	23.7	1.3	31.4	16.0	37.1	39.3	33.1	2.0	37.0	10.2	49.5	55.2	45.2
13:00	-	-	-	-	-	-	-	2.1	23.5	25.8	35.3	41.7	26.2	2.0	31.9	14.2	41.6	46.4	35.9	1.8	37.9	8.2	51.1	56.7	46.8
14:00	-	-	-	-	-	-	-	2.1	23.7	27.3	26.6	28.4	21.9	2.6	33.0	13.5	44.6	51.2	38.6	2.7	38.4	8.3	50.7	57.5	47.4
15:00	-	-	-	-	-	-	-	2.2	23.8	26.0	26.4	28.0	21.7	2.3	32.9	11.6	40.9	45.3	36.2	2.3	39.3	8.5	50.4	55.9	47.7
16:00	-	-	-	-	-	-	-	1.9	23.9	25.3	25.5	26.4	21.6	2.7	32.9	11.8	41.9	47.3	36.7	1.7	38.0	9.3	51.8	57.4	47.3
17:00	-	-	-	-	-	-	-	2.2	23.5	25.0	23.8	23.9	20.1	2.2	32.5	12.2	34.8	36.2	32.1	3.3	37.7	8.8	40.6	42.7	40.5
18:00	-	-	-	-	-	-	-	1.6	22.7	27.2	22.0	21.6	19.2	2.1	31.7	13.6	31.9	32.0	29.7	2.0	37.3	9.9	38.7	39.4	38.7
19:00	-	-	-	-	-	-	-	1.5	21.7	31.2	21.0	20.6	18.0	2.3	30.7	17.2	30.4	30.2	27.9	2.6	36.2	10.2	36.2	36.2	36.3
20:00	-	-	-	-	-	-	-	1.7	20.9	34.0	20.2	19.7	16.8	2.1	29.8	19.8	29.7	29.6	26.8	2.7	35.3	11.7	34.8	34.5	34.6
21:00	-	-	-	-	-	-	-	1.2	20.4	35.3	19.5	19.1	16.8	2.1	28.8	21.4	28.4	28.1	25.1	2.6	34.4	12.8	33.9	33.6	33.3
22:00	-	-	-	-	-	-	-	1.1	19.4	37.4	18.7	18.4	15.8	1.3	28.1	22.9	27.7	27.5	25.1	1.8	33.8	13.9	33.3	33.1	32.6
23:00	-	-	-	-	-	-	-	1.2	18.4	39.8	17.8	17.5	14.5	1.3	27.6	23.6	26.7	26.3	24.1	1.1	33.4	14.9	32.7	32.5	32.1
AVERAGE	-	-	-	-	-	-	-	1.2	19.2	40.5	20.4	21.1	16.7	1.5	28.0	23.4	30.3	31.5	26.8	1.5	33.6	14.4	37.2	38.9	35.4

**A6. 10: Detailed hourly microclimatic data in the low urban density area (winter).**

<b>Field measurements for Winter (1st to 7th of January 2013) in the Low Density Area (Case 3)</b>							
<b>Date</b>	<b>Time</b>	<b>Wind (m/s)</b>	<b>Ta (°C)</b>	<b>RH (%)</b>	<b>Tg (°C)</b>	<b>MRT (°C)</b>	<b>Wind Direction</b>
<b>1st of January 2013</b>							
01/01/2013	00:00	0.4	18.6	48.0	18.3	18.2	NNW
01/01/2013	01:00	0.2	18.1	49.3	17.4	17.3	NNW
01/01/2013	02:00	0.0	16.9	53.4	16.4	16.4	S
01/01/2013	03:00	0.0	16.4	54.0	15.8	15.8	SW
01/01/2013	04:00	0.0	15.5	58.5	15.1	15.0	W
01/01/2013	05:00	0.3	15.1	61.8	14.4	14.3	S
01/01/2013	06:00	0.5	15.0	61.3	14.4	14.2	S
01/01/2013	07:00	1.1	15.6	56.1	15.2	15.0	W
01/01/2013	08:00	0.8	16.8	49.8	17.1	17.2	NW
01/01/2013	09:00	1.3	18.5	46.3	19.6	20.0	N
01/01/2013	10:00	1.3	21.2	38.1	27.5	30.1	NNE
01/01/2013	11:00	1.4	22.8	35.8	25.2	26.2	NNW
01/01/2013	12:00	1.2	25.0	31.0	34.6	38.0	NW
01/01/2013	13:00	2.0	26.5	25.2	42.2	49.7	WNW
01/01/2013	14:00	0.5	27.2	25.0	31.1	31.8	WSW
01/01/2013	15:00	0.9	28.3	25.6	30.8	31.6	S
01/01/2013	16:00	1.4	27.6	26.5	29.6	30.4	NNE
01/01/2013	17:00	2.8	27.4	29.8	27.4	27.3	ESE
01/01/2013	18:00	1.6	26.2	31.8	25.5	25.1	ESE
01/01/2013	19:00	1.5	25.1	32.4	24.2	23.8	ESE
01/01/2013	20:00	1.1	24.3	33.9	23.6	23.3	SE
01/01/2013	21:00	1.2	24.2	35.6	23.1	22.6	SE
01/01/2013	22:00	0.4	22.5	41.0	22.0	21.8	NW
01/01/2013	23:00	0.5	21.4	44.4	20.6	20.4	WNW
<b>2nd of January 2013</b>							
02/01/2013	00:00	0.0	20.0	48.2	19.3	19.3	NW
02/01/2013	01:00	0.2	18.8	53.9	18.1	18.0	WNW
02/01/2013	02:00	0.0	17.9	57.5	18.0	18.0	S
02/01/2013	03:00	0.3	17.9	59.0	17.0	16.8	SSW
02/01/2013	04:00	0.0	16.4	66.5	15.9	15.9	SSW
02/01/2013	05:00	0.0	16.0	69.8	15.3	15.3	NNW
02/01/2013	06:00	0.0	15.4	73.3	15.0	15.0	N
02/01/2013	07:00	0.2	16.0	70.9	15.5	15.4	ESE
02/01/2013	08:00	0.6	16.8	69.5	16.9	16.9	WNW
02/01/2013	09:00	0.2	19.6	61.6	20.2	20.3	ESE
02/01/2013	10:00	0.3	23.1	45.7	28.9	29.7	NE
02/01/2013	11:00	0.6	23.6	38.7	26.9	27.6	ESE
02/01/2013	12:00	0.8	26.0	30.6	34.1	36.3	SSE
02/01/2013	13:00	1.0	27.4	15.9	41.4	45.5	SE
02/01/2013	14:00	0.9	26.8	22.8	29.1	29.9	NNE
02/01/2013	15:00	0.9	26.0	22.9	28.5	29.3	N
02/01/2013	16:00	1.3	26.1	21.5	27.5	28.0	N
02/01/2013	17:00	1.6	26.0	21.3	25.9	25.9	NNW
02/01/2013	18:00	0.6	25.1	22.2	24.4	24.2	N
02/01/2013	19:00	0.7	24.4	22.9	23.7	23.4	ENE
02/01/2013	20:00	1.0	23.7	22.3	22.6	22.2	ENE
02/01/2013	21:00	0.4	22.8	20.9	22.0	21.9	N
02/01/2013	22:00	0.5	22.0	19.0	21.3	21.1	NNW
02/01/2013	23:00	0.6	20.8	20.7	19.8	19.5	ENE



Date	Time	Winds. (m/s)	Ta (°C)	RH (%)	Tg (°C)	MRT (°C)	Wind Direction
<b>3rd of January 2013</b>							
03/01/2013	00:00	0.7	18.8	27.0	18.3	18.2	N
03/01/2013	01:00	0.2	16.8	32.7	16.0	15.9	W
03/01/2013	02:00	0.7	16.1	34.3	15.2	14.9	N
03/01/2013	03:00	0.4	14.5	42.5	13.7	13.5	WNW
03/01/2013	04:00	0.0	13.9	42.4	13.3	13.3	SW
03/01/2013	05:00	0.9	14.8	43.4	14.2	14.0	WSW
03/01/2013	06:00	1.5	16.6	44.8	15.8	15.4	SW
03/01/2013	07:00	1.5	16.4	47.7	15.9	15.6	NNW
03/01/2013	08:00	1.9	16.5	48.8	16.4	16.3	NNW
03/01/2013	09:00	0.8	17.2	47.5	18.6	19.0	NW
03/01/2013	10:00	0.8	18.8	42.2	25.2	27.1	N
03/01/2013	11:00	0.4	21.0	39.2	23.3	23.7	WNW
03/01/2013	12:00	1.3	21.8	34.6	32.9	37.2	N
03/01/2013	13:00	1.1	23.9	31.1	36.2	40.2	NW
03/01/2013	14:00	1.3	23.5	30.1	27.2	28.8	WNW
03/01/2013	15:00	1.0	23.3	27.8	26.3	27.4	SSW
03/01/2013	16:00	1.1	23.8	24.7	25.8	26.5	N
03/01/2013	17:00	1.1	23.6	23.7	23.8	23.9	S
03/01/2013	18:00	1.6	22.8	24.9	22.2	21.9	SW
03/01/2013	19:00	0.8	21.9	32.0	21.4	21.2	N
03/01/2013	20:00	0.8	20.6	36.4	20.1	19.9	NW
03/01/2013	21:00	1.0	19.4	40.6	18.7	18.4	NNW
03/01/2013	22:00	1.0	17.9	46.8	17.4	17.1	NNW
03/01/2013	23:00	0.8	17.1	49.7	16.5	16.3	NNW
<b>4th of January 2013</b>							
04/01/2013	00:00	1.1	16.3	52.1	15.9	15.7	NW
04/01/2013	01:00	1.3	15.6	54.0	15.1	14.9	SW
04/01/2013	02:00	2.0	14.7	55.7	14.3	14.0	W
04/01/2013	03:00	2.1	14.0	57.6	13.6	13.2	SW
04/01/2013	04:00	2.4	13.7	58.5	13.2	12.9	WSW
04/01/2013	05:00	1.9	13.2	60.2	12.7	12.3	SW
04/01/2013	06:00	0.0	12.7	60.4	12.2	12.2	WSW
04/01/2013	07:00	0.0	12.4	60.4	11.9	11.9	WNW
04/01/2013	08:00	1.3	13.0	54.5	13.2	13.3	SSW
04/01/2013	09:00	1.0	14.2	47.4	15.6	16.1	NNW
04/01/2013	10:00	0.4	16.9	39.0	22.8	23.8	WSW
04/01/2013	11:00	0.5	17.7	37.4	20.5	21.1	NNW
04/01/2013	12:00	1.8	19.0	32.5	30.4	36.1	SW
04/01/2013	13:00	2.0	20.4	29.6	34.2	41.5	WNW
04/01/2013	14:00	1.6	21.8	27.8	25.8	27.8	NW
04/01/2013	15:00	0.2	23.1	24.9	26.1	26.5	NNW
04/01/2013	16:00	0.5	23.5	25.0	25.3	25.7	W
04/01/2013	17:00	0.7	23.2	25.3	23.3	23.3	NW
04/01/2013	18:00	0.5	22.2	28.6	21.2	21.0	NW
04/01/2013	19:00	0.9	20.2	35.2	19.8	19.7	NNW
04/01/2013	20:00	0.2	19.5	39.5	18.7	18.6	N
04/01/2013	21:00	0.6	19.3	38.2	18.5	18.3	NW
04/01/2013	22:00	0.5	18.3	42.2	17.4	17.2	NW
04/01/2013	23:00	0.7	17.0	46.5	16.6	16.5	S

Date	Time	Winds. (m/s)	Ta (°C)	RH (%)	Tg (°C)	MRT (°C)	Wind Direction
<b>5th of January 2013</b>							
05/01/2013	00:00	0.9	16.6	44.1	15.6	15.2	WNW
05/01/2013	01:00	0.0	15.5	47.6	14.7	14.7	NW
05/01/2013	02:00	0.3	14.4	54.3	14.1	14.0	SW
05/01/2013	03:00	0.0	13.6	56.6	13.2	13.2	WNW
05/01/2013	04:00	0.3	13.4	57.7	12.6	12.5	WNW
05/01/2013	05:00	0.0	12.5	63.3	12.0	11.9	NW
05/01/2013	06:00	0.4	13.5	62.5	12.9	12.7	NNW
05/01/2013	07:00	0.5	13.6	65.6	13.1	13.0	NNW
05/01/2013	08:00	0.8	15.5	63.9	15.5	15.5	WNW
05/01/2013	09:00	1.2	18.2	61.4	19.2	19.6	W
05/01/2013	10:00	1.4	21.4	51.5	26.8	29.2	ESE
05/01/2013	11:00	0.5	22.6	41.2	24.6	25.0	NNW
05/01/2013	12:00	1.9	25.0	31.2	34.1	38.7	SSE
05/01/2013	13:00	3.4	24.2	18.7	34.2	41.7	SE
05/01/2013	14:00	3.3	24.6	20.3	27.2	29.3	E
05/01/2013	15:00	3.9	24.9	16.4	27.4	29.7	S
05/01/2013	16:00	2.1	25.1	15.6	26.4	27.1	S
05/01/2013	17:00	3.0	24.1	12.0	24.5	24.9	SSE
05/01/2013	18:00	1.6	23.4	17.3	22.7	22.3	SSE
05/01/2013	19:00	2.5	22.1	24.9	21.2	20.6	NNE
05/01/2013	20:00	3.0	21.4	29.0	20.6	19.9	SSE
05/01/2013	21:00	0.9	20.8	31.8	19.8	19.4	E
05/01/2013	22:00	0.3	19.8	33.9	19.0	18.9	NNE
05/01/2013	23:00	0.3	19.1	34.6	18.7	18.6	SW
<b>6th of January 2013</b>							
06/01/2013	00:00	0.6	17.7	40.7	17.0	16.8	N
06/01/2013	01:00	0.2	16.3	45.1	15.2	15.1	S
06/01/2013	02:00	0.4	15.0	53.2	14.1	13.9	SSW
06/01/2013	03:00	0.0	14.4	58.5	13.9	13.9	SW
06/01/2013	04:00	0.0	13.3	63.8	12.7	12.7	N
06/01/2013	05:00	0.6	13.5	64.4	12.5	12.2	SSW
06/01/2013	06:00	0.0	12.6	67.2	11.9	11.9	NW
06/01/2013	07:00	0.5	14.2	58.8	13.6	13.4	WSW
06/01/2013	08:00	1.0	16.2	43.7	16.2	16.2	SW
06/01/2013	09:00	0.7	17.5	43.2	18.2	18.4	ENE
06/01/2013	10:00	0.8	18.9	38.4	24.6	26.2	NNE
06/01/2013	11:00	1.5	19.4	32.7	22.6	24.2	NNW
06/01/2013	12:00	3.4	20.8	29.6	31.5	39.7	ENE
06/01/2013	13:00	2.6	21.6	34.9	29.1	34.1	SSE
06/01/2013	14:00	4.0	20.9	40.0	23.2	25.4	SSE
06/01/2013	15:00	4.9	21.1	38.9	23.3	25.7	SE
06/01/2013	16:00	4.3	21.2	38.9	22.4	23.6	SSE
06/01/2013	17:00	3.3	20.6	38.9	20.9	21.2	SE
06/01/2013	18:00	2.9	20.0	39.9	19.5	19.1	S
06/01/2013	19:00	2.2	19.7	41.9	19.0	18.5	SE
06/01/2013	20:00	2.4	19.3	44.7	18.6	18.1	SSE
06/01/2013	21:00	3.0	18.9	46.4	18.3	17.7	ESE
06/01/2013	22:00	3.3	18.6	46.0	18.0	17.5	SSE
06/01/2013	23:00	3.6	18.2	48.5	17.5	16.9	SE



Date	Time	Winds. (m/s)	Ta (°C)	RH (%)	Tg (°C)	MRT (°C)	Wind Direction
<b>7th of January 2013</b>							
07/01/2013	00:00	1.8	17.5	50.3	16.7	16.2	E
07/01/2013	01:00	2.2	16.8	46.9	16.1	15.6	ESE
07/01/2013	02:00	1.5	16.4	44.6	15.5	15.0	ESE
07/01/2013	03:00	1.4	16.0	43.4	15.0	14.4	SE
07/01/2013	04:00	1.4	15.6	40.5	14.5	14.0	ENE
07/01/2013	05:00	0.0	13.0	50.3	12.5	12.4	ESE
07/01/2013	06:00	0.4	12.9	49.7	11.7	11.5	NW
07/01/2013	07:00	0.3	13.8	41.1	13.0	12.9	N
07/01/2013	08:00	0.5	14.6	39.7	14.5	14.4	ENE
07/01/2013	09:00	1.1	15.8	34.6	16.3	16.5	NE
07/01/2013	10:00	1.4	17.0	31.5	24.1	27.3	NNE
07/01/2013	11:00	1.9	19.3	31.0	21.1	22.1	SSE
07/01/2013	12:00	4.8	19.5	27.7	26.5	33.9	SSE
07/01/2013	13:00	2.9	20.6	25.2	30.1	36.8	ENE
07/01/2013	14:00	3.2	21.1	25.0	23.1	24.7	NNE
07/01/2013	15:00	3.4	20.4	25.6	22.5	24.4	E
07/01/2013	16:00	3.0	20.4	25.1	21.9	23.1	ESE
07/01/2013	17:00	3.0	19.9	24.3	20.6	21.1	SE
07/01/2013	18:00	2.5	19.2	26.0	18.5	17.9	ESE
07/01/2013	19:00	2.1	18.5	29.2	17.7	17.2	SSE
07/01/2013	20:00	3.3	17.7	32.5	17.0	16.3	SSE
07/01/2013	21:00	1.7	17.5	33.6	16.4	15.8	E
07/01/2013	22:00	1.9	16.5	33.0	15.7	15.1	SE
07/01/2013	23:00	1.8	15.4	34.2	14.9	14.5	SE

**A6. 11: Detailed hourly microclimatic data in the low urban density area (spring).**

<b>Field measurements for Spring (1st to 12th of April 2013) in the Low Urban Density Area (Case 3)</b>							
<b>Date</b>	<b>Time</b>	<b>Wind (m/s)</b>	<b>Ta (°C)</b>	<b>RH (%)</b>	<b>Tg (°C)</b>	<b>MRT (°C)</b>	<b>Wind Direction</b>
<b>1st of April 2013</b>							
01/04/2013	00:00	0.5	25.6	9.4	25.4	25.3	NNW
01/04/2013	01:00	0.6	24.8	16.2	24.2	24.0	NE
01/04/2013	02:00	1.5	23.9	19.7	23.3	23.0	NE
01/04/2013	03:00	1.6	23.2	20.0	22.9	22.7	NNE
01/04/2013	04:00	1.5	22.5	20.8	22.3	22.2	NNE
01/04/2013	05:00	1.2	21.9	22.0	21.9	21.9	N
01/04/2013	06:00	0.9	21.8	22.8	21.9	21.9	NE
01/04/2013	07:00	1.7	21.4	24.2	22.1	22.5	NE
01/04/2013	08:00	1.8	21.7	24.6	23.8	24.9	NNW
01/04/2013	09:00	1.7	22.4	24.0	26.8	29.1	NNE
01/04/2013	10:00	1.1	24.3	23.1	28.8	30.5	ENE
01/04/2013	11:00	1.4	25.5	22.2	31.5	34.0	ENE
01/04/2013	12:00	1.8	26.9	22.0	33.8	37.2	ENE
01/04/2013	13:00	3.0	27.0	22.1	35.4	41.3	SSE
01/04/2013	14:00	0.8	29.9	21.6	38.8	41.2	ENE
01/04/2013	15:00	1.7	29.6	20.9	35.8	38.7	NE
01/04/2013	16:00	1.2	29.9	19.9	35.1	37.0	E
01/04/2013	17:00	0.9	30.0	18.5	32.0	32.6	NE
01/04/2013	18:00	0.9	29.3	18.2	29.8	29.9	N
01/04/2013	19:00	1.0	28.9	17.9	28.5	28.3	NNE
01/04/2013	20:00	0.8	28.5	18.4	28.1	27.9	NNE
01/04/2013	21:00	1.1	27.8	20.6	27.8	27.8	ENE
01/04/2013	22:00	1.3	27.1	22.7	26.9	26.8	NE
01/04/2013	23:00	2.1	26.2	23.5	26.0	25.9	NE
<b>2nd of April 2013</b>							
02/04/2013	00:00	1.7	25.0	25.4	24.8	24.6	ENE
02/04/2013	01:00	1.5	24.1	25.2	23.8	23.7	ESE
02/04/2013	02:00	2.0	23.2	23.2	22.9	22.7	NE
02/04/2013	03:00	1.6	22.6	23.5	22.2	21.9	E
02/04/2013	04:00	1.1	22.0	24.7	21.7	21.5	NE
02/04/2013	05:00	1.0	21.2	26.2	20.9	20.8	NNE
02/04/2013	06:00	0.5	21.0	26.8	20.7	20.6	NE
02/04/2013	07:00	1.7	21.2	27.8	21.5	21.6	N
02/04/2013	08:00	0.9	21.9	29.6	23.8	24.4	NW
02/04/2013	09:00	1.3	24.1	29.9	27.3	28.6	NE
02/04/2013	10:00	0.2	26.7	30.7	29.6	29.8	NNW
02/04/2013	11:00	0.9	27.6	31.1	33.6	35.5	NNE
02/04/2013	12:00	1.9	30.1	31.1	35.1	37.7	ENE
02/04/2013	13:00	1.0	31.6	27.5	40.9	43.7	WNW
02/04/2013	14:00	0.6	32.3	24.6	40.6	42.2	NNW
02/04/2013	15:00	2.0	31.8	15.5	38.3	41.5	SSW
02/04/2013	16:00	2.2	32.0	16.1	35.5	37.5	SW
02/04/2013	17:00	2.9	31.5	18.3	33.6	35.1	NW
02/04/2013	18:00	1.7	31.2	18.4	31.6	31.8	NW
02/04/2013	19:00	2.5	30.4	22.0	30.6	30.7	W
02/04/2013	20:00	2.6	29.3	31.3	29.2	29.0	WSW
02/04/2013	21:00	1.2	29.0	29.8	28.6	28.5	W
02/04/2013	22:00	0.5	28.6	30.8	28.2	28.1	NW
02/04/2013	23:00	1.6	27.9	33.1	27.7	27.5	WNW

Date	Time	Winds. (m/s)	Ta (°C)	RH (%)	Tg (°C)	MRT (°C)	Wind Direction
<b>3rd of April 2013</b>							
03/04/2013	00:00	0.5	27.5	36.9	27.1	27.0	NNE
03/04/2013	01:00	0.5	27.0	39.4	26.4	26.3	SSE
03/04/2013	02:00	0.9	25.2	40.1	25.0	24.9	ENE
03/04/2013	03:00	0.3	24.2	42.1	23.8	23.7	ESE
03/04/2013	04:00	0.6	22.9	47.5	22.8	22.7	NE
03/04/2013	05:00	0.0	22.8	50.3	22.4	22.4	E
03/04/2013	06:00	0.5	22.3	53.1	22.4	22.4	NE
03/04/2013	07:00	0.4	23.1	55.7	23.4	23.4	NE
03/04/2013	08:00	0.9	24.7	55.4	26.0	26.4	ENE
03/04/2013	09:00	0.6	26.9	50.7	28.7	29.1	S
03/04/2013	10:00	1.0	29.3	42.4	32.1	33.0	SSE
03/04/2013	11:00	1.2	29.6	38.0	34.1	35.7	WSW
03/04/2013	12:00	1.2	31.7	29.7	35.6	37.0	SSW
03/04/2013	13:00	2.8	32.1	24.3	40.3	45.5	S
03/04/2013	14:00	2.9	33.1	22.1	40.0	44.6	WSW
03/04/2013	15:00	4.3	33.0	20.5	40.0	46.0	N
03/04/2013	16:00	3.3	33.4	20.4	43.1	49.8	WNW
03/04/2013	17:00	3.0	32.6	19.4	35.6	37.6	SW
03/04/2013	18:00	3.3	31.9	24.6	32.1	32.3	SSE
03/04/2013	19:00	4.2	30.6	29.9	30.5	30.4	WSW
03/04/2013	20:00	2.9	29.5	34.2	29.3	29.2	SW
03/04/2013	21:00	3.5	28.8	32.5	28.5	28.2	SSW
03/04/2013	22:00	2.3	28.3	33.3	27.8	27.5	NW
03/04/2013	23:00	1.1	27.8	33.5	27.5	27.3	SW
<b>4th of April 2013</b>							
04/04/2013	00:00	1.4	27.6	33.8	27.2	27.0	S
04/04/2013	01:00	0.6	26.6	34.8	26.2	26.1	SSE
04/04/2013	02:00	1.0	24.9	42.4	24.7	24.6	ENE
04/04/2013	03:00	0.0	24.1	44.4	24.0	24.0	SSE
04/04/2013	04:00	0.6	24.0	44.1	23.5	23.4	SE
04/04/2013	05:00	2.1	23.0	55.0	23.0	22.9	SSE
04/04/2013	06:00	1.0	22.9	58.4	22.6	22.5	E
04/04/2013	07:00	1.5	23.0	57.4	23.3	23.5	NE
04/04/2013	08:00	1.4	24.6	50.5	25.8	26.4	SE
04/04/2013	09:00	1.4	26.2	40.1	29.0	30.2	ESE
04/04/2013	10:00	1.0	28.6	27.1	33.2	34.6	W
04/04/2013	11:00	0.6	30.5	19.7	33.5	34.1	NW
04/04/2013	12:00	1.2	32.6	18.9	36.5	37.9	SE
04/04/2013	13:00	1.1	33.9	15.3	43.5	46.4	NNE
04/04/2013	14:00	0.9	35.4	12.8	57.7	63.1	NE
04/04/2013	15:00	1.5	34.7	11.9	42.3	45.3	E
04/04/2013	16:00	1.7	34.0	12.3	45.0	49.7	SSW
04/04/2013	17:00	1.6	34.0	10.5	37.0	38.3	WNW
04/04/2013	18:00	2.6	33.3	10.6	33.7	34.0	N
04/04/2013	19:00	3.7	31.4	24.9	31.2	30.9	NNE
04/04/2013	20:00	2.2	30.5	26.4	30.4	30.4	S
04/04/2013	21:00	1.5	30.3	25.8	29.7	29.3	SW
04/04/2013	22:00	2.1	29.1	26.5	28.7	28.5	WNW
04/04/2013	23:00	0.7	29.1	25.8	28.4	28.2	SW

Date	Time	Winds. (m/s)	Ta (°C)	RH (%)	Tg (°C)	MRT (°C)	Wind Direction
<b>5th of April 2013</b>							
05/04/2013	00:00	1.5	28.4	21.0	27.7	27.4	SW
05/04/2013	01:00	0.7	27.6	21.2	26.9	26.7	NW
05/04/2013	02:00	1.0	27.7	19.7	26.9	26.6	NNE
05/04/2013	03:00	0.5	26.8	20.9	26.3	26.1	NNE
05/04/2013	04:00	0.2	25.5	24.1	25.1	25.1	E
05/04/2013	05:00	0.7	24.1	29.0	23.8	23.7	E
05/04/2013	06:00	1.1	23.1	33.3	22.6	22.4	S
05/04/2013	07:00	0.8	23.2	32.5	23.4	23.4	SSE
05/04/2013	08:00	1.0	24.8	31.5	25.8	26.2	ESE
05/04/2013	09:00	1.0	27.2	22.9	29.6	30.3	S
05/04/2013	10:00	0.6	30.0	16.3	32.6	33.1	S
05/04/2013	11:00	1.0	30.6	15.2	34.8	36.1	SSW
05/04/2013	12:00	1.4	31.7	12.1	36.9	38.9	SW
05/04/2013	13:00	1.5	32.6	11.7	41.6	45.3	NW
05/04/2013	14:00	2.1	33.9	11.9	56.5	66.2	N
05/04/2013	15:00	1.8	34.2	11.2	41.9	45.4	NE
05/04/2013	16:00	3.3	33.3	11.7	45.9	54.3	ESE
05/04/2013	17:00	2.2	32.9	13.7	35.7	37.2	ESE
05/04/2013	18:00	1.0	31.9	16.7	32.4	32.6	N
05/04/2013	19:00	2.5	30.8	20.7	30.8	30.8	NW
05/04/2013	20:00	2.9	29.8	25.4	29.7	29.6	SSW
05/04/2013	21:00	3.0	29.2	28.0	28.6	28.2	S
05/04/2013	22:00	2.1	28.5	30.9	27.8	27.3	SW
05/04/2013	23:00	1.4	27.7	32.9	27.2	27.0	WSW
<b>6th of April 2013</b>							
06/04/2013	00:00	1.5	27.0	33.1	26.5	26.2	W
06/04/2013	01:00	0.8	26.2	33.7	25.3	25.0	WNW
06/04/2013	02:00	0.3	24.3	39.1	24.0	23.9	WSW
06/04/2013	03:00	0.7	24.0	40.1	23.6	23.5	NNW
06/04/2013	04:00	0.4	22.8	42.8	22.4	22.3	NNE
06/04/2013	05:00	0.0	21.7	46.8	21.5	21.5	ENE
06/04/2013	06:00	0.5	21.6	48.3	21.5	21.5	NNE
06/04/2013	07:00	0.7	22.7	48.9	22.8	22.8	NE
06/04/2013	08:00	1.4	24.6	46.2	25.9	26.4	NNE
06/04/2013	09:00	0.5	27.3	36.3	28.5	28.8	E
06/04/2013	10:00	0.7	29.4	25.4	31.9	32.5	ENE
06/04/2013	11:00	0.6	30.5	20.6	33.9	34.6	NE
06/04/2013	12:00	0.6	31.4	15.9	36.0	37.0	NNW
06/04/2013	13:00	1.4	32.9	11.1	42.1	45.6	N
06/04/2013	14:00	2.6	34.1	12.4	47.2	54.6	E
06/04/2013	15:00	2.6	33.1	12.2	41.5	46.5	SW
06/04/2013	16:00	3.6	33.4	13.7	44.2	52.1	S
06/04/2013	17:00	2.6	33.0	14.0	35.3	36.8	S
06/04/2013	18:00	2.5	32.0	15.1	32.4	32.7	SSW
06/04/2013	19:00	2.4	31.8	15.6	31.2	30.8	WSW
06/04/2013	20:00	2.9	29.8	25.4	29.7	29.6	SW
06/04/2013	21:00	3.0	29.2	28.0	28.6	28.2	SSW
06/04/2013	22:00	2.1	28.5	30.9	27.8	27.3	NW
06/04/2013	23:00	1.4	27.7	32.9	27.2	27.0	SW

Date	Time	Winds. (m/s)	Ta (°C)	RH (%)	Tg (°C)	MRT (°C)	Wind Direction
<b>7th of April 2013</b>							
07/04/2013	00:00	0.6	28.3	19.3	28.0	27.9	***
07/04/2013	01:00	0.0	27.8	21.1	27.3	27.3	***
07/04/2013	02:00	0.0	26.1	23.4	26.1	26.1	***
07/04/2013	03:00	0.0	25.6	23.4	24.5	24.5	***
07/04/2013	04:00	1.1	23.0	25.5	22.6	22.4	***
07/04/2013	05:00	0.6	23.0	22.2	23.9	24.1	***
07/04/2013	06:00	0.3	22.8	26.9	21.9	21.8	***
07/04/2013	07:00	0.4	24.0	27.9	24.0	24.0	***
07/04/2013	08:00	0.0	26.1	21.3	26.5	26.5	***
07/04/2013	09:00	0.7	28.4	17.4	29.8	30.2	***
07/04/2013	10:00	1.0	29.4	12.1	33.4	34.7	***
07/04/2013	11:00	0.6	32.6	8.7	37.5	38.6	***
07/04/2013	12:00	1.1	36.0	5.4	39.4	40.5	***
07/04/2013	13:00	4.8	34.7	4.8	44.8	53.7	***
07/04/2013	14:00	5.4	35.1	4.5	38.0	41.0	***
07/04/2013	15:00	4.5	34.3	5.4	42.6	49.8	***
07/04/2013	16:00	4.0	34.0	7.0	42.9	50.0	***
07/04/2013	17:00	1.3	34.0	8.5	36.7	37.8	***
07/04/2013	18:00	2.2	32.0	10.9	31.8	31.7	***
07/04/2013	19:00	2.1	31.7	11.9	30.8	30.3	***
07/04/2013	20:00	0.9	30.2	14.4	30.1	30.1	***
07/04/2013	21:00	2.2	30.2	14.8	29.2	28.6	***
07/04/2013	22:00	2.1	29.0	15.8	28.6	28.4	***
07/04/2013	23:00	1.4	28.9	17.1	28.2	27.9	***
<b>8th of April 2013</b>							
08/04/2013	00:00	0.9	27.9	18.5	27.4	27.2	***
***	01:00	***	***	***	***		***
***	02:00	***	***	***	***		***
***	03:00	***	***	***	***		***
***	04:00	***	***	***	***		***
***	05:00	***	***	***	***		***
***	06:00	***	***	***	***		***
***	07:00	***	***	***	***		***
***	08:00	***	***	***	***		***
08/04/2013	09:00	1.3	26.7	31.7	28.8	29.7	***
08/04/2013	10:00	3.5	28.3	28.8	32.6	36.1	***
08/04/2013	11:00	0.6	32.9	20.5	36.8	37.7	***
08/04/2013	12:00	2.3	32.0	14.6	34.7	36.3	***
08/04/2013	13:00	1.3	33.3	11.3	40.9	43.7	***
08/04/2013	14:00	6.5	33.0	8.8	43.7	55.4	***
08/04/2013	15:00	2.3	33.4	6.9	38.6	41.6	***
08/04/2013	16:00	3.8	34.1	6.2	42.8	49.5	***
08/04/2013	17:00	2.7	33.5	8.3	35.9	37.5	***
08/04/2013	18:00	3.2	32.7	15.1	33.2	33.6	***
08/04/2013	19:00	3.2	31.5	18.7	31.1	30.8	***
08/04/2013	20:00	2.8	30.8	13.7	30.5	30.3	***
08/04/2013	21:00	3.4	29.9	19.4	29.4	29.0	***
08/04/2013	22:00	1.5	29.1	21.5	28.8	28.7	***
08/04/2013	23:00	1.3	28.9	18.6	27.9	27.5	***



Date	Time	Winds. (m/s)	Ta (°C)	RH (%)	Tg (°C)	MRT (°C)	Wind Direction
<b>9th of April 2013</b>							
09/04/2013	00:00	1.3	28.9	18.6	27.9	27.5	***
***	01:00	***	***	***	***		***
***	02:00	***	***	***	***		***
***	03:00	***	***	***	***		***
***	04:00	***	***	***	***		***
***	05:00	***	***	***	***		***
***	06:00	***	***	***	***		***
***	07:00	***	***	***	***		***
***	08:00	***	***	***	***		***
09/04/2013	09:00	2.8	26.6	23.9	34.9	40.5	***
09/04/2013	10:00	0.6	27.6	23.6	33.5	34.9	***
09/04/2013	11:00	0.8	29.3	18.6	32.8	33.8	***
09/04/2013	12:00	3.2	32.3	7.6	39.0	43.8	***
09/04/2013	13:00	3.2	32.3	7.6	39.0	43.8	***
09/04/2013	14:00	5.0	31.6	12.8	40.5	48.9	***
09/04/2013	15:00	4.6	31.3	9.6	35.0	38.6	***
09/04/2013	16:00	5.7	31.6	7.8	43.4	55.1	***
09/04/2013	17:00	6.0	29.6	13.7	33.5	38.1	***
09/04/2013	18:00	4.7	28.5	11.9	29.3	30.1	***
09/04/2013	19:00	3.2	27.3	18.0	28.0	28.6	***
09/04/2013	20:00	4.8	25.7	20.2	27.1	28.6	***
09/04/2013	21:00	1.8	25.4	22.9	24.5	24.0	***
09/04/2013	22:00	1.1	25.8	24.0	24.8	24.4	***
09/04/2013	23:00	1.8	24.8	24.9	22.8	21.7	***
<b>10th of April 2013</b>							
10/04/2013	00:00	0.3	24.9	22.2	24.2	24.1	***
***	01:00	***	***	***	***		***
***	02:00	***	***	***	***		***
***	03:00	***	***	***	***		***
***	04:00	***	***	***	***		***
***	05:00	***	***	***	***		***
***	06:00	***	***	***	***		***
***	07:00	***	***	***	***		***
***	08:00	***	***	***	***		***
10/04/2013	09:00	1.7	21.9	22.8	24.2	25.4	***
10/04/2013	10:00	1.3	23.3	20.8	26.7	28.2	***
10/04/2013	11:00	1.6	25.9	18.0	30.6	32.8	***
10/04/2013	12:00	0.8	27.7	15.9	31.8	33.0	***
10/04/2013	13:00	2.7	27.7	14.9	38.7	45.6	***
10/04/2013	14:00	1.2	30.7	12.2	42.6	46.7	***
10/04/2013	15:00	1.2	28.9	11.5	44.6	49.9	***
10/04/2013	16:00	0.9	32.6	9.8	38.0	39.6	***
10/04/2013	17:00	1.3	30.3	9.2	33.8	35.2	***
10/04/2013	18:00	0.6	30.2	8.3	30.6	30.7	***
10/04/2013	19:00	0.5	29.4	7.0	28.5	28.3	***
10/04/2013	20:00	1.3	29.3	7.3	28.2	27.7	***
10/04/2013	21:00	2.1	28.0	8.2	27.6	27.4	***
10/04/2013	22:00	0.8	27.3	9.6	26.3	26.0	***
10/04/2013	23:00	1.1	26.7	11.3	24.5	23.6	***



Date	Time	Winds. (m/s)	Ta (°C)	RH (%)	Tg (°C)	MRT (°C)	Wind Direction
<b>11th of April 2013</b>							
11/04/2013	00:00	0.9	25.6	13.1	24.6	24.3	***
***	01:00	***	***	***	***		***
***	02:00	***	***	***	***		***
***	03:00	***	***	***	***		***
***	04:00	***	***	***	***		***
***	05:00	***	***	***	***		***
***	06:00	***	***	***	***		***
***	07:00	***	***	***	***		***
***	08:00	***	***	***	***		***
11/04/2013	09:00	0.9	24.5	16.4	26.7	27.4	***
11/04/2013	10:00	0.9	25.6	16.1	30.6	32.2	***
11/04/2013	11:00	0.7	27.1	14.1	37.1	39.6	***
11/04/2013	12:00	0.7	27.1	14.1	37.1	39.6	***
11/04/2013	13:00	1.2	30.0	11.2	43.8	48.5	***
11/04/2013	14:00	1.4	31.0	11.6	43.0	47.6	***
11/04/2013	15:00	0.4	34.1	9.2	42.0	43.3	***
11/04/2013	16:00	2.5	31.1	9.8	42.2	48.6	***
11/04/2013	17:00	1.2	32.5	8.8	33.8	34.3	***
11/04/2013	18:00	0.5	31.6	9.7	31.8	31.8	***
11/04/2013	19:00	0.0	32.0	11.3	32.3	32.3	***
11/04/2013	20:00	0.0	32.0	11.3	32.3	32.3	***
11/04/2013	21:00	0.9	28.3	16.0	29.4	29.8	***
11/04/2013	22:00	0.0	26.6	17.0	27.5	27.5	***
11/04/2013	23:00	1.1	26.0	17.8	23.1	21.9	***
<b>12th of April 2013</b>							
12/04/2013	00:00	0.5	25.4	18.2	23.8	23.4	***
***	01:00	***	***	***	***		***
***	02:00	***	***	***	***		***
***	03:00	***	***	***	***		***
***	04:00	***	***	***	***		***
***	05:00	***	***	***	***		***
***	06:00	***	***	***	***		***
***	07:00	***	***	***	***		***
***	08:00	***	***	***	***		***
12/04/2013	09:00	0.8	28.5	12.7	35.0	36.8	***
12/04/2013	10:00	2.4	30.4	10.1	33.1	34.8	***
12/04/2013	11:00	1.1	31.6	8.3	45.8	50.2	***
12/04/2013	12:00	0.0	37.9	5.4	48.8	48.8	***
12/04/2013	13:00	0.0	35.2	9.0	48.4	48.4	***
12/04/2013	14:00	1.6	35.8	6.7	46.2	50.4	***
12/04/2013	15:00	0.8	36.1	4.1	47.9	50.8	***
12/04/2013	16:00	0.0	35.1	7.5	44.3	44.3	***
12/04/2013	17:00	0.9	36.2	4.0	35.2	34.9	***
12/04/2013	18:00	1.9	35.4	3.6	33.8	33.0	***
12/04/2013	19:00	2.7	32.9	9.1	31.3	30.2	***
12/04/2013	20:00	1.1	32.5	9.8	31.6	31.3	***
12/04/2013	21:00	1.9	30.0	11.4	29.1	28.6	***
12/04/2013	22:00	0.4	29.6	12.1	29.5	29.5	***
12/04/2013	23:00	0.6	29.7	11.7	30.1	30.2	***

**A6. 12: Detailed hourly microclimatic data in the low urban density area (summer).**

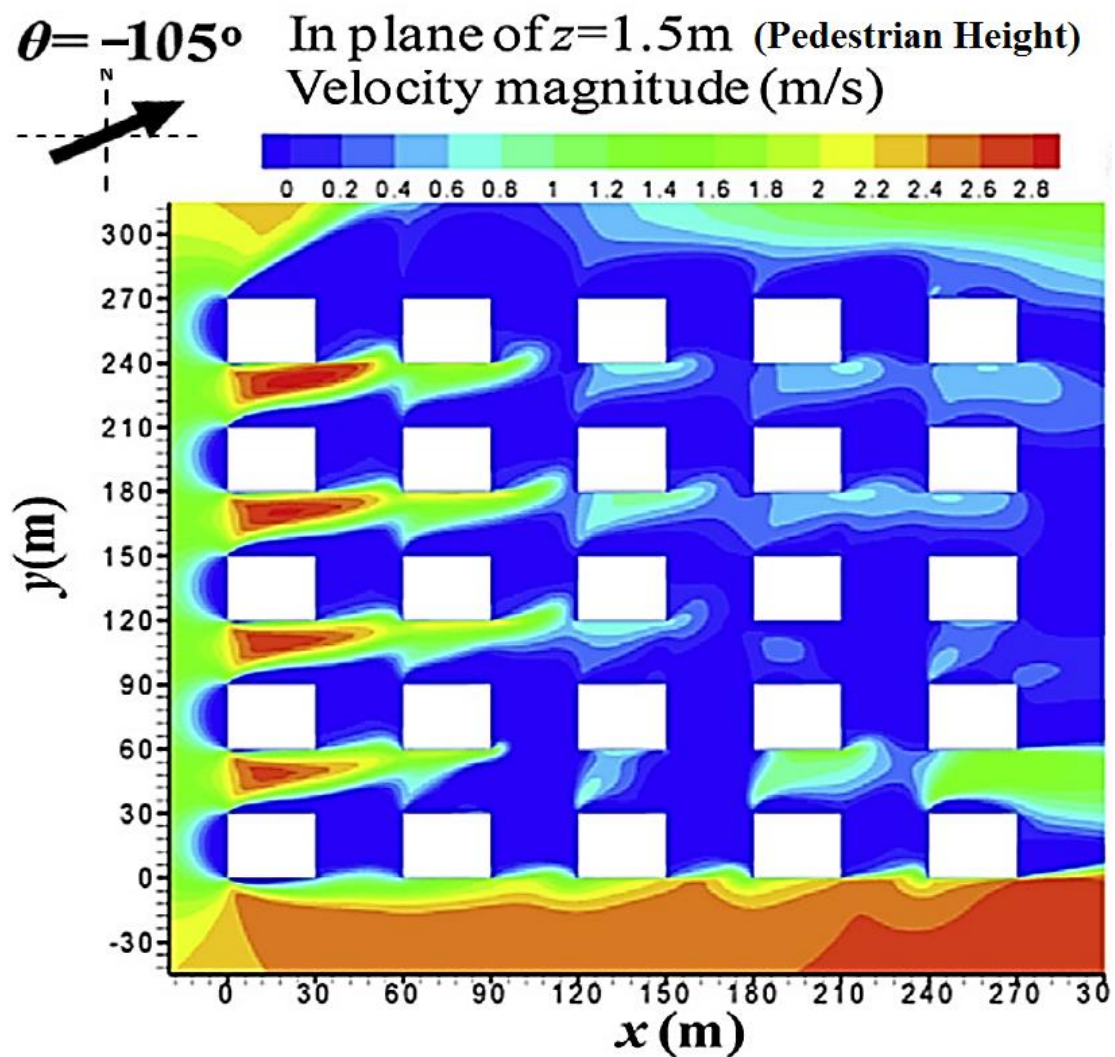
<b>Field measurements for Summer (17th to 22nd of June 2013) in the Low Urban Density Area (Case 3)</b>							
<b>Date</b>	<b>Time</b>	<b>Wind (m/s)</b>	<b>Ta (°C)</b>	<b>RH (%)</b>	<b>Tg (°C)</b>	<b>MRT (°C)</b>	<b>Wind Direction</b>
<b>17th of June 2013</b>							
17/06/2013	00:00	1.9	32.1	14.2	31.1	30.6	***
17/06/2013	01:00	1.3	31.3	15.5	30.1	29.6	***
17/06/2013	02:00	0.4	30.7	16.7	29.8	29.6	***
17/06/2013	03:00	0.8	29.9	18.3	28.8	28.5	***
17/06/2013	04:00	0.7	28.2	20.2	27.9	27.8	***
17/06/2013	05:00	1.3	27.4	20.8	27.0	26.8	***
17/06/2013	06:00	1.3	27.4	20.8	27.0	26.8	***
17/06/2013	07:00	1.3	27.7	22.1	28.2	28.4	***
17/06/2013	08:00	0.5	30.5	17.3	31.8	32.1	***
17/06/2013	09:00	1.2	31.6	19.3	34.2	35.2	WSW
17/06/2013	10:00	0.0	34.1	18.5	45.7	45.7	WNW
17/06/2013	11:00	0.7	36.8	14.7	48.7	51.4	NNW
17/06/2013	12:00	2.9	36.0	10.5	48.5	56.0	SW
17/06/2013	13:00	1.6	38.3	3.5	49.3	53.7	W
17/06/2013	14:00	5.1	38.5	4.7	49.6	59.3	NW
17/06/2013	15:00	2.5	39.1	5.0	48.4	53.5	NNW
17/06/2013	16:00	3.2	38.0	5.8	71.3	88.1	WSW
17/06/2013	17:00	3.0	37.5	5.9	40.5	42.5	SW
17/06/2013	18:00	2.0	37.0	7.6	37.7	38.1	SW
17/06/2013	19:00	2.4	35.6	8.7	35.5	35.4	WSW
17/06/2013	20:00	3.3	34.8	11.9	34.6	34.4	SW
17/06/2013	21:00	1.7	34.3	13.2	33.9	33.7	S
17/06/2013	22:00	3.0	33.9	14.5	33.1	32.5	SSW
17/06/2013	23:00	2.2	32.2	19.8	32.0	31.9	WNW
<b>18th of June 2013</b>							
18/06/2013	00:00	0.5	32.0	20.3	31.1	30.9	***
18/06/2013	01:00	1.2	31.5	19.0	30.4	30.0	***
18/06/2013	02:00	0.9	30.1	18.8	29.3	29.0	***
18/06/2013	03:00	1.6	30.2	17.8	29.2	28.7	***
18/06/2013	04:00	0.6	29.0	19.4	28.6	28.5	***
18/06/2013	05:00	0.0	27.4	22.4	26.3	26.3	***
18/06/2013	06:00	0.4	27.0	23.4	26.5	26.4	***
18/06/2013	07:00	0.6	27.9	22.3	28.0	28.0	***
18/06/2013	08:00	0.0	30.3	19.3	31.5	31.5	***
18/06/2013	09:00	1.0	31.8	17.3	34.0	34.7	NW
18/06/2013	10:00	2.0	33.9	12.8	46.5	52.4	NW
18/06/2013	11:00	1.5	35.0	9.8	46.2	50.6	S
18/06/2013	12:00	0.8	37.1	9.3	49.9	53.0	N
18/06/2013	13:00	1.8	37.7	8.5	49.3	54.3	SSW
18/06/2013	14:00	2.8	38.3	8.9	47.8	53.4	WSW
18/06/2013	15:00	4.1	38.2	9.5	47.2	54.2	S
18/06/2013	16:00	3.0	37.5	8.9	47.3	53.4	SW
18/06/2013	17:00	3.3	37.2	9.0	40.7	43.2	SSW
18/06/2013	18:00	0.0	36.9	11.6	37.6	37.6	SSW
18/06/2013	19:00	2.0	35.3	10.5	35.2	35.1	S
18/06/2013	20:00	1.9	35.1	11.4	34.1	33.6	SW
18/06/2013	21:00	2.6	33.8	13.3	33.1	32.6	SSW
18/06/2013	22:00	2.2	33.0	12.0	32.5	32.2	WSW
18/06/2013	23:00	0.6	33.7	13.0	32.4	32.1	SSW

Date	Time	Winds. (m/s)	Ta (°C)	RH (%)	Tg (°C)	MRT (°C)	Wind Direction
<b>19th of June 2013</b>							
19/06/2013	00:00	0.0	31.1	14.8	30.7	30.7	***
19/06/2013	01:00	1.0	31.3	15.7	30.7	30.5	***
19/06/2013	02:00	0.0	30.2	17.4	30.0	30.0	***
19/06/2013	03:00	0.0	29.1	19.1	28.2	28.2	***
19/06/2013	04:00	0.0	27.9	22.5	27.0	27.0	***
19/06/2013	05:00	0.0	26.4	23.6	25.7	25.7	***
19/06/2013	06:00	0.8	26.2	22.3	25.8	25.7	***
19/06/2013	07:00	0.4	26.0	27.4	26.7	26.8	***
19/06/2013	08:00	0.0	30.1	23.3	31.8	31.8	***
19/06/2013	09:00	1.3	32.2	15.9	33.6	34.2	WNW
19/06/2013	10:00	1.2	34.2	13.1	45.5	49.3	WNW
19/06/2013	11:00	1.7	35.4	12.1	47.4	52.4	W
19/06/2013	12:00	3.9	36.0	11.7	48.6	57.8	NNW
19/06/2013	13:00	3.0	36.8	11.2	48.1	55.1	SW
19/06/2013	14:00	2.4	38.3	10.7	50.8	57.2	SSW
19/06/2013	15:00	3.1	37.4	10.1	50.4	58.4	SSW
19/06/2013	16:00	0.3	38.4	10.6	49.2	50.5	WSW
19/06/2013	17:00	2.9	37.0	10.1	39.6	41.3	SSW
19/06/2013	18:00	3.7	36.2	11.4	37.8	39.1	SW
19/06/2013	19:00	3.6	35.7	11.2	35.5	35.3	SW
19/06/2013	20:00	1.3	35.2	12.1	34.6	34.4	SSW
19/06/2013	21:00	2.6	34.4	12.5	33.7	33.2	SSW
19/06/2013	22:00	1.3	33.4	15.5	33.1	33.0	S
19/06/2013	23:00	***	***	***	***	***	SSW
<b>20th of June 2013</b>							
20/06/2013	00:00	1.3	32.3	15.1	31.6	31.3	***
20/06/2013	01:00	1.0	31.9	15.3	31.1	30.8	***
20/06/2013	02:00	0.9	31.6	14.9	30.7	30.4	***
20/06/2013	03:00	1.0	31.0	16.4	29.4	28.8	***
20/06/2013	04:00	0.0	28.6	21.3	27.8	27.8	***
20/06/2013	05:00	0.0	27.8	23.1	27.0	27.0	***
20/06/2013	06:00	0.0	26.7	25.2	26.1	26.1	***
20/06/2013	07:00	0.7	28.0	23.4	27.8	27.7	***
20/06/2013	08:00	1.2	32.1	19.5	32.8	33.1	***
20/06/2013	09:00	0.8	33.1	15.5	34.7	35.2	NW
20/06/2013	10:00	0.9	35.5	12.2	47.2	50.4	WSW
20/06/2013	11:00	0.7	36.4	11.8	48.0	50.6	W
20/06/2013	12:00	0.4	36.4	12.1	46.9	48.2	NW
20/06/2013	13:00	0.5	36.4	12.0	47.5	49.4	NNW
20/06/2013	14:00	0.3	36.3	12.2	46.6	47.6	NW
20/06/2013	15:00	0.1	36.3	12.3	46.2	46.7	N
20/06/2013	16:00	0.0	36.3	12.4	45.8	45.8	NNW
20/06/2013	17:00	0.9	38.4	10.1	40.8	41.5	NW
20/06/2013	18:00	2.4	37.7	10.2	39.2	40.1	SW
20/06/2013	19:00	2.1	36.0	12.0	36.6	36.9	SW
20/06/2013	20:00	3.2	35.2	12.0	35.1	35.0	WSW
20/06/2013	21:00	5.8	34.5	12.3	34.2	33.9	SW
20/06/2013	22:00	1.4	34.2	13.1	33.6	33.3	NW
20/06/2013	23:00	1.5	33.7	13.5	33.1	32.8	WSW

Date	Time	Winds. (m/s)	Ta (°C)	RH (%)	Tg (°C)	MRT (°C)	Wind Direction
<b>21st of June 2013</b>							
21/06/2013	00:00	***	***	***	***	***	***
21/06/2013	01:00	***	***	***	***	***	***
21/06/2013	02:00	***	***	***	***	***	***
21/06/2013	03:00	***	***	***	***	***	***
21/06/2013	04:00	***	***	***	***	***	***
21/06/2013	05:00	***	***	***	***	***	***
21/06/2013	06:00	***	***	***	***	***	***
21/06/2013	07:00	***	***	***	***	***	***
21/06/2013	08:00	***	***	***	***	***	***
21/06/2013	09:00	0.0	33.7	11.8	35.0	35.0	NE
21/06/2013	10:00	2.3	35.4	10.5	48.5	55.2	NW
21/06/2013	11:00	0.5	36.1	11.0	48.4	50.6	NW
21/06/2013	12:00	1.5	37.6	9.1	49.5	54.0	SW
21/06/2013	13:00	0.6	37.6	8.2	53.9	57.0	WNW
21/06/2013	14:00	2.3	37.4	8.4	51.4	58.3	NNW
21/06/2013	15:00	0.9	40.9	8.7	52.8	55.8	NNE
21/06/2013	16:00	0.4	38.2	9.0	48.5	50.1	NNW
21/06/2013	17:00	***	***	***	***	***	NW
21/06/2013	18:00	2.0	37.9	9.1	39.9	40.9	NW
21/06/2013	19:00	2.2	37.2	9.5	37.2	37.2	NNE
21/06/2013	20:00	3.8	36.0	11.0	35.5	35.1	SW
21/06/2013	21:00	0.4	35.0	12.6	34.7	34.6	SW
21/06/2013	22:00	1.1	34.3	14.4	34.3	34.3	WNW
21/06/2013	23:00	0.0	34.1	13.1	33.4	33.4	SW
<b>22nd of June 2013</b>							
22/06/2013	00:00	***	***	***	***	***	***
22/06/2013	01:00	***	***	***	***	***	***
22/06/2013	02:00	***	***	***	***	***	***
22/06/2013	03:00	***	***	***	***	***	***
22/06/2013	04:00	***	***	***	***	***	***
22/06/2013	05:00	***	***	***	***	***	***
22/06/2013	06:00	***	***	***	***	***	***
22/06/2013	07:00	***	***	***	***	***	***
22/06/2013	08:00	***	***	***	***	***	***
22/06/2013	09:00	0.4	34.5	13.8	35.6	35.8	SE
22/06/2013	10:00	5.5	34.9	12.2	47.7	59.6	NNW
22/06/2013	11:00	0.5	36.1	11.0	48.4	50.6	NW
22/06/2013	12:00	0.9	38.5	10.5	51.0	54.3	NNW
22/06/2013	13:00	2.0	39.0	9.6	54.9	61.8	SSE
22/06/2013	14:00	0.9	39.7	8.6	53.8	57.4	E
22/06/2013	15:00	0.7	41.1	9.0	53.1	55.7	NW
22/06/2013	16:00	3.3	39.5	8.9	48.9	55.1	SSW
22/06/2013	17:00	6.2	38.2	8.8	41.3	44.8	SW
22/06/2013	18:00	2.1	38.2	9.4	39.7	40.5	SW
22/06/2013	19:00	3.2	37.5	9.3	37.2	37.0	SW
22/06/2013	20:00	***	***	***	***	***	SW
22/06/2013	21:00	***	***	***	***	***	SSW
22/06/2013	22:00	***	***	***	***	***	SW
22/06/2013	23:00	***	***	***	***	***	SSW

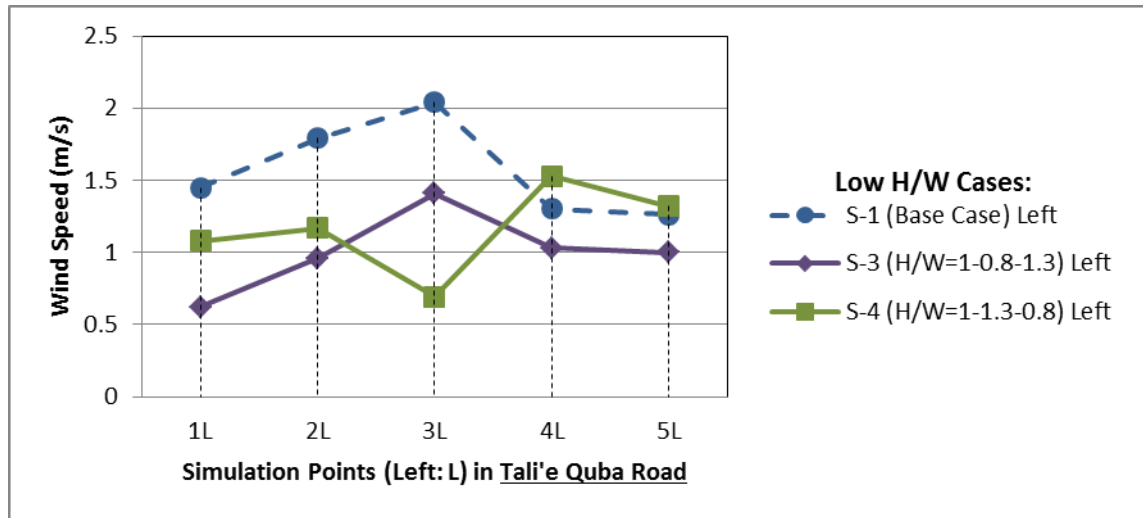


In the S-2 model (symmetrical aspect ratio scenario), the wind velocity in the windward canyon (between the first two rows of the buildings, i.e. Tali'e Quba Road) is higher compared to the leeward canyon (between the second and third rows of the buildings, i.e. Nazil Quba Road) (refer to section 7.3.1). This result has been confirmed in previous investigations on symmetrical rows of buildings, including a study by Yuan and Ng (2012) and Hang et al. (2015). According to Hang et al. (2015), the wind speed in the urban area was accelerated in the windward canyon when the prevailing wind direction was approximately perpendicular to the canyon (i.e.  $-105^\circ$  from north), while wind speed was significantly decreased at the leeward canyons, as illustrated in A7.1a.

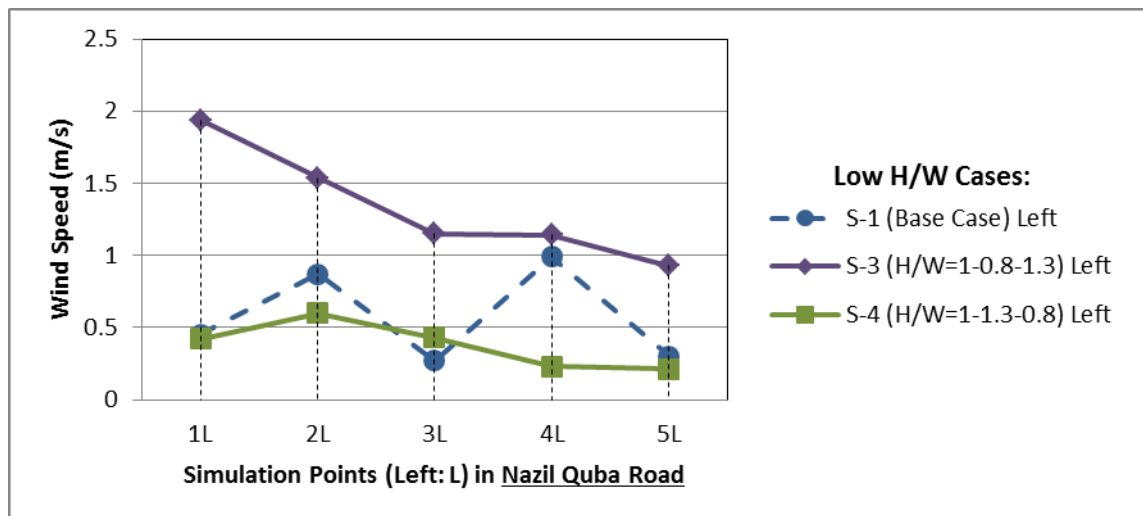


A7. 1: Contours of velocity magnitude for symmetrical urban canyons with  $H/W$  of 1, wind direction of  $-105^\circ$  from north. The graph shows lower wind velocities in leeward canyons compared to windward canyon. Source: adapted from Hang et al. (2015).

**A7: Appendices for Chapter 7 (From A7.2 to A7.7): Results of Wind Velocity in the Low Aspect Ratio Cases (S-3 and S-4)**

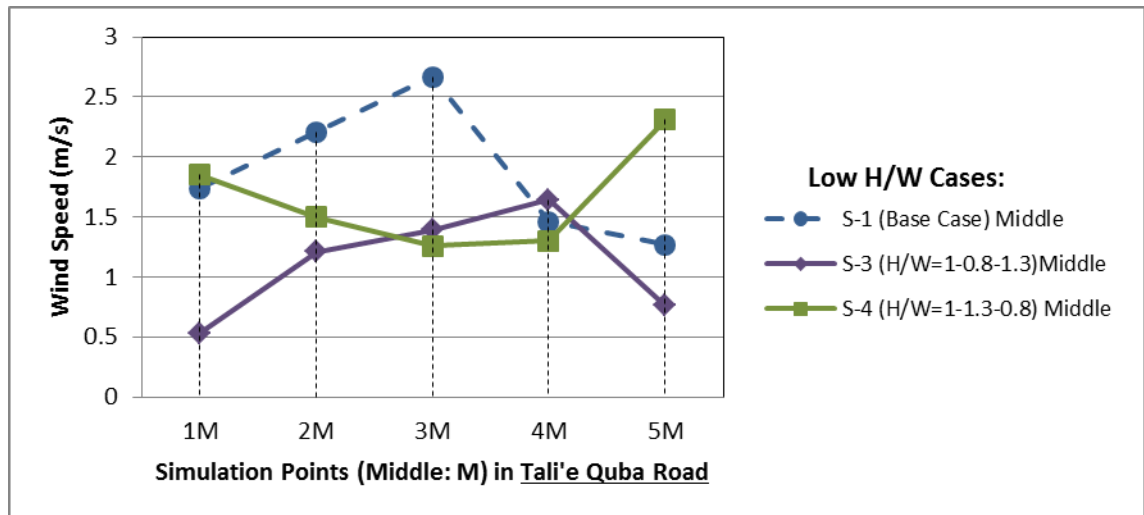


A7. 2: Wind velocity at the left (leeward) simulation points in the low asymmetrical aspect ratio scenarios, particularly in the Tali'e Quba Road, and compared with the base case S-1 scenario.

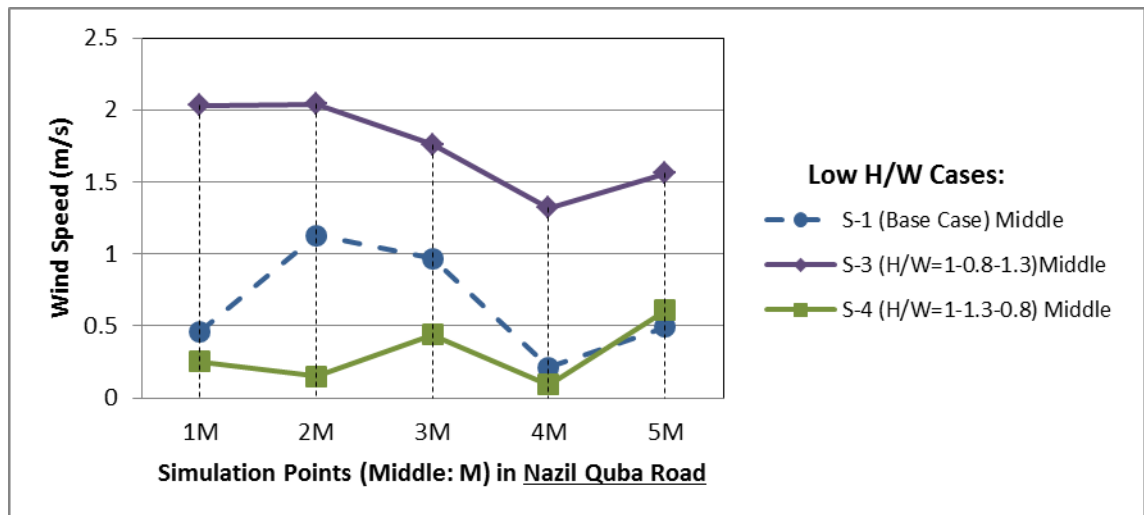


A7. 3: Wind velocity at the left (leeward) simulation points in the low asymmetrical aspect ratio scenarios, particularly in the Nazil Quba Road, and compared with the base case S-1 scenario.

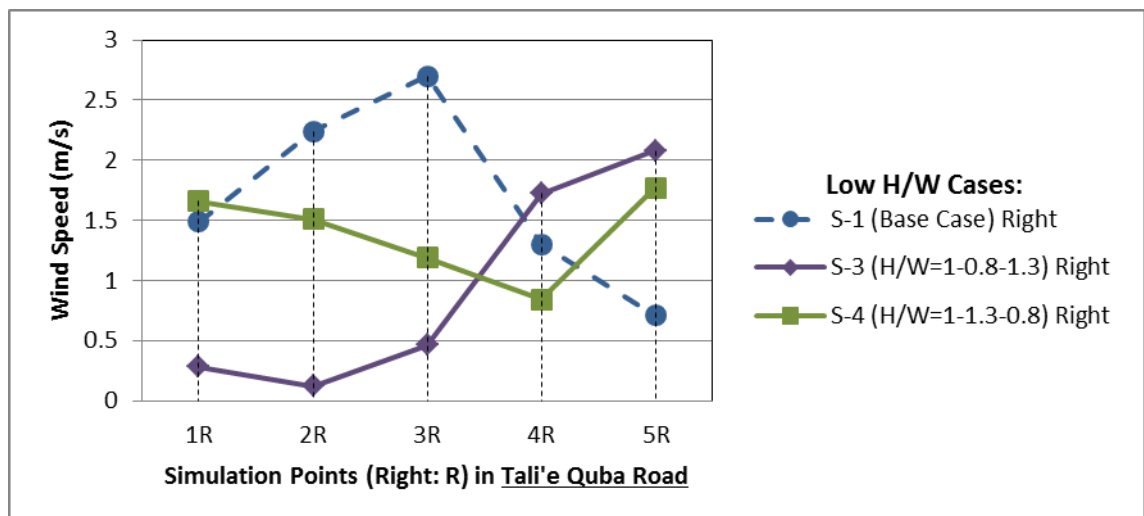




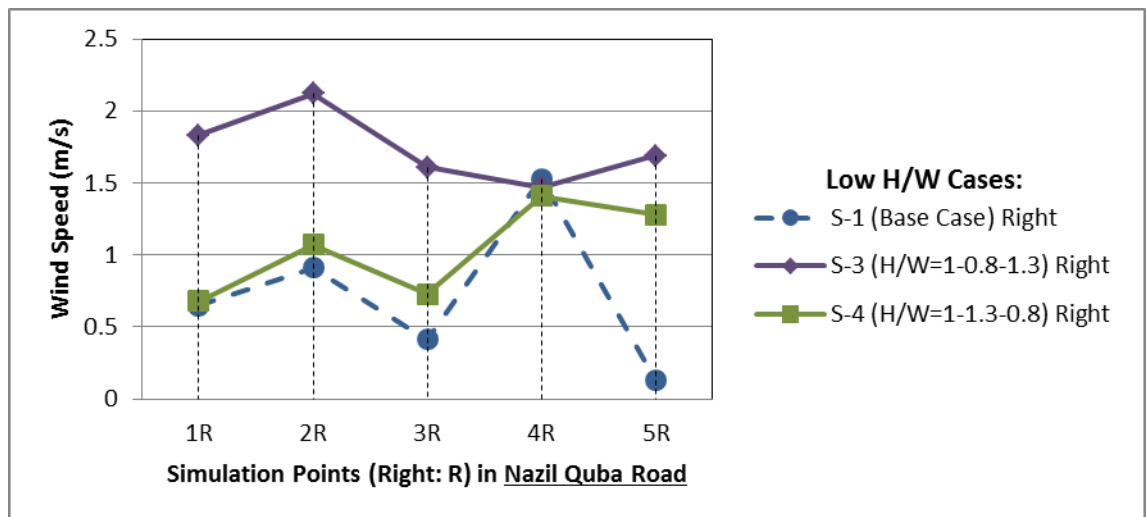
A7. 4: Wind velocity at the middle simulation points in the low asymmetrical aspect ratio scenarios, particularly in the Tali'e Quba Road, and compared with the base case S-1 scenario.



A7. 5: Wind velocity at the middle simulation points in the low asymmetrical aspect ratio scenarios, particularly in the Nazil Quba Road, and compared with the base case S-1 scenario.

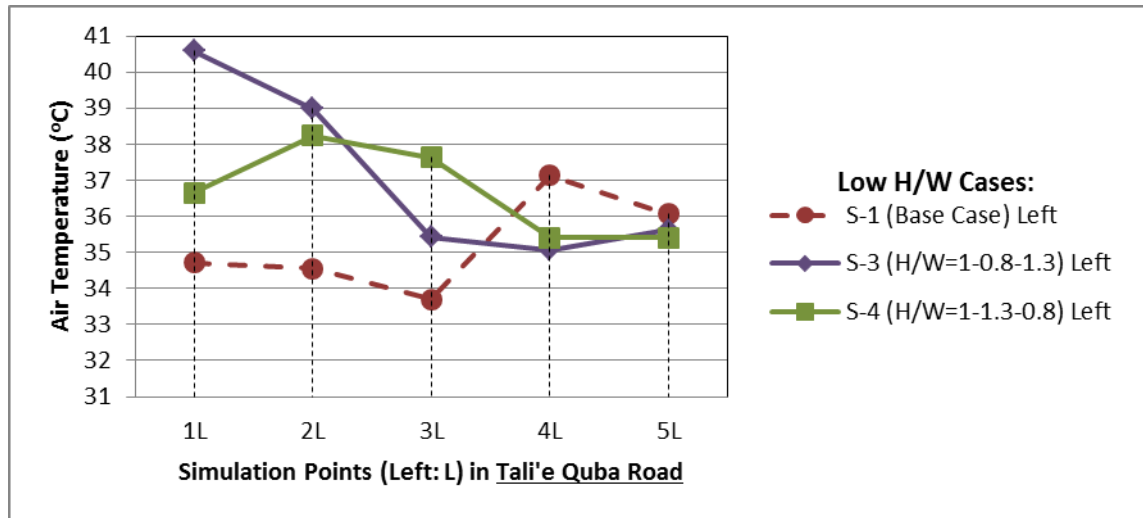


A7. 6: Wind velocity at the right (windward) simulation points in the low asymmetrical aspect ratio scenarios, particularly in the Tali'e Quba Road, and compared with the base case S-1 scenario.

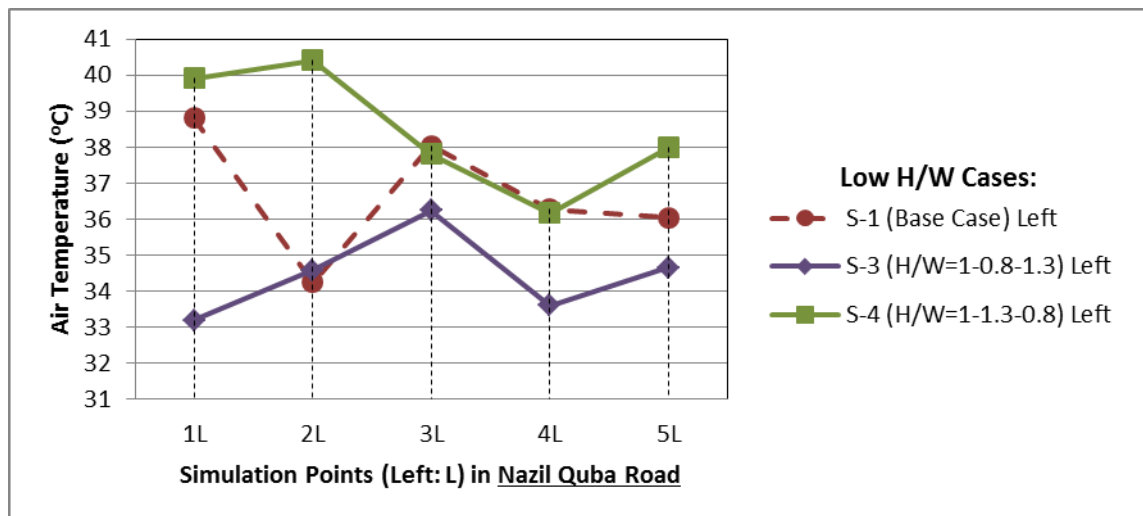


A7. 7: Wind velocity at the right (windward) simulation points in the low asymmetrical aspect ratio scenarios, particularly in the Nazil Quba Road, and compared with the base case S-1 scenario.

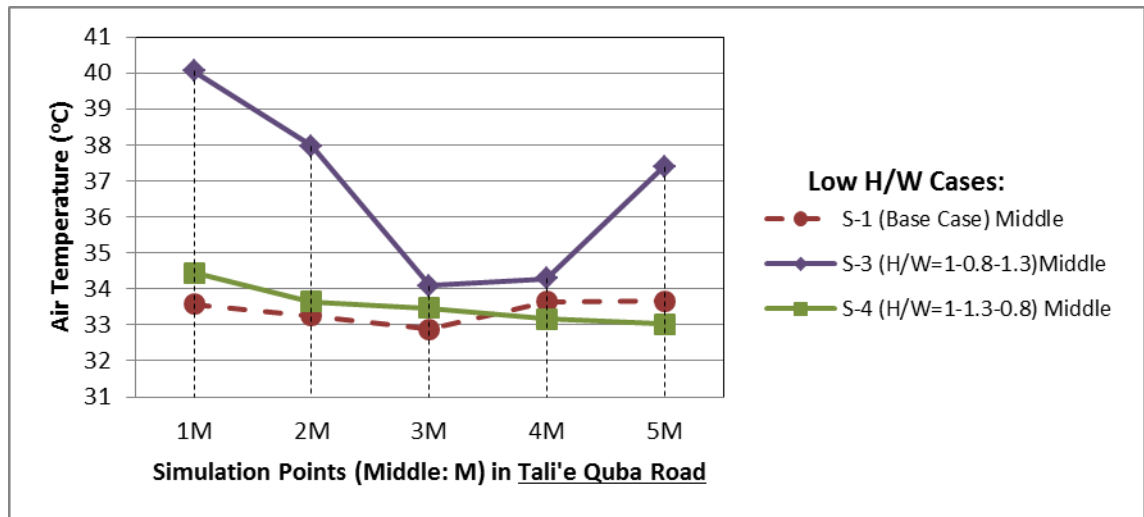
**A7: Appendices for Chapter 7 (From A7.8 to A7.13): Results of Air Temperature in the Low Aspect Ratio Cases (S-3 and S-4)**



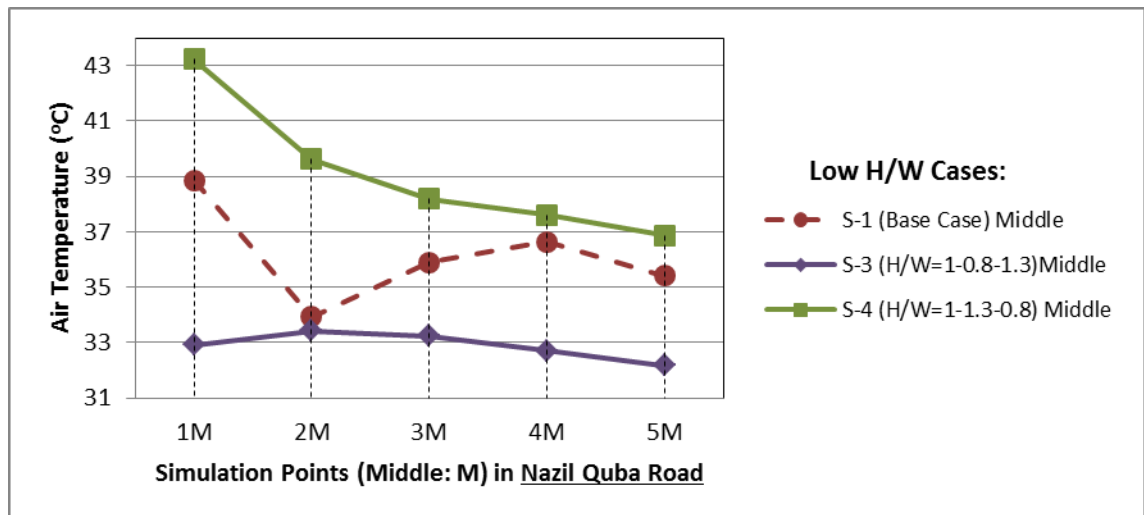
A7. 8: Air temperature at the left (leeward) simulation points in the low asymmetrical aspect ratio scenarios, particularly in the Tali'e Quba Road, and compared with the base case S-1 scenario.



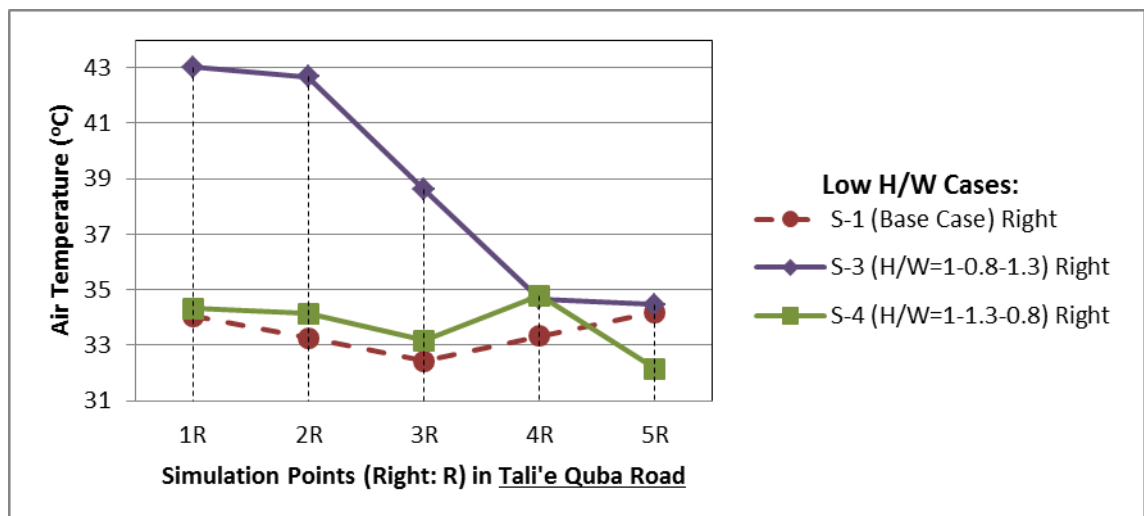
A7. 9: Air temperature at the left (leeward) simulation points in the low asymmetrical aspect ratio scenarios, particularly in the Nazil Quba Road, and compared with the base case S-1 scenario.



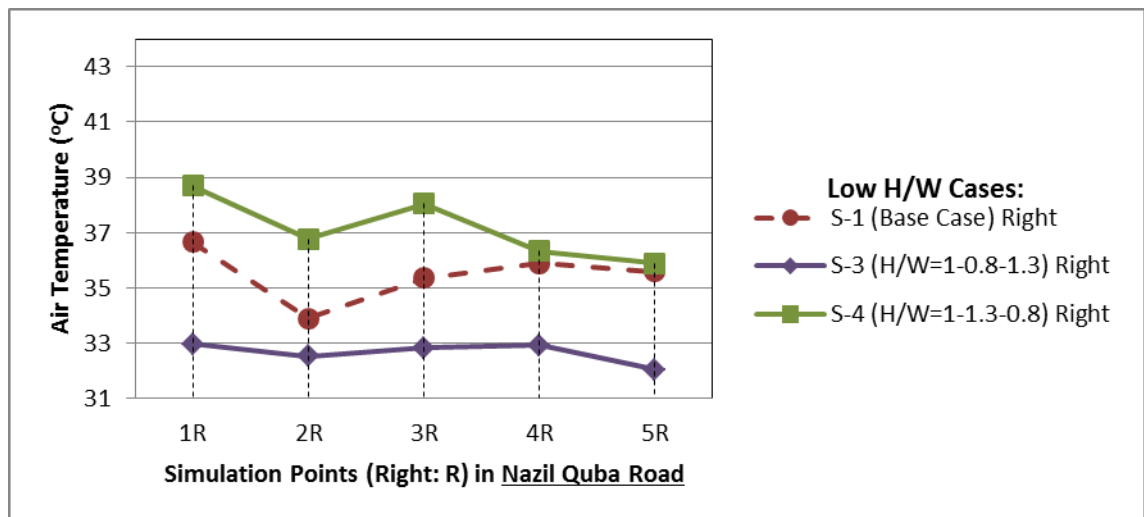
A7. 10: Air temperature at the middle simulation points in the low asymmetrical aspect ratio scenarios, particularly in the Tali'e Quba Road, and compared with the base case S-1 scenario.



A7. 11: Air temperature at the middle simulation points in the low asymmetrical aspect ratio scenarios, particularly in the Nazil Quba Road, and compared with the base case S-1 scenario.

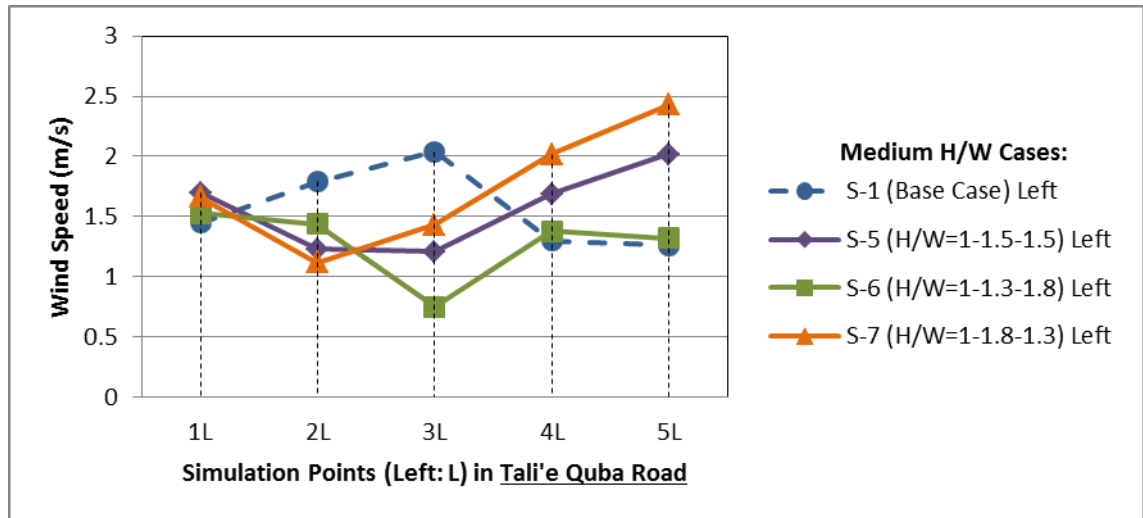


A7. 12: Air temperature at the right (windward) simulation points in the low asymmetrical aspect ratio scenarios, particularly in the Tali'e Quba Road, and compared with the base case S-1

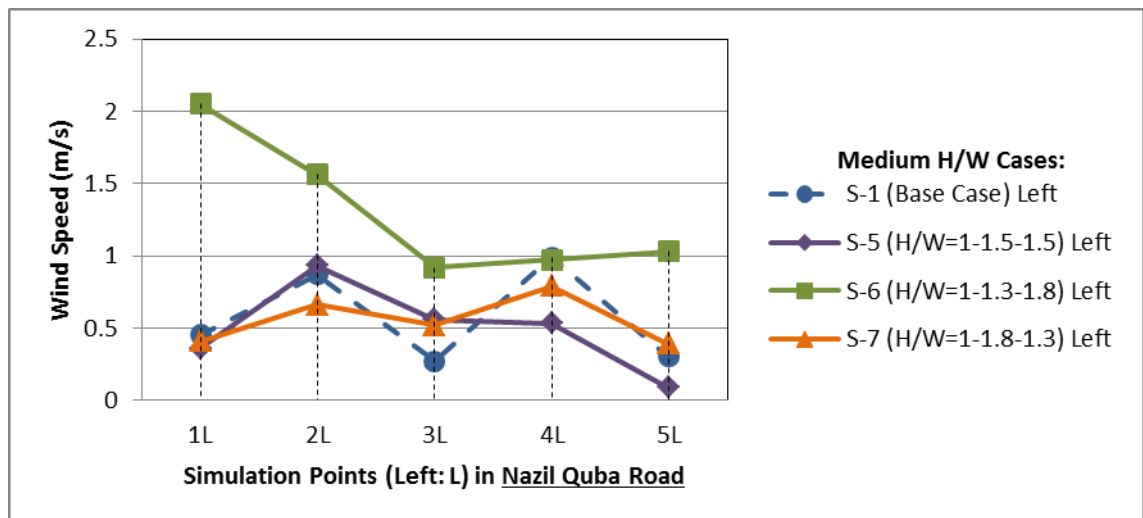


A7. 13: Air temperature at the right (windward) simulation points in the low asymmetrical aspect ratio scenarios, particularly in the Nazil Quba Road, and compared with the base case S-1

**A7: Appendices for Chapter 7 (From A7.14 to A7.19): Results Wind Velocity in the Medium Aspect Ratio Cases (S-5, S-6, and S-7)**

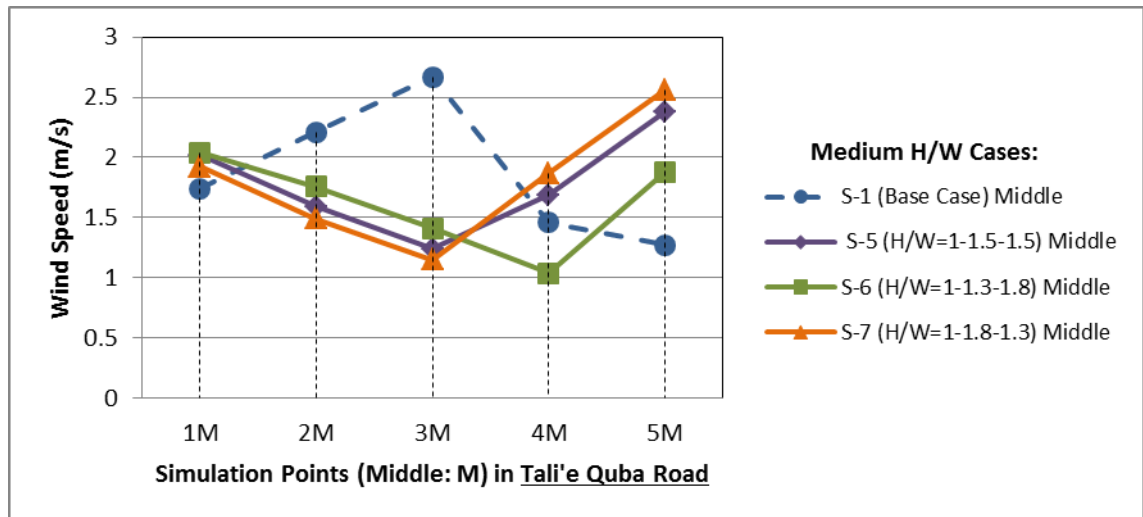


A7. 14: Wind velocity at the left (leeward) simulation points in the medium asymmetrical aspect ratio scenarios in the Tali'e Quba Road, and compared with the base case S-1 scenario.

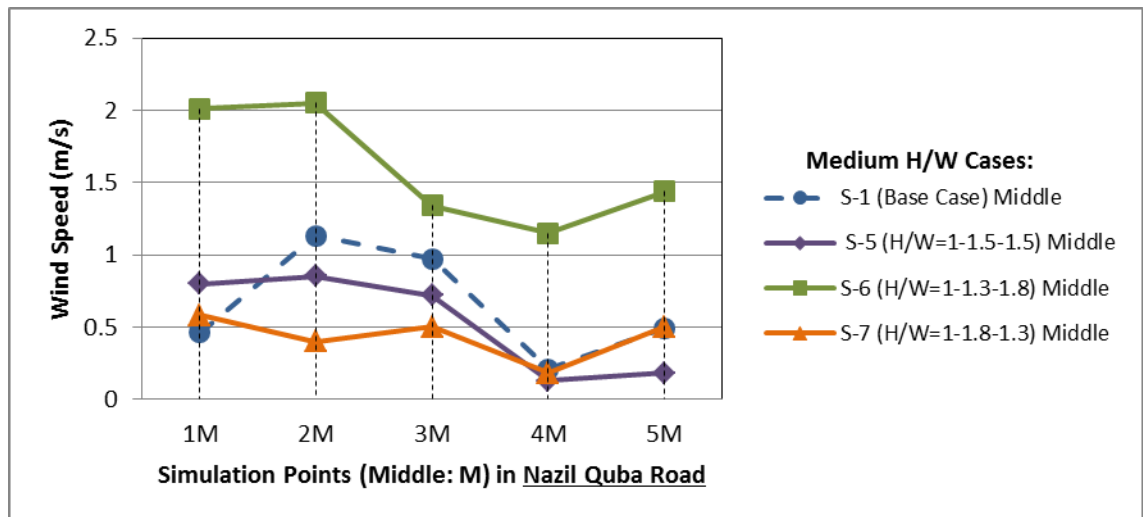


A7. 15: Wind velocity at the left (leeward) simulation points in the medium asymmetrical aspect ratio scenarios in the Nazil Quba Road, and compared with the base case S-1 scenario.

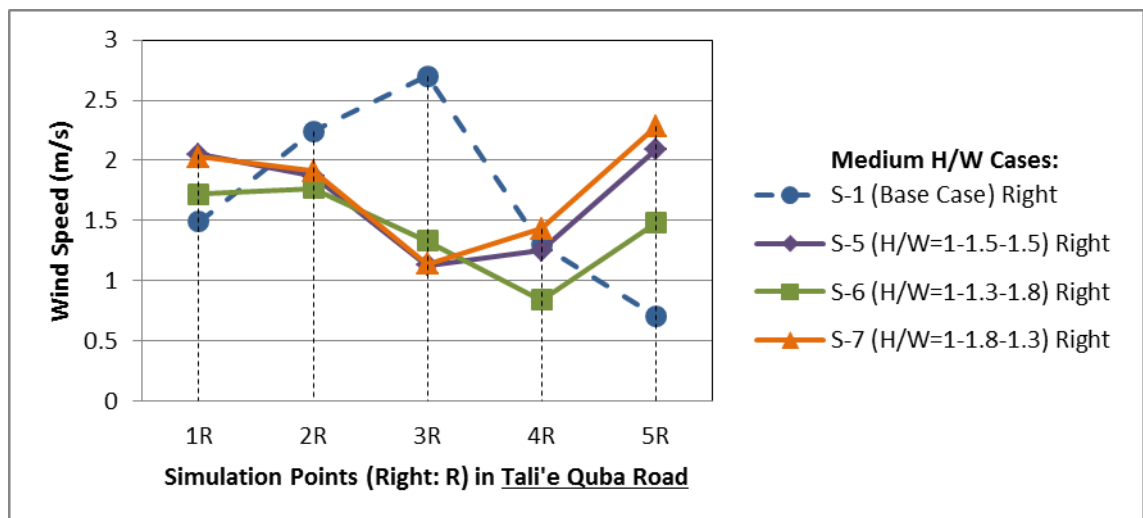




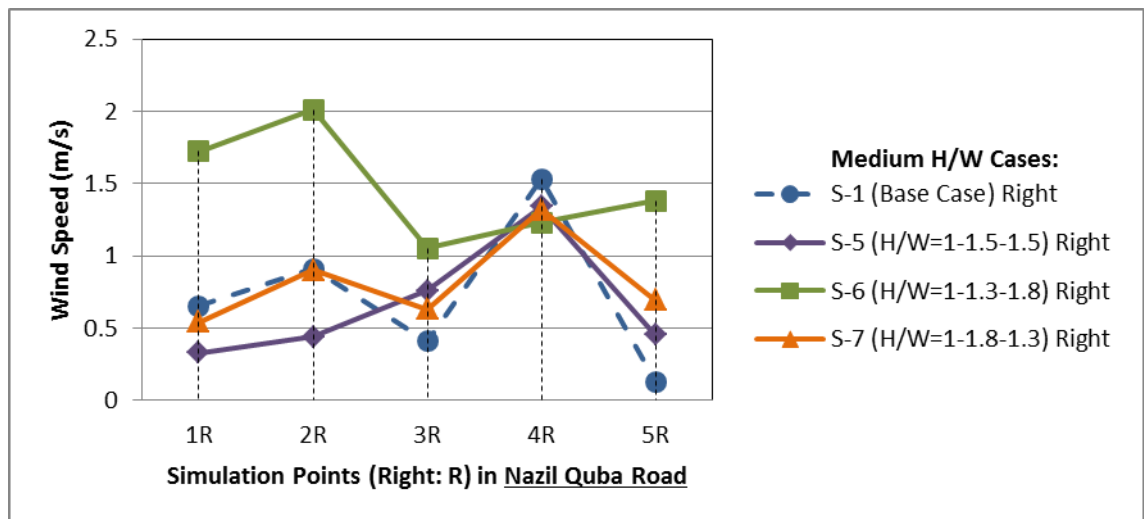
A7. 16: Wind velocity at the middle simulation points in the medium asymmetrical aspect ratio scenarios in the Tali'e Quba Road, and compared with the base case S-1 scenario.



A7. 17: Wind velocity at the middle simulation points in the medium asymmetrical aspect ratio scenarios in the Nazil Quba Road, and compared with the base case S-1 scenario.

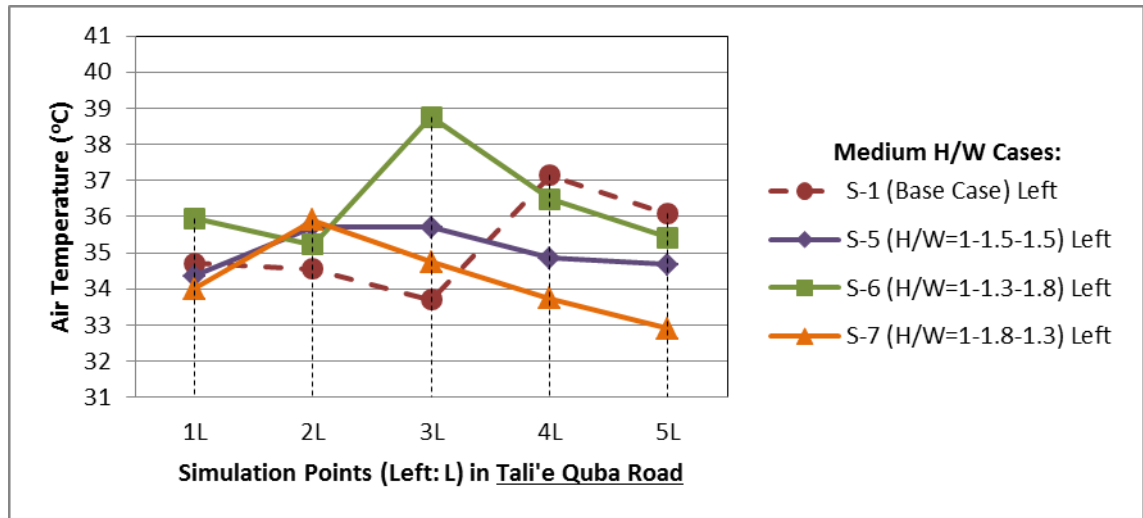


A7. 18: Wind velocity at the right (windward) simulation points in the medium asymmetrical aspect ratio scenarios in the Tali'e Quba Road, and compared with the base case S-1 scenario.

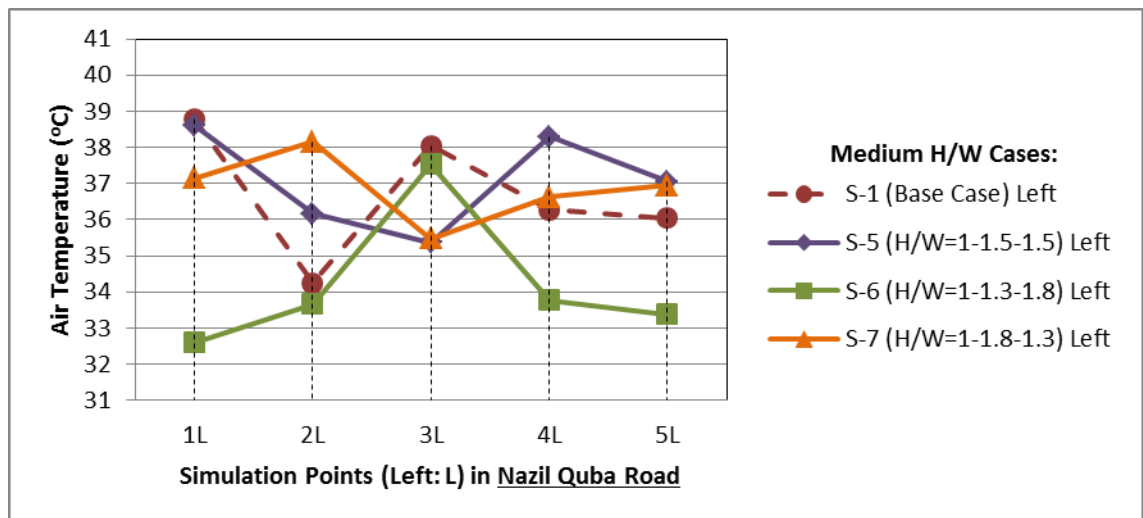


A7. 19: Wind velocity at the right (windward) simulation points in the medium asymmetrical aspect ratio scenarios in the Nazil Quba Road, and compared with the base case S-1 scenario.

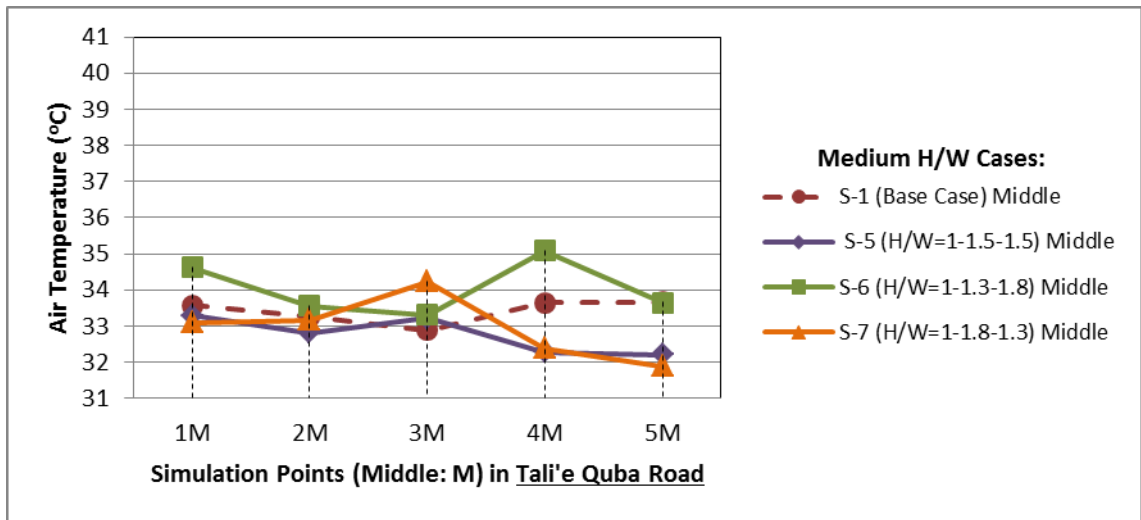
**A7: Appendices for Chapter 7 (From A7.20 to A7.25): Results of Air Temperature in the Medium Aspect Ratio Cases (S-5, S-6, and S-7)**



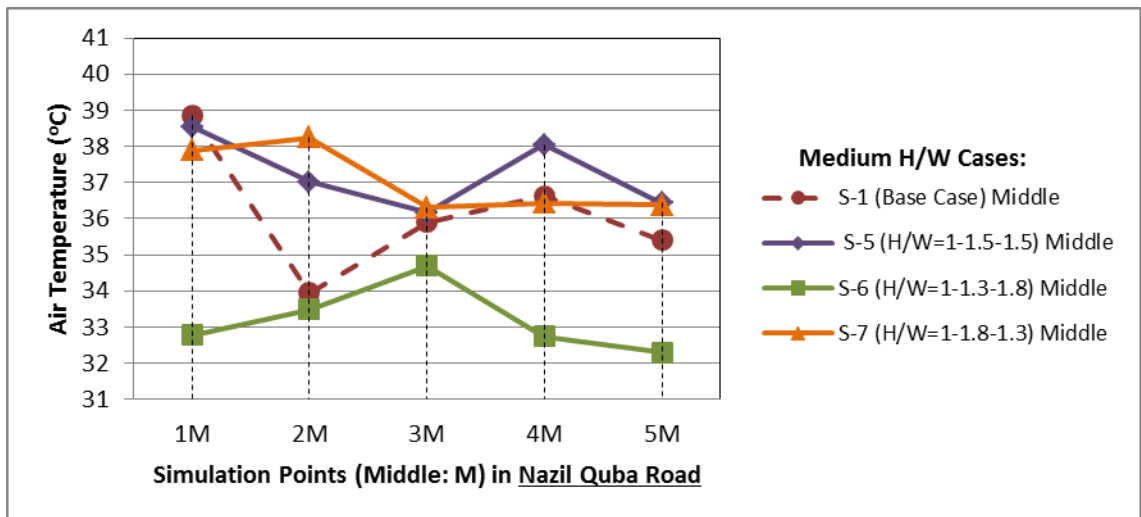
A7. 20: Air temperature at the left (leeward) simulation points in the medium asymmetrical aspect ratio scenarios in the Tali'e Quba Road, and compared with the base case S-1 scenario.



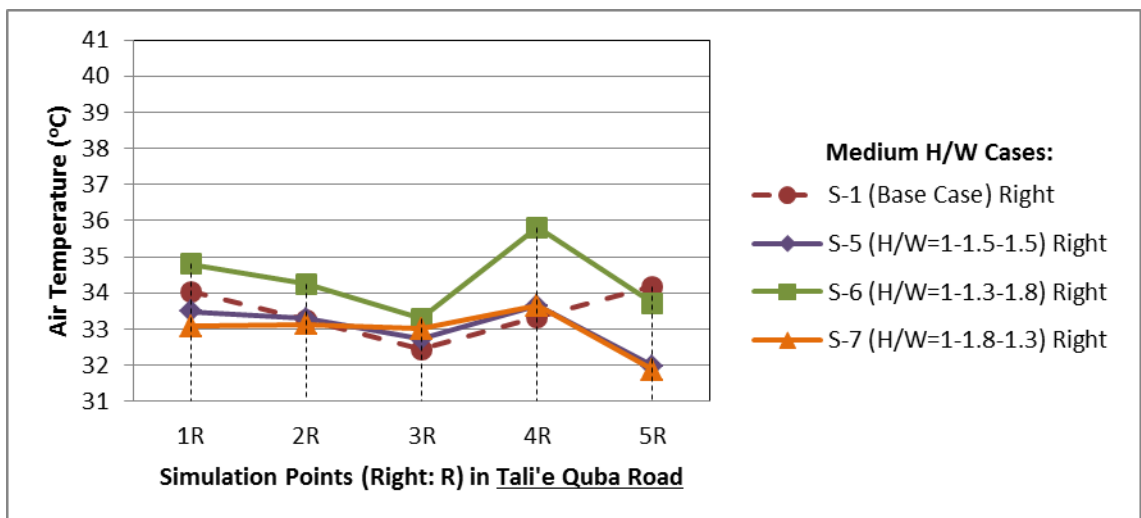
A7. 21: Air temperature at the left (leeward) simulation points in the medium asymmetrical aspect ratio scenarios in the Nazil Quba Road, and compared with the base case S-1 scenario.



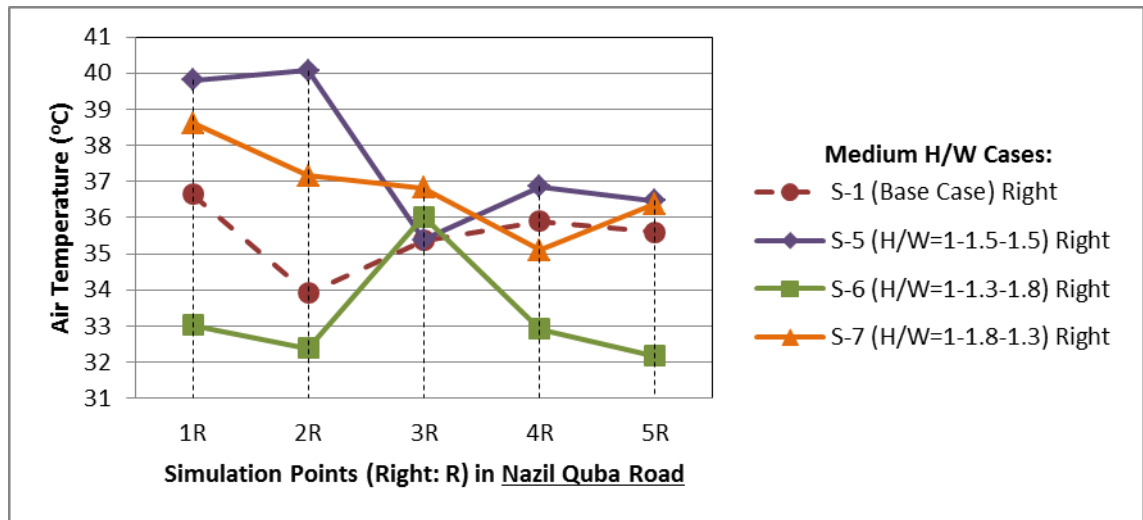
A7. 22: Air temperature at the middle simulation points in the medium asymmetrical aspect ratio scenarios in the Tali'e Quba Road, and compared with the base case S-1 scenario.



A7. 23: Air temperature at the middle simulation points in the medium asymmetrical aspect ratio scenarios in the Nazil Quba Road, and compared with the base case S-1 scenario.



A7. 24: Air temperature at the right (windward) simulation points in the medium asymmetrical aspect ratio scenarios in the Tali'e Quba Road, and compared with the base case S-1 scenario.

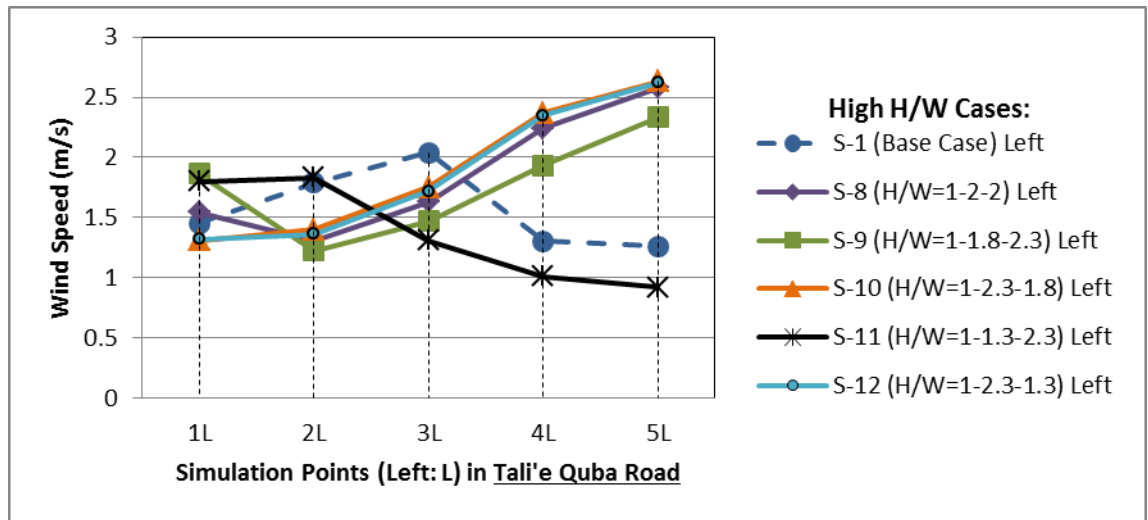


A7. 25: Air temperature at the right (windward) simulation points in the medium asymmetrical aspect ratio scenarios in the Nazil Quba Road, and compared with the base case S-1

Figures A7.26 and A7.27 demonstrate the wind flow patterns for the five measurement locations (1 through 5) in the Tali'e Quba Road (i.e. the windward canyon) and the Nazil Quba Road (i.e. the leeward canyon), respectively, for the higher type of multi-asymmetrical aspect ratio scenarios S-8, S-9, S-10, S-11 and S-12 scenarios compared to the base case, particularly for the left row of measurement points that are aligned near the leeward elevations at the pedestrian height. In the Tali'e Quba Road in Figure A7.26, it is found that the wind velocity patterns is different from the base case S-1 scenario but similar between most of the high aspect ratios scenarios (except in S-11 where lowest windward elevation). The highest wind velocity values in the Tali'e Quba Road is found in S-10 ( $H/W=1-2.3-1.8$ ), followed by S-12 ( $H/W=1-2.3-1.3$ ), then S-8 ( $H/W=1-2-2$ ), S-9 ( $H/W=1-1.8-2.3$ ) and the base case S-1, while S-11 ( $H/W=1-1.3-2.3$ ) is found to be the lowest, with average left measurement values of 1.9m/s, 1.9m/s, 1.9m/s, 1.8m/s, 1.6m/s and 1.4m/s, respectively. The reason for the S-11 being the lowest value is due to its lowest aspect ratio on windward elevation of the second row of buildings compared to the rest of the scenarios (e.g. Lee et al., 2013).

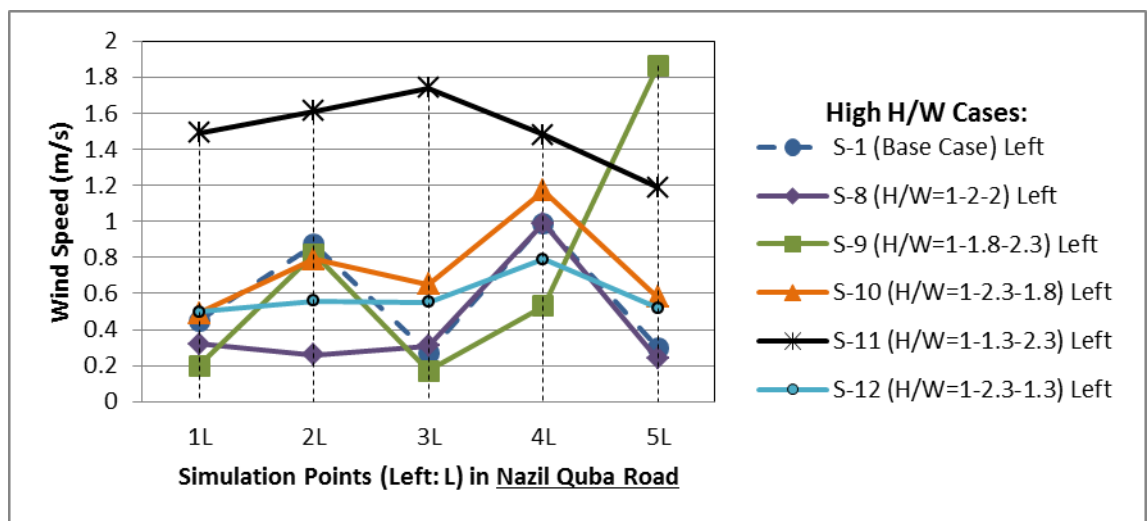
However, the overall difference in wind velocities between S-11 and the base case (S-1), at the left measurement points (near the leeward elevations) in the Tali'e Quba Road, is minor (i.e. 0.2m/s). Whereas the difference in wind velocity at measurement location 4 and 5 is high in S-10, S-12, S-8, and S-9 scenarios when compared to the base case, with approximate difference value reaches between 1.1m/s to 1.4m/s, which is due to higher aspect ratios on the second row of buildings, while the S-11 scenario with lower aspect ratio on the second row of buildings is having the lowest difference values at these two locations (difference value of 0.5m/s at location 4, and 0.9m/s at location 5). In addition, measurements locations 4 and 5 in the Tali'e Quba Road are positioned opposite to a widest windward elevation, particularly in the interest area, compared to the other measurement locations, which can capture more wind compared to the narrower windward elevations (e.g. Blocken and Carmeliet, 2004b).





A7. 26: Wind velocity at the left simulation points (leeward) in the high asymmetrical aspect ratio scenarios, particularly in the Tali'e Quba Road (between the first and the second rows of buildings).

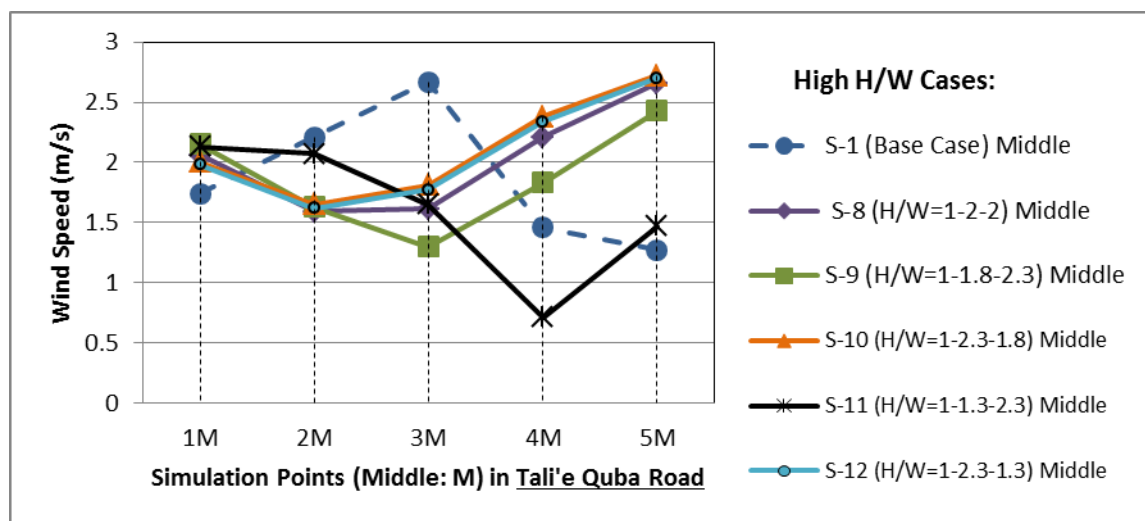
On the other hand, in the Nazil Quba road the wind velocities is found significantly higher in S-11 scenario when compared with the base case (S-1) at all the five measurement locations near the leeward walls (left points). The maximum difference found at location 3 with a difference value of 1.5m/s, followed by location 1, 5, 2 and 4 with a value of 1.0m/s, 0.9m/s, 0.7m/s and 0.5m/s, respectively. However, the rest of the scenarios (i.e. S-8, S-9, S-10, and S-12) have minor difference in wind velocity values in comparison to the base case.



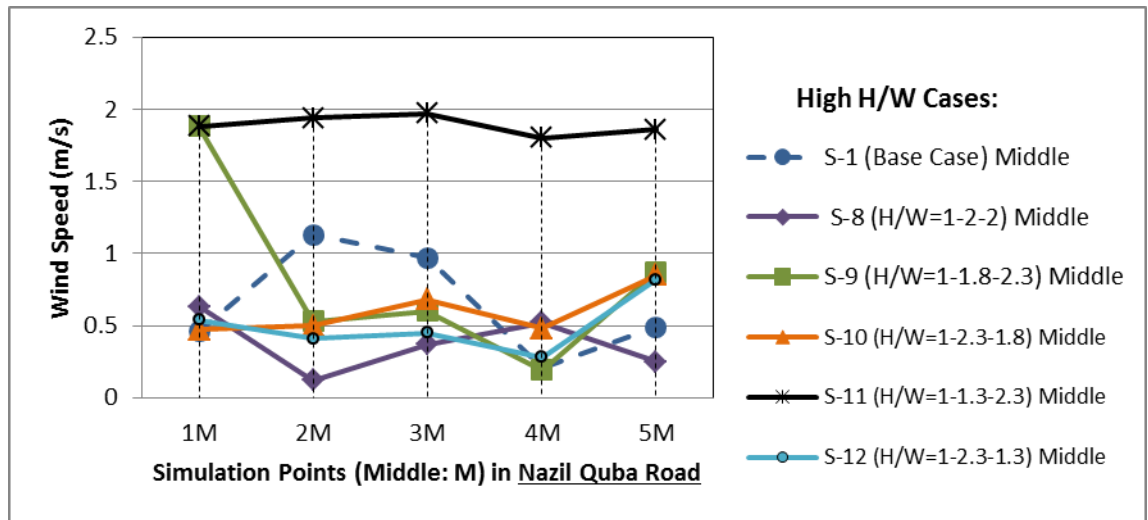
A7. 27: Wind velocity at the left simulation points (leeward) in the high asymmetrical aspect ratio scenarios, particularly in the Nazil Quba Road (between the second and the third rows of buildings).

Figures A7.28 and 7.29 demonstrate the wind speed values along the middle points of the Tali'e and the Nazil Quba Roads canyons, respectively. In the Tali'e Quba Road, it is found that the wind speeds pattern is similar in most of the high aspect ratio scenarios, with highest wind speed values found in S-10 (H/W=1-2.3-1.8), followed by S-12 (H/W=1-2.3-1.3), then S-8 (H/W=1-2-2) and S-9 (H/W=1-1.8-2.3), while S-11 (H/W=1-1.3-2.3) is the lowest. However, there is no major difference in wind speeds at the middle points of this road in S-11, which is lower than the base case (S-1) scenario with maximum difference of about 0.8-1m/s at location 3 and 4. The difference in wind speed in the Tali'e Canyon at location 4 and 5 is significantly high in S-10, S-12, S-8, and S-9 scenarios when compared with the base case, with approximate difference reached up to 1.5m/s at location 5, followed by 0.92m/s at location 4 in S-10 scenario.

On the other hand, in the Nazil Quba road, it is found that the wind speed is significantly higher in S-11 scenario when compared with the base case (S-1) at all the five locations near in the middle of the road. The maximum difference found at location 4 with a difference value of 1.6m/s, followed by location 1, 5, 3 and 2 with a value of 1.4m/s, 1.4m/s, 1m/s and 0.8m/s, respectively. However, the rest of the scenarios (i.e. S-8, S-9, S-10, and S-12) have minor difference in wind velocity values in comparison to the base case. It is found that the middle points receive higher wind velocities at pedestrian level than those points located at the leeward and windward sides of the buildings, followed by the near windward wall points (right points), while leeward (left) points are the worst.

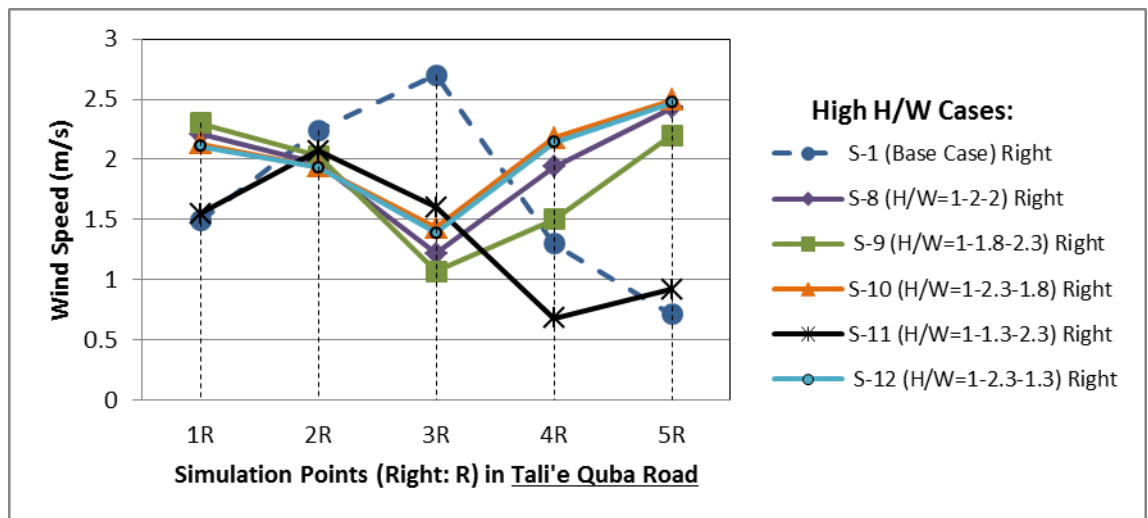


A7. 28: Wind velocity at the middle simulation points in the high asymmetrical aspect ratio scenarios, particularly in the Tali'e Quba Road (between the first and the second rows of buildings).



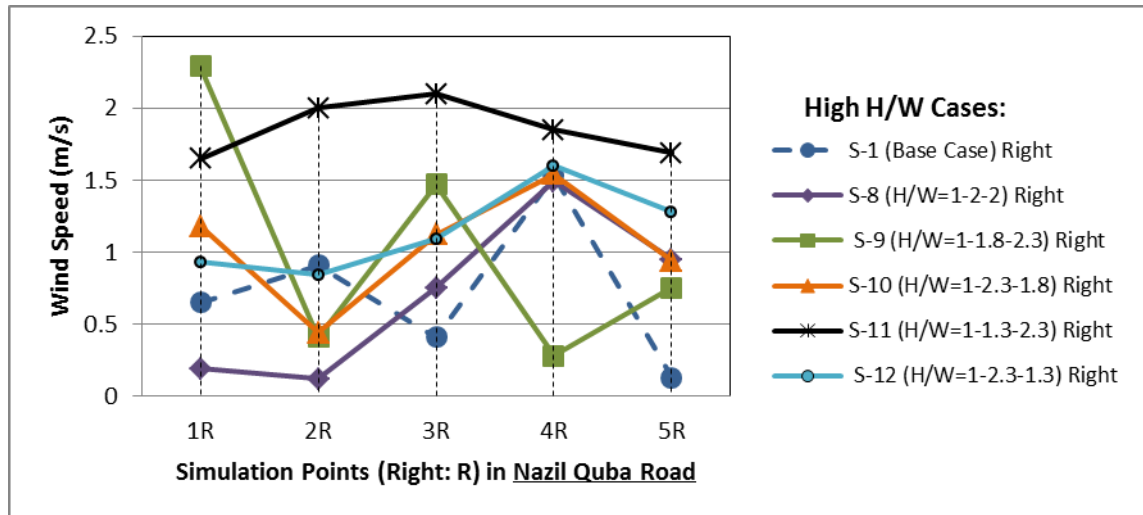
A7. 29: Wind velocity at the middle simulation points in the high asymmetrical aspect ratio scenarios, particularly in the Nazil Quba Road (between the second and the third rows of buildings).

Figures A7.30 and A7.31 demonstrate the wind speed values at points near the windward walls (right points) of the Tali'e and the Nazil Quba Roads canyons, respectively. In the Tali'e Quba Road, it is found that the wind speeds pattern is similar in most of the high aspect ratio scenarios, with highest wind speed values found in S-10 (H/W=1-2.3-1.8), followed by S-12 (H/W=1-2.3-1.3), then S-8 (H/W=1-2-2) and S-9 (H/W=1-1.8-2.3), while S-11 (H/W=1-1.3-2.3) is the lowest. Major difference in wind speeds reduction at location 3 near the windward side is found in all the five high asymmetrical scenarios when compared to the base case, while the wind flow rate greatly increases in these scenarios at location 5, except for scenario S-11.



A7. 30: Wind velocity near the windward walls (right points) in the high asymmetrical aspect ratio scenarios, particularly in the Tali'e Quba Road (between the first and the second rows of buildings).

On the other hand, in the Nazil Quba road, it is found that the wind speed is significantly higher in S-11 scenario when compared with the base case (S-1) at all the five locations near the windward walls (right points). The maximum difference found at location 3 with a difference value of 1.69m/s, followed by location 5, 2, 1 and 4 with a value of 1.6m/s, 1.1m/s, 1m/s and 0.3m/s, respectively.

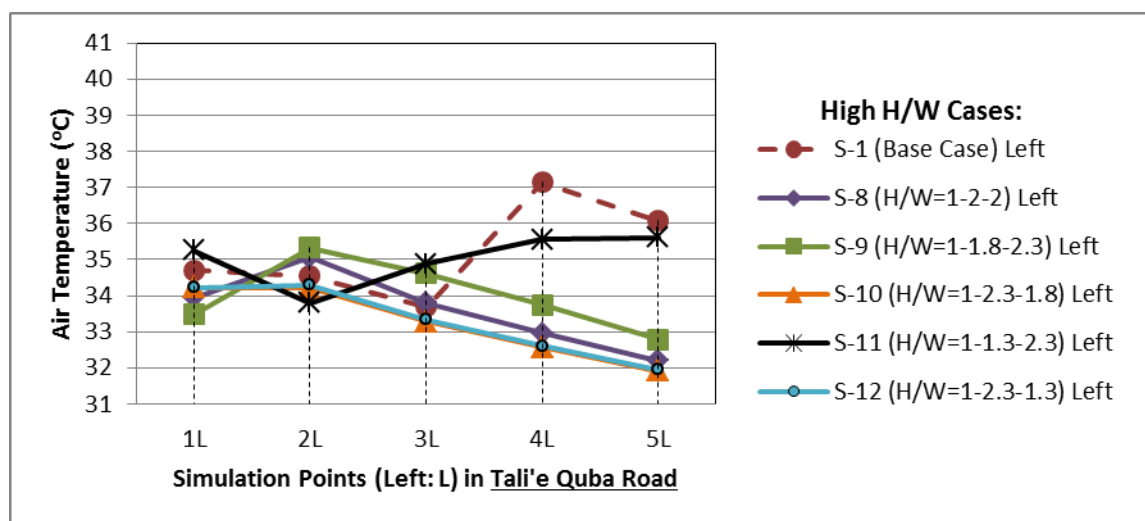


A7. 31: Wind velocity near the windward walls (right points) in the high asymmetrical aspect ratio scenarios, particularly in the Nazil Quba Road (between the second and the third rows of buildings).

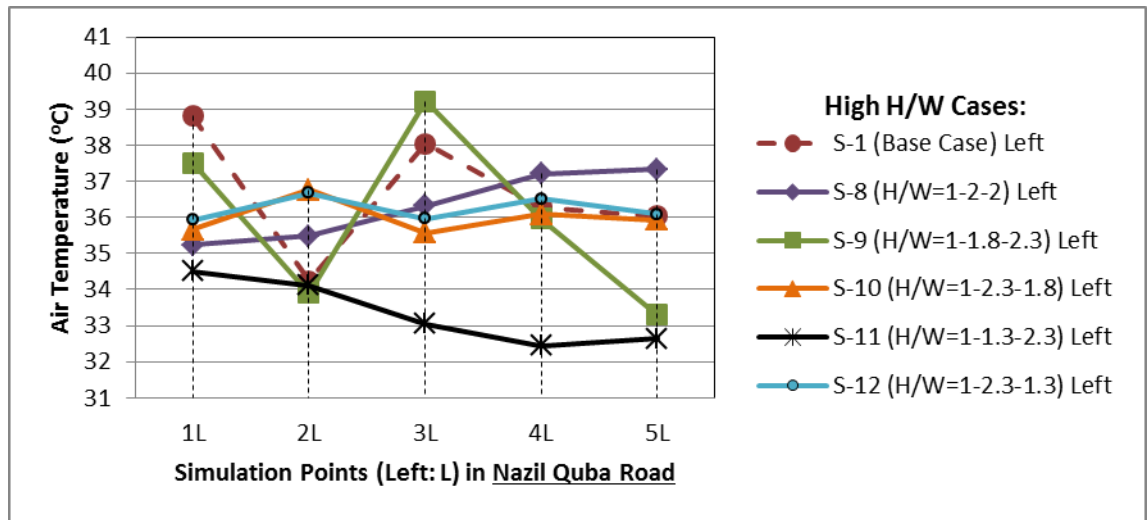
**A7: Appendices for Chapter 7 (From A7.32 to A7.37): Results of Air Temperature in the High Aspect Ratio Cases (S-8, S-9, S-10, S-11, and S-12)**

Figures A7.32 and A7.33 demonstrate the air temperature values near the leeward walls (left points) of the Tali'e and the Nazil canyons, respectively at the pedestrian level. In the Tali'e Quba Road, it is found that air temperature pattern in S-8, S-9, S-10 and S-12 is similar in almost all of the locations, with the highest values found at location 2. While S-11 has different temperature pattern than all of the rest of the proposed scenarios in the Tali'e canyon, with the highest values found at location 1, 3, 4 and 5 (while location 2 is the lowest). However, S-11 is lower than S-1 in location 2, 4 and 5. The average air temperatures at the Tali'e leeward side of the canyon for S-8, S-9, S-10, S-11 and S-12 are 33.6°C, 34.0°C, 33.2°C, 35.0°C and 33.3°C, respectively.

On the other hand, in the Nazil Quba road, it is found that the air temperature near the leeward walls is significantly lower in S-11 scenario when compared with the base case (S-1) and the rest of the scenarios at all the five measurement locations. The maximum difference found at location 3 with a difference value of 5.6°C, which is due to the highest wind speed been recorded at this location. The average air temperatures at the leeward side of the Nazil canyon for S-8, S-9, S-10, S-11 and S-12 are 36.3°C, 36.0°C, 36.0°C, 33.4°C and 36.2°C, respectively.



A7. 32: Air temperature at the left simulation points (leeward) in the high asymmetrical aspect ratio scenarios, particularly in the Tali'e Quba Road (between the first and the second rows of buildings).

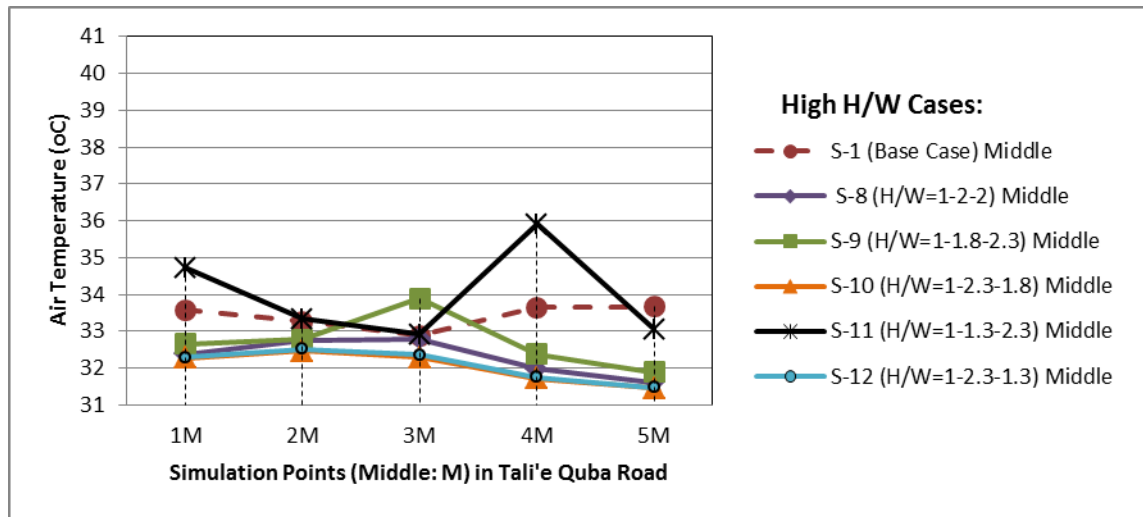


A7. 33: Air temperature at the left simulation points (leeward) in the high asymmetrical aspect ratio scenarios, particularly in the Nazil Quba Road (between the second and the third rows of buildings).

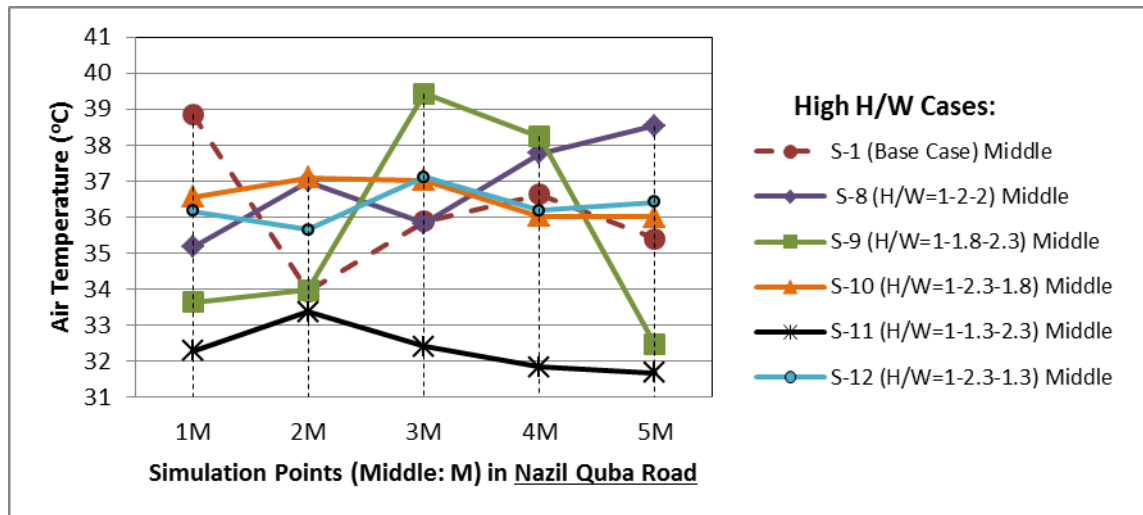
Figures A7.34 and A7.35 demonstrate the air temperature values along the middle row of points in the Tali'e and the Nazil canyons, respectively at the pedestrian level. In the Tali'e Quba Road, it is found that air temperature pattern is similar and stable for approximately all of the high aspect ratio scenarios, and the lowest average temperature being S-10 with a value of 32.04°C, followed by S12, S-8, and S-9 with a value of 32.1°C, 32.3°C, and 32.7°C, respectively. While S-11 has the highest temperature value with slightly different temperature pattern than the rest, with the value of 34.0°C.

On the other hand, in the Nazil Quba road, it is found that the air temperature in the middle row of extracted points is significantly lower than all of the proposed scenarios and the base case S-1 scenario. It is even lower than the leeward row of points that mentioned above, which is as a result of higher wind vortices found here than the leeward side, thus leading to reduced air temperature by convective heat transfer (e.g. Defraeye et al., 2010). The average air temperatures in the middle points of the Nazil canyon for S-8, S-9, S-10, S-11 and S-12 are 36.7°C, 35.6°C, 36.5°C, 32.3°C and 36.3°C, respectively. Thus, S-11 achieved significant air temperature reduction in the middle of the Nazil canyon as well as along the leeward row of points.





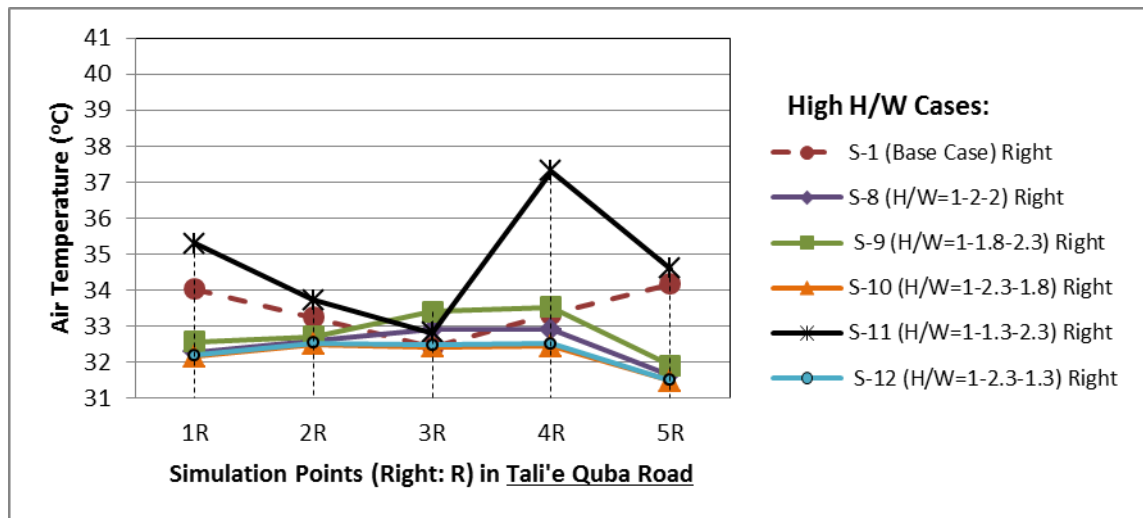
A7. 34: Air temperature at the middle simulation points in the high asymmetrical aspect ratio scenarios, particularly in the Tali'e Quba Road (between the first and the second rows of buildings).



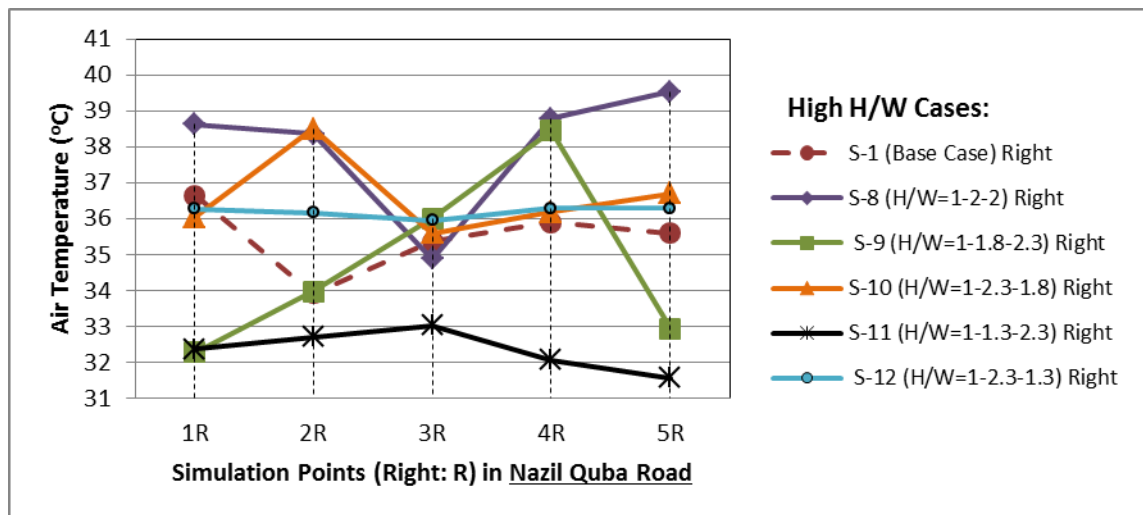
A7. 35: Air temperature at the middle simulation points in the high asymmetrical aspect ratio scenarios, particularly in the Nazil Quba Road (between the second and the third rows of buildings).

Figures A7.36 and A7.37 demonstrate the air temperature values along the right row of points, near the windward walls, in the Tali'e and the Nazil canyons, respectively at the pedestrian level. Air temperature pattern in the windward is similar to the middle row of points that mentioned above, particularly in the Tali'e canyon. The lowest average temperature is found in S-10 within all the five locations with an average value of 32.2°C, followed by S12, S-8 and S-9 with a value of 32.3°C, 32.5°C, and 32.8°C, respectively. However, S-11 scenario is found has the highest temperature and different pattern than the rest with a value of 34.6°C. On the other hand, in the Nazil Quba road, it is found that the air temperature at the windward row of extracted points is

significantly lower than all of the proposed scenarios and the base case S-1 scenario. It is even lower than the leeward row of points and slightly above the readings of the middle points that mentioned above, which is as a result of higher wind vortices found here than the leeward and wind windward sides, thus leading to reduced air temperature by convective heat transfer. The average air temperatures at the windward points of the Nazil canyon for S-8, S-9, S-10, S-11 and S-12 are 38.0°C, 34.7°C, 36.6°C, 32.4°C and 36.2°C, respectively. Thus, S-11 achieved significant air temperature reduction in the middle, left and right sides of the Nazil canyon.

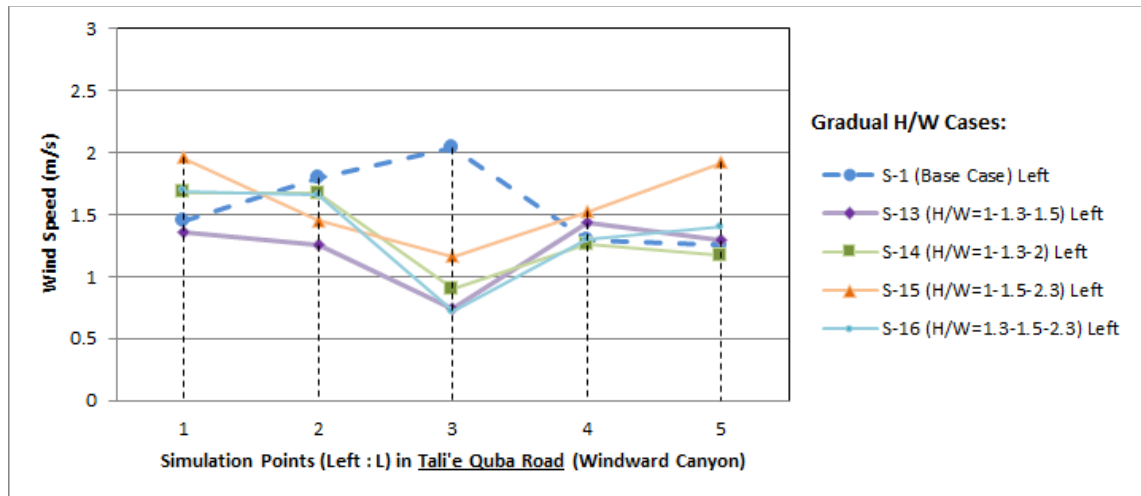


A7. 36: Air temperature near the windward walls (right points) in the high asymmetrical aspect ratio scenarios, particularly in the Tali'e Quba Road (between the first and the second rows of buildings).

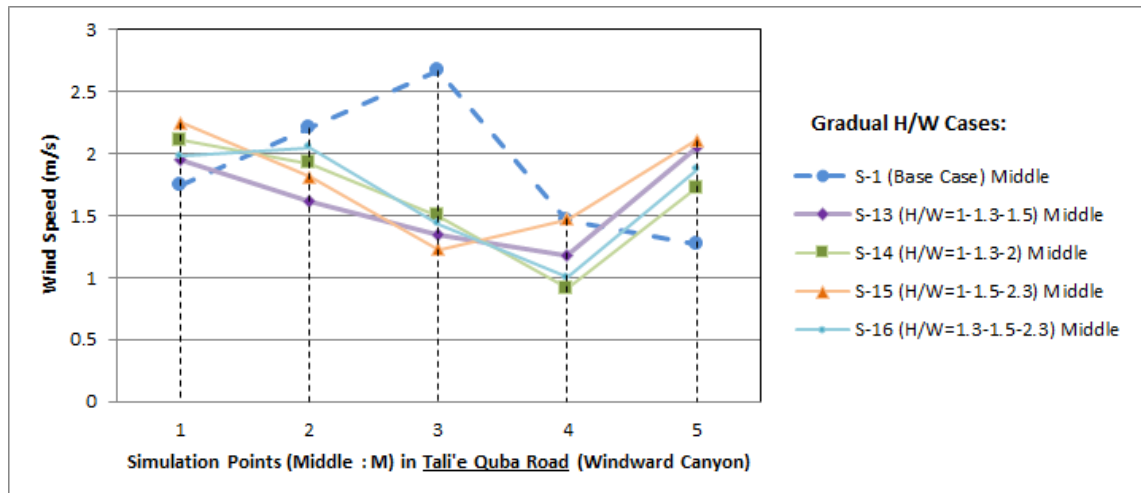


A7. 37: Air temperature near the windward walls (right points) in the high asymmetrical aspect ratio scenarios, particularly in the Nazil Quba Road (between the second and the third rows of buildings).

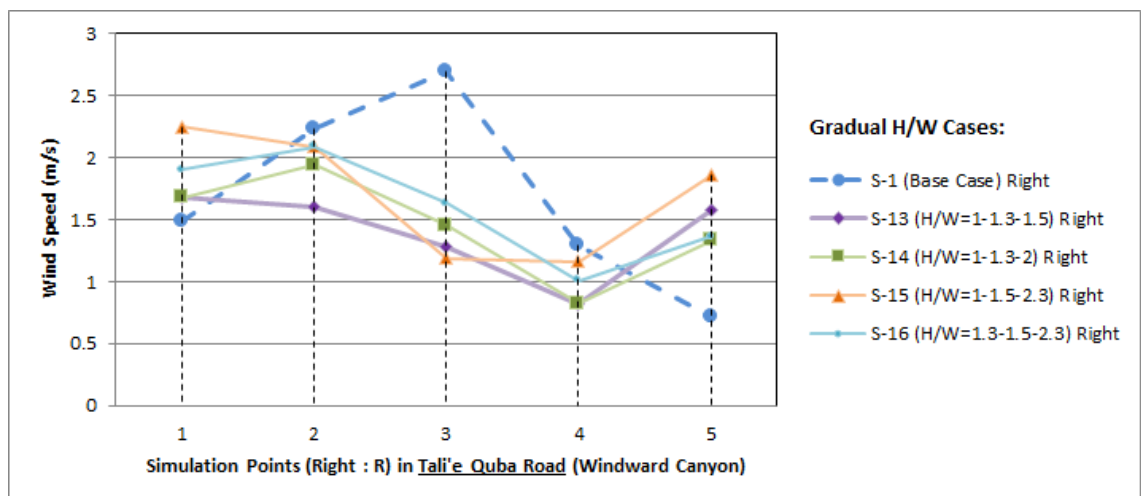
**A7: Appendices for Chapter 7 (From A7.38 to A7.43): Results of Wind Velocity in the Leeward Gradual Increase in Aspect Ratio Cases (S-13, S-14, S-15, and S-16)**



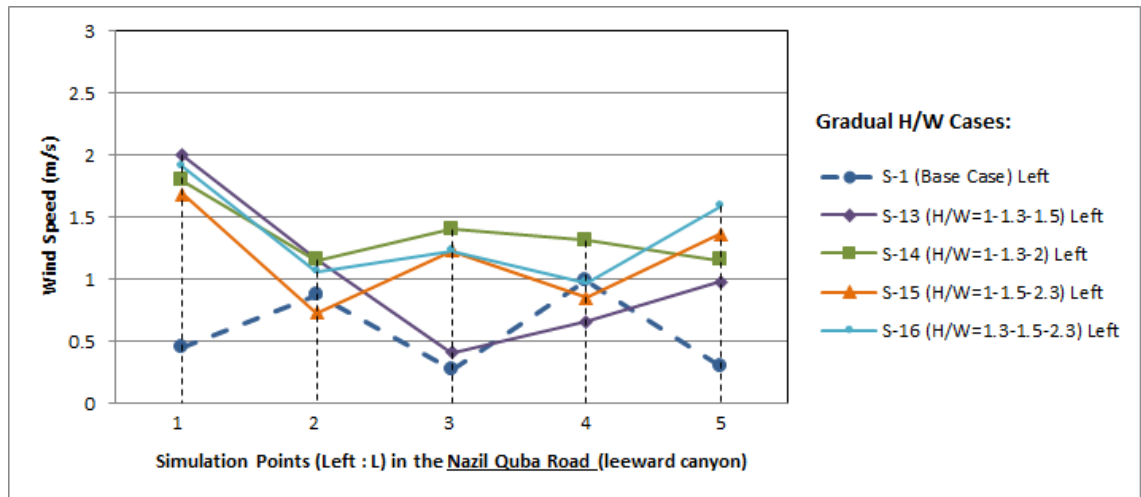
A7. 38: Wind velocity at the left side (near leeward elevations) of Tali'e Quba Road (windward canyon) in the the gradual increase in aspect ratios models (S-13 to S-16) and compared with the base case S-1 scenario.



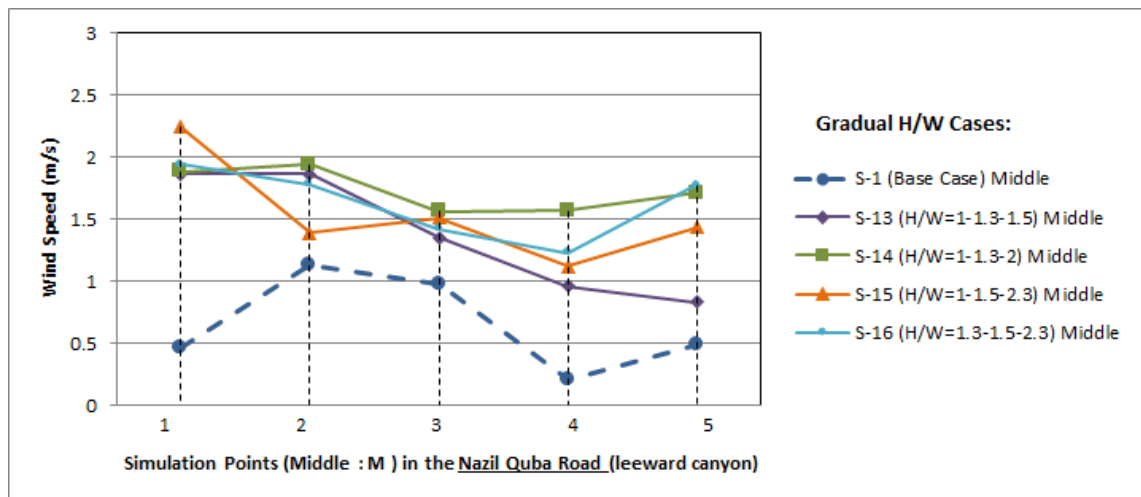
A7. 39: Wind velocity in the middle of Tali'e Quba Road (windward canyon) in the the gradual increase in aspect ratios models (S-13 to S-16) and compared with the base case S-1 scenario.



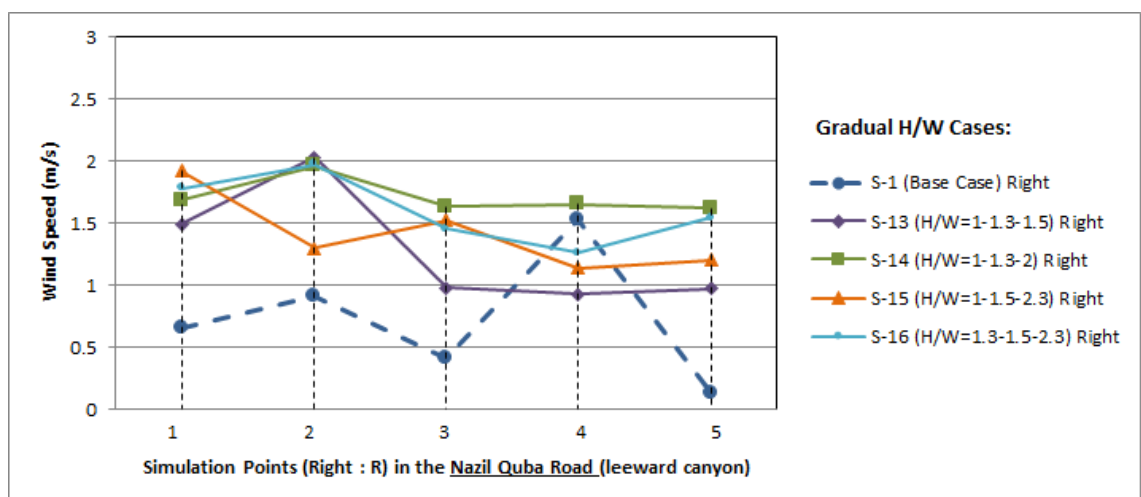
A7. 40: Wind velocity at the right side (near windward elevations) of Tali'e Quba Road (windward canyon) in the the gradual increase in aspect ratios models (S-13 to S-16) and compared with the base case S-1 scenario.



A7. 41: Wind velocity at the left side (near leeward elevations) of Nazil Quba Road (leeward canyon) in the the gradual increase in aspect ratios models (S-13 to S-16) and compared with the base case S-1 scenario.

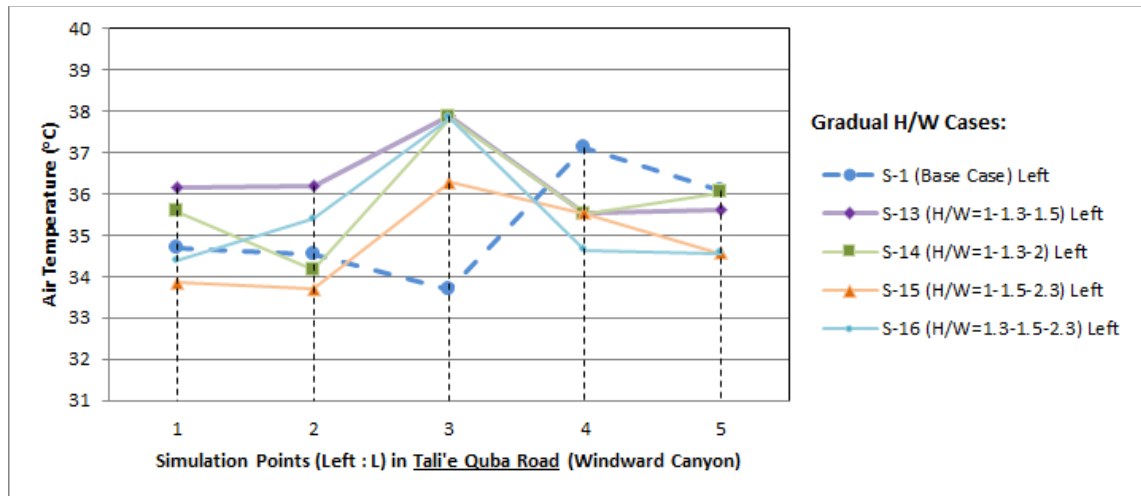


A7. 42: Wind velocity in the middle of Nazil Quba Road (leeward canyon) in the the gradual increase in aspect ratios models (S-13 to S-16) and compared with the base case S-1 scenario.

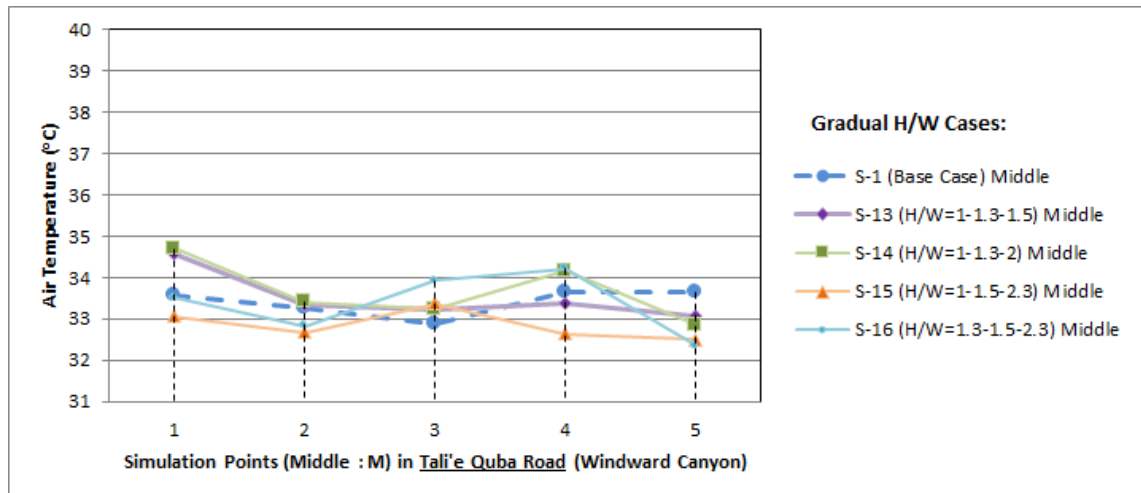


A7. 43: Wind velocity at the right side (near windward elevations) of Nazil Quba Road (leeward canyon) in the the gradual increase in aspect ratios models (S-13 to S-16) and compared with the base case S-1 scenario.

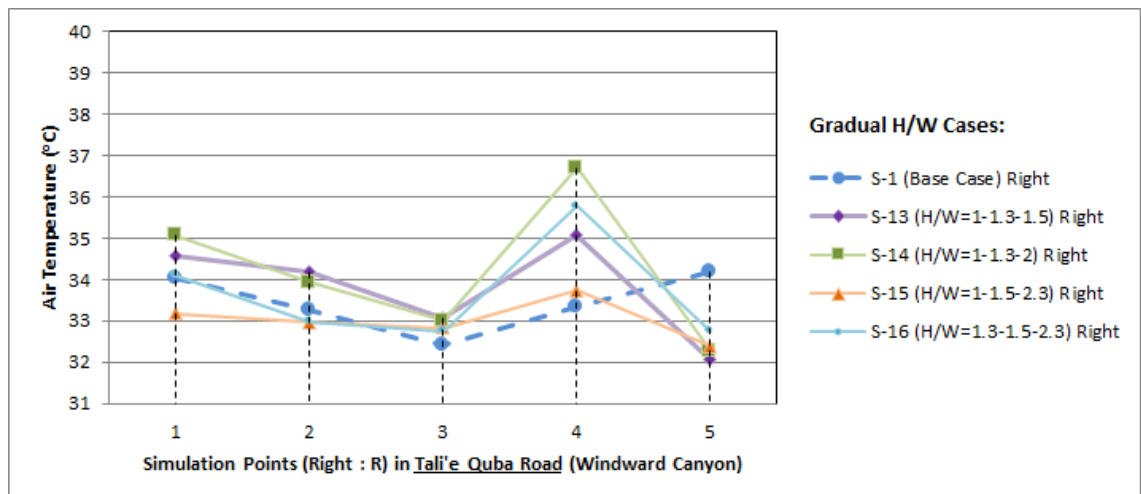
**A7: Appendices for Chapter 7 (From A7.44 to A7.49): Results of Air Temperature in the Leeward Gradual Increase in Aspect Ratio Cases (S-13, S-14, S-15, and S-16)**



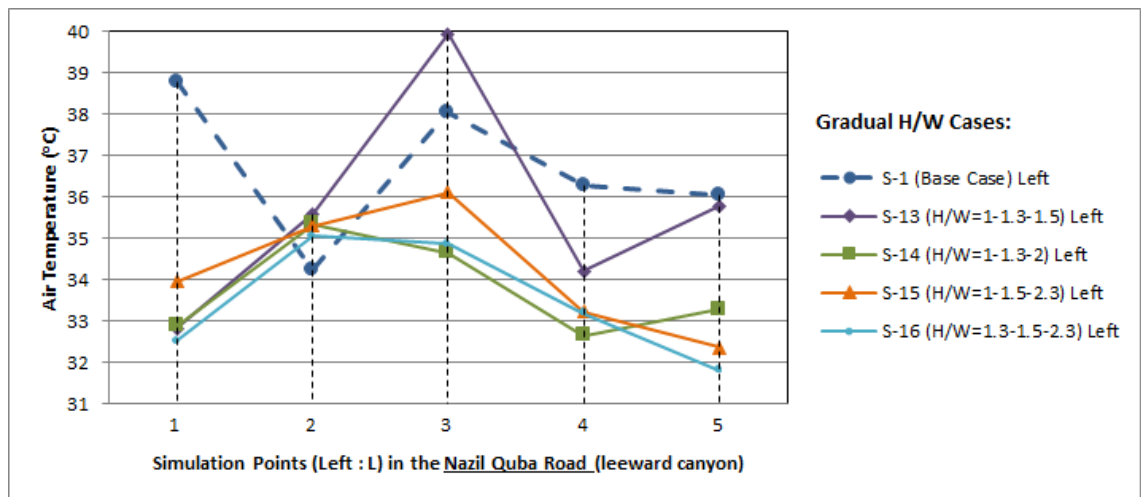
A7. 44: Air temperature at the left side (near leeward elevations) of Tali'e Quba Road (windward canyon) in the the gradual increase in aspect ratios models (S-13 to S-16) and compared with the base case S-1 scenario.



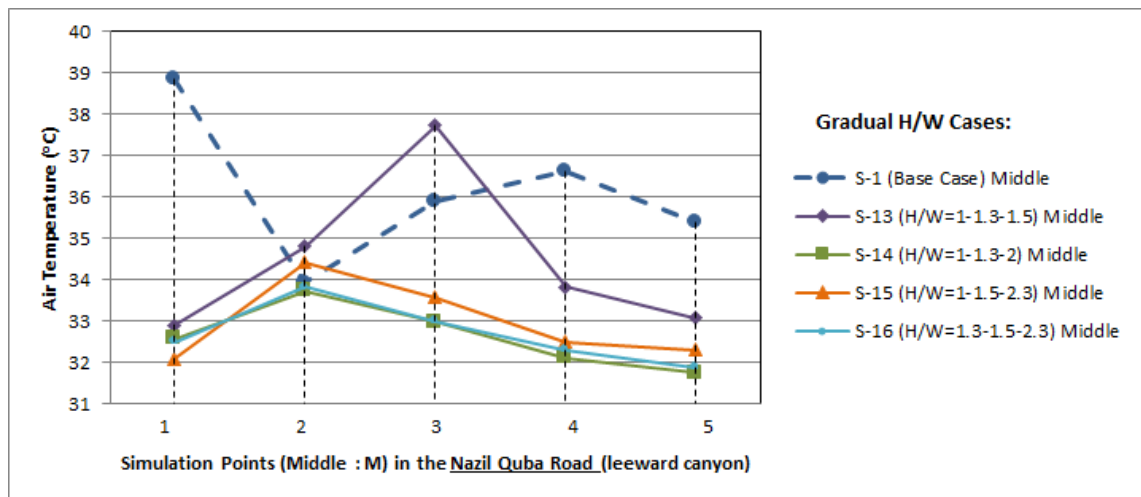
A7. 45: Air temperature in the middle of Tali'e Quba Road (windward canyon) in the the gradual increase in aspect ratios models (S-13 to S-16) and compared with the base case S-1 scenario.



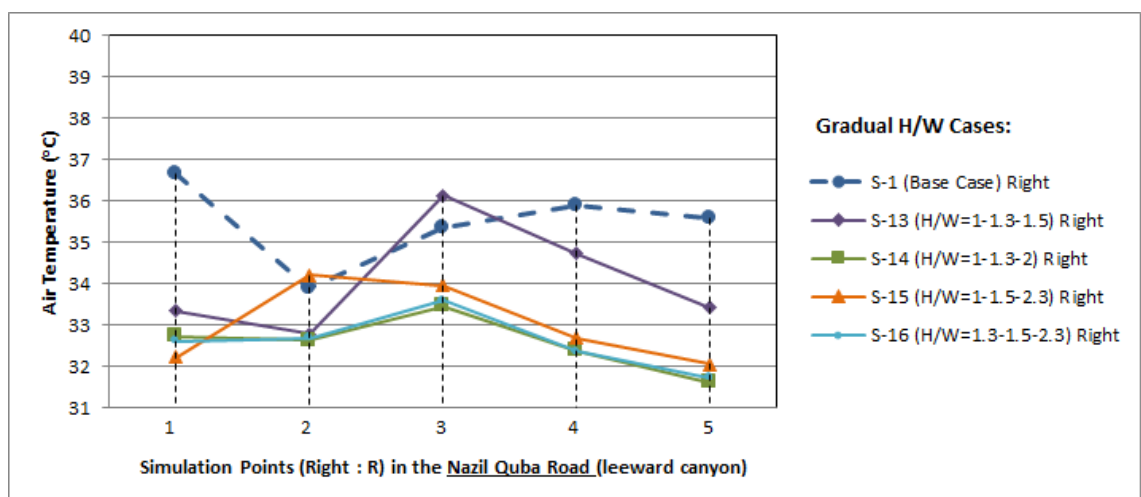
A7. 46: Air temperature at the right side (near windward elevations) of Tali'e Quba Road (windward canyon) in the the gradual increase in aspect ratios models (S-13 to S-16) and compared with the base case S-1 scenario.



A7. 47: Air temperature at the left side (near leeward elevations) of Nazil Quba Road (leeward canyon) in the the gradual increase in aspect ratios models (S-13 to S-16) and compared with the base case S-1 scenario.



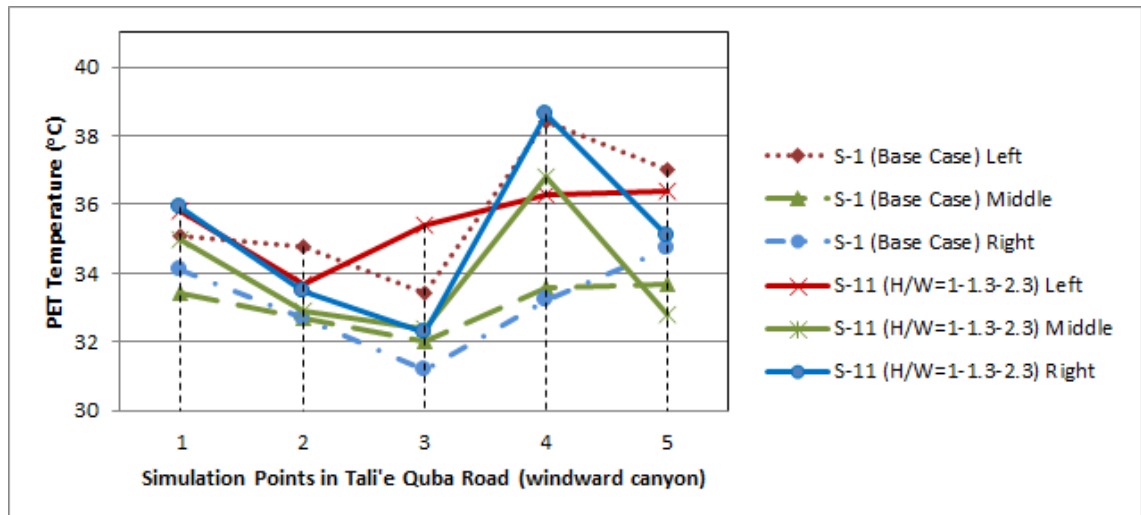
A7. 48: Air temperature in the middle of Nazil Quba Road (leeward canyon) in the the gradual increase in aspect ratios models (S-13 to S-16) and compared with the base case S-1 scenario.



A7. 49: Air temperature at the right side (near windward elevations) of Nazil Quba Road (leeward canyon) in the the gradual increase in aspect ratios models (S-13 to S-16) and compared with the base case S-1 scenario.

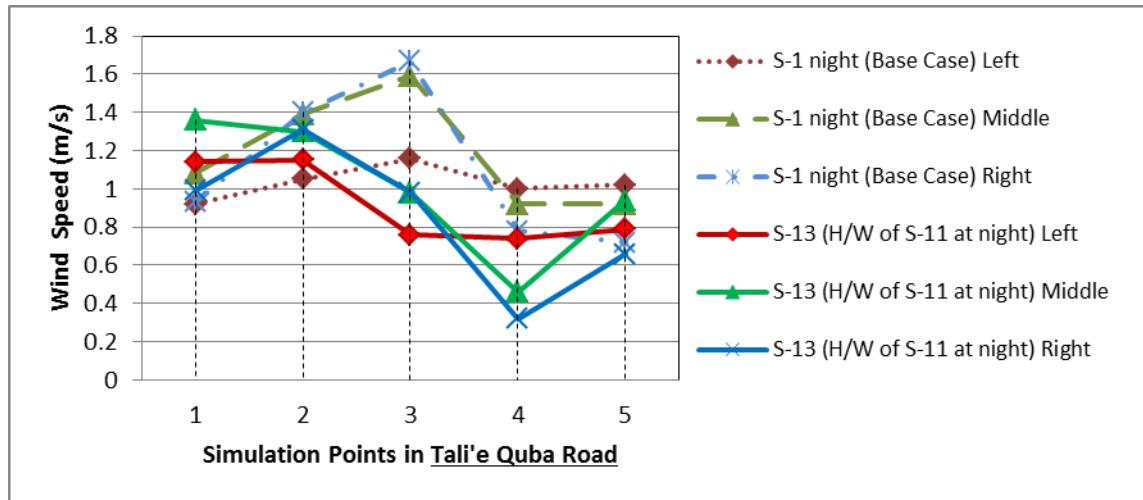


**Appendix 7.50: Results of the PET temperature for the windward canyon (Tali'e Quba Road) in the S-11 scenario compared to the base case S-1 model, particularly at the Left, Middle and Right measurement point locations.**

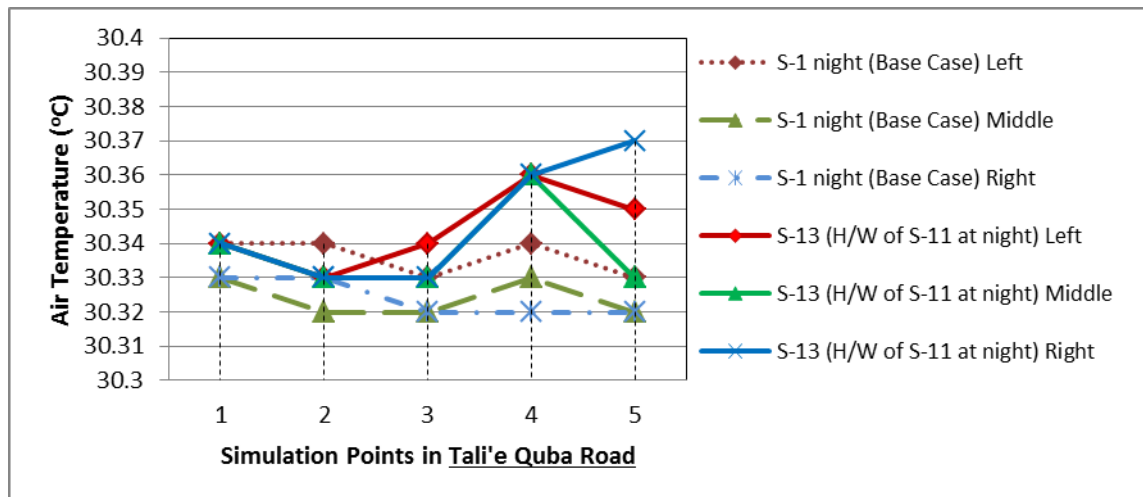


*A7. 50: PET temperature in the windward canyon (i.e. Tali'e Quba Road) near the windward walls (right points), leeward walls (left points) and middle of the canyon in the high asymmetrical aspect ratio scenario of S-11.*

**A8: Appendices A8.1 – A8.2 for Chapter 8: microclimatic results in the Tali'e Quba Road (i.e. the windward canyon) for the Night wind flow variation scenario (S-13) for the optimum H/W model, and compared with the existing situation at night (i.e. S-1 Night).**

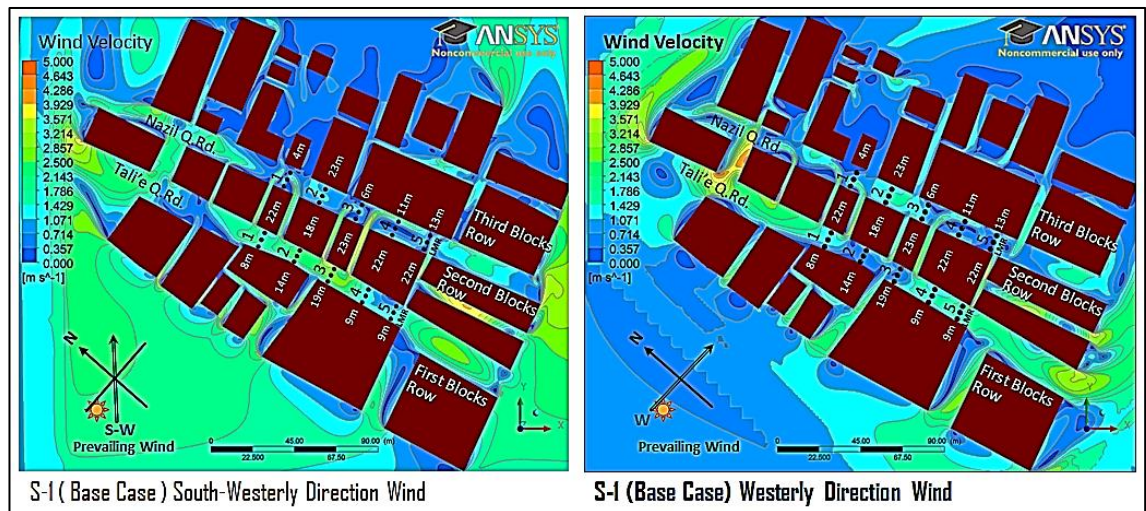


*A8. 1: Wind velocity at pedestrian height (2m) for S-13 that represents the night time (21:00pm) case based on the best H/W of (S-11), and compared with the base case (S-1) at night in the Tali'e Quba Road along five cross-sections at the left (leeward), middle and right (windward) rows of points*

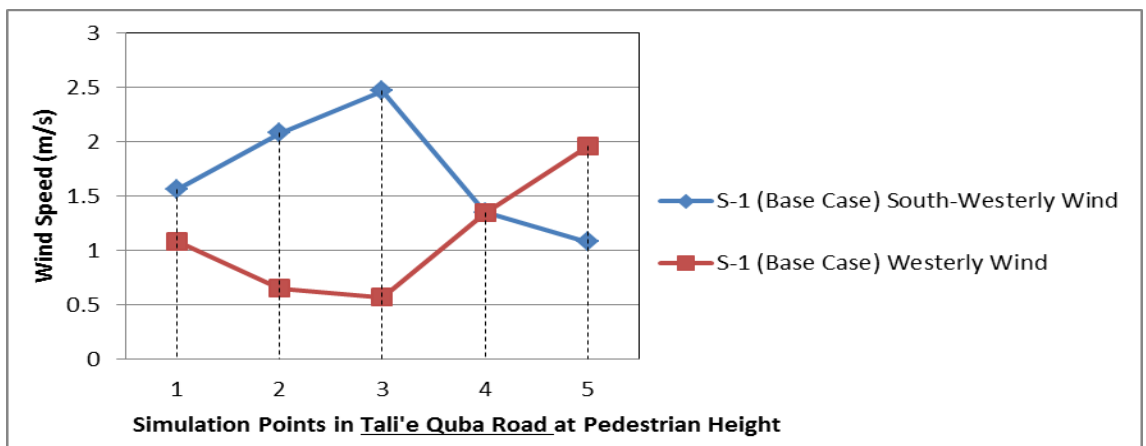


*A8. 2: Air temperature at pedestrian height (2m) for S-13 that represents the night time (21:00pm) case based on the best H/W of (S-11), and compared with the base case (S-1) at night in the Tali'e Quba Road along five cross-sections at the left (leeward), middle and right (windward) rows of points.*

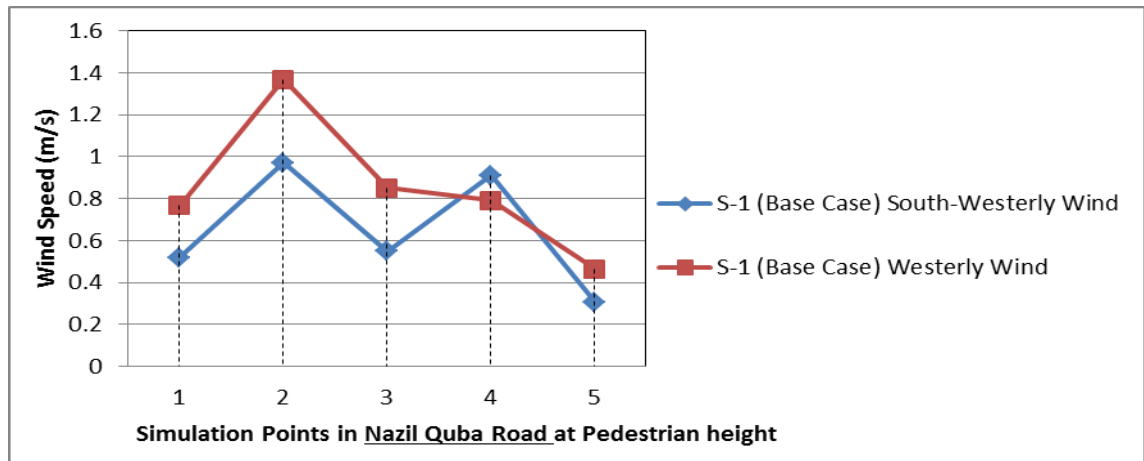
**A8: Appendices A8.3 to A8.8 for Chapter 8: Base Cases (S-1) scenarios of the existing conditions with westerly less prevailing wind direction**



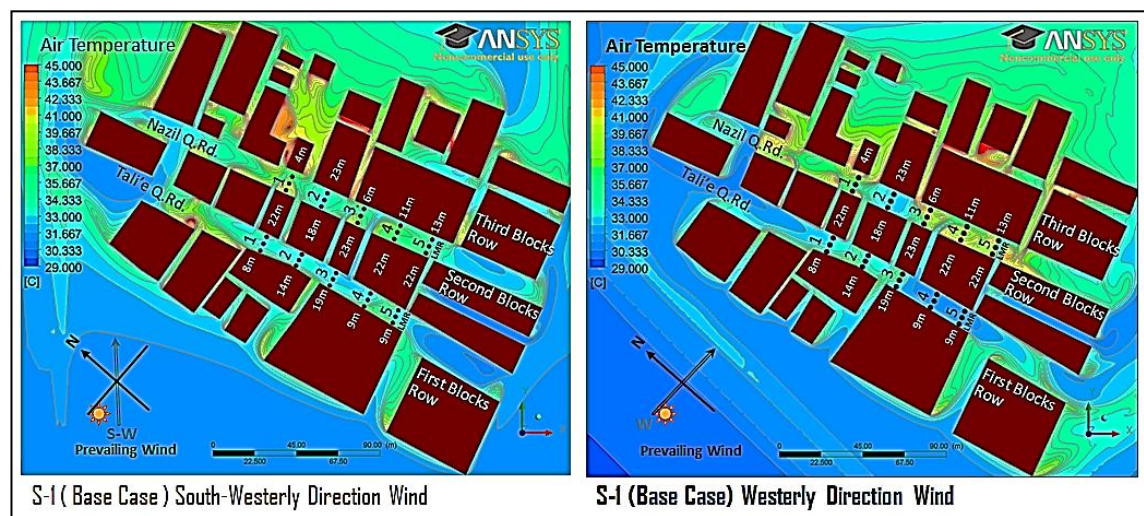
*A8. 3: Contours of velocity magnitude (m/s) at pedestrian height (2m) for the base case with South-Westerly wind direction (S-1 south-west) and Westerly wind direction (S-1 west) scenarios*



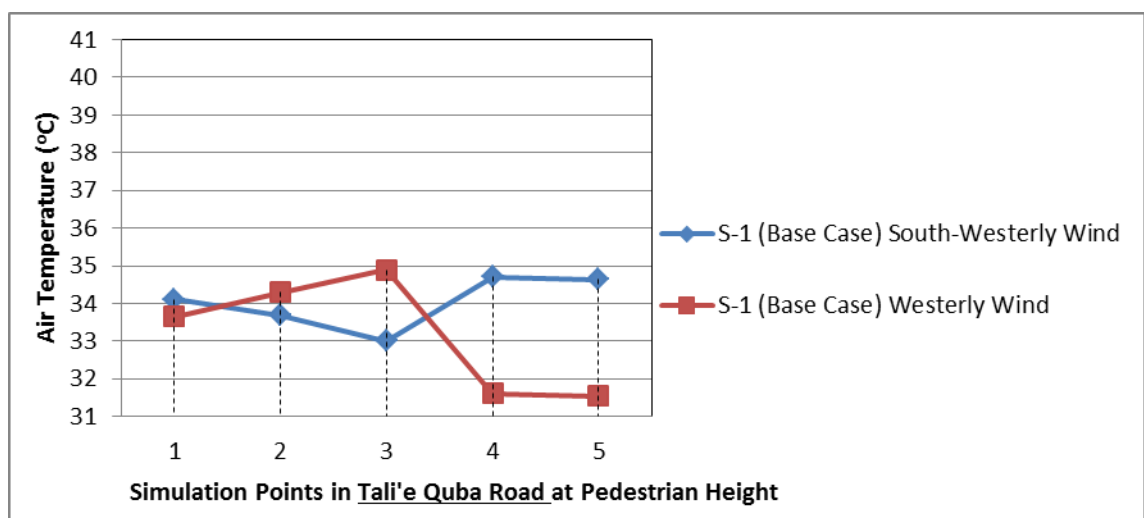
*A8. 4: Wind velocity in the Tali'e Q.Rd. at pedestrian height (2m) for the base case with South-Westerly wind direction (S-1 south-west) and Westerly wind direction (S-1 west) scenarios.*



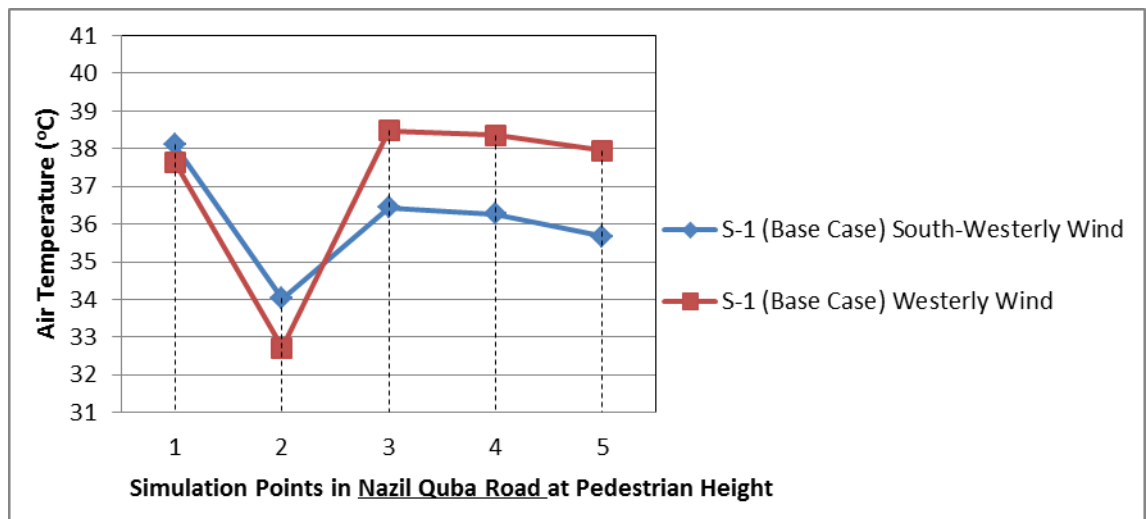
A8. 5: Wind velocity in the Nazil Q.Rd. at pedestrian height (2m) for the base case with South-Westerly wind direction (S-1 south-west) and Westerly wind direction (S-1 west) scenarios.



A8. 6: Contours of air temperature degrees (oC) at pedestrian height (2m) for the base case with South-Westerly wind direction (S-1 south-west) and Westerly wind direction (S-1 west) scenarios



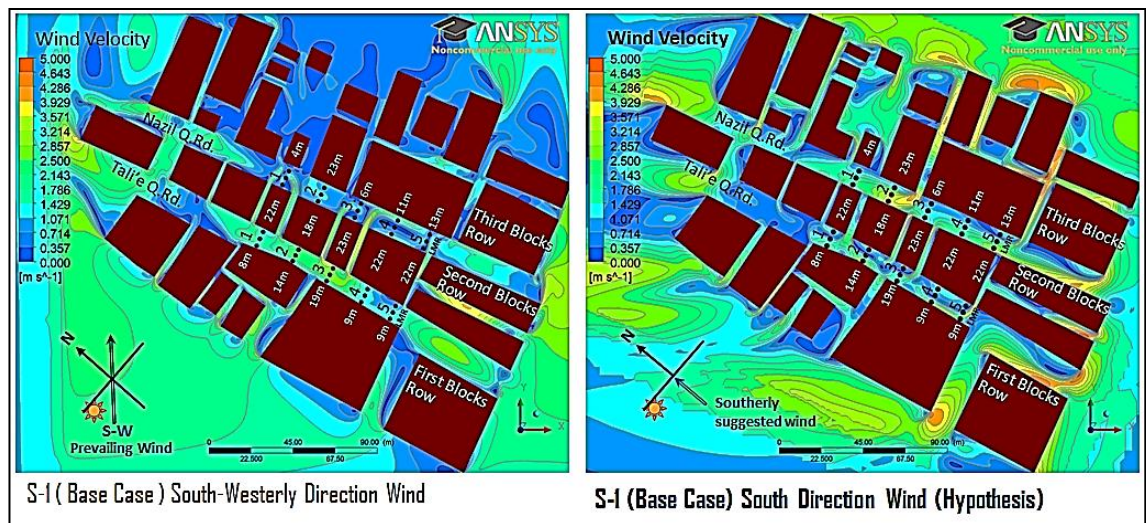
A8. 7: Air temperature in the Tali'e Q.Rd. at pedestrian height (2m) for the base case with South-Westerly wind direction (S-1 south-west) and Westerly wind direction (S-1 west) scenarios.



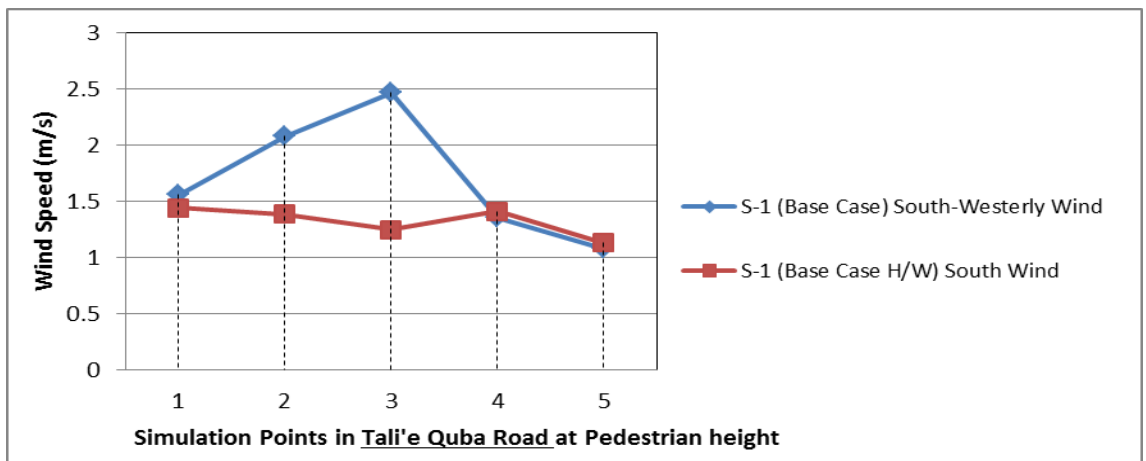
A8. 8: Air temperature in the Nazil Q.Rd. at pedestrian height (2m) for the base case with South-Westerly wind direction (S-1 south-west) and Westerly wind direction (S-1 west) scenarios



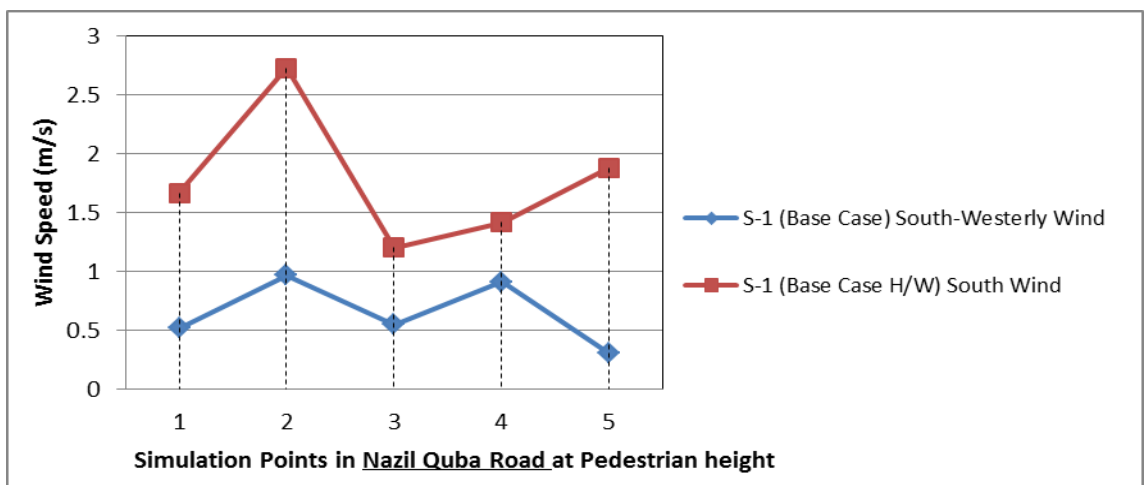
**A8: Appendices A8.9 to A8.14 for Chapter 8: Parallel Wind Direction (from South) with Urban Canyons in the Base Case**



A8. 9: Contours of velocity magnitude (m/s) at pedestrian height (2m) for the base case with a hypothesised South wind direction (S-1 South) parallel with the urban canyons, and compared with south-westerly wind direction.

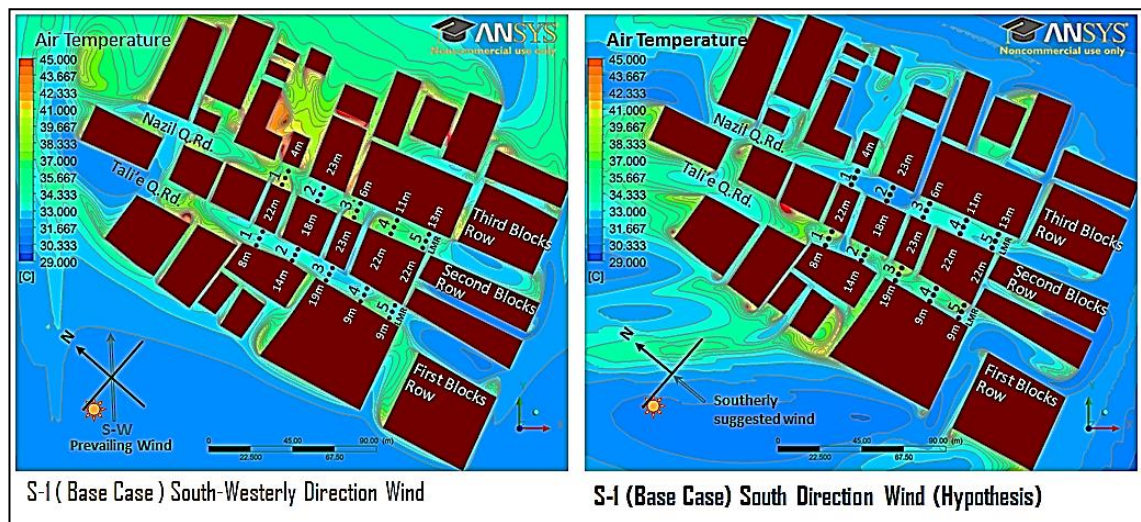


A8. 10: Wind velocity in the Tali'e Q.Rd. at pedestrian height (2m) for the base case with hypothesised South wind direction (S-1 south) i.e. parallel with the urban canyons, and compared with the prevailing south-westerly direction.

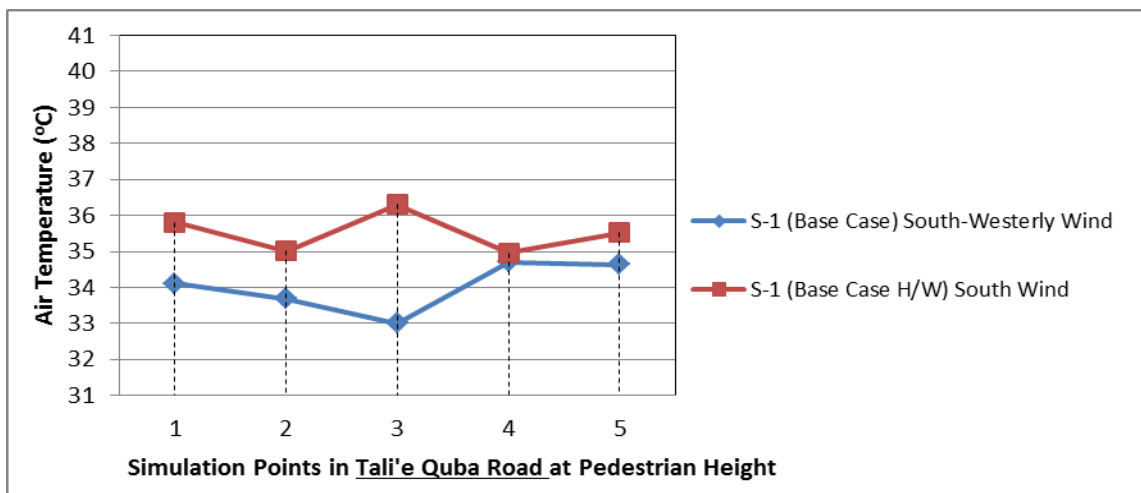


A8. 11: Wind velocity in the Nazil Q.Rd. at pedestrian height (2m) for the base case with hypothesised South wind direction (S-1 south) parallel with the urban canyons, and compared with the prevailing south-westerly direction.

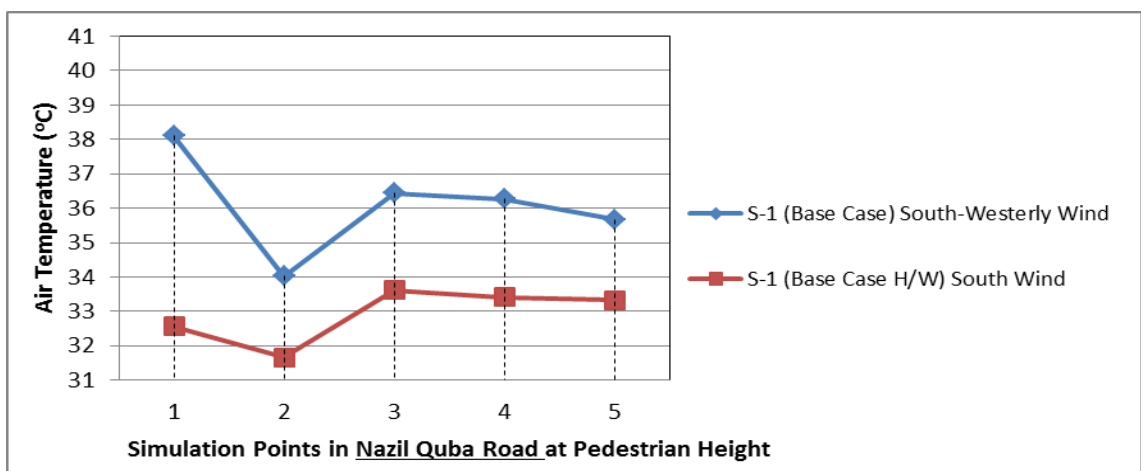




A8. 12: Contours of air temperature degrees (oC) at pedestrian height (2m) for the base case with a hypothesised South wind direction (S-1 South) parallel with the urban canyons, and compared with south-westerly wind direction.

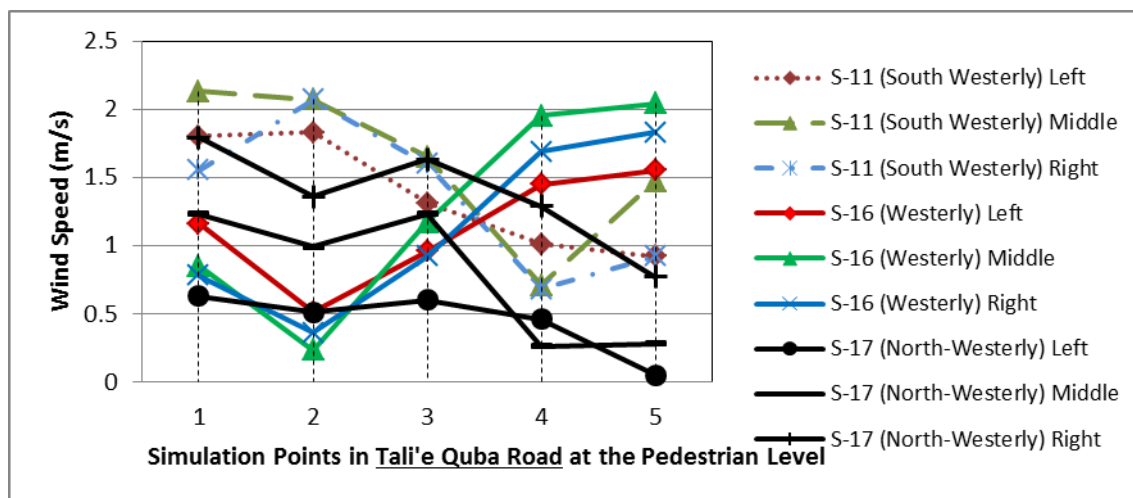


A8. 13: Air Temperature in the Tali'e Q.Rd. at pedestrian height (2m) for the base case with hypothesised South wind direction (S-1 south) parallel with the urban canyons, and compared with the prevailing south-westerly wind direction.

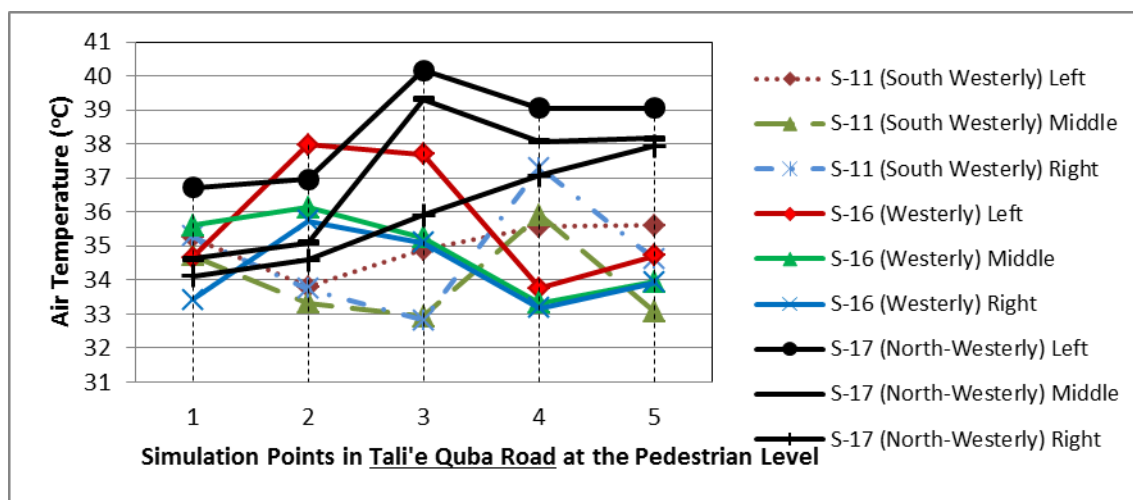


A8. 14: Air Temperature in the Nazil Q.Rd. at pedestrian height (2m) for the base case with hypothesised South wind direction (S-1 south) parallel with the urban canyons, and compared with the prevailing south-westerly wind direction.

**A8: Appendices A8.15 and A8.16 for Chapter 8. Orientation of the Urban Geometry with the Prevailing Wind Directions for the Best H/W Ratio Scenarios in the Tali'e Quba Road.**

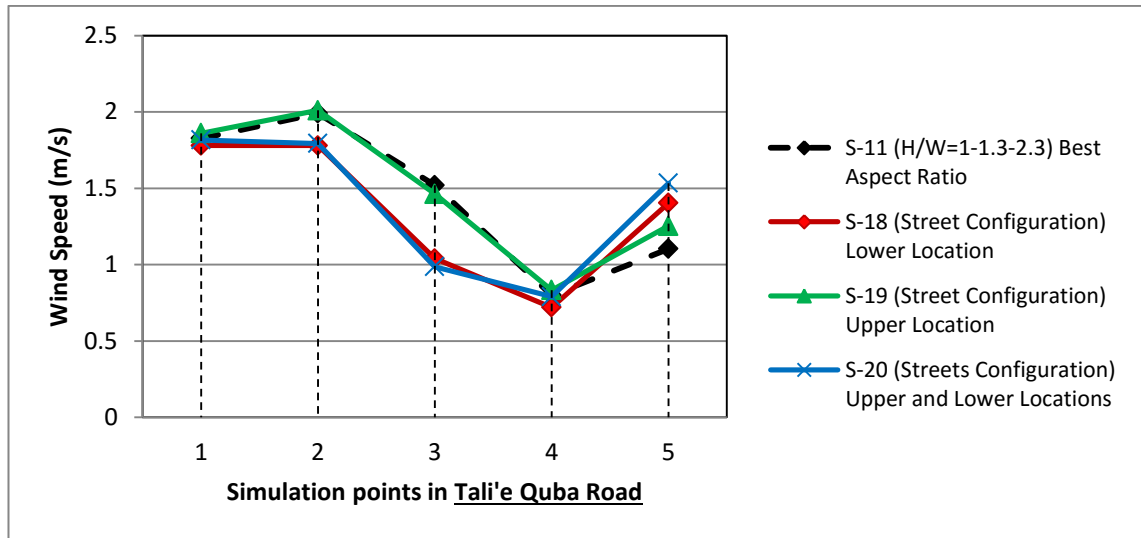


A8. 15: Wind speed at pedestrian height (2m) in the Tali'e Quba Road for the best aspect ratio with scenarios of Westerly prevailing wind direction (S-16) and North-Westerly prevailing wind (S-17), and compared with the best aspect ratio (S-11) scenario with South-Westerly prevailing wind.

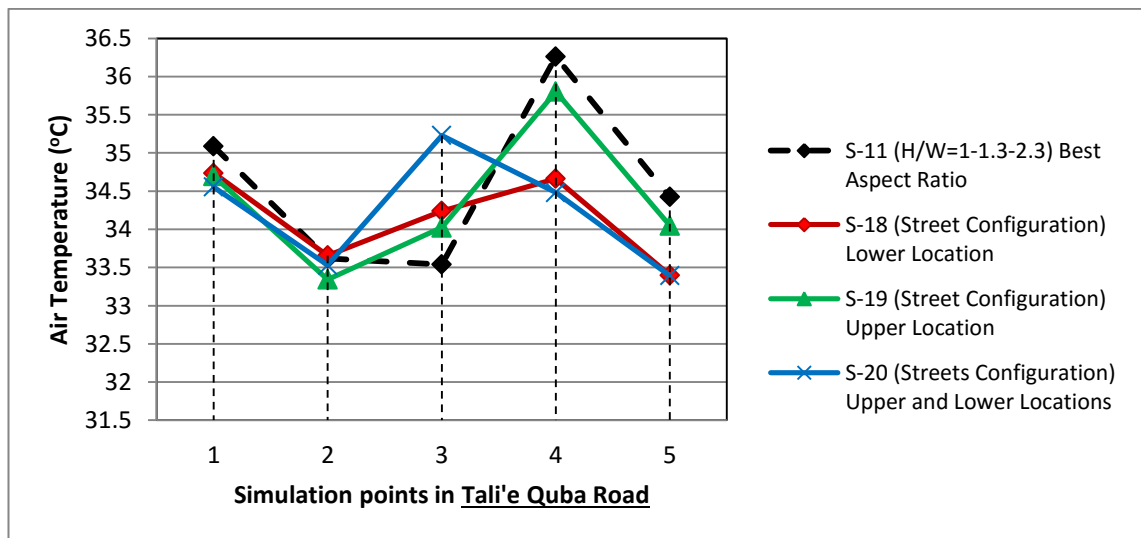


A8. 16: Air temperature at pedestrian height (2m) in the Tali'e Quba Road for the best aspect ratio with scenarios of Westerly prevailing wind direction (S-16) and North-Westerly prevailing wind (S-17), and compared with the best aspect ratio (S-11) scenario with South-Westerly prevailing wind.

**A8: Appendices A8.17 and A8.18 for Chapter 8. Streets Configuration with S-W Prevailing Wind Direction (results for Tali'e Quba Road for the best aspect ratio scenarios).**



A8. 17: Wind velocity for the streets configuration with different prevailing wind directions



A8. 18: Air Temperatures for the streets configuration with different prevailing wind directions